7th Hull Performance & Insight Conference

HullPIC'22

Edited by Volker Bertram

Sponsored by

www.jotun.com

tutech.de

www.hasytec.com

albis-mp.com

i-tech.se

www.vpsolutions.dk

www.marorka.com

www.mirosmocean.com

www.hempel.com

www.enamor.pl

www.hullwiper.co

www.ppg.com

www.kyma.no

www.wartsila.com

www.hoppe-marine.com

www.coach-solutions.dk

www.idealship.de

www.c-leanship.com

Veinland.net

www.deepsea.ai

Index

Frederik Hammer Berthelsen, Ulrik Dam Nielsen 4
Assessment of Ships' Speed-Power Relationship at Lower Sailing Speeds

Volker Bertram 16
Capabilities and Limits of Machine Learning

Volker Bertram 24
A Discussion of the Weather Factor in the EEDI/EEXI

Inno Gatin, Milan Kalajdžić 30
Energy Saving Devices Performance Assessment Using CFD

Naoto Sogihara, Mariko Kuroda, Masaru Tsujimoto 36
Lifecycle Assessment of Fuel Oil Consumption of a Ship in Service

Amy Parkes, Edwin Pang 50
Uncertainty Quantification and its Effect on Compliance Accuracy for Different Data Collection Methods

Malte Mittendorf, Ulrik D. Nielsen, Harry B. Bingham, Ditte Gundermann, Daniel Schmode, Cedric Deymier 63
Performance Analysis of a Gas Carrier using Continual Learning in a Data Stream Context

Nikolaos Bekiaris, Zacharias Zervos, Ioannis Tolias, Christos Giordamlis 75
Suggestion and Evaluation of Alternative Indexes for Estimating Hull Performance Degradation Trendlines

Maria G.N. Tsompanoglou 91
A Case Study Approach on CII Rating: Understanding the Role of Annual Sailing Activity and Operational Speeds

Falko Fritz 107
Detecting Hull Degradation - Current Practice and Future Challenges

Soren Vinther Hansen, Richard Marioth 111
How CII ratings (A to E) are Linked to Energy Efficiency

Sofia Werner, Jonny Nisbet, Fredrik Olsson 124
Sea Trial Methodology for Wind Assisted Ships

Jan Richter, Jonas Wagner, Florian Kluwe 141
Correlating Laboratory with Full-Scale Data

Irma Yeginbayeva, Angelika Brink, Vilde Emilie Aas 149
New Measurement Facility: Enhanced Skin-Friction Measurement over Large-Scale Plates in a Channel Flow

Markus Hoffmann 161
The Impact of 'Fouling Idling' on Ship Performance and Carbon Intensity Indicator (CII)

Wojciech Górski, Jerzy Michniewicz 169
Continuous Monitoring and Predicting CII based on Ship Operational Data

Dimitris Georgousis, Najmeh Montazeri, Jakob Buus Petersen 181
Improving Performance Prediction using Hindcast Weather and AIS Data

Keng Khoon Tan, Sergiu Paereli, Angelika Brink 190
Impact of hull coating on EEXI and CII

Camille Colle, Casimir Morobé 198
Saving AI from its Own Hype: Getting Real about the Benefits and Challenges of Machine Learning for Ship Performance Modelling Aimed at Operational Optimizations

Alex A. Shiri, Sofia Werner, Rickard Bensow 207
Full-Scale Power Prediction for Vessel Equipped with Energy Saving Device

Efthymia Ofelia Tsompopoulou, Andreas Athanassopoulos, Elli Sivena, Kyriakos Polymenakos, Vasileios Tsarsitalidis, Antonis Nikitakis 218
On the Evaluation of Uncertainty of AI models for Ship Powering and its Effect on Power Estimates for Non-ideal Conditions

Dmitriy Ponkratov, Gijs Struijk, Miloš Birvalski, Martijn Elbertsen 234
A Journey to Unique PIV Flow Measurements at Ship Scale

JanWienke 244
From Performance Monitoring to ShaPoLi System

Martin Karlstad 249
Data Models for Environmental and Safety Improvements and Innovation

Martin Köpke 254
Increasing Fuel Efficiency by Sharing Operational Insights with the Crew

Vemund Svanes Bertelsen, Alfredo Carella, Rune Gangeskar, Gunnar Prytz, Michael Schmidt 260
Vessel Technical Performance Analysis using Accurate Weather and Speed Through Water Data

Hauke Hendricks, Andre Blaurock 275
To What Extent can ShaPoLi Accelerate Digitalization of the Shipping Industry

Solène Guéré, Nicolas Gambini 280
Hull Data is Big Data – How Much Can We Improve Hull Performance Using Real Hull Data?

Call for paper for next conference
List of authors

Assessment of Ships' Speed-Power Relationship at Lower Sailing Speeds

Frederik Hammer Berthelsen, DFDS, Copenhagen/Denmark, frber@dfds.com
Ulrik Dam Nielsen, Technical University of Denmark, Copenhagen/Denmark, udn@mek.dtu.dk

Abstract

This study assesses the relationship between speed and power of ships, and is based on operational data derived from more than 50,000 noon reports retrieved from 88 tankers. The analysis is made with a data-driven model based on principles from naval architecture and an econometric framework. The model facilitates the determination of a draught- and speed-dependent exponent. It is shown that the exponent is significantly lower than 3 at speed intervals below the design speed. The finding of a (much) smaller exponent, relative to 3, at low speed intervals is important in the slow steaming debate, since slow steaming will not be as good as often stated when the cubic speed-power relationship does not hold. On a practical level, the developed method can be used to set a more reliable benchmark in the performance monitoring of ships.

1. Introduction

Fuel consumption is typically the major costs of the running expenses in shipping companies; thus profit depends on its minimisation. Even more important than maximising profit, is the minimisation of emissions in order to make the shipping industry greener and more sustainable. The emissions of most concern are CO2, SOx, NOx and particular matters, *IMO (2014)*. Altogether, this has led to vessel performance monitoring in order to control the fuel consumption by intervention before the performance is too low and therefore unsustainable and unprofitable.

In vessel performance monitoring, ships' speed-power relationship is key; noticing that, generally, the relationship yields the necessary main engine power (MEP) to attain a constant sailing speed under given operational conditions. In many cases, it is normal practice to assume that the MEP is proportional to speed cubed, equivalent to assume that the exponent equals 3. This assumption relies on the hypothesis that the calm-water resistance of a ship, sailing around the design speed, is proportional to speed squared, following principles of classical hydrodynamics, e.g. *Newman (2017)*. However, ships rarely sail in calm water (no waves) and, furthermore, ships will more than often be sailing at speeds (significantly) lower than the design speed. In combination, the cubic speed-power relationship will not be a good model for the performance. In fact, analysis of in-service data shows that the exponent typically is significantly smaller than 3, *Adland et al. (2020)*, when the sailing speed is in ranges lower than the design speed. The consequence of this is that it is difficult to establish a good and reliable benchmark in the performance monitoring processes. In addition, and maybe more importantly, the effect of reducing speed, when assessing fuel consumption, appears much better than reality is if the cubic relationship is used. Fig.1 can be used to illustrate the addressed concerns. In the plot, operational data from a large group of tankers, all sister ships, is plotted together with speed-power curves derived from towing tank tests of the corresponding parent ship at different draughts. First of all, the plot shows that the majority of the operational data is in a speed range not covered by the results from the towing tank tests. Secondly, attempting a (mathematical) extrapolation of the speed-power curves will lead to a significant underestimation of required power.

This paper presents the main results obtained in the study by *Berthelsen and Nielsen (2021)*. As such, the paper outlines the findings made from an analysis of operational data consisting of more than 50,000 noon reports retrieved from 88 tankers. The data has been cast into a combined econometric and naval architectural model, which can be used to assess the speed-power relationship for ships sailing in real seaways, accounting for the effect of wind and waves. In a nutshell, the paper brings empirical evidence that ships' main engine power is not proportional to the speed cubed for the lower speed ranges relative to the design speed.

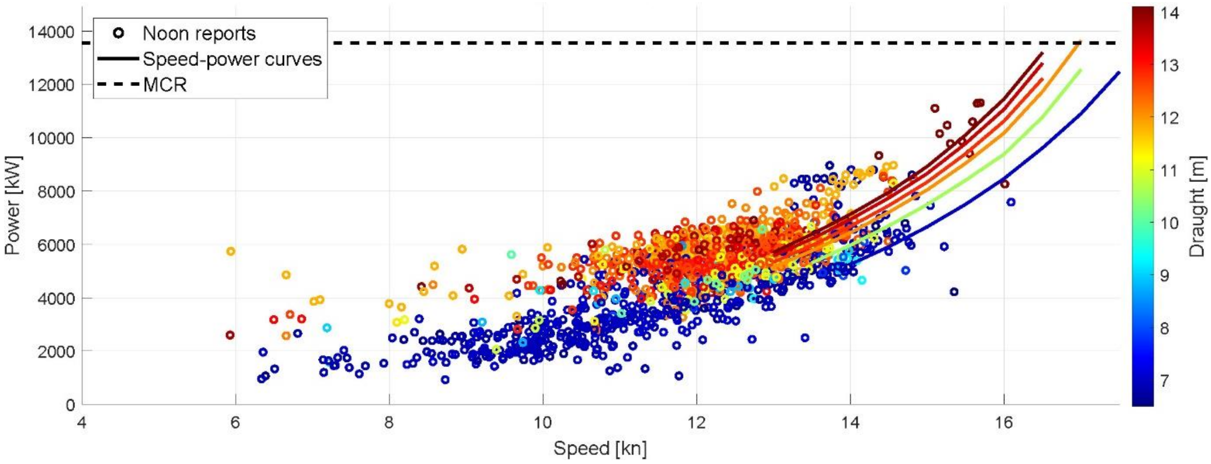

Fig.1: Illustration of the operational profile of two sister ships (74,000 DWT) with respect to speed-through-water, power, and draught compared to the corresponding towing tank curves for different draughts. The colour scale (draughts) is the same for noon report data and towing tank curves.

2. Modelling

2.1. Practical remarks

The reported speed in the noon reports is the GPS speed, i.e. speed-over-ground. In subsequent analyses, this speed is corrected for sea current to give the speed-through-water. Throughout the paper, for convenience, speed-through-water is referred to just as 'speed'. Similarly, before the regression modelling, reported power measurements are corrected for wind and waves in accordance with *ITTC (2017)*.

2.2. Speed-power relationship

The starting point for the model generation is the simplest power law model describing the relationship between power P and speed V:

$$P = x_1 V^{x_2} \tag{1}$$

where x_1 and x_2 are the unknown variables. x_2 is the exponent which is the focal point of this study, and it is emphasised that both x_1 and x_2 must be determined from the analysis of data. The nonlinear model is made linear in x_2 by a variable transformation using the natural logarithm:

$$\ln(P) = \ln(x_1) + x_2 \ln(V) \tag{2}$$

As shown subsequently, the model can be extended in order to take other relevant variables into account. First, however, note that in practice, the model is given by:

$$\begin{bmatrix} \ln(P_1) \\ \ln(P_2) \\ \ln(P_3) \\ \vdots \\ \ln(P_n) \end{bmatrix} = \begin{bmatrix} 1 & \ln(V_1) \\ 1 & \ln(V_2) \\ 1 & \ln(V_3) \\ & \vdots \\ 1 & \ln(V_n) \end{bmatrix} \begin{bmatrix} \ln(x_1) \\ x_2 \end{bmatrix} \tag{3}$$

when a set of corresponding observations $\{P_i, V_i\}$, $i = 1, 2, \cdots, n$ exists from n noon reports. This means that the unknown coefficients x_1, x_2 can be easily determined by formulating a least-squares problem.

The simple model is the basis for an extended model that take the draught and speed-dependency of the exponent into account. The simple model is therefore gradually extended.

As realised from speed-power curves, e.g. Fig.1, the ballast curve (smallest draught) and scantling curve (largest draught) will generally differ relatively much. It is therefore sensible to introduce the draught as an independent parameter in the model:

$$\ln(P) = \ln(x_1) + x_2 \ln(V) + x_3 T \tag{4}$$

noticing that T is the mean of the reported fore and aft draughts. This extended model, with draught as a parameter, implies that speed-power curves at different draughts will be parallel but shifted when studied in a log-log plot. Qualitatively speaking, draught is thus an additive effect. In order to take into account that speed-power curves obtained from towing tank tests are not parallel in log-log domain, an interaction term is introduced, since the exponent x_2 must be dependent on the draught:

$$\ln(P) = \ln(x_1) + x_2 \ln(V) + x_3 T + x_4 \ln(V)\, T \tag{5}$$

Rewriting, it is seen that the exponent now depends on the draught, too:

$$P = x_1 V^{(x_2 + x_4 T)} \exp(x_3 T) \tag{6}$$

A speed-dependent exponent is introduced through piecewise linear regression. This is done by introducing a dummy variable V_d assigning the noon reports to different speed intervals, hence introducing a "breakpoint" B_p separating different speed intervals. As an example, the speed-power regression model with one breakpoint reads:

$$\ln(P) = \ln(x_1) + x_2 \ln(V) + x_3 T + x_4 \ln(V)\, T + x_5\big(\ln(V) - B_p\big)V_d \tag{7}$$

where the breakpoint(s) will be determined from the data in question (see later).

3. Noon report data

The dataset contains noon reports and speed-power curves from model tests for 88 ships divided into 15 vessel groups. All the ships are tankers, and all the data is from the same shipping company. Roughly, the noon reports cover a five-year period (2016–2020) with vessels operating worldwide. In total, 51,826 filtered noon reports are available. (Different filtering rules are applied. The "raw" data set contains 53,017 noon reports.) Each vessel group consists of between 2 and 13 sister vessels. In order to work with these vessels and vessel groups and, at the same time, keep them anonymous, a naming convention has been introduced, e.g. TXXX-YY where XXX indicates the deadweight and YY indicates the number of vessels in each vessel group. This means that T035-03 is a 35,000 DWT vessel group consisting of 3 vessels.

As the very initial step, before analysing the noon reports, they are populated with hindcast data describing sea current, wind, and wave conditions. Specifically, the hindcast data assigned to the noon reports is a weighted average of the conditions during the duration of the single noon report by use of AIS data.

All data has been retrieved by COACH Solutions, https://coachsolutions.com/, that kindly provided the data to the authors. COACH Solutions also prepared the initial merge of hindcast data to the noon reports, including the subsequent correction of power accounting for environmental effects (wind, waves, sea current).

4. Results

4.1. Descriptive statistics

In order to give an overview of all the noon report data, descriptive statistics have been prepared. As the data set is comprehensive, with many vessel groups with large numbers of vessels within, the presented statistics will just be a glimpse of the larger picture. The vessel group T050-12 is considered somewhat representative and will be covered in the following.

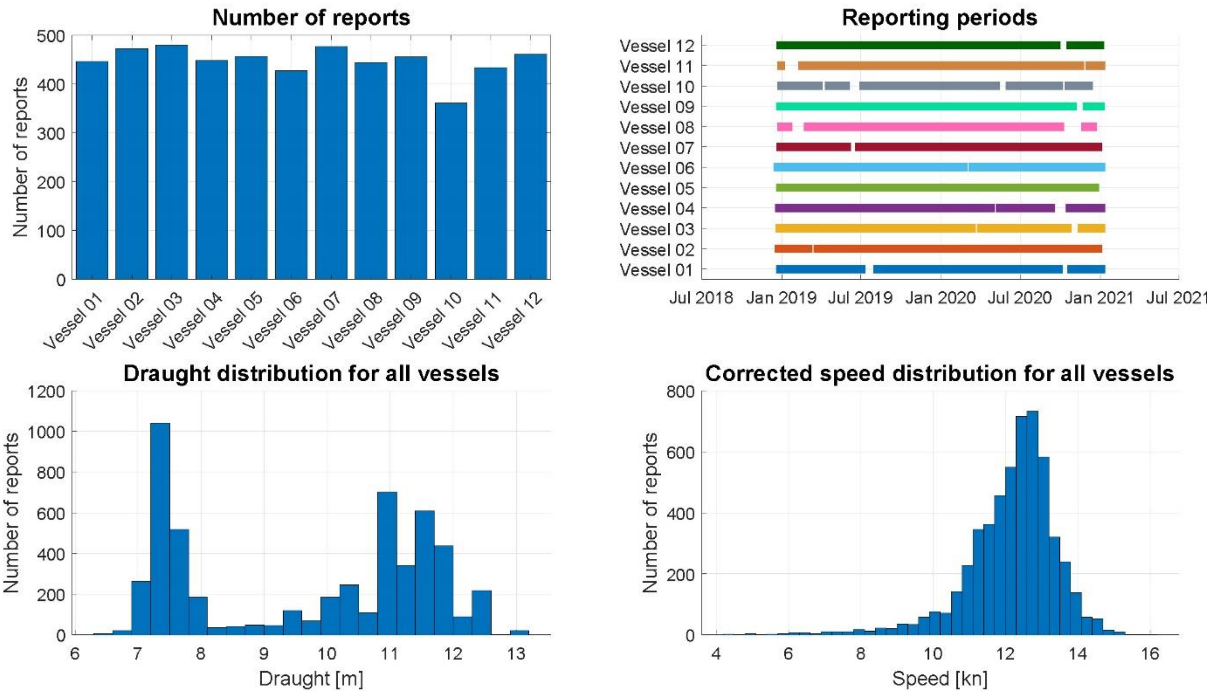

Fig.2: Descriptive statistics for the vessel group T050-12

Vessel group T050-12 has many vessels with many noon reports for each vessel. This can be seen in Fig.2 where the number of reports and reporting periods are shown. The vessels were not reporting every day due to port stays, idle periods, drydocking, etc. The draught and speed distributions can also be seen for all 12 vessels. It is seen that the vessels sail mostly at 2-3 draughts where the first is a ballast draught at around 7.5 m and the two others are laden draught(s) at around 11-11.5 m which agrees with the design draught T_d = 11.0 m. The draught distribution can be seen for every single vessel in Fig.3 which shows that the vessels have individual draught distributions that agree well with the draught distribution for the group as a whole (cf. Fig.2).

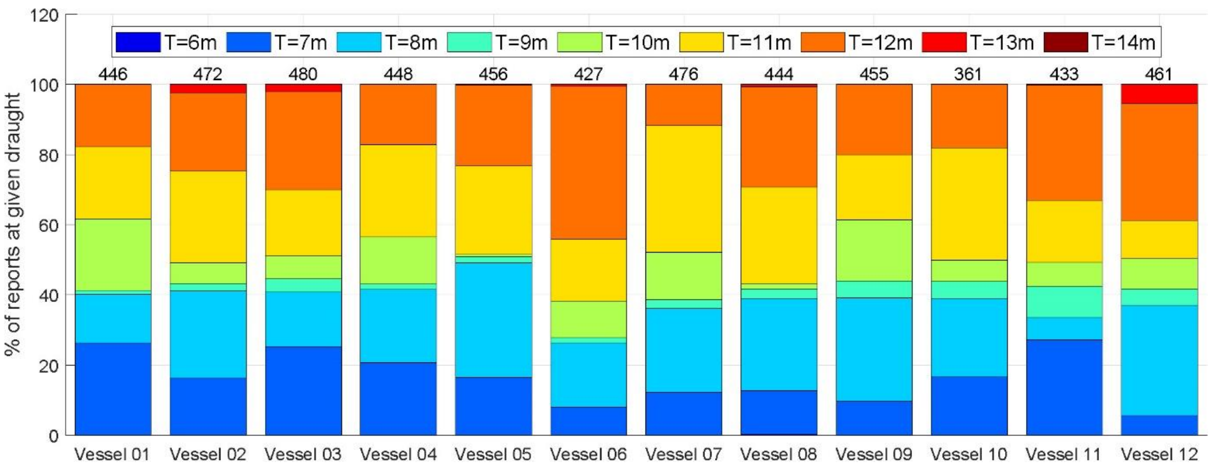

Fig.3: Draught distributions for all vessels in T050-12

A similar observation is seen from the speed distribution in Fig.4 which shows that the vessels primarily sail at 12–13 kn. Overall it can be concluded that the vessels operate relatively similar with regard to draught and speed which means that similar levels of power are expected for the vessels.

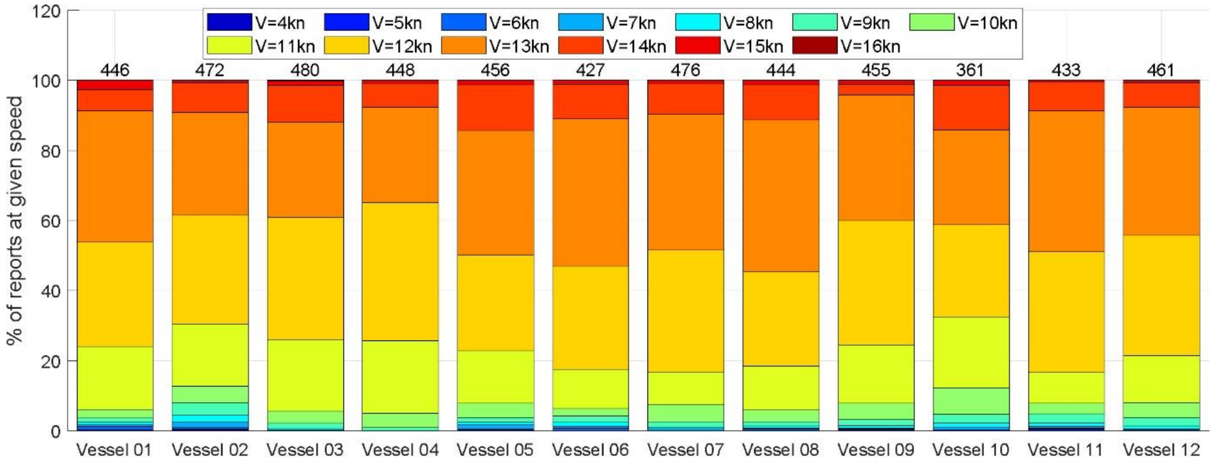

Fig.4: Draught distributions for all vessels in T050-12

4.2. Draught-dependent speed-power model

Initially, Eq.(5) is used for each and every vessel to determine the exponent when this is dependent on draught but not speed.

Table I gives the exponents for all vessels at ballast (T_b), design (T_d) and scantling (T_s) draughts. The exponent is determined for the single vessel in a group, but the exponent is also determined when the model, cf. Eq.(5), considers noon reports for all vessels collectively in a given vessel group (denoted by "Group"). To emphasize, this means that the exponent for the individual vessel groups is not an average of the vessel specific exponents of ships in a given group but independently modelled on all ship-specific data from the given group. This way, the regression is based on much more data, which makes its outcome more reliable. The group-wise regression is justified by the descriptive statistics presented earlier, where it was observed that the vessels within given groups are sailing with relatively similar draught, speed and power. The exponents of the individual groups were included in Table I, and they are presented graphically in Fig.7.

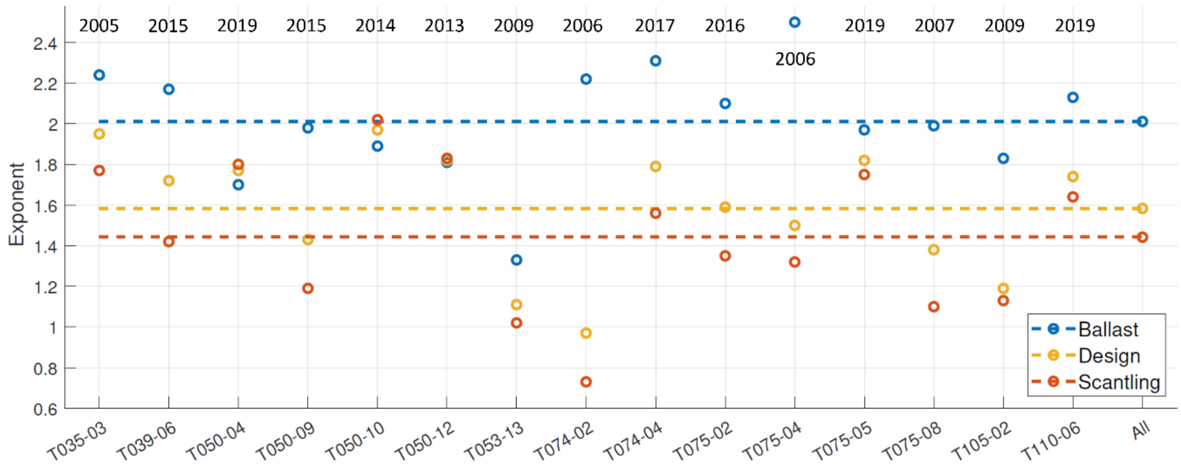

Fig.5: Exponents as determined from the draught-dependent model, cf. Eq.(5), for the single vessel groups considered at three draughts (ballast, design, scantling). The dashed lines indicate the average exponent, for a given draught, over all vessel groups. The year of construction is indicated for each group at the top of the plot.

Fig.5 reveals that the exponent is significantly lower than 3 for all studied vessel groups. It is seen that the value is in general decreasing with increasing draught for the individual vessel group. Thus, the exponent depends on draught but for some of the vessel groups there are less dependency, e.g. T050-12. As noticed from Table I, some vessels are "outliers" compared to the group-wise result, because too little data is available for the particular vessels; for instance, this is the case for Vessel 01 in T050-09 which has only 30 noon reports, and Vessel 01 in T105-02 that has just two ballast noon reports. Fig.5 shows that there is no size dependency, as the plot reveals no trend in the data, noticing that deadweight increases going from left to right on the x-axis. Similarly, when comparing with the year of construction (indicated at the top of the plot), no age dependency is observed for the exponent.

Table I: Specification of the exponent for all single vessels at ballast (T_b), design (T_d), and scantling (T_s) draughts; emphasizing that the simple model expressed by Eq.(5) is studied. The result when considering all the vessels, collectively, in the group is also included.

Vessel	T_b	T_d	T_s
T035-03			
V01	1.79	1.83	1.85
V02	1.19	1.66	1.95
V03	2.54	2.05	1.74
Group	2.24	1.95	1.77
T039-06			
V01	2.02	1.54	1.22
V02	2.35	1.95	1.68
V03	1.85	1.66	1.53
V04	2.23	1.80	1.51
V05	2.13	1.85	1.66
V06	2.37	1.45	0.84
Group	2.17	1.72	1.42
T050-04			
V01	1.76	2.39	2.71
V02	1.52	2.12	2.42
V03	1.85	2.25	2.44
V04	1.52	1.40	1.33
Group	1.70	1.77	1.80
T050-09			
V01	3.46	2.37	1.88
V02	1.91	1.38	1.14
V03	2.04	1.42	1.14
V04	2.23	1.35	0.96
V05	1.21	1.38	1.46
V06	1.92	1.56	1.40
V07	2.32	1.47	1.09
V08	1.74	1.19	0.95
V09	1.78	1.73	1.70
Group	1.98	1.43	1.19
T050-10			
V01	1.94	1.91	1.89
V02	2.51	1.83	1.42
V03	2.19	1.72	1.44
V04	1.70	1.87	1.98
V05	1.68	1.99	2.17
V06	1.94	2.41	2.69
V07	1.57	1.86	2.05
V08	1.54	2.17	2.55
V09	2.19	2.25	2.28
V10	1.49	1.93	2.20
Group	1.89	1.97	2.02

Vessel	T_b	T_d	T_s
T050-12			
V01	1.73	1.27	1.01
V02	2.11	1.93	1.82
V03	2.30	2.45	2.54
V04	2.59	2.89	3.06
V05	1.79	1.80	1.81
V06	1.58	2.31	2.72
V07	1.72	2.27	2.58
V08	2.44	1.88	1.56
V09	1.74	2.28	2.59
V10	1.62	1.34	1.18
V11	0.94	1.38	1.63
V12	1.59	1.73	1.81
Group	1.81	1.82	1.83
T053-13			
V01	1.04	1.34	1.46
V02	1.84	1.92	1.95
V03	1.55	2.85	3.40
V04	1.52	1.00	0.79
V05	1.25	0.95	0.83
V06	1.41	1.15	1.04
V07	2.23	1.53	1.24
V08	1.18	1.42	1.51
V09	0.88	0.95	0.98
V10	1.41	1.17	1.07
V11	1.33	0.80	0.57
V12	2.73	2.33	2.16
V13	1.44	1.02	0.84
Group	1.33	1.11	1.02
T074-02			
V01	2.30	0.66	0.35
V02	2.30	1.65	1.52
Group	2.22	0.97	0.73
T074-04			
V01	2.31	1.64	1.36
V02	2.25	1.61	1.34
V03	2.06	2.00	1.98
V04	2.62	2.35	2.23
Group	2.31	1.79	1.56

Vessel	T_b	T_d	T_s
T075-02			
V01	2.25	1.09	0.56
V02	2.12	1.79	1.64
Group	2.10	1.59	1.35
T075-04			
V01	2.53	1.61	1.43
V02	2.48	1.39	1.19
Group	2.50	1.50	1.32
T075-05			
V01	1.84	1.64	1.55
V02	2.81	2.06	1.71
V03	1.58	1.72	1.78
V04	2.26	1.88	1.70
V05	2.20	1.69	1.45
Group	1.97	1.82	1.75
T075-08			
V01	1.49	1.06	0.86
V02	1.59	1.64	1.66
V03	2.35	2.03	1.88
V04	1.62	1.25	1.09
V05	2.02	1.48	1.23
V06	2.11	1.34	0.98
V07	2.38	2.09	1.96
V08	2.79	1.77	1.31
Group	1.99	1.38	1.10
T105-02			
V01	-2.21	2.07	2.40
V02	1.82	1.16	1.11
Group	1.83	1.19	1.13
T110-06			
V01	2.21	2.17	2.15
V02	1.91	1.83	1.81
V03	2.01	1.45	1.31
V04	1.97	1.48	1.36
V05	2.38	1.46	1.23
V06	2.49	1.86	1.70
Group	2.13	1.74	1.64

The application of the simple model shows that the exponent cannot generally be assumed to be 3. Taking the vessel group T050-12 as an example, the simple regression model is plotted together with the noon reports and speed-power curves from model test in Fig.6, where the noon reports have been grouped based on draught for clarity. Clearly, the regression model does not capture the relationship for the higher speeds, but it does for the bulk of the noon reports; noticing that about 75–90% of the reported speeds generally are in the range 11–13 kn. It is appreciated (“confirmed”) that the model test curves follow the steeper path exhibited by the noon reports at the higher speeds.

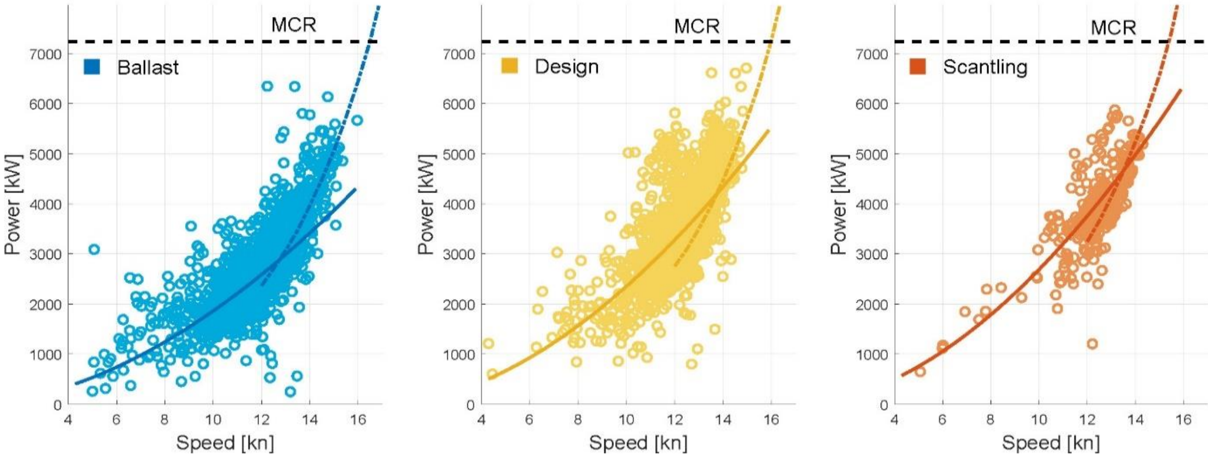

Fig.6: Speed-power curves [full lines] based on Eq.(5), plotted together with the draught-grouped noon report data [circles]. The corresponding curves from towing tank tests are also shown [dashed lines].

4.3 Speed- and draught-dependent speed-power model

The extended model, as expressed by Eq.(7), considers the exponent to also be dependent on speed. In practice, depending on the studied vessel group, a number of speed-breakpoints is set. In current implementation, the MATLAB function `findchangepts` is used to determine the breakpoints, based on the speed-sorted noon reports. Thus, modelling by Eq.(7) is made in the individual intervals limited by the respective breakpoints.

In the following, the resulting speed-power curves at the ballast, the design and the scantling draughts are computed, thus enabling a comparison with the curves from towing tank tests. Note that it is possible to model and compute speed-power curves at <u>any</u> given draught with the regression model. Specifically, for T050-12 the speed-power curve as a function of draught T and speed V is modelled as:

$$\ln(P) = \ln(x_1) + x_2 \ln(V) + x_3 T + x_4 \ln(V)\, T + x_5(\ln(V) - 10.8)V_{d,1} + \\ x_6(\ln(V) - 12.4)V_{d,2} + x_7(\ln(V) - 13.2)V_{d,3} \quad (8)$$

with the coefficients x_1 = 4.117, x_2 = 1.294, x_3 = 0.066, x_4 = -0.003, x_5 = 0.827, x_6 = 0.010, and x_7 = 1.333. The dummy variables $V_{d,i}$ are defined as

$$V_{d,1} = \begin{cases} 0, & \text{if } V \leq 10.8 \text{ kn} \\ 1, & \text{if } V > 10.8 \text{ kn} \end{cases} \quad (9)$$

$$V_{d,2} = \begin{cases} 0, & \text{if } V \leq 12.4 \text{ kn} \\ 1, & \text{if } V > 12.4 \text{ kn} \end{cases} \quad (10)$$

$$V_{d,1} = \begin{cases} 0, & \text{if } V \leq 13.2 \text{ kn} \\ 1, & \text{if } V > 13.2 \text{ kn} \end{cases} \quad (11)$$

which means that the expression, i.e. Eq.(8), contains the more terms, the higher the speed. It is noticed that, for V = 14 kn and ballast draught T_b = 7 m, the (“total”) exponent ε, as per Eq.(8), becomes,

$$\varepsilon = x_2 + 7x_4 + x_5 + x_6 + x_7 = 3.45 \quad (12)$$

Thus, the model predicts a result in line with physical expectation; that is, if the speed is around or above the design speed, the exponent is, indeed, 3 or larger.

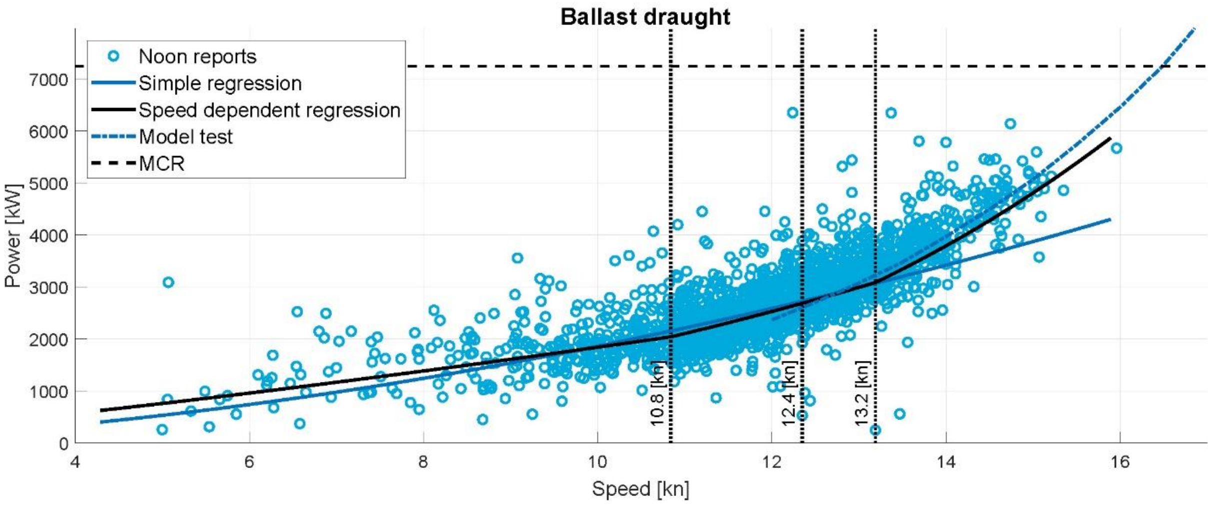

Fig.7: Outcome from the draught- and speed-dependent regression model, cf. Eq.(8), plotted together with noon reports, towing tank test curve, and the draught-dependent regression model, cf. Eq.(5), for T050-12 in ballast conditions.

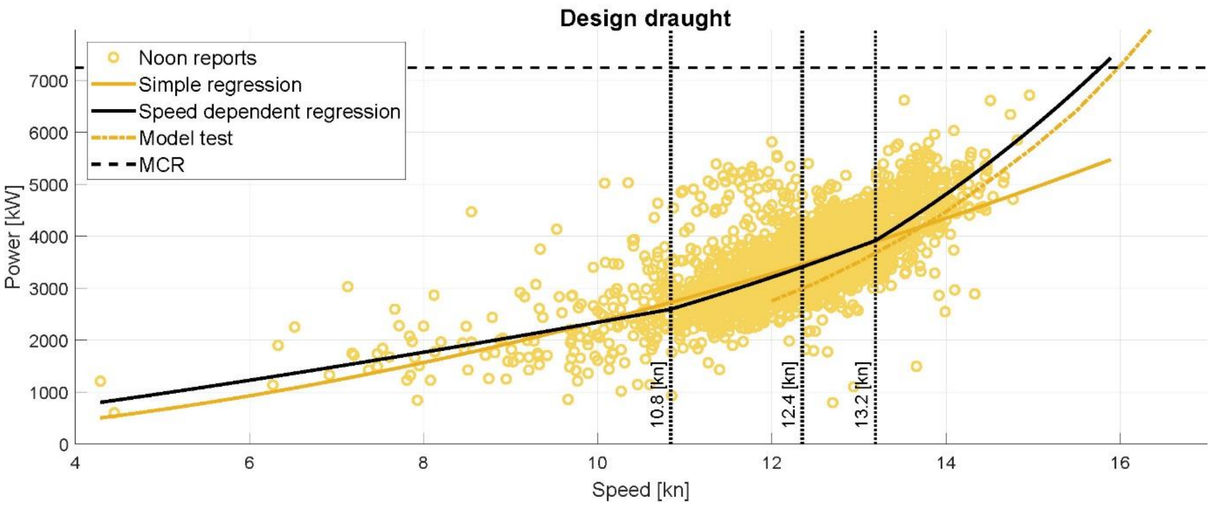

Fig.8: Outcome from the draught- and speed-dependent regression model, cf. Eq.(8), plotted together with noon reports, towing tank test curve, and the draught-dependent regression model, cf. Eq.(5), for T050-12 in design draught conditions.

In Figs.7 and 8, the draught- and speed-dependent regression model, cf. Eq.(8), is plotted at ballast and design draughts, respectively, together with the draught-grouped noon reports; noticing that the vessel group T050-12 is considered. The single plots also include the outcome of the simpler regression model, cf. Eq.(5), and, in addition, the speed-power curves from towing tank tests. It is seen that the speed-dependent model estimates the power better at the higher speed intervals compared to the simpler model that underestimates the power, see also Fig.6. This observation applies both to the noon-report data and the speed-power curves from towing tank tests; emphasising that data from the latter exists only in the (high-speed) interval 12–16+ [kn]. Albeit the speed-power curves from the speed-dependent regression do not exactly coincide with the towing tank test curves, the set of curves are nearly parallel which means that the exponents are relatively close to each other in their numerical values. At lower speed intervals the speed-dependent regression model deviates only slightly from the simple model, capturing the speed-power relationship in the noon-report data well.

The numerical values of the speed-dependent exponents, as determined for the single vessel groups, are presented in Table II. The main observations from the table, including Figs.7 and 8, are the following: (a) Only a very few cases reveal an exponent equal to or larger than 3; in most cases, the exponent is smaller. (b) Just three out of fifteen exponents at the scantling draught are above 3 at the highest speed interval. These three vessel groups are T050-04, T050-10 and T050-12 which have been shown to be very similar. In the ballast condition, for the highest speed interval, seven out of fifteen exponents are above 3. (c) For the particular case of T050-12, the exponent is 3.45, 3.44 and 3.43 for the ballast, design and scantling conditions, respectively, when the speed is above 13.2 kn. It can be informed that the exponents for the towing tank test curves for the same draughts are 3.57, 3.44 and 3.31. (d) Generally, the speed-dependent regression, cf. Eq.(8), with two or more speed intervals increases the exponent at the high-speed intervals compared to the simpler regression model, cf. Eq.(5), only taking draught into account, cf. Table I. At the same time, it is seen that the exponent is significantly higher for the ballast draught than for the scantling draught for many of the vessel groups.

Table II: Exponent and speed intervals from the speed-dependent regression model, cf. Eq.(8), for all vessel groups at three draughts: ballast (T_b), design (T_d) and scantling (T_s).

Vessel Group	**Speed interval** [kn]	**Exponent** [-]			**No. of NR** [-]
		Tb	***Td***	***Ts***	
T035-03					
Interval 1	$V \leq 9.1$	1.38	1.13	0.98	208
Interval 2	$9.1 < V \leq 11.0$	3.48	3.23	3.08	223
Interval 3	$11.0 < V \leq 13.1$	1.83	1.58	1.42	1207
Interval 4	$13.1 < V$	2.77	2.52	2.37	175
T039-06					
Interval 1	$V \leq 11.3$	1.90	1.34	0.95	1881
Interval 2	$11.3 < V \leq 12.2$	3.26	2.69	2.31	1682
Interval 3	$12.2 < V \leq 13.2$	1.93	1.36	0.98	2310
Interval 4	$13.2 < V$	3.38	2.81	2.43	880
T050-04					
Interval 1	$V \leq 11.9$	1.08	1.10	1.11	277
Interval 2	$11.9 < V$	3.01	3.04	3.05	799
T050-09					
Interval 1	$V \leq 10.0$	1.46	0.85	0.58	425
Interval 2	$10.0 < V \leq 11.4$	2.50	1.89	1.62	807
Interval 3	$11.4 < V \leq 13.0$	2.23	1.62	1.35	3762
Interval 4	$13.0 < V$	1.98	1.37	1.10	1765
T050-10					
Interval 1	$V \leq 9.8$	1.11	1.12	1.12	222
Interval 2	$9.8 < V \leq 11.8$	2.10	2.11	2.11	1239
Interval 3	$11.8 < V \leq 13.1$	2.38	2.39	2.39	2148
Interval 4	$13.1 < V$	3.17	3.18	3.19	517
T050-12					
Interval 1	$V \leq 10.8$	1.28	1.27	1.26	570
Interval 2	$10.8 < V \leq 12.4$	2.10	2.09	2.09	2016
Interval 3	$12.4 < V \leq 13.2$	2.11	2.10	2.10	1911
Interval 4	$13.2 < V$	3.45	3.44	3.43	862
T053-13					
Interval 1	$V \leq 10.6$	1.05	0.81	0.70	922
Interval 2	$10.6 < V \leq 12.0$	1.63	1.39	1.28	2518
Interval 3	$12.0 < V \leq 13.2$	1.36	1.11	1.00	5192
Interval 4	$13.2 < V$	2.11	1.87	1.76	1601
T074-02					
Interval 1	$V \leq 11.6$	1.91	0.57	0.31	490
Interval 2	$11.6 < V$	2.76	1.42	1.17	1080
T074-04					

Interval 1	$V \leq 11.5$	1.85	1.23	0.96	404
Interval 2	$11.5 < V$	2.98	2.35	2.08	1528
T075-02					
Interval 1	$V \leq 10.7$	1.09	0.50	0.23	170
Interval 2	$10.7 < V$	2.64	2.05	1.78	979
T075-04					
Interval 1	$V \leq 11.7$	2.32	1.18	0.96	626
Interval 2	$11.7 < V$	2.93	1.79	1.58	1547
T075-05					
Interval 1	$V \leq 11.5$	1.33	0.81	0.57	460
Interval 2	$11.5 < V$	3.28	2.76	2.51	1207
T075-08					
Interval 1	$V \leq 10.9$	1.60	0.93	0.63	711
Interval 2	$10.9 < V \leq 14.0$	2.28	1.61	1.30	3498
Interval 3	$14.0 < V$	3.76	3.09	2.79	362
T110-06					
Interval 1	$V \leq 11.5$	1.70	1.20	1.08	504
Interval 2	$11.5 < V \leq 13.5$	2.89	2.40	2.27	1570
Interval 3	$13.5 < V$	3.25	2.75	2.63	244

4.4 Overall evaluation

Table III shows the r^2 (R-squared) for the two regression models when the models are applied on every vessel group. It is seen that both models lead to an r^2 value of 0.60–0.80 for most of the vessel groups. It is noted that T053-13 is an outlier, with $r^2 = 0.376$ and $r^2 = 0.381$ for the two models, although a lot of noon reports are available for this group. The explanation for this odd behaviour is a result of the fact that the group consists of older vessels installed with relative large engine power, thus designed to go at a higher speed than what they have been actually sailing during the considered reporting period. In turn, this means that the performance varies significantly depending on encountered conditions; altogether making the outcome of this group much more scattered than what is observed the other vessel groups.

Table III: Resulting r^2 values for, respectively, the draught-dependent regression model, cf. Eq.(5), and the draught- and speed-dependent regression model, cf. Eq.(8).

Vessel Groups	**r^2** – Eq.(5) ("simple" model)	**r^2** – Eq.(8) (Extended model)	**No. of NR**
T035-03	0.694	0.704	1813
T039-06	0.681	0.687	6753
T050-04	0.662	0.722	1076
T050-09	0.609	0.616	6759
T050-10	0.668	0.693	4126
T050-12	0.652	0.675	5359
T053-13	0.376	0.381	10233
T074-02	0.751	0.760	1570
T074-04	0.776	0.791	1932
T075-02	0.699	0.716	1149
T075-04	0.725	0.727	2173
T075-05	0.719	0.757	1667
T075-08	0.665	0.678	4571
T105-02	0.824	-	327
T110-06	0.790	0.812	2318

Overall, the r^2 values increase for all vessel groups when the speed-dependent, extended regression model is considered. This was noticed also by visual inspection of the plots in Figs.7 and 8. Indeed, the piecewise regression model did capture the trend of the NR data, and, at the same time, the modelled output matched the towing tank test curves at the higher speed intervals. In fact, although not shown in the paper, similar visual observations can be made for the other vessel groups considered in the study.

5. Conclusions

This paper has studied the relationship between attained speed and used power by ships sailing at sea. The paper was focused on the exponent of this relationship. A data-driven analysis was made on the basis of a model established from principles of naval architecture and an economic framework.

Based on noon report data from 88 tankers in the 35,000–110,000 DWT segment, and the development of a draught- and speed-dependent regression model, it can be concluded that the exponent for this vessel type is significantly lower than 3 at speed intervals below the design speed. It has been shown that the regression model yields results in good agreement with the reported operational data. In a context of practical vessel performance monitoring, the study showed that resistance towing tank curves, often used as benchmark, cannot blindly be (mathematically) extrapolated to the full operational speed range by assuming a constant exponent. In this respect, it is imagined that models, like presented in this paper, could be a useful tool to produce more reliable benchmarks in fuel performance evaluations if, say, results from towing tank tests are not available or not covering the relevant range of sailed speeds.

In the literature, the speed-power exponent is almost always stated to be at least 3, and the International Maritime Organization reports, *IMO (2014)* “to ensure simplicity of analysis, the speed-resistance relationship is held as a cubic and no uncertainty is applied”. This gives, erroneously, a good reason for slow steaming when the fuel consumption is to be decreased. However, as empirically confirmed by this study, neither is the exponent constant nor is it close to 3, when sailing at speed intervals below the design speed. Therefore, speed <u>optimization</u> is a better strategy than (blind) speed reduction towards more sustainable shipping; somewhat logical and reasonable to experienced performance analysis teams but not necessarily to government officers and politicians discussing future regulations of shipping.

It is important to mention that the modelled output, i.e. basically the speed-power exponent, depends on the correction of power where account for environmental effects (wind, waves, sea current) is made. In the present study, the noon report data was pre-corrected by COACH Solutions <u>before</u> being cast into the regression models. While *ITTC (2017)* is the basis for the correction, in-house details with regards to, e.g., computation of the added resistance in waves are not known to the authors. Clearly, the level of complexity in the individual correction procedure, notably for waves, can induce uncertainties in the final output of the regression model(s). As such, it would be interesting to study, in a future work, the sensitivity to the correction of power in the modelled output.

Acknowledgement

Data for this study was kindly provided by COACH Solutions, and their assistance in the initial data preparation is highly appreciated. The work by the second author has been supported by the Research Council of Norway through the Centres of Excellence funding scheme, project number 223254 AMOS.

References

ADLAND, R.; CARIOU, P.; WOLFF, F.C. (2020), *Optimal ship speed and the cubic law revisited: Empirical evidence from an oil tanker fleet*, Transportation Research Part E 140, https://www.sciencedirect.com/science/article/pii/S1366554520306232

BERTHELSEN, F.H; NIELSEN, U.D. (2021), *Prediction of ships' speed-power relationship at speed intervals below the design speed*, Transportation Research Part D 99, https://www.sciencedirect.com/science/article/pii/S1361920921002947

IMO (2014), *Third IMO Greenhouse Gas Study 2014*, IMO, London

ITTC (2017), *Preparation, Conduct and Analysis of Speed/Power Trials*, ITTC Recommended Procedures and Guidelines 7.5-04-01-01.1

NEWMAN, J.N. (2017), *Marine Hydrodynamics*, MIT Press

Capabilities and Limits of Machine Learning

Volker Bertram, DNV, Hamburg/Germany, volker.bertram@dnv.com

Abstract

This paper looks at a key technology of Artificial Intelligence (AI), namely machine learning. Capabilities and especially limits of capabilities of machine learning are discussed. Techniques are illustrated by maritime examples taken from personal experience and literature. The conclusion is that machine learning techniques are a useful tool of advanced numerical statistics. We should use it selectively and wisely, but not expect miracles.

1. What is AI?

You've heard of it, and it is powerful, maybe threatening. Artificial Intelligence or "AI" is a term often used, yet little understood. What we don't know, often scares us; but sometimes we also have unrealistic hopes. Much of the common perception of AI comes through Hollywood movies, Fig.1: AI seems to have a nice female voice which lulls us into trusting "her", until "she" starts killing off humans, because somehow "she" developed "her" own mind. This makes generally for most entertaining movies but has little in common with my experience and view of AI. It just seems to be a new version of the 1970s' misconception of computers and software: "he" (back then, it was generally a "he") says so and therefore it must be true.

Fig.1: Common perception of AI from Hollywood movies – a powerful and deadly super-technology

The engineering truth behind the term or misnomer "Artificial Intelligence" is a set of tools that may do jobs better or handle tasks we could not handle at all in the past. The tools as such may fascinate; you may also worry what might be done when the tools are used by the wrong people; but the tools as such do not scare me.

There is no coherent definition of what "Artificial Intelligence" is. In its broadest sense, AI is concerned with the investigation and simulation of human intelligence with the ambition to replicate the processes in machines. A (not exhaustive) list of sub-branches of AI encompasses:

- machine learning / artificial neural nets / machine vision
- natural language processing / gesture processing
- knowledge-based systems (expert systems, case-based reasoning, Bayesian networks)
- robotics
- ...

And as the context is performance monitoring of ships, we will focus on machine learning. In the following, I will try to show that machine learning (or AI in a broader sense) is a useful 'numerical statistics' technique, useful but not performing miracles.

2. Principles of Machine Learning

Machine learning and data mining are closely related to computational statistics. In essence, we have glorified statistics here with new, catchy labels attached to it.

Traditionally, the human brain is very good at pattern recognition. Table I shows some x-y combinations which would remain meaningless if shown only for a second. Fig.2 shows the corresponding visualisation, *Zelasny (2011)*. Here we see immediately trends and unusual deviations. Such trend spotting and pattern recognition is a human intelligence ability that machine learning tries to mimic (and take further and to higher dimensions).

Table I: Sample x-y combinations

I		II		III		IV	
X	Y	X	Y	X	Y	X	Y
10.0	8.04	10.0	9.14	10.0	7.46	8.0	6.58
8.0	6.95	8.0	8.14	8.0	6.77	8.0	5.76
13.0	7.58	13.0	8.74	13.0	12.74	8.0	7.71
9.0	8.81	9.0	8.77	9.0	7.11	8.0	8.84
11.0	8.33	11.0	9.26	11.0	7.81	8.0	8.47
14.0	9.96	14.0	8.10	14.0	8.84	8.0	7.04
6.0	7.24	6.0	6.13	6.0	6.08	8.0	5.25
4.0	4.26	4.0	3.10	4.0	5.39	19.0	12.50
12.0	10.84	12.0	9.13	12.0	8.15	8.0	5.56
7.0	4.82	7.0	7.26	7.0	6.42	8.0	7.91
5.0	5.68	5.0	4.74	5.0	5.73	8.0	6.89

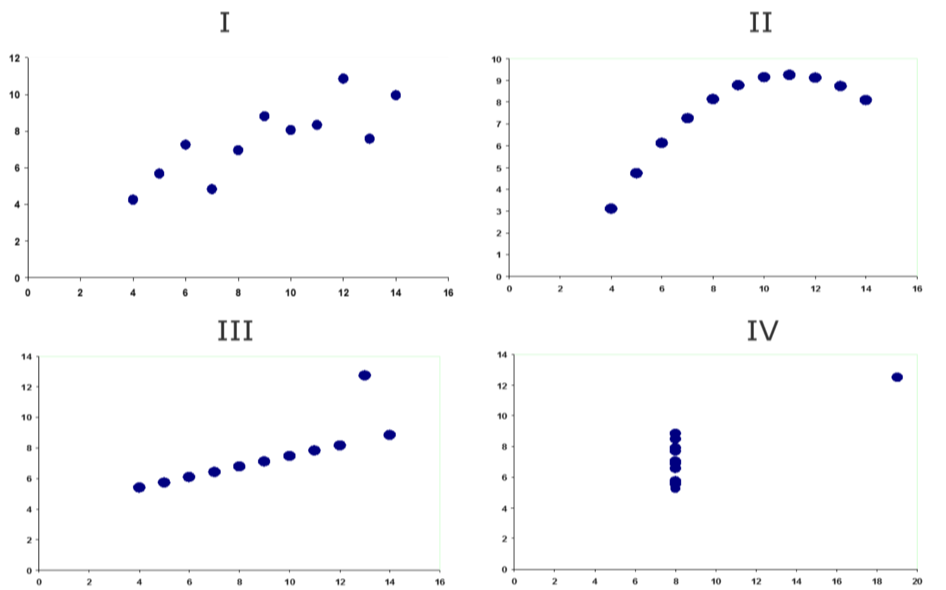

Fig.3: Visual equivalents to Table I – Here we see immediately the patterns, *Zelasny (2001)*

Our standard tools for evaluating such data, e.g. for simple design methods, have been rather primitive and inaccurate. We might have averaged to a single value (coefficient), used linear regression or nonlinear regression analysis based on polynomials, which have the unfortunate tendency to introduce unphysical oscillations for higher orders. These are the standard options Excel offers. And they all fail at least for some of the data sets in Table I, in the sense that at for some parts of the range of x-variables they give much larger errors than what we would estimate with the human eye. The 'failure' stems from the inappropriate choice of inherent function, not the least-square fitting algorithm, used in statistics. In the language of Germans and mathematicians, we fail from the 'ansatz'.

Wouldn't it be nice to have some mathematical way of mimicking the curve we would instinctively draw through such data sets, ignoring implausible outliers and following the trends our eye sees, something flexible yet smooth and free of inappropriate oscillations? For the naval architect, this is old hat. We have approximated arbitrary point sets for centuries, Fig.4, using first flexible thin beams (splines), Fig.4, and later using aptly named spline curves, which do not oscillate and form smooth curves and surfaces. See e.g. *Veelo (2004)* for an overview of such techniques for ship design, automotive engineering or the movie industry.

Fig.3: Rembrandt painting of shipbuilder using smooth curves to describe ship lines

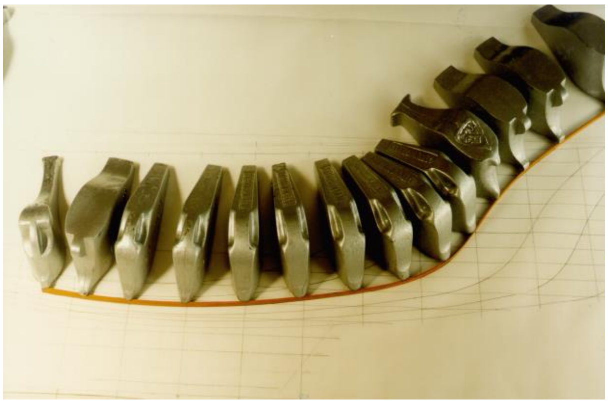

Fig.4: Traditional splines for ship design, source: TU Berlin

The machine learning community prefers other functions, such as sigmoid functions, Fig.5. Combining many of these, we have similar basic qualities of flexible approximation and avoiding oscillations.

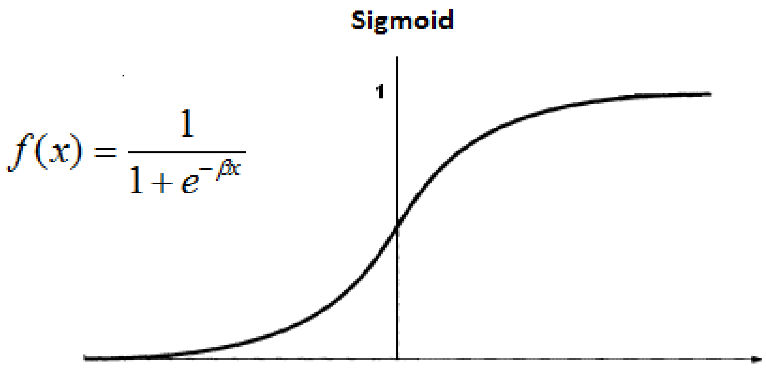

Fig.5: Sigmoid function

Conventional regression analysis has been extensively used in naval architecture in system identification to provide required factors and coefficients. Based on databases of existing designs, coefficients are then interpolated or even extrapolated to calculate coefficients for a new application. This procedure requires the engineer to specify not only which input parameters mainly influence one or more output parameters, but also to specify the type of functional relation between input and output parameters. Most often in the past, simple linear relations (or even worse just constants) have been chosen. Designers plotted data and by visual inspection sometimes chose also simple polynomial relations. This approach is cumbersome and unsuitable for many nonlinear relations. Shortcomings are especially apparent for multi-dimensional input/output data sets.

Artificial neural networks (ANNs) are the most popular technique in machine learning, *Mesbahi (2003)*, https://en.wikipedia.org/wiki/Artificial_neural_network. ANNs can generally represent the mapping of multi-dimensional input/output data sets, i.e. an arbitrary number of input variables x_i and output variable y_i. An ANN structure consists of several layers; each layer consists of several nodes. In the example shown in Fig.6, we have the input layer, the output layer, and one hidden layer. The ANN is "trained" on data sets. This training process results in mathematical relationship output variables y_i and input variables x_i, e.g. of the form (for a single-input, single-output ANN):

$$y = c_0 + c_1 \cdot \text{sig}\,[b_0+b_1 \cdot \text{sig}(a_{10}+a_{11} \cdot x_1+a_{12} \cdot x_{2+\ldots}) + b_2 \cdot \text{sig}(a_{20}+a_{21} \cdot x_1+a_{22} \cdot x_{2+\ldots}) + \ldots] \qquad (1)$$

Here, sig denotes the sigmoid function, Fig.5. After sufficient training, adjusted values for the coefficients *a*, *b*, and *c* are derived and the non-linear relationship is determined. Now the ANN can very rapidly determine values y_i for given values x_i. One might also use the general functional expression of Eq.(1) and use least-square fit methods to determine the coefficients *a*, *b* and *c*. But then we would lose out on a wealth of wonderful jargon and might not be that impressed anymore.

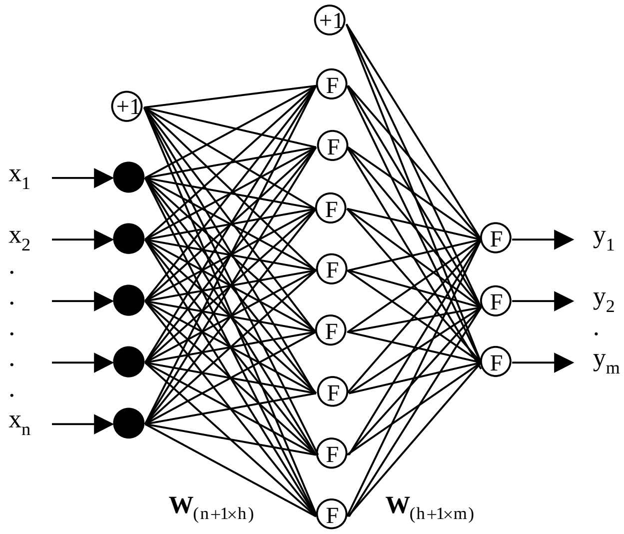

Fig.6: General structure of an Artificial Neural Network

There are countless applications for ANNs in the literature, as pattern matching or trending is needed in countless fields. Popular TV series may show fingerprint matching, facial recognition or machine reading of licence plates – all based on neural nets. General data mining, as found in major internet companies such as Google, Yahoo, Amazon, etc. will involve neural nets, and much of the large financial trading industries will rely on them. Game playing and decision making in some strategic games (chess, backgammon, poker, Go) is another popular application of ANNs.

Finally, "Deep Learning", https://en.wikipedia.org/wiki/Deep_learning, is a more recent buzz word used when neural nets with two or more hidden layers are used. Having an additional layer means that the transfer function (e.g. the sigmoid function) is calling in itself a transfer function, as shown in the example in Eq.(1). This adds more flexibility in approximating functions.

The ANN software ICE (Intelligent Calculations of Equations) is provided free-of-charge by William Faller (Applied Simulation Technologies), *Roddy et al. (2006)*. The software is easy to use, tries automatically different architectures (i.e. number of layers and nodes per layer) to get best fits, and allows exporting the resulting mathematical formulas directly to source code of widely used programming languages, *Bertram and Herradon (2016).*

3. Maritime applications

ANNs are increasingly used in the maritime industries for system identification. *Hess and Faller (2000)* give an overview of early maritime ANN applications. *Mesbahi (2003)* gives an introduction to ANNs and some applications from ship design and marine engineering.

ANNs have been used in

- system identification, e.g. deriving body-force coefficients in ship manoeuvring from model tests or sea trials, e.g. *Moreira and Guedes Suares (2003),* or diesel engine monitoring, *Mesbahi and Atlar (2000)*
- deriving design formulas from narrow-domain databases, e.g. power prediction for tugs, Fig.7, *Mesbahi and Bertram (2000),* semi-planing hulls, *Bertram and Mesbahi (2004),* or cargoships, *Couser et al. (2004)*
- meta-modelling using ANNs to interpolate between data sets generated in expensive simula-tions, e.g. *Harries (2010), Couser et al. (2011)*; in a similar vein, ANNs can be used to create response surfaces for interpolation of simulation results; e.g. in DNV GL's ECO Assistant for trim optimization, 300-500 CFD (Computational Fluid Dynamics) results of power as function of speed, draft and trim are connected smoothly in such a response surface. The knowledge base thus created can be re-used in performance monitoring, *Bertram (2013).*
- Automatic ship type identification, Fig.8, *Kumlu (2012)*
- Economic predictions, e.g. of freight rates, *Bruce and Morgan (2006)*

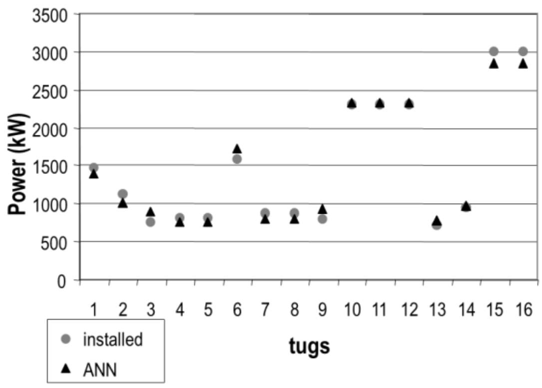

Fig.7: Tug power prediction, *Mesbahi and Bertram (2000)*

Fig.8: Automatic ship identification, *Kumlu (2012)*

ANNs have been used by various authors for performance monitoring applications, such as *Pedersen and Larsen (2009), Petersen et al. (2011), Haranen et al. (2016), Bal Besikci et al. (2016), Paereli and Levantis (2018), Parkes et al. (2018), Jeon et al. (2018), Gonzalez and Arango (2019), Petersen et al. (2020).*

4. Limitations

Artificial Neural Nets (as the most popular machine learning technique) have in principle no problem in handling arbitrary numbers of input variables. Hence the progress through them that has sometimes fuelled mythical confidence in what they can do. As any other tool, ANNs have their limitations:

- They can't predict the unpredictable. Random events, such as lottery numbers of next week, are by definition unpredictable. Many events involving highly nonlinear ("chaotic") behaviour are quasi-random. For example, crash-stop manoeuvres of ships are highly non-linear; small changes in the ambience at the begin of the manoeuvre result in largely varying tracks for the stopping manoeuvre, *Söding (1995),* Fig.9. Subsequently, attempts to predict crash-stop paths using ANNs cannot succeed. If satisfactory agreement is published, e.g. *Moreira and Guedes Suares (2003),* Fig.10, it is the luck of the draw taking only one of the possible tracks in sea trials for comparison.

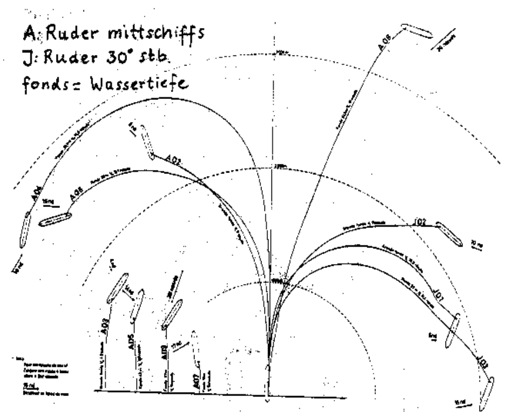

Fig.9: Sea trial results of repeated crash-stop manoeuvres for a tanker, *Söding (1995)*

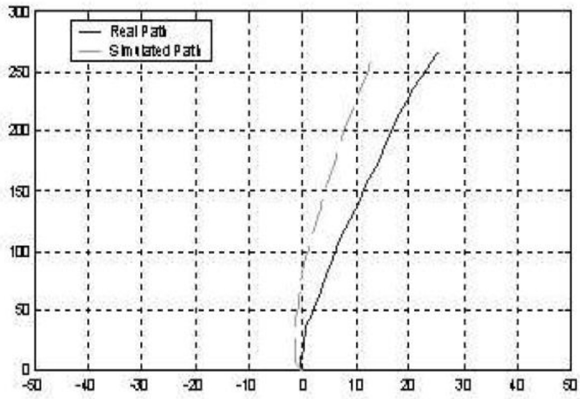

Fig.10: Satisfactory ANN prediction of crash-stop manoeuvre, *Moreira and Guedes Suares (2003)*

- Machine Learning is data greedy. Imagine an arbitrary curve, e.g. the sin-function sin(x) over one period. For us to recognize the function (= pattern), we would probably need ~10 points equidistantly spaced, and twice as many if we have some random selection. For a function of 2 input variables, we would then need 100-400 points to see the pattern or train a neural network. For *n* input variables, then 10^n-20^n data points are needed. For many real-world problems, we have many factors driving the problem; e.g. for hull performance monitoring we may look at changing operational conditions (speed, draft, trim, rudder angle) and ambient conditions (water depth, significant wave height, wave direction, wind speed, wind direction, possibly also current speed, current direction), leading to billions of data points to train a neural network properly. For many maritime problems, e.g. in ship design (as used in baseline curves), we may have O(10)-O(100) data points. Then brute-force machine learning no longer works and we have to use natural intelligence, e.g. reducing the number of free variables using physical insight.
- Machine learning is not good for rare events. The relations found are fine for interpolating, especially in regions where we have many data points (= frequently occurring cases). Extra-polating often results in wrong predictions. Machine learning is based on experience, not theoretical reasoning. This may lead to problems in practice, *Bertram (2014)*: "[…], there was a shipowner who was looking for the best trim optimisation for his […] ships. He looked for suitable candidates and installed a CFD-based system [i.e. based on systematic simulations based on fluid dynamics physics] and a machine-learning system on one of his ships. One fine day, the captain asked both systems for advice. The CFD-based system said: 1m down by the bow. The machine learning system said: 1m down by the stern. […] the solution to the puzzle was that the comparison was made shortly after installation. The captain had never before driven the ship on that draft and at that speed other than with trim by stern. The machine learning system had, therefore, never "seen" that by trimming by bow the fuel consumption was lower and picked the best solution from its limited experience. Its knowledge base was patchy and thus its recommendation not good."

5. Conclusion

Artificial Intelligence is a tool, sometimes using unnecessarily pretentious jargon. The progress in numerical statistics allows better approximations of data clouds, but require large data sets. As with all statistics, functional approximations will show “random” fluctuations (errors) if factors affecting the results are not included in the variables (e.g. trim for power predictions).

As with other statistical methods, extrapolations beyond the original data sets remain dangerous. The approximations are ‘optimum’ for the given data sets, but beyond those approximation function often diverge. Unfortunately, software applications generally do not suppress extrapolations. This may lead to ‘hidden’ errors in performance monitoring applications.

References

BAL BEŞIKÇI, E., ARSLAN, O., TURAN, O.; ÖLCER, A. (2016), *An artificial neural network based decision support system for energy efficient ship operations*, Computers & Operations Research 66, pp.393-401

BERTRAM, V. (2013), *Trim Optimization Meets Hull Performance*, Lloyds List Seminar “Hull Management and Performance”, London

BERTRAM, V. (2014), *Trim optimisation – Don’t blind me with science!*, The Naval Architect, September, pp.66-68, www.dnvgl.com/Images/2014_TheNavalArchitect_Bertram_TrimOptimization_tcm8-21468.pdf

BERTRAM, V.; HERRADON, E. (2016), *Predicting added resistance in wind and waves employing artificial neural nets*, 1st Hull Performance & Insight Conf. (HullPIC), Pavone, pp.14-22, http://data.hullpic.info/HullPIC2016.pdf

BERTRAM, V.; MESBAHI, E. (2004), *Estimating resistance and power of fast monohulls employing artificial neural nets*, 4th Conf. High-Performance Marine Vehicles (HIPER), Rome, pp.18-27, http://data.hiper-conf.info/Hiper2004_Rome.pdf

BRUCE, G.; MORGAN, G. (2006), *Artificial neural networks – Application to freight rates*, 5th Conf. Computer and IT Applications in the Maritime Industries (COMPIT), Oegstgeest, pp.146-153, http://data.hiper-conf.info/compit2006_oegstgeest.pdf

COUSER, P.; MASON, A.; MASON, G.; SMITH, C.R.; KONSKY, B.R. von (2004), *Artificial neural networks for hull resistance prediction*, 3rd Conf. Computer and IT Applications in the Maritime Industries (COMPIT), Sigüenza, pp.391-402, http://data.hiper-conf.info/compit2004_siguenza.pdf

COUSER, P.; HARRIES, S.; TILLIG, F. (2011), *Numerical hull series for calm water and seakeeping*, 10th Conf. Computer and IT Applications in the Maritime Industries (COMPIT), Berlin, pp.206-220, http://data.hiper-conf.info/compit2011_berlin.pdf

GONZALEZ, C.; ARANGO, D.L. (2019), *Techniques for the Automated Detection of Anomalies and Assessment of Quality in High-Frequency Data Collection Systems*, 4th Hull Performance & Insight Conf. (HullPIC), Gubbio, pp.143-153, http://data.hullpic.info/HullPIC2019_gubbio.pdf

HARANEN, M.; PAKKANEN, P.; KARIRANTA, R.; SALO, J. (2016), *White, grey and black-box modeling in ship performance evaluation*, 1st Hull Performance & Insight Conference, Pavone, pp.115-127, http://data.hullpic.info/HullPIC2016.pdf

HARRIES, S. (2010), *Investigating multi-dimensional design spaces using first principle methods*, 7th Conf. High-Performance Marine Vehicles (HIPER), Melbourne, pp.179-194, http://data.hiper-conf.info/Hiper2010_Melbourne.pdf

HESS, D.; FALLER, W. (2000), *Simulation of ship maneuvers using recursive neural networks*, 23rd Symp. Naval Hydrodynamics, Val de Reuil

JEON, M.; NOH, Y.; SHIN, Y.; LIM, O. K.; LEE, I.; CHO, D. (2018), *Prediction of ship fuel consumption by using an artificial neural network*, J. Mechanical Science and Technology 32(12), pp.5785-5796

KUMLU, D. (2012), *Autonomous ship recognition from color images*, MSc Thesis, Univ. Southern California, http://digitallibrary.usc.edu/cdm/ref/collection/p15799coll3/id/64052

MESBAHI, E. (2003), *Artificial neural networks – Fundamentals,* 39th WEGEMT School OPTIMISTIC – Optimization in Marine Design, Mensch & Buch Verlag, Berlin, pp.191-216, www.wegemt.com/?wpfb_dl=45

MESBAHI, E.; ATLAR, M. (2000), *Artificial neural networks: Applications in marine design and modelling*, 1st Conf. Computer and IT Applications in the Maritime Industries (COMPIT), Potsdam, pp.276-291, http://data.hiper-conf.info/compit2000_potsdam.pdf

MESBAHI, E.; BERTRAM, V. (2000), *Empirical design formulae using artificial neural nets,* 1st Conf. Computer and IT Applications in the Maritime Industries (COMPIT), Potsdam, pp.292-301, http://data.hiper-conf.info/compit2000_potsdam.pdf

MOREIRA, L.; GUEDES SUARES, C. (2003), *Comparison between Manoeuvring Trials and Simulations with Recursive Neural Networks*, Ship Technology Research 50/2, pp.77-84

PAERELI, S.; LEVANTIS, M. (2018), *Quantification of Changes in Propeller Performance – Method Validation*, 3rd Hull Performance & Insight Conf. (HullPIC), pp.285-295, http://data.hullpic.info/hullpic2018_redworth.pdf

PARKES, A.I.; SOBEY, A.J.; HUDSON, D.A. (2018), *Physics-based shaft power prediction for large merchant ships using Neural Networks*, J. Ocean Eng. 166, pp.92-104

PEDERSEN, B.P.; LARSEN, J. (2009), *Prediction of full-scale power using artificial neural networks*, 8th Conf. Computer and IT Applications in the Maritime Industries (COMPIT), Budapest, pp.537-550, http://data.hiper-conf.info/compit2009_budapest.pdf

PETERSEN, J.P.; JACOBSEN, D.J.; WINTHER, O. (2011), *A machine-learning approach to predict main energy consumption under realistic operational conditions*, 10th Conf. Computer and IT Applications in the Maritime Industries (COMPIT), Berlin, pp.305-316, http://data.hiper-conf.info/compit2011_berlin.pdf

PETERSEN, J.P.; FREDERIKSEN, J.S.; JACOBSEB, D.J. (2020), *Bridging the Gap Between Noon Data and Automated Data*, 5th Hull Performance & Insight Conf. (HullPIC), Hamburg, pp.64-70, http://data.hullpic.info/HullPIC2020_Hamburg.pdf

RODDY, R.F.; HESS, D.E.; FALLER, W.E. (2006), *Neural Network Predictions of the 4-Quadrant Wageningen B-Screw Series*, 5th Conf. Computer and IT Applications in the Maritime Industries (COMPIT), Oestgeest, pp.315-324, http://data.hiper-conf.info/compit2006_oegstgeest.pdf

SÖDING, H. (1995), *Manövrierfähigkeit von Schiffen*, Lecture Notes, Institut für Schiffbau, Univ. Hamburg

VEELO, B. (2004), *Variations of Shape in Industrial Geometric Models*, PhD thesis, NTNU, Trondheim, https://www.sarc.nl/publications/variations-of-shape-in-industrial-geometric-models/

ZELASNY, G. (2001), *Say It with Charts: The Executive's Guide to Visual Communication*, McGraw-Hill

A Discussion of the Weather Factor in the EEDI/EEXI

Volker Bertram, DNV, Hamburg/Germany, volker.bertram@dnv.com

Abstract

This paper critically discusses the weather factor in the calculation of EEDI and EEXI. The basic intent of the weather factor is good, reflecting the fact that ships usually operate not in sea trial conditions with calm weather, and that ships with lower energy requirements in realistic ambient conditions should be rewarded with a better energy efficiency index. The problem lies in the uncertainties in determining the speed loss in waves and the flexibility given in the regulations. The deliberate choice of assessment tool and parameters could be used to improve the energy efficiency index on paper without corresponding improvement in real energy efficiency of the ship.

1. Introduction

The EEDI (Energy Efficiency Design Index) provides a newbuilding standard, ensuring that ship designs achieve a certain level of efficiency and decrease carbon emissions. The EEDI was made mandatory by IMO for most newbuilds more than a decade ago. For newbuilds that require an EEDI, shipyards are responsible for the calculation of the EEDI, which is then verified by classification societies. For this purpose, shipyards have to prepare a technical file containing the EEDI calculation.

Calculating the EEDI or EEXI of a ship is complex. The basic formula is straightforward enough, but for many of the variables in the formula, there are various ways of calculating them, using default values or alternative assessment methods, such as measurements or calculations. These in turn are subject to lengthy descriptions trying to balance flexibility in assessment methods with the overall goal of having a level playing field in assessment.

For the simplest case, using default values wherever applicable, the EEDI calculation can be performed using DNV's EEDI Calculator, https://www.dnv.com/services/energy-efficiency-design-index-calculator-140598. The EEDI Calculator supports shipyards and ship owners in calculating the EEDI of their vessels and in preparing the associated technical file. The complexity of EEDI calculation has been reduced to a minimum of required input fields. Shipyards as well as ship owners who want to apply a voluntary EEDI to their ships can easily use the EEDI Calculator to check their designed energy efficiency. The technical file is provided as an MS Word file and can be freely edited.

For existing ships, an equivalent energy efficiency design index dubbed EEXI (Energy Efficiency Existing Ship Index) will become mandatory from 1st January 2023 on. The calculation guidelines refer to corresponding EEDI guideline for newbuildings with some adaptations regarding limited access to design data. Again, for the simplest approach, using default values wherever possible instead of tailored alternatives, the EEXI can be calculated using an online tool, DNV's EEXI Calculator, https://www.dnv.com/maritime/insights/topics/eexi/class-service-portfolio.html.

Calculating EEDI or EEXI is akin to tax declarations. For the simple cases, you can use simple software tools, for very complex cases or if you want to play the system, you need a dedicated consultant. Especially for the EEXI, there will be a significant demand to lower the obtained (= calculated) value to meet the thresholds.

One option may be to implement energy saving measures, e.g. applying ultra-smooth coatings reducing friction resistance in sea trials, https://glomeep.imo.org/technology/hull-coating/, or retrofitting a propulsion improving device (PID), https://glomeep.imo.org/technology/propulsion-improving-devices-pids/. Another option may be to exploit leeway or loopholes in the calculation procedures, gaining energy efficiency only on paper.

2. The weather factor f_w

2.1. General description

On a very high level, the EEDI (like the EEXI) is to be computed by:

$$\mathrm{EEDI_{attained}} = \frac{\mathrm{CO_2\ emissions}}{\mathrm{Cargo\ capacity} \cdot f_w \cdot V_{ref}} \quad (1)$$

$$f_w = \frac{V_w}{V_{ref}} \quad (2)$$

V_w is the speed of the vessel in Beaufort 6 (corresponding to 3 m significant wave height and 12.6 m/s wind speed) and V_{ref} is the speed of the ship in calm water. Eqs.(1) and (2) mean that the EEDI is based on the attained speed of the ship in Bft 6. The idea behind the weather factor f_w is to assess the ship's energy efficiency in more realistic ambient conditions and reward hull designs with lower added resistance or speed loss in waves.

Ships are frequently designed with a "sea margin" of 15% regardless of actual seakeeping performance. In reality, different hull shapes, particularly different bow shapes, will significantly impact speed losses in waves. "A […] case study indicates the potential for further fuel savings if performance in waves is considered in hull design, especially for bulk carriers and tankers. Two hull variants of a Handymax bulk carrier were investigated: one with a conventional bulbous bow, one with a rather straight bow profile. The assessment considered a typical trade and a simplified operational profile with two load conditions (fully loaded and in ballast) and two speeds (service speed and slow steaming). The design with the straight bow contour reduced average fuel consumption by 3%," *Shigunov and Bertram (2014)*, Fig.1.

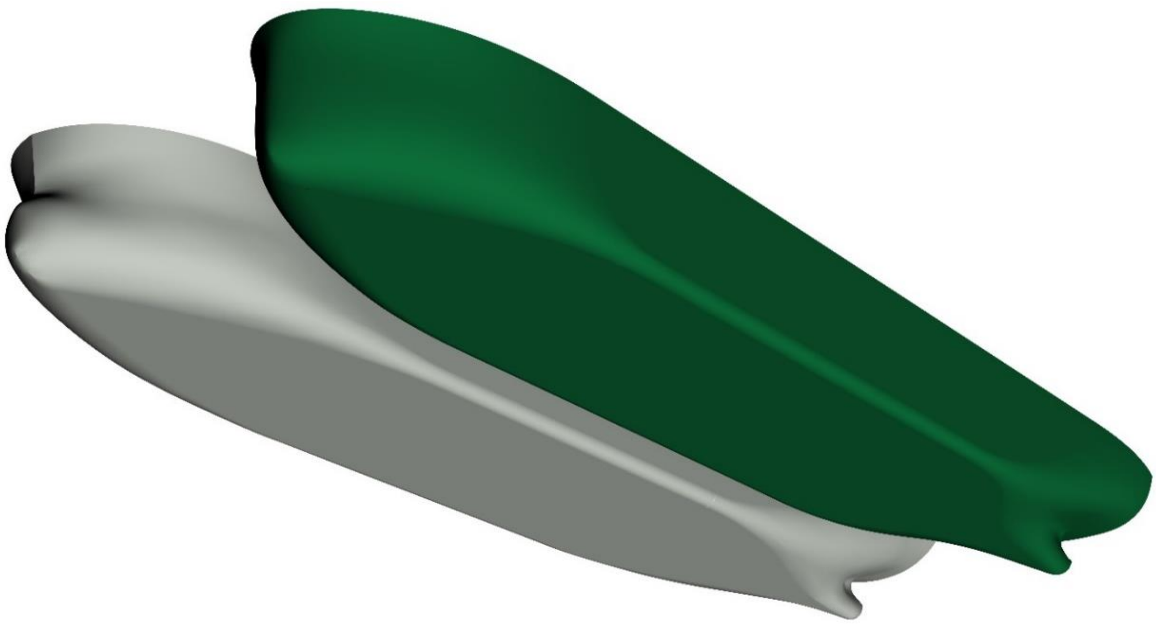

Fig.1: Classical bulbous-bow (left) and optimized straight-bow (right) design for bulk carrier bows

2.2. Assessment options

"Two things are required to obtain a more realistic and above all ship-specific value of f_w: determination of the calm water speed and determination of the ship speed in Beaufort 6," *Gerhardt (2017)*. The calm-water speed is standard fare for ship model basins. For the EEXI, there may not be any old model test results for the required conditions (e.g. draft at 70% deadweight for containerships). In those cases, model tests may be performed just for that condition; but more pragmatically, CFD (computational fluid dynamics) simulations may be used. These are deemed to be comparatively accurate for full-scale prediction by now, *Bertram (2020)*, and are generally the cheaper and faster option. For attained speed in waves, there are various possible options for assessment, discussed in the following.

2.2.1. IMO standard curves for f_w

"A very simple, if somewhat rough, method of obtaining an initial estimate for f_w is described in IMO Circular MEPC.1/Circ.796. The method is based on regression analysis of full-scale measurements, i.e. on the actual speed reduction of existing ships, and only requires ship type and cargo capacity as input. Three kinds of standard f_w curves are provided for bulk carriers, tankers and containerships. The disadvantage of this simplistic method is obvious: it will not give a ship-specific f_w value, i.e. it cannot distinguish between a good and a bad design," *Gerhardt (2017)*.

For ships that need to attain a better EEDI/EEXI, we then have to resort to more accurate approaches to prove ship-specific better performance for the weather factor.

The wind resistance part of the weather factor may be determined through wind tunnel testing. Although CFD is in principle an option with equivalent accuracy, economic arguments usually make wind tunnel tests at least an equivalent, if not better, option, *Bertram (2020)*. Alternatively, semi-empirical methods may be employed, e.g. as recommended for sea trials and performance monitoring, *Herradon de Grado and Bertram (2016)*. The rest of the discussion will then focus on the speed (loss) in waves.

2.2.2. Model tests

Added resistance in waves, or attained speed in waves, can be measured in dedicated model tests. Seakeeping model tests are time consuming and expensive (due to the long waiting time between tests before water is sufficiently calm again, and the relatively rare installations that can investigate oblique waves). For motions with strong viscous effects (yaw, sway and to lesser degree also roll), model test behavior differs from full-scale ship behavior. For practical purposes, model tests are then often limited to head waves, implicitly assuming that the highest speed loss occurs in head waves (which is not true) or that the added resistance distribution over encounter angles is fairly similar for most ships (which may be a more reasonable assumption).

Speed loss in waves, particularly in shorter waves, is difficult to measure. In other words, it comes with high errors, as discussed by *Söding et al. (2012a,b)*: "Model test methods use either self-propelled or towed models. The former method ensures minimum distortion of model motions by the carriage; however, the influence of motions and waves on thrust deduction factor (required to estimate the added resistance) remains an uncertain factor. Methods with towed models either restrain the model's surge motion or use springs that connect the model to the towing carriage. Restraining the surge motion may disturb heave and pitch motions and thus influence the added resistance. The arrangement with springs appears more appropriate; however, springs may introduce additional, low-frequency oscillations in the longitudinal direction.

Another difficulty in model tests is that the added resistance (average force over time) is small compared to the amplitude of the oscillations of the longitudinal force. Thus, errors in the measurement and averaging of these forces in time might be comparable to or even exceed the average force itself. Finally, added resistance is sensitive to the quality of wave generation and wave measurement, especially in short waves. As a consequence, added resistance results from various model basins for the same case often exhibit large scatter, especially for shorter waves and oblique waves," *Bertram (2016)*. In addition, the wave height reaching the ship model adds an additional uncertainty, particularly for shorter waves, which feature smaller attainable wave heights than longer waves.

2.2.3. Computational seakeeping methods

Since the 1950s, a range of computational seakeeping methods has evolved. *Beck and Reed (2001)* and *Bertram (2012)* are recommended for structured overviews. The most important approaches for hull performance were already discussed by *Bertram (2016)*.

ITTC (2018) gives in principle the choice between simulation tools based on slender-body theory ("strip methods"), 3D panel methods, and CFD methods:

- Strip methods are simple, fast and widely available. The very formulation of the underlying theory means that the three-dimensional flow in bow area cannot be captured. Instead, one tries semi-empirical corrections to obtain the added resistance in waves. *ITTC (2018)* states that strip methods provide "[…] engineering accuracy of added resistance in waves." I don't know what constitutes engineering accuracy for a quantity as hard to determine as added resistance in waves, but in my experience with strip methods and added resistance the typical errors are 20-60% in head waves, and significantly higher in oblique waves.
- 3D panel methods may use Green functions or Rankine singularities. Codes based on Rankine singularities, namely FATIMA (MARIN) and Rankine (DNV), *Shigunov and Bertram (2014),* have presented good results for added resistance in validation studies, outperforming all other codes. Both FATIMA and Rankine are used for commercially offered analyses, but are not commercially available, restricting access for a wider community. For accurate pressure integration, the bow region needs to be resolved in much finer detail for added resistance than for motion analyses. *Söding and Shigunov (2015)* show that much finer hull grids are needed for mesh-independent results for added resistance than for motions. Probably, in many cases typical grid resolution, Fig.2, used will be too coarse for accurate prediction of added resistance. Alternatively, the added resistance may be determined using control surface integration in the far field. Here, numerical damping introduces large errors as the "far field" needs to be further removed from the ship than in steady wave resistance computations, where the control surface approach already introduces errors of similar magnitude as the direct pressure integration.
- State-of-the-art CFD (Computational Fluid Dynamics) codes solve the Reynolds-Averaged Navier-Stokes Equations (RANSE), modeling turbulent fluctuations by semi-empirical turbulence models, Fig.3. This approach captures all relevant physics, but is computationally expensive. One might assume that a superior underlying model for the physics would also yield better results. That is a false conclusion, *Bertram et al. (2016)*: "In RANSE-based seakeeping simulations, the calm-water resistance needs to be computed separately (preferably on the same grid) and subtracted from the average total resistance to obtain the value of the added resistance. Resolution and unphysical numerical damping are challenges. A strategy needs to be set for how to control the vessel; soft springs or an autopilot are required to maintain speed and average position and course, unless first-order horizontal motions are prevented." In practice, with affordable resolution, we often get more accurate results with the 3D panel code Rankine.

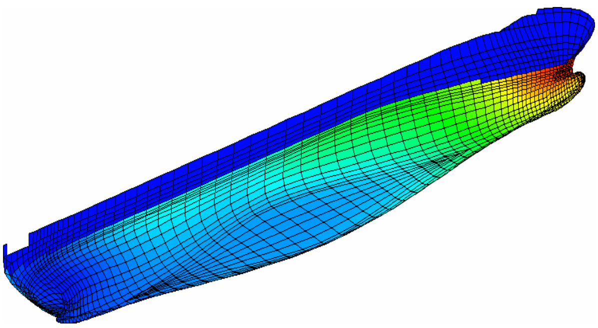

Fig.2: 3D panel method with typical grid

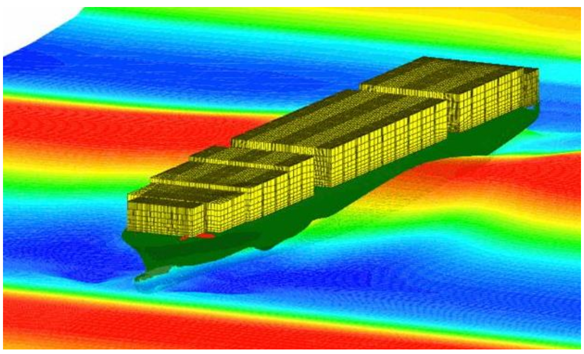

Fig.3: RANSE seakeeping simulation

2.3. Objective uncertainties

The experts in the field of added resistance of ships in waves are well aware of the difficulties. *ITTC (2018)* requires V&V (Verification and Validation) for all numerical codes used, meaning showing adequate accuracy for predicted results compared to other results, typically model tank tests. The problem is "good agreement" shown in such V&V studies has only limited significance for how well the speed loss in waves is predicted for the actual ship where the weather factor is used to determine the EEDI/EEXI:

- The fact that heave and pitch motions are "in good agreement" with benchmark results does not mean that added resistance is calculated well. Added resistance is numerically much more sensitive and difficult to predict than heave and pitch motions.
- The fact that good agreement is shown for head waves and longer wave lengths does not mean that added resistance is calculated well, where oblique waves contribute most to the added resistance. For longer ships, larger parts of the wave spectrum will be relatively short.
- The fact that added resistance is predicted well does not mean that speed loss in waves is predicted just as well. Indirect resistance parts, like induced rudder forces to keep course, and changes in propulsive efficiency of the propeller are mostly neglected in the computational models.
- Published and documented validation of seakeeping codes generally show best cases, often for computationally friendly hull shapes (e.g. without transom sterns), wave lengths and directions and for process parameters (e.g. grids) that yielded best results.

In summary, added resistance is difficult to predict, regardless what approach is taken, especially in short or oblique waves. Even when following best practice, uncertainties of at least 20-30% in added resistance are to be accepted.

2.4. How one could play the system

Improving the EEDI/EEXI by 3-5% in reality requires generally significant effort coming at significant cost. Getting a high-performance coating instead of a low-cost coating on a large tanker may cost 300,000 – 500,000 USD more [Andreas Krapp of Jotun in personal communication]. The price for a Mewis Duct as a high-end PID is estimated to be in the same order of magnitude, based on a press release giving payback times of 1 year and fuel savings of 930 t in 2012.

One might be tempted to play the system instead and exploit the margins of uncertainties in the assessment of "proving" the actual weather factor when not using the IMO standard values. Various computational methods (all validated and formally acceptable) and computational parameters could be tried and the results with the smallest speed loss taken and submitted for formal approval:

- Variations in computational methods, e.g. strip methods or 3D methods; strip methods use crude or semi-empirical corrections for the flow at the bow which may give favorable errors for the weather factor
- Computing or testing just in head waves, as allowed by *ITTC (2018)*: "the wind and wave encounter angle for the f_w calculation should be taken as the direction which results in the largest speed loss; i.e. yields the smallest f_w value. Should this require too much computational or experimental effort then the head sea condition can be used to represent the ocean environmental condition for computing f_w."
- Variation in grids for a given (good) code can yield large changes in the computed added resistance: "From experience, you need an extremely fine resolution on the hull: panel size should be ~1% of L_{pp} in the middle of the ship and 1.5 times finer at bow and stern. If you make it coarser, you greatly reduce the additional drag in short waves and somewhat at the peak. How bad the results can be if you selectively coarsen panels, I don't know, but a factor 2 error is easy to make," [Dr. Vladimir Shigunov (DNV) in personal communication].

3. Conclusion

The weather factor in the EEDI/EEXI is a well-intended attempt to improve energy efficiency performance of ships in realistic ambient conditions. As so often, the devil lurks in the details. The difficulties in determining speed loss in waves accurately, particularly for shorter waves, respectively longer vessels, lead to relatively large uncertainties. These could be exploited to achieve a better EEDI/EEXI on paper than achieved in reality.

Acknowledgements

My colleague Dr. Vladimir Shigunov generously and openly shared his expertise on the uncertainties in even the best numerical tools when calculating added power requirements or speed loss in waves. I am very grateful for this unique insight.

References

BECK, R.F.; REED, A.M. (2001), *Modern computational methods for ships in a seaway*, SNAME Trans. 109, pp.1-52

BERTRAM, V. (2012), *Practical Ship Hydrodynamics*, Butterworth-Heinemann, Oxford

BERTRAM, V. (2016), *Added Power in Waves – Time to Stop Lying (to Ourselves)*, 1st HullPIC Conf., Pavone, pp.5-13, http://data.hullpic.info/HullPIC2016.pdf

BERTRAM, V. (2020), *CFD for Performance Monitoring – Current Capabilities and Limits*, 5th HullPIC Conf., Hamburg, pp.13-21, http://data.hullpic.info/HullPIC2020_Hamburg.pdf

BERTRAM, V.; ZORN, T.; ROGNEBAKKE, O. (2016), *Advanced Simulations = Better Results. Really?*, 19th Numerical Towing Tank Symp., Oleron, https://www.uni-due.de/imperia/md/content/ist/nutts_19_2016_st_pierre.pdf

GERHARDT, F. (2017), *f_w – the unknown factor*, SSPA, Gothenburg, https://www.sspa.se/sites/www.sspa.se/files/field_page_files/2017_sspa_highlights_64_fw_the_unknown_factor.pdf

HERRADON DE GRADO, E.; BERTRAM, V. (2016), *Predicting added resistance in wind and waves employing artificial neural nets*, 1st HullPIC Conf., Pavone, pp.14-22, http://data.hullpic.info/HullPIC2016.pdf

ITTC (2018), *Calculation of the weather factor fw for decrease of ship speed in wind and waves*, Recommended Procedures and Guidelines 7.5-02-07-02.8, Int. Towing Tank Conf., https://ittc.info/media/8248/75-02-07-028.pdf

SHIGUNOV, V.; BERTRAM, V. (2014), *Prediction of added power in seaway by numerical simulation*, 9th Int. Conf. on High-Performance Marine Vessels (HIPER), Athens, pp.102-113, http://data.hiper-conf.info/Hiper2014_Athens.pdf

SÖDING, H.; SHIGUNOV, V. (2015), *Added resistance of ships in waves*, Ship Technology Research 62/1, pp.2-13

SÖDING, H.; GRAEFE, A.v.; EL MOCTAR, O.; SHIGUNOV, V. (2012a), *Rankine source method for seakeeping predictions*, 31st Int. Conf. Ocean, Offshore and Arctic Eng. (OMAE), Rio de Janeiro

SÖDING, H.; SHIGUNOV, V.; SCHELLIN, T.E.; EL MOCTAR, O.; WALTER, S. (2012b), *Computing added resistance in waves – Rankine panel method vs RANSE method*, 15th NuTTS Symp. (NuTTS), Cortona, http://www.uni-due.de/imperia/md/content/ist/nutts_15_2012_cortona.pdf

Energy Saving Devices Performance Assessment Using CFD

Inno Gatin, In silico d.o.o., Zagreb/Croatia, inno.gatin@cloudtowingtank.com
Milan Kalajdžić, University of Belgrade, Belgrade/Serbia, mdkalajdzic@mas.bg.ac.rs

Abstract

In the wake of the new EEXI regulations, a lot of attention has been given to quantifying power savings (or losses) generated by various Energy Saving Devices available on the market. These come in many different variations, while the most popular and effective ones are typically based on pre-swirl and/or equalization of the ship wake upstream from the propeller. The new regulations and trends in shipping pressure shipowners to quantify the effect of these devices, giving rise to an uptake in CFD application for this purpose. In this paper we will share our findings on this topic gathered during the past 10 months of intense activity on the topic, in the attempt to draw general observations on the effectiveness of different ESDs.

1. Introduction

The sudden rise in stringency of greenhouse gas emission regulations caused an intensification of studying various propulsion efficiency increase methods. This process is ongoing and initiated mostly by shipowners worrying about meeting the EEXI and CII requirements without damaging their bottom line. Many energy saving methods are being reviewed and scrutinized to levels unseen before. This is because "greenwashing" is not sufficient in the light of the new regulations, and the shipowners need the savings to be real and provable. Moreover, since many are now considering installation of different Energy Saving Devices for ships that are bordering economic viability at reduced speed or ones that are close to satisfying EEXI without Engine Power Limitation, making the right choice when it comes to ESD-s has rarely been as important as it is now.

Naturally, CFD presents a cost-effective method for predicting the benefits that different ESD-s can provide, even if its role in creating an approved EEXI Technical File is less certain at this point. Nonetheless many shipowners chose to use it to help them make the right choice when it comes to selecting the ESD or installing one in the first place. The scientific literature concerning application of CFD to ESD performance prediction is currently growing, and many publications deal with optimising the ESDs using CFD, *Korkmaz (2015), Dang et al. (2011), Furcas et al. (2020), Kim et al. (2015), Nadery and Ghassemi (2020), Nowruzi and Najafi (2019).* In most cases the problem is considered in model scale, to provide grounds for comparison against experimental measurements, but some authors pay special attention to scale effects that influence the performance of ESD-s in full scale, compared to model scale predictions. For example, *Kim et al. (2014)*, compared four different ESDs, and found that the predicted model scale savings in power reduce from 3-6 % to 0-2% in full scale. The largest difference is observed for a duct type ESD without pre-swirl stator finds, which shows 0% savings in full scale, and more than 4% in model scale. In our experience, presented in this paper, it is often the case that the performance of duct-type ESDs is lower than expected.

In this paper a study for five different vessels is given, showing relative changes in required power delivered to the propeller with and without several types of ESDs. The five vessels are typical representatives of cargo vessels, comprising two tankers, two bulk carriers, and one container vessel. The considered ESDs are a Propeller Boss Cap Fin (PBCF), a Wake equalising duct, and a Wake equalising duct with stator fins.

2. Numerical method

The Naval Hydro Pack is a CFD software based on collocated Finite Volume method which uses Level Set for interface capturing. Special discretisation techniques are employed based on the Ghost Fluid Method to guarantee high accuracy of the two-phase flow model, *Vukčević et al. (2017).*

The main goal of the numerical simulations discussed in this paper is to calculate the propulsive characteristics where the rotative nature of the flow around the propeller is taken into account, as well as the non-uniform propeller inflow distribution. To achieve this, the propeller geometry needs to be discretized and simulated while rotating in its designated position at the stern, with and without the presence of the ESD. The transient nature of this sort of simulations makes them computationally expensive, serving as a motivation for developing procedures that will minimize the real time that needs to be simulated. More specifically, the methodology attempts to eliminate large temporal scales from these computations in order to reduce the time scale difference between the propeller rotation and overall behavior of the flow around the hull. This can be achieved by splitting the problem of self-propulsion calculation into two main steps:

1. Calculating the required thrust to propel the vessel at certain speed, together with dynamic sinkage and trim, using the Actuator Disc approach,
2. Calculating the required rotation rate and torque of the propeller to achieve the thrust calculated in 1, using the discretized propeller rotation approach.

In the first step, two degrees of freedom are allowed for the motion for the vessel, namely pitch and heave, allowing for dynamic trim and sinkage of the vessel. The present CFD approach uses a pressure-jump based actuator disc approach where the disc is represented by an infinitely thin surface of circular shape position roughly at the position of the actual propeller. Across the surface, a pressure jump is enforced that when integrated is equal to the thrust of the propeller. The thrust of the propeller is controlled to counteract the resistance of the hull and appendages, i.e. to achieve longitudinal force equilibrium. The control of the propeller is performed using a Proportional-Integral (PI) controller that adjusts the rotation rate of the propeller to achieve the required thrust. The relationship between thrust, rotation rate, torque and propeller inflow velocity are governed by open water characteristics of the propeller at hand. The propeller disc inflow velocity is calculated based on the measured inflow during the simulation when the disc is active, by subtracting the dynamic effect of the pressure jump of the actuator disc, thus obtaining the inflow velocity that corresponds to the calm water resistance condition (without the action of the propeller). The actuator disc model used in this method is explained in detail in *Jasak et al. (2018).*

In the second step, the trim and sinkage of the vessel are fixed to the values obtained in step one. The propeller is geometrically represented, while the Overset grid approach is utilized to model relative motion of the propeller and the hull with appendages. Overset allows automatic, parallelized overlap fringe assembly based on run–time selectable Donor Suitability Functions (DSF). In this work, DSF based on cell volumes of similar sizes has been used to find the overlap. The library offers run–time selection of interpolation schemes, where first order injection scheme is used in this work. Velocity and Level Set fields are interpolated implicitly within the linear system solver, while the pressure is interpolated explicitly to ensure region–wise and fringe mass conservation in a straightforward way. A specialized two–phase model is used supporting overset grid, within the Naval Hydro Pack. The propeller RPM is adjusted to find the thrust calculated in step one, or in some cases, three fixed RPM simulations are carried out and the propulsion point is found using interpolation.

The above-described procedure is repeated with and without the ESD for each vessel, to calculate the relative differences in propulsive power. For this purpose, numerical grids with and without the device need to be generated, Fig.1.

For calculating the effect of the PBCF in isolation, open water simulations are carried out with and without the PBCF, for ships where it was considered. Single phase steady state simulations are used with Multiple Reference Frame approach for this purpose.

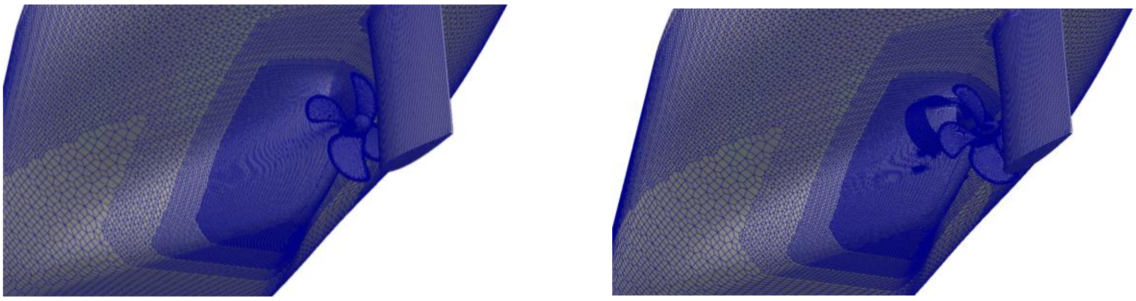

Fig.1: Example of the computational grid with and without the ESD

3. Vessel characteristics

We present here results of relative ESD performance calculated using CFD for five different ships. Typical hull forms are considered for two tankers, two bulk carriers and one container vessel. Length between perpendiculars range between 170 and 200 m for tankers, 200 and 230 m for bulk carriers, and around 180 m for the container vessel. Table I lists the vessels and corresponding ESDs considered in this work. Fig.2 shows the side view of different hull forms. The number of speeds tested for different vessels varies from 1 to 3, while the considered loading conditions are either design or scantling.

Table I: Vessels and ESDs studied in this paper

	Vessel Type	**Displacement**	**Energy Saving Devices**
Ship 1	Tanker	~45 000 tons	PBCF, Wake equalising duct
Ship 2	Bulk Carrier	~60 000 tons	Wake equalising duct
Ship 3	Container Vessel	~45 000 tons	PBCF, Wake equalising duct
Ship 4	Tanker	~72 000 tons	Wake equalising duct
Ship 5	Bulk Carrier	~95 000 tons	Wake equalising duct with stator fins, Wake equalising duct

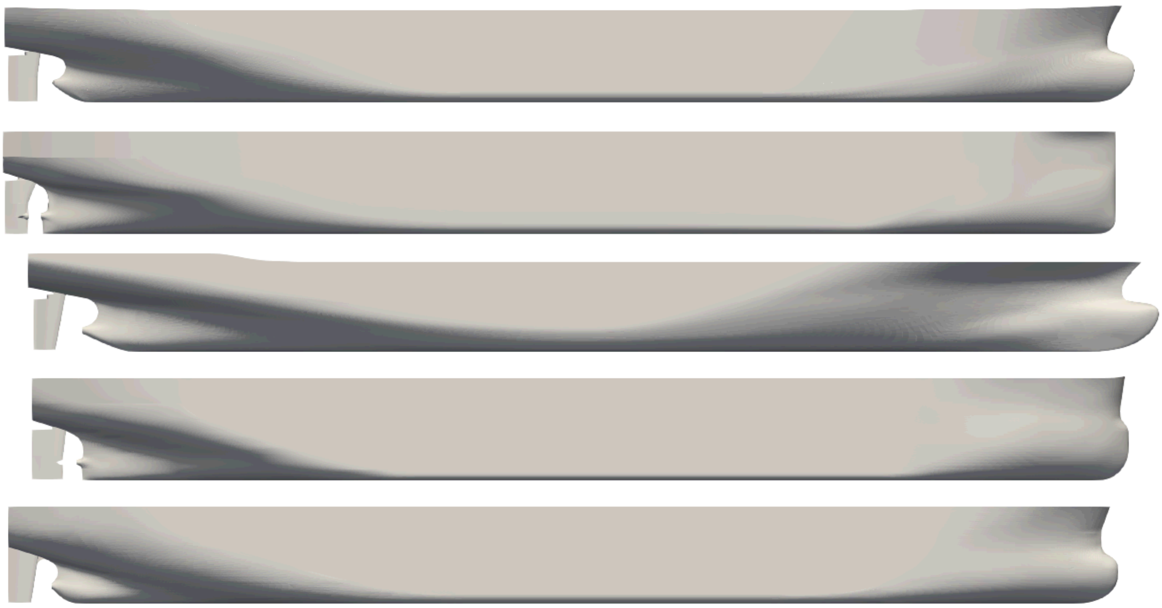

Fig.2: Side view of different hull forms listed in Table I, showing Ship 1 to Ship 5, from top to bottom

4. Analysis and results

The achieved change in delivered power to the propeller for different vessels and ESDs is presented in this section. Differences are given relative to the baseline power, obtained for the condition without the ESD: Power difference = $(P_{D,ESD} - P_{D,BSL})/P_{D,BSL}$, where $P_{D,BSL}$ denotes the baseline delivered power to the propeller (without the ESD) and $P_{D,ESD}$ denotes power with ESD. Positive values of power difference indicate that the ESD causes increase in power, and negative denote a power reduction. The table also shows the difference in thrust, calculated in an analogous way.

Table II: shows relative power differences for the five vessels. It can be observed that all but one tested point predicts an increase in power demand from installing the ESD. The power losses range between 0.8 to 5.2 %, often being above 2%. The container vessel, Ship 3, showed the smallest losses with the Wake equalising duct, indicating that it is the best candidate for this type of ESD. Power reduction is achieved only in the case of the Wake equalising duct with stator fins with Ship 5, where a 2.2 % power reduction is predicted. Ship 1 and Ship 3 are studied for both the Wake equalising duct and the PBCF being installed at the same time.
Table III: shows power savings achieved when the PBCF is installed in isolation, as predicted by the open water test simulations. Here a small reduction in power is predicted for both ships, staying below 1% for all advance ratios. Note that when paired up with the Wake equalising duct, the two ESDs do not produce a power reduction, as shown in Table II:. When it comes to thrust, an increase is calculated in all simulations, even with the Wake equalising duct with stator fins where a power reduction is achieved. This indicates that the ESD increases the resistance in all cases, while in the case of the Wake equalising duct with stator fins manages to increase the efficiency of the propeller at the same time. The increase in efficiency compensates for the increase in thrust and gives additional power reduction.

Table II: Relative power differences predicted with different ESDs using self-propulsion simulations

	ESD	**Speeds**	**Power difference**	**Thrust difference**
Ship 1	PBCF and Wake equalising duct	12 kn	3.4%	3.1%
		14 kn	1.7%	1.9%
		15 kn	1.3%	2.3%
Ship 2	Wake equalising duct	14 kn	4.0%	3.1%
Ship 3	PBCF and Wake equalising duct	21.2 kn	0.8%	2.7%
Ship 4	Wake equalising duct	14 kn	2.5%	4.1%
Ship 5	Wake equalising duct	12.5 kn	5.2%	5.6%
	Wake equalising duct with stator fins	12.5 kn	-2.2%	3.1%

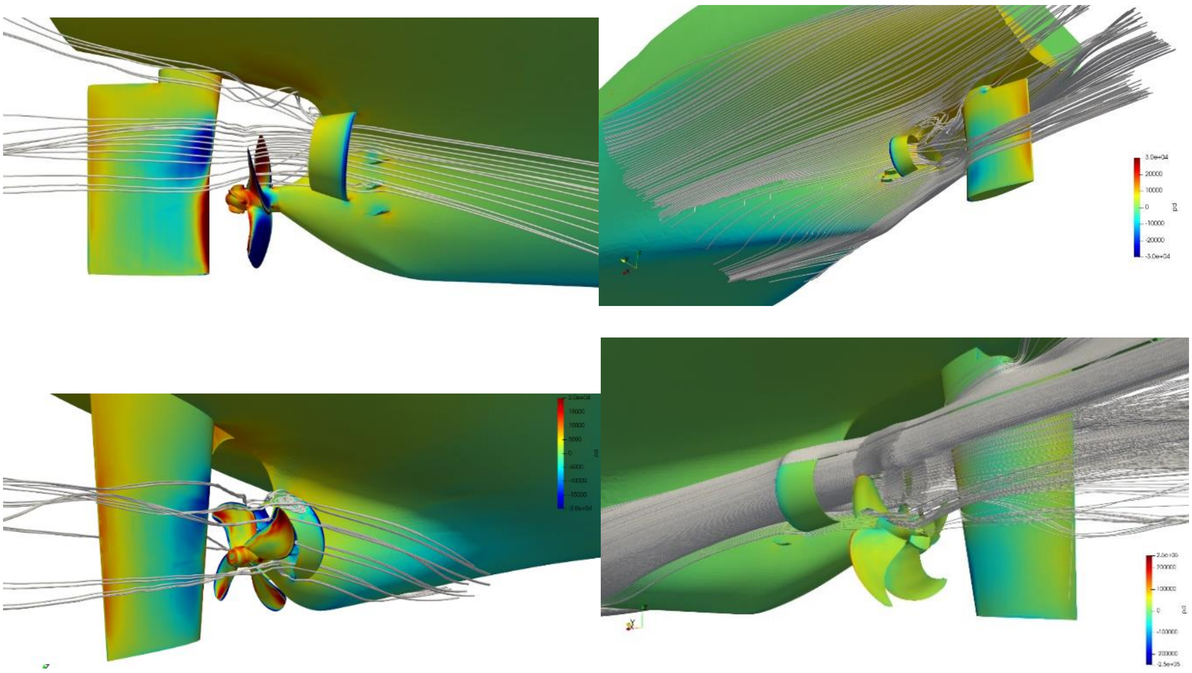

Fig.3: Selected images from the CFD simulations with ESDs

Table III: Relative power differences achieved with PBCF, calculated using open water CFD simulations

	ESD	Advance coefficient J	Power difference
Ship 1	PBCF	0.4 to 0.9	-0.85 to -0.45 %
Ship 3	PBCF	0.34 to 0.64	-0.8 to -0.66 %

Note that the Wake equalising duct is a duct type ESD that has no pre-swirl fins, i.e. its function is based on homogenization and/or change in the average inflow velocity to the propeller. In model scale, thrust generated by these kinds of ducts has been reported, even though we see little evidence of this in full scale simulations. The Wake equalising duct with stator fins is located closer to the propeller and is equipped with fins designed to create a pre-swirl and reduce rotational losses in this way.

6. Conclusion

A study of effectiveness of different ESDs is conducted for five different vessels. Three different ESDs are considered: PBCF, Wake equalising duct, and Wake equalising duct with stator fins. The study is conducted using Finite Volume based RANSE CFD approach, where discretized propeller geometry is used to conduct the individual self-propulsion simulations. Two sets of calculations are carried out for each vessel and ESD combination: with and without the ESD.

Results show that in most cases the ESD increases power consumption, with one exception. The increases in delivered power to the propeller range between 0.8% and 5.6%, and are exhibited by the Wake equalising duct, or a combination of the Wake equalising duct and PBCF. The one case that showed a benefit was when the hull was equipped with the Wake equalising duct with stator fins, with a power reduction of 2.2%. Note that the same hull experienced increase in power with the Wake equalising duct of 5.6%. The PBCF in isolation showed a reduction in power up to 0.85%.

The results presented in this paper are indicative, as they are not validated against sea trial and performance monitoring data for these vessels. To gain more confidence in them, a systematic comparison against sea trials and long-time performance monitoring is recommended. Comparing to sea trials is in most cases not practical, since usually the ESD is not the only factor of change between the baseline and the new trial results. This is due to the fact that hull cleaning, and sometimes application of low surface roughness paint, are also a factor. This makes it difficult to directly compare CFD results against measurements. Nonetheless they serve as indications of relative performance of different devices. Additionally, they pose a question regarding model scale prediction of duct-type ESDs without pre-swirl effects, that should be studied further.

References

DANG, J.; CHEN, H.; DONG, G.; VAN DER PLOEG, A.; HALLMANN, R.; MAURO, F. (2011), *An Exploratory Study on the Working Principles of Energy Saving Devices (ESDs*), Greenship Conf., Wuxi

FURCAS, F.; VERNENGO, G.; VILLA, D.; GAGGERO, S. (2020), *Design of Wake Equalizing Ducts using RANSE-based SBDO*, Applied Ocean Research 97

JASAK, H.; VUKČEVIĆ, V.; GATIN, I.; LALOVIĆ, I. (2018), *CFD validation and grid sensitivity studies of full scale ship self propulsion*, Int. J. Naval Architecture and Ocean Engineering 11/1, pp.33-43, https://doi.org/10.1016/j.ijnaoe.2017.12.004

KIM, J.H.; CHOI, J.E.; CHOI, B.J.; CHUNG, S.H.; SEO, H.W. (2015), *Development of Energy-Saving devices for a full Slow-Speed ship through improving propulsion performance*, Int. J. Naval Architecture and Ocean Engineering 7(2), pp.390–398

KIM, K.; LEER-ANDERSEN, M., ORYCH, M. (2014), *Hydrodynamic Optimization of Energy Saving Devices in Full Scale*, 30th Symp. Naval Hydrodynamics, pp.2-7, http://www.sspa.se/news/hydrodynamic-optimization-energy-saving-devices-full-scale

KORKMAZ, K.B. (2015), *CFD Predictions of Resistance and Propulsion for the JAPAN Bulk Carrier (JBC) with and without an Energy Saving Device*, MSc thesis, Chalmers Techn. Univ. Gothenburg

NADERY, A.; GHASSEMI, H. (2020), *Numerical Investigation of the Hydrodynamic Performance of the Propeller behind the Ship with and without WED*, Polish Maritime Research 27(4), pp.50–59

NOWRUZI, H.; NAJAFI, A. (2019), *An experimental and CFD study on the effects of different pre-swirl ducts on propulsion performance of Series 60 ship*, Ocean Engineering 173, pp.491–509

VUKČEVIĆ, V.; JASAK, H.; GATIN, I. (2017), *Implementation of the Ghost Fluid Method for free surface flows in polyhedral Finite Volume framework*, Computers and Fluids 153, pp.1–19

Lifecycle Assessment of Fuel Oil Consumption of a Ship in Service

Naoto Sogihara, National Maritime Research Institute, Tokyo/Japan, sogihara@m.mpat.go.jp
Mariko Kuroda, National Maritime Research Institute, Tokyo/Japan, kuroda@m.mpat.go.jp
Masaru Tsujimoto, National Maritime Research Institute, Tokyo/Japan, m-tsuji@m.mpat.go.jp

Abstract

This paper describes the outcomes from the OCTARVIA project in which 25 stakeholders in Japan Maritime Cluster participated. The first outcome is a standard monitoring method of ship performance in actual seas, which enables an objective evaluation of the performance. The second outcome is an objective method of lifecycle assessment of fuel oil consumption of a ship in service. Further, the evaluation method can clarify the fouling and aging effect on fuel oil consumption in service. The outcomes are expected to contribute the reduction of GHG emission from ships in service.

1. Introduction

A reduction of the greenhouse gas emission from shipping sector is an urgent issue and to achieve that it is required to make efforts to build eco-friendly ships and operate ships with energy saving. To validate the effectiveness of such efforts, an evaluation method of ship performance in actual seas should be established.

The OCTARVIA project where 25 stakeholders in Japan Maritime Cluster participated discussed and established the evaluation method, *Tsujimoto et al. (2020*). This method can assess fuel consumption in the lifecycle taking account of the fouling and aging effect on the propulsive performance and deal with retrievals of the performance due to dock-in.

The OCTARVIA project also focused to an establishment of an analysis method for ship performance monitoring, which results in a development of Resistance Criteria Method (RCM). An application of RCM can provide a reliable solution of ship performance in calm seas and actual seas. This paper presents the lifecycle assessment of fuel oil consumption in service based on a ship performance in calm seams derived from the performance monitoring.

2. Ship performance evaluation in calm seas

2.1 Outline of standard monitoring method

Onboard monitoring has widely spread in shipping sector and effective for evaluating ship performance. In order to evaluate ship performance objectively, a standard monitoring method is necessary. The OCTARVIA project has established the standard monitoring method for evaluating the ship performance and consolidated the outcomes into a document. The standard monitoring method is comprised of three parts; measurement, analysis, and evaluation. The flowchart of the method is illustrated in Fig.1. The standard monitoring method is packaged into a web application 'SALVIA-OCT.-web', shown in Fig.2.

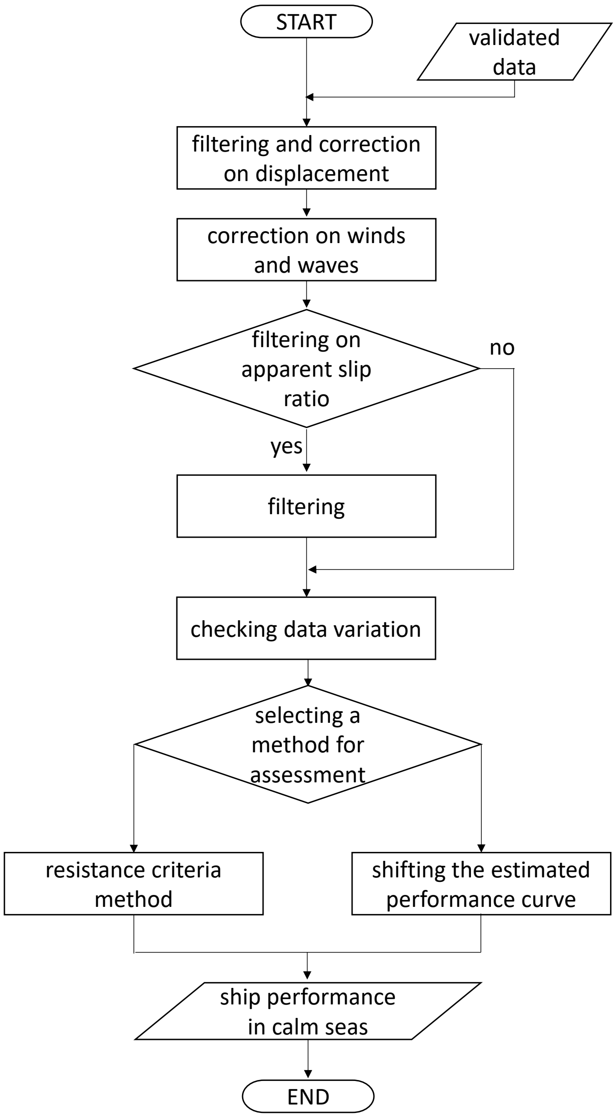

Fig.1: Flowchart of standard monitoring method

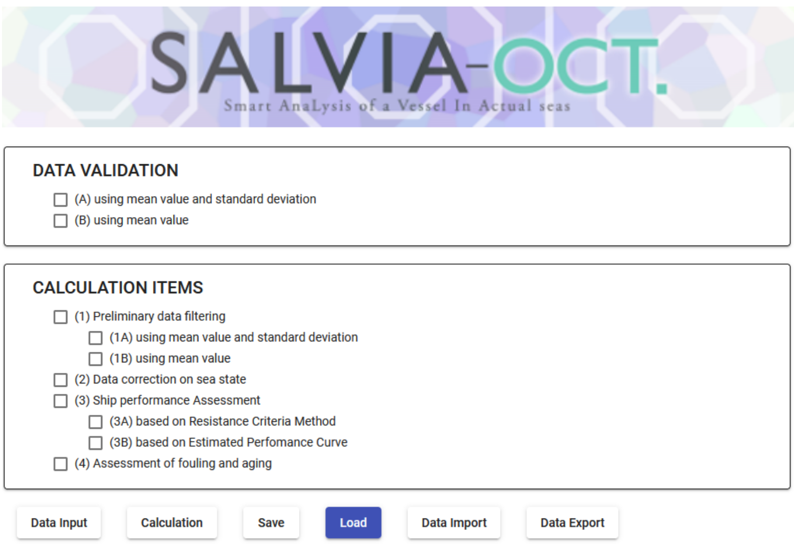

Fig.2: Top page of SALVIA-OCT.-web

2.1.1 Measurement

The standard monitoring method recommends the items listed in Table I as those measured in ship performance monitoring. Taking into consideration that, with auto-logging system, each measurement item is generally collected with high sampling frequency such as 1 Hz, the mean value in a certain period should be used for the analysis and the evaluation of the performance, not instantaneous value.

Table I: Recommended items in the standard monitoring method

Item	Instrument, data source	allowable error
Ship speed over ground	GPS	2%
Course over ground	GPS	
Ship speed through water	Doppler log	1%
Shaft horsepower	Shaft horsepower meter	0.5%
Engine revolution	Revolution counter	1%
Heading angle	Gyro compass	
Wind	Anemometer	Relative wind speed: 5% Relative wind direction: 5°
Sea state	Wave data (hindcast or nowcast data is available), onboard measurement (radar, visual observation, etc.)	Wave height: 0.1m Wave direction: 5°
Rudder angle	Rudder angle indicator	
Draft	Visual observation at departure	
Longitudinal radius of gyration	Measured value or simplified estimation	

The standard monitoring method recommends that the certain period should be set within 10 to 30 minutes. Further, for ensuring data validation, criteria listed in Table II are applied. N_{EMCR} means the engine revolution at Maximum Continuous Rate (MCR). The data collected in the ship performance monitoring should be screened according to the criteria and the screened data (validated data) is used for the analysis.

Table II: Criteria for data validation

Item	Criteria	Intent
Engine revolution [rpm]	40%N_{EMCR}	Eliminate the unsteady data measured under the acceleration after departure and the deceleration before arrival
Drift angle [deg.]	3.0*	Eliminate the data under rudder operation
Rudder angle [deg.]	5.0*	
Difference between ship speed over ground and through water [knot]	0.5*	Eliminate the data affected by the current Ensure the accuracy of speed through water

* denotes an absolute value.

2.1.2 Analysis

Analysis consists of two corrections. The first correction is for displacement. In general, the displacement of a ship in service varies due to the change in the amount of cargo. Since the standard monitoring method aims to evaluate the ship performance in a representative displacement, the validated data close to the representative displacement should be extracted. The standard monitoring method permits the displacement within 3% of the representative displacement. The screened data is corrected for displacement as defined by Eq.(1).

$$V_{rep} = V_{voy}\left(\frac{\Delta_{voy}}{\Delta_{rep}}\right)^{\frac{2}{9}} \qquad (1)$$

V and Δ is ship speed through water and displacement, respectively. Subscripts '*voy*' and '*rep*' denote the value in voyage and representative displacement, respectively.

The second correction is for the effects of environmental factors. specifically winds and waves. The correction is conducted in compliance with Resistance-Thrust Identify Method, *ITTC (2014)*. Added resistance in winds is estimated by the empirical formula, *Fujiwara et al. (2006)* and added resistance in waves is estimated by the theoretical method with simplified tank tests in short waves or empirical formula, *Tsujimoto et al. (2008)* which can be expanded to any wave direction, *Tsujimoto et al. (2013)*.

Estimation on added resistance in winds and that in waves requires superstructure parameters and hull form parameters such as ship sectional data and waterplane, respectively. Authors prepared such parameters by the simplified method, *Sogihara et al. (2019),* in which these parameters can be estimated by ship type and ship principal parameters. Further, self-propulsion factors and propeller open characteristics which are required in the correction based on Resistance-Thrust Identify Method can be estimated by the simplified method. The simplified method can be used on a web application 'EAGLE-OCT.-web', Fig.3. The input and output of EAGLE-OCT.-web are summarized in Table III. Using the EAGLE-OCT.-web, the party not having the detail hull form and performance data, such as ship owner, operator, and paint maker can evaluate the ship performance.

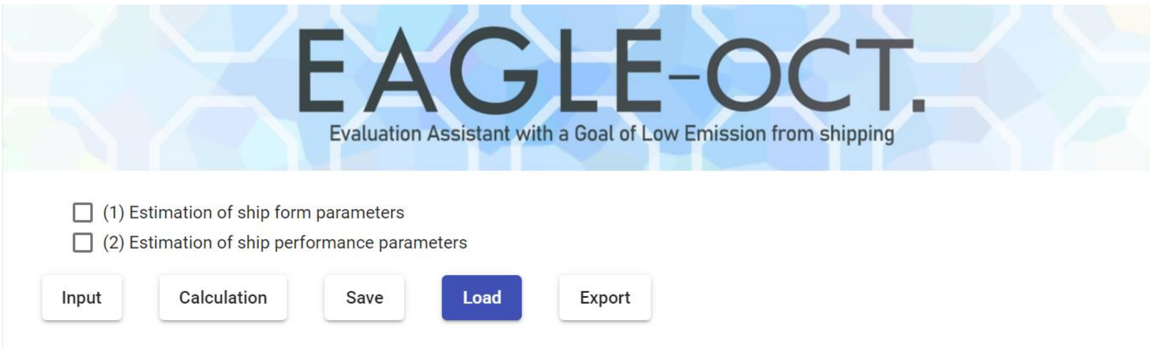

Fig.3: Top page of EAGLE-OCT.-web

Table III: Input and output of EAGLE-OCT.-web

Input	Output
✓ Ship type (Container ship, PCC, bulk carrier, and tanker are available.) ✓ Length overall, length between perpendiculars, maximum breadth ✓ Draft at mid, fore, aft in design full and operation condition ✓ Design speed ✓ Propeller diameter ✓ Transmission efficiency and gear ratio of main engine ✓ MCR of main engine and engine revolution at MCR	✓ Sectional data (draft, half breadth, and area), waterplane ✓ Blockage coefficient （C_B, C_P etc.） ✓ Superstructure parameters ✓ Longitudinal and vertical center of gravity ✓ Height of transverse metacenter and natural roll period ✓ Radius of gyration (pitch, roll, and yaw) ✓ Self-propulsion factors ✓ Propeller open characteristics

2.1.3 Evaluation

The corrected data for displacement and environmental factors are used for the evaluation. The standard monitoring method includes two methods for evaluating ship performance in calm seas; resistance criteria method (RCM), *Sakurada et al. (2020),* and the method shifting the estimated performance curve derived from numerical or experimental investigations. This paper outlines RCM which effectiveness is validated, *Sogihara et al. (2021)*.

RCM has a unique filtering by an apparent slip ratio. This filtering aims to extract the data having a sufficient accuracy for evaluating the ship performance. In other words, the data with poor accuracy of the speed should not be used.

RCM is characterized by introducing increase rate of resistance δR as defined Eq.(2) and Eq.(3) for enhancing the accuracy of the evaluated performance.

$$\delta R = \frac{\Delta R}{R_{id}} \tag{2}$$

$$R_{id} = R_{ms} - \Delta R \tag{3}$$

In these equations, ΔR is the added resistance due to waves and winds, R_{ms} is the total resistance in waves and winds, and R_{ms} is the resistance in calm seas. ΔR and R_{ms} are obtained in the process of the correction for the effects of environmental factors.

The outline of evaluation by increase rate of resistance in RCM is shown in Fig.4. The evaluation includes the process of 'two-way' evaluation involving the increase rate of resistance δR. On the first way, the data measured in the condition where the effects of waves and winds are negligible are extracted by small δR (δR_{eval} in Fig.4) such as less than 5%. These data are used for the evaluation of the performance curve, which named 'evaluation data'.

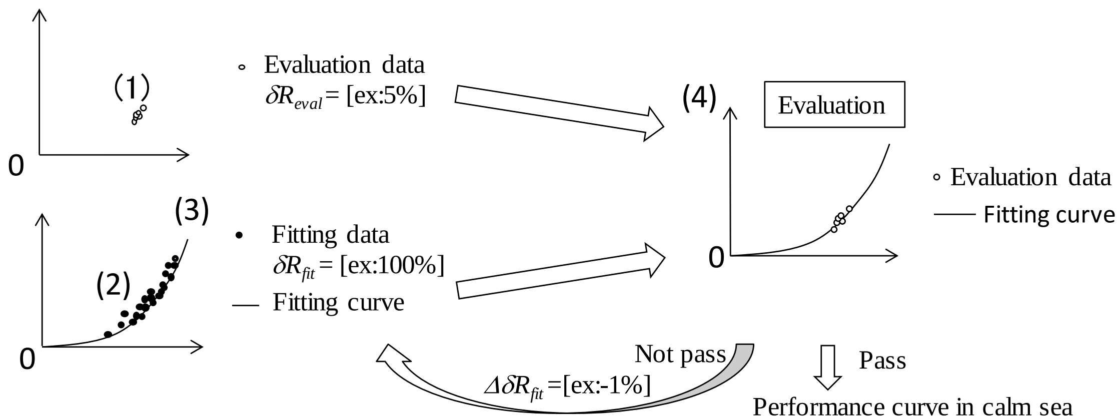

Fig.4: Outline of evaluation by increase rate of resistance in RCM

On the second way, the data are extracted by large δR (δR_{fit} in Fig.4) such as less than 100% for estimating the performance curve in wide range of engine output which is required for the performance evaluation in lower output. These data are used for the curve fitting, which named 'fitting data'. Applying the numerical model (*SAKURADA et al, 2021*) expressed as Eq.(4) and Eq.(5) to the fitting data gives a tentative performance curve, where V_S, N_E, and P indicate ship speed through water, engine revolution, and engine output, respectively.

$$N_E = d_{nv} \cdot V_S \tag{4}$$

$$P = a_n \cdot {N_E}^{b_n} \tag{5}$$

After two ways above, the tentative performance curve is evaluated by the evaluation data. Based on a deviation of the evaluation data around the tentative performance curve, the effectiveness of the tentative performance curve is examined. If the deviation is smaller than the criteria, the tentative performance curve is regarded as a result of the evaluation by RCM. Otherwise, it is necessary to return to the second way and the fitting data is re-extracted with the smaller δR_{fit}. Based on the re-extracted fitting data, the tentative performance curve is obtained again and validated by the evaluation data in similar way, which is iteratively conducted till the deviation satisfies the criteria.

Furthermore, RCM provides quality information based on the results of the evaluation, *Sogihara et al. (2020)*. The quality information is listed in Table IV.

Table IV: Quality information by RCM

ID	Rank	Quality
Passed	1	RCM is finished completely.
Grade1	2	RCM is not finished completely. The performance curve is obtained by the initial fitting data.
Grade2	3	RCM is not finished completely. The performance curve is obtained by the initial fitting data with b_n = 3.0
Grade3	4	RCM is not finished completely. The performance curve is obtained by all the data with b_n = 3.0

2.2 Application of standard monitoring method

The standard monitoring method is applied to simulated monitoring data of Cape-size bulk carrier shown in Table V. This study addresses a route from Gladstone to Tokyo shown in Fig.5. The simulated monitoring data on the route in design full load condition is shown in Fig.6, including significant wave height (H), mean wave period (T_w), primary wave direction (θ_w), true wind speed (U_{wind}), true wind direction (γ_{wind}), ship speed over ground (V_G), ship speed through water (V_S), engine revolution (N_E), engine output (P), drift angle (β), and rudder angle (δ).

Table V: Principal particulars of Cape-size bulk carrier

Item	Design full load	Ballasted	Unit
Length overall	280.0		m
Length between perpendiculars	285.0		m
Breadth	45.0		m
Draft at midship	16.5	8.6	m
Trim by stern	0.0	2.8	m
Design speed	14.5		knot
Amount of cargo	150,000	0	ton
Maximum Continuous Rate (MCR)	15610		kW
Engine revolution at MCR	83.0		rpm

The interval of data sampling is one hour. Wave and wind data in Fig.6 are nowcast data provided by Japan Meteorological Agency. Ship performance data except ship speed over ground are provided by ship performance simulator VESTA, *Tsujimoto et al. (2015)*. Ship speed over ground is generated by adding uniform random numbers to the simulated speed through water.

Fig.5: Route of navigation from Gladstone to Tokyo

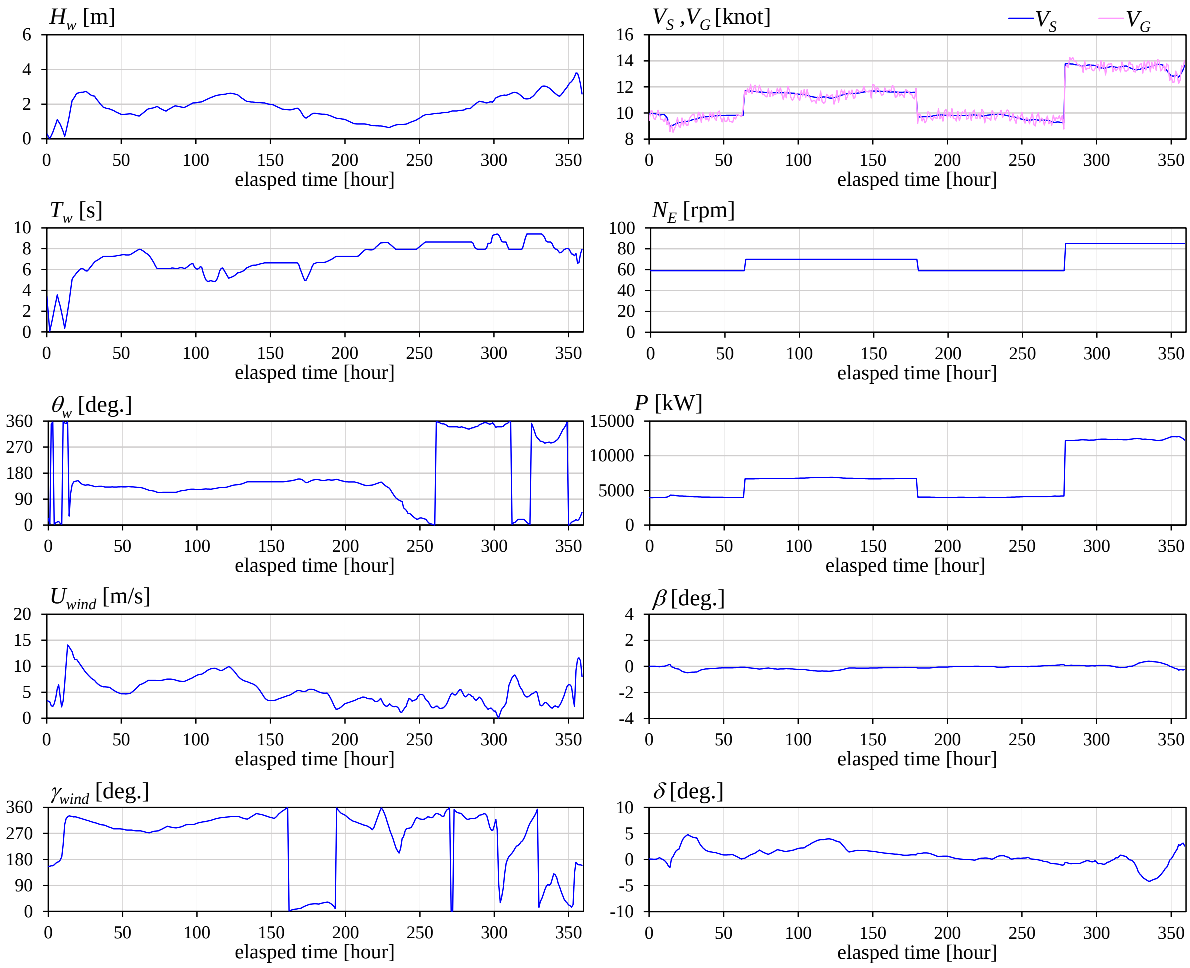

Fig.6: Simulated monitoring data in design full load condition

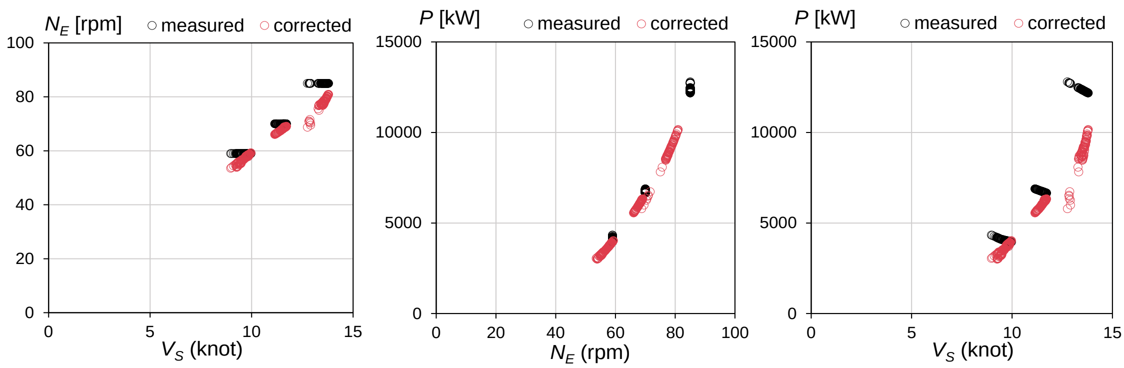

Fig.7: Correction of engine revolution and power for winds and waves

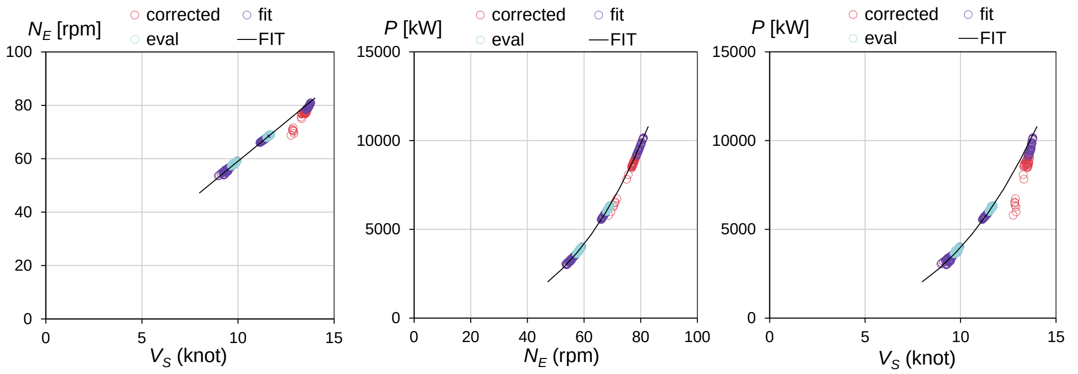

Fig.8: Evaluation of ship performance in calm seas according to the standard monitoring method

Based on the simulated monitoring data, the performance of the cape-size bulk carrier in calm seas is evaluated. Engine revolution and output at constant speed are corrected for the effects of winds and waves, which results in Fig.7. The performance evaluation results in Fig.8 where 'corrected', 'fit', 'eval', and 'FIT' means corrected data for environmental factors, fitting data, evaluation data, and the resultant performance by RCM.

3. Lifecycle assessment of fuel oil consumption in service

3.1 Methodology

The methodology of lifecycle assessment of fuel oil consumption in service is explained in *Kuroda and Sugimoto (2021)* and its outline is described in this paper. The methodology is packaged into 'OCTARVIA-web' shown in Fig.9 and available as a web application.

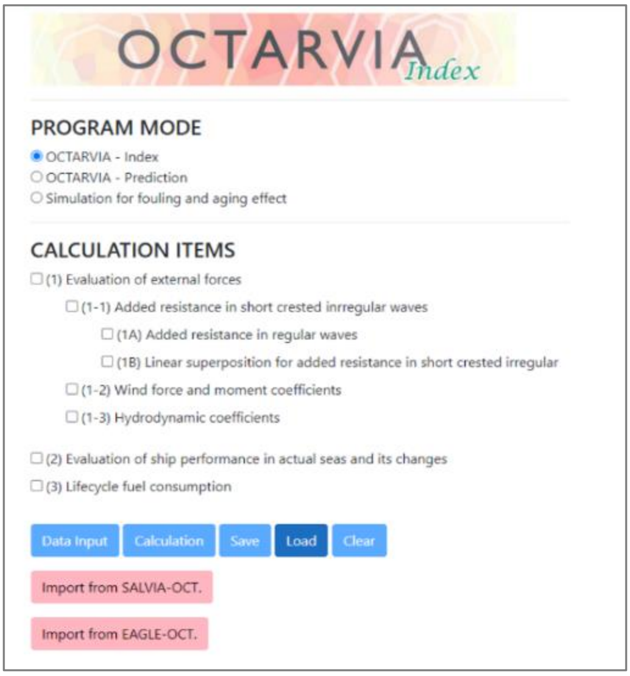

Fig.9: Top page of OCTARVIA-web

3.1.1 Short-term prediction of ship speed and fuel oil consumption

Ship performance in winds and wave is calculated by solving equilibrium equations expressing the external forces acting on a ship. After solving the equilibrium equations, the relationship between propeller revolution (equivalent to engine revolution in cases of low-speed diesel) and engine output and that between ship speed and engine output are obtained. Taking the engine characteristics into consideration, ship speed and fuel oil consumption in the evaluation conditions indicated in Table VI are predicted as shown in Fig.10 for the cape-size bulk carrier.

Table VI: Evaluation conditions

EC	True wind speed U [m/s]	Significant wave height H [m]	Mean wave period T [s]
1	4.4	1.25	4.3
2	6.9	2.00	5.5
3	9.8	3.00	6.7
4	12.6	4.00	7.7
5	15.7	5.50	9.1
6	19.0	7.00	10.2

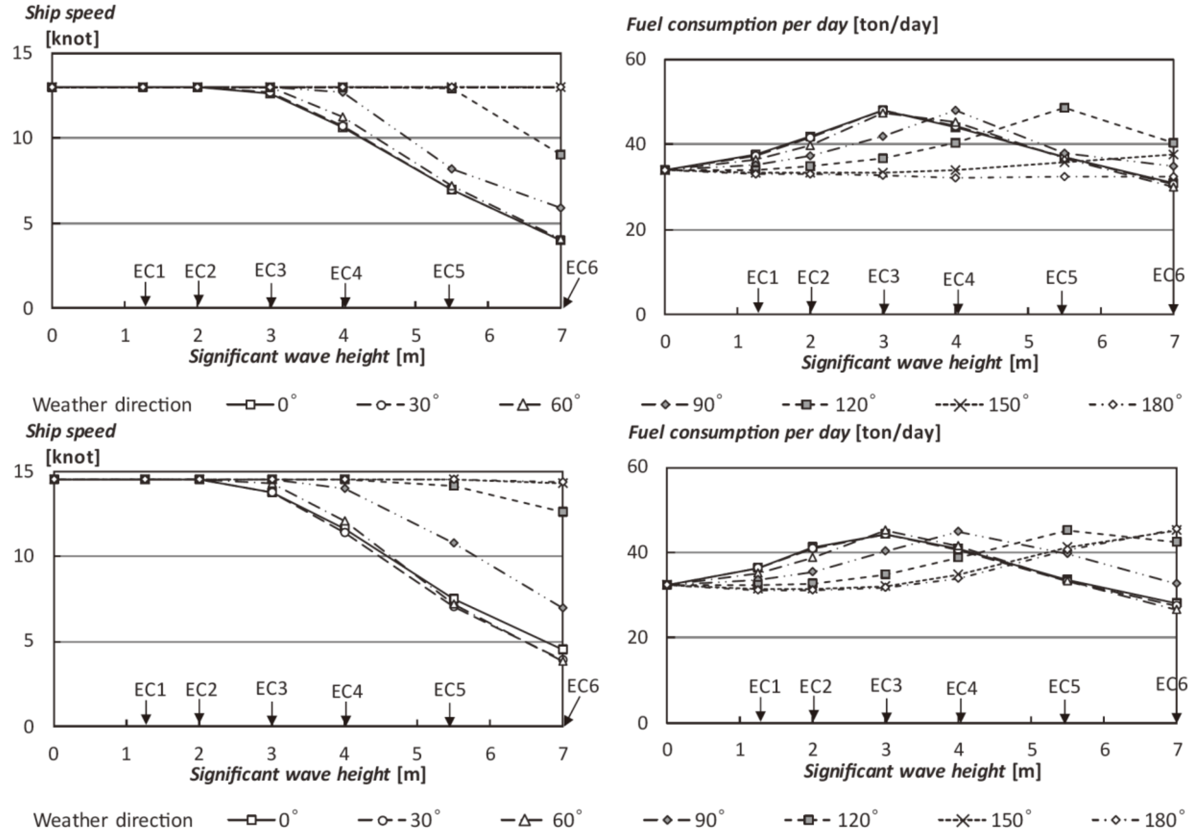

Fig.10: Ship speed and fuel oil consumption, *Kuroda and Sugimoto (2021)*, (top: design full load condition, bottom: ballasted condition)

3.1.2 Long-term prediction of ship speed and fuel oil consumption

Based on the results of short-term prediction of ship speed and fuel oil consumption and occurrence probability distribution on a ship route, the long-term prediction can be conducted by Eqs.(6) and (7). Since the long-term prediction considers the effects of fouling of hull and propeller and those of aging of hull and engine governor, the expectation value of ship speed and fuel oil consumption, $V_E(t)$ and $FPD_E(t)$, respectively, becomes a function of elapsed time after put in service.

$$V_E(t) = \sum_{k=1}^{km} \left\{ p_{dk} \cdot \left(\sum_{j=1}^{jm} p_{wj} \cdot V_{j,k} \right) \right\} \tag{6}$$

$$FPD_E(t) = \sum_{k=1}^{km} \left\{ p_{dk} \cdot \left(\sum_{j=1}^{jm} p_{wj} \cdot FPD_{j,k} \right) \right\} \tag{7}$$

Definitions of the variables in Eqs.(6) and (7) are as follows:

- t : elapsed time after put in service
- P_{dk} : probability distribution for weather direction
- P_{wj} : probability distribution for weather scale
- $V_{j,k}$: ship speed under weather condition j and weather direction k
- $FPD_{j,k}$: fuel oil consumption under weather condition j and weather direction k

Weather scale means EC in Table VI. Weather direction is the direction of winds and waves. $V_{j,k}$ and $FPD_{j,k}$ are the results of the short-term prediction shown in Fig.10.

3.1.3 Evaluation of Lifecycle ship performance

In general, the performance of a ship in service become worse than that of a newly-built ship since the roughness of ship surface under the waterline increases. Such roughness increase is derived from effects of fouling and aging on hull. In the evaluation of fuel oil consumption in ship's lifecycle, these effects should be taken into account. The developed evaluation method treats the effects of fouling and aging as an increase rate of hull resistance in calm seas and expresses the hull resistance in service $R_t(t)$ as shown in Eq.(8).

$$R_t(t) = R_{t0}\{1 + p_{as}t + p_{fs}(t - t_{ch})\} \tag{8}$$

Definitions of the variables in Eq.(8) are as follows:

- t : elapsed time after put in service
- R_{t0}: hull resistance in calm seas at $t = 0$
- p_{as}: aging deterioration for hull
- p_{fs}: fouling deterioration for hull
- t_{ch}: latest time of hull cleaning

The effect of propeller fouling is considered as a deterioration ratio of propeller efficiency in open water. The propeller thrust and torque $T_p(t)$ and $Q_p(t)$ are expressed in Eqs.(9) and (10).

$$T_p(t) = (1 - a)T_{p0} \tag{9}$$

$$Q_p(t) = (1 + a)Q_{p0} \tag{10}$$

$$a = \frac{p_{fp} \cdot (t - t_{cp})}{2 - p_{fp} \cdot (t - t_{cp})} \tag{11}$$

Definitions of the variables from Eqs.(9) to (11) are as follows:

- t : elapsed time after put in service
- T_{p0}: propeller thrust at $t = 0$
- Q_{p0}: propeller torque at $t = 0$
- p_{fp}: fouling deterioration for propeller
- t_{ch}: latest time of propeller cleaning

The aging of engine governor is treated as an increase rate of the specific fuel oil consumption (SFC). The formulation of engine governor aging is explained in detail in *Kuroda and Sugimoto (2021)*.

3.2 Estimation of the effects of fouling and aging on hull resistance

Eq.(8) means that the fouling deterioration for hull can be retrieved by hull cleaning while the aging deterioration is assumed not to be retrieved. p_{as} and p_{fs} can be estimated based on the surface roughness increase of the hull. The relation between the roughness and ship frictional resistance coefficient is expressed as Eq.(12), *Himeno (1983)*.

$$\Delta C_F = 1.8 \times 10^{-5} \cdot R_n^{\ 0.75} \times \frac{k_A}{L} \tag{12}$$

where R_n is Reynolds number, L is ship length, and k_A is apparent roughness height. p_{as} and p_{fs} can be expressed using the increase rate of the roughness (dk_A/dt), which is indicated in Eq.(13).

$$\left.\begin{array}{l} p_{as} \\ p_{fs} \end{array}\right\} = \frac{1.8 \times 10^{-5} \cdot R_n^{\ 0.75}}{C_{T0} L} \cdot \frac{dk_A}{dt} \tag{13}$$

where C_{T0} is the total resistance coefficient in calm seas at newly-built condition. Total resistance for each condition is based on the evaluation of the onboard monitoring data explained in the previous section. p_{as} and p_{fs} at V_S = 12.0 and 14.5 result in Fig.11. There is not remarkable difference between design full load condition and ballasted condition.

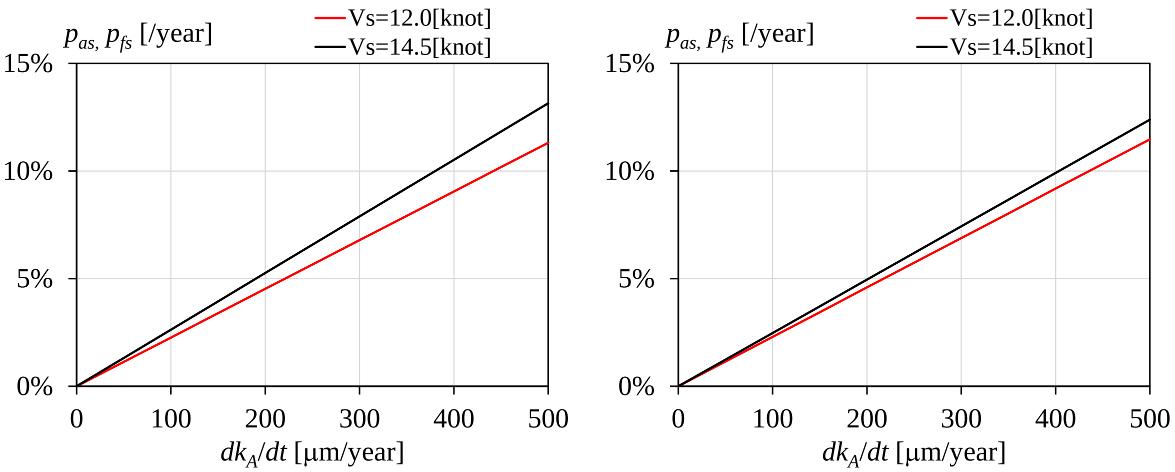

Fig.11: Aging and fouling deterioration (left: design full load condition, right: ballasted condition)

On the roughness effects on the total resistance, an example on a frigate is reported, *Schultz (2007)*. The report shows that, the change in total resistance for an Oliver Hazard Perry-class frigate is 2.0% for anti-fouling coating and 11.0% for deteriorated coating or light slime, respectively, at ship speed 7.7 m/s.

Referring above, the increase rate of the roughness due to fouling (p_{fs}) at ship speed 12.0 kn of the cape-size bulk carrier in the design full load condition corresponds to be 90 μm/year and 485 μm/year which are corresponding to p_{fs} = 2.0% and 11.0%, respectively. Similarly, that in ballasted condition corresponds to be 88 μm/year and 480 μm/year. In addition, on the increase rate of the roughness due to aging (p_{as}) at ship speed 12.0 kn, 15 μm/year, *Miyamoto (2007)*, is given which yields p_{as} = 0.3%.

3.3 Evaluation of hull fouling effects on lifecycle assessment of a ship

A lifecycle assessment on fuel oil consumption is conducted according to the method indicated by Kuroda and Sugimoto. In this study, this assessment assumes that fouling deterioration for propeller is 0.5% per a year and there is no deterioration for engine governor. The assessment also takes cleaning for a hull and propeller into consideration and assumes that the fouling deterioration for a hull and propeller are perfectly retrieved by the cleaning. The evaluation period is set 15 year and cleaning interval for a hull and propeller is assumed to be the combination of 2 and 3 years.

Time variation of the expectation value of ship speed and fuel oil consumption, $V_{ave}(t)$ and $FPD_{ave}(t)$, respectively, are calculated by Eqs.(14) and (15).

$$V_{ave}(t) = \frac{2}{1/V_{E,H}(t) + 1/V_{E,O}(t)} \tag{14}$$

$$FPD_{ave}(t) = \frac{FPD_{E,H}(t)/V_{E,H}(t) + FPD_{E,O}(t)/V_{E,O}(t)}{2/V_{ave}(t)} \tag{15}$$

$V_{E,H}$ and $V_{E,O}$ are the expectation value of ship speed per homeward and outward voyage, respectively. $FPD_{E,H}$ and $FPD_{E,O}$ are the expectation value of fuel oil consumption per homeward and outward voyage, respectively. There four values are calculated by Eqs.(6) and (7). Finally, total fuel oil consumption in lifecycle FOC is given by Eq.(16).

$$FOC = \int_0^{t_E} FPY(t)\, dt \tag{16}$$

$$FPY(t) = FPD_{ave}(t) \cdot Day(t) \cdot OPE_{rate} \tag{17}$$

In Eq.(17), $Day(t)$ means the number of days per year and usually given 365 and 366 on intercalary year. OPE_{rate} indicates the rate of operation per year and OPE_{rate} = 1.0 means a ship runs all year around.

The cape-size bulk carrier is assumed to be put into West Pacific Route between Japan and Australia. The distance on the route is assumed to be 4400NM. The operation rate is set as 100%, which means OPE_{rate} = 1.0. Ship performance such as ship speed and fuel oil consumption in actual seas and occurrence probability distribution on the objected route are taken from *Kuroda and Sugimoto (2021)*.

Lifecycle assessment on fuel oil consumption results in Fig.13 where ship speed in calm seas is given 12.0 kn. V_{ave} and FPD_{ave} express a round trip average of expected values of ship speed and fuel consumption per day, respectively. The expected values are calculated by a superposition of the ship performance in actual seas and occurrence probability distribution on West Pacific Route shown in Fig.12 derived from statistical database of global winds and waves, *Tsujimoto et al. (2018)*. The expected ship speed in Fig.13 is less than 12.0 kn due to the effects of winds and waves and that due to hull surface aging.

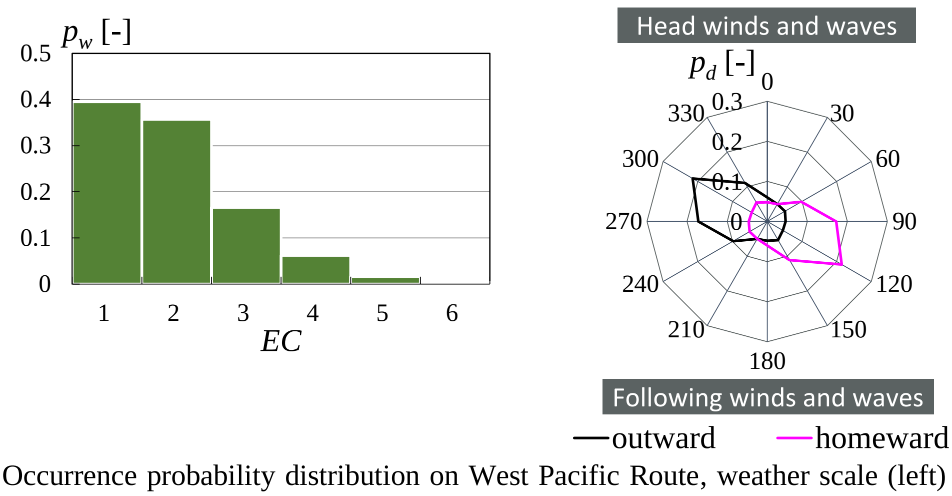

Fig.12: Occurrence probability distribution on West Pacific Route, weather scale (left) and direction (right)

Fig.13 shows that a decrease of V_{ave} and an increase of FPD_{ave} are the largest in the three conditions of fouling deterioration for a hull and have a linear response to the deterioration. Fig.14 indicates the total fuel oil consumption in lifecycle calculated by the integration of FPD_{ave} in Fig.13. At p_{fs} = 6.5% and 11.0%, the total fuel oil consumption is about 8,500 ton and 17,000 ton larger, respectively, than that at p_{fs} = 2.0%. This means that the deterioration due to fouling on a hull has a significant impact on the total fuel oil consumption and implies that efforts should be made for developing high-performance paints which are capable preventing the fouling on a hull.

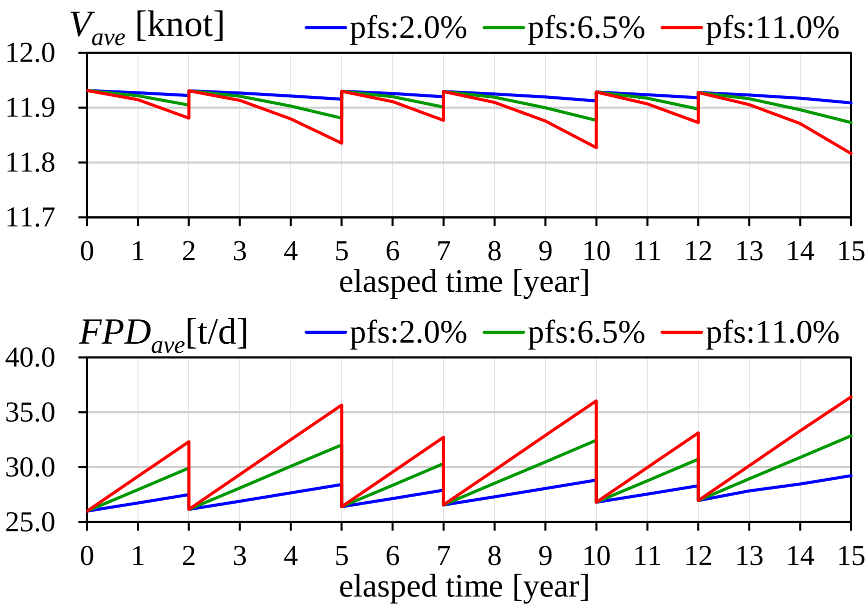

Fig.13: Time variations of expected values (left: ship speed, right: fuel oil consumption per day)

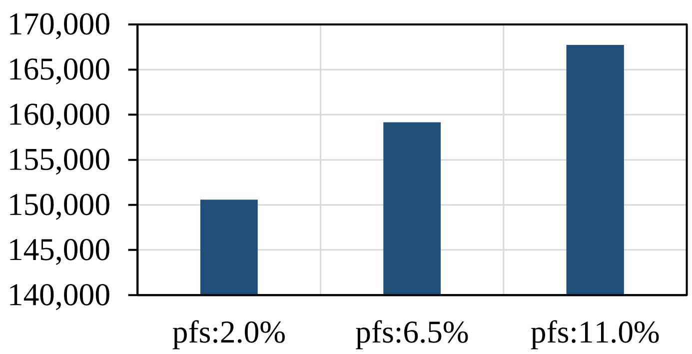

Fig.14: Total fuel oil consumption [t] in lifecycle of the cape-size bulk carrier

4. Concluding remarks

The regulations for protecting marine environments have been strengthened, which requires shipyards to design eco-friendly ships and ship owners to operate with low GHG emission. In 2023, the regulations of energy efficiency existing ship index (EEXI) and carbon intensity indicator (CII) will be entered into force, which increases the needs for monitoring the performance of ships in service. In this respect, the standard monitoring method developed in the OCTARVIA project can be utilized as an effective solution.

For addressing measures to the regulation of EEXI and CII, the prediction method of ship lifecycle performance is necessary. The OCTARVIA project has developed an objective method of lifecycle assessment of fuel oil consumption of a ship in service. This method can take into account not only the effects of winds and waves but also those of fouling and aging for a hull, propeller fouling and aging of engine governor on the fuel oil consumption throughout a ship's life. The lifecycle assessment is required in the stage of ship design or ship operation, which can contribute to GHG reduction from shipping sector.

References

FUJIWARA, T.; UENO, M.; IKEDA, Y. (2006), *Cruising performance of a large passenger ship in heavy sea*, ISOPE2006, San Francisco

HIMENO, Y. (1983), *A study on Frictional Resistance of Painted Rough Surface*, J. Kansai Society of Naval Architects, Vol. 191, pp.11-15. (in Japanese)

KURODA, M.; SUGIMOTO, Y. (2021), *Development of the Evaluation Method for Life Cycle Ship Performance*, J. Japan Society of Naval Architects and Ocean Engineering, Vol. 34, pp.19-28

ITTC (2014), *Prediction of Power Increase in Irregular Waves from Model Test* (RP.7.5.-02-07-02.2), International Tank Test Conference

MIYAMOTO, M. (2007), *Estimation and Evaluation of Ship Performance in Actual Seas* -Review and Evaluation of Fouling, Aging Effect and Sea Condition-, J. Japan Society of Naval Architects and Ocean Engineering, Vol. 6, pp.205-214. (in Japanese)

SAKURADA, A.; SOGIHARA, N.; TSUJIMOTO M. (2020), *Development of a Filtering Method for the Evaluation of Performance in Calm Sea Based on Onboard Monitoring Data*, J. Japan Society of Naval Architects and Ocean Engineering, Vol. 31

SAKURADA, A.; SOGIHARA, N.; TSUJIMOTO, M.; SATO, H. (2021), *Development of resistance criteria method for ship performance evaluation by onboard monitoring data*, Conf. Full Scale Ship Performance, pp.19-26

SCHULTZ, M.P. (2007), *Effects of coating roughness and biofouling on ship resistance and powering*, Biofouling 23, pp.331-341

SOGIHARA, N.; KURODA, M.; SAKURADA, A.; YOKOTA, S.; TSUJIMOTO, M. (2019), *UNITAS: Tool for supporting evaluation of ship performance in actual seas*, Papers of National Maritime Research Institute 19/1, pp.101-122

SOGIHARA, N.; SAKURADA, A.; TSUJIMOTO, M.; SATO, H. (2020), *Validation of the Evaluation Method of Ship Performance Using Onboard Monitoring Data -Development of Resistance Criteria Method with Apparent Slip Ratio and Quality Management-*, 5th Hull Performance & Insight Conference, pp.82-95

SOGIHARA, N.; SAKURADA, A.; TSUJIMOTO, M. (2021), *Validation of Filtering Method for Evaluating Ship Performance in Calm Sea Using Onboard Monitoring Data*, J. Japan Society of Naval Architects and Ocean Engineering, Vol. 33

TSUJIMOTO, M.; SHIBATA, K.; KURODA, M.; TAKAGI, K. (2008), *A Practical Correction Method for Added Resistance in Waves*, J. Japan Society of Naval Architects and Ocean Engineering, Vol. 8.

TSUJIMOTO, M.; KURODA, M.; SOGIHARA, N. (2013), *Development of a calculation method for fuel consumption of ships in actual seas with performance evaluation*, OMAE2013, Nantes

TSUJIMOTO, M.; SOGIHARA, N.; KURODA, M.; SAKURADA, A. (2015), *Development of a ship performance simulator in actual seas*, OMAE2015, Newfoundland

TSUJIMOTO, M.; MATSUZAWA, T.; KUME, K. (2018), *Statistical Characteristics of Global Winds and Waves*, 28th International Offshore and Polar Engineering Conference, pp.379-386

TSUJIMOTO, M.; SOGIHARA, N.; SATO, H.; KUME, K.; ORIHARA, H.; SUGIMOTO, Y.; KURODA, M. (2020), *Development of Performance Evaluation of Ships in Actual Seas*, 5th Hull Performance & Insight Conference, pp.54-63

Uncertainty Quantification and its Effect on Compliance Accuracy for Different Data Collection Methods

Amy Parkes, Arcsilea, Barking/UK, amy@arcsilea.com
Edwin Pang, Arcsilea, Barking/UK, ed@arcsilea.com

Abstract

Data collection and analysis will be required for ships to illustrate compliance to new greenhouse gas regulation coming into effect from 2023. Vessels often have multiple sources of operational data and at different levels of frequency and fidelity but there is a limited understanding of the uncertainties in the data from each collection approach. How these translate into compliance metric uncertainties is also unknown. This paper compares three of the major data collection setups, namely: yearly and voyage reporting; Automatic Identification System (AIS); and any onboard high frequency monitoring. Using data from the same set of 45 bulk carriers, the expected bias and uncertainty are quantified in each approach. Uncertainty is quantified and propagated using skewed distributions which more accurately represents the uncertainty compared to previous studies which use Gaussian distributions. The results show that, for the ships investigated, using a high frequency dataset to calculate carbon intensity metrics results in a bias of 9-14% less than the more manual yearly and voyage data. The uncertainty of which is around 30% - which spans all rating bands for bulk carriers. This clearly illustrates that any claim to provide a sustainability assessment for a vessel based solely off publicly available data such as AIS is likely to contain a level of uncertainty rendering the estimation useless.

1. Introduction

Amendments to MARPOL Annex VI, *IMO (2021a)*, adopted by the 76th session of the International Maritime Organisation (IMO) Maritime Environment Protection Committee will require ships to calculate and report a Carbon Intensity Indicator (CII) value from 2023 onwards, building on the existing requirement to report annual fuel consumption and distance travelled to the IMO Fuel Oil Consumption Database (DCS). The CII value attained by the ship is required to be at or below a required CII, which changes based on vessel type and capacity. The required values are based on quantile regression analysis of attained CII value against ship capacity using data from IMO DCS.

The median quantile regression produces the baseline and approximations of the 15th, 35th, 65th and 85th quantiles produce rating band boundaries to categorise ships from A-E, with C and better the only compliant bands, *IMO (2021b)*. Any ships which report attained CII values in rating bands D for three years or E will be required to submit and implement corrective action plans designed to bring them back into compliance by the following year, essentially allowing around 19 months for changes to be made.

To calculate the attained CII of any given ship the following three values are required: total CO_2 emitted, total distance travelled and vessel capacity which is either the deadweight or the gross tonnage depending on the ship type. The calculation of this metric therefore requires accurate measurement of fuel consumed by the vessel and distance travelled over the time period desired; it is assumed that an accurate value for ship gross tonnage and deadweight are available. The metric to be reported to the IMO is the CII of the ship for an entire year, every year, however calculation of the attained CII for individual routes is desirable to aid a ship owner in decision making to ensure compliance at the end of the year.

Although operational data has been collected onboard ships for many years in the form of noon reports and is increasingly collected at higher frequencies for performance monitoring, this regulation is the first time that operational performance data collected onboard will have regulatory implications for the ship and shipowner. The attained CII of a ship is also expected to be used as part of chartering decisions, and sustainability assessments. Understanding the quality of the data collected onboard is therefore essential for fairness and transparency.

A technical report which discusses the accuracy but not uncertainty of fuel consumption measures, *Faber (2013)*, suggests that an average fuel bias (error) between 3-5% should be expected. However, this reported bias is based on manufacturers quoted instantaneous accuracy for specific sensors and does not provide any guidance on what level bias should be expected for a voyage or a full year. There is an IMO technical report attempting to analyse fuel consumption uncertainty, *Hunsucker (2018)*, which concludes that average fuel bias ranges from 0.33% to 12% depending on the measurement method, and that fuel uncertainty ranges between 1.8-6.5%. However, this report uses Gaussian distributions to model data error, which is inappropriate given the highly skewed nature of fuel consumption measurement differences.

There are more sophisticated approaches to quantifying uncertainties surrounding analysis of onboard ship operations data, *Aldous (2015a,b)*. However, these omit to discuss fuel consumption measurements and distance measurements. There are no known studies which quantify bias or uncertainty of distance measurements onboard a ship. This paper therefore aims to quantify the expected uncertainty of both fuel consumption and distance measurements, using appropriate distributions, and propagate this uncertainty to produce the expected CII uncertainty for different data collection methods.

There are multiple different schools of thought with regards to characterising data error and how this affects model uncertainty. The most common characterisation of data error is the distinction between precise and accurate data. To illustrate these terms, it is common to use the analogy of a dartboard. If data is gathered by taking multiple repeated measurements such as throwing multiple darts at a dartboard, then precision refers to how close or spread out datapoints or darts are, and accuracy refers to how close to the real value or bullseye the darts are. Data with a lack of precision can be thought of as data without repeatability or reproducibility and data with a lack of accuracy can be thought of as data with a systematic error. For data which is accurate but not precise, an increase in data frequency can allow data certainty to be improved. As no systematic error is present the average of the measurements will be the true value, no matter how wide the scatter is. Therefore, more certain lower frequency traces can be derived from imprecise higher frequency traces.

Data error and CII uncertainty are closely related, uncertainty can be thought of as the unexplainable variation inherent in any calculation based on real data. In this context the ‘model’ can be considered the CII framework: the required CII and the CII calculation itself. The combination of data from different sensors with different error profiles and the interaction of these separate error profiles can be quantified as the uncertainty of the attained CII value. Uncertainty is characterised into two groups: epistemic and aleatoric, *Hüllermeier (2021)*, these are often thought of as model uncertainty and data uncertainty respective.

Epistemic (model) uncertainty is uncertainty which is due to factors which could be known but are not known in practice. The primary focus of this paper is the aleatory (data) uncertainty, which is the uncertainty due to factors which affect the data but cannot be known, such as the sensitivities of the flow meters to different pressures or compositions of fluids. In this context ‘cannot be known’ means what cannot be measured sufficiently with current measurement devices, in theory the invention or installation of a sufficient measurement device would turn the aleatory uncertainty to an epistemic one.

This paper takes three different aggregation levels and ways of measuring distance and fuel consumption for 45 bulk carriers. It quantifies the uncertainty surrounding CII calculation dependant on which data acquisition method is used. Finally, these uncertainties are propagated forwards to produce the expected bias and associated uncertainties for the attained CII value of a given ship.

2. Data

Data used in this study is from 45 different bulk carriers of varying size and operating profile. All data is for the year 2019. There are multiple different ways that ship data is measured onboard and then processed, in this paper these methods are grouped based roughly on data frequency, availability and level of human involvement in the process. The groups of data sources are: onboard monitoring, AIS (Automatic Identification System) data, and journey aggregated data which is either reported to the MRV (Monitoring, Reporting and Verification, *EMSA (2019)*, or the DCS (IMO Fuel Oil Consumption Database, *IMO (2016)*. The variables relevant to the CII calculation which are available in each group and the frequency are visualised in

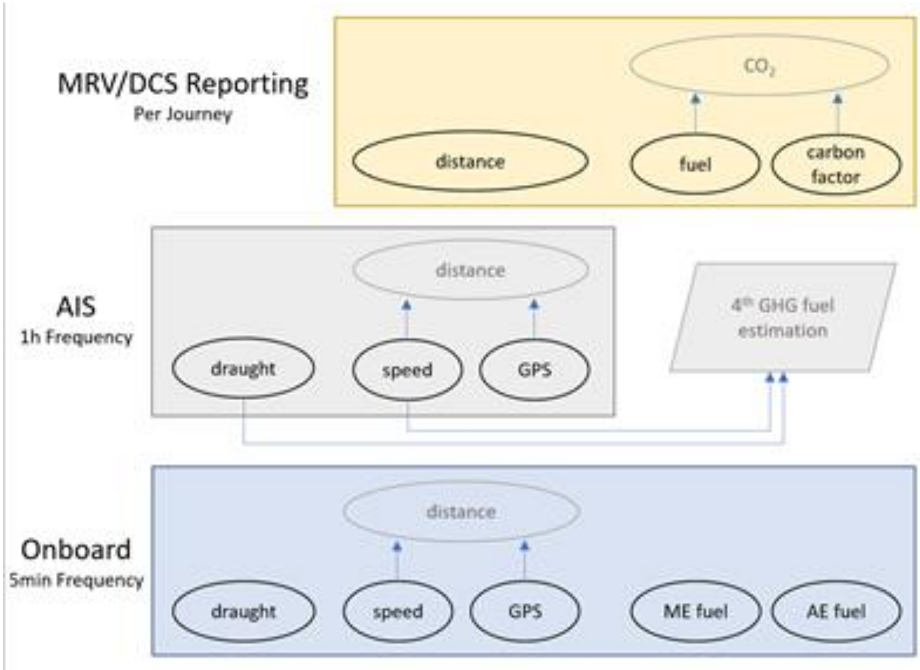

Fig.1: Diagram illustrating the data collection method groupings used in this paper. Black outlined shapes indicated measured variables and grey outlined shapes indicate derived variables

Although a ship owner reports journey-based consumption and distance to the DCS and MRV, the journey granularity is only for verification purposes and the databases themselves only contain the full year attained CII. DCS data is confidential, only the IMO have access to the full dataset which contains the yearly attained CII of all ships which are party to MARPOL. Full year attained CII is also present in the MRV data, which is publicly available, but the MRV data only contains journeys which are within, from or to countries in the European Union.

Multiple other variables, not visualised or discussed, are available in all datasets. However, for conciseness only the speed, location, fuel consumption, and draught variables are analysed in this paper. The speed and location are analysed as they are directly used to derive the distance travelled, the fuel consumption is similarly analysed as it is used to derive the CO_2 and the draught is analysed as it is required to use the 4^{th} GHG fuel estimation method, *IMO (2020)*, for the AIS data. Each dataset available is briefly discussed below.

2.1 Onboard

Data measured onboard the ship at 5-minute frequency using either pre-existing or specially installed sensors. The data is automatically sent to an ‘Vessel Performance Optimisation Platform’ which is available to the ship owners by web browser.

No information regarding:

- the type of sensors;
- sensitivities of sensors;
- the data handling processes;
- whether the datapoints are averaged from a higher frequency or sampled every 5 minutes or
- whether any validation or verification is performed,

is provided by the onboard data management company. It also cannot be assumed that the same type of sensor is used across all ships. All variables are reported to 6 decimal places in the onboard monitoring system.

The following variables from onboard monitoring are analysed in this paper:

- GPS
  - data appears to be pre-smoothed; on analysing times when ships are drifting and so moving less than 1 knot there is no evidence of the normal ‘jittering’ associated with unsmoothed navigational traces, *Gade (2009)*.
- Speed Over Ground
  - it is verified that speed over ground data is measured onboard and not derived from GPS signals.
- Draught
  - data is from a pressure sensor and therefore varies by ~0.25 m during a single voyage.
  - Some voyages show infeasible or highly unlikely draught values; it is suggested the draught sensor has periods of poor calibration.
- Fuel consumption
  - data is from flow meters to the main and auxiliary engines, in the system studied these cannot be attributed to a specific fuel type, so derivation of CO_2 is not possible.
  - In addition, there was no data available for boiler consumption for any of the ships, so all fuel consumption estimates will underestimate the true quantity of fuel consumed by the ship or boiler consumption will need to be added manually.
  - Traces include infeasibly large, infeasibly small or negative values for fuel consumption.

2.2 Automatic Identification System (AIS)

Data is transmitted to AIS receivers at varying frequencies depending on vessel operating mode. The data used for analysis in this paper is provided from an AIS data provider at hourly frequency. This provider does not specify whether datapoints are averaged across all datapoints within the hour, or the point value on the hour. It is clear from investigation of GPS traces, and comparison to the onboard data, that the GPS data is not the ships position on the hour.

- GPS
  - data appears to not be pre-smoothed when compared to the onboard GPS traces.
- Speed Over Ground
  - it is verified that speed over ground data is measured onboard and not derived from GPS signals.
  - Traces include very occasional infeasibly large values, one ship reports a speed over ground of 40 kn for multiple timepoints, when bulk carriers should not be capable of sailing much faster than 15 kn.
- Draught
  - data is suggested to be human input as it does not vary at all through the course of a voyage. A constant draught for the entirety of a voyage is not realistic, as the effect of fuel consumption and any ballast changes are expected to be reflected in the draught.
- Fuel consumption

- is not available from the AIS dataset.
- It is derived using the fuel consumption estimation method detailed in the IMOs 4th Greenhouse Gas Study which is briefly outlined below. The method splits consumption into three parts: main engine, auxiliary engine, and boiler.
- Hourly main engine consumption is calculated in a quasi-fundamental (resistance based) manner where hourly draught and speed are combined with numerous assumed values to calculate the approximated fuel consumption for the hour.
- Hourly auxiliary and boiler consumptions are assumed constant for each of the ship operating modes: at berth, anchored, manoeuvring and at sea.
- These assumed values used throughout the calculation are different for different ship: types, age, and size. They are said to be derived from real consumption data, although no detail of this data is provided in the 4th Greenhouse Gas Study.

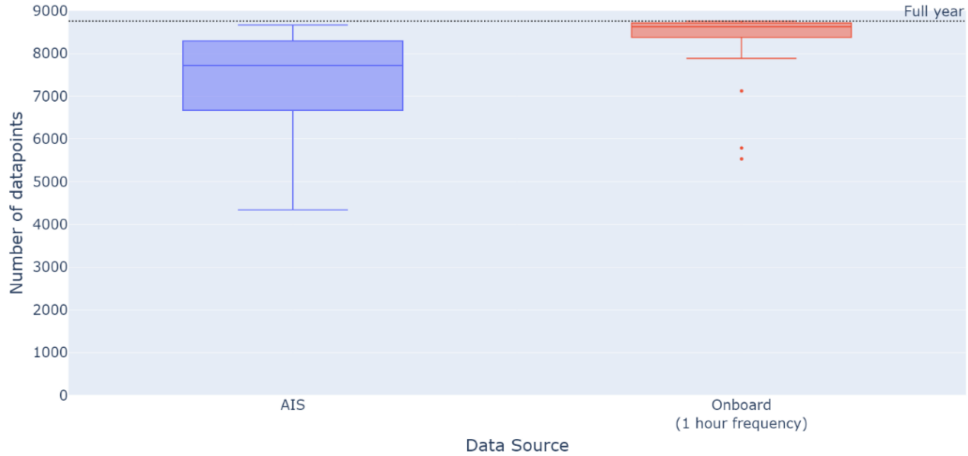

Fig.2: Quantity of hours with data, or number of valid datapoints, in the year for AIS and onboard monitoring for the 45 bulk carriers analysed.

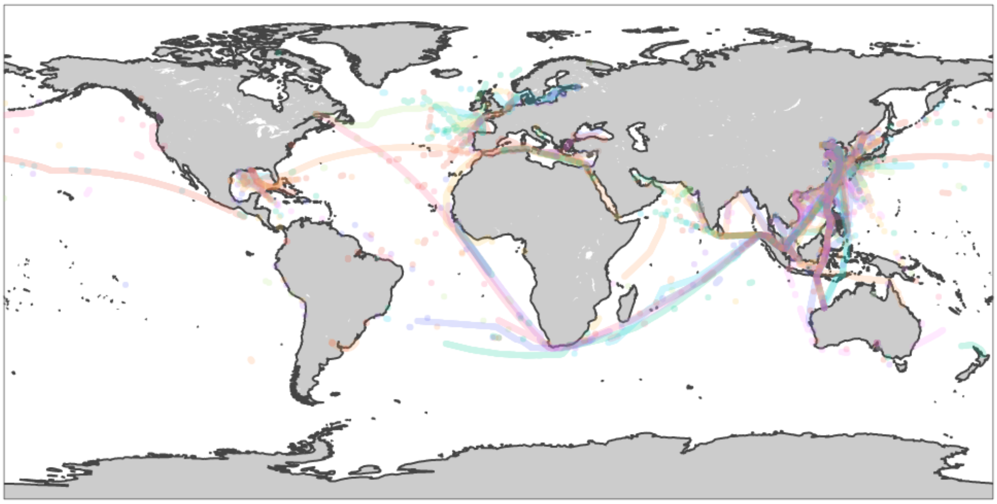

Fig.3: Locations where AIS data is invalid or missing for all 45 ships. A different colour is used for each ship.

There is significantly less coverage of the year from the AIS data compared to the high frequency, as the AIS data contains more invalid or missing points compared to onboard monitoring data when taken at hourly frequencies, Fig.2. For the onboard monitoring data taken at hourly frequencies 34 out of 45 ships analysed have more than 90% coverage compared to AIS data where 34 ships have less than 90% coverage, with one ship only having data for half the year.

The geographic locations where AIS data is invalid or missing are mostly in the East and South China Seas, where congestion is known to interfere with transmission, Fig.3. Also note that from late 2021 a new Chinese law shut down international access to Chinese based AIS stations, therefore AIS data from 2022 onwards not from Chinese sources will be expected to have a larger proportion of invalid datapoints. However, there are also whole cross Atlantic, Pacific and Indian Ocean voyages which are missing, and this loss of multiple multi-week voyages is surprising. It is not clear why the quantity of AIS datapoints are so low in comparison to the onboard monitoring; the AIS provider claimed to provide full AIS data for the year 2019. It is not possible to identify if the missing AIS datapoints were never received by an AIS receiver, or if the AIS provider failed to provide full years to the authors.

2.3 Journey aggregated (MRV and DCS)

For the ships studied, data is aggregated manually per journey to report to the MRV database. This manual step introduces a different type of uncertainty to the onboard and AIS datasets. Human intervention can be beneficial to identify infeasible values but it can also cause more data error are values are not copied across correctly. These errors are also more difficult to identify as they do not follow any reliable rules. If a speed sensor has error between ±0.5 kn the speed value can always be expected to be within 0.5 kn of the true value, whereas if a number is copied across wrong into a new spreadsheet the new value could have any two digits reversed, or additional/missing trailing zeros which could alter the value significantly.

- Distance
  - is calculated using distances from noon reports. This process involves such a large quantity of manual intervention that access to the noon reports themselves for the purpose of this paper was not possible.
- Fuel consumption
  - is calculated using period stock takes, verified by bunker delivery notes for the ships used in this study. These can have inherent errors due to inaccurate flow meters on the bunkering barge, aerated fuel, or an error in the manual processes surrounding the calculation.

There is no consistency in the MRV reporting on whether the fuel for cargo operations are included in the relevant voyage or as a separate entry. This adds another level of uncertainty to the CII calculation for a single journey, as it is impossible to determine from the MRV entry if cargo operations fuel are included.

3. High Frequency Uncertainty Analysis

To quantify the uncertainty of the AIS and onboard monitoring datasets they need to be compared at the same frequency. However, the increased frequency of onboard monitoring data (every 5 minutes) increases its certainty, so sampling the onboard monitoring at 1-hour frequencies would reduce the analysis to sensor and data pipeline comparisons and not provide a true assessment of the data uncertainties. A method is therefore required to include the information from the 11 other datapoints in an hour into the hourly reading for onboard monitoring data.

A standard approach in sensor research is to use a *Kalman (1960)* filter, a recursive Bayesian filter, to smooth raw data streams from a sensor. These are often used to smooth out jumping in GPS signals and is almost certainly used on the onboard monitoring GPS data before it is sent to the online platform to be accessed by the ship owner. In simple terms, a Kalman filter works chronologically along a data trace, making an initial guess of the distribution of numbers a single datapoint could be, then updating its estimation based on the actual datapoint value and finally producing an estimate of the true trace value at this point.

The use of a Kalman filter on the onboard monitoring data before sampling at an hourly frequency ensures that the extra information available because onboard monitoring works at a higher frequency is implicitly included in the hourly samples. The two variables from these datasets required to calculate CII is distance and fuel consumption. Distance can be calculated in two ways from the available variables: from the speed over ground or from the GPS trace. Fuel consumption is measured in the onboard monitoring system but is not available from the AIS data. To perform a full uncertainty analysis between onboard monitoring and AIS data, an approximation of fuel consumption is used for the AIS data, replicating the scenario where only AIS data is available. The fuel consumption is approximated using the IMOs 4th Greenhouse Gas Study method which is based on minimal vessel specifics, draught, speed, and location.

The speed over ground from AIS and onboard monitoring agree well, Fig.4. The violin plots show the distribution of values in two ways: on the right, the mirrored probability distribution shape which is wider where there is more data and narrower where there is less data; and on the left, a scatter plot of datapoints at a constant width. Although the two data sources have almost identical distributions the AIS speed over ground has some values which occur more regularly than others, presenting as horizontal lines on the scatter graph, Fig.4. This is indicative of errors in the AIS data where the speed over ground reading gets 'stuck' and is constant for an infeasible amount of time.

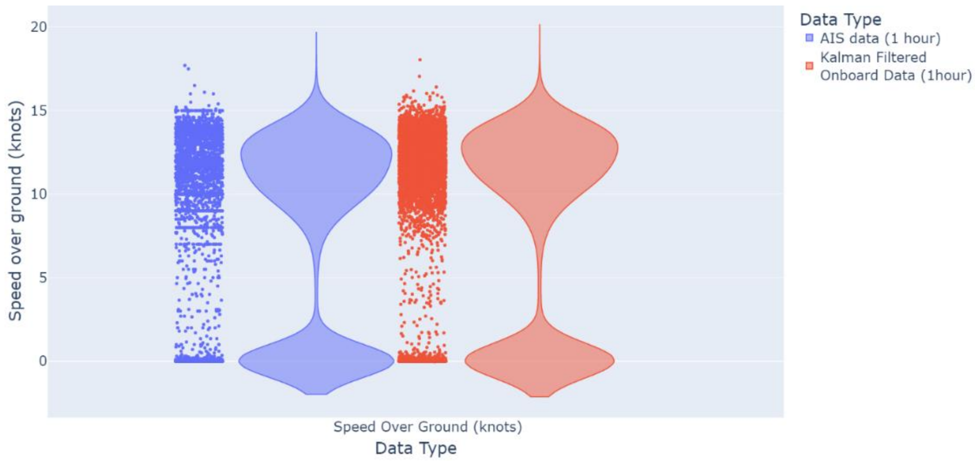

Fig.4: Violin plot showing the distribution of speed over ground from AIS data and the smoothed onboard monitoring data sampled at 1 hour frequency.

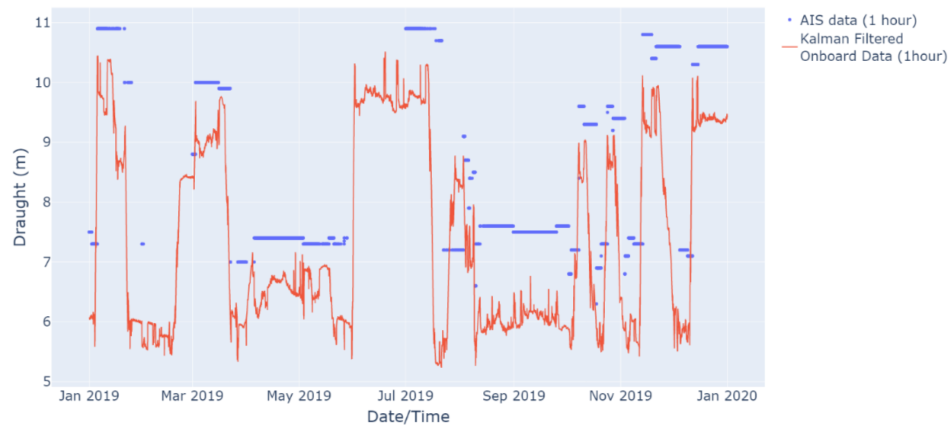

Fig.5: Draught data for one of the 45 bulk carriers for the year 2019 from both AIS and smoothed onboard monitoring data.

A comparison of the draught from AIS and onboard data shows that the AIS draught is on average 1.44m higher than the onboard monitoring draught across all ships. With the 4.76 m the largest average difference and 0.6 m the lowest average distance. The dynamics of the traces are also notably different, Fig.5, with AIS data having little to no variance for the length of a journey. It is suggested this is due to the AIS draught values being manually input at the beginning and end of each voyage which is akin to the measurement having a frequency of once a journey. Whereas the onboard monitoring draught is measured directly from the draught pressure sensor, which shows high variability. It is suggested this variability is the combination of the effect of weather and a sensor which initially over-shoots the draught, automatically recalibrating itself after a couple of hours at sea.

The AIS draught could be considered precise, due to being manually input and consistently feasible. Also, that the onboard monitoring draught could be considered accurate because of the limited human involvement and Kalman filtering allowed by the higher frequency. Hence a data fusion of both traces would improve the certainty of these measurements. However, this fusion is out of scope of the current study.

4. Journey Based Uncertainty Analysis

Although regulation is based on a CII calculation for a full year, understanding of the effect single journeys have on CII is important for a ship owner to optimise operation to improve their ships attained CII. There may be some routes which give particularly bad CII because they include multiple stops or prevailing weather or currents, so the fuel used with no associated distance travelled is much larger in proportion to the fuel consumption for propulsion. It is important for ship owners or operators to understand this so they can distribute the poor CII journeys across a fleet.

A)

B)

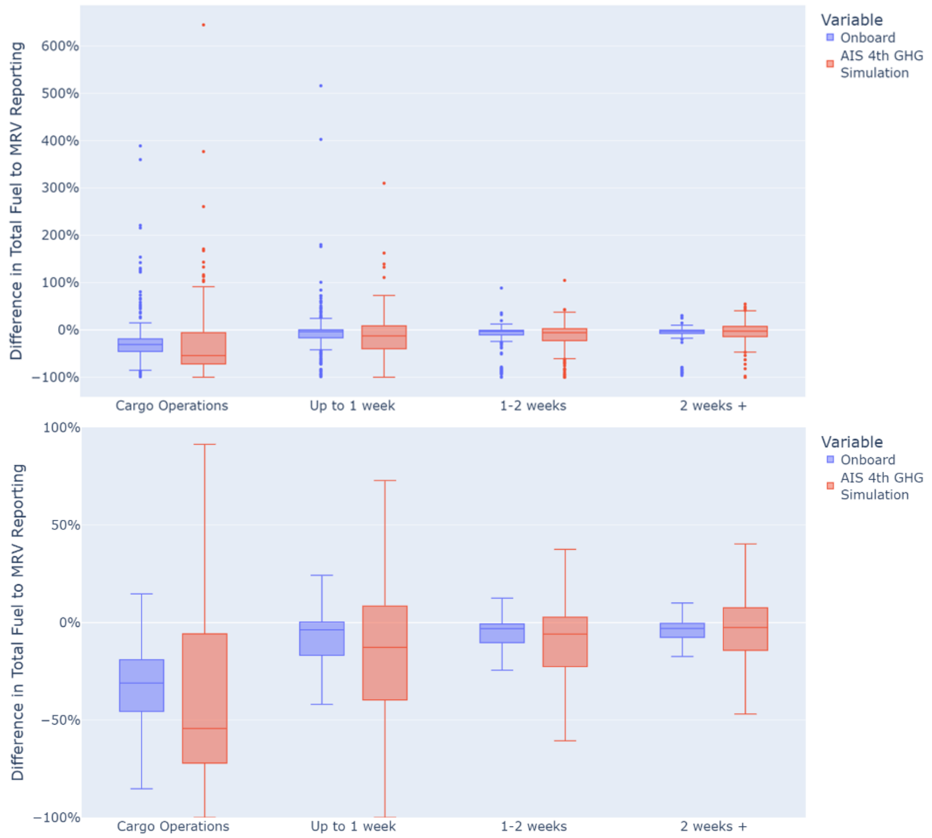

Fig.6: Percentage uncertainty, or percentage difference between MRV and aggregated higher frequency data types of total fuel consumption for different length journeys. Uncertainty can be quantified as the range or distribution of biases. A) Full box plots including outliers and B) zoomed in on the interquartile range of boxplots without outliers visible.

For the remainder of the paper the uncertainty of an AIS or an onboard variable is quantified by analysing the difference between the values found in the journey-based records for MRV/DCS and the value from the AIS or the onboard dataset. The average difference between journey-based and high frequency is called the bias of the high frequency data and the variability of this difference is called the uncertainty. The journey-based reporting is chosen as the baseline in this study as the characteristics of it differ greatly to the higher frequency data types, therefore comparison of AIS to onboard directly is more meaningful, it has also been verified by an independent verifier as part of the reporting.

This section takes all journeys in the MRV/DCS dataset for all 45 ships and separates them into 3 different journey types: cargo operation, voyages under 1 week, voyages between 1-2 weeks and voyages over 2 weeks. The cargo operation ‘journeys’ are the entries in the database which refer only to fuel used in a cargo operation or port stays and not to any associated voyage, as discussed previously for some voyages the fuel consumed in and around port is included but for others it is not. This will increase the uncertainty of fuel consumption for all journeys as there is no way to determine which voyages do or not include fuel from a cargo operation.

There is a clear trend in uncertainty (or range of bias) based on length of journey, Figs. 6 and 7, where longer voyages have less uncertainty and short journeys and the entries for cargo operation only have larger uncertainties. The bias of fuel consumed for all journey types are negative, Fig.6, meaning both AIS data with fuel consumption approximated with the 4th GHG method and onboard monitoring of fuel consumption underestimate the fuel consumed for a given journey. For the onboard monitoring, this underestimation was expected, as there is no consumption data for the boiler.

The 4th GHG simulation however explicitly includes boiler consumption which is on average 36% of the total simulated consumption for cargo operations, 9% for journeys under 1 week, 4% for journeys between 1 and 2 weeks, and 3% for journeys over 2 weeks in length. Over all MRV entries, this is an average of 15%. Since the 4th GHG fuel simulation underestimates the fuel consumed significantly, these percentages are presented purely to contextualise the lack of boiler consumption, and will not be used in this study in an attempt to replace the lack of boiler consumption data for the onboard monitoring data.

The fuel bias for AIS is larger than the bias for onboard monitoring for all journey types apart from journeys over 2 weeks where the biases are inline, Fig.6. However, for all journey types the uncertainty of AIS fuel consumption is over 3 times the level of uncertainty than that of the onboard monitoring. This is probably due to the fuel approximation, and that the 4th GHG fuel consumption approximation may not be reliable enough to be used for single journey analysis of attained CII.

There are two different ways to calculate the distance travelled from each data type: based on GPS and based on speed over ground, in theory these methods should produce identical results as speed over ground is derived from the GPS trace. However, for short journeys there is a notable difference in distance travelled between speed over ground and GPS. All ways of approximating distance travelled, apart from the AIS speed over ground, overestimate the distance travelled on any given route. All four approaches produce very similar bias and uncertainty values, with the AIS speed over ground having marginally larger uncertainty than the other three, Fig.7. There is also a similar trend for the uncertainty of all methods for differing length journeys, that the shortest journeys have the largest uncertainty. The similarity in uncertainty for all four distance measures suggests that the journey-based MRV/DCS distance reporting is likely to be inaccurate, especially for the voyages lasting less than a week.

Both fuel consumption and distance have skewed distributions of the difference between journey-based and high frequency. This is most apparent in Figs.6A and 7A where the outliers, the datapoints in the top and bottom 5th percentile, form the large upwards tails of the distributions. This means that the mean and standard deviation (the standard way to summarise the uncertainty or the distribution of biases) will not give a good description of the distribution. To accurately capture the skewness a separate measure of upwards and downwards spread is needed.

The approach taken in this study is to use the median bias as the expected bias and calculate the standard deviation of the upwards and downwards tails as if they were different normal distributions, explicitly mirroring each distribution which forces it to be normally distributed. To propagate the uncertainty from the fuel consumption and distance into the uncertainty for the attained CII, the upwards and downwards uncertainties need to be propagated separately. Due to the CII formula containing a quotient the upwards uncertainty of attained CII is the sum in quadrature, *Palmer (2003)*, of the upwards uncertainty of fuel and the downwards uncertainty of distance.

A)

B)

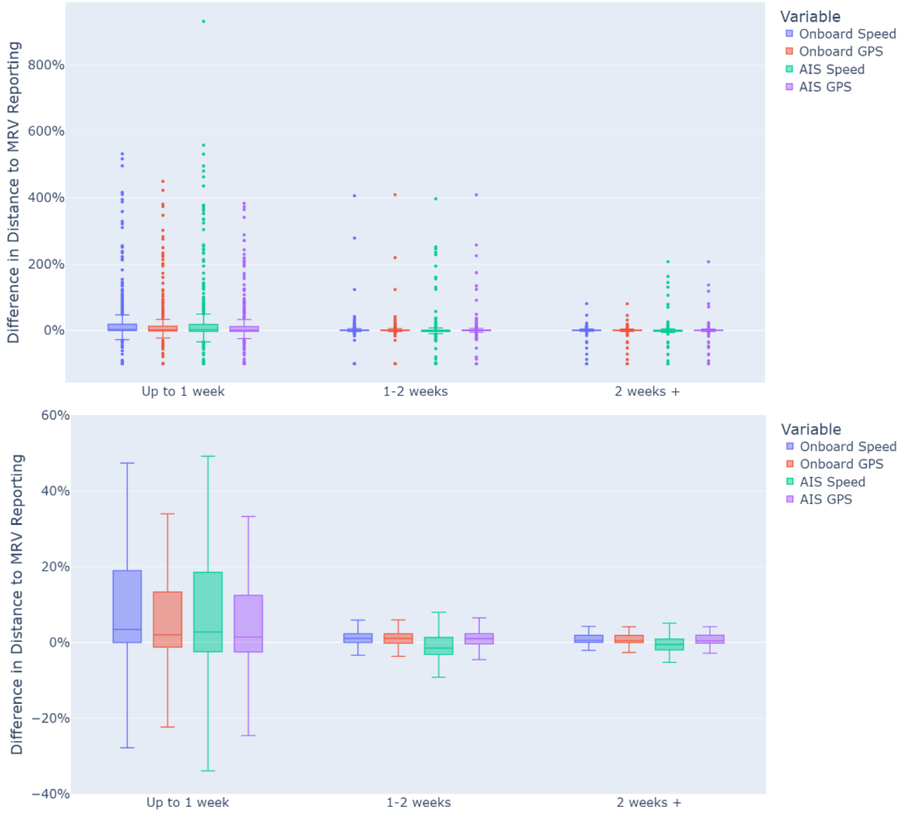

Fig.7: Percentage bias, or percentage difference between MRV and aggregated higher frequency data types of total distance travelled for different length journeys. Uncertainty can be quantified as the range or distribution of biases. A) Full box plots including outliers and B) zoomed in on the interquartile range of boxplots without outliers visible.

No fusion of data types is performed for the propagation, it is assumed that the uncertainty for a single data type is most of interest due to availability of onboard monitoring data. For both AIS and onboard monitoring the distance used in the propagation is the GPS derived distance as these distances have slightly lower uncertainties than the speed over ground derived distances. The propagated expected bias in attained CII is all negative, meaning the high frequency approximations of CII underestimate compared to the journey-based data, Table I. For the shorter journeys, this bias is as high as 14% underestimate, reducing to underestimates of around 3% for the journeys lasting over 2 weeks.

Table I: Quantified uncertainty for the attained CII of a single voyage

Journey Type	Data Type	Average bias (percent under estimated)	+ Uncertainty (standard deviation of upwards bias)	- Uncertainty (standard deviation of downwards bias)
Up to 1 week	Onboard	6.4%	55.2%	105.8%
Up to 1 week	AIS	14.1%	54.6%	105.8%
1-2 weeks	Onboard	4.2%	17.5%	50.7%
1-2 weeks	AIS	6.9%	28.6%	50.7%
2 weeks +	Onboard	3.5%	12.2%	40.4%
2 weeks +	AIS	2.9%	31.4%	43.4%

Uncertainty for CII attained in a single journey is as high as 161%, with upwards uncertainty of 105.8% and downwards uncertainty of 55.2%, this again reduces to 52.6% for the longest journeys. For every journey type apart from over 2 weeks the AIS with IMO simulated fuel produces more biased CII approximations than the onboard monitoring. As well as this the AIS uncertainties are the same as or larger than the onboard monitoring uncertainties.

5. Yearly Reporting Uncertainty

When aggregating to the full year, all approximations of total distance travelled converge to the same distribution which has an expected bias of overestimating by 2.5% with upwards uncertainty of 7% and downwards uncertainty of 4.5%. On aggregating the full year total fuel consumption there is a notable increase in accuracy, or decrease in bias, and decrease in uncertainty for the onboard monitoring data compared to the AIS, Fig.8.

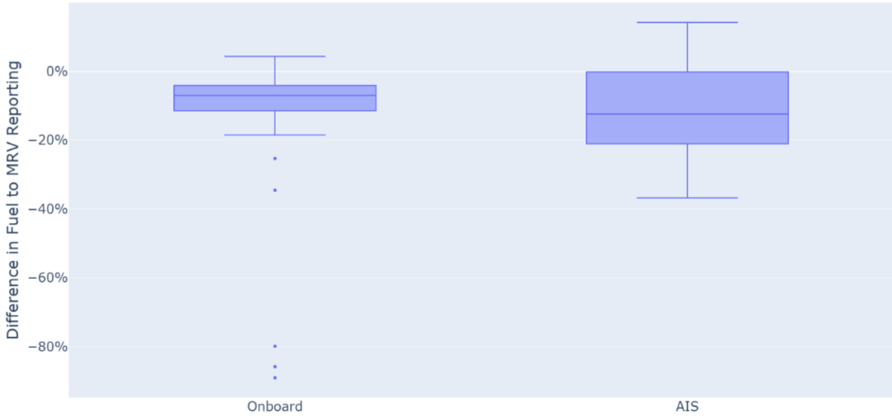

Fig.8: Percentage bias between MRV and aggregated higher frequency data of fuel consumption for the full year. Uncertainty can be quantified as the range or distribution of biases.

When the uncertainty is propagated forwards to produce the uncertainty of the attained yearly CII the bias increases compared to that of the longer journeys, but the uncertainty decreases notably, Table II. On average the onboard monitoring approximation of CII underestimates by 9%, with a upwards uncertainty of 6% therefore there is minimal chance that the onboard monitoring will overestimate the CII. The onboard monitoring has a skewed distribution, as downward uncertainty is 30%.

Contrastingly, the AIS approximation of attained CII has no skew at all and is a normal distribution. The expected bias is a 14% underestimate of fuel consumption, with upwards and downwards uncertainty of 15%, which also means that it is highly unlikely that the AIS approximation will ever overestimate the attained CII.

Note that the onboard monitoring data does not include boiler consumption, and that the 4th GHG fuel consumption estimation method suggests this should comprise around 15% of the total fuel consumed for the 2019 data. Thus if boiler consumption was available, the onboard monitoring AER bias may be reversed from underestimating to overestimating and reduced from 9% to 4%.

6. Contextualise Uncertainty

There are multiple companies claiming to provide CII estimations for ships based purely on publicly available data – namely AIS and MRV - for benchmarking or Environmental, Social and Governance (ESG) purposes, *Wood Mackenzie (2021), Climate Trace (2021).* The CII estimations are either sold as part of ESG analysis products, *Scope Group (2021)* or used as the foundation of white papers, *Wärtsilä (2022)*. This section briefly contextualises the bias and uncertainty of these estimations compared to the percentage distances between rating bounds, Table III. The publicly available MRV data is aggregated yearly and only concerns journeys within, from or to countries in the European Union. Since there is no way to quantify fuel burnt outside of the EU, attained CII in the MRV database has little meaning from a compliance perspective. The uncertainty associated with using AIS data to estimate yearly CII has been quantified in previous sections of this study.

The expected attained CII using only AIS data would have a bias of underestimating by 14% and therefore erroneously put the ship 2 rating bands better (from C to A) than the DCS with an uncertainty of nearly the entire range from A-E. As the rating bands from A-E were designed to hold 15%, 20%, 30%, 20% and 15% percent of the fleet respectively, a CII estimate with an uncertainty of 36% means that over 70% of ships could be misclassified by more than one rating band.

Onboard monitoring is not an automatic panacea, as the expected attained CII from onboard monitoring data would erroneously put the ship a rating band better than it should be, with an uncertainty larger than the entire span from A-E bands. Ships at the extreme ends of categories A or E are more likely to be classified 'correctly' - or in the same way as the DCS - but with uncertainty levels as large as the rating bound span, very little can be concluded from any estimation.

As there is no way to confirm the specific source of the uncertainty quantified in this study it is hard to propose methods to reduce uncertainty. However, based on an understanding of the data collection and processing for the bulk carriers used in this study, the authors suggest the following: routine sensor calibration; internal sense checking to remove infeasible values from high frequency sensors and coverage estimation to quantify what proportion of a voyage has valid data. As well as more targeted triangulation, for example using a flow meter for fine grained fuel consumption, comparing these values weekly to tank dips, to identify when the flow meters fall out of calibration, and then comparing to bunker delivery notes for fully validated fuel consumption.

Essentially, high frequency data has the potential to be very useful for improving ship operations for compliance and efficiency purposes. But it cannot be blindly relied on and requires significant and continuous validation to reduce its uncertainty. It is also suggested that further research should be performed into data fusion methods to reduce uncertainty, as often multiple sources of data are available for the CII calculation.

8. Conclusion

To conclude there is increasing pressure to calculate accurate compliance metrics such as attained CII and there are multiple sources of data which could be used for this calculation. This study quantifies the levels of uncertainty of the attained CII calculated from each data collection method, by comparing two high frequency methods: onboard monitoring and AIS, to the journey-based reporting for MRV/DCS. Both data collection methods underestimate the CII compared to MRV/DCS by around 10%, with an uncertainty range the size of all rating bands combined. Therefore any CII estimation based on AIS or onboard monitoring alone is unlikely to be representative of the value reported to the MRV or DCS.

References

ALDOUS, L. (2015a), *Ship Operational Efficiency: Performance Models*, PhD thesis, University College London

ALDOUS, L. (2015b), *Uncertainty analysis in ship performance monitoring*, Ocean Engineering

CLIMATE TRACE (2021), *Transport: Shipping Emissions Methodology*, https://drive.google.com/file/d/1ZBdyKfjNEYTHPTg7xviUkGCM_ppysP9A/view

EMSA (2019), *THETIS-MRV*, https://mrv.emsa.europa.eu/#public/eumrv

FABER, J.N. (2013), *Monitoring of bunker fuel consumption*, CE Delft

GADE, K. (2009), *Introduction to Inertial Navigation and Kalman Filtering*, Tutorial for IAIN World Congress, Stockholm

HÜLLERMEIER, E.W. (2021), *Aleatoric and epistemic uncertainty in machine learning*, Machine Learning

HUNSUCKER, T.J. (2018), *Uncertainty Analysis of Methods Used to Measure Ship Fuel Consumption*, Shipwright LLC, https://wwwcdn.imo.org/localresources/en/OurWork/Environment/Documents/Uncertainty_Analysis_in_Ship_Fuel_Oil_Consumption.pdf

IMO (2016), *Data collection system for fuel oil consumption of ships*, Amendments to MARPOL Annex VI, Resolution MEPC.278(70), IMO, London

IMO (2020), *Fourth IMO GHG Study*, IMO, London

IMO (2021a), *Guidelines on the Reference Lines for use with Operational Carbon Intensity Indicators (CII Reference Lines Guidelines, G2)*, MARPOL Annex V-Resolution MEPC.337(76), IMO, London

IMO (2021b). *Guidelines on the Operation Carbon Intensity Rating of Ships (CII Ratings Guidelines, G4)*, MARPOL Annex VI-Resolution MEPC.339(76), IMO, London

KALMAN, R.E. (1960), *A New Approach to Linear Filtering*, Trans. ASME

PALMER, M. (2003), *Propagation of Uncertainty through Mathematical Operations*, Massachusetts Institute of Technology Module Program for Fluid Mechanics

SCOPE GROUP (2021), *Scope launches Ship Review: 70,000 ESG ship-assessments, 40,000 CII Ratings*, https://scopegroup.com/media-centre/Scope-launches-Ship-Review--70-000-ESG-ship-assessments--40-000-CII-Ratings

WÄRTSILÄ (2022), *Is the global fleet ready for CII?*, https://www.wartsila.com/insights/whitepaper/is-the-global-fleet-ready-for-cii

WOOD MACKENZIE (2021), *Why Fishtail trusts Vesseltracker to power its sustainable finance platform for suppliers and traders*, https://www.woodmac.com/news/editorial/why-fishtail-trusts-vesseltracker-to-power-its-sustainable-finance-platform-for-suppliers-and-traders/

Performance Analysis of a Gas Carrier using Continual Learning in a Data Stream Context

Malte Mittendorf, Technical University of Denmark, Lyngby/Denmark, mamit@mek.dtu.dk
Ulrik D. Nielsen, Technical University of Denmark, Lyngby/Denmark, udn@mek.dtu.dk
Harry B. Bingham, Technical University of Denmark, Lyngby/Denmark, hbb@mek.dtu.dk
Ditte Gundermann, Hempel, Lyngby/Denmark, digu@hempel.com
Daniel Schmode, Wärtsilä Voyage, Hamburg/Germany, daniel@schmode.eu
Cedric Deymier, Wärtsilä Voyage, Paris/France, cedric.deymier@wartsila.com

Abstract

In the present study, model drift – mostly driven by biofouling – is mitigated by applying continual learning and the hydrodynamic performance of a large LNG tanker trading in worldwide service is assessed in parallel. The available auto-logged sensor data spans five years including two dry docking intervals. An adaptive training methodology of an artificial neural network is established, and the drift score is derived from simulated data under sea trial conditions. In addition, hindcast metocean data from ERA5 is included in the model's feature space for capturing environmental conditions. Crucially, it was found that the obtained drift estimate is in general accordance to ISO 19030 results, proving the method's validity. Still, the methodology itself is subject to considerable uncertainty. Finally, limitations and possible extensions of the proposed methodology are presented.

1. Introduction

Although shipping is considered as the most efficient transport mode; it is still predominantly dependent on fossil fuels and contributes ~3% of global CO_2 emissions raising societal, environmental and economic issues, *IMO (2014)*. Minimizing fuel consumption is directly linked to the reduction of the associated environmental and economic cost of ship operation. For this reason, monitoring the state of the ship's hull and propellers is an imperative throughout its life cycle. One key aspect of performance monitoring is the estimation of the prevalent degree of biofouling and scheduling maintenance accordingly. For detailed information pertaining to in-service ship performance and hull/propeller fouling, see *Carlton (2018).*

Traditionally, in-situ ship performance is analysed using (semi-)empirical expressions and/or experimental data. Decomposing the measured shaft power into subcomponents is still considered as the default method in this domain and builds upon superposition, i.e. the assumption of *linearity*. For reference, the contributions from *Hansen (2011)* and *Nielsen et al. (2019)* rely on empirical estimates of the individual resistance components. However, decomposing the ship resistance only facilitates human understanding and preliminary design calculations according to *Bertram (2012)*. In fact, a ship in a natural seaway is a complex non-linear system and several resistance/propulsive components are highly interrelated, i.e. superposition is not strictly valid in theory. Furthermore, the uncertainty of the employed estimation methods is mostly unknown and disregarded in spite of its magnitude, which is visualized by *Mittendorf et al. (2022c)* in the case of added resistance. On the other hand, significant practical expertise has been acquired over the years employing decomposition methodologies for hull performance analysis and empirical corrections are frequently applied. Nonetheless, a machine learning-based approach without any assumptions or biases is applied in the present contribution. Machine learning techniques are widely adopted in the realm of overall ship hydrodynamics, e.g. *Mittendorf and Papanikolaou (2021)*. In addition, data-driven models are increasingly deployed as digital representations in the field of ship performance monitoring as well. *Petersen et al. (2012)* and *Coraddu et al. (2019)*, for instance, apply neural networks to high frequency data, whereas *Pedersen and Larsen (2009)* as well as *Laurie et al. (2021)* employ noon report data for machine learning-based performance monitoring. From the presented literature, it stands out that, artificial neural networks are most frequently used, which may be attributed to their high generalization capability and versatility.

Still, the majority of state-of-the-art publications violate vital assumptions of machine learning: The samples have to be independent and identically distributed (i.i.d.) and stationary when using gradient-based optimization techniques for training. Broadly speaking, it is assumed that the underlying data generating process remains invariant throughout time. In reality, however, in-situ ship sensor data is subject to concept drift and subsequently *not* time-invariant. Concept drift refers to the scenario, in which the same set of features (or inputs) lead to different labels (or outputs) in different time instances. The phenomenon of concept drift results from sensor drift and predominantly from hull deterioration, which may be impermanent or permanent. Therefore, *quantification* of concept drift is the overarching goal and novelty of the present paper. In addition, the application of continual learning for mitigating model drift allows the consideration of a data stream, i.e. adding new sensor data continuously, which reflects another novelty. Hence, the focus of the present contribution is the application of continual learning in the ship performance monitoring domain for providing a drift score, which is a proxy variable for hull and propeller biofouling. We propose an end-to-end-learning approach using an artificial neural network trained on auto-logged data as well as metocean hindcast data obtained from ERA5, which is part of the Copernicus EU project, *Copernicus (2021)*. Additionally, the developed model will be compared to the de-facto industry standard ISO 19030 for performance analysis, similar to the work of *Coraddu et al. (2019)*. As a demarcation, it is stressed that no distinction between hull and propeller fouling is made in this work, but an aggregated score is provided. A discussion on whether the decomposition of hull and propeller performance is sensible and/or even feasible, is beyond the scope of this contribution.

2. Fundamentals of continual learning

In common practice, e.g. in IoT (Internet of Things) applications, the dataset is generally not fixed, but samples are continuously acquired in a sequential data stream. In theory, a data stream is considered as a potentially infinite sequence $Z = (z_1, \dots, z_t)$ of tuples $z_t = \{x_i, y_i\}$. It is noted that t represents the timestamp and y_i is the label for a given feature vector x_i. Mathematically speaking, if a joint distribution changes with t, this phenomenon is considered as concept drift, i.e. $\exists x: P_{t0}(x,y) \neq P_{t1}(x,y)$, referring to *Losing et al. (2018).* Concept drift may have different types, namely incremental or abrupt drift rates. Interestingly, both are observed in hull performance analysis: An incremental concept drift is a result of biofouling and an abrupt one is due to hull or propeller cleaning. However, fouling might lead to abrupt changes in performance as well due to idle periods. Sensor drift and calibration may also lead to incremental and abrupt concept drift, respectively. Ultimately, concept drift leads to model drift, i.e. decay in accuracy over time.

According to *Jaworski et al. (2020)* concept drift may be detected in a univariate case using, e.g. the Kolmogorov Smirnov windowing approach or a Boltzmann machine. In doing so, it is investigated, whether the data distribution remains the same over time. However, in ship performance monitoring, we are facing a multivariate problem, i.e. speed through water depends on a multitude of predictors, such as engine power or draft. Moreover, fouling is a latent variable, i.e. not measurable, and is expressed herein using a proxy variable, which quantifies the change within a data-driven representation of the ship, e.g. a state space model or neural network. The underlying idea draws inspiration from *Antola et al. (2017)*, where they propose a state space model for sensor fusion of noon reports and auto-logged data. The method was extended and applied in a performance monitoring context in *Schmode and Antola (2020)*. As a side note, Wärtsilä Voyage implemented their so-called virtual fuel flow meter in the Fleet Operations Solution software suite.

Artificial neural networks are considered as composite functions and rely on two basic building blocks: The weight matrix and activation functions. The combination of affine functions, i.e. matrix operations followed by a non-linear activation function, lead finally to the universal approximation theorem. For mathematical intricacies of deep learning, i.e. ANN with more than one hidden layer, see *Goodfellow et al. (2016)*. In comparison to traditional machine learning, deep learning is characterized by increased versatility and scalability, which comes at the cost of increased computational effort. In theory, deep learning is optimized for static, large-scale datasets, i.e. for learning in stationary and self-contained environments. Additionally, gradient-based optimization, which is applied for parameter updating during training, assumes the dataset as balanced or independent and identically distributed (i.i.d.). In reality, however, these assumptions are rarely met in real data and the increasing demand of machine learning in industrial and practical applications requires adaptive and robust methodologies. The concept of continual learning is mimicking human abilities to continually acquire and transfer knowledge and skills throughout their lifespan. In case of neural networks, this is achieved in applying transfer learning repetitively, i.e. retraining a pre-trained model on newly obtained data after certain time intervals. For more elaborate details of continual learning using neural networks, cf. *Parisi et al. (2019)*. The occurrence of catastrophic forgetting (or interference) is the main concern when applying continual learning. The phenomenon describes that a model, which is trained continually, unlearns patterns of prior training instances. Reasons for catastrophic forgetting and several mitigation strategies are provided in *Ramasesh et al. (2021)*. In short, they observed that the higher layers suffer most from the associated decay in accuracy and that parameter freezing is a simple, yet effective way of minimizing catastrophic forgetting. In turn, freezing the upper layers may lead to reduced robustness indicating the so-called plasticity-stability-dilemma. The model will be trained batch-wise and not incrementally for minimizing catastrophic forgetting as well as computational effort. The utilization of advanced measures for minimizing catastrophic forgetting, such as elastic weight consolidation, are an important aspect of future work.

3. Methodology

Herein, a large gas carrier is taken as the case study and its GPS position history between May 2015 and July 2020 is presented in Fig.1, in which it is observed that the ship is in worldwide operation. The data comprises of two dry docking intervals and it is assumed that propeller polishing is conducted on a fixed schedule, but there is no additional information about other cleaning events.

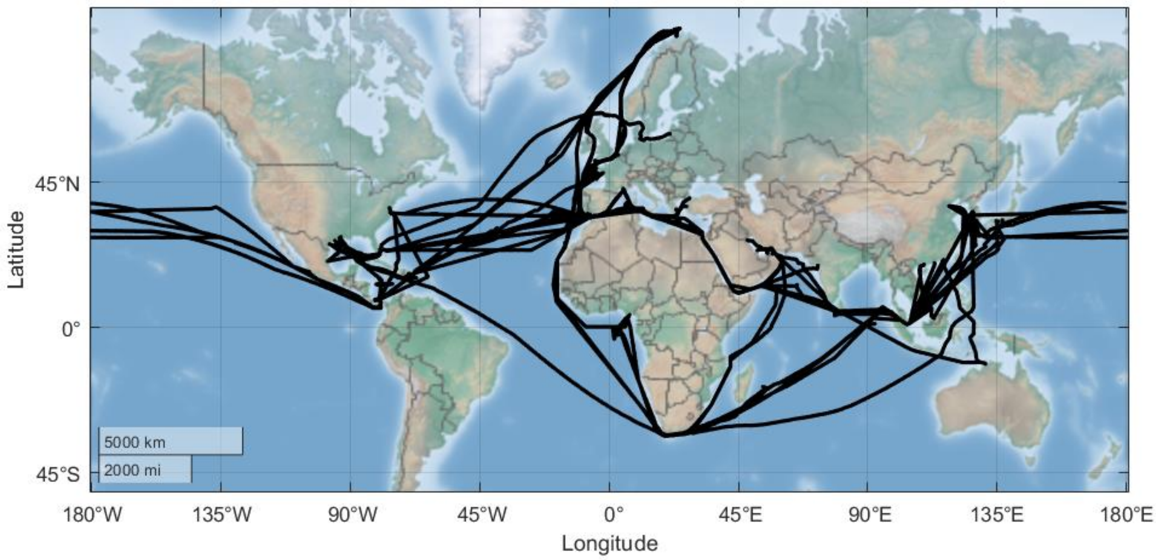

Fig.1: GPS position history of the LNG carrier in 5 years according to AIS data

The world map in Fig.1 conveys a spatially widespread operational area, but it appears that the vessel sails predominantly in regions with relatively high water temperature and sun exposure, i.e. with a higher biofouling potential. In contrast, the histogram of the mean draft T_m indicates a rather discrete profile, which is typical of tankers (cf. Fig.2). It can be seen that the ballast draft is at T/T_{max}=0.75 and the laden draft is at T/T_{max}=0.9. Obviously, the actual measurement samples are arranged around the two conditions in a stochastic manner. As can also be inferred from Fig.2, the non-dimensional speed *Fn* distribution is skewed towards higher values and indicates notable influence of wave resistance to the total hull resistance.

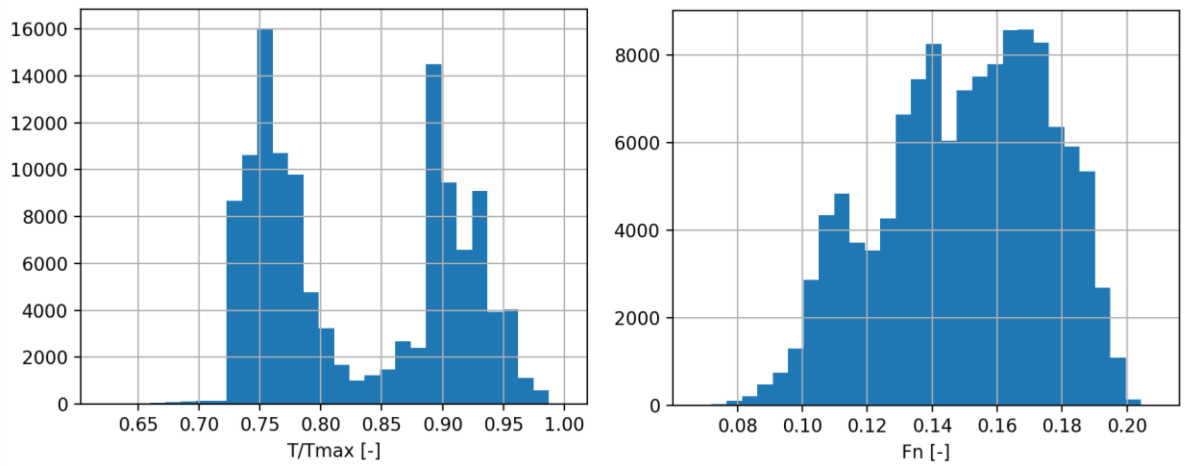

Fig.2: Histogram of relative draft T/T_{max} and Froude number *Fn* taken from the filtered dataset.

The speed-power-relationship of a vessel is heavily influenced by the presence of waves. The involuntary speed loss or added power results from the second order force of the added-wave resistance. *Mittendorf et al. (2022a)* provide a study about machine learning methods for the prediction of the associated quadratic transfer function using data derived from potential flow theory calculations. In the present study, however, the added resistance is considered indirectly and will be inferred by the model using the significant wave height H_S of combined wind and swell waves obtained from ERA5, *Hersbach et al. (2018)*. The metocean data is retrieved in an hourly interval according to the GPS position history of the vessel, cf. Fig.1. Subsequently, the hindcast data is upsampled by linear interpolation in order to match the 10-minute frequency of the remaining dataset. Due to the worldwide service of the case study, the comparison of the empirical data to global wave climate statistics seems worthwhile. The reference long-term statistics were obtained from British Maritime Technology (BMT) as provided in *DNV GL (2018)*. In Fig.3, the joint distributions of the significant wave height H_S and zero-upcrossing period T_Z are compared. It is noted that the left plot is an overlay of scatter, kernel density and two-dimensional histogram plots for showing the overall data distribution and potential outliers in parallel.

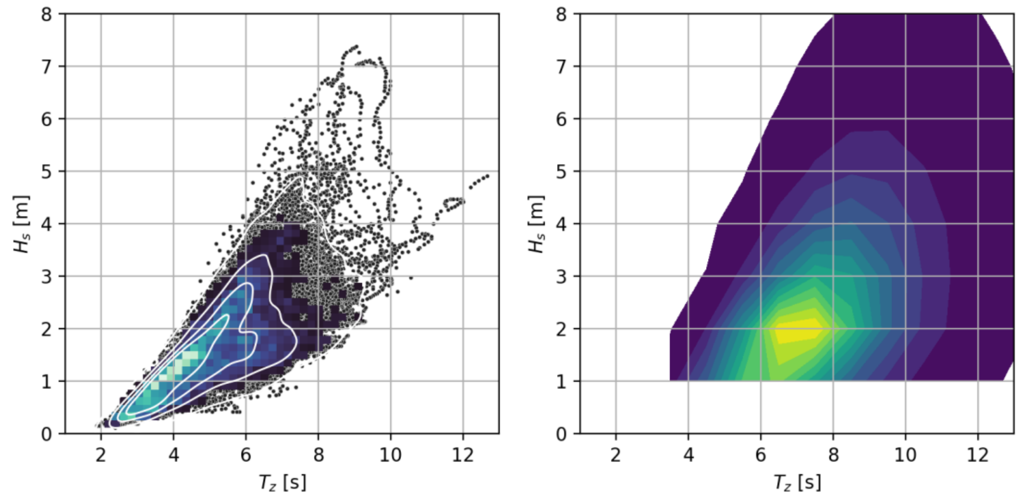

Fig.3: Joint distributions of H_S and T_Z obtained for the case ship from ERA5 (left) and worldwide long-term statistics from BMT as presented in *DNV GL (2018)* (right).

Initially, the effect of weather routing and seamanship is appreciated as the empirical distribution (left) is skewed towards much lower values in comparison to the theoretical one (right). Hence, the conclusions drawn in *Nielsen and Ikonomakis (2021)* are found in this case as well. However, it is stressed that both joint distributions have been acquired using different methodologies and thus have different sources and magnitudes of uncertainty. As it can be inferred from Fig.3, there is substantial epistemic or systematic uncertainty for H_S<1m, i.e. no available data, in case of the long-term statistics. Interestingly, outlier samples in the empirical distribution obtained in higher sea states have a seemingly coherent character and it is assumed that they have been acquired sequentially in both time and space.

3.1. Preprocessing and filtering

The initial dataset has a sample size of approximately 10^7, but the data is resampled from 0.07 Hz sample frequency to 10-minute intervals by window wise averaging. In addition, erroneous and instationary samples are disregarded by a rigorous filtering methodology as explained in the following. Initially, samples where *STW* and *SOG* are below 5 knots are dropped, as it is thought that this speed regime is mostly characterized by manoeuvering. Additionally, shallow water cases were filtered by dismissing samples with a depth Froude number $Fn_H > 0.5$. Conversely, the Froude number of depth could have been part of the feature space, in order to train the model on shallow water effects. Furthermore, samples with unavailable sea state data from ERA5 where filtered. In this contribution, only steady state conditions are considered as the used multilayer perceptron has no spatial invariance, i.e. treats each time step individually and not as coherent. For extracting steady state samples, *Hansen (2011)* applies the CUMSUM filter. In this work, however, the hourly rolling relative variances of rudder angle and speed through water are considered for filtering. Ultimately, the sample size was reduced to 1.24×10^5.

It is a common misconception that more features directly lead to higher model performance. Peculiarly, even the GPS position has been considered in the feature space in recent publications pertaining to hull performance monitoring. In fact, it is essential to keep the feature space as efficient as possible due to the curse of dimensionality, i.e. the more dimensions a search space comprises, the sparser the data becomes. Simultaneously, the features are supposed to be as meaningful to the model as possible. Feature selection is performed either in an iterative elimination procedure as demonstrated by *Mittendorf et al. (2022a)* or by domain knowledge, which is done in this case. The target variable is the measured speed through water *STW* and the feature vector has the following shape:

$$x_i=\left\{T_m,\delta,P_B,H_S,V_{rel},\psi_{rel}\right\}. \tag{1}$$

In Eq.(1), δ denotes the rudder angle, V_{rel} and ψ_{rel} indicate the relative wind speed and direction, respectively. As a side note, only the mean draft T_m is provided and neither trim nor heel are part of the sensor readings. In addition, propeller revolutions and shaft torque have been acquired during the measurement campaign; however, these particular sensor readings are considered as *collinear* to shaft power and thus not part of the feature space. Therefore, the model is solely dependent on operational conditions and environmental influences resulting from wind and waves.

3.2. Training procedure

A multilayer perceptron with four hidden layers is utilized as the underlying regression model. Moreover, no baseline data is available and therefore the model has to derive a baseline from data obtained during the first 3 months. The so-called warm-up period is used for training the entire network, whereas at times after only the last layers were adapted based on a random subsample drawn from the time interval. Therefore, the present concept of continual learning has a resemblance to active learning using random sampling. The adaptive training methodology is conducted window-wise, i.e. a 3-month window is shifted every month (i.e. 40 days). It is noted that this may introduce a lagging behavior of the performance estimate. Neural networks are not scale-invariant and, thus, the data is normalized according to the extrema of the warm-up period, in order to minimize look-ahead-bias. Despite the applied filtering conditions, the data is still characterized by significant variance and therefore the choice of loss function and regularization is of high importance. Strong focus was placed on minimizing the risk of overfitting. Therefore, shuffled 5-fold cross validation was applied and the maximum number of epochs is set to 50. In addition, an early stopping callback was implemented, which is triggered after 25 epochs without improvement of the cross validation loss. The second callback is the so-called model checkpoint saving the models parameters with the smallest cross validation loss, in order to store the model parameters with the highest generalization capability before overfitting occurs. The computations were performed on an Intel Core i7-8565U CPU, 1.80GHz with 16 GB physical memory (RAM). Moreover, the utilized deep learning framework is TensorFlow 2.6 as proposed by *Abadi et al. (2015)*.

3.3. Estimation of drift score

In several papers, explanatory variables or predictors for fouling are sought and implemented in the feature space, such as the days since last dry docking. However, it is thought that there is, in fact, no sufficient number of features for capturing the degree and development of biofouling. In addition, a recurrent neural network, such as the Long Short-Term Memory (LSTM) network, would be necessary for storing long-term developments. More importantly, we are facing a multiscale problem, in which the accumulation of fouling is of relatively small magnitude and develops over larger time scales than, e.g. the effect of wind and waves or draft changes. For this reason, a proxy variable of fouling is derived from the change of the model over time. Following the work of *Schmode and Antola (2020)*, vessel performance is assessed using simulated data under the same conditions for maintaining consistency. The enforced conditions roughly reflect sea trial conditions, i.e. a moderate seaway (5 m/s head wind and 1 m of H_S). Additionally, the laden draft and the mean rudder angle are considered. For minimizing variance, the speed loss at multiple speeds in the approximate range $STW \in [13, 20]$kts were taken as the mean value. The speed loss indicator SL is defined in Eq. 2.

$$SL = \frac{U_m - U_{ref}}{U_{ref}} \tag{2}$$

In Eq.(2), U_m refers to the measured ship speed and U_{ref} is considered as baseline data from either model test or CFD data. The de-facto standard for ship performance monitoring is *ISO 19030 (2016)*. The ISO guidelines are much debated and multiple extensions have been proposed by e.g. *Schmode et al. (2018)* mainly addressing the speed dependency issue. The overall procedure is divided into four steps: (1) Data filtering, (2) Correcting for environmental factors, (3) Calculating performance values and (4) Calculating performance indicators. The filtering step is carried out using Chauvenet's criterion and enforcing thresholds to ship and absolute wind speed. Lastly, the ISO 19030 methodology relies on baseline data extracted from e.g. model tests and empirical corrections for the calculation of the speed loss indicator according to Eq.(2).

4. Results and discussion

In the following, the results of the developed methodology are presented and discussed. Initially, the model's accuracy in the warm-up period is depicted in Fig.4. On the left, a correlation plot of normalized measured and predicted *STW* are presented both for a training and an unseen validation set. In addition, the generated baseline speed-power curve under the aforementioned conditions and an exemplary curve after 3 months (estimate) are shown on the right.

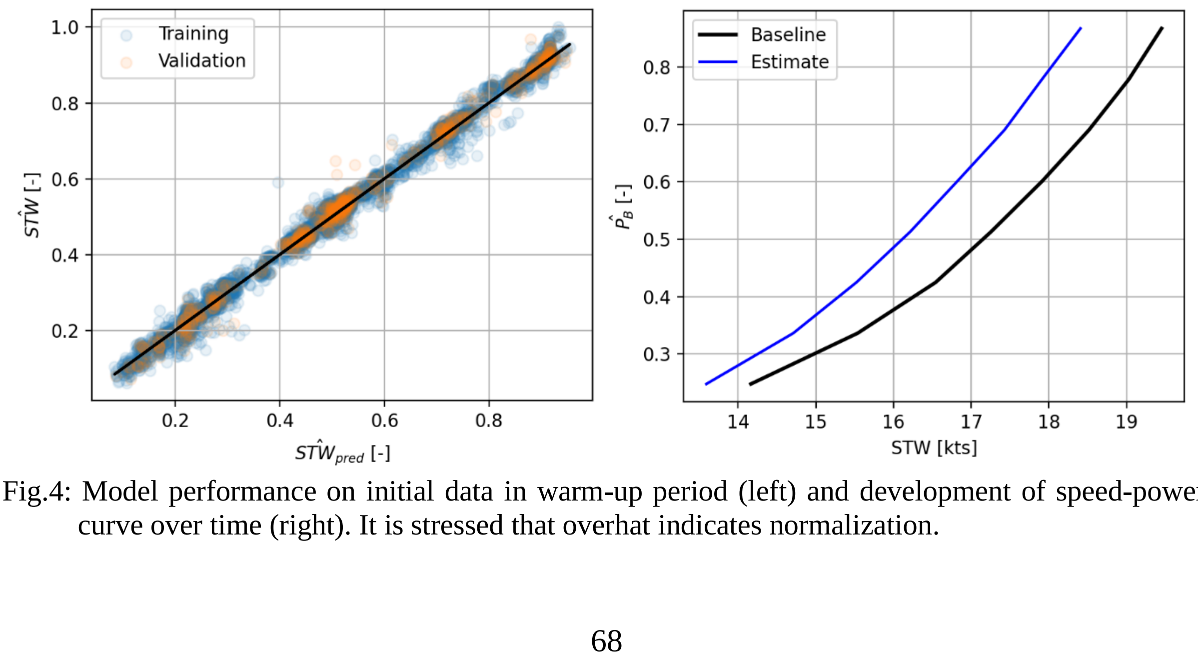

Fig.4: Model performance on initial data in warm-up period (left) and development of speed-power curve over time (right). It is stressed that overhat indicates normalization.

In view of Fig.4, it is stated that the relatively shallow multilayer perceptron is capable of establishing a satisfactory non-linear mapping from operational and environmental conditions to the actual *STW*. Still, minor outliers stand out in the medium speed regime, which may be due to possible sea currents or other uncaptured effects, such as changes in water temperature. In fact, water temperature affects both density and viscosity. The latter subsequently has a direct influence on frictional as well as viscous pressure resistance components. Overall, the model exhibits adequate out-of-sample performance. In the left hand plot of Fig.4, the cubic speed power relationship is conveyed sufficiently in both cases. It is stressed that the baseline curve is obtained from the first 3 months of data and comparison to model test data may be beneficial for validation. A significant performance decrease is visible from the second speed-power curve, which is generated 3 months after the initial warm-up period. Furthermore, minor inconsistent offsets are obvious throughout the speed range in case of the estimate of the adapted model underlining the necessity of averaging the speed loss for the entire speed range for diminished uncertainty (or variance).

The validation of a biofouling indicator is considered complex, as the ground truth is unknown and thus a latent variable. For this reason, the applied procedure is compared to the ISO 19030 method. The speed loss indicator is presented in Fig.5 and the inherent speed dependency issue of the ISO guidelines is indicated using a colorbar of *STW*. In addition, the method is subject to considerable variance and a lack of data is visible in early 2018. The first dry docking interval is divided into two phases, where the former corresponds to the first year of the analysis and the latter spans until dry docking. The third period reflects the time since dry docking. The prevalent trend of decaying ship performance is visible, but only mean values of the speed loss samples are provided for all three periods by the ISO 19030 analysis.

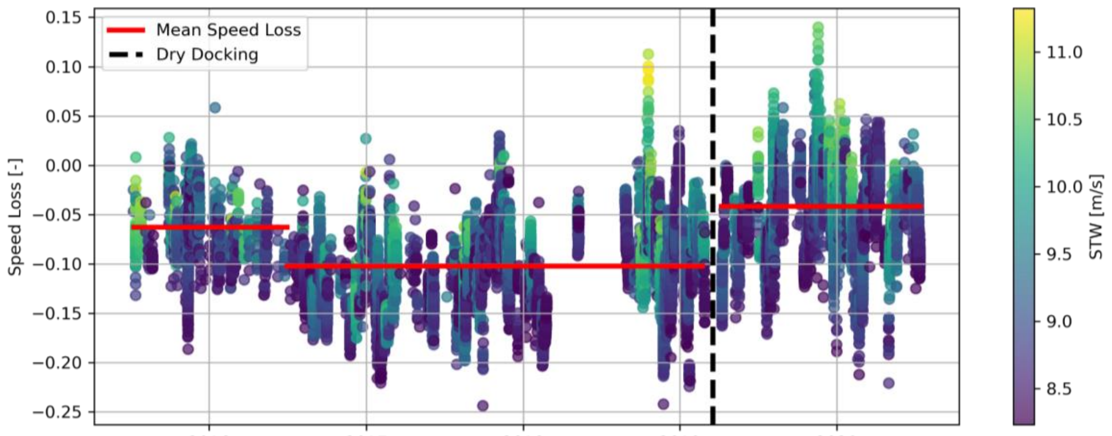

Fig.5: Speed loss according to ISO 19030 including *STW* in the colorbar

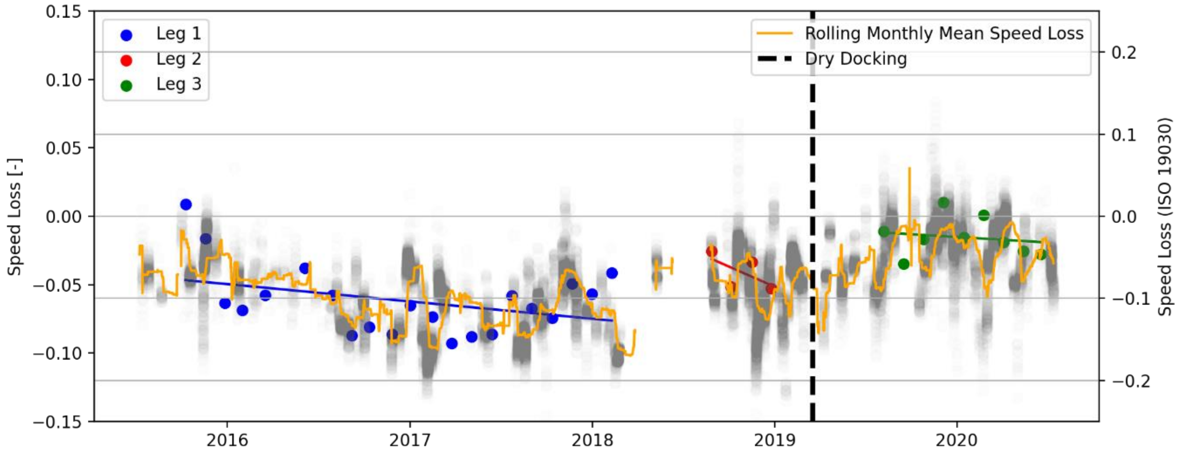

Fig.6: Comparison of model estimate (primary axis) indicated as dots in 40-day intervals to ISO 19030 speed loss data (secondary axis) for laden draft

In Fig.6, the machine learning estimates are subdivided into three periods or legs and their ordinates are presented on the primary axis, whereas the magnitude of the ISO 19030 data is presented on the secondary axis. There is one estimate every 40 days. It is stressed that the ISO 19030 speed loss samples taken from Fig.5 are included in a transparent grey color and the monthly rolling mean is indicated in orange to show the time-dependent performance decay. The first dry docking interval is split into two legs due to the period of missing data in the beginning of 2018. Additionally, linear regression is performed for the model's estimates. Crucially, it is appreciated that the proposed method and ISO 19030 are in accordance, underlining the validity of the proposed methodology. However, the agreement is only qualitative, as the primary and secondary axes have different limits. The apparent offset is a result of different baseline data: The ISO 19030 method is based on model test data, whereas the continual learning method derives its baseline from sensor data of the first 3 months. Interestingly, a structural break of estimated performance is visible after the warm-up period in leg 1, which is due to the application of continual learning, i.e. parameter updating. Moreover, the model estimates show significantly less variance as compared to ISO 19030. Unfortunately, no additional information about other cleaning events is available for a more detailed analysis.

For the discussion of the results, the uncertainty categories of epistemic and aleatoric uncertainty are introduced: (1) *Epistemic* or systematic uncertainty is due to limited data availability and reduces, as additional data is acquired. (2) *Aleatoric* or statistical uncertainty, however, is an inherent part of the data and reflects the noise and variance within the data. Hence, the latter is unaffected by increasing data availability. Both categories are important in the present case and are visualized using Fig.7.

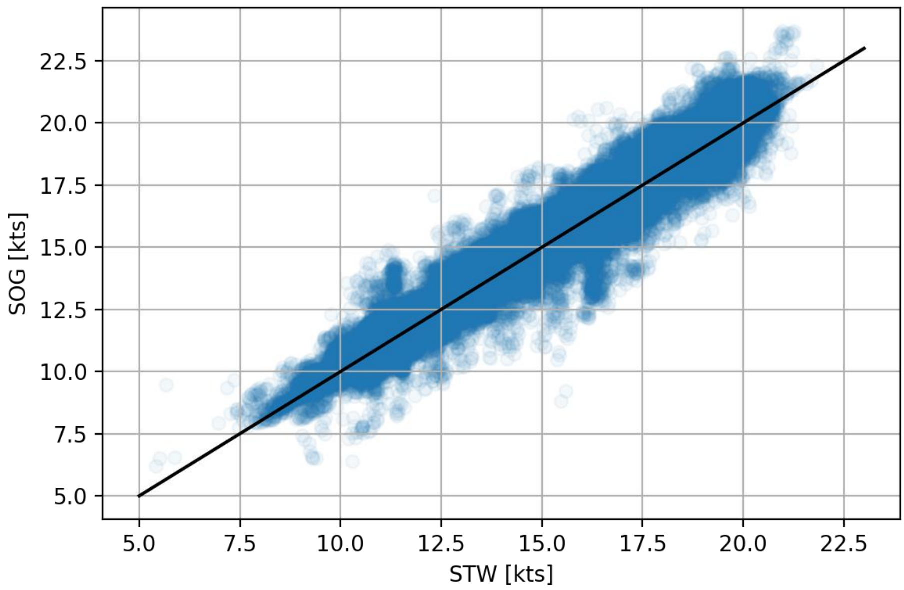

Fig.7: Correlation plot of *STW* and *SOG* of the filtered dataset including identity

In view of Fig.7, it is stated that both speed sensor readings – *SOG* and *STW* – are subject to uncertainty. Moreover, we notice a homoscedastic behavior of the residuals, i.e. no variance increase with increasing speed. The deviations result from sea currents and sensor drift, as discussed by *Ikonomakis et al. (2021).* However, the focus is on visualizing the two different uncertainty categories: Epistemic uncertainty, for instance, is present for *STW*<7.5kts, i.e. no available data. Aleatoric uncertainty, on the other hand, is considered as the "structureless" white noise present around identity.

Initially, a result of epistemic uncertainty can be observed in Fig.4, in which inconsistent offsets between both speed-power curves are visible. This inconsistency is a result of unbalanced sensor data, i.e. more samples have been measured in a certain speed interval, which leads to a shift in this particular speed regime. For the lower speed regime, it is vice versa. Furthermore, no data of trim or heel is obtained and thus no information about bulbous bow immersion is available leading to additional epistemic uncertainty. Systematic uncertainty has a significant impact on the generation of baseline data in the warm-up period due to the unbalanced exploration of the multidimensional search space. For combating epistemic uncertainty in the warm-up period, a design of experiments of synthetic data, as shown in *Mittendorf et al. (2022b)*, seems favorable. In this case, a sampling technique, such as Latin Hypercube Sampling, is applied to a parameterized simulation framework based on, e.g. semi-empirical expressions. In doing so, the baseline data and the resulting model are derived from simulated data and the continual learning procedure is then applied to in-situ sensor data.

Aleatoric uncertainty results from the insufficiencies of the sensor infrastructure, i.e. measurement uncertainty, and data aggregation uncertainty caused by window-wise averaging. Moreover, the spatio-temporal interpolation of hindcast data and the hindcast data itself increases statistical uncertainty within the data, *Nielsen (2021)*. In addition, it was shown by *Ikonomakis et al. (2022)* that GPS data as such may be erroneous and hence introduce further uncertainty in the hindcast data. For practical applications, a trustworthy estimate of aleatoric uncertainty is of high importance. Therefore, two individual approaches show potential for future work: (1) Following *Mittendorf et al. (2022c)* a quantile regression approach, i.e. training the neural network on quantile loss functions, seems promising in a deterministic attempt. (2) Conversely, establishing a Bayesian or probabilistic model using the Monte Carlo dropout method as shown in *Gupta et al. (2021)* has potential as well, but may be limited by increased computational effort.

Ultimately, strictly decomposing uncertainty types is considered as complex and not only is the data characterized by uncertainty, but also the machine learning model as well as the continual learning methodology, which is summarized in model form uncertainty. This uncertainty type is affected by random sampling in the continual learning process, the application of shuffled cross validation and the use of stochastic gradient descent for neural network training.

5. Conclusions

In the present contribution, it has been shown that ship performance data is subject to concept drift, a methodology for its quantification was proposed, and the procedure has been applied to a real-world case study. It is assumed that the degree of concept drift is highly correlated to biofouling accumulation on hull and propeller. The methodology is built upon continual learning of an artificial neural network and showed sufficient accuracy both when predicting the actual speed through water, but also when estimating the long-term performance decay due to biofouling. Herein, an adaptive digital representation of an LNG tanker is utilized for biofouling estimation, but may also be applied in bunker forecast or routing optimization. In general, the presented methodology is considered as relatively modular and robust. It may work in a solely data-driven manner, but the drift score calculation may also be based on model test or CFD results. In addition, different hyperparameters were studied and the obtained results suggest sufficient robustness – even for possible application in practice. The present methodology may be a leap forward towards data-driven predictive maintenance in the maritime sector, but the methodology as such is not limited to the domain of ship operation.

Moreover, the presented procedure shows significant potential for future work. For instance, the method exhibits satisfactory applicability in case of a gas carrier, but the application to container vessels having more widespread operational conditions appears to be challenging. The real time estimation of sea state parameters as in the study of *Mittendorf et al. (2022b)*, i.e. employing the wave buoy analogy as described by *Nielsen (2018)*, may enhance the accuracy and diminish the uncertainty of the proposed method resulting from hindcast data and its spatio-temporal interpolation. Furthermore, the extension towards fleet performance analysis appears as advantageous considering the individual ship as a node within a network, i.e. as an edge device. Non-transparency is the key issue of neural networks and turning the model into a so-called grey box model may reduce opaqueness. For this reason, estimates of (semi-)empirical formulae or derived quantities such as propeller slip could be part of a modified feature vector for training a physically informed model.

Acknowledgments

The first author wishes to acknowledge the fruitful collaboration of DTU, Hempel and Wärtsilä Voyage. The financial support from The Danish Maritime Fund (case number 2019-043), A/S D/S Orient's Fond and the Department of Mechanical Engineering (DTU) is highly appreciated. The second author has received funding by the Research Council of Norway through the Centres of Excellence scheme, project number 223254 AMOS.

References

ABADI, M.; AGARWAL, A.; BARHAM, P.; BREVDO, E.; CHEN, Z.F.; CITRO, C.; CORRADO, G.S.; DAVIS, A.; DEAN, J.; DEVIN, M.; GHEMAWAT, S.; GOODFELLOW, I.; HARP, A.; IRVING, G.; ISARD, M.; JIA, Y.Q.; JOZEFOWICZ, R.; KAISER, L.; KUDLUR, M.; LEVENBERG, J.; MANE, D.; MONGA, R.; MOORE, S.; MURRAY, D.; OLAH, C.; SCHUSTER, M.; SHLENS, J.; STEINER, B.; SUTSKEVER, I.; TALWAR, K.;TUCKER, P.; VANHOUCKE, V.; VASUDEVAN, V.; VIEGAS, F.;VINYALS, O.; WARDEN, P.; WATTENBERG, M.; WICKE, M.; YU, Y.; ZHENG, X.Q. (2015), *TensorFlow: Large-scale machine learning on heterogeneous systems*, http://download.tensorflow.org/paper/whitepaper2015.pdf

ANTOLA, M.; SOLONEN, A.; STABOULIS, S. (2017), *The Art of Scarcity: Combining High-Frequency Data with Noon Reports in Ship Modelling*, 2nd Hull Performance and Insight Conference (HullPIC'17), Ulrichshusen

BERTRAM, V. (2012), *Practical Ship Hydrodynamics*, Butterworth & Heinemann

CARLTON, J.S. (2018), *Marine Propellers and Propulsion.* Butterworth & Heinemann

CORADDU, A.; ONETO, L.; BALDI, F.; CIPOLLINI, F.; ATLAR, M.; SAVIO, S. (2019), *Data-driven Ship Digital Twin for Estimating the Speed Loss Caused by the Marine Fouling.* Ocean Engineering 186, No. 106063.

COPERNICUS (2021), *ERA5: Fifth Generation of ECMWF Atmospheric Reanalyses of the Global Climate.* Copernicus Climate Change Service, https://cds.climate.copernicus.eu/cdsapp#!/home

DNV GL (2018), *Class Guideline: Wave loads (DNVGL-CG-0130)*, DNV, Hovik

GOODFELLOW, I.; BENGIO, Y.; COURVILLE, A. (2016), *Deep Learning*, The MIT Press

GUPTA, P.; RASHEED, A.; STEEN, S. (2021), *Ship Performance Monitoring using Machine-learning*, Ocean Engineering

HANSEN, S.V. (2011), *Ship Performance Monitoring.* Ph.D. thesis, Technical University of Denmark

HERSBACH, H.; BELL, B.; BERRISFORD, P.; BIAVATI, G.; HORÁNYI A.; MUÑOZ SABATER, J.; NICOLAS, J.; PEUBEY, C.; RADU, R.; ROZUM, I.; SCHEPERS, D.; SIMMONS, A.; SOCI, C.; DEE, D.; THÉPAUT, J.-N. (2018), *ERA5 hourly data on single levels from 1979 to present.* Copernicus Climate Change Service (C3S) Climate Data Store (CDS), https://doi.org/10.24381/cds.adbb2d47

IKONOMAKIS, A.; NIELSEN, U.D.; HOLST, K.K.; DIETZ, J.; GALEAZZI, R. (2021), *How Good Is the STW Sensor? An Account from a Larger Shipping Company*, J. Marine Science and Eng. 9/465

IKONOMAKIS, A.; NIELSEN, U.D.; HOLST, K.K.; DIETZ, J.; GALEAZZI, R. (2022), *Validation and correction of auto-logged position measurements*, Communications in Transportation Research Vol. 2. No. 100051

IMO (2014), *Reduction of GHG emissions from ships – Third IMO GHG Study 2014*, Final Report (MEPC 67/INF3)

ISO 19030 (2016), *Ships and marine technology – Measurement of changes in hull and propeller performance Standard*, Int. Organization for Standardization, Geneva

JAWORSKI, M.; RUTKOWSKI, L.; ANGELOV, P. (2020), *Concept Drift Detection Using Autoencoders in Data Streams Processing*, Artificial Intelligence and Soft Computing, ICAISC 2020

LAURIE, A.; ANDERLINI, E.; DIETZ, J.; THOMAS, G. (2021), *Machine learning for shaft power prediction and analysis of fouling related performance deterioration*, Ocean Eng. 234, No. 108886.

LOSING, V.; HAMMER, B.; WERSING, H. (2018), *Tackling heterogeneous concept drift with the Self-Adjusting Memory (SAM)*, Knowledge and Information Systems 54, pp.171–201

MITTENDORF, M.; PAPANIKOLAOU, A.D. (2021), *Hydrodynamic Hull Form Optimization of Fast Catamarans using Surrogate Models*, Ship Technology Research 68/1, pp.14-26.

MITTENDORF, M.; NIELSEN, U.D.; BINGHAM, H.B. (2022a), *Data-Driven Prediction of Added-Wave Resistance on Ships in Oblique Waves - A Comparison between Tree-Based Ensemble Methods and Artificial Neural Networks*, Applied Ocean Research 118, No. 102964

MITTENDORF, M.; NIELSEN, U.D.; BINGHAM, H.B. (2022b), *The Prediction of Sea State Parameters by Deep Learning Techniques using Ship Motion Data*, 7th World Maritime Technology Conference (WMTC'22), Copenhagen

MITTENDORF, M.; NIELSEN, U.D.; BINGHAM, H.B.; LIU, S. (2022c), *Towards the Uncertainty Quantification of Semi-empirical Formulas Applied to the Added Resistance on Ships in Arbitrary Heading*, Ocean Engineering 251, No. 111040

NIELSEN, U.D. (2018), *Sea State Estimation Based on Measurements of Wave-induced Ship Responses*, PhD thesis, DTU, Lyngby

NIELSEN, U.D.; JOHANNESEN, J.R.; BINGHAM, H.B.; BLANKE, M.; JONCQUEZ, S. (2019), *Indirect Measurements of Added-wave Resistance on an In-service Container Ship*, 14th Int. Symp. Practical Design of Ships and Other Floating Structures (PRADS'19), Yokohama

NIELSEN, U.D. (2021), *Spatio-temporal Variation in Sea State Parameters along Virtual Ship Route Paths*, J. Operational Oceanography

NIELSEN, U.D.; IKONOMAKIS, A. (2021), *Wave Conditions Encountered by Ships – A Report from a Larger Shipping Company based on ERA5*, Ocean Engineering 237, No. 109584

PARISI, G.I.; KEMKER, R.; PART J.L.; KANAN, C.; WERMTER, S. (2019), *Continual lifelong learning with neural networks: A review*, Neural Networks 113, pp.54-71

PEDERSEN, B.P.; LARSEN, J. (2009), *Prediction of full-scale propulsion power using artificial neural networks*, 8th COMPIT Conf., Budapest

PETERSEN, J.P.; WINTHER, O.; JACOBSEN, D.J. (2012), *A machine-learning approach to predict main energy consumption under realistic operational conditions*, Ship Technology Research 59, pp.64–72

RAMASESH, V.V.; DYER, E.; RAGHU, M. (2021), *Anatomy of catastrophic forgetting: Hidden representations and task semantics*, 9th Int. Conf. on Learning Representations (ICLR'21), Virtual

SCHMODE, D.; HYMPENDAHL, O.; GUNDERMANN, D. (2018), *Hull Performance Prediction beyond ISO 19030*, 3rd Hull Performance and Insight Conference, Redworth

SCHMODE, D.; ANTOLA, M. (2020), *Fusion of High-Frequency Navigational Data and Noon-Reported Data to Predict Hull Condition*, 5th Hull Performance and Insight Conference, Hamburg

Suggestion and Evaluation of Alternative Indexes for Estimating Hull Performance Degradation Trendlines

Nikolaos Bekiaris, Prisma Electronics, Athens/Greece, nikos.bekiaris@prismael.com
Zacharias Zervos, Prisma Electronics, Athens/Greece, zacharias.zervos@prismael.com
Ioannis Tolias, Prisma Electronics, Athens/Greece, ioannis.tolias@prismael.com
Christos Giordamlis, Prisma Electronics, Athens/Greece, christos@prismael.com

Abstract

A High Frequency Data Collection System (HFDCS) can monitor continuously and accurately the performance of the vessel where it is installed. For calculating vessel's performance degradation ISO 19030, suggests two coefficients, Power Deviation and Speed Loss. The minimum parameters required for calculating these two coefficients are the shaft power, the speed through water and the vessel's drafts. The sensors or equipment that are measuring the speed through water and the shaft power are usually very reliable. On the contrary, the sensors that are measuring vessel's drafts are usually very susceptible to fault measurements due to external factors (sensors age, water salinity, calibration etc.). For this reason though, in many cases – since the automatically collected data for the vessel's draft from an installed HFDCS are not considered reliable – these data are being entered manually to the HFDCS, as direct entries, or through external systems as an EPR software, AIS data, a noon report etc. However, again in all these alternatives, the vessels' drafts estimation by vessels' crew – especially when the vessel is underway – include many uncertainties and they deviate significantly from the actual. In this paper, alternative ways for estimating vessels' hull performance degradation trendlines without the use of drafts data are presented, and through the use of almost two years of operational data from 8 vessels will be, analyzed, evaluated and finally compared with the suggested by ISO 19030 coefficients. For the calculation of the relevant indexes/coefficients, filtering techniques and regression modeling will also be employed. Finally, a comparative study and conclusions between the alternatives and the ISO suggested indexes will critically be presented, together with best practices and models about the applicability and the usability of these alternatives.

1. Introduction

Hull and propeller performance refers to relationship between the condition of a ship's underwater hull and propeller and the power required to move the ship through water at a given speed. Hull and propeller performance is related to variations in power, because ship hull resistance and propeller efficiency are not directly measurable quantities. ISO 19030 suggests two basic performance indicators.

1.1. ISO 19030 Performance Indicators

ISO 19030, outlines two general principles for the measurements of changes in hull and propeller performance indicators for hull and propeller maintenance, repair and retrofit activities. These two principles/indicators are:

Power Deviation: The deviation between the actual measured shaft power and the theoretical from a vessel's baseline, for the same speed.

Speed Loss**:** The deviation between the actual measured vessel's speed and the theoretical from a vessel's baseline for the same power.

Moreover, ISO 19030-2 describes in detail the primary and secondary parameters that a HFDCS should collect for calculating these indicators.

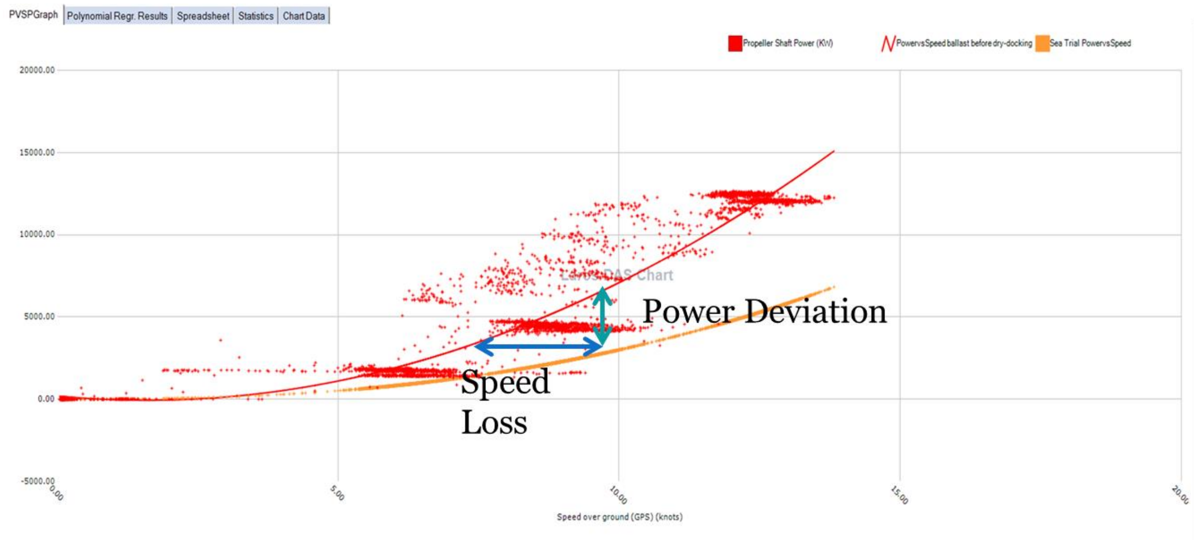

Fig.1: Graphical representation of ISO 19030 performance indicators

1.2. Primary parameters required

The defined primary required collected parameters are:

- Speed Through Water
- Delivered Power

1.3. Secondary parameters required

The defined secondary suggested collected parameters are:

- Shaft revolutions
- Relative wind speed/direction
- Speed over ground
- Heading
- Rudder angle
- Water depth
- Static draughts (fore & aft)

From these values the calculation of the "Power Deviation" and/or the "Speed Loss", requires also the selection/availability of the relative baseline. From vessel's sea trials, three are the most common provided baselines (in some cases though, only two – ballast/laden – are available):

a. Speed/Power Curve for Ballast draft
b. Speed/Power Curve for Design draft
c. Speed/Power Curve for Scantling draft

In order to select the correct baseline, the knowledge of vessel's actual draft is imperative. Most of the times, the actual vessel's draft is not coincide with one of the above, so interpolations are required for the selection of the best fitted baseline for intermediate drafts.

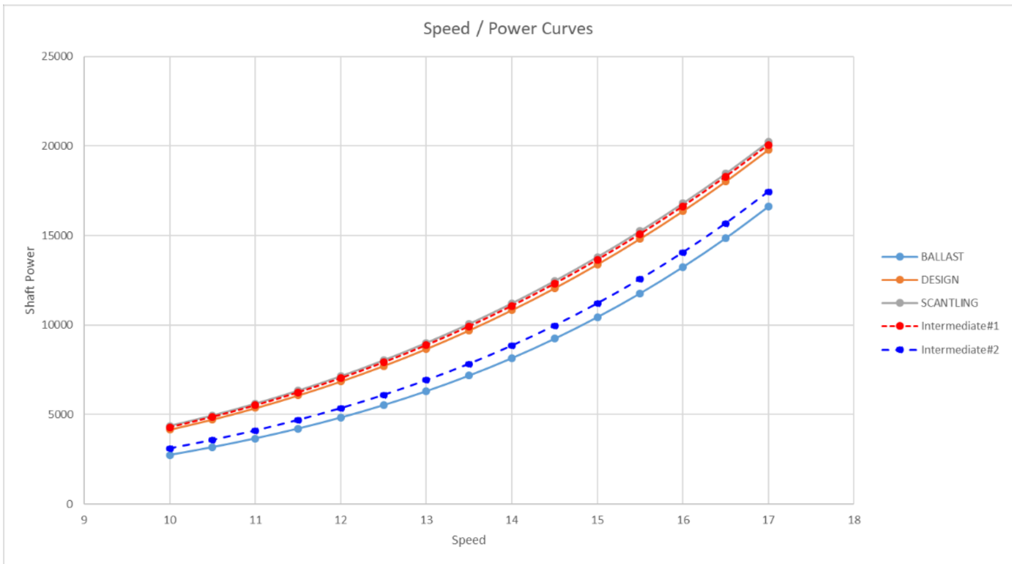

Fig.2: Interpolated baselines

1.4. Filtering of Data

All collected data, should also be filtered under the conditions that table A.1 of ISO 19030-1 describes and more specific for:

- True Wind Speed of less than 7.9 m/sec
- Absolute difference of (SOG – STW) less than 1 knot
- Sea depth criteria – usually for depth higher than 50m
- Vessel's speed within limits according the available baselines

1.5. ISO 19030 Performance Indicators outputs

Under the above described conditions, the HFDCS calculates continuously both of these two performance indicators.

When vessel's resistance is increasing (mostly due to hull & propeller fouling), the vessel in order to achieve the same speed requires higher shaft power (power increase), or at the same shaft power, the vessel is achieving lower speeds (speed loss). So:

Power Deviation (%): Positive values/Increasing by time (positive trendline)
Speed Loss (%): Negative values/Increasing (in absolute values) by time (negative trendline)

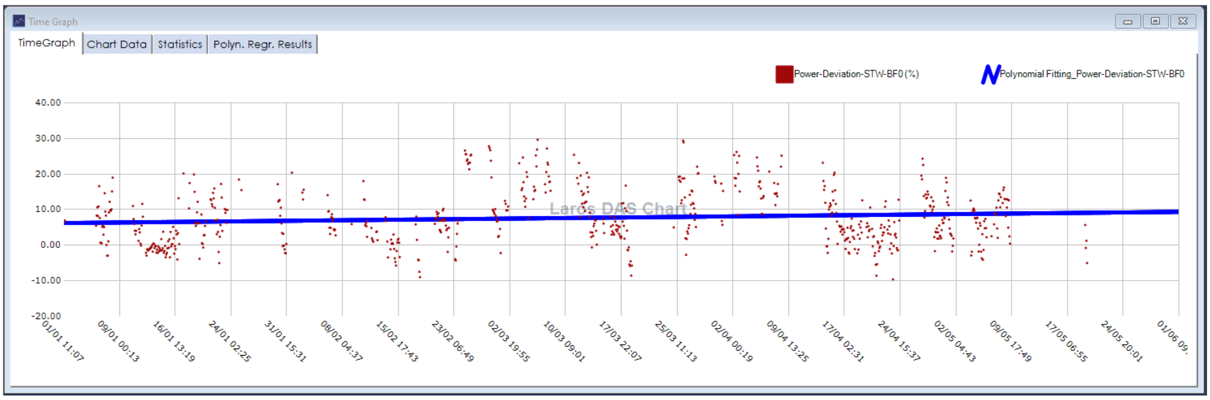

Fig.3: Power Deviation

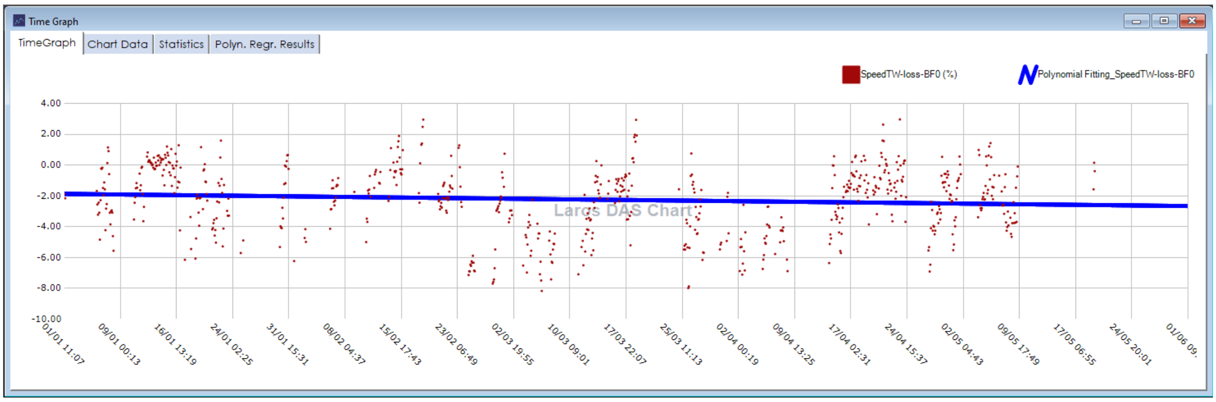

Fig.4: Speed Loss

1.6. Accuracy of collected data

All sensors and equipment that are measuring the above required for the calculations parameters, usually are very accurate with the exception of the drafts. The sensors that are measuring vessel's drafts are often very susceptible to fault measurements due to external factors (sensors age, water salinity, calibration etc.). For this reason though, in many cases – since the automatically collected data for the vessel's draft from an installed HFDCS cannot be considered reliable – these data are being entered manually to the HFDCS, as direct entries, or through external systems as an EPR software, AIS data, noon reports etc. However, again in all these cases, the vessels' drafts estimation by vessels' crew – especially when the vessel is underway – include many uncertainties and they deviate significantly from the actual.

For this reason, without having accurate draft measurements (especially for older vessels), the outputs of these indicators – and not only – may provide wrong conclusions regarding vessel's previous performance, as well as predictions for vessel's future performance.

2. Alternative Indexes for Estimating Hull Performance Degradation

In addition to the performance indicators that ISO 19030 describes, alternative indexes have been extensively used in order to provide an estimation of vessel's performance degradation. The most used of them are:

1.1. Percentage of slip

Slip is considered as the difference between the speed of the engine and the actual speed of the ship. It is always calculated in percentage. Positive slip is influenced by various reasons such as fouled bottom or hull part which offers resistance to the movement of the ship, environmental factors such as water current and wind against the ship direction. The slip may be negative if the ship speed is influenced by following sea or wind.

If the propeller had no slip, i.e. if the water which the propeller "screws" itself through did not yield, the propeller would move forward at a speed of:

$$V_p = p\ x\ n \qquad \text{where:}$$

p: Vessel's propeller pitch and
n: Propeller's rate of revolution

Under increased resistance, this involves that the propeller speed (rate of revolution) has to be increased in order to maintain the required ship speed.

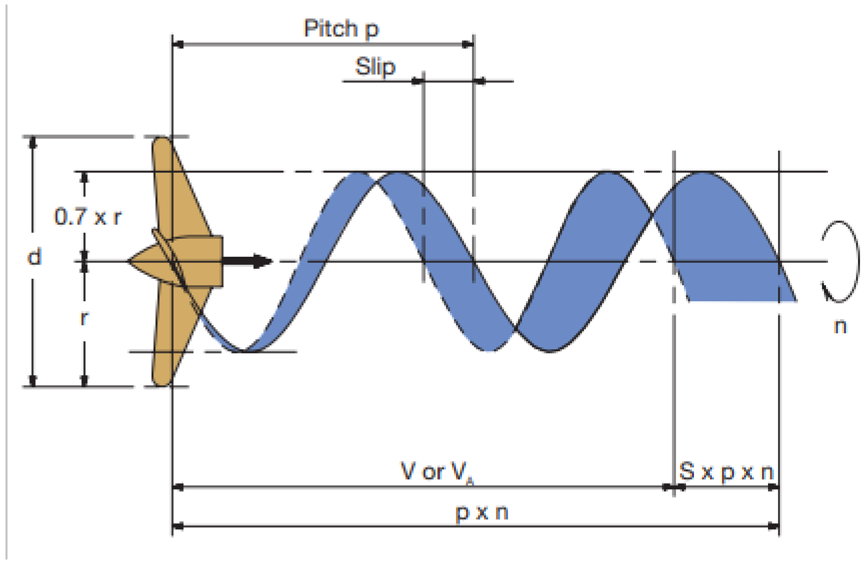

Fig.5: Percentage of Slip

So the percentage of slip is:

$$Slip(\%) = \frac{(V_p - V)}{V_p} \qquad \text{where:}$$

V: Vessel's actual speed

While vessel's performance deteriorates through time due to hull & propeller fouling (considering good weather conditions), vessel's slip is increasing.

1.2. Engine (Load) margin & Propeller margin

Engine (Load) Margin: The available percentage engine load for overcoming additional encountered resistance. This margin is required to achieve reasonable maintenance intervals of the engine, to enable a higher ship speed than design speed in case the ship is behind schedule and to cope with increased loads due to more fouling or a higher sea state than in design condition.

$$EM = \frac{MCR \,.\, \left(\frac{rpm}{RPM}\right)^3 - shp}{MCR \,.\, \left(\frac{rpm}{RPM}\right)^3} \qquad \text{where:}$$

EM: Engine (Load) Margin
MCR: Engine's power at Maximum Continuous Rating
RPM: Engine's RPM at Maximum Continuous Rating
shp: Operational engine's power
rpm: Operational engine's rpm

Propeller Margin: The available rpm (or percentage rpm) at a specific power for overcoming additional encountered resistance. It relates the engine speed difference between the service propeller curve and the propeller curve at light running conditions.

$$PM = rpm - RPM \,.\, \sqrt[3]{\frac{shp}{MCR}} \qquad \text{or} \qquad PM\% = \left(\sqrt[3]{\frac{MCR}{shp}} \,.\, \frac{rpm}{RPM} - 1\right) x\ 100 \qquad \text{where:}$$

PM: Propeller Margin
MCR: Engine's power at Maximum Continuous Rating

RPM: Engine's RPM at Maximum Continuous Rating
shp: Operational engine's power
rpm: Operational engine's rpm

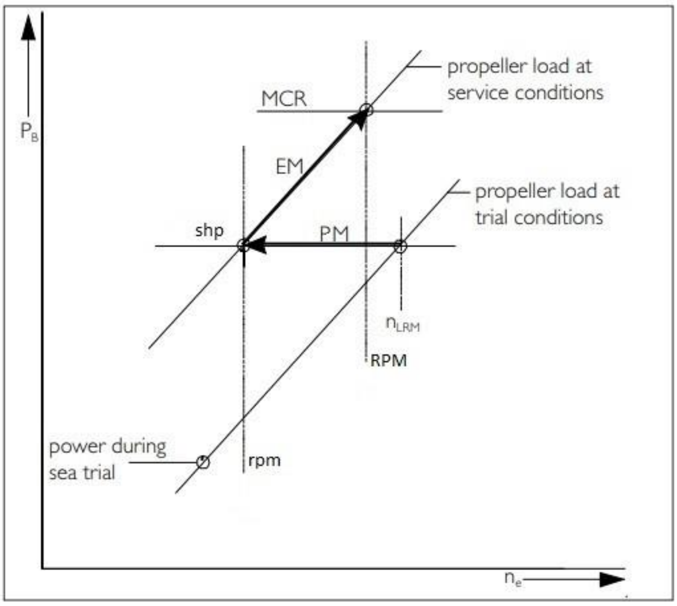

Fig.6: Engine Margin/Propeller Margin

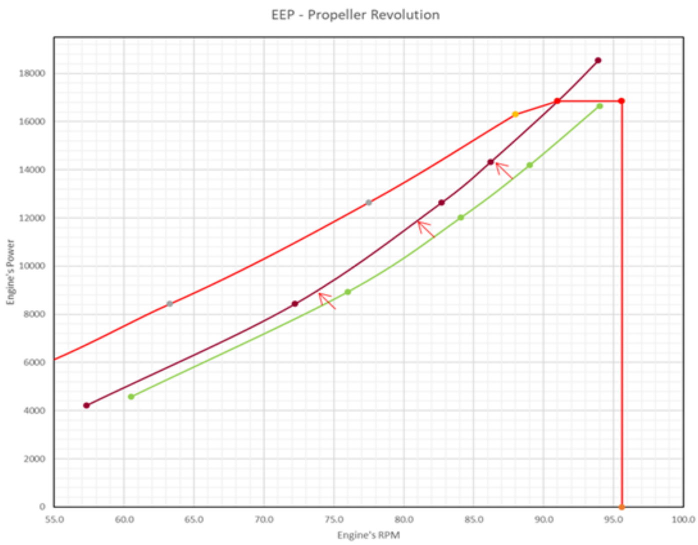

Fig.7: Shift of the light propeller running margin towards heavy propeller running

The vessel, in calm seas and with a clean hull and propeller, has a positive engine load margin and propeller margin, which is needed to overcome any additional encountered resistance. Considering good weather conditions, due to hull and propeller fouling both these margins are decreasing.

1.3. Laros Combined Power (P)/RPM (N)/Speed (V) analysis for performance deviation

Through this analysis a concurrent "power deviation" and "speed loss" indexes can be calculated from a combined Power (P), RPM (N) and Speed (V) analysis (PNV).

For this analysis, again the speed/power curves from vessel's sea trials are considered, together with vessel's shaft rpm. With these three parameters, the parabolic curves of speed vs power can be converted to linear as *f(P,V)* vs *f(V,N)*. Through this transformation, all data for either ballast & scantling drafts – as well as for all the intermediate drafts – have the same linear trendline in the form of Ax+B

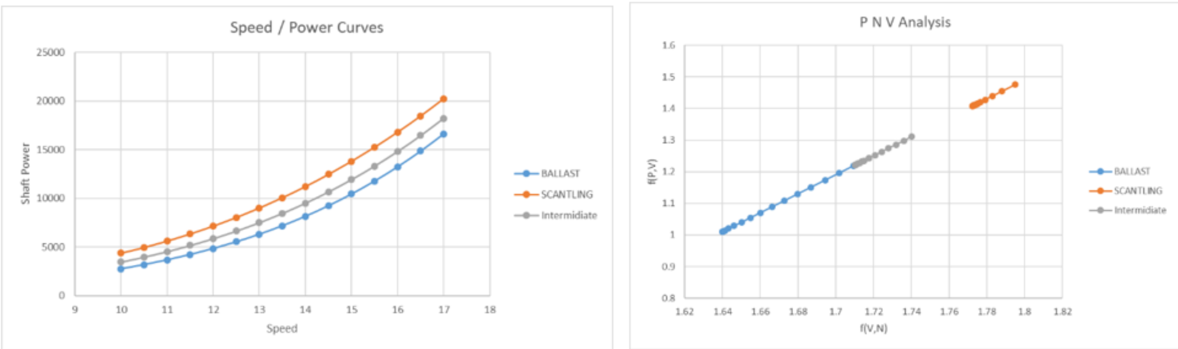

Fig.8: Parabolic to linear baseline curves conversion

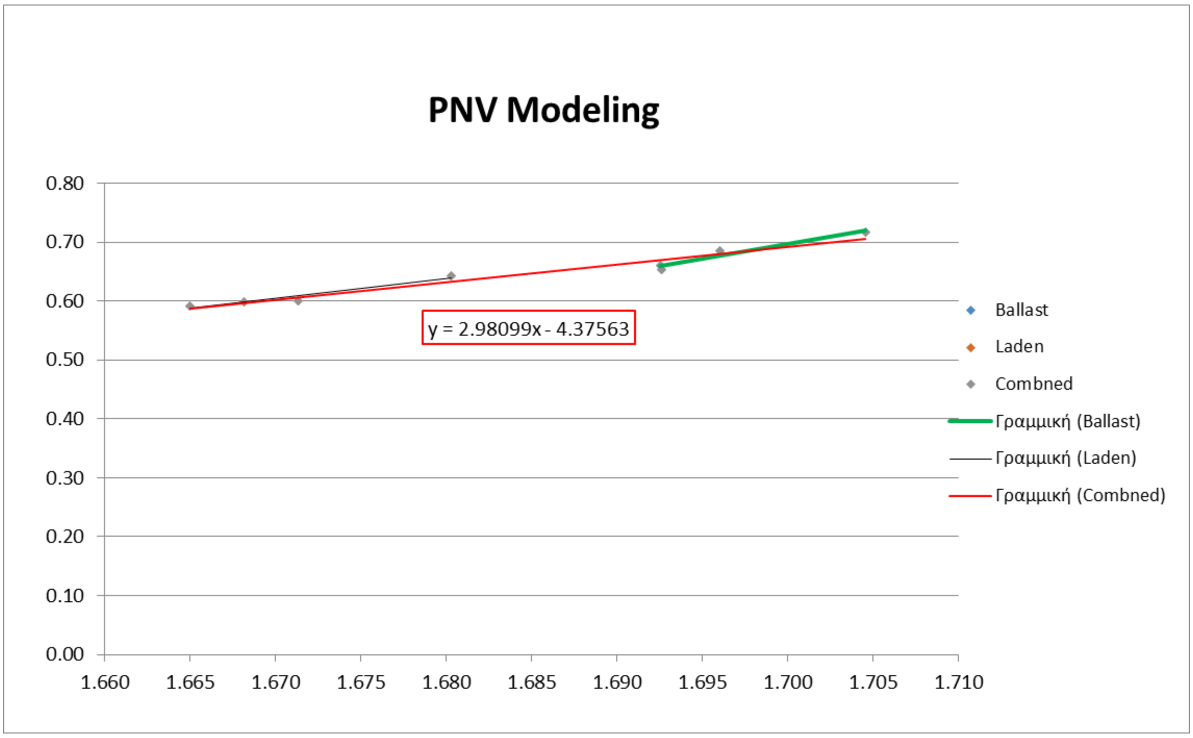

Fig.9: Parabolic to linear baseline curves conversion from an actual vessel

More specific: $f(P,V) = ln\left(\frac{P}{V^3}\right)$ and $f(V,N) = -ln\left(\frac{V}{N}\right)$ where:

P: Shaft Power
V: Vessel's Speed
N: Shaft rpm

By comparing the $f(P_{act},V_{act})$ with the output of the equation $A \times f(V_{act},N_{act}) + B$ a "%Power deviation" and a "%Speed loss" can be calculated. When vessel's resistance is increasing (mostly due to hull & propeller fouling), the vessel is achieving lower speed while concurrently she requires increased power, thus the "%Power deviation" is increasing by time (positive trendline), while "%Speed Loss" has negative values and decreasing by time (negative trendline)

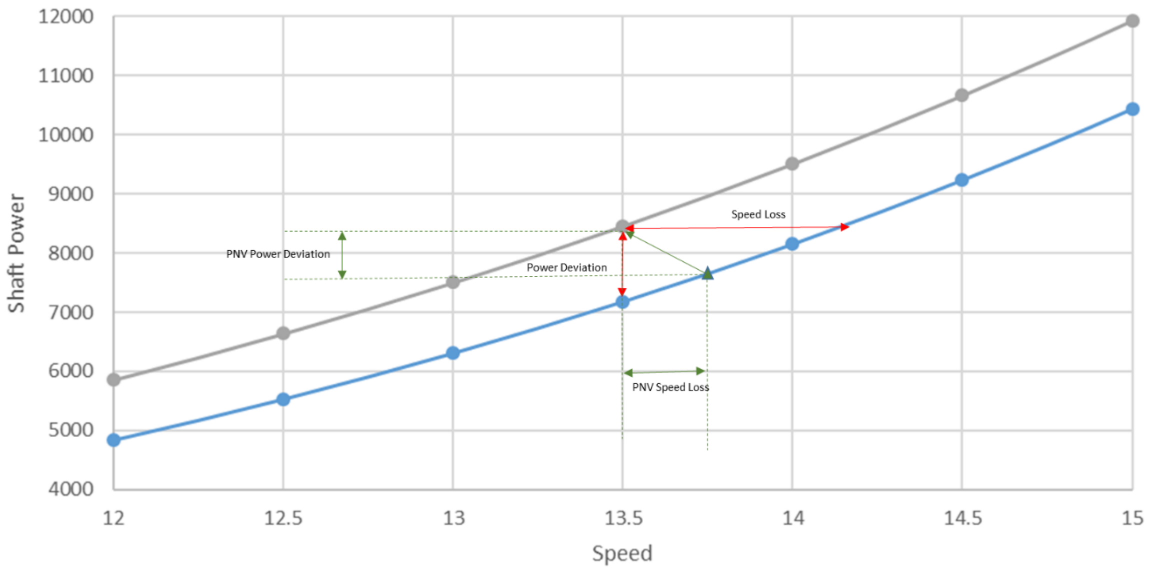

Fig.10: Concurrent “Power Deviation” & “Speed Loss”

3. Data Selection and acquisition

3.1. Data Selection

In this paper we proceeded in the calculations and comparison of all the above-described indexes. The collected/calculated parameters that were used in the analyses and the calculations were the following, and as suggested by ISO 19030:

- Speed Through Water
- Speed Over Ground
- Propeller Shaft Power
- Propeller Shaft revolutions
- Relative wind Speed/Direction
- Heading
- Rudder Angle
- Water Depth
- Static Draughts (fore & aft)

The time period for the analysis was two years between 01/01/2020 and 01/01/2022

3.2. Data acquisition

All data have been collected through LAROS$^{TM©}$, which is a Holistic High Frequency Data Acquisition System, independent from main vendors. LAROS$^{TM©}$ is a system where wireless/wired smart collectors are connected on any existing vessel’s sensors, SCADA or equipment, for collecting the agreed datasets in a single and integrated approach and transmitting them to a centrally installed server. Then the collected data can be analyzed and presented on vessel’s crew – if required, and transmitted – even in real time – to vessel’s headquarters for further and more detailed analyses and storing. Below figure shows a graphical representation of LAROS$^{TM©}$ system.

The collected data from LAROS$^{TM©}$ system may have a time resolution of 3 s stored in the database, but for this specific analysis, a time resolution of 1 min was used. The accuracy of all collected data from LAROS$^{TM©}$ system is relative to the accuracy of each sensor/equipment providing the specific measurement. Machine Learning (ML) and Artificial Intelligence (AI) through the high frequency data collections can also decrease significantly the uncertainty of the collected measurements.

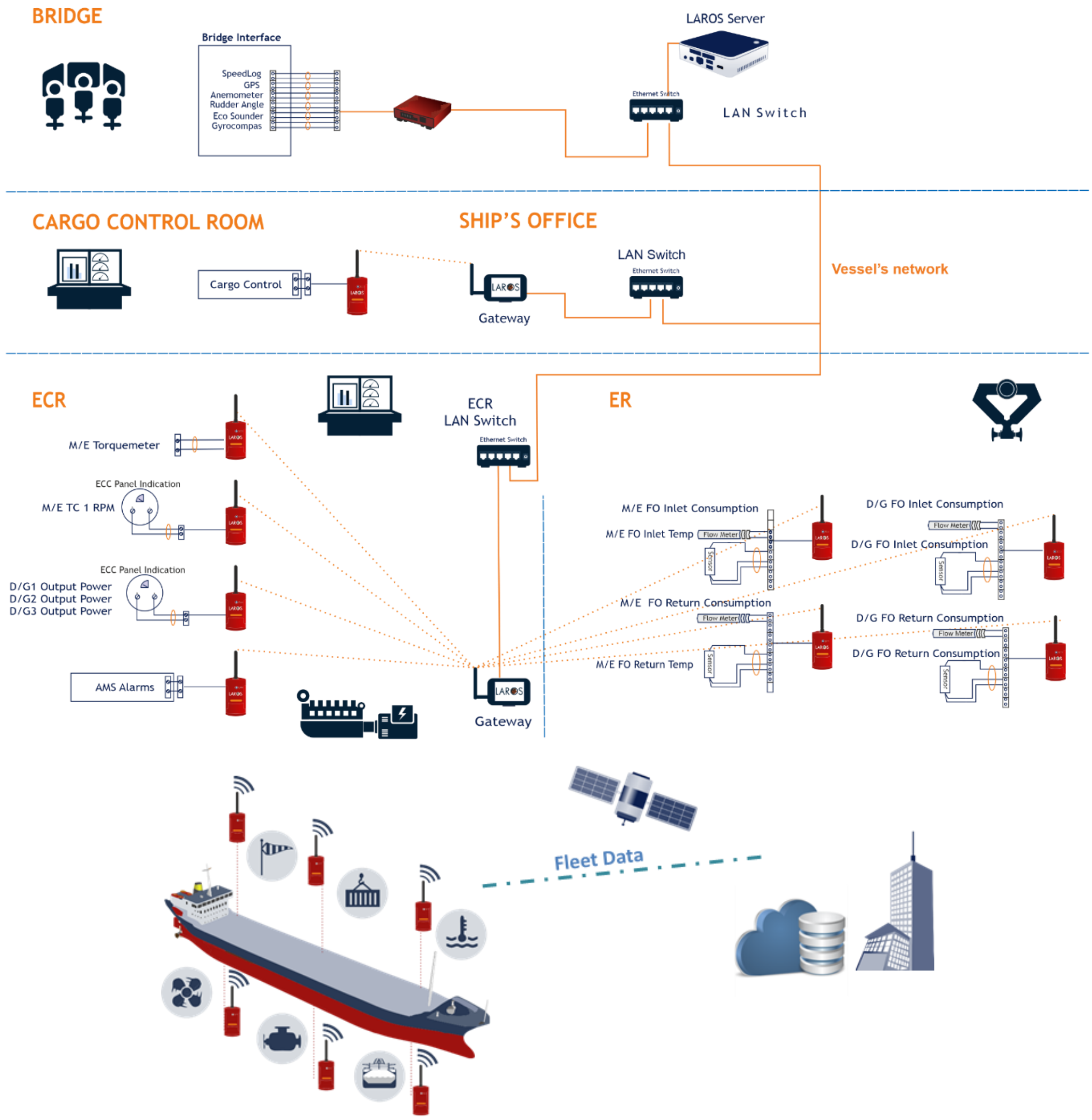

Fig.11: Graphical representation of LAROS™© system

3.3. Vessels Selections

For the analysis and comparison, data from eight different vessels have been used, both bulker and tanker vessels of several sizes. Since one of the requirements for the selection of the vessels was the collection of the draft measurements, five of them were new buildings, two of them were older vessels that completed their dry dock at the end of 2019 (at these seven vessels Laros data collectors were connected directly at the output of the draft sensors or the relevant equipment), while for the final (older) vessel the draft measurements were entered – almost daily – manually. Before selecting the vessels, no validation for the accuracy of the draft measurements was conducted, in order to check if system's output could identify possible irregular outcomes. Finally, the vessels that were used in this analysis were also selected for the reliability of the manufacturer's and the types of sensors and equipment installed.

Table I presents a summary of these vessels. For the analysis, all collected data for the years 2020 and 2021 were used.

Table I: Selected vessels summary data

A/A	Type	Size	Built (year)	Latest DD (mm/year)
1	Bulker	Panamax	2010	10/2020
2	Bulker	Kamsarmax #1	2019	N/A
3	Bulker	Kamsarmax #2	2019	N/A
4	Tanker	Suezmax	2010	01/2020
5	Tanker	VLCC	2009	12/2019
6	Tanker	Coastal Tanker #1	2019	N/A
7	Tanker	Coastal Tanker #2	2019	N/A
8	Tanker	Coastal Tanker #3	2019	N/A

4. Data Analyses

For the analyses of the data – verification of the received data, analyses, estimation of indexes, comparisons – as well as for the majority of the graphical representations, LAROS™© Digital Analysis Software was used. Below steps were followed:

4.1. Collection of Data – Filtering of Data – Aggregation

All required data for the calculation of the relevant indexes were collected as described in chapter 3, and used for the calculation of below indexes as analytically described in chapters 1& 2:

- ISO Power Deviation
- ISO Speed Loss
- Percentage of Slip
- Engine Load Margin
- Propeller Margin
- PNV – "Power Deviation"
- PNV – "Speed Loss"

The collected data were filtered initially under the conditions that table A.1 of ISO 19030-1 describes and more specific for:

- True Wind Speed of less than 7.9 m/s
- Absolute difference of (SOG – STW) less than 1 knot
- Sea depth criteria – usually for depth higher than 50m
- Vessel's speed within limits according the available baselines

Especially for the true wind speed a further filtering was used for wind speed of less than 5.5 m/s (Beaufort 3). Additionally, to that, for each parameter the outliers have been identified and removed and specific filters have been added, as specified below:

- Speed Through Water: Between 10 and 16 knots
- Speed Over Ground: Between 10 and 16 knots
- Propeller Shaft Power: Between 20% and 100% of MCR
- Propeller Shaft revolutions: Only outliers
- Relative wind Speed/Direction: Only outliers. The filter has been added to the calculated True Wind Speed
- Heading: Only outliers
- Rudder Angle: ± 2.5°
- Water Depth: Higher than 100m
- Static Draughts (fore & aft): Between ballast and scantling drafts

Finally, even that all the indexes have been calculated with 1 minute time resolution, for the analysis and comparisons, all outcomes have been averaged for three hours with an activation threshold of 70%, meaning that an average value has been accepted only when 70% of data are available in these three hours of time resolution (at least 180 x 70% = 126 measurements available for every 3 h = 180 min)

4.2. Analysis procedure

For the analysis procedure below steps were followed:

1. For each vessel all above-described performance indicators were calculated for two years' time period. The calculated results then were filtered and aggregated as described in paragraph 4.1.
2. Relevant time graphs of all indicators were plotted for each vessel together with the derived linear trendlines, presenting the performance degradation of the vessel.
3. Finally, the derived trendlines of the non-ISO indicators were compared with same from the ISO indicators for analogies/patterns.

4.3. Indicators Plots and trendlines

For all indicators the relevant time graphs were plotted and checked for their validity, meaning that the calculated values and the slope of the relative trendlines were as expected and described in the above analysis.

For five of these vessels the relevant indicators with their linear trendlines show the same hull and propeller degradation, similar to the outputs of ISO suggested indicators, regardless the loading condition of the vessel (knowing the vessel's draft). Of course the limits for each indicator in order for them to be considered "off", are vessel specific regarding the considered/selected baselines and the age/condition of the vessel.

Fig.12-16, the relevant plots from all vessels are being presented.

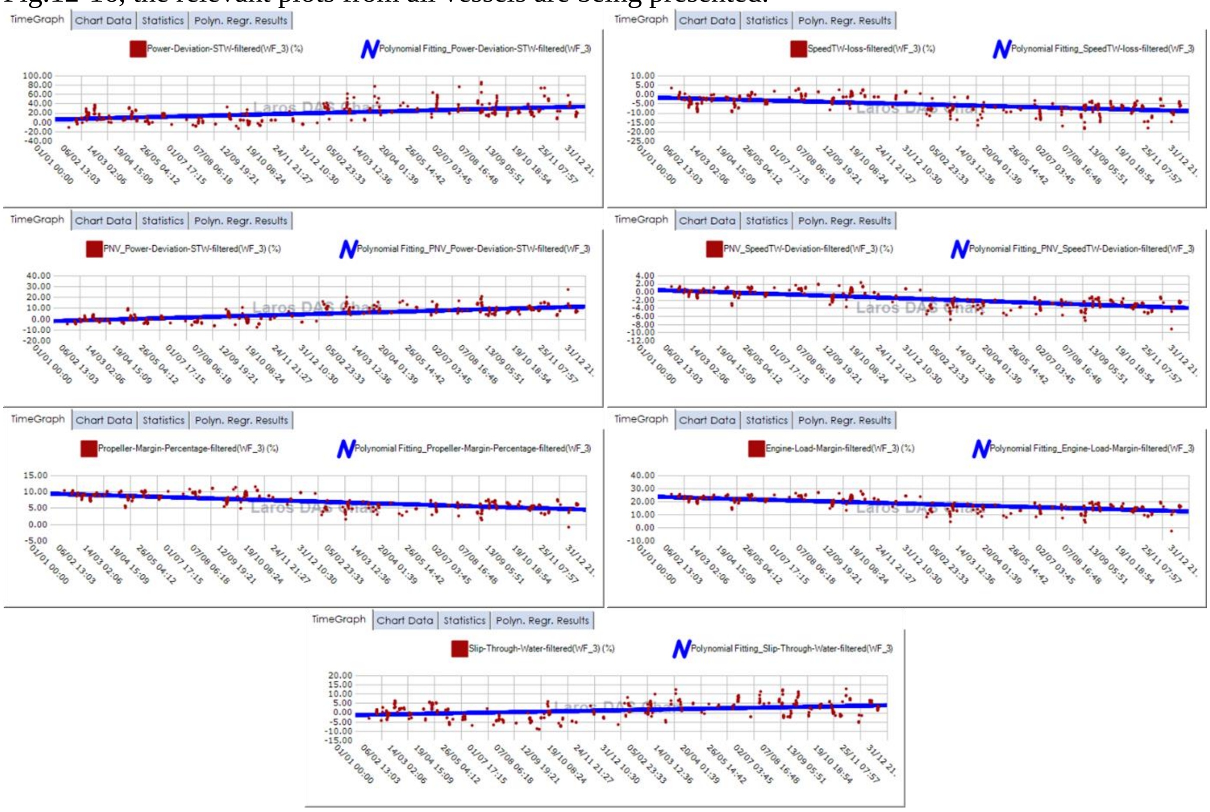

Fig.12: Indicators of Coastal Tanker #1

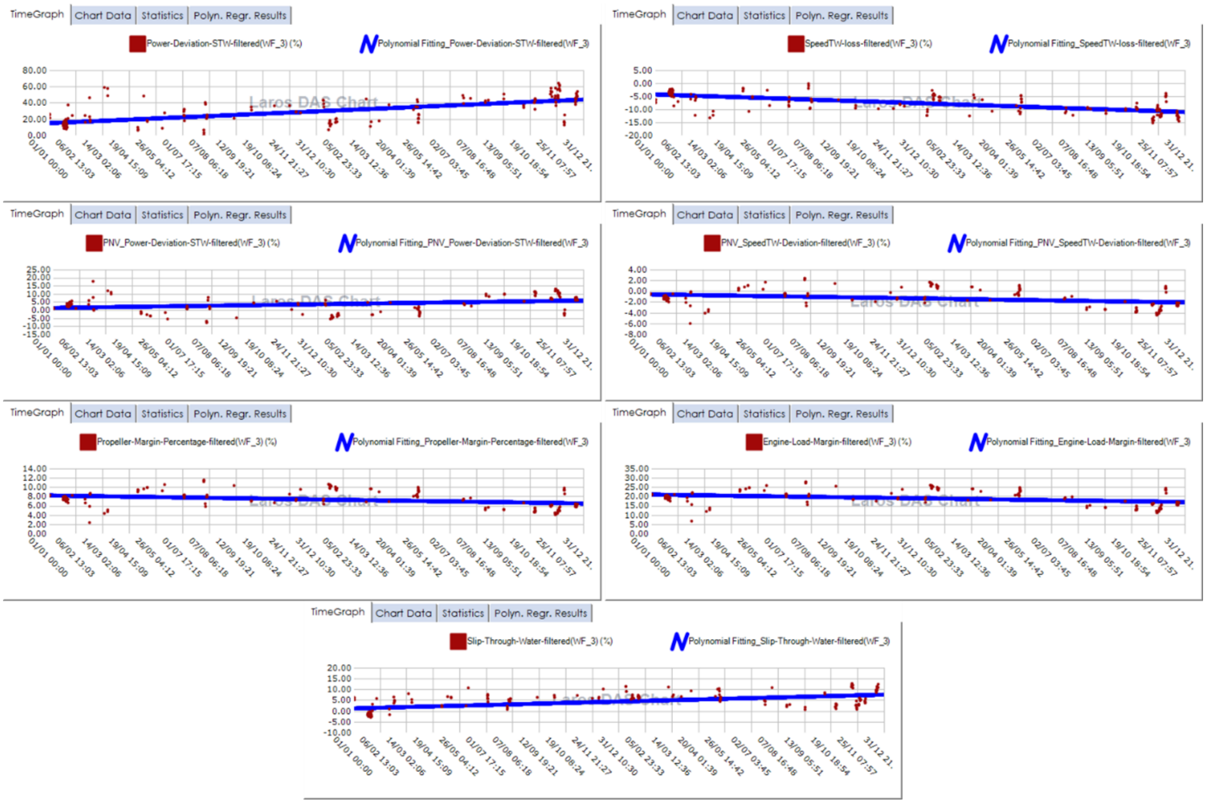

Fig.13: Indicators of Coastal Tanker #2

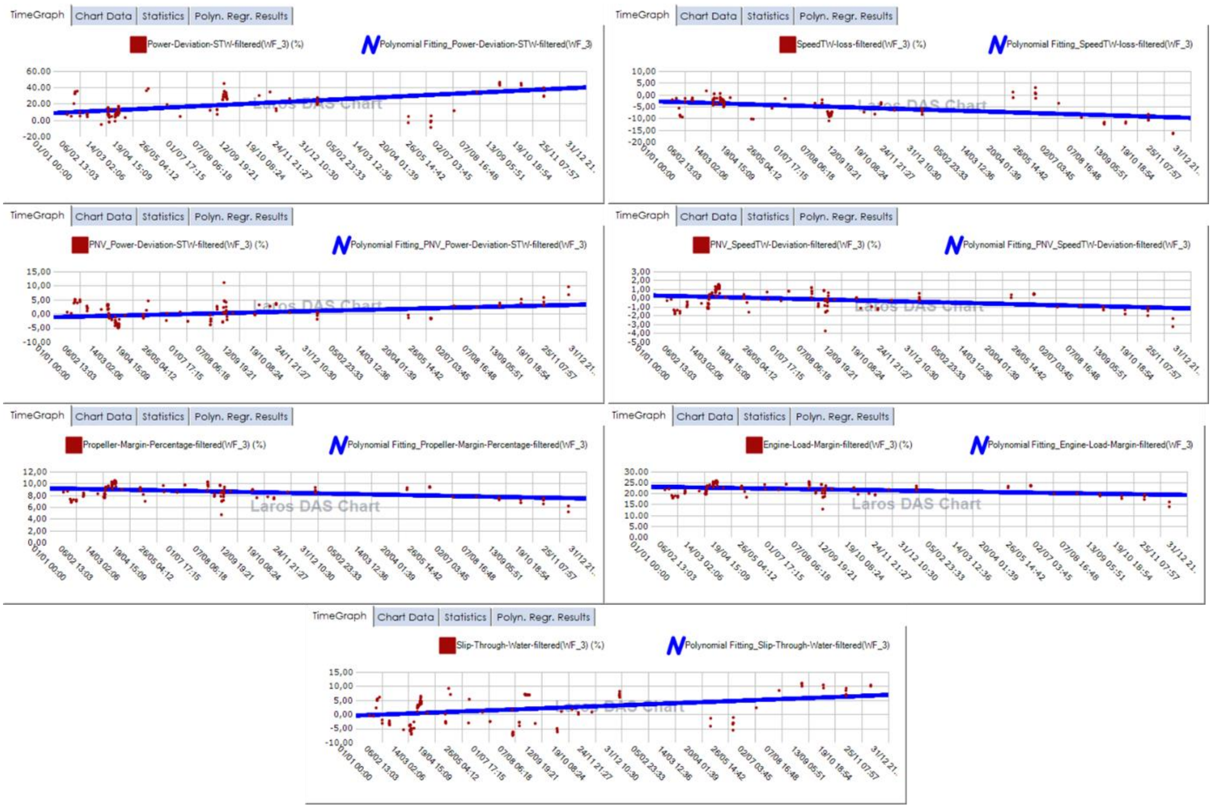

Fig.14: Indicators of Coastal Tanker #3

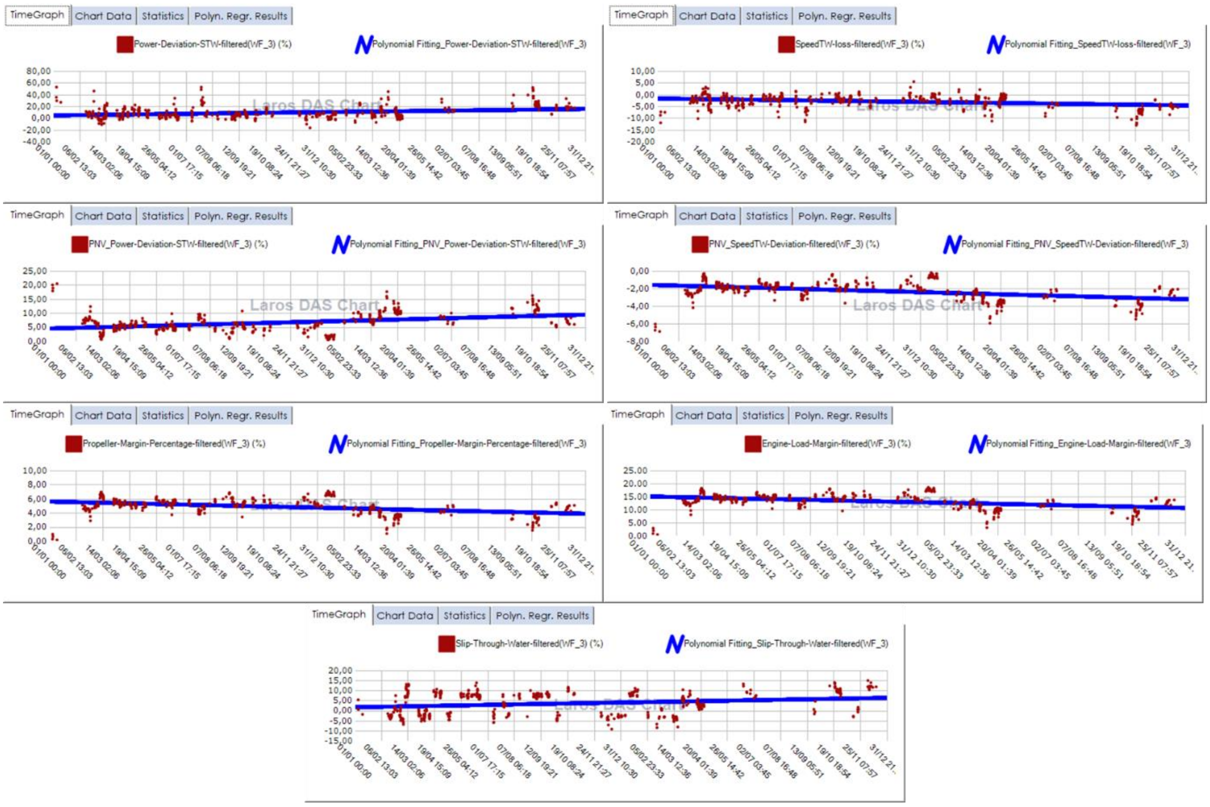

Fig.15: Indicators of Suezmax

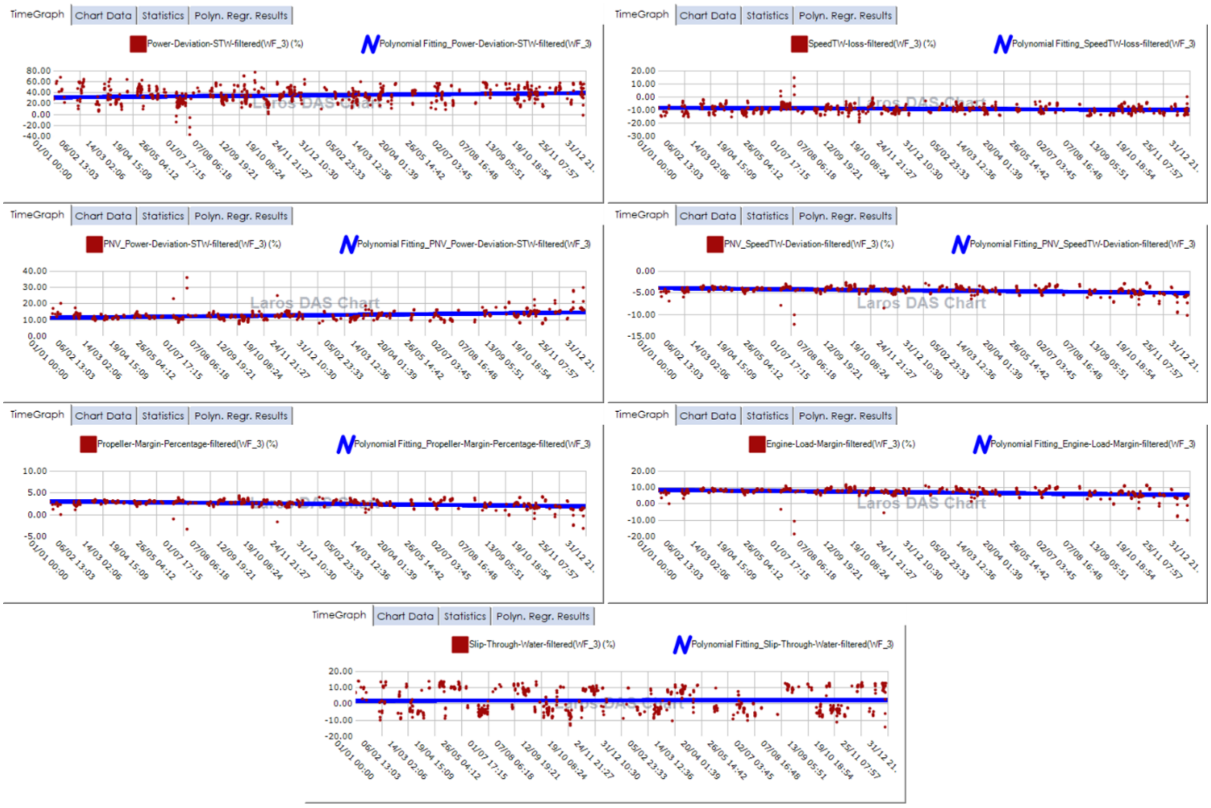

Fig.16: Indicators of VLCC

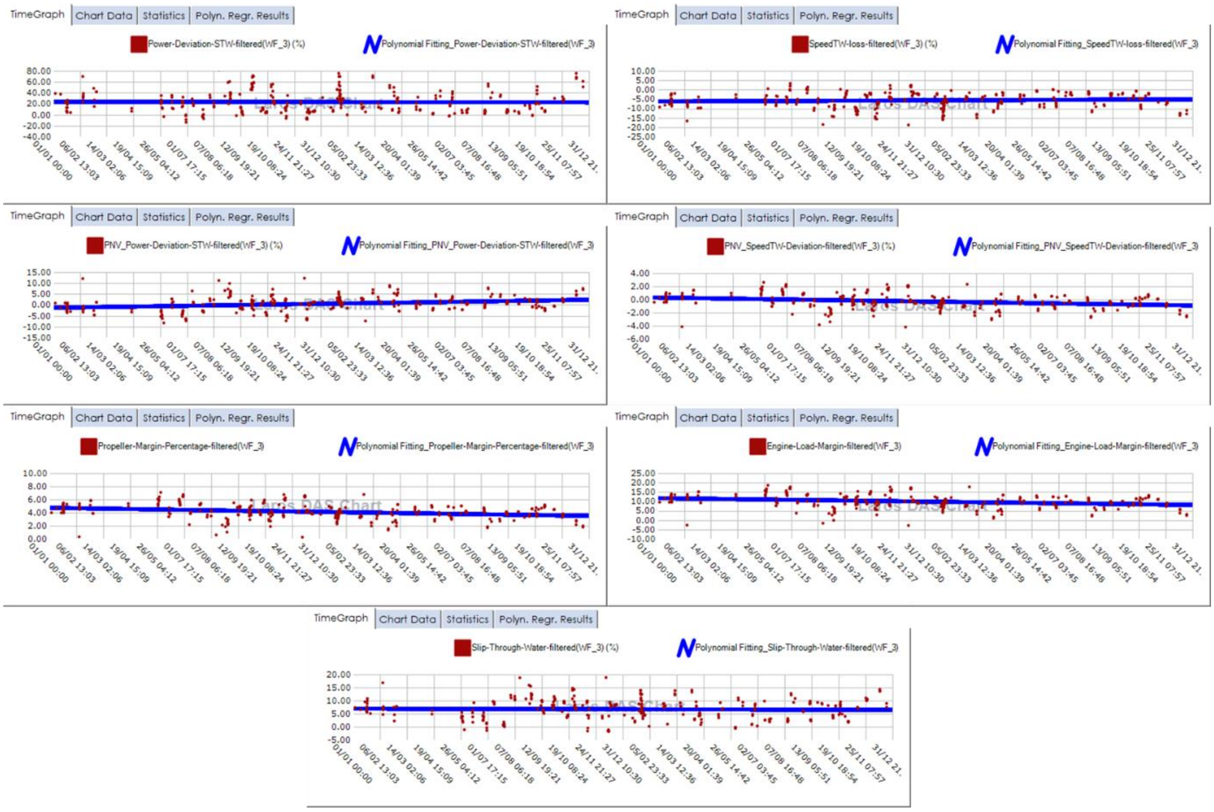

Fig.17: Indicators of Kamsarmax #1 (irregular ISO Indicators)

4.4. Irregular values

During the validity check, in one vessel (Kamsarmax #1) was noticed that the ISO Indicators have not the expected values. More specific both ISO Indicators were showing an improvement of vessel's performance through time, while all other indicators were showing a deterioration of vessel's performance, which was the expected. After contacting the company and check the accuracy of the draft measurements, it was verified that indeed often the draft sensors were malfunctioning, even since the first day of vessel's delivery. Fig.17 shows the exported time graphs with the relevant trendlines from the specific vessel.

For the second Kamsarmax vessel, it was noticed that all indicators had irregular outcomes. ISO indicators were showing an improvement of vessel's performance, similar though to the outcomes of the Combined Power (P)/RPM (N)/Speed (V) analysis. Increasing Propeller margin indicators, increasing Engine margin indicator, stable slip. After contacting the shipping company, it was verified that for the specific vessel, since her delivery, often several equipment were malfunctioning, so the measurements for both shaft power and speed through water were inaccurate. Fig.18 shows the plots with the relevant trendlines from all indicators for the specific vessel.

4.5. Irregular values – Second case

The selected Panamax vessel for the examined period had a dry dock. Before the dry dock, due to the condition of the vessel, many equipment were malfunctioning (torque meter, speed log, etc), so no accurate data could be collected. During the dry dock repairs, all equipment necessary for the data collection were serviced and repaired. On the specific vessel, the draft measurements were entering manual into the system through the AIS data, but they were also examined from shipping company's personnel for their accuracy. The analysis was divided into two time periods. Before the dry dock and after the dry dock. As it can be seen in the relative time graphs, Fig.19, all indicators before the dry dock had irregular values, while after the dry dock, all of them were consistent.

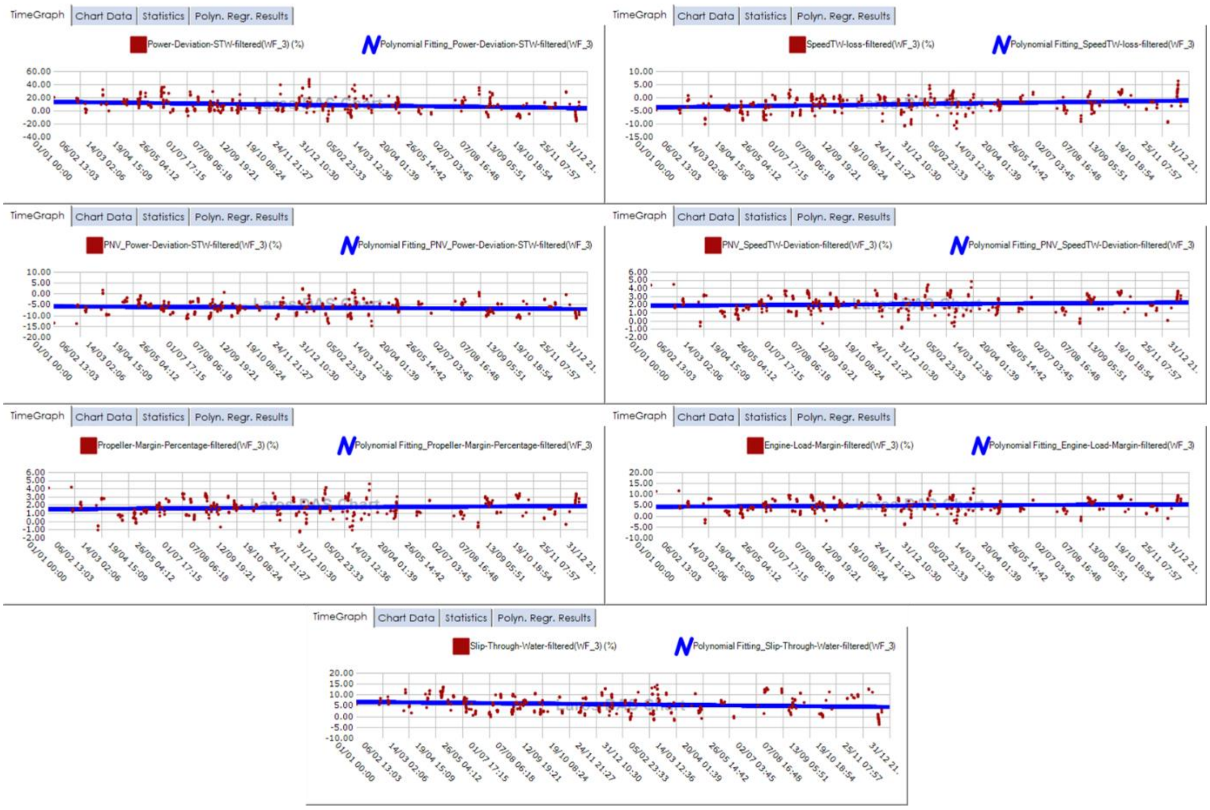

Fig.18: Indicators of Kamsarmax #2 (irregular all Indicators)

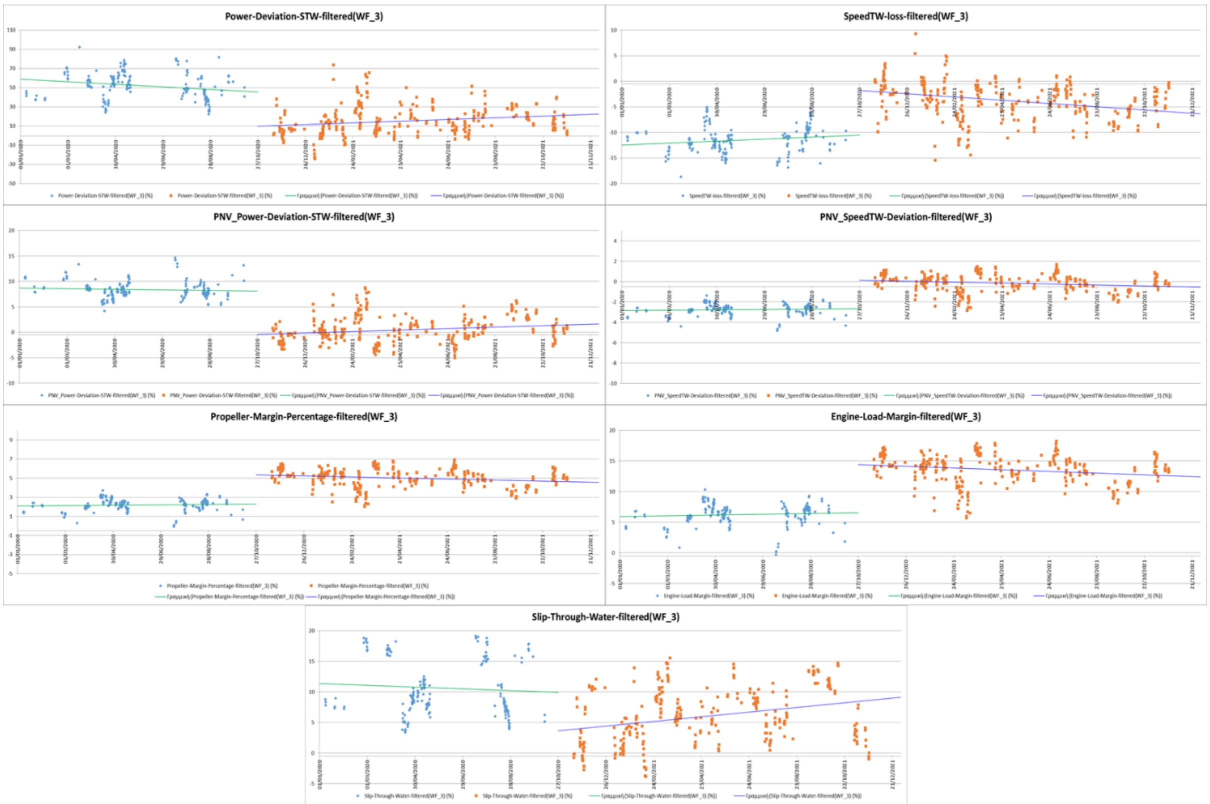

Fig.19: Indicators of Panamax (before & after dry dock)

5. Conclusions

After analyzing all the above, below conclusion can be derived.

1. In order to have accurate calculations for the suggested ISO indicators, it is required to have accurate draft measurements. Often though, the relevant sensors are not operating correctly, so – especially for older vessels – the calculations of these indicators through a HFDCS are not providing accurate indications for the performance of the vessel.
2. The Propeller Margin and the Engine Margin are independent from vessel's draft and may provide indications regarding the performance of the vessel, but they are also independent from vessel's speed.
3. Vessel's slip is independent from vessel's draft and may provide indications regarding vessel's performance, but it is also independent from shaft power.
4. The Combined Power (P)/RPM (N)/Speed (V) analysis for performance deviation is independent from vessel's draft measurements, while at the same time it takes under consideration all three basic parameters (power, speed, rpm) and it provides similar conclusions to the ISO suggested indicators. A HFDCS can easily calculate these indicators and depending the selected baseline, accurate conclusions regarding vessel's performance can be derived, so these indicators can be considered as alternative to ISO suggested, especially for vessels where drafts are not known.

From all the above it can be concluded that, the two basic indicators suggested by ISO 19030 – Power Deviation & Speed Loss – are not unique for monitoring vessel's performance. Alternative indicators can be use in order to have similar or even better/more accurate conclusions.

References

ISO 19030-1 (2016), *Ships and marine technology – Measurement of changes in hull and propeller performance*, Int. Standard Org., Geneva

A Case Study Approach on CII Rating: Understanding the Role of Annual Sailing Activity and Operational Speeds

Maria G.N. Tsompanoglou, Pantheon Tankers & Alpha Bulkers, Athens/Greece, performance@pantheontankers.com, performance@alphabulkers.com

Abstract

The IMO MEPC76 introduced a new emissions reduction requirement, which is to come into force in 2023, the Carbon Intensity Indicator (CII), which classifies vessels based on their factual carbon emissions in relation to the distance sailed. Given the dynamic character of the new indicator, this paper deals with the vessel service speed and operating parameters as contributing factors to CII changes and investigates the possibility of drastic CII improvements by appropriately regulating these parameters. This paper also incorporates certain operating scenarios in an attempt to outline best CII monitoring routines and their applicability on commercial decisions.

1. Introduction

In July 2011, IMO adopted mandatory measures to improve the energy efficiency of international shipping. Since then, IMO have imposed several measures on energy efficiency, forming the first global mandatory and legally binding GHG-reduction regime for the international industry sector. The culmination of IMO's effort towards shipping decarbonization takes place ten years after the first efforts, with the enforcement of the Energy Efficiency Index for Existing Ships (EEXI) and the Carbon Intensity Indicator (CII) as environmental performance indices, both enacted within IMO's 76th Marine Environment Protection Committee in July 2021 and taking effect as of January 2023.

The two new emissions reduction requirements, share the same calculation rule where the vessel's total carbon emissions are divided by vessel's transportation work, the latter expressed as the DWT capacity multiplied by the distance sailed. The main difference between the two indicators lies in the fact that the EEXI utilizes the design characteristics of the vessel and must fall below a specific max threshold level. In contrast, the CII is related with the factual carbon emissions and sailing distance over a year and classifies vessels in environmental categories ranging from level A for the most environmental-efficient vessels to level E indicating the worst polluters, each category having certain boundaries. Furthermore, while the compliance with the EEXI limit is to be satisfied once in a rather irreversible way, the observance of the acceptable CII ratings requires continuous monitoring tailored to both freight market requirements and ship's physical condition. In this paper, we focus mainly on the CII rating and the parameters affecting it.

A compliant CII rating is either A, B, or C and corrective actions are needed if a vessel receives D for three consecutive years or E for one year. IMO do not stipulate penalties for a low CII rating. According to MEPC 76, ships rated D or E will have to submit a plan for corrective action, however, if the CII improvement plan is not followed, there is no provision for penalization as the correction plan is not subject to rules and requirements. Nonetheless, a satisfactory CII rating may be attractive for the charterers, thus important commercially-wise, which should incentivize Owners into putting efforts and capital to improve the fleet operational and design performance, *Psaraftis (2021)*. Furthermore, financing stakeholders exert great interest in emissions performance within a certain threshold, and therefore a poor environmental rating could negatively influence Owner's access to capital, making the ever-going improvement of fleet efficiency a business-critical procedure and a vessel's emissions performance a contract differentiator, *DNV (2020)*.

To date, neither charter nor vessel's resale prices reflect the economic benefit of fuel saving offered by an energy efficient vessel. This is gradually changing however, as the high-energy-efficient ships are better described to charterers in terms of speed-consumption ratio, thus achieving higher fares. It is already clear, therefore, that the future of charters will include and cover the issue of ship's energy efficiency, not only in relation to ship's construction (via EEDI for the newbuilding vessels and EEXI for the existing ones) but also to its commercial operation over time via CII rating.

Being directly calculated from the actual operating parameters of the ship, the CII rating constitutes a completely dynamic scheme of environmental classification with quite unexpected outcomes in many instances. Vessel evaluations based on CII may present noteworthy contradictions such as poor scores for new or relatively young ships incorporating advanced technological features, and high scores for older vessels with conventional hull design and propulsion. These inconsistencies confirm the fundamental principle of this indicator that voyage operational characteristics (e.g. speed, route, ambient conditions, draft, etc.) are stronger influencing factors than the vessel's technical characteristics (e.g. hull design, propulsion technology, energy saving technologies, etc.), *Poulsen et al. (2022)*. This ascertainment raises reasonable questioning whether ship management companies could act proactively in voyage planning to maintain a satisfactory index, what are the degrees of freedom with regards to the commercial decisions and whether there are pertinent lessons to be learned from the CII results of recent years.

Boosting fleet overall performance with energy-saving technologies to ensure a high attained CII score is not always a practicable or realistic solution: specific hull designs do not offer the option to install an energy efficiency device, whereas quite a few energy efficiency technologies are currently very expensive, with poor Internal Rate of Return (IRR), or complicated in their installation, and therefore prohibitive for ships of certain age and/or size. The issue has been examined by many experts in maritime business, *Rehmatulla and Smith (2015)* and the basic outcome is that among the measures with the most significant emissions abatement potential, speed reduction stands out together with alternative fuels and hull shape optimization, *Oliveira et al. (2022)*.

The CII definition suggests that speed reduction is the easiest approach for compliance within the acceptable band limits, because the lower the speeds the lower the consumptions and emissions. Many maritime technology experts also point to speed limitation as a way for the reduction of fuel emissions, however, speed reduction as key solution to mitigate emissions has been challenged by many researchers, *Psaraftis and Kontovas (2013), Walsh et al. (2017), Psaraftis (2019)*, especially in relation to the optimal speed that maximizes the Time Charter Equivalent (TCE) of a voyage charter i.e. the average earnings of a vessel net of voyage-related costs, *Adland and Jia (2016).*

Undoubtedly, a vessel's operating speed determines emissions level to a major extent, but it is heavily susceptible to commercial drivers (e.g. freight rates) rather than to vessels design and technical characteristics. That means certain market conditions may lead to operational speed increase and consequently fuel consumption along with higher emissions, which evidently brings about a major turbulence in emission intensity achieved up to that point, *IMO (2012,2020).*

In a market that requires high speeds and offers respectively high freight rates, speed reduction as main solution for satisfying CII regulation may not be feasible. If the market experiences an ongoing upturn of freight rates, speed will inevitably increase to follow the market demand, *Changa et al. (2019), Poulsen et al. (2022)*. In such case, Owners would need to adjust their fleet speed profile to benefit from the higher freight rates while at the same time comply with the CII regulatory requirements. To keep the scales tilting equally between revenue and environmental conformity, it is important for the operator to know the margins for CII compliance in the event that a fleet would need to accelerate.

Many studies conducted to determine the CII influencing factors use assumptions on voyage characteristics that are often not representative of the freight market conditions nor realistic with regards to the actual sailing profile of a fleet. As such, these studies cannot assist the operator to decide the appropriate vessel operating speed, in order to maintain a high revenue and a superior CII score at the same time.

Based on observations from actual voyage profiles of typical tankers and bulk carriers of large capacities, this paper attempts to take a broad perspective and, if possible, draw practical inferences, on how the vessel's yearly sailing and idling periods, as well as its operating speeds, affect its CII rating.

2. Methodology

This work is focused on the voyage charter – time charter constitutes a separate area of research on the subject – and comprises of two parts. The first part is a brief comparison of CII percentage changes between years 2020 and 2021 for a sample of vessels, with the purpose to identify correlations between CII fluctuations and fluctuations of the parameters participating in CII calculation. The second part investigates the CII Rating changes in relation to different combinations of vessel operating speeds and sailing activities in ballast and laden condition over a year, in an attempt to connect the commercial performance of the vessel with its environmental performance.

2.1. Vessel selection and data source

With regards to the first part of this paper, sample vessels are tankers and bulk carriers trading worldwide, aged about or over 10 years, with conventional propulsion machinery (2-stroke mechanically-controlled engines) and not retrofitted with energy efficiency technologies. The main criteria for choosing the vessels' sample were their age and expected remaining trading life. The rationale behind this selection was that ships of conventional design and propulsion technology are not usually Owners' primary selection when it comes to decisions on energy efficiency investments. The vessels of this age are still highly profitable to justify their removal from fleet by resale or scrapping, but not young enough to attract an expensive investment for retrofitting energy efficiency technologies. Very often, these ships are not prominent candidates for such expensive modifications and so their energy efficiency and emissions performance (CII) is more challenging as it depends upon the proper voyage planning and execution.

The sample vessels of this work are tankers and bulk carriers that bear similarities with reference to time since last dry/dock and did not face particular issues of underperformance due to hull/propeller fouling or main engine underperformance during the years 2020 and 2021, Table I.

Table I: Sample vessels

Vessel Type	Vessel Size	No of Vessels	Age of Vessel
Tankers	VLCC	3	9 – 13 years
	Suezmax	5	13 – 18 years
	Aframax	1	15 years
Bulk Carriers	Capesize	9	11-15 years
	Kamsarmax	5	10-15 years

In this part, the research model uses the CII results based on the aggregated IMO DCS annual voyage data of the years 2020 & 2021. Actual CII values and ratings are out of the present paper purposes, and the paper solely focuses on the percentage changes of the CII indicator in relation to the percentage changes of the parameters included in CII calculation formula.

With regards to the second part, the reference vessel is one of the Suezmax tankers, 13 years old, with 158,270 tdw. The vessel's speed-consumption curves were derived from the vessel's model tests results and adjusted with the results of sea trials. In addition, results of dedicated in-service speed tests, as well as combined noon report data and high-frequency digital data, were incorporated to increase the curves' reliability. Although some inaccuracies cannot ruled out, the daily monitoring of vessel's performance based on these reference curves provides a high level of confidence that the curves represent satisfactorily the vessel's expected sailing consumptions at different operating speeds and drafts.

2.2. Part I: CII %change per vessel 2020-2021

In the first part of this paper, an attempt is made, without delving into the components involved in the calculation of CII, to observe how the CII changes in relation to the main variables of an annual vessel operation. This approach, although simple, may indicate obvious features of the indicator.

Table II compares the relative changes of CII 2021 compared to CII 2020 are correlated with the respective relative changes of the CII variables, namely the hours in "Port" (not-sailing time), the hours sailing in ballast and laden, the total annual fuel oil consumption (FOC) and the ballast and laden speeds.

Table II: CII 2021 % change compared to CII 2020

Sample	$\%\Delta CII_{2021}$	Modes (hours)			FOC_{TOTAL}	Speed	
		Port	Ballast	Laden		V_B	V_L
TK1	-2.3%	-5.0%	+11.7%	-6.5%	-5.4%	-7.8%	-2.3%
TK2	+1.4%	+2.9%	-22.8%	+23.7%	-1.6%	-8.8%	+1.7%
TK3	-5.8%	-33.8%	+3.5%	+20.5%	-7.3%	-23.4%	-1.7%
TK4	+11.0%	174.9%	-29.5%	-6.5%	-13.6%	-3.8%	-5.7%
TK5	+6.2%	-59.4%	+36.0%	+18.1%	+24.5%	-8.6%	-5.2%
TK6	+5.3%	-52.0%	+66.4%	+6.7%	+63.5%	+65.8%	+32.0%
TK7	-0.9%	+38.3%	-0.8%	-11.7%	-13.9%	-15.5%	+1.4%
TK8	+4.5%	+12.4%	-4.5%	-3.9%	-11.1%	-21.3%	-1.9%
TK9	+17.1%	+34.4%	-7.1%	-22.4%	-15.1%	-22.1%	-6.6%
BC1	+4.9%	-20.1%	+20.1%	-0.1%	+11.6%	+2.2%	-6.2%
BC2	+17.9%	+6.6%	-4.2%	-2.2%	+14.9%	-0.7%	+1.2%
BC3	+6.7%	+0.2%	-12.9%	+9.4%	+15.0%	+10.3%	+6.9%
BC4	-1.0%	+90.6%	-39.5%	-20.0%	-24.0%	+10.4%	+7.0%
BC5	+5.5%	-15.3%	-30.3%	+39.8%	+22.5%	+2.0%	+11.6%
BC6	+15.4%	+25.8%	-18.8%	-1.7%	+12.1%	+5.1%	+10.7%
BC7	+2.7%	+164.3%	-6.2%	-30.2%	-15.7%	-3.2%	+6.2%
BC8	+7.6%	-16.2%	+27.2%	-6.1%	+20.4%	-0.4%	+10.4%
BC9	-4.7%	-5.1%	-4%	+13.5%	-9.0%	+1.3%	-17.6%
BC10	-6.2%	+32.0%	-16.2%	-10.6%	-15.8%	+2.3%	+5.4%
BC11	+7.1%	-16.1%	+6.9%	+10.0%	+29.5%	+9.7%	+13%
BC12	-2.7%	+26.1%	-2%	-18.6%	-10.4%	+1.9%	+4.1%
BC13	+4.3%	+66.0%	-20.1%	-30.6%	-21.8%	+1.1%	+0.3%
BC14	+14.3%	+83.9%	-41.2%	-4.0%	-7.0%	+2.1%	+11.9%

By means of comparisons between the two consecutive years, the results presented in Table II indicate some noticeable correlations, as follows:

1. Increased port (non-sailing) time relates to increased CII (TK4, TK5, TK9, BC6, BC14)
2. Decreased activity in laden seems to counterbalance the negative effect of increased port time on CII, (TK7, BC4, BC7, BC12, BC13)
3. High total sailing activity with higher share in ballast seems to counterbalance the negative effects of increased speeds, thus consumptions, on CII (TK6, BC8)
4. Increased sailing time in laden, even at increased speeds, do not affect CII remarkably if the annual sailing activity is high (TK3, BC5)
5. Fuel consumption increase as result of an increased sailing activity does not seem to decisively affect CII (TK5, TK6, BC5, BC11).

The identified correlations derived from the CII percentage changes between two continuous calendar years are in line with some general conclusions that have emerged so far from studies on the nature of the CII indicator, stating among others that, ballast voyages and lower speeds favor the indicator. In addition, some interesting observations emerge with respect to the impact of the vessel's sailing activity. The second part of this paper sheds more light on these conclusions.

2.3. Part II: CII Rating Matrix

The second part of this work investigates the CII changes in relation to combinations of total sailing time over a year and its distribution in ballast and laden condition, as well as vessel operating speeds. As already mentioned, the sample vessel is a Suezmax tanker, 13 years old, with 158,270 tdw.

Vessel's annual operation is distinguished in "Sailing" and "Not Sailing" modes. "Sailing" mode relates to the time of main engine in operation, with vessel sailing in either ballast or laden condition. "Not sailing" mode is the time when main engine is stopped, and involves the port activities, including cargo operations, idling, anchorage, maneuvering and drifting conditions. For simplicity purposes, the "Not Sailing" mode is identified in this work as "Port".

The following assumptions are made to simplify the annual CII calculation:

- Vessel consumes Light Low Sulphur Fuel Oil (LSFO) at the "Sailing" mode and Marine Gas Oil (MGO) at the "Port" mode.
- Laden voyages are performed at design draft and ballast voyages at the normal ballast draft. No intermediate drafts (partial laden and/or heavy ballast) have been taken into account in the calculations.
- The total consumption in sailing includes the consumption of main engine and aux diesel generators only; no other consumption, i.e. for cargo heating, incineration, etc., is included.
- Vessel is trading worldwide, therefore, the average annual wind/sea conditions have been taken to correspond roughly to Wind Beaufort Scale 5, Sea State 4 (wave height 1.25 to 2.5 m) and swell 2 m. The ballast and laden fuel consumptions versus speeds is based on these weather characteristics and have also been incremented by 5% to consider any additional unforeseen sailing consumption during the year.

Based on the assumptions outlined above, the CII calculation is given by Eq.(1).

$$\mathrm{CII} = \frac{\mathrm{C_{LSFO}} * \mathrm{FOC_{SAILING}} + \mathrm{C_{MGO}} * \mathrm{FOC_{PORT/IDLE}}}{\mathrm{DWT} * \mathrm{NM}} \qquad (1)$$

Where DWT = 158,270 tdw

$\mathrm{C_{LSFO}} = 3.151\ \frac{\mathrm{mt{-}CO_2}}{\mathrm{mt{-}LSFO}}$ (Carbon content of LSFO)

$\mathrm{C_{MGO}} = 3{,}206\frac{\mathrm{mt{-}CO_2}}{\mathrm{mt{-}MGO}}$ (Carbon content of MGO)

$\mathrm{FOC_{SAILING}} = \mathrm{FOC_{B-ANNUAL}} + \mathrm{FOC_{L-ANNUAL}}$ (2)

$\mathrm{FOC_B/FOC_{L-ANNUAL}}$: the annual total sailing consumptions in ballast/laden mode respectively

$\mathrm{FOC_{PORT/IDLE}}$: the fuel consumption during "Port" (not-sailing) activities, which results by an average fuel consumption in mt/h multiplied with the "Port" time represented as $\mathrm{HRS_{PORT}}$. The average "Port" fuel consumption in mt/h has been derived from the actual annual not-sailing consumptions of the five sample Suezmax tankers used in this work and equals to about 0.7t/h. $\mathrm{FOC_{PORT/IDLE}}$ equals then to 0.7t/h multiplied by the $\mathrm{HRS_{PORT}}$.

NM : nautical miles travelled, equal to $\mathrm{V_B} * \mathrm{HRS_B} + \mathrm{V_L} * \mathrm{HRS_L}$,

V_B is the ballast speed,

V_L is the laden speed, and

HRS_B, HRS_L the hours sailing in ballast and in laden correspondingly.

Based on the above definitions, CII equation is formulated as follows:

$$\mathrm{CII} = \frac{3.151 * (\mathrm{FOC_{B-ANNUAL}} + \mathrm{FOC_{L-ANNUAL}}) + 3.206 * 0.7 * \mathrm{HRS_{PORT}}}{158{,}270 * (\mathrm{V_B} * \mathrm{HRS_B} + \mathrm{V_L} * \mathrm{HRS_L})} \qquad (1a)$$

or,

$$\mathrm{CII} = \frac{3.151 * (\mathrm{HRS_B} * \mathrm{FOC_B} + \mathrm{HRS_L} * \mathrm{FOC_L}) + 3.206 * 0.7 * \mathrm{HRS_{PORT}}}{158{,}270 * (\mathrm{V_B} * \mathrm{HRS_B} + \mathrm{V_L} * \mathrm{HRS_L})} \qquad (1b)$$

Eq.(1b) outlines CII as function of three variables: i) fuel consumption at the numerator, ii) vessel's speed at the denominator, and iii) sailing activity modes over a year at both sections of the fraction.

Fuel consumption is a function of vessel's speed. Propulsion law reveals that fuel consumption is proportional to vessel's speed to the power of three, known as "cubic law", however, service results indicate that the relation between fuel consumption and vessel's speed is dependent on the speed itself and the "cubic law" applies only near the vessel's design speed, whereas in the lower speed range, where ships mostly operate, fuel consumption is proportional to speed to a power lower than 3, *Adland et al. (2020)*.

Actual voyage data of sailing fuel consumptions and operating speeds of the sample Suezmax tanker and fuel consumption-speed curves adjustment as described in Section 1, indicate that the connection of total fuel consumption with operating speed of this specific vessel is proportional to a power between 2 and 3 as indicated in the following equations, which give total sailing consumption is t/h:

$$\mathrm{FOC_B} = 0.001363 * \mathrm{V_B}^{2.7961} \qquad (3)$$

$$\mathrm{FOC_L} = 0.004633 * \mathrm{V_L}^{2.4252} \qquad (4)$$

By replacing in Eq.(1b) the Eqs.(3) & (4) then three parameters remain in the CII fraction: operating speeds $\mathrm{V_B}$, $\mathrm{V_L}$ in knots, sailing hours$\mathrm{HRS_B}$, $\mathrm{HRS_L}$ in ballast and laden modes and non-sailing/idle hours $\mathrm{HRS_{PORT}}$.

$$\mathrm{CII} = \frac{3.151 * \left(\mathrm{HRS_B} * 0.001363 * \mathrm{V_B}^{2.7961} + \mathrm{HRS_L} * 0.004633 * \mathrm{V_L}^{2.4252}\right) + 3.206 * 0.7 * \mathrm{HRS_{PORT}}}{158{,}270 * (\mathrm{V_B} * \mathrm{HRS_B} + \mathrm{V_L} * \mathrm{HRS_L})} \qquad (1c)$$

Eq.(1c) is applied in six different sailing activity scenarios over the course of a year to give insight on how the combination of ballast and laden speeds and not-sailing time affects CII rating. The six scenarios illustrate different possible cases of annual ship operation and all scenarios reflect possible market activities of the tanker sector.

Scenarios as described below are summarized in Table III:

- Scenario 1: high sailing activity, equally distributed to ballast & laden legs
- Scenario 2: low sailing activity, equally distributed to ballast & laden legs
- Scenario 3: high sailing activity, ballast activity < laden activity
- Scenario 4: high sailing activity, ballast activity > laden activity
- Scenario 5: low sailing activity, ballast activity < laden activity
- Scenario 6: low sailing activity, ballast activity > laden activity

Table III: Annual Operational Scenarios

Scenario No	Annual Sailing Activity		Ballast mode		Laden mode			Port/idle
	(%)	(hrs)	(%)	(hrs)	(%)	(hrs)	(%)	(hrs)
1	80	7008	50	3504	50	3504	20	1752
2	60	5256	50	2628	50	2628	40	3504
3	80	7008	30	2102	70	4906	20	1752
4	80	7008	70	4906	30	2102	20	1752
5	60	5256	30	1577	70	3679	40	3504
6	60	5256	70	3679	30	1577	40	3504

For each scenario, CII equation is formulated as follows:

Scenario 1 (80% B50 L50):

$$\mathrm{CII} = \frac{\left(\mathrm{V_B^{2.7961}} + 3.3991 * \mathrm{V_L^{2.4252}}\right) + 261.2687}{36851429.8527 * (\mathrm{V_B} + \mathrm{V_L})} \qquad (Sc1)$$

Scenario 2 (60% B50 L50):

$$\mathrm{CII} = \frac{\left(\mathrm{V_B^{2.7961}} + 3.3991 * \mathrm{V_L^{2.4252}}\right) + 696.7164}{36851429.8527 * (\mathrm{V_B} + \mathrm{V_L})} \qquad (Sc2)$$

Scenario 3 (80% B30 L70):

$$\mathrm{CII} = \frac{\left(\mathrm{V_B^{2.7961}} + 7.9334 * \mathrm{V_L^{2.4252}}\right) + 435.5306}{36851429.8527 * \mathrm{V_B} + 86010045.1272 * \mathrm{V_L}} \qquad (Sc3)$$

Scenario 4 (80% B70 L30):

$$\mathrm{CII} = \frac{\left(\mathrm{V_B^{2.7961}} + 1.4561 * \mathrm{V_L^{2.4252}}\right) + 186.6052}{36851429.8527 * \mathrm{V_B} + 15789177.6499 * \mathrm{V_L}} \qquad (Sc4)$$

Scenario 5 (60% B30 L70):

$$\mathrm{CII} = \frac{\left(\mathrm{V_B^{2.7961}} + 7.9298 * \mathrm{V_L^{2.4252}}\right) + 1161.0467}{36851429.8527 * \mathrm{V_B} + 85971090.9500 * \mathrm{V_L}} \qquad (Sc5)$$

Scenario 6 (60% B70 L30):

$$\mathrm{CII} = \frac{\left(\mathrm{V_B^{2.7961}} + 1.4570 * \mathrm{V_L^{2.4252}}\right) + 497.6816}{36851429.8527 * \mathrm{V_B} + 15796331.8504 * \mathrm{V_L}} \qquad (Sc6)$$

By using the aforementioned equations, a CII Rating Matrix is plotted for each scenario with combinations of laden and ballast speeds. CII versus V_L curves for constant V_B speeds are plotted, depicting how the variance of laden speeds affects CII Rating for different constant V_B options. The (CII, V_L) curves are polynomials of 3rd degree.

The CII Rating Matrices are shown in Tables IV to IX. The (CII, V_L) curves are shown in Figs.1-6.

Note that CII limits change every year, however, for illustration purposes we will use specific figures; as such, the CII ratings are based on the 2024 CII limits.

Table IV: CII Matrix Scenario 1, 80% sailing activity, ballast = laden

	VB8	VB9	VB10	VB11	VB12	VB13	VB14	VB14.5
VL8.0	A	A	A	A	A	B	B	C
VL8.5	A	A	A	A	A	B	B	C
VL9.0	A	A	A	A	A	B	B	C
VL9.5	A	A	A	A	A	B	C	C
VL10.0	A	A	A	A	B	B	C	C
VL10.5	A	A	A	A	B	B	C	C
VL11.0	A	A	A	B	B	B	C	C
VL11.5	A	A	B	B	B	C	C	C
VL12.0	B	B	B	B	C	C	C	C
VL12.5	B	B	B	B	C	C	C	D
VL13.0	B	B	C	C	C	C	D	D
VL13.5	C	C	C	C	C	C	D	D
VL14.0	C	C	C	C	C	D	D	D
VL14.5	C	C	C	C	D	D	D	D
VL15.0	D	D	D	D	D	D	D	D

Table V: CII Matrix Scenario 2, 60% sailing activity, ballast = laden

	VB8	VB9	VB10	VB11	VB12	VB13	VB14	VB14.5
VL8.0	A	A	B	B	C	C	C	D
VL8.5	B	B	B	B	C	C	C	D
VL9.0	B	B	B	B	C	C	C	D
VL9.5	B	B	B	C	C	C	D	D
VL10.0	B	B	B	C	C	C	D	D
VL10.5	B	B	C	C	C	C	D	D
VL11.0	C	C	C	C	C	D	D	D
VL11.5	C	C	C	C	C	D	D	D
VL12.0	C	C	C	C	D	D	D	D
VL12.5	C	C	C	C	D	D	D	D
VL13.0	C	C	D	D	D	D	D	D
VL13.5	D	D	D	D	D	D	D	D
VL14.0	D	D	D	D	D	D	E	E
VL14.5	D	D	D	D	D	D	E	E
VL15.0	D	D	D	D	D	E	E	E

Table VI: CII Matrix Scenario 3, 80% sailing activity, ballast < laden

	VB8	VB9	VB10	VB11	VB12	VB13	VB14	VB14.5
VL8.0	A	A	A	A	A	A	B	B
VL8.5	A	A	A	A	A	A	B	B
VL9.0	A	A	A	A	A	A	B	B
VL9.5	A	A	A	A	A	B	B	B
VL10.0	A	A	A	A	B	B	B	C
VL10.5	A	A	B	B	B	B	C	C
VL11.0	B	B	B	B	B	C	C	C
VL11.5	B	B	B	B	C	C	C	C
VL12.0	B	C	C	C	C	C	C	C
VL12.5	C	C	C	C	C	C	D	D
VL13.0	C	C	C	C	C	D	D	D
VL13.5	C	C	D	D	D	D	D	D
VL14.0	D	D	D	D	D	D	D	D
VL14.5	D	D	D	D	D	D	D	D
VL15.0	D	D	D	D	D	D	E	E

Table VII: CII Matrix Scenario 4, 80% sailing activity, ballast > laden

	VB8	VB9	VB10	VB11	VB12	VB13	VB14	VB14.5
VL8.0	A	A	A	A	A	B	C	C
VL8.5	A	A	A	A	A	B	C	C
VL9.0	A	A	A	A	A	B	C	C
VL9.5	A	A	A	A	A	B	C	C
VL10.0	A	A	A	A	A	B	C	C
VL10.5	A	A	A	A	B	B	C	C
VL11.0	A	A	A	A	B	B	C	C
VL11.5	A	A	A	A	B	C	C	C
VL12.0	A	A	A	B	B	C	C	C
VL12.5	A	A	A	B	B	C	C	D
VL13.0	A	A	A	B	B	C	C	D
VL13.5	A	A	B	B	C	C	D	D
VL14.0	B	B	B	B	C	C	D	D
VL14.5	B	B	B	C	C	C	D	D
VL15.0	B	B	B	C	C	C	D	D

Table VIII: CII Matrix Scenario 5, 60% sailing activity, ballast < laden

	VB8	VB9	VB10	VB11	VB12	VB13	VB14	VB14.5
VL8.0	B	B	B	B	B	C	C	C
VL8.5	B	B	B	B	C	C	C	C
VL9.0	B	B	B	C	C	C	C	C
VL9.5	B	B	C	C	C	C	C	C
VL10.0	C	C	C	C	C	C	C	D
VL10.5	C	C	C	C	C	C	D	D
VL11.0	C	C	C	C	C	D	D	D
VL11.5	C	C	C	C	D	D	D	D
VL12.0	D	D	D	D	D	D	D	D
VL12.5	D	D	D	D	D	D	D	D
VL13.0	D	D	D	D	D	D	D	D
VL13.5	D	D	D	D	D	D	E	E
VL14.0	D	D	D	D	E	E	E	E
VL14.5	E	E	E	E	E	E	E	E
VL15.0	E	E	E	E	E	E	E	E

Table IX: CII Matrix Scenario 6, 60% sailing activity, ballast > laden

	VB8	VB9	VB10	VB11	VB12	VB13	VB14	VB14.5
VL8.0	A	A	B	B	C	C	D	D
VL8.5	A	A	B	B	C	C	D	D
VL9.0	A	A	B	B	C	C	D	D
VL9.5	A	B	B	B	C	C	D	D
VL10.0	A	B	B	B	C	C	D	D
VL10.5	B	B	B	C	C	C	D	D
VL11.0	B	B	B	C	C	C	D	D
VL11.5	B	B	B	C	C	C	D	D
VL12.0	B	B	C	C	C	D	D	D
VL12.5	B	C	C	C	C	D	D	D
VL13.0	C	C	C	C	C	D	D	D
VL13.5	C	C	C	C	D	D	D	D
VL14.0	C	C	C	C	D	D	D	D
VL14.5	C	C	C	D	D	D	D	E
VL15.0	C	C	D	D	D	D	D	E

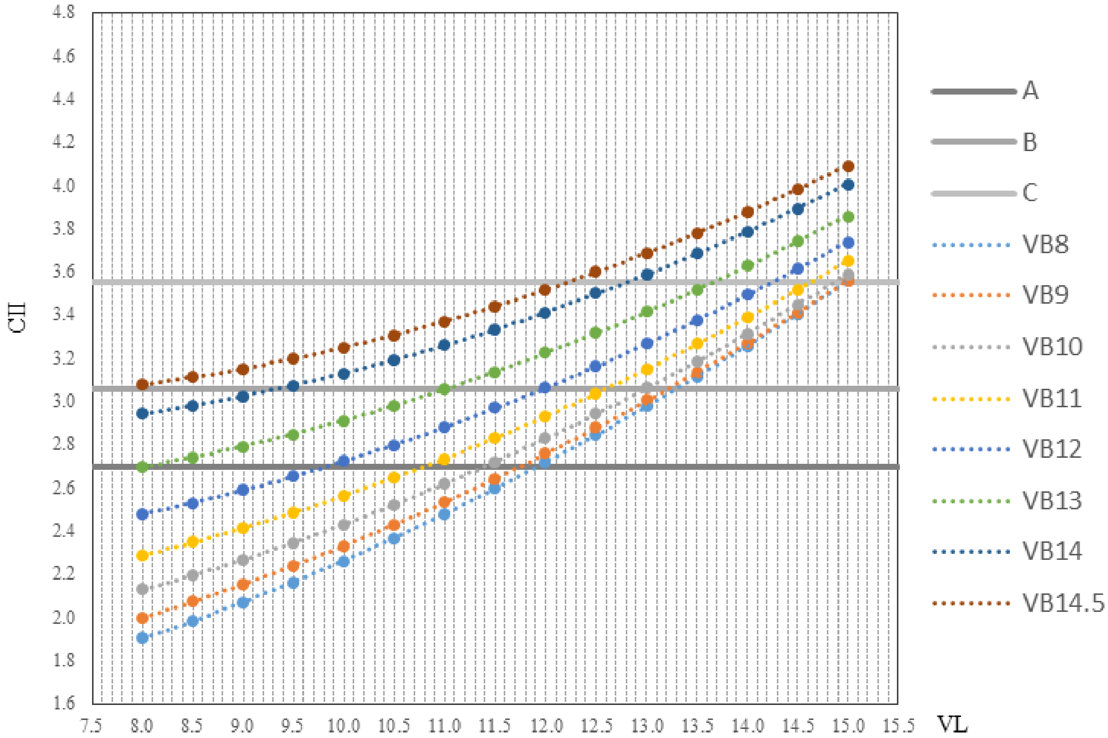

Fig.1: Scenario 1, CII vs V_L curves for Constant V_B

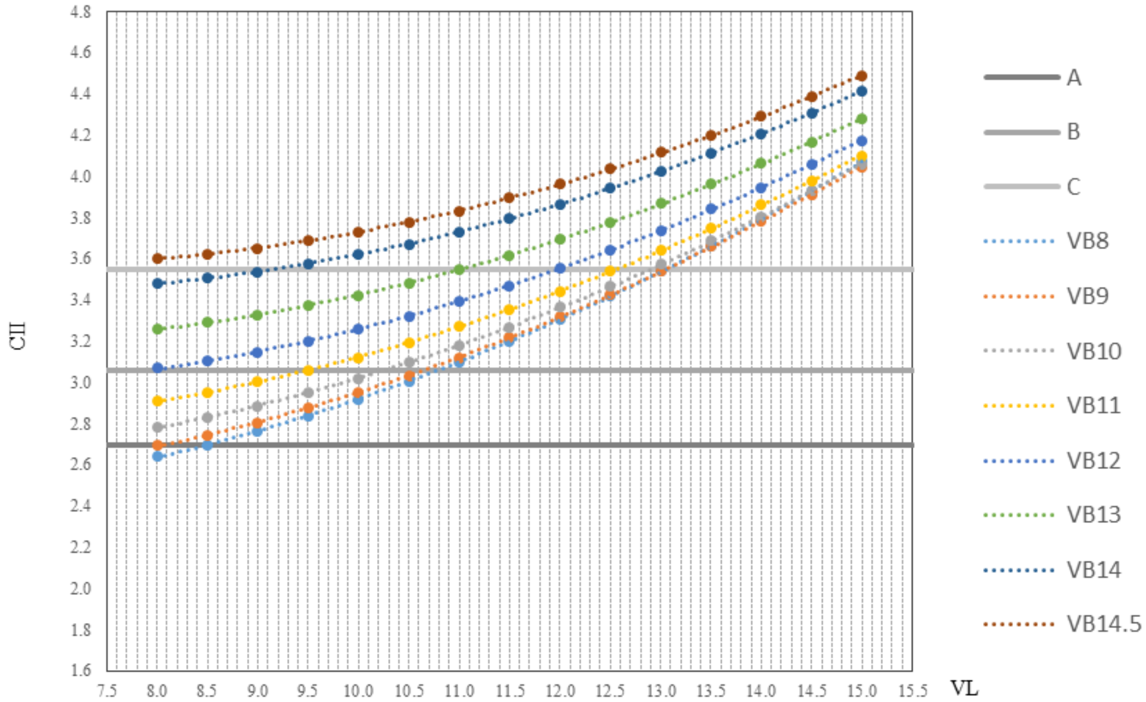

Fig.2. Scenario 2, CII vs V_L curves for Constant V_B

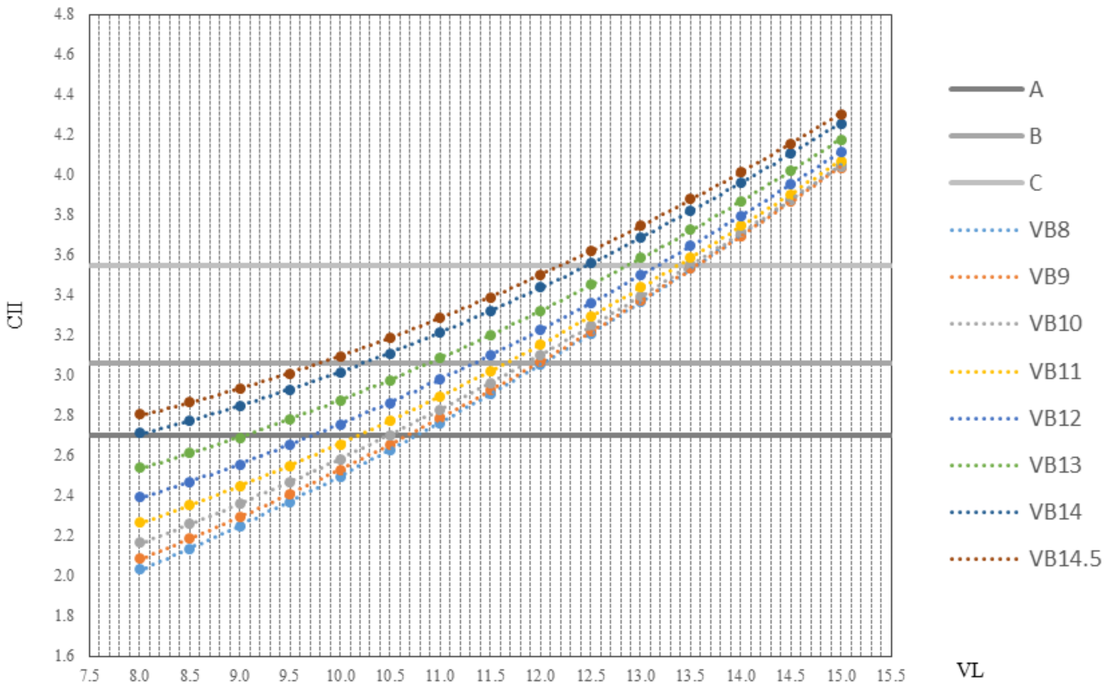

Fig.3. Scenario 3, CII vs V_L curves for Constant V_B

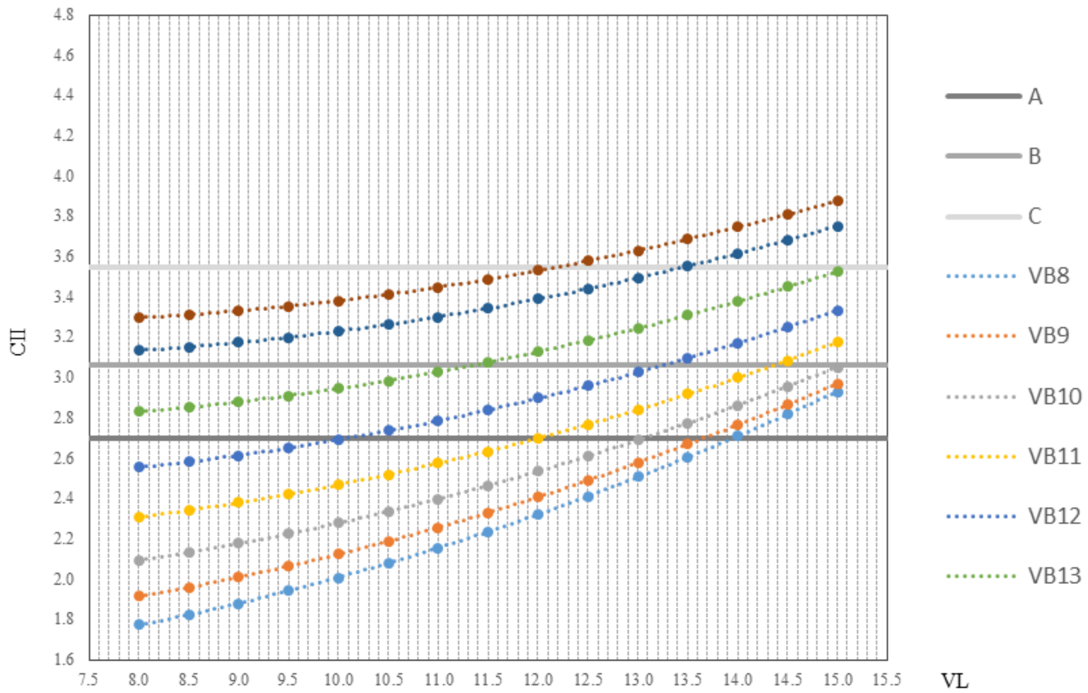

Fig.4. Scenario 4, CII vs V_L curves for Constant V_B

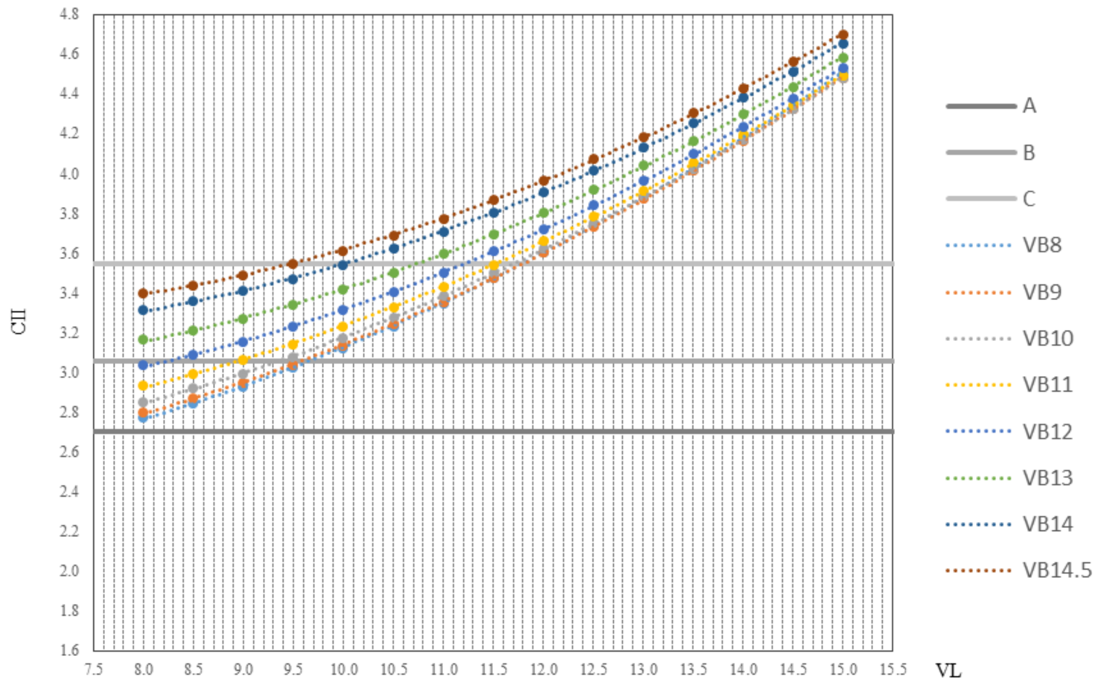

Fig.5: Scenario 5, CII vs V_L curves for Constant V_B

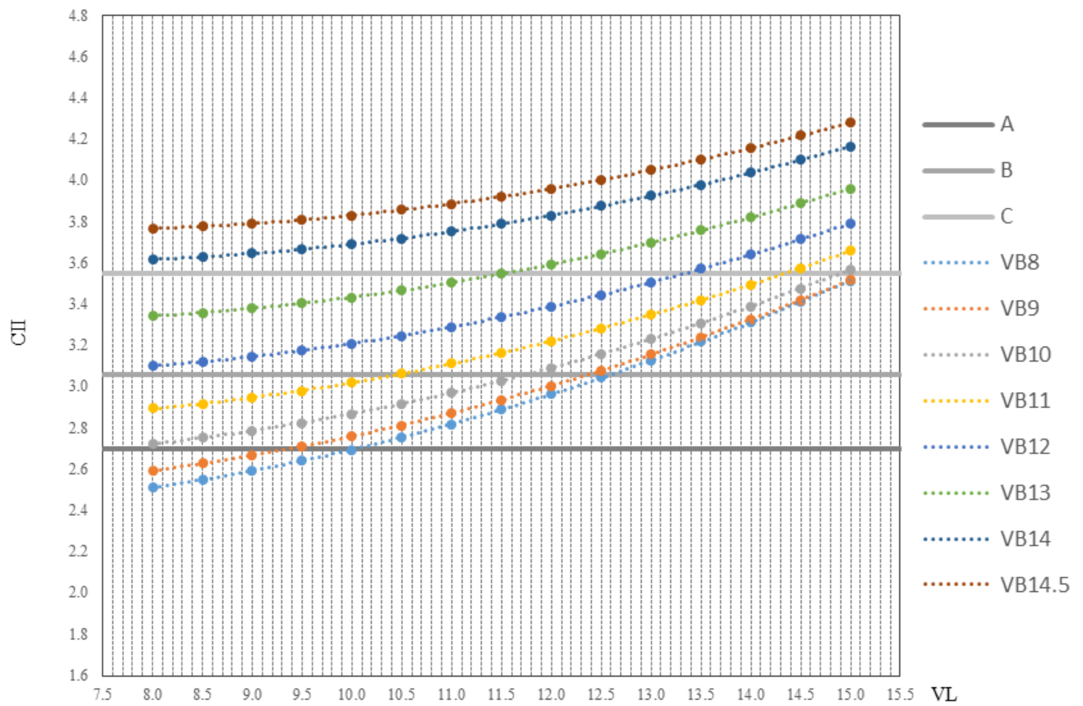

Fig.6: Scenario 5, CII vs V_L curves for Constant V_B

3. Results and Discussion

The CII Matrices results give clear indications of the positive impact the high sailing activity exerts on CII rating. Another explicit indication is that CII rating deteriorates as speeds increase, especially for the laden speeds.

It is noticeable that in the high sailing activity scenarios 1, 3, 4, Table IV, VI and VII, the lowest CII rating E is almost non-existent: only two combinations of very high ballast and laden speeds result in E, namely the ballast speeds 14-14.5 kn combined with 14.5-15 kn in laden mode. However, the operating pattern involving such high speeds in both laden and ballast modes is not likely to characterize the average annual ship operation, but rather individual voyages. Additionally, scenarios 1, 3, 4 indicate a wider range of speed combinations that result in high CII ratings: ballast speeds from 8 to 11 kn combined with laden speeds of up to 13 kn result in the highest possible CII ratings of A and B. Scenario 4, in particular (high sailing, ballast > laden), indicates that if the annual sailing activity in ballast exceeds the laden, the speeds range that bring about high CII ratings is even greater: with average annual ballast speeds of up to 10-11 kn, an excellent CII score can yet be achieved even with high laden speeds over 14 kn. This finding obviously weakens the theory of speed reduction as a means of emissions mitigation.

The results of CII matrices in scenarios 2, 5, 6, Tables V, VIII, and IX, relating to low annual sailing activity are clearly worse: high scores are achieved almost exclusively at the lowest laden speeds while the presence of the worst CII rating E is more evident than in the high sailing activity scenarios, even at the ultra-slow steaming ballast speeds of 8-10 kn. CII rating A appears only in scenarios 2 and 6. In scenario 2, where the annual distribution of ballast and laden legs is equal, CII rating A is possible only for the combination of ultra-slow steaming speeds 8-9 kn in both sailing modes. Scenario 6, where ballast condition exceeds the laden, allows slightly higher laden speeds of up to 10 knots, but still requires ultra-slow steaming ballast speeds of 8-9 kn to achieve the highest CII score A.

The results of the CII matrices recommend that the higher the total sailing activity and the higher the ballast condition share, the greater the range of speeds that can be combined to lead to high CII scores. These findings confirm that the annual sailing activity and CII rating are directly correlated, and provide useful information about the extent to which the combination of ballast and laden speeds affect the indicator. More importantly however, it shows that sailing inactivity is neither financially beneficial nor actually feasible in times of increased cargo transportation demand.

While ship operators are generally aware of the effect of speed on CII rating, they have not accumulated sufficient experience yet in relation to indicator's influencing factors, so their understanding is limited to a vague knowledge of a general rule that implies that ballast voyages favor high CII scores. In the context of emissions performance, this interpretation very often leads to the tentative and erroneous conclusion that "idling is good". The annual CII matrices of this work suggest that sailing inactivity may be equally detrimental to CII ratings as other related influencing factors, such as the high operational speeds – that elevate fuel consumptions - or the speed and consumption underperformance.

At this point, one should not overlook the fact that the physical condition of the ship, together with other design and operational characteristics, play a distinctive role in CII rating. The CII matrices of the present work refer to a certain ship type, size and age, with satisfactory hull and engine performance and annual voyages covering a worldwide trading. The results would be different for hull, propeller and main engine underperformance or for another ship type and size trading in specific world regions.

4. Concluding Remarks

Shipping industry is characterized by unpredictable situations driven by multi-variables that do not allow operators and crews to fully control the energy efficiency of their fleet, *Poulsen and Johnson (2016).* The sector's volatility does not always create a fertile ground for precautionary measures, so pre-estimating the CII fluctuations that will result from an operational and commercial decision is an extremely demanding task. In such a dynamic market, scenarios illustrating possible future realities could assist shipping company executives, charterers and crews in planning and decision-making, *Psaraftis (2021),* with regards to CII compliance.

In the event that administrations, port authorities, and other stakeholders provide incentives for high CII performing vessels, operators shall inevitably follow certain commercial, operational and technical practices to achieve the required scores. If a fleet is not intended to be upgraded with energy efficiency technologies, and since the margins of commercial flexibility are often narrow, candidate solutions for high CII scores are more likely to combine voyage optimization practices with appropriate service speeds' adjustments. The question is what the proper speed combinations to fulfil this objective are. The CII Matrices resulted from specific sailing activity scenarios serve the purpose to clear up that, under certain market conditions, there are certain speed combinations that could lead to better CII ratings than others.

Although the paper focuses on a certain type of vessel and uses a limited sample of tankers and bulk carriers with certain technical specification, size and age, the input data are based on actual operational information. The outcome, therefore, constitute a reliable database of interactions between ballast and laden speeds, annual sailing activity and CII rating. This work could be extended to other tankers and bulk carries designs and sizes to investigate in more detail how the voyage execution and ship's technical performance affect CII rating. Another interesting study would be to account for the ballast and laden speeds combination that concurrently maximize the Time Charter Equivalent and CII of a voyage charter.

References

ADLAND, R.; JIA, H.Y. (2016), *Dynamic speed choice in bulk shipping*, Maritime Economics & Logistics 20(3)

ADLAND, R.; CARIOU, P.; WOLFF, F.C. (2020), *Optimal Ship Speed and the Cubic Law Revisited: Empirical Evidence from an Oil Tanker Fleet*, Transportation Research Part E

CHANGA, C.C.; HUANGA, P.C.; HSIEHA, C.C. (2019), *Carbon Allowance Allocation in the Shipping Industry under Different Economic Activities*, 14th Global Congress on Manufacturing and Management

DNV (2020), *Maritime Forecast to 2050, Energy Transition Outlook 2020*, DNV, Hovik

IMO (2012), *Third GHG Study,* Int. Maritime Org., London

IMO (2020), *Fourth GHG Study*, Int. Maritime Org., London

OLIVEIRA, M.A.N. De; SZKLO, A.; CASTELO BRANCO, D.A. (2022), *Implementation of Maritime Transport Mitigation Measures according to their marginal abatement costs and their mitigation potentials,* Energy policy

POULSEN, R.T.; JOHNSON, H. (2016), *The logic of Business vs. the logic of Energy Management Practice: understanding the choices and effects of Energy Consumption Monitoring Systems in Shipping Companies*, J. Cleaner Production

POULSEN, R.T.; VIKTORELIUS, M.; VARVNE, H.; RASMUSSEN, H.B.; VON KNORRING, H. (2022), *Energy efficiency in ship operations - Exploring voyage decisions and decision-makers*, Transportation Research Part D

PSARAFTIS, H.N. (2019), *Speed Optimization vs Speed Reduction: the choice between speed limits and a bunker levy*, Sustainability article

PSARAFTIS, H.N. (2021), *Shipping Decarbonization in the aftermath of MEPC 76,* European Maritime Transport Environmental (EMSA) Report

PSARAFTIS, H.N.; KONTOVAS, C.A. (2013), *Speed models for energy-efficient maritime transportation: A taxonomy and survey*, Transportation Research Part C: Emerging Technologies

REHMATULLA, N.; SMITH, T. (2015), *Barriers to Energy Efficient and Low Carbon Shipping,* Ocean Engineering

WALSH, C.; MANDER, S.; LARKIN, A. (2017), *Charting a low carbon future for shipping: A UK perspective*, Marine Policy

Detecting Hull Degradation - Current Practice and Future Challenges

Falko Fritz, Albis Marine Performance GmbH, Hamburg/Germany, falko.fritz@albis-mp.de

Abstract

Current hull condition monitoring systems are able to detect even small overconsumptions or ship speed losses due to fouling relatively quickly. The simpler the propulsion system on a vessel is, the easier it is to obtain reliable results quickly. Already now, changing e.g. the combinator setting on a vessel may require a different normalization function for ship speed, which means that the combinator setting should be monitored. With the need to reduce fuel consumption further, new technologies will be introduced and vessels will become more complex. Alternative fuels, active hull friction reduction methods, harvesting energy from the sun and wind, etc. may all contribute to the energy balance on future vessels. While alternative fuels or electric modifications don't influence the evaluation of shaft power vs. ship speed directly, air lubrication or wind propulsion will. To understand their effects and enable the computation of their influence, the main operational parameters of these systems should be recorded on board and in high frequency.

1. Introduction

The condition of a ship's hull is usually monitored in two ways:

1. by taking pictures or videos of the hull and inspecting them for slime, fouling, paint damage, etc., also taking the distribution on the different areas on the hull into account,
2. by continuously monitoring ship speed, propulsion power and other parameters and using this information for an evaluation according to ISO 19030 or a similar method.

While method 1 gives the best information for planning and preparing for a hull cleaning with divers, the strong point of method 2 is the evaluation of the financial and ecological impacts of the hull degradation. It links the hull condition to the costs and emissions of burning fossil fuel.

The ability to detect hull degradation and fouling by measuring propulsion power or fuel consumption vs. ship speed depends on the accuracy of the measuring methods used and the calculation process employed to filter, normalize and compare data over an extended period of time. Some of these calculation methods are well understood and fairly standardized, while other influences on the propulsion efficiency are not yet in wide use and therefore not implemented in current hull condition monitoring systems.

2. Current Practice

In 2020, the IMO launched a Global Industry Alliance (GIA) for Marine Biosafety to support the development of technologies to prevent hull fouling. For the COP26 Conference on Climate Change, GIA published a preliminary report of the effect of biofouling on greenhouse gas emissions, *GIA (2021)*. According to this study, even very thin layers of slime or degraded paint may cause increasing emissions in the range of 10-20%, see Fig.1. The goal for hull condition monitoring systems should be to reach a level of confidence where even these small effects can be detected reliably.

Most hull condition monitoring systems today work by measuring the mechanical power on the shaft that drives the propeller and set it in perspective with the attained ship speed through water (STW), as measured by the ship's log and distributed with the NMEA protocol. A drawback of using a torque meter as the primary parameter for vessel propulsion is that many of these instruments suffer accuracy losses when the shaft torque is getting smaller. In a time when power reduction and slow steaming are rather the norm than the exception, torque meters often deliver readings with significant error margins. According to the manufacturers' specifications, they also need to be calibrated frequently, which is often neglected in practice.

Some monitoring systems therefore use mass flow meters to measure the main engine fuel flow in addition or as a proxy for shaft power. Typically, other influencing factors like the weather or the vessel's draft will then be added to the dataset from additional sensors, manual inputs in noon reports on board or third-party sources like weather services.

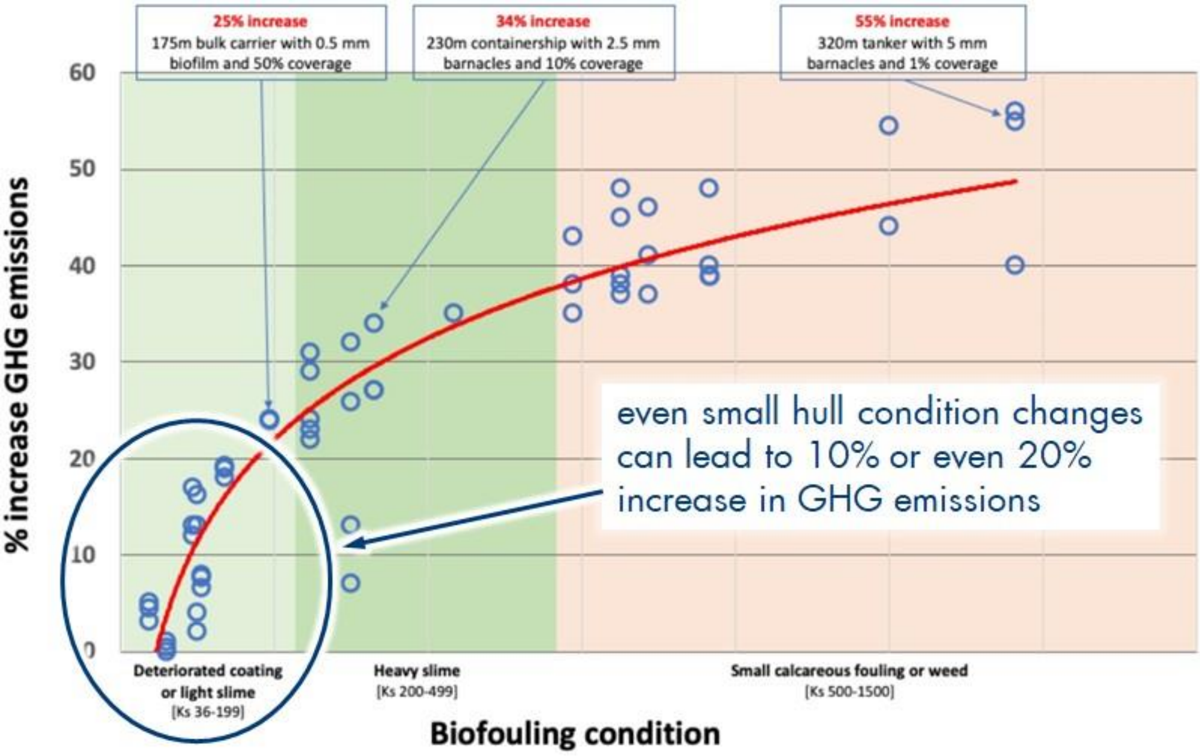

Fig.1: Effect of biofouling on GHG emissions, *GIA (2021)*

2.1. Optimal Conditions for Hull Condition Monitoring

To get optimal results in the monitoring of hull condition, a vessel should go through as few changes as possible and have a propulsion system that is as simple as possible. This means, a vessel with a single main engine driving a fixed pitch propeller, operating at the same speed and draft on the same route in comparable weather conditions all the time. Of course, this is not what most vessels look like or normally do. Most change speed and draft according to trades and market situation, many have controllable pitch propellers or shaft generators, etc. Consequently, data filters and normalization or correction functions come into play.

2.2. Fuel Types

If fuel meters are used instead of a torque meter or in addition to it, the fuel quality may influence the calculation. Running the main engine on MGO may give a higher power output per kg of fuel than burning VLSFO due to the higher calorific value of MGO. Thankfully, the calorific value of VLSFO can be approximated relatively well if the density is known, *IF (2019).* Coriolis mass flow meters are commonly used by now and they also measure density continuously, so that the calorific value can be accounted for when switching between fuel types.

If the main engine drives the propeller shaft only, Coriolis fuel meters can either be used as a proxy for shaft power or for checking the plausibility of the torque meter readings continuously. If a shaft generator is installed on the main engine's flywheel, its electric power output must be measured and reflected in the calculation.

2.3. Combinator Settings

If a vessel is equipped with a controllable pitch propeller and a combinator, the setting of the combinator curve has an influence on the ship's consumption over speed dependency. If the settings are changed, the normalization function to account for different speeds must be changed accordingly. For this to happen, the provider of the condition monitoring services must first be aware of the change, otherwise it could easily be mistaken as a change in hull condition. Awareness and frequent communication between the ship operator and the service provider are essential to keep the monitoring results consistent.

3. Future Challenges

Besides the fuel costs, the demands of the CII regulation are an important incentive to keep the hull in good condition. Hull cleanings are one method among others to comply with the CII limits in the future. For example, DNV lists the following energy saving methods in four categories, *DNV (2021)*:

1. Logistics and Digitalization: speed reduction, vessel utilization,
2. Hydrodynamics: hull coating, hull-form optimization, air lubrication, cleaning,
3. Machinery: machinery improvements, waste-heat recovery, engine de-rating, battery hybridization,
4. Fuels and Energy: LNG, LPG, biofuels, electrification, methanol, ammonia, hydrogen, harvesting from the surroundings.

Some of these measures to reduce the carbon footprint directly influence the hull condition monitoring, particularly those in the categories 2 and 4, hydrodynamics and fuel/energy.

3.1. Alternative Fuels

If a torque meter is used as the primary source of propulsion data, the use of alternative fuels does not affect the hull condition monitoring. If fuel meters are used in addition, their use should be recorded in high frequency to account for their effects, much in the same way as it is already done on vessels that frequently switch between VLSFO and MGO.

3.2. Solar Panels, Waste-Heat Recovery, Batteries

Solar panels, waste-heat recovery and batteries all have in common that they improve the use of electrical power rather than propulsion power. If torque meters are used to determine propulsion power, the electrical energy balance on the vessel does not influence the hull condition monitoring. If fuel meters are used in addition and electrical power is either taken from or fed back to the propulsion drive train, this influence should be measured and accounted for in the calculation.

3.3. Air Lubrication

Air lubrication works be reducing the hull friction while underway. But quantifying precisely by how much under which exact circumstances might be a serious challenge. How much of the hull is affected by the air bubbles depends on the amount of air used, the pressure, bubble size, ship motions and possibly further factors. There is a risk that hull fouling and changing properties on the air lubrication system could be hard to differentiate on vessels that steam with air lubrication most of the time.

At the very least, any hull condition monitoring installed on these vessels should also record the main operational parameters of the air lubrication system in high frequency to enable a computation of its use and influence.

3.4. Wind Propulsion

Wind propulsion systems like kites, sails, rigid wings or Flettner rotors transmit forces to the hull which counteract the ship's hydrodynamic resistance and thereby reduce the required propeller thrust to reach the desired speed. To account for this effect during hull condition monitoring, the forces of these systems should be measured in high frequency and transmitted along with the other ship performance data. However, measuring the forces may be a challenge. Sails, wings and Flettner rotors commonly have larger installation structures and measuring the magnitude and direction of the forces they transfer to the vessel structure may not be an easy task. Kites on the other hand are tethered to a single rope and the rope force and the direction of its pull are easy to measure in the pulley where the kite is connected.

The influence of wind propulsion systems may still be relatively easy to tackle, though, since most hull condition monitoring systems filter out bad weather conditions anyways. Wind propulsion systems have their greatest potential between 5 and 8 Bft, and these data are often not used for trend monitoring in the first place. Even when wind propulsion systems are installed, they will often be inactive in 0-3 or even 0-4 Bft wind conditions, so that these data can be used normally without being influenced by the wind propulsion system's forces.

4. Conclusion

New technologies to reduce the fuel consumption of cargos ships are quickly emerging. Some of them are easy to integrate into existing hull condition monitoring systems, while others will pose a significant challenge. What they all have in common, though, is that a continuous recording of their operational parameters in high frequency is the first step to evaluate their influences on the vessel. This will eventually make it possible to compensate their effects in the calculation of the hull condition. Setting the vessels up for this future task of systematic data gathering and transmission, possibly by upgrading the IT infrastructure and ship to shore communication if required, is an important step in the process of improving the energy efficiency of the fleet.

References

DNV (2021), *The carbon intensity indicator (CII)–a closer look*, https://www.dnv.com/maritime/webinars-and-videos/on-demand-webinars/Carbon-Intensity-Indicator-CII-A-closer-look.html

GIA (2021), *Impact of Ships' Biofouling on Greenhouse Gas Emissions*, Global Industry Alliance for Marine Biosafety, https://wwwcdn.imo.org/localresources/en/MediaCentre/Documents/Biofouling%20report.pdf

IF (2019), *Buying fuel on calorific value as means to achieve savings*, Integr8 Fuels, https://integr8fuels.com/wp-content/uploads/2019/12/Integr8-Research-2019-12-Calorific-value-analysis.pdf

How CII ratings (A to E) are Linked to Energy Efficiency

Soren Vinther Hansen, VesOPS, Svendborg/Denmark, info@vesops.dk
Richard Marioth, Idealship, Itzehoe/Germany, rm@idealship.de

Abstract

Decarbonization of the maritime sector is one of the main missions of the next decades. To lower the carbon footprint of shipping, IMO has introduced the Carbon Intensity Index Indicator (CII) which is defined as the Annual Efficiency Ratio (AER). A vessel will be rated on the CII and if the rating is bad, it will have to improve. Such ratings will lead to possible restrictions in the vessels ability to operate which may lead to loss of value in the market. The actual energy efficiency of a vessel is impacted by many factors, the CII however is determined by a quite simple formula only based on IMO DCS data. What do the ratings say about energy efficiency? Were physics possibly oversimplified and does the CII incentivize potentially wrong behavior? This paper uses case studies to give an overview of the parameters that affect the CII. The paper also shows how comparable ships in the same trade will benefit of retrofits and proper hull maintenance for the improvement of the rating. Finally, the paper will highlight the importance of keeping track of a vessel rating over a reporting period. This to being able to keep the ranking target setting and to maintain transparency of the vessel's energy efficiency towards stakeholders with interests in the vessel operations.

1. Introduction

1.1. Regulatory background

On the MEPC 76 (June 2021), the International Maritime Organization (IMO) adopted amendments of the MARPOL Annex VI regulation. The amendments include a new regulation 28, which sets the requirement to demonstrate operational carbon intensity reduction through the Carbon Intensity Indicator (CII), *IMO (2021a)*. The CII judges the carbon intensity of a trading vessel based on the yearly Annual Efficiency Ratio (AER]). The AER is defined as:

$$AER = \frac{Annual\ Fuel\ Consumption\ \cdot\ CO_2\ Emission\ Factor}{Annual\ Distance\ Sailed\ \cdot\ Capacity}\left[\frac{gCO_2}{tnm}\right] \quad (1)$$

The capacity is in general defined as the summer deadweight. Only for cruise passenger ships, vehicle carriers and RO/RO passenger ship the technical cargo-carrying capacity is used. The rating of CII works by a comparison of the vessels individual AER within the year of compliance as compared to baselines of the vessel. The baselines are the average AER values for that vessel class of 2019 reduced by a certain factor which is defined by the year of compliance. Depending on the outcome of this comparison, a vessel is rated as A, B, C, D or E. Where A stands for a very carbon efficient vessel and vessels which get a rating of D or lower will need to agree with the regulators upon an action plan, *IMO (2021b)*. Fig.1 illustrates the rating scheme and how IMO has set the boundaries.

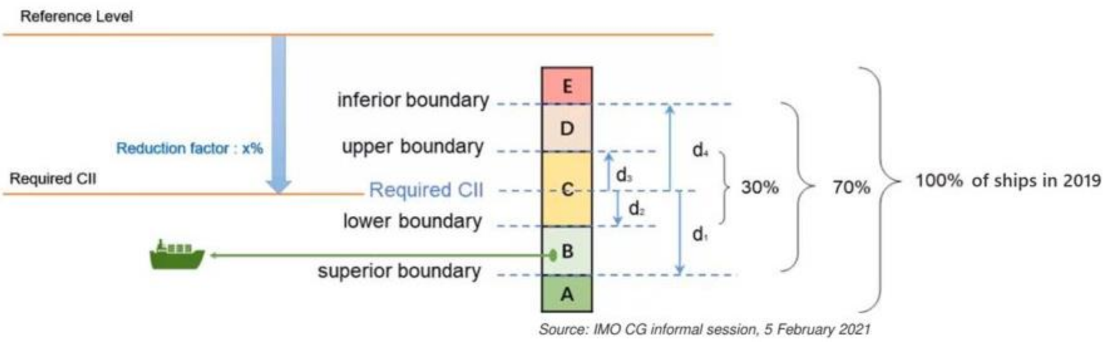

Fig.1: CII evaluation scheme, source: DNV webinar

The AER baselines get stricter over time so it will be more and more difficult to comply to the regulation. Table I shows the reduction factors of the current decade as they are defined by IMO so far, *IMO (2021c)*:

Table I: Reduction factors for CII compliance

Year	Reduction factor from 2019
2023	5 %
2024	7 %
2025	9 %
2026	11 %
2027-2030	To be decided

An AER value which would be rated as "C" in 2023 would get a D rating in 2025. In order to comply the vessel would need to undergo some measures. A study from the Korean Register (webinar) indicated that more than 75% of the KR verified Tanker and Bulk carrier vessels would get a C, D or E rating in 2023. So for a large part of the world fleet, it will be challenging to comply to the regulation and vessel operation will need to change in order to be compliant within the next years.

1.2. CII as compared to EEXI

CII and the Energy Efficiency Existing Ship Index (EEXI) have the date of enforcement and the technical measurement unit $\left(\frac{g(CO_2)}{tnm}\right)$ in common. EEXI has however no relation to the actual vessel operation and focuses on the theoretical CO_2 emissions a vessel has based on her technical equipment and the theoretical speed vs. power curves. Compliance to EEXI is usually ensured by limiting the operational speeds of the vessel through an Engine Power Limitation (EPL). The CII does not consider the technical equipment at all but focuses on the actual fuel consumptions. So, vessels with a very good EEXI may still get a poor CII rating, it is just less likely.

1.3. CII as compared to EEOI

Another KPI, which was introduced as a "voluntary" KPI for operational emissions performance when the SEEMP and the EEDI were agreed on, is the EEOI, the Energy Efficiency Operational Indicator. The EEOI is calculated for each voyage as:

$$EEOI = \frac{\sum_j (FuelConsumption)_j \cdot (CO_2EmissionFactor)_j}{VoyageDistance \cdot m_{Cargo}} \quad (2)$$

The average EEOI is just the average for multiple voyages is defined as:

$$EEOI_{Avg} = \frac{\sum_i \left(\sum_j (FuelConsumption)_j \cdot (CO_2EmissionFactor)_j\right)_i}{\sum_i VoyageDistance_i \cdot m_{Cargo,i}} \quad (3)$$

The differences between the EEOI and the AER are that the transported cargo is used instead of the deadweight and that the EEOI regulation is voluntary.

1.4. Structure of this document

A practical analysis approach was chosen for this paper. Firstly, the CII figures for three different vessel types are analyzed through case studies. Case study 1 is related to a bulk carrier, case study 2 to a fleet of 7 sister vessels and case study 3 to a bulk carrier vessel fleet. A short summary gives then an overview of the findings. As details of the CII regulation, like the operational exemptions, are yet not finalized an overview of the current status as per early April 2022 is given. To widen the view a small outlook is given in chapter 4 and some alternative options to the current CII regulation are suggested.

2. CII impact - Case Studies

2.1. Case Study 1: Bulkers – operational profile

The CII figures of a medium size bulk carrier fleet were analyzed using 2020 operational data. The results of this analysis are shown in Fig.2 over the deadweight. The CII ratings in the figure are shown as colored areas. The dark green area in the bottom means a rating of A then the color changes for each rating number to the dark red area in the top which means rating of E. One can observe that the Handy and Supra class are lying completely in the E area, so they fail to comply to the CII regulation. Overall, the ratings vary from ship to ship and from ship class to ship class.

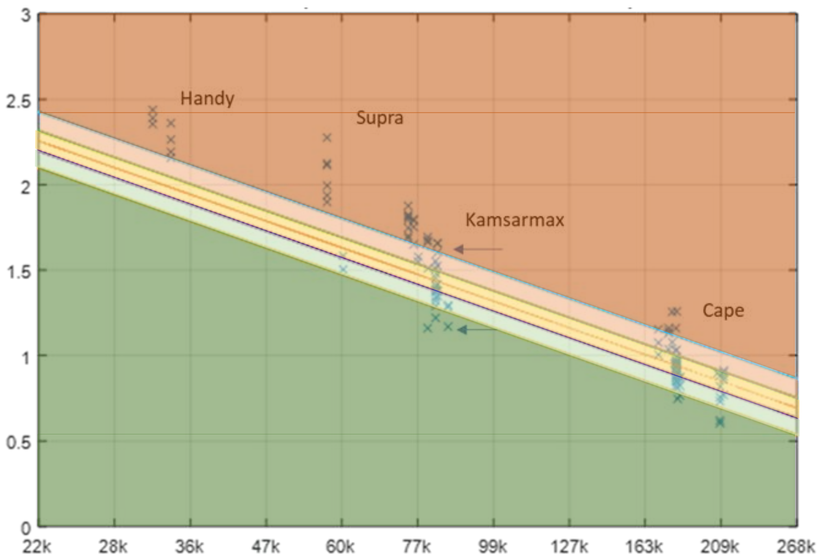

Fig.2: CII of Bulk Carrier fleet over deadweight

Looking specifically at the Kamsarmax class, Fig.2, it can be seen that some ships are rated A and some are rated E. Three samples were taken out to identify the reasons for the different ratings. Details are given in Table II. One (vessel #1) has a fuel-efficient design, and two others (vessels #2 & #3) are less efficient and somewhat similar to each other.

Table II: Comparison of ratings for three Kamsarmax vessels

Vessel	CII (AER)	Built year	Fuel efficient design	CO2 emissions for the year
#1	3.39 – Rating A	2014	YES	16998 ton
#2	5.24 – Rating E	2012	NO	18168 ton
#3	5.25 – Rating E	2010	NO	23834 ton

Vessel #2 and vessel #3 have the approximately the same CII, but vessel #3 emitted about 30% more CO2 than vessel #2. In principle one would expect that vessel #2 should be rewarded for emitting less CO2. This is not the case due to the vessel’s operational profiles, shown in Table III. Further details regarding the operational profile of the 2 vessels can be found in Fig.3.

Table III: Analysis of ratings for three Kamsarmax vessels

Vessel	At Sea mean speed	Average draught	Number of voyage legs	Sailed distance
#2	11.4 knots	9.4 m	31	42251 nm
#3	10.9 knots	10.3 m	24	55369 nm

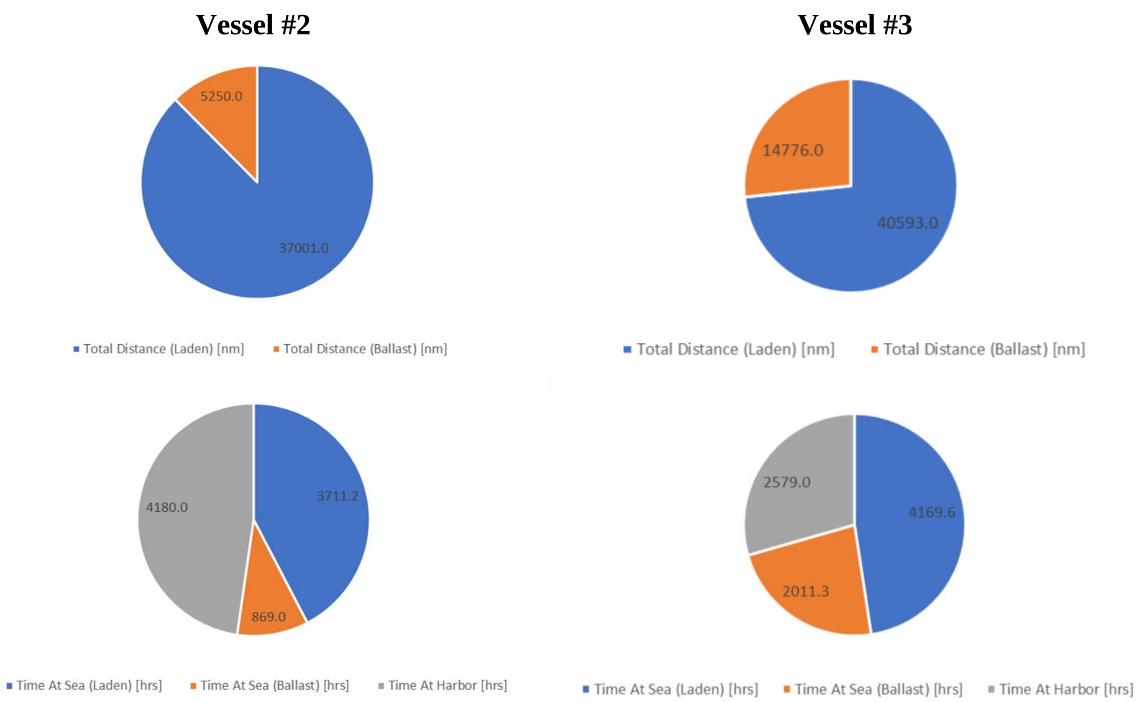

Fig.3: Operational profile of 2 Kamsarmax vessels

It is obvious that what makes vessel #2 to get the E rating even though the CO2 emission is so low, it is the lower distance that it sails compared to vessel #3, the considerable idle time (almost half of the year) and the higher average speed when it is at sea. In this case the operational profile is the driver for the CII rating.

In a second step the CII of vessel #1 and vessel #3 was compared. Their operational profiles are shown in Fig.4 and Table IV. Here the time distribution is more or less the same, the draught and speed likewise, but the total distance sailed is about 10% higher for vessel #1.

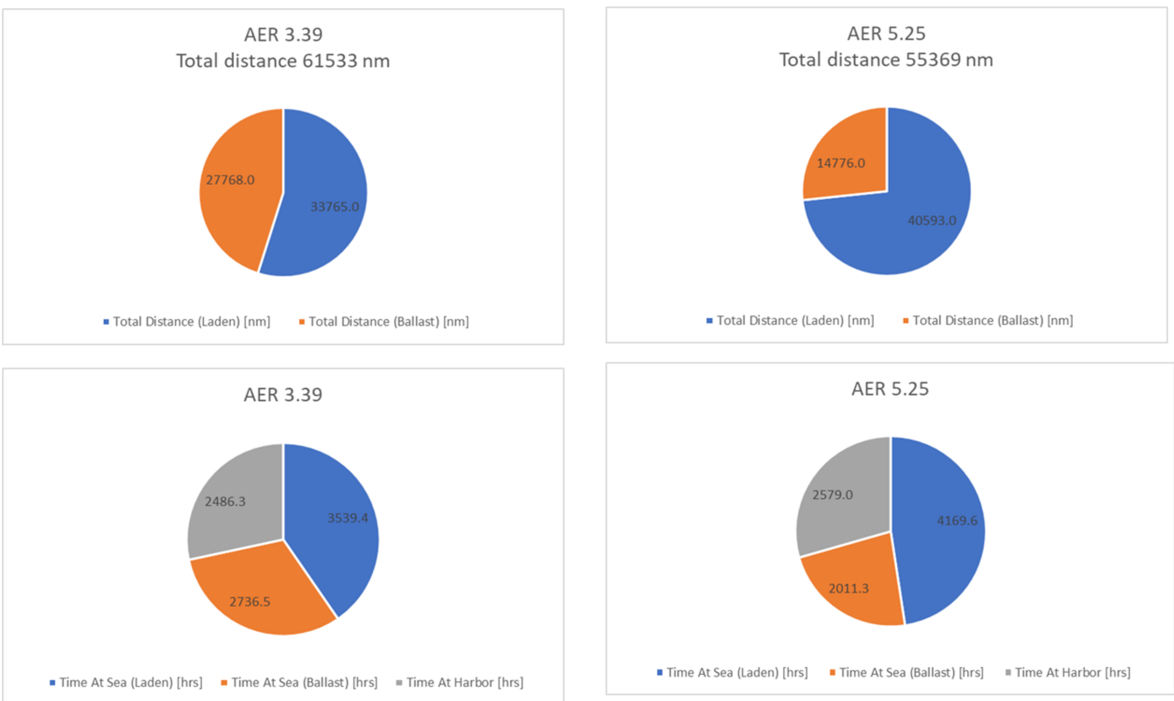

Fig.4: Operational profile of 2 Kamsarmax vessels (vessel #1 left, vessel #3 right)

Table IV: Comparison of 2 Kamsarmax vessels

Vessel	At Sea mean speed	Average draught	Number of voyage legs	Sailed distance
#1	11.0 knots	10.4 m	17	61533 nm
#3	10.9 knots	10.3 m	24	55369 nm

At this comparison the bigger distance, the lower number of voyages, the higher percentage of sailing time in ballast and the higher fuel efficiency for vessel #1 makes the rating significantly better than vessel #3. So in this case it is the fuel efficiency that the main driver for the good CII rating of vessel #1, but it is not the only cause.

2.2 Case Study 2: 7 Sister vessels – Energy Efficiency improvements effect on the CII

Seven 22k tanker (sister) vessels were included in a second study. The study includes the vessels operations in 2019 and 2020. The vessels operational profile related to CII parameters are given as in the Fig.5.

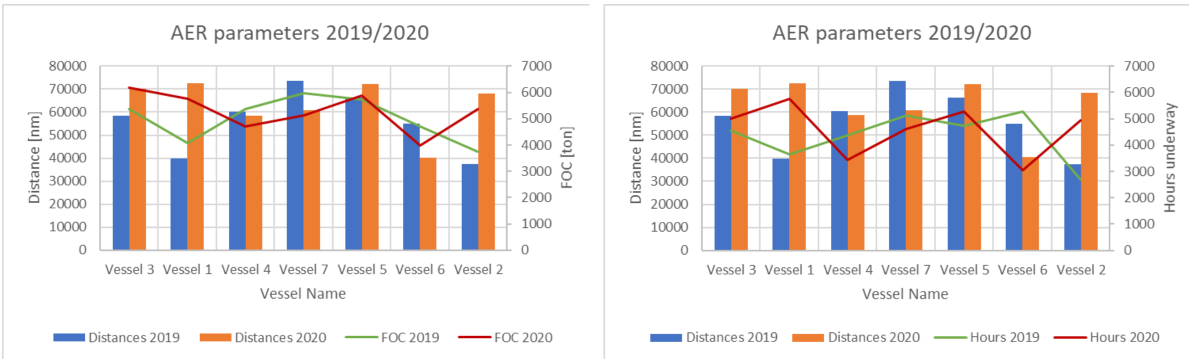

Fig.5: Operational profile parameters 2019/2020

In general, the fleet is utilized better and busier in 2020 than in 2019. The days at sea are increased with 6% and the total distance sailed is increased with 13% overall on the fleet level. There are variations in the vessel specific figures, and this is reflected also in the CII ratings.

The operational parameters are used in a calculation of the CII and the vessels are categorized in the A to E scheme and the result is as in the Fig.6

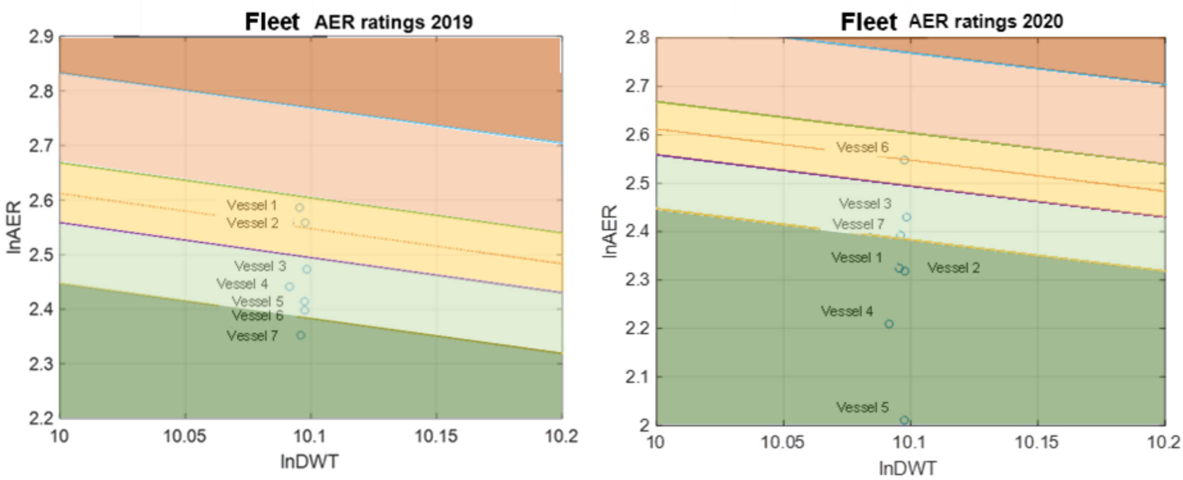

Fig.6: Fleet CII ratings for 2019/2020

None of the vessels are rated critical (D to E). There are some changes in the ratings from 2019 to 2020 and the changes for some of the vessels can be explained with different factors and events.

Vessels 1, 2, 4 & 5	The CII rating is in general improved in 2020. Rating have changed from B/C to A for all 4 vessels. Some can be explained by changes in the operational profile even though the profile changes do not justify the ratings improvement that is seen. Main CII change is due to all 4 vessels went to drydock 2019/2020 and operated with clean hull and new antifouling paint in 2020. The improvements are in the range of 21% to 33%.
Vessels 3 & 7	The CII rating does not differ much from 2019 to 2020. Vessel 3 improves 4% and vessel 7 drops 4%.
Vessel 6	The CII rating drops 16% from a B to a C rating and this is mainly because of shorter time at sea and a higher average voyage speed in 2020.

This case study shows that the benefit of a drydock as well as a good hull and propeller maintenance and an energy efficiency improvement also is reflected in the CII rating and can be seen as an efficient instrument to control the rating of a vessel. In general, the vessels are rated quite high which partly is due to an energy efficient design and partly because the vessels are included in a vessel performance monitoring scheme based on high frequency sensor data where operators are given information to operate the vessels to their optimum.

2.3 Case Study 3: Dependencies of the AER

A fleet of 19 Kamsarmax Bulk carriers was analyzed with the goal of revealing the dependencies of the AER on vessel operation parameters and the Energy Efficiency Operational Indicator. Noon report data of about a year was used for this, only completed voyages were taken into account. Fig.**7** shows the AER over the total percentage of sailing time as well as separated in Ballast and Laden sailing time.

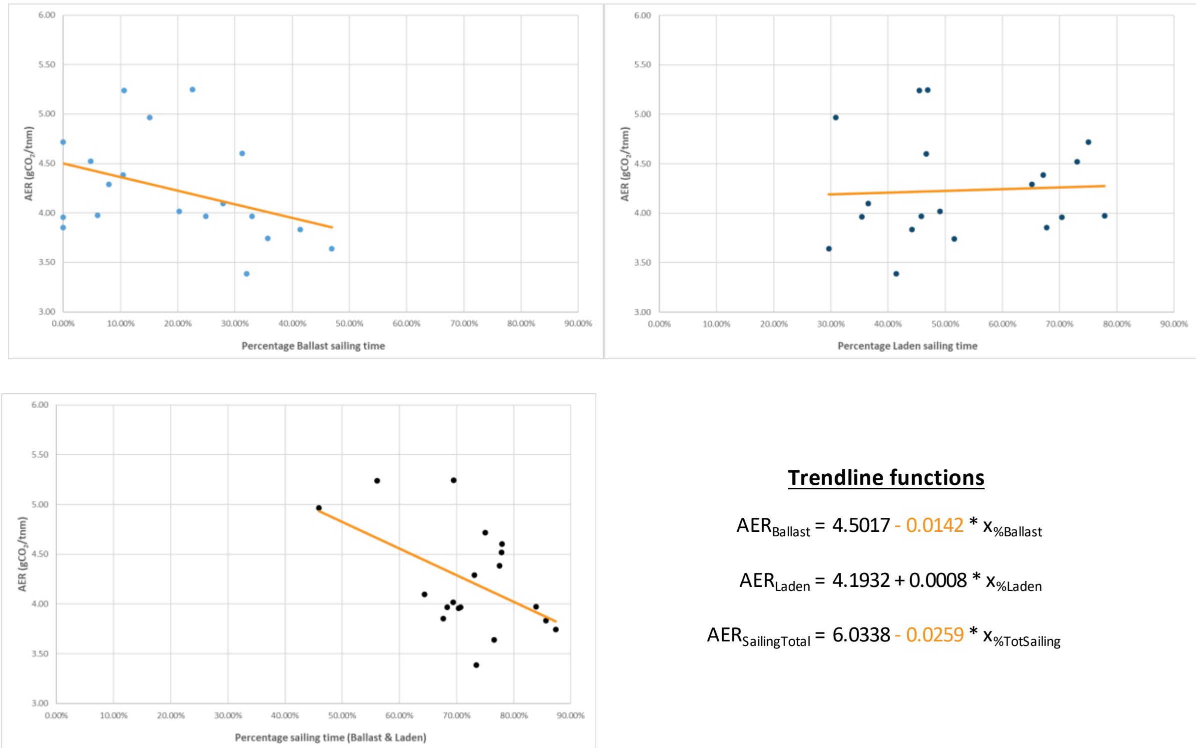

Trendline functions

$AER_{Ballast} = 4.5017 - 0.0142 * x_{\%Ballast}$

$AER_{Laden} = 4.1932 + 0.0008 * x_{\%Laden}$

$AER_{SailingTotal} = 6.0338 - 0.0259 * x_{\%TotSailing}$

Fig.7: AER over percentage sailing time and the related trendline functions with slopes

The slope of the trendline $AER_{SailingTotal}$, highlighted orange in the formulas, indicates that the more a vessel sails, the better the AER figure will be. At this case study the sailing time has a very strong impact on the AER 4% more sailing time would lead roughly to a reduction of 0.1 gCO_2/nm at the AER figure. In other words: "About a percent of more sailing time means about a percent lower AER value." However, as one can see from the slopes of $AER_{Ballast}$ and AER_{Landen} only the Ballast sailing time leads obviously to lower AER figures. The Laden sailing time has little impact. A similar observation can be made when analyzing how the utilization of the vessel, average percentage of Deadweight, impacts the AER. This is done in Fig.8. One can observe that a lower utilization, i.e. less cargo transportation, has a slightly positive impact on the AER and with this the CII. The reason for this is that such vessels consume about 10-30% less fuel for propulsion when they sail in Ballast instead of Laden.

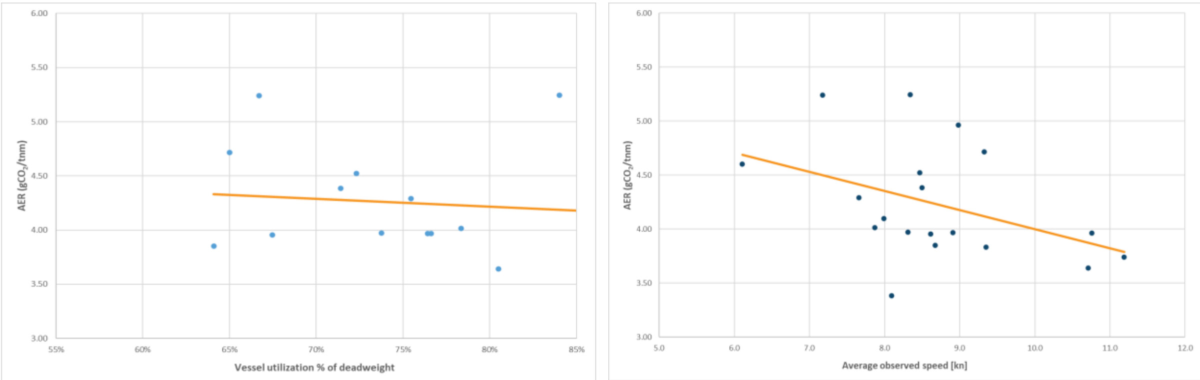

$AER_{Deadweight} = 4.7911 - 0.00719 * x_{\%Deadweight}$ $AER_{Speed} = 5.768 - 0.1769 * x_{SpeedKnots}$

Fig.8: AER over utilization % deadweight (left) and over average observed vessel speed (right)

When checking how different average vessel operation speeds have impacted the AER one can observe that higher average speeds seem to have had a positive impact on the AER. This is remarkable as physical principles assume an almost cubical relationship between propulsion power and speed and contradict this observation ($PropulsionFuelConsumption \sim v^{x\approx 3}$).

The main reason for the given slope is the averaging over the whole voyage. The voyage time includes some idle and maneuvering time and not only the time when the vessel was sailing at Sea. The little impact of Speed on the AER indicates however that Engine Power Limitations, an approach frequently used to comply to the EEXI regulation, will have a limited impact on the AER values.

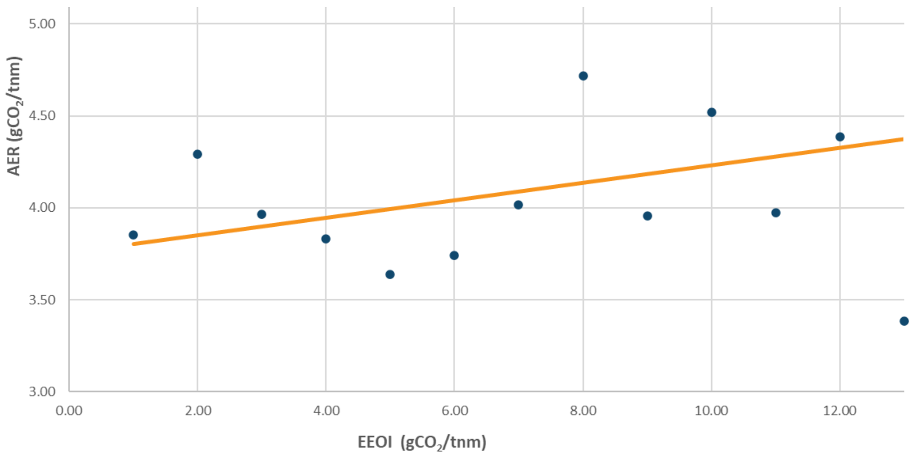

Fig.9: AER over EEOI

The voluntary vessel KPI, EEOI which is described in chapter 1.3 determines the carbon emissions of each voyage as compared to the transported amount of cargo. A comparison between the EEOI and the AER for this set of vessels is shown in Fig.9. The incline of the trendline indicates that a low EEOI leads in average to a low AER, there is however a high scatter as the average deviation of the AER values from the trendline value is 10.2%. An outlier is for instance the vessel on the right side of Fig.9, which has $EEOI = 11.99 \frac{gCO_2}{tnm}$ and an $AER = 3.64 \frac{gCO_2}{tnm}$, the difference is caused by the high amount of Ballast voyages.

Overall the EEOI behaves differently in regard to Ballast and Laden voyage. In Fig.10 one can observe that a lot of sailing time in Ballast has clearly a negative impact on the EEOI figure whereas sailing time in Laden has a positive impact.

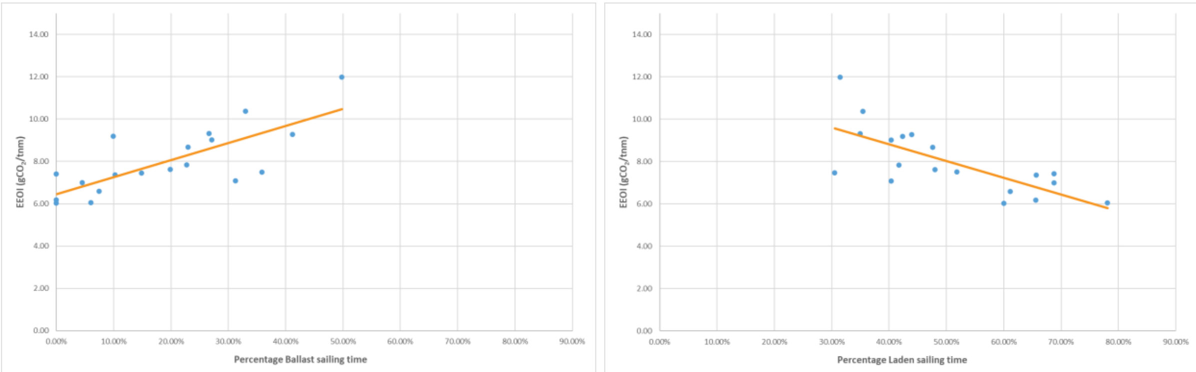

Fig.10: EEOI over percentage sailing time

2.4 Summary of case studies

It has been highlighted through the case studies that certain types of vessels with certain operational profiles would get a penalty in their CIIs by the way they were operated and therefore end up with worse CII ratings than other vessels of the same type and size. The CII rating as it is defined as of now by IMO does not always favor the fuel-efficient vessels. It is possible to speculate in the operations in order to control the rating. It can even be an advantage to categorize routes from the benefit of the CII, an example is shown in two routes selected Fig.11.

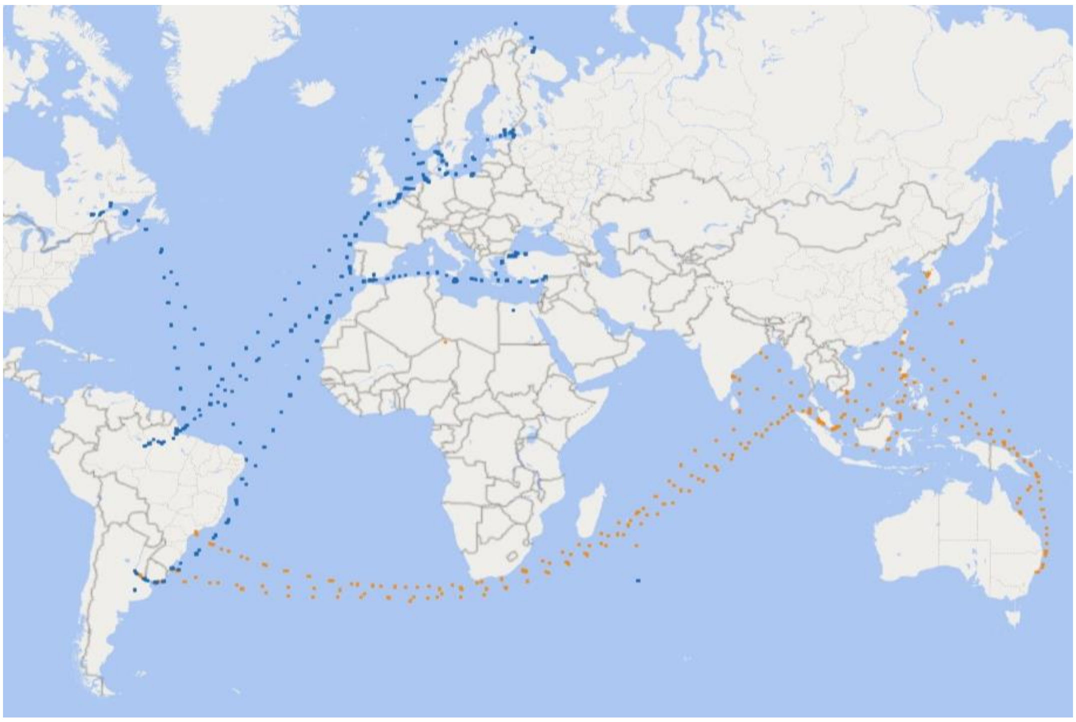

Fig.11: Comparison of favorable and less favorable trades for CII

The route with the orange dots is the CII favorable route with long distances equal split in ballast/laden voyages. The route with the blue dots has a large number of voyage legs and a lot of idle time and is the CII non favorable route.

The main driver of the CII rating is the operational profile and time spent at Sea, but energy efficiency has also an impact on the CII, case study 2 showed that Dry Dockings with new paint applications have an impact on the CII rating. Same can be found for hull maintenance events. Having the hull condition under control and avoidance of fouling will become even more important with the CII regulation in place.

It is always favorable for a shipowner to operate fuel efficient vessel. They operate with lower costs and emits less CO2, which is again to the benefit for the environment. Fuel efficient vessels will also come out with a better CII rating in general, it is however the operational profile which has a more significant impact.

3. CII exemptions, current status

Since the reported data are few, the parameter to rate ships will therefore also be simple. The simplicity of the CII makes it easy to handle but as it has seen in the previous case studies it may also be too simple and there are cases where it might not have the desired effect. To compensate for some cases where the CII rating will give a different outcome for vessels of same size and type due to different operations, several exemption rules have been suggested. A correspondence group under IMO was formed to handle incoming suggestions to exemptions in the CII and the group has ended up with several suggestions for exemptions for the circumstances. The work of the correspondence group is not completed, yet. The following list is based on the suggestions and represents our best knowledge, *IMO (2022)*. The following exemptions are likely to come:

- A correction factor for shuttle tankers in DP (Dynamic Positioning) mode or tankers involved in STS (Ship To Ship) operations where TF_j represents the quantity of fuel removed for these operations.

- A correction factor for specific voyages, where FC_{voyage} represents the quantity of fuel for voyages where a vessel is involved in the following situations:

    1. Scenarios specified in regulation 3.1 of MARPOL Annex VI, which may endanger safe navigation of a ship;
    2. Sailing in ice conditions, which means sailing of an ice-classed ship in a sea area within the ice edge

- A correction factor for distance adjustments where D_x represents the distance for voyage periods as defined in 1 & 2 above.

- A correction for time in port, specifically for cruise vessels, where AF_{PT} represents the quantity of fuel used when cruise vessels have long port stays during the reporting period.

- A correction factor for cases where vessels have high electrical consumption, where a consumption factor ($FC_{electrical}$) represents the quantity of fuel used for operations that require high electrical loads e.g. when sailing with a high number of reefer containers or where cooling of cargo is essential or where discharge pumps are used to a high level.

- A correction factor for boilers where the term FC_{boiler} represents the quantity of fuel used in operations where boilers are used to a high level, e.g. for cargo heating and for discharge operations.

- A correction factor used for "other" deductions where FC_{others} represents the fuel used in other deductible operations e.g. load/discharge with own cargo handling gear.

A more specific description on how the different exemption factors are calculated are given in the correspondence group documents and will presented for approval at the MEPC 78 in June 2022. The adjusted CII formula would then include the correction factors:

$$\frac{\sum_j C_{Fj} \cdot \left\{FC_j - \left(FC_{voyage,j} + TF_j + (0.75 - 0.03y_i) \cdot \left(FC_{electrical,j} + FC_{boiler,j} + FC_{others,j}\right)\right)\right\}}{f_i \cdot f_m \cdot f_c \cdot f_{iVSE} \cdot Capacity \cdot (D_t - D_x) \cdot AF_{PT}} \quad (4)$$

To get the exemptions it is required that the values are reported according to the descriptions in the rules documentation and the reporting is sent the verifying body where the data is included in the final calculation of the attained CII. This layer of additional reporting complicates the original simplicity of the CII and adds a layer of additional verification effort for the verifier. Since manual reporting of consumption via tank sounding or flow meter readings is allowed in the rules, the verification process can be difficult.

4. Outlook and suggestions

4.1 CII's foreseen impact on the charter market

Historically it has only been responsible shipowners/operators that have developed reporting systems with the intent to optimize operations both to the benefit of reduced operational costs and to the reduction of GHG emissions.
However, the main part of shipping companies has been operating in a market where commercial terms were the driver and where the focus has been keeping the charter contract terms. Since the fuel costs very often were included in the contract there has been no further incentive for many owners to optimize or reduce the fuel oil consumption/GHG emissions.

On the other hand, the charterer had focused on the commercial operations as well. Fuel consumptions are a very technical matter and improvements often have rather long return of investment periods, therefore also the charter had not put focus on consumption/emissions, at least not outside of the commercial boundaries of operations. With the CII ratings coming into play, the owners will have to pay more attention to how their vessels are operated in the charter contracts. In principle, the way how it is operated is up to the charterers, but if the charterer is operating the vessel in a way where it will come out with a bad CII rating (D or E) after a year, then the owner would have an issue. Landing in these two categories will first of all set restrictions on the future operations of the vessel. Furthermore it will be difficult to go out into the market and charter the vessel out while having these restrictions. So, the two stakeholders will need to align on targets, communicate during the chartering period and essentially incorporate these concerns into their contracts.

4.2 Use of EEOI instead of AER

Since 2019, vessels have reported their carbon emissions through the IMO DCS scheme. The implementation of the IMO DCS reporting scheme is generally a big achievement in getting an impression of the global shipping fleet's CO2 emissions. The verification procedure is in place, and it is logic to use the data in a regulation scheme to lower the CO2 emissions from ships. The choice of the AER as the CII for shipping is based on the availability of data in the IMO DCS.

However essentially ships are sailing to fulfill the needs of our societies, which is to transport cargo efficient and with very low emissions. One can argue that the current CII regulation does not always support this, as the theoretical vessel deadweight but not the amount of transported cargo is used in the equation. This means that Ballast voyages have a positive impact on the rating. A small comparison between the CII and EEOI and how they are aligned with the need of efficient and fast cargo transportation is shown in Table V.

Table V: CII and EEOI vs. needs of the society

	Useful for society?	Good for CII Rating?	Good for EEOI figure?
Sailingtime in Ballast	No	Yes	No
Sailingtime in Laden	Yes	Marginal	Yes
Idle in port	No	No	No

As the EEOI is in line with the needs of our societies the authors see it as a better parameter, in particular when it is considered over the whole transport chain. The criteria set in the EU MRV would allow the calculation of the EEOI figure. The EU MRV and IMO DCS reporting schemes should be aligned. As such processes in IMO need time, the authors believe that it would be a possibility to include this in the planned evaluation of the CII rating system in 2026. At that time there will be a reasonable overview on the CII rating system, how it has been received in the market and what effect it has had on the CO2 reductions from shipping.

4.3 Track and monitor vessels actual efficiency

The previous work shows that the AER as a CII to some extent is a relevant measure for the reporting of CO2 emissions. However, as the CII figure is impacted heavily by the vessel's operation profile, it has a limited meaning in terms of a vessel's actual energy efficiency. A vessel may have just received an "A" rating because she was sailing long Ballast legs last year.

The optimization of energy efficiency of a ship requires more detailed logging and observations combined with some target base models. Energy efficiency onboard can be optimized by a well-trained crew, which complies to targets and possibly a benchmark towards the crews of sister vessels. The crew has however limited impact on the hull & propeller performance, which is primarily impacted by the fouling status, the vessel age and the coating which was applied during the last dry docking.

Shipping companies shall address both fields. The hull and propeller performance can be tracked using methodologies such as the ISO 19030, *ISO (2016)*, or other. The majority of suppliers in the field of vessel performance analytics offer hull performance tracking solutions similar to this standard, some methodologies are already better.

Fig.**12**: CII tracking system, VesOPS 2021

The case study 2 includes vessels operated assisted by a performance monitoring system, Fig.12, and due to the high attention towards energy efficiency for this fleet, continuous attention to the energy efficiency has led to the vessels being rated in the better end of the scale. The ability to act on any deviations from the targets set for the efficiency is key to success on energy efficiency related matters.

4.4 Enforce the acquisition of better data

Introducing the CII as a measure of CO2 emissions from ships is the beginning of the regulations of GHG emissions from ships. One figure per year and vessel will however not be sufficient for an active improvement scheme within shipping companies, neither will it allow charterers to screen and select efficient vessels.

Already now many service providers desire to estimate the fuel consumption of unknown vessels to sell their services, like proving the effectiveness of a Hull Cleaning. Today we have a well-functioning and mandatory AIS system that is used in vessels for anti-collision and besides the original intended use, it is now used to collect information about vessel operations, vessel identification and fleet intelligence. The AIS system lacks however data that can be converted to fuel consumption or CO_2 emissions. This data is however most of the time available on board, so it is just not transmitted. There should be initiated some work in analyzing how automatic logged emission related data could be integrated in the AIS reporting process.

Many shipping companies have already set up data collection processes outside of AIS with high frequency and the experiences so far show that:

- Using data direct from sensors in the vessels increases the accuracy of the measured data.
- Operators get quicker response time, since data are updated continuously, and this will assist in making operations more efficient towards costs and energy efficiency.
- It is in a relief to the crews since there so many reporting systems already and there is no good reason to add another.
- The verifying tasks for the verifier would also be more efficient and it would be easy to automatize the verifying process.

Mandatory high frequency emission reporting, even without targets, would support the existing regulations and ensure that owners invest into the efficiency of their fleet. The market would undergo a change as it would be more evident which vessel operates efficient and which vessel does not.

In principle, the AIS system could be expanded to include the data that now are included in the mandatory reporting schemes. IMO DCS, EU/MRV and other – and since there is a standard for the information available in the existing system, this could very well be used for adding additional data.

5. Summary and conclusions

The beauty of the CII is that it reveals the carbon efficiency of transportation as a whole. IMO has set a goal of reducing annual greenhouse gas emissions in shipping by at least 40 % by 2030 as compared to 2008, hence the industry is very much in a need of having such a measure. However, due to the complexity of logistics, a one-size-fits-it-all regulation has its challenges in particular as the IMO DCS data is only giving a rough indication about the vessel's trade and most frequently based on manual vessel reporting.

The CII is linked to energy efficiency, but the energy efficiency of a single vessel cannot fully be described by the CII rating. A shipowner/operator will not be able to operate and optimize the energy efficiency of their vessels based on the CII values alone. For this, a more detailed vessel performance scheme must be used, where a system is fitted to the type of vessels included and where the monitoring is based on a higher frequency of data.

In principle, the CII differs from the original idea of GHG reductions from Shipping when the EEDI and the EEOI were introduced. In these indexes/indicators the term “to the benefit of society” was included and the EEDI rewarded vessels with large capacities and the EEOI rewarded the vessels which were able to operate with fully laden ships as much as possible. Our case studies show that the CII chosen rewards the opposite and it should be considered to also include the amount of transported cargo in the IMO DCS reporting and to move from AER to EEOI as the CII rating base.

An additional measure to IMO DCS could be a mandatory emission reporting with a high frequency (e.g. AIS frequency), with a verification scheme in place. Such a measure would reveal the actual performance of the worlds fleet and allow real optimization upon it.

References

ISO (2016), *Ship and marine technology – Measurement of changes in hull and propeller performance*, Int. Standard Org., Geneva

IMO (2021a) *Resolution MEPC.337(76) - Guidelines on Reference Lines for use with Carbon Intensity Indicators (G2),* IMO, London

IMO (2021b), *Resolution MEPC.338(76) - Guidelines on Operational Carbon Intensity Reduction Factors (G3),* IMO, London

IMO (2021c), *Resolution MEPC.339(76) - Guidelines on Operational Intensity Rating of Ships (G4),* IMO, London

IMO (2022), *MEPC 78-X4 Report of CG on tech.GL on carbon intensity*, IMO, London

Sea Trial Methodology for Wind Assisted Ships

Sofia Werner, **Jonny Nisbet,** SSPA, Gothenburg/Sweden, sofia.werner@sspa.se
Fredrik Olsson, RISE, Gothenburg/Sweden

Abstract

Wind propulsion technology has the potential to significantly lower the fuel consumption of cargo vessels and improve the EEDI/EEXI. The number of wind propulsion installations is predicted to increase rapidly the coming years, and thereby the number of different technologies and makers. This development calls for standardised procedures for validation of the wind propulsor performance in full-scale. However, such standard procedures or guidelines are still lacking. This paper proposes a methodology based on short sea trials, combined with digital twin modelling and statistical voyage analysis. The method is demonstrated using full scale trials for three cargo vessels with wind assistance technology. Various strategies for conducting as well as analysing the trials are discussed.

1. Introduction

In response to IMO's request to reduce green-house gas emissions from shipping, *IMO (2017)*, many ship owners now consider wind propulsion as one way to reduce the fuel consumption and improve the EEDI/EEXI. There are already a number of cargo vessels equipped with wind assistance technology and the number is predicted to increase rapidly the coming years according to *UK Clean Maritime Plan (2019)* and *Nelissen (2016)*.

As with all new technologies, there is a need to verify the performance of wind propulsion solutions in real life. Not only does the ship owner who made the investment request confirmation of the power savings. The technology provider can also make use of the validation data to improve the design and prediction methods for future installations. Last but not the least, authorities request trustworthy verification of energy reduction for legal indicators such as EEDI *IMO (2021)*, and other voluntary notifications of sustainable shipping.

Since the wind propulsion in modern commercial shipping is still a novelty, the community has not converged towards a standard procedure for conducting full scale verification tests. As the industry matures and the number of manufacturers and installations increases, there is a growing need for standardisation of full-scale verification.

The present work aims at contributing to the development of methods for full-scale verification of wind assistance vessels. The long-term goal is to develop a sea trial methodology that is transparent and feasible to conduct, and that results in useful performance indicators. In this paper, some optional methods are proposed, discussed, and demonstrated for the three vessels shown in Fig.1.

Fig.1: m/v Copenhagen with a Norsepower rotor, m/v Annika Braren with EcoFlettner rotor and m/v Frisian Sea with Econowind suction wings.

Recently published full-scale campaigns for wind assisted ships have mainly been based on long-term monitoring data, such as for m/v Viking Grace *Paakkari (2019)* and for m/v Maersk Pelican *Paakkari (2020).* An advantage of this type of data is that it reflects the variety of weather conditions and operational profile that the ship encounters, as well as the real operability factors like idling time due to maintenance, weather routing, and crew skills. A challenge of using long-term monitoring data to detect even moderate power savings is the large scatter of such data, together with difficulties to find a comparable reference period with all other conditions except the wind propulsion installation unchanged. The main disadvantage is, however, the long period of time that such campaign requires. This is both costly and impractical in a commercial context and for EEDI verification.

Another strategy for performance verification of wind propulsion is to carry out short, dedicated tests over a few hours, compare the ship's speed and power when the wind device is turn on and off, and carefully record the environmental conditions. This methodology is reported for m/v E-Ship 1 *Smidth (2013)* and for m/v Fehn Pollux *Vahs (2019),* but showing only one selected (favourable) condition with no explanation on how to extrapolate this to a useful KPI.

The three sea trials in this work were conducted within the EU Interreg North Sea Region project *WASP* with the primary aim of demonstrating the energy saving of the wind propulsion installations. It should be stressed that the results should <u>not</u> be used to compare and rank the tested technologies. The power saving of an installation depends to a large extent on the shape of the ship hull, limitations related to cargo handling, limited air draft, and the ship's speed. The detailed results of the three sea trial assessments, plus two more to come, will be published by the *WASP* project on a later occasion.

Apart from verification of power saving, other aspects of the wind powered ship's functionality such as manoeuvrability, stability, noise, and human machine interface should be tested in real life. This paper focus entirely on power consumption, which is directly linked to green-house gas emissions. The scope is limited to wind <u>assisted</u> ships, i.e. ships with wind propulsion devices that reduce the engine power, as opposed to wind powered ships, which can be completely driven by wind.

2. Ship cases

The RoPax hybrid ferry m/v Copenhagen, owned by Scandlines, (L=156.45m, B=24.6m, dwt=5000t, IMO 9587867) operates the route Gedser-Rostock. She is equipped with a 5m x 30m Norsepower rotor sail with top end plate. (See *Paakkari* (2020) for a description of the rotor technology.) The rotor is positioned longitudinally around mid-ship, 17.2 m above design water line. The rotation speed of the rotor is set automatically by its control system, based on the measured apparent wind speed. The anemometer is positioned in the top of the signal mast over the bridge. The vessel is driven by two Azimuth thrusters and a centre propeller with controllable pitch.

The bulk carrier m/v Annika Braren, owned by Rörd Braren Bereederungs-GmbH & Co. KG, (L=84.95m, B=15m, dwt=5035t, IMO 9849148) operates mainly in the North Sea region and the Baltic Sea. She sails with a 3m x 18m Eco Flettner rotor with top and bottom end plates, positioned at the fore castle. The rotor is driven by an electric motor and the rotation speed is set automatically, based on the measured apparent wind speed. The anemometer is positioned in the top of the signal mast over the bridge. The ship has a ducted, controllable pitch propeller.

The general cargo vessel m/v Frisian Sea, owned by Boomsma shipping (L=118m, B=13.4m, dwt=6446t, IMO 9534547) operates mainly in the North Sea region and Baltic Sea. She is fitted with two 3m x 10m suction wings from Econowind. (See *Charrier (1985)* for a description on suction wings*).* The wings are fitted with flat racks and they are tiltable sideways over the hatch covers. Air suction is created using fans driven by electric motors. The sheet angle is set automatically based on the apparent wind measured in the mast. The ship has a ducted, controllable pitch propeller.

3. Sea trials

3.1 Settings

The three sea trials were planned and conducted by Sofia Werner, SSPA Sweden AB, in cooperation with the ship's masters and in the case of the ferry Copenhagen, also in cooperation with Scandlines' naval architect Rasmus Nielsen. The trials took 5-6 hours. The trial with the ferry Copenhagen was carried out at night between ordinary schedules trips. With Frisian Sea and Annika Braren the trials were conducted on route between two load ports in the Baltic Sea.

The environmental conditions and settings are given in Table I. The sea trial of Copenhagen has been reported earlier in *Werner (2021)*. Further details on the trial conditions, data accusation, the measured data and detailed results are available in three project reports, which will be made available from the EU Interreg project WASP. There is unsignificant tidal current in the trial area, but weak, constant currents reported.

Table I: Trial conditions. Wave condition reported by external provider, wind as measured onboard

	m/v Copenhagen	m/v Annika Braren	m/v Frisian Sea
Trial date	March 6-7, 2021	September 25, 2021	October 11, 2021
Ship's Master	Alan Bach	Capt Mehrens	Oleksandr Pasatiuk
Location	South of Gedser	North of Gotland	South of Gotland
Wave height	1 m	0.7-1.5 m	1.7 m
Wave direction	W	NW	WSW
True wind speed	8-9 m/s	9-12 m/s	7-9 m/s
True wind direction	W	NW	SW

3.2 Data acquisition

The measured data was recorded using the three ships standard equipment for performance monitoring according to Table II. Some signals were recorded manually on the bridge during trial, by reading the display every 60 s. On Annika Braren, the "trial function" of the performance monitoring system was used to get the averaged fuel consumption over each run. Since Annika Braren is not equipped with a shaft torque meter, the delivered power in kW had to be derived from the fuel oil consumption, the main engines SFOC and subtracting the shaft generator power. On Frisian Sea, the suction wing fan engine power could not be registered. The theoretical curve from the provider is used in the analysis.

Table II: Data acquisition, source, and sampling frequency.

	m/v Copenhagen	m/v Annika Braren	m/v Frisian Sea
Speed through water	Doppler log manual reading, 60s	Doppler log 60s	Doppler log 3 min running average
Speed over ground	GPS 60s	GPS 60s	GPS 3 min running average
Ship engine power	electric engine power output, 5s	Volumetric fuel flow meters, inlet and outlet, manual reading of time average value	Shaft torque meter 3 min running average
Wind anemometer	Mast top 60s	Mast top 60s	Mast top 3 min running average
Wind propulsor power	Electric engine power	Electric engine power	Not measured

3.3 Sea trial procedure

The trials were conducted as close as possible according to the well-recognised standards for speed-trials ISO 15016 / ITTC 7.5-04-01-01.1. The trial programs included a number of short runs, 10-15 minutes long. Constant heading was kept during the runs using the ships' autopilots. Before the measurements started for each run, it was check that the heading and speed was steady with an external GPS by plotting over time. The rotor and wing settings were adjusted automatically by the control system throughout the trial. The wings were activated and dis-activated by raising and lowered them down, which takes just a few minutes. The two rotors were activated by turning the spinning on or off.

Different approaches to test program were tried for the three trials, in order to study pros and cons of each method. A discussion will follow in Section 7.

<u>Copenhagen.</u> The trial was executed as a conventional sea trial using doubles runs in reciprocal directions. One complete double run was done without the rotor on and the wind at 90° from the bow, followed by a double run with the rotor on. This was repeated for one other wind direction, about 40/140° true wind. The ship's thrusters were set to constant shaft rate.

<u>Frisian Sea.</u> Reciprocal double runs were *not* used. Instead, two runs with and without the wings were done in series, with the ship's heading and main engine shaft rate and propeller pitch fixed. After two such runs, the heading was changed to get another wind angle, and the procedure repeated. For some headings, the order was opposite (wings first, without wings second). Additionally, two runs were conducted without the wings straight into and following the wind.

<u>Annika Braren.</u> A similar program as for Frisian Sea, without reciprocal double runs were used for Annika Braren. The difference is that 3 runs were done for each wind direction: i) without rotor, ii) rotor turned on, main engine fixed as in first run (which means ship's speed increases) iii) ship's propeller pitch reduced to get similar speed as the initial run.

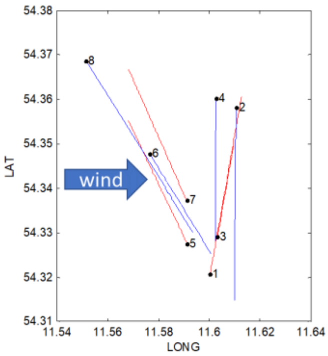

m/v Copenhagen

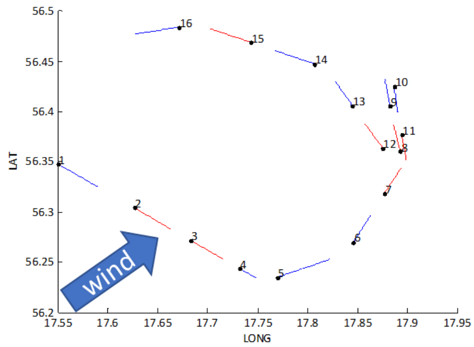

m/v Frisian Sea

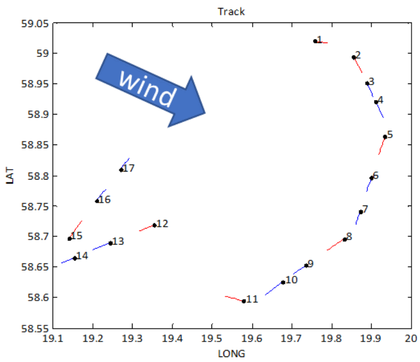

m/v Annika Braren

Fig.2: Trial programs. Red=without wing/rotor, blue=with wing/rotor. Black dot is the start of each run.

4. Sea trial analysis

4.1 Current

The three trials presented here were all conducted in areas with unsignificant tidal current, but with weather driven currents that change slowly compared the trial time frame. Since the purpose of the trials here was to measure differences (with and without wind propulsor), no correction for current was needed.

4.2 Superstructure and idling rotor air resistance

The measured power for each single run is corrected for the resistance of the superstructure based on ISO/ITTC standard procedure.

Since the purpose is to derive the effect of the wind propulsor compared to the ship without any wind propulsor, the resistance of the idling propulsor must be subtracted from the runs when the wind propulsor was not used. For Frisian Sea, the wings were folded down when idling, so this is only required for the two ships with rotors. The rotor resistance is estimated as:

$$R_{rotor} = C_{\mathrm{D\ rotor}} \frac{1}{2} \rho_{air} \cdot H \cdot D \cdot {AWS_x}^2 \qquad (1)$$

The resistance coefficient of the idling rotor, $C_{\mathrm{D\ rotor}}$, is estimated to be 0.5 *Kramer (2016)*. AWS_x is the apparent wind speed in the ships longitudinal direction at the height of the rotor.

4.3 Power correction

The correction of propulsive efficiency due to the added resistance corrections and idling rotor resistance is derived according to the ISO/ITTC standard using the Direct Power Method, see *ITTC (2021)* for details.

5. Performance analysis

After the corrections described above are done, the effect of the wind propulsors can be derived by comparing the runs with and without propulsor, for the same wind angle. As shown in Fig.3 for Copenhagen, this results in an increased speed AND a reduced power (due to higher propeller efficiency when off-loading). To be useful, the results need to be processed further.

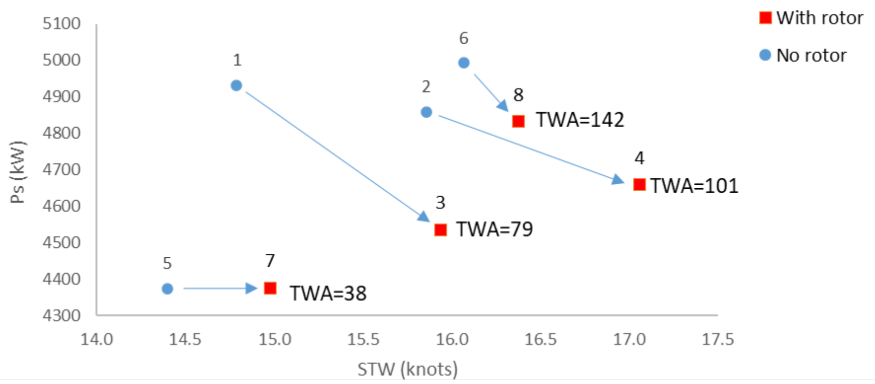

Fig.3: Speed and corrected power from the m/v Copenhagen trial

5.1 Normalisation Method 1 - using the speed-power curve

The simplest way to translate the speed and power differences found at the sea trial into a single power loss is to use the ship's speed-power curve. This can be done in the following way:

1. Fit a polynomial to a part of the Baseline curve that covers the measured points.
2. Shift this polynomial vertically so that it intersects the sea trial point for the no wing/no rotor case, as shown in Fig.4.
3. Evaluate the shifted polynomial at the reference speed. This gives P1.
4. Repeat for the case with rotor/wing. This gives P2.
5. The delta power is the difference between P1 and P2.

For the present vessels, baseline curves were obtained from earlier sea trials or model test, adjusted to the actual condition.

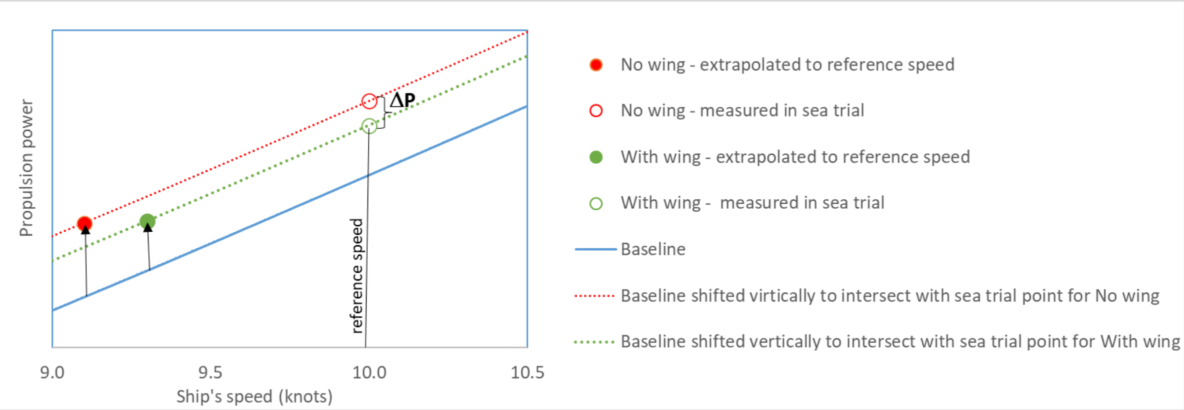

Fig.4: Example of how sea trial result is extrapolated to nominal speed using the Baseline curve shape

The derived power difference is corrected to a nominal wind speed using:

$$\Delta P_{TWS_{ref}} = \Delta P \cdot \frac{TWS_{ref}^{\;2}}{TWS^2} \cdot \frac{\rho_{a\,ref}}{\rho_{a\,trial}} \tag{2}$$

where TWS_{ref} is the reference wind speed and TWS is the true wind speed during the sea trial, at the same height. The wind variation over height is computed according to ISO 15016 using exponent 1/7. $\rho_{a\,ref} = 1.24\ \mathrm{kg/m^3}$.

Normalisation Method 1 above includes several simplifications. The propulsive efficiency is not necessarily the same when moving along the power curve as when changing the net longitudinal force for a given speed (as when adding a rotor). A second simplification is that the changed apparent wind due to a changed ship speed is not included. It will be shown below that these possible error sources are significantly smaller than the measurement uncertainty, at least when the reference condition is close to the sea trial condition. However, using this method for extrapolation to any wind condition is questionable. Therefore, a more advanced method is proposed in the next section.

5.2 Normalisation Method 2 - using a propulsion model

In order to extrapolate the trial results to any arbitrary speed and wind condition, a ship simulation program is used. The program is part of SSPA's inhouse simulation code SEAMAN. The part that is used here is a static 4DOF VPP including propeller and power models. The important point is that it can model the relation between speed, resistance, power and propeller efficiency. The process includes, in short, the following steps (further details are given in *Werner (2021)*):

1. Ensure by correlation that the output of the VPP is equal to the ship's baseline curve (speed-power-rpm curve at the actual condition, without wind propulsor)
2. Use the VPP to find the additional force in the longitudinal direction that matches the measured change in speed AND corrected power between two runs *with* and *without* wind propulsor. That

force is assumed to be the wind thrust, T . Derive the coefficient Ct by nondimensionalising T using the apparent wind speed and air density, while considering the atmospheric boundary layer assuming 1/7 power.
3. Regress Ct against apparent wind angle by adapting a theoretical Ct curve of a generic wind propulsor (rotor or suction wing) derived by CFD. The same correction is applied to the side force, assuming that the ideal rotor/wing Cl/Cd is preserved. This is an assumption, but since side forces is not measured at the sea trial, it is the best possible approach. However, the magnitude of the side force has only a marginal effect on the power gain for the current cases.

The VPP can now be used to derive power savings for any wind condition, using the correlated wind propulsor thrust coefficient, under the assumption that the coefficient is independent on wind speed. (Algorithm to find rotor optimal spin ratio at different wind speeds is included). The power consumption from spinning the rotor or driving the air fans in the suction wings is added to get the net power saving. Fig.5 shows the result of normalisation Method 2, together with the results from the more simplified normalisation described earlier. The two methods coincide within the uncertainty level, which indicates that the simplified method is acceptable, at least for wind and ship speed close to the trial condition. However, this needs to be studied further with more test cases.

The performance model can now be used to predict the power saving at any wind condition. For wind conditions that results in negative wind propulsor thrust, it is assumed that it is turned off. In head wind, the rotor will give an added resistance according to Eq.(1), but the suction wings will be lowered on deck and give no idling resistance.

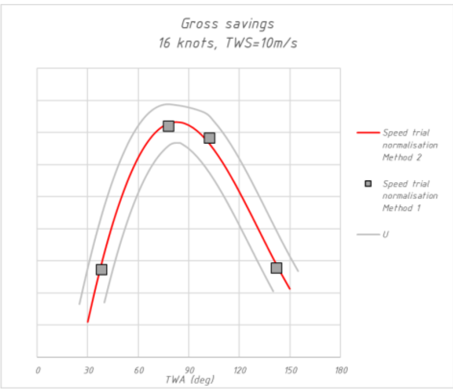

m/v Copenhagen

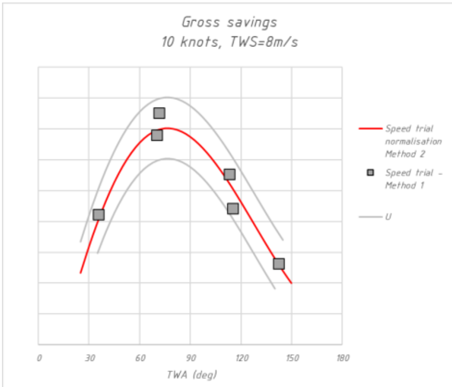

m/v Frisian Sea

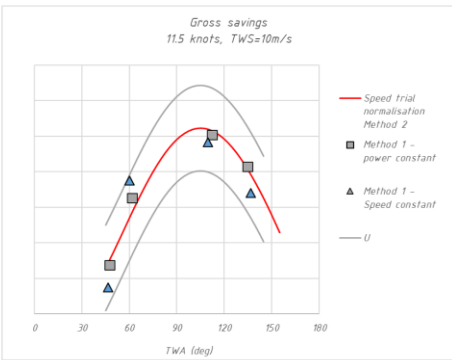

m/v Annika Braren

Fig.5: Sea trial results with two different normalisation methods. Uncertainty estimates described in Section 7.5.

The drift and rudder forces are introduced in the ship simulation tool in terms of manoeuvring coefficients based on the bis system model due to *Norrbin (1970)*. In the present cases, the manoeuvring coefficients are extracted from SSPA's database of manoeuvring model tests of similar ships. Added resistance in waves are derived using spectral superposition of response amplitude operators (RAO) using ITTC and wave spectrum (ITTC) to find mean added resistance in an irregular sea state.

The results are shown in Fig.6. These graphs should not be used to rank the devices between each other. The result is highly dependent on ship's speed, ship size, hull shape and limitations due to cargo handling. However, optimum performance of the rotor sails is at wind angles aft of beam compared to wing sails; it moves forward for higher ship's speed. The wings give positive thrust for wind angles up to about 30° (17° apparent wind), and are folded down in head winds, whereas the rotors cost additional resistance for wind directions less than 30°, since the rotors of these ships cannot be folded.

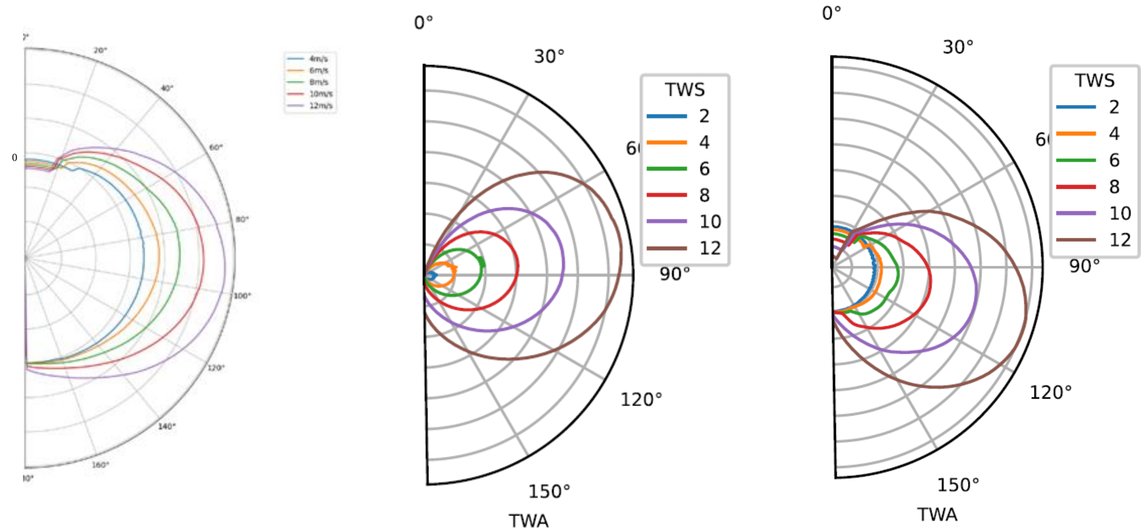

Fig.6: Net power saving at various wind speeds. Copenhagen (16 kn), Frisian Sea (10 kn), and Annika Braren (11.5 kn)

6. Fuel and emission saving potential

6.1 Settings

The final step in the analysis is to estimate the fuel and emission savings on given routes. This is achieved by combining the ship and wind propulsor model described above with weather statistics and a Monte-Carlo based voyage simulation tool.

There are several simplifications in the simulations:

- One fixed speed per ship (16 kn for Copenhagen, 11.5 kn for Annika Braren and 10 kn for Frisian Sea)
- Air density 1.24 kg/m^3 all year around
- Two typical loading conditions according to ships expected operational profile.
- The main engine is assumed to always deliver enough power and torque to reach the intended speed, i.e. no involuntary speed reductions.
- Engine efficiency variation with load not accounted for.
- Voluntary speed reductions are not accounted for.
- Hull fouling is not accounted for.

6.2 Routes and wind statistics

The ferry m/v Copenhagen traffics the route Gedser – Rostock. The two other vessels are tramping in the Baltic Sea, North Sea, English Channel and Biscay. Four typical routes in their operational profile are selected for illustration of the fuel saving potential.

The routes are divided into legs, and for each leg a discrete joint weather distribution (True wind speeds and True wind angles) is derived from the ERA5 reanalysis dataset available in the Copernicus Climate Data Store, https://cds.climate.copernicus.eu. Each leg is treated independently, and leg-wise distributions are assumed to be uncorrelated. For Copenhagen's route Gedse-Rostock, there were not enough suitable datapoints in the Copernicus data set for this short route. Instead, the wind distribution is obtained from the Global Wind Atlas, https://globalwindatlas.info/. The Global Wind Atlas use the reanalysis ERA5 statistics and apply both mesosacale and microscale modelling in order to get a 250x250m grid of local wind climate. As a complement, the wind statistics from EEDI Global Weather matrix is included, *IMO (2021)*. It represents the wind on the mayor world-wide trade routes.

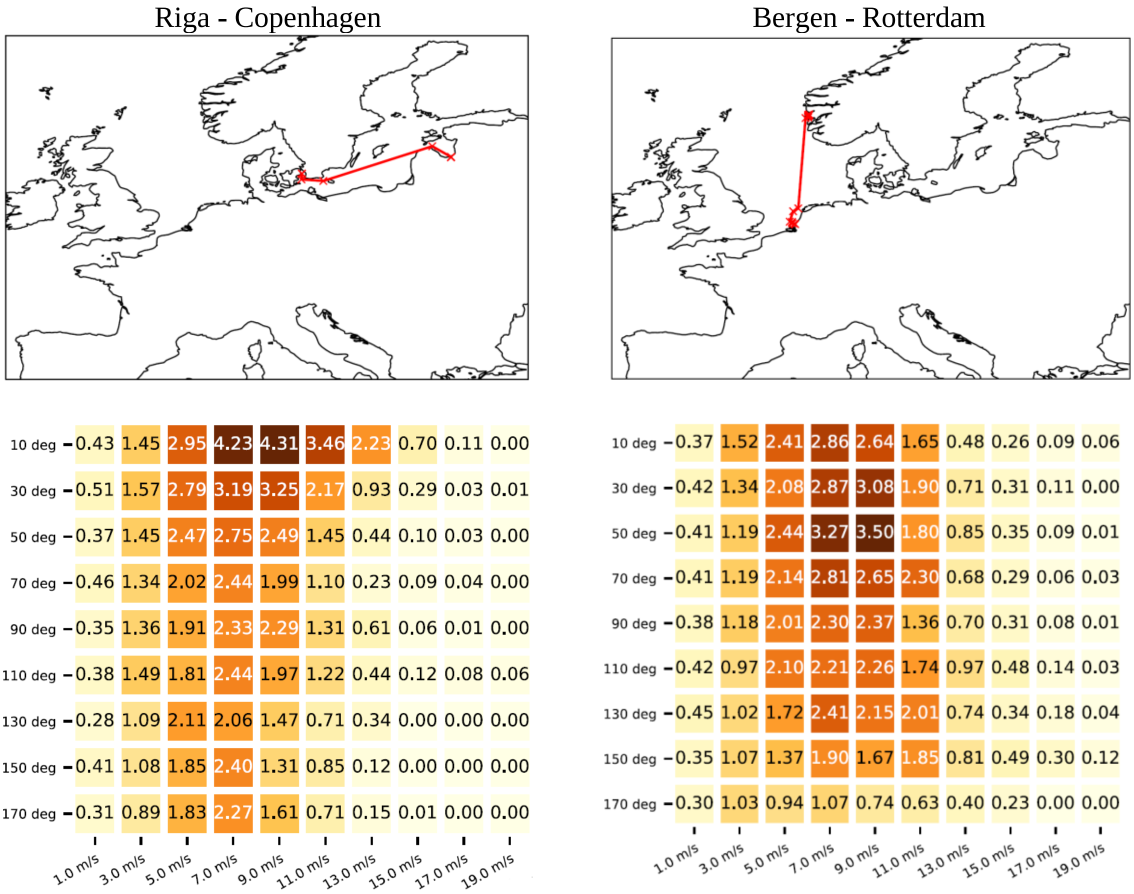

Fig. 7: Example of weather distribution on two routes (one way). The heat maps show joint probability of true wind speed and true wing angle relative to route heading.

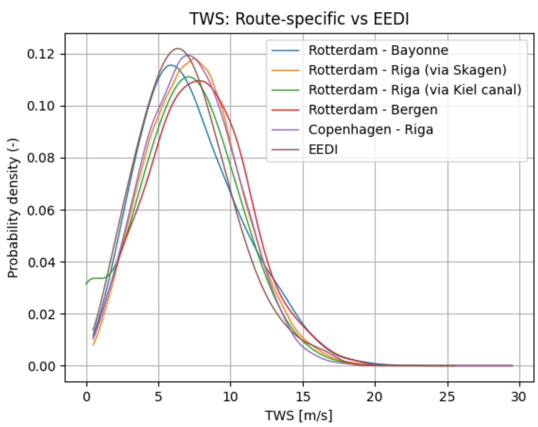

Fig.8: Probability of true wind speed on Frisian Sea's routes (two-ways) from external weather source.

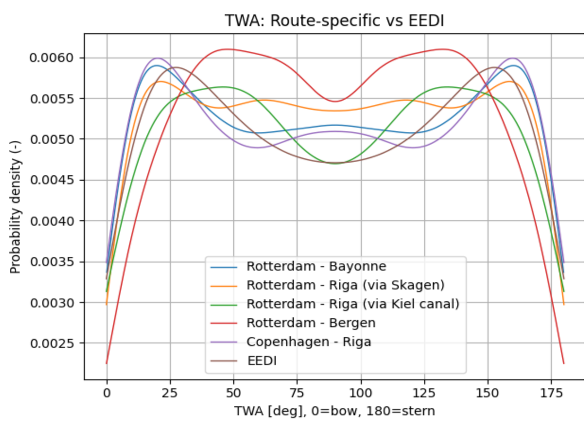

Fig. 9: Probability of true wind angle relative to ship heading on Frisian Sea's routes (two-ways) from external weather source.

As an example, two of Frisian Sea's routes are shown in Fig.7. The joint probability distribution heat maps indicate that the Riga-Copenhagen route has prevailing winds straight against the bow, whereas at the Bergen- Rotterdam route the winds are generally more open and also stronger. Fig.8. shows the assembled (two-ways) weather distribution for a number of routes of the actual ship. It can be noted that the EEDI Global Weather matrix has lower wind speeds than most of the routes.

6.3 Route simulation technique

Route simulations are carried out by performing statistical simulations of Monte Carlo type over different combinations of environmental conditions along the route to estimate statistical properties of route energy requirement. See *Olsson (2020)* for further details.

6.4 Fuel saving potential

The power saving potential is derived by executing the voyage simulating with and without the wind propulsor and comparing the average power requirement, keeping the ship's speed fixed. This represents the average value of letting the ship sail the route 100 000 times in randomly chosen weather conditions based on weather statistics from the full year of 2019. Some days the weather will be favourable with large power savings, some days it will be adverse.

For the ferry Copenhagen, the simulation shows that the power saving potential is around 4%. The corresponding value when using the EEDI Global Weather Matrix as the weather source is 2.0 %. The two other vessels sail on many different routes without a fixed schedule. As an example, the fuel savings for some of the typical routes are shown in Figs.10 and 11.

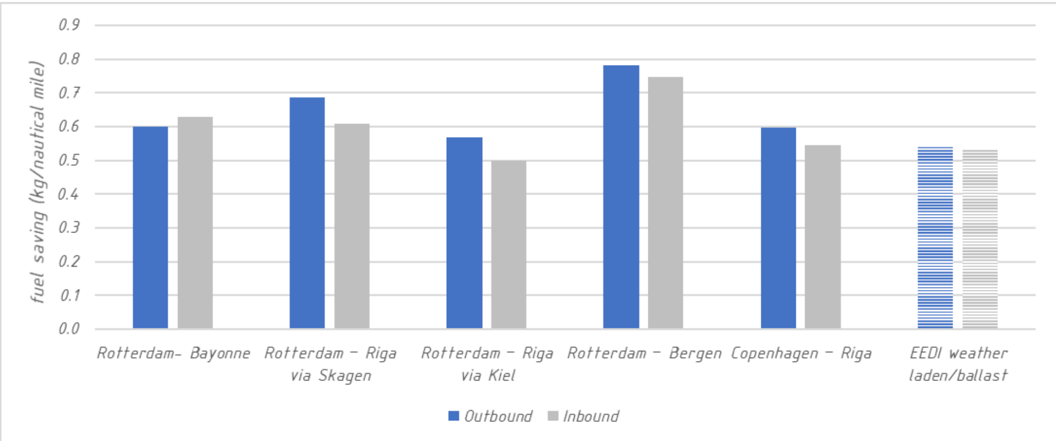

Fig.10: Frisian Sea, average fuel saving per route, ships speed 10 kn

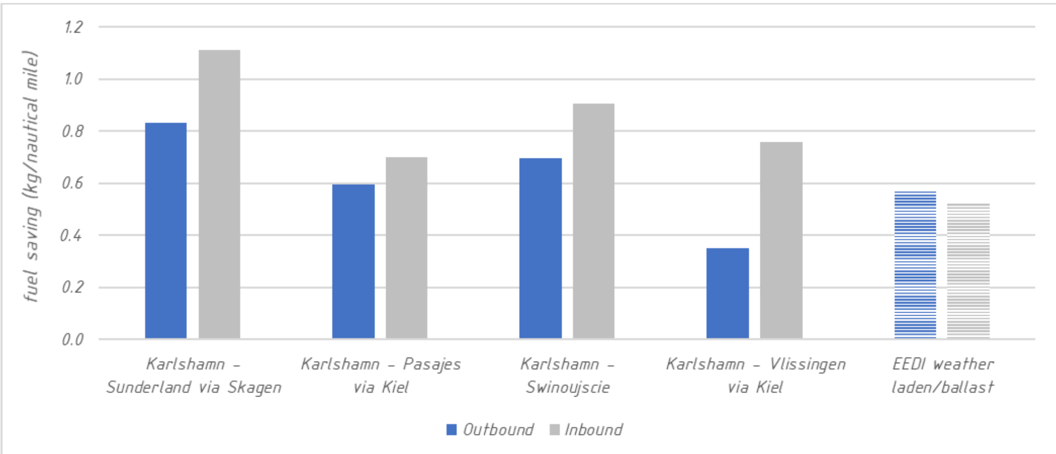

Fig.11: Annika Braren, average fuel saving per route, ships speed 11.5 kn

For Frisian Sea, the largest power saving per mile is achieved on the route Bergen-Rotterdam. On this route the prevailing wind directions are further towards the beam than for the other routes and with generally stronger winds speeds. The route Copenhagen – Riga is east-west bound and the prevailing winds are either head or stern winds. The power savings are therefore smaller.

Annika Braren has a very favourable route from Sunderland (UK) to Karlshamn, with dominating wind from aft beam, which is very suitable for the rotor performance profile. On the other hand, the west-southwest bound route Karlshamn-Vlissingen via Kiel is not a favourable route for any wind sailor.

7. Discussion on methodology

The purpose of this work is to test and evaluate different methodologies and strategies for wind propulsion sea trials. Here follows a discussion on some aspects that has been considered.

7.1 Speed constant or power constant

The conventional ISO 15016 procedure prescribes that the power setting (propeller shaft rate and propeller pitch) is kept constant for both runs in a double run. An alternative approach for the wind propulsion sea trial would be to keep the speed constant between two subsequent runs by adjusting the power. The benefit would be to limit the need for correction in the normalisation to reference speed.

In an attempt to compare the feasibility of the two approaches, the sea trial program of Annika Braren included both types of power settings. It is, however, difficult to achieve a given speed in practice on a large vessel. The ship's speed reading is constantly varying, and it is not until the end of a trial run that the averaged value can be derived. The ship's large inertia makes the response to a changed engine load setting very slow and therefore it is not possible to fine tune the speed by hand.

It is observed that the result as presented in Fig.5 does not show any benefit of either method in terms of scatter or difference between Method 1 and Method 2. Somewhat larger scatter can be seen for the runs where constant speed was attempted, but it could just as well relate to measurement uncertainty.

There is an advantage of keeping the power setting constant when analysing with Method 2: even if the true propeller pitch setting is not measured accurately, at least it is known that it was the same setting in the two runs. This reduces some uncertainty. Another advantage is that it is faster to conduct the trial with constant power, since the adjustment and trying to find the right speed takes some time. Finally, the advantage of keeping the power constant is that it follows the ISO standard. The conclusion is that constant power is recommended for wind propulsion sea trials.

7.2 Current

One of the key outputs from a sea trial is of course the ship's speed through water (STW). However, speed logs are in general too inaccurate be usable for performance assessment *Øksnes (2021), ITTC (2014)*. Measuring the speed over ground (SOG), historically by using landmarks and accurate timing, and nowadays using DGPS, is much more accurate. The problem is that the SOG readings are affected by current. In the standard ISO/ITTC sea trial procedure *ISO (2014), ITTC (2021)*, current is eliminated using double runs, i.e. two runs in reciprocal direction with the same engine power setting. The correction method, either the so-called Means of Means or the Iterative method (see *Strasser (2007)* for further details) effectively compensate for the current, under the condition that the engine power is constant over the two runs, and that the effect of wind and waves can be estimated and subtracted.

The problem for wind propulsion sea trials is that the first condition cannot be fulfilled for other wind directions than exactly ±90° from the bow! For all other wind directions, there is an additional, unknown, propulsive power that is different between the two runs. This can be solved in several ways:

i) to use the ship's log directly instead of the GPS SOG, and thereby avoid the need to correct for current. Since the aim of the wind propulsion trial is to compare the runs with and without rotor, a small bias error in the speed log readings will have no influence on the result. However, if the precision of the speed log is poor, it will increase the uncertainty of the trial result.
ii) to use the GPS SOG to derive the speed differences between two consecutive runs. This works only if the current changes slowly enough to be regarded as constant during the ~30 minutes of the two runs.
iii) to do three or four runs in a series with wind propulsion device (on-off-on-off), instead of just two (on-off). This option has not yet been used by us.

The three trials presented here were all conducted in areas with unsignificant tidal current, but with weather driven currents that change slowly compared the trial time frame. Therefore, any of the options i) or ii) could be used. Option iii) will be investigated in the near future.

7.3 Why not just test at 90° wind angle then?

A fourth solution to the problem with current correction would be to carry out the sea trials at 90° wind angle only. There are two good reasons why wind propulsion sea trials should include a range of wind directions.

The first reason is the difference in performance over wind directions between different devices, as was seen in Fig.6. Verifying the performance at 90° only could be misleading or unfair.

The second reason is the influence of the hull on the wind propulsor performance. Predictions of the performance have up to now often been based on wind tunnel tests or CFD simulations of a propulsor (rotor, wing) in isolation, without any hull. The performance of a wind propulsor standing on a ship hull has been reported to be quite different from that of one a floor. CFD studies by *Garneaux (2020)* showed both increased and decreased performance depending on the wind angle. *Vahs (2019)* reported an increased performance compared to the ideal case for a rotor positioned in the bow of a coaster measured in full-scale. *Jones (2019*) on the other hand, observed a decreased performance when placing rotors on tanker ship hull.

The sea trial in the present study showed a large deviation between the theoretical lift and drag curves of rotors and wings and the actual results. More research is underway on the physical explanations, but so far it is noted that:

i) The influence of the hull varies substantial with wind angle
ii) The trend is completely different between the three ships

It can be concluded that sea trials at a range of wing angles are very important to verify the hull interaction. On top of that, the latest version of the EEDI regulations *IMO (2021)* request that a validated method is used for the interaction effects between wind propulsors and ship.

7.4 Normalisation Method 1 and Method 2

A comparison between the two normalisation methods presented in Fig.5 shows that they correspond well. The scatter is probably related to the poor precision uncertainty of the measurements.

Method 2 can be used not only for the sea trial assessment but also for further use such as weather routing, fleet optimisation. This method requires that the ship's resistance curve, propulsive factors and propeller characteristics are known. If such data is not available, good enough estimates can be done by tuning data from similar ships against the actual trial. An initial sensitivity check showed that the influence of these assumptions on the result is small, but this should be investigated more in a systematic way.

Method 1 is simple and transparent and does not require any ship simulation tool as Method 2 does. Therefore, it can be a useful method in praxis for example for EEDI verification, but it should be limited to cases with small contribution of wind propulsion and when the sea trial wind speed is close to the nominal. Further research should be done on the limitation of Method 1 and Method 2 for more powerful wind propulsion installations.

7.5 Uncertainty assessment

Assessing the uncertainty of full-scale test is very challenging, let alone for a completely new application as wind propulsion. An attempt is made here, but is should be stressed that more research and data from sea trials is needed.

The bias uncertainty of a speed trial is stated in the ISO and ITTC standards to be 2% *ISO (2015, ITTC 2021)*. The precision error of speed trials in general is estimated by Werner (2020) and Insel (2008) to be around 7-8%. A large part of the precision probably relates to geometrical difference between the sister ships, and that the trials are conducted at different occasions. These number is of little use to the uncertainty estimation of the wind propulsion sea trial. The purpose is here to derive a power *difference* and therefore, the bias error can be assumed to cancel out. The exception is the wind measurements. A bias error of the anemometer will affect the comparison of the runs with wind propulsor and the runs without.

The uncertainty of the derived power difference has been estimated for the three sea trials, following ITTC 7.5-02-01-01 (Type A). We do not claim it to be a complete uncertainty assessment, but rather an indication of the magnitude of the larger error sources. The analysis leads to the 95% uncertainty interval indicated in Fig.5.

The three largest sources of uncertainty were estimated to be the precision of the speed log, precision of the power measurement and the total uncertainty of the wind measurements. The three tested vessels have different data logging equipment for speed and power, some with higher precision the others. On Annika Braren for example the power was measured indirectly from volumetric fuel flow meter, which is known to be less accurate that shaft torque meters.

The total uncertainty of the measured wind is estimated to be 5% based on the standard deviation of the time signal, and guessed bias due to calibration error, variation of the atmospheric boundary layer and disturbances of the superstructure, mast and other antennas. The bias error estimate could well underestimated. This should be studied further using CFD and further wind measurements using alternative techniques such as LIDAR.

8. Using the sea trial results

The results of a wind propulsion sea trial can be used for several purposes.

8.1 Performance guarantee, contract confirmation

In the current “innovative phase” of the growing wind propulsion industry, the buyer and sellers of wind propulsion technology often mutually understand that the promised performance is really a best guess. Those days are soon over. As the competition grows, the providers must sell their solution with an expected performance, and the buyers will request a confirmation on delivery. There are two ways that the sea trial methodology described above can be used in this context.

i) The provider states the performance at a number of reference conditions, for example 8, 10, 12 m/s true wind speed and a range of wind angles. An independent 3rd party organisation conducts a sea trial at wind speeds between 6-14 m/s and normalised using the method described above to the reference conditions.

ii) The provider states the fuel saving potential for an agreed route. An independent third-party organisation conducts a sea trial and extrapolate to fuel saving potential using their voyage simulation tool or agreed weather matrix.

8.2 EEDI and EEXI

Currently, improvement of EEDI/EEXI from wind propulsion does not need to be verified in full scale, (whereas sea trial is required for air lubrication). However, as shown in this paper, sea trial verification is both possible and feasible. EEDI verification could be done by carrying out a sea trial at any wind speed between say, 6-14 m/s, including ~5 wind directions, and normalise to the closest wind speed in the EEDI matrix. If the submitted force matrix this does not match the derived power gain, the ship owner (i.e. the technology provider) must adjust it.

8.3 Operation optimisation

The digital twin model of the ship and wind propulsor used for the sea trial normalisation and extrapolation can be re-used for other purposes. Example of investigations that require, or get better, if the ship owner has access to a correlated digital twin ship model includes:

- weather routing
- speed optimisation
- fleet optimisation with respect to wind propulsion potential over season and geographical areas
- CII strategy and CO2 budget
- business case and decision support for investment of wind propulsion for similar ships

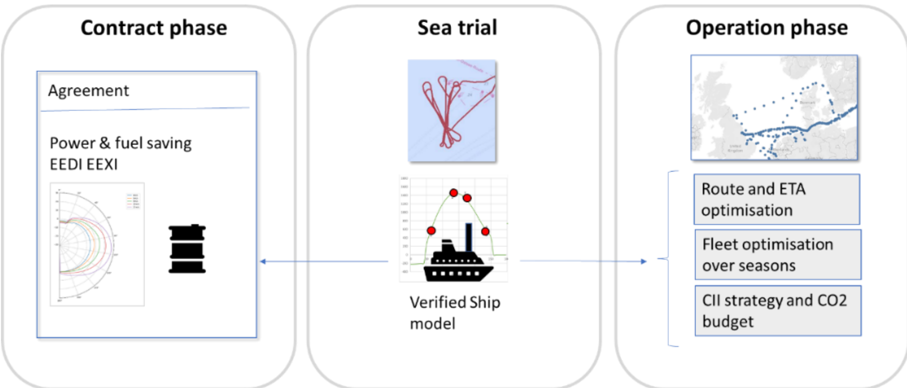

Fig. 12: Wind propulsion sea trial results can be used both for contract performance verification and for operational simulation tools.

9. Conclusions

The purpose of the present work is to discuss methodologies for sea trial assessment of wind assisted ships. A methodology based on a short, dedicated trial is suggested. The trial is complemented with a voyage simulation and weather statistics to extrapolate the trial result to average fuel saving for a specific route. The proposed method is demonstrated for three ships with wind assistance technologies, two ships with Flettner rotors and one with suction wings. The detailed results of the three sea trial assessments, plus two more to come, will be published by the WASP project on a later occasion.

The sea trials are conducted as a series of short runs, with and without the wind assistance propulsors in active mode. The runs can be laid out as reciprocal double runs, as in a conventional sea trial, or as a circular track, changing the wind angle gradually. The advantage of the reciprocal double runs option is that it uses less space, which can be an advantage in areas with heavy traffic.

The sea trials results showed that there can be a large difference between the measured performance and the theoretically expected performance. The disparity varies with wind angle in a unique way for each tested vessel. It is assumed that this effect is due to the disturbance of the ships' freeboard and superstructure on the air flow over the wind propulsors. This gives a strong motivation for requesting sea trial verification of theoretical performance numbers, and for including a range of wind directions.

According to conventional sea trial standards, the ship's power setting should be constant during the speed runs. The effect of activating a wind propulsor while the power is fixed is that the ship speed increases. However, the sea trial result is often requested in terms of *power loss* for a given speed. Two methods to normalise the trial results to a reference speed are proposed. The first method uses the shape of the ship's speed power curve to extrapolate to nominal condition. This method involves several simplifications including the effect on propulsive efficiency due to changed propeller load. The second method is more complex and makes use of a ship simulation model. The difference between the results of the two methods are well within the estimated uncertainty margin of the three test cases.

In order to reduce the uncertainties related to the translation of a speed increase into a power loss, it was investigated whether wind propulsion sea trials should aim for constant *speed* between the runs instead of constant *power*. However, this did not turn out to be beneficial. The conclusion is that constant power is recommended for wind propulsion sea trials.

The mayor uncertainties of the sea trial assessment include the wind measurement onboard the vessel. It is recommended that the ship's anemometer is calibrated before trial, or that a second, calibrated, anemometer is temporarily fitted during the trial.

The sea trial assessment and voyage simulation result in a power saving *potential*. The *real* achieved saving will be a result of operational factors such weather routing, speed optimization, and wind propulsor idling due to maintenance and failure.

The proposed methodology is shown to be a feasible way to perform full scale verification for commercial vessels with wind assistance technologies. Trustworthy results can be derived at a feasible cost, within a limited time frame, and using transparent, commercially available tools and established procedures.

10. Further work

Sea trial procedures

The International Towing Tank Conference (ITTC) identified in 2021 that the industry would benefit from a standardised methodology for full scale evaluation of wind assisted ships. A Specialist Committee for Wind Powered and Wind Assisted Ships was established with that objective (among other). The work in this paper could contribute to the development of new Recommended Procedures for sea trials of wind assisted ships. However, more research will be required to establish such standards. For example: sensitivity and requirement of sensors, in particular wind sensors, sensitivity on parameters in the normalisation process, limitations for current variation, and limiting wind conditions.

Uncertainty analysis

Understanding the uncertainty level of wind propulsion sea trials is very important in the context of performance guarantee and contract confirmation. Further work is needed on the precision of such sea trials. This includes the uncertainty of anemometers, and how this error source can be minimised.

Key performance indicators

The performance of wind powered and wind assisted ships can be expressed in number of ways, for example percentage power reduction over a year, kW per miles, kW per hour, EEDI, power reduction at beam wind in a gale, etc. These numbers can be derived based on a number of assumptions, such as weather statics from actual logging or from IMO, with or without sea margin, including weather routing or not, etc. We will investigate the effect, pros and cons of the different options, and hopefully be able to give some recommendations to the community.

Acknowledgement

We would like to thank Boomsma Shipping, Scandlines and Rörd Braren for assisting with arranging the trials, and the three Masters of the tested vessels: Captain Bach, Captain Mehrens, Captain Pasatiuk and their crew. We also thank Econowind, EcoFlettner and Norsepower for technical discussions. The work is funded by EU Interreg North Sea Region.

References

CHARRIER, B.; CONSTANS, J.; COUSTEAU, J.; DAÏF, A.; MALAVARD, L.; QUINIO, J. (1985), *Fondation Cousteau and Windship Propulsion 1980-1985 System Cousteau – Pechiney*, J. Wind Engineering and Industrial Aerodynamics 20, pp.39-60

GARENAUX, M.; SCHOT, J.; EGGERS, R., (2020), *Numerical Analysis of Flettner Rotors Performances on the MARIN Hybrid Transition Coaster*, 12th HIPER Conf.

IMO (2017), *Strategic plan for the organization for the six-year period 2018 to 2023*, IMO, London

IMO (2021), *MEPC.1-Circ.896, Guidance on treatment of innovative energy efficiency technologies for calculation and verification of the attained EEDI and EEXI*, IMO, London

INSEL, M. (2008), *Uncertainty in the analysis of speed and powering trials*, Ocean Engineering 35

ISO (2015), *15016:2015 Ships and marine technology – Guidelines for the assessment of speed and power performance by analysis of sea trial data*, Int. Standard Org., Geneva

ITTC, (2014), Specialist Committee on Performance of Ships in Service, *Final report and recommendation to the 27th ITTC*, 27th Int. Towing Tank Conf.

ITTC (2021), *Recommended Procedure 7.5-04-01-01, Preparation, Conduct and Analysis of Speed/Power Trials*, Int. Towing Tank Conf.

JONES, L.; PRINCE, M.; HUDSON, D.; COCKS, J., (2019) *Predicted Fuel-Savings for a Flettner Rotor Assisted Tanker Using Computational Fluid Dynamics*, RINA Wind Propulsion, London

KRAMER, (2016), *Drift Forces –Wingsails vs Flettner Rotors*, HIPER Conf.

NELISSEN, D. (2016), *Study on the analysis of market potentials and market barriers for wind propulsion technologies for ships*, CE Delft

NORRBIN, N. H, (1970), *Theory and Observations on the Use of a Mathematical Model for Ship Manoeuvring in Deep and Confined Waters*, 8th Symp. Naval Hydrodynamics, Pasadena

ØKSNES, Ø.; DALHEIM, S., (2021) *Uncertainty in the real-time estimation of ship speed through water*, Ocean Engineering 235

OLSSON, F.; MARIMON GIOVANNETTI, L.; WERNER, S.; FINNSGÅRD, C. (2020), *A performance depowering investigation for wind powered cargo ships along a route*, INNOVSAIL 2020, Gothenburg

PAAKKARI, V. (2019), *Performance verification of a recent rotor sail installation*, RINA Wind Propulsion, London

PAAKKARI, V.; HURFORD, A.; CRADDOCK, C., (2020) *Rotor sail GHG reduction potential, modelling and sea trial validation*, 5th Int. Conf. Innovation in High Performance Sailing Yachts and Sail-Assisted Ship Propulsion, Gothenburg

REHMATULLA, N.; CALLEYA, J.; SMITH, T. (2019), *The implementation of technical energy efficiency and CO2 emission reduction measures in shipping*, Ocean Engineering 139, pp.184-197

SCHMIDT, A.; VAHS, M. (2013) *Entwicklung eines innovativen Schiffsantriebes gekennzeichnet durch den Einsatz von Magnus-Rotoren zur Windenergienutzung in Kombination mit einem hierauf abgestimmten Antriebspropeller,* Final report for the development project promoted under the Az .: 25741 -24/0 by the German Bundesstiftung Umwelt

STRASSER, G.; TAKAGI, K.; WERNER, S.; HOLLENBACH, U., (2015) *A verification of the ITTC/ISO speed/power trials analysis*, J. Marine Science and Technology

UK GOVERNMENT (2019), *Clean Maritime Plan* 2019, Department for Transport, UK

VAHS, M., (2019), *Retrofitting of Flettner rotors – results from sea trials of the general cargo ship "Fehn Pollux*", Int. Conf. Wind Propulsion, London

WERNER, S.; NISBET, J.; HÖRTEBORN, A.; NIELSEN, R., (2021), *Sea trial Verification for a Wind Assisted Ship*, RINA Int. Conference on Wind Propulsion, London

Correlating Laboratory with Full-Scale Data

Jan Richter, Hamburg Ship Model Basin, Hamburg/Germany, richter@hsva.de
Jonas Wagner, Hamburg Ship Model Basin, Hamburg/Germany, wagner@hsva.de
Florian Kluwe, Hamburg Ship Model Basin, Hamburg/Germany, kluwe@hsva.de

Abstract

Within this publication, the difficulties of correlating laboratory and full-scale data with respect to quality and consistency of the respective data sets are outlined. First, the latest standards of on-board performance monitoring and performance prediction according to ITTC'78 are summarised and the uncertainty of model testing and extrapolation is put into perspective with the uncertainty of long-term full scale recordings and environmental corrections. While it can be shown that the uncertainty of model tests is significantly lower than those of full-scale measurements, the paper subsequently focusses on how to deal with the latter by analysing the monitoring data of an exemplary vessel in service that has previously been tested at HSVA. Based on these findings, recommendations regarding the parameters that should be monitored and possible corrections that could be included within the ISO standards for speed trial corrections are provided. The overall goal is to provide means for estimating and ensuring the quality and consistency of the on-board recordings and in the long run to further improve the model test extrapolation procedures especially on loaded draughts through a better coverage.

1. Introduction

Both calm water model test and numerical predictions strongly depend on full scale data for a correlation allowance CA, which covers the factors that are insufficiently or not at all included in the respective procedure.

In the case of physical model testing, this parameter is model basin specific as it does not, as originally intended, only cover differences in hull roughness but also includes facility dependent parameters. Exemplary factors are wall and bottom effects which are naturally dependent on the tank and model dimensions. Another example is the inevitable wind resistance on a model, which is dependent on the model height above the water line and test speed. Even the quality of the model hull surface, model test setup assumptions, such as omitting or including certain appendages, or different approaches in calculating surface areas can have an influence that may be covered insufficiently by applying a form factor in conjunction with the correlation allowance and roughness allowance recommended by the latest *ITTC (2017)* guidelines.

Typically, the correlation allowance is derived from speed trial recordings of vessels tested at the respective facility. The majority of speed trials are conducted on a ballast draught leading to the most accurate correlation for those conditions owing to the size of the underlying data base. The loaded draughts are usually backed by fewer data, leading to a larger uncertainty which might even affect the correlation for these conditions. In order to better quantify and mitigate these uncertainties, an in-depth correlation study based not only on speed trials but also on on-board performance monitoring data is contrived. The advantage of using monitoring data is its capability of providing performance information for all operational draughts, increasing the correlation data base for the loaded conditions. The drawback of these data is the environmental impact that cannot be corrected as thoroughly as for clearly defined speed trials, increasing the uncertainty of the on-board performance monitoring recordings which in consequence reduces the accuracy of the findings.

2. ITTC'78 Performance Prediction Method – The Basics

Model testing is an established means for a cost-efficient prediction of a vessels power demand, its seakeeping behaviour, manoeuvring characteristics, propeller cavitation, noise, vibration or even the ship handling in ice. The international towing tank conference (ITTC) provides guidelines for carrying out and analysing model tests and the leading facilities around the world follow these procedures to a certain extent. Most institutes incorporate custom modifications or extensions of the recommendations - based on experience and decades of research - for improving the predictions further and accounting for their individual towing tank characteristics.

Calm water model tests generally consist of resistance and self-propulsion tests as well as propeller open water tests. The measured data is converted to full scale using certain assumptions, such as Froude similarity and thrust identity for resistance and propulsion tests and Reynolds similarity for the propeller open water tests. The final predictions may be for ideal trial conditions as well as for service conditions that include the effect of wind and wave resistance on the vessel's performance. Even the impact of shallow water may be included in model test predictions, where necessary.

The most prominent parameter in a performance prediction is the correlation allowance CA, a facility dependent parameter that accounts for any factors that are not fully considered in the scaling process. The correlation allowance typically is based on customer feedback in form of full scale speed trial data for vessels tested at the corresponding basin. It is used to determine the correct self-propulsion point of the model and applied in the scaling process itself. Ideally, the correlation allowance should be updated regularly if new trends in the correlation of the ever increasing full scale data become apparent. At this point, it should be stressed that correlation updates do not necessarily imply that previous correlations were incorrect. The modifications in correlation may reflect general changes in hull designs, as for example during the years of transitioning from fast delivery to slow steaming, *Faber et al. (2012)*, as well as improvements in the manufacturing process of shipyards.

Other typical correction parameters that vary between model basins are the propeller open-water scaling, *Streckwall et al. (2013)*, and the full-scale wake scaling. The combination of scaling procedures used for a full-scale prediction naturally affects the correlation allowance to be applied.

3. On-Board Performance Monitoring – The Basics

The general principle and recommended methods for the evaluation of on-board monitoring data is presented in the draft International Standard ISO 19030, *ISO (2016*). It outlines the data acquisition, storage and preparation including data filtering and correction procedures. The resulting performance indicator is usually used to monitor changes in performance and to better plan the operation profile, routes and docking periods.

For the present study, the corrected and filtered on-board performance monitoring data is directly compared to the corresponding model test predictions in order to assess the quality of the correlation itself. The relation of the measured power demand to the one predicted by model tests is labelled prediction correctness PC and is a value used to estimate the deviations between model and full-scale. In the best case, an average PC should be close to one; i.e. the average monitored power demand is equal to the power demand that has been predicted in the model tests. The scatter of that value gives an indication for the stationarity of the recordings. Even though filtering and corrections are applied, a large scatter is usually to be expected. This may be due to critical parameters not being recorded or the logging interval being too large to capture peak values in time, which is especially true for values that typically average around a fixed value, such as the rudder angle.

The absolute minimal required data for comparing full scale monitoring data to numerical or model test predictions consists of the draught readings, speed through water and engine power. Additional ship and environmental data allow for better filtering and correction of the recorded information and a reduction in the scatter of the comparison to the performance predictions. The ISO in its draft version is rather limited in data that is used as it corrects only for the effect of wind and disregards any other unfavourable environment effects. Table I summarises these and other effects as well as the means for using the information in an on-board performance analysis.

Table I: List of parameters and their use for on-board performance analyses.

Parameter	Used for/as
Speed through water	Reference to the underlying performance predictions
Engine / delivered power	Reference to the underlying performance predictions
Draughts / displacement	Reference to the underlying performance predictions Interpolation between or correction to known displacements
Latitude / longitude	Filtering of adverse trial areas (e.g. constrained waterways, traffic) Estimation of water depth Calculation of ground speed, if necessary
Speed over ground Course over ground	Wind speed correction Filtering for currents (in combination with speed through water)
Water depth	Shallow water correction Filtering of shallow water regions
Wind speed Wind direction	Correction for wind resistance
Wave / swell height Wave / swell direction	Filtering for seaways Potentially correction for seaways
Water temperature Water density	Correction of the friction resistance
Rudder angle	Filtering for significant rudder actions Correction for stationary rudder angles deviating from zero
Heading	Filtering or correction for drift (in combination with the course)
Engine / Propeller revolutions	Filtering of instationary revolutions (accelerations, etc.) Filtering for engine loads (in combination with power and speed)
Propeller pitch (controllable pitch propeller)	Filtering or correction to underlying performance prediction pitch

4. Uncertainties in Model Test Extrapolation and Long-Term Full Scale Monitoring

The uncertainties of model testing are quite low when compared to full scale recordings due to the laboratory conditions of the model test setup. In a 95 % confidence interval model test setup and conduct uncertainties typically are situated around one percent. The total expanded uncertainty of speed trial analyses, including model and full scale uncertainties, is almost 10 %. Based on the comparison of recordings for 41 sister vessels the uncertainty of full scale trial recordings has been identified in the order of magnitude of 8 %. From these figures it is concluded that, again in a 95 % confidence interval, about 5 % uncertainty may be attributed to the scaling procedure of model test results to full scale itself (e.g. full scale wake correction). The relationships outlined above are elaborated in detail by *Richter and Kluwe (2019)*.

Speed trials are carried out in favourable weather conditions, at a suitable trial area and at several power settings, each setting with and against the primary wind or wave direction (whichever is the dominant factor), so called double-runs. Using this approach, insufficient corrections (too optimistic as well as too conservative) are slightly compensated by combining both directions of a double-run to a single speed-power value for each power setting. Furthermore, several approaches exist to calculate the speed of the water currents based on double-runs. Long-term full scale monitoring lacks these well-defined test conditions, further increasing the scatter of the recordings.

An in-depth analysis of the confidence intervals of on-board performance monitoring is pending but qualitative observations may be given, quantified in form of exemplary data. The scatter strongly depends on the quality and properties of the provided data. The exemplary sample given by Fig.1 shows standard deviations of individual prediction correctness values with respect to the corresponding moving mean of up to 20 %. It should be emphasised that the sample data is not ideal, as its logging interval is larger than recommended and some information that would be useful for filtering are missing. For this sample, no seaway information and water properties have been available. Even though the track is known, filtering and correction for confined water, such as shallow sea or routes along rivers and canals, has not yet been carried out explicitly. It has been chosen as representative example data nonetheless, as most on-board performance monitoring data are incomplete in one way or another.

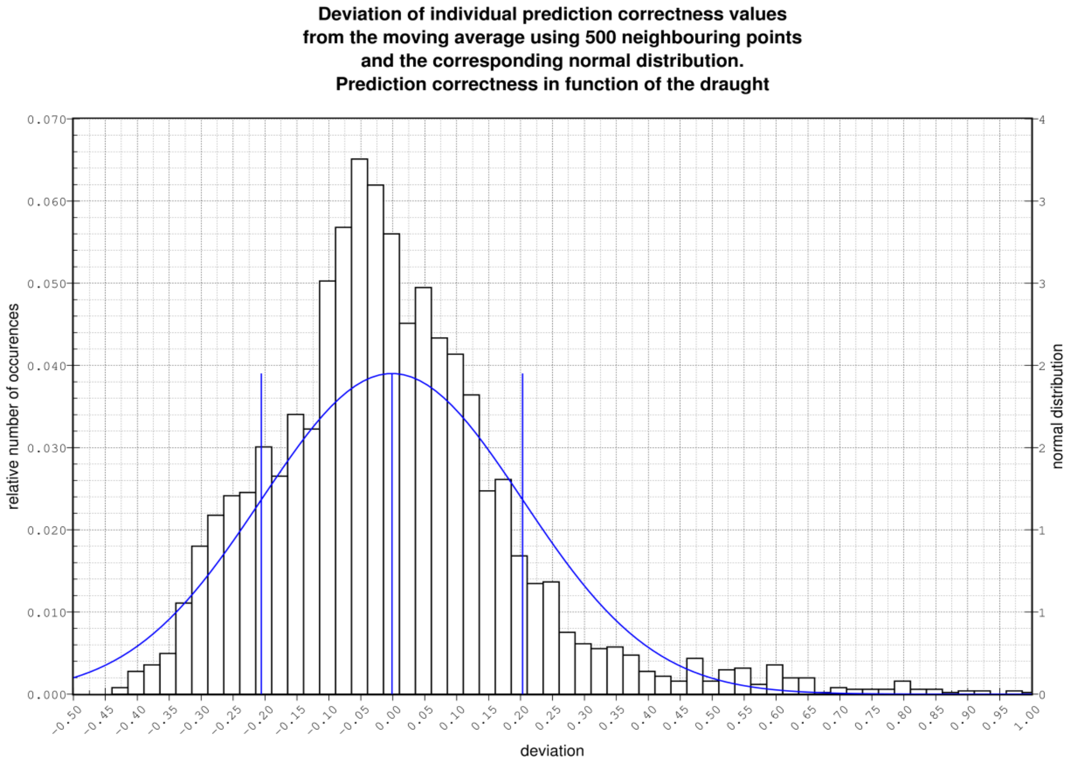

Fig.1: Sample deviation of prediction correctness

5. Lessons Learned: How to improve Monitoring Analyses

Consistency checks of the provided data are an essential step prior to the analysis. It is most important that the units and coordinate systems used in the provided data are well defined and consistent, especially when combining multiple data sets into one evaluation. Examples for potentially changing coordinate systems are the trim, which may have different signs for bow-down trim in different recordings, the zero-degree angle of the apparent wind or the incident wave direction. Especially the waves should be checked closely because the definition of the incident wave angle has been reversed between the ISO standard for speed trial corrections of 2002, *ISO (2002)*, and the standard of 2015, *ISO (2015)*. An incident wave angle of zero degrees now corresponds to head waves.

Where possible, redundancies should be produced and checked in order to ascertain the validity of the available data. If the data provides, for example, the speed of the currents, these information should be checked against the difference between the recorded speed trough water and ground speed. Similarly, apparent and true wind recordings should be laid side by side. Where possible, one could also use wind and wave recordings of nearby stations or hind-cast data to check the plausibility of the on-board recordings. Water depth readings may be confirmed using sea charts and the recorded location of the vessel. It is also always sensible to compare the recorded power demand to the corresponding fuel consumption, if shop test data are available.

Fig.2 shows samples of such comparisons. In the provided example it is noted that there are issues for some of the apparent wind recordings, manifesting in form of deviations of calculated true wind when compared to the recorded true wind information. The speeds of current correlate flawlessly while the recorded trim changes its sign at some point in time. With this information available it is recommended to use the recorded true wind information and the calculated trim data for further analysis.

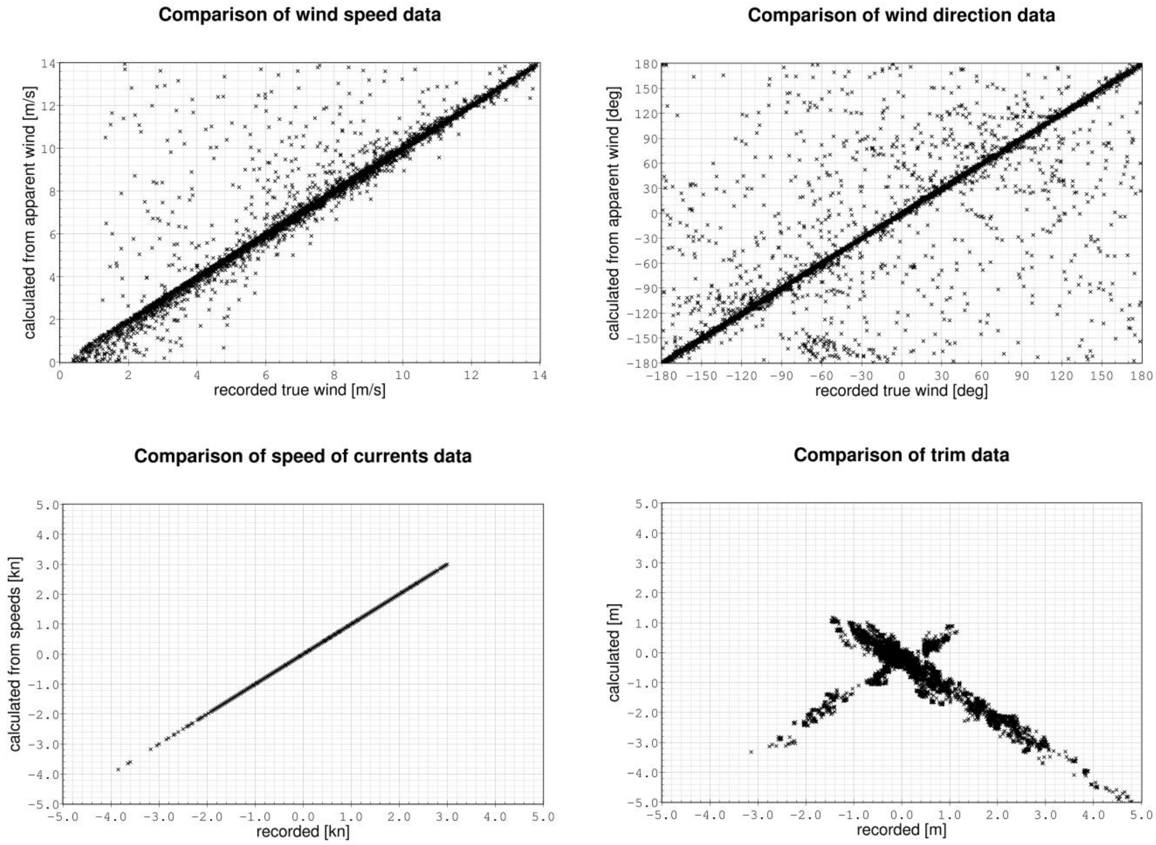

Fig.2: Comparison of recorded (x-axis) and calculated (y-axis) parameters

The draft ISO standard 19030 strongly relies on filtering instead of data correction. In the default method, the only environmental factor that is corrected is the effect of wind. If sufficient data are available, radical filtering might pose less of a problem but for cases in which the original data set already is limited, further reduction may lead to a non-Gaussian distribution in the data base – a fact that needs to be considered in any summary statistics applied to the data. As showcase, table II displays the number of recordings of the example data set before, during and after filtering. In that particular case, the initial dataset's usable information consists of about 22000 entries. After filtering for sensible environmental and operational conditions, only 43 % of the data are still available, further reduced to about a quarter of the initial number of recordings when only accounting for load cases and speeds which are within the range that has been tested in the model basin.

Table II: Reduction in data points during filtering

Applied filtering	**Number of recordings**
Filtered for missing data	22079
Filtered for valid wind conditions	18987
Filtered for seaway (seaway not available in this example)	18987
Filtered for propeller load (combination of power and revolutions)	10894
Filtered for exceeding speeds of current	10866
Filtered for track/location (w/o consideration of shallow and constrained waterways)	9548
Filtered for speed and draught range of model test conditions (w/o consideration of trim)	5058

In order to improve data significance, additional corrections need to be introduced within the draft ISO standard. Of particular interest in this case would be parameters that require little or no additional measurement data or instrumentation, such as corrections for shallow water, *Raven (2016)*, or water temperature in combination with salinity. While the first can be carried out without additional measurements by mapping GPS data to nautical charts, the second needs additional and – in order to prevent recording unintentionally misleading values such as the temperature of ballast water – carefully placed temperature sensors and a means for estimating or obtaining the water salinity (e.g. regular manual recordings or obtaining the information from nearby stations). Seaway corrections would improve the validity of the data significantly, but as it can only be done by the help of additional (costly) monitoring equipment and/or use of external tools and services, they might not be as easy to apply as the previous methods. When considering corrections of seaway, it should be kept in mind that, in contrast to conventional speed trials, the vessel is not only exposed to head and beam seas. Most simplified correction methods are only valid for these conditions, even though more complex empiric procedures exist, *Blume (1977)*. If special efforts are to be taken to correctly monitor the present sea state on board of a vessel, it should also be recommended to conduct reference model tests or numerical computations of the added resistance due to waves for this specific hull. The additional effort is rewarded by improved corrections when compared to the abovementioned empiric and more generic correction procedures.

Another useful criterion for quality control or filtering that is presently not emphasised in literature is the propeller load; a combination of power demand, ship speed and propeller revolutions in form of a torque coefficient in function of the speed of advance. Knowing the typical load range of a vessel may be used as an additional filter for stationary conditions, Fig.3. Data points with extreme speed of advance values correspond to situations in which the propeller speed and the ship speed do not match well. One possible reason may be changes in revolutions which are not yet reflected in the ship speed due to inertia. Extremes on the torque coefficient indicate power demands above the typical propeller load range as is often the case during manoeuvres, particularly in confined waters.

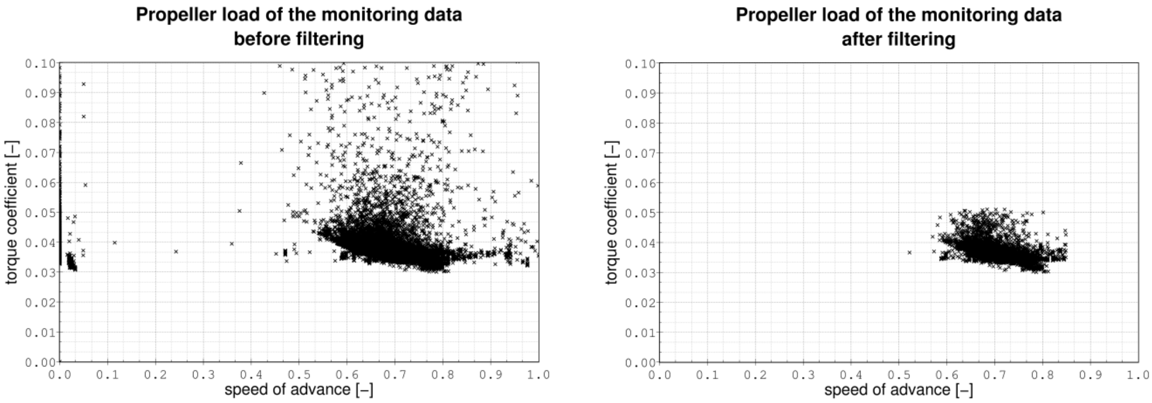

Fig.3: Propeller load in a typical range before (left) and after (right) filtering

6. Lessons Learned: How to improve Model Test Extrapolation

The goal of any reputable model test basin is to further improve their model test extrapolation procedure to full scale. To achieve this goal, feedback of the full scale data, not only on the trial but on all draughts, is essential. The broader the data base, the more reliable extrapolation methods can be established. Ideally, the findings should not only be reflected in the individual model basins extrapolation procedures but should also find their way into the ITTC guidelines and recommended procedures. This implies sufficiently generic relationships that are valid for all facilities and will not substitute the individual correlation allowances. In order to enable the broad public to extrapolate model test data according to the ITTC recommendations, it should always be kept in mind that too complex procedures should not be incorporated into the general guidelines. This is especially true for methodologies that rely on closed-source algorithms or require special equipment.

One straightforward means for improving model test extrapolations might be realised by adjusting the default average hull roughness to the expected full scale values. But in cases in which a facility's custom correlation allowance is applied, it should be taken care that this effect is not already covered by the CA.

Improvements in the ITTC recommendation could possibly be formulated for the propeller open water scaling, the wake scaling or even in form of additional resistance components that incorporate resistance changes that are not fully covered by the current standard procedures and form factor method. Such separate resistance components may be of special interest for unusual hull forms, transom stern immersion, propeller tunnels or maybe even for vessels with and without a bulbous bow. Prior to introducing any of the mentioned improvements, detailed studies on the individual topics as well as on their effects towards the entire scaling process need to be investigated.

The propeller open water scaling recommended by the ITTC guidelines is rather simplified and dependent on only a few geometric propeller properties. Alternatives which promise improved scaling typically require more details about the propeller geometry itself. As an example, HSVA's standard procedure requires integration over the propeller blade radii. The additional effort is earning positive feedback from the majority of the customers. An improved wake scaling poses more of a problem, as an in-depth full scale wake analysis would be necessary. Since measuring the wake on a ship in service requires special equipment on the vessel itself, comparably few benchmark cases are available. A full-scale wake study therefore will mainly rely on numerical comparisons of model and full scale computations.

If the extrapolation procedure itself is to remain untouched, there is always the possibility for updating the correlation allowance based on the ever increasing customer feedback in form of speed trial reports. Even a more dynamic correlation allowance should not be discounted. Instead of a fixed equation, the CA could be re-defined in function of a suitable collection of reference vessels for which both model tests and speed trial (or high-quality on-board monitoring) data on all relevant draughts are available.

7. Conclusions

Correlation of model test to full scale measurements is impaired by multiple uncertainties that result especially from a lack of data quality of full scale measurements (including amongst others inconsistencies, missing observations, too low logging frequencies). In the presented example, these uncertainties lead to a scatter of the prediction correctness with a standard deviation of up to 20 %. In order to improve the correlation allowance especially on loaded draughts, not only speed trial but also long-term on-board monitoring data should be used. Since the ISO standard procedures for the evaluation of on-board monitoring mainly rely on filtering instead on corrections, even comparatively large data sets are reduced significantly – in the presented example to about a quarter of its initial size. It should be noted that any filtering needs to be carried out carefully, since too much might reduce the data to a point that doesn't allow for drawing meaningful conclusions (e.g. when it comes to non-Gaussian distributions). It is therefore recommended to check and validate the data before the application of filters. A good example for the benefits of this approach is the check for trim data with respect to its sign.

Beyond these rather basic procedures, there is still much room for reducing uncertainty and improving data significance by applying additional corrections for environmental factors that are currently not addressed within the ISO standard procedures. Easy to apply examples are shallow water, water temperature and salinity corrections. More elaborate procedures like sea state corrections might not be suitable to include within the ISO standards but still offer the potential to notably increase significance of the provided data.

Resulting, future work with respect to further improve model test extrapolation should in a first step focus on improving the data basis: more extensive and better full-scale measurements – be it speed trials or long-term on-board monitoring data – are required. In a second step, advanced filtering and correction procedures need to be developed, applied and validated. The last step consists in mapping the processed data to the corresponding model test results in order to allow for an even more sophisticated – possibly even dynamic – correlation allowance that keeps track of as many relevant factors as possible.

Acknowledgement

We would like to thank NSB GROUP for providing the valuable on-board monitoring recordings as well as operational and academic insights regarding these data.

References

BLUME, P. (1977), *Berechnung des Seeverhaltens für eine systematisch variierte Formfamilie, Teil A: Allgemeine Beschreibung*, HSVA Bericht 1505

FABER, J.; NELISSEN, D.; HAN, G.; WANG, H.; TSIMPLIS, M. (2012), *Regulated slow steaming in maritime transport - an assessment of options, costs and benefits,* CE Delft

ISO (2002), *ISO 15016: Ships and marine technology – Guidelines for the assessment of speed and power performance by analysis of speed trial data*, Int. Standard Org., Geneva

ISO (2015), *ISO 15016: Ships and marine technology – Guidelines for the assessment of speed and power performance by analysis of speed trial data*, Int. Standard Org., Geneva

ISO (2016), *ISO 19030: Ships and marine technology – Measurement of changes in hull and propeller Performance,* Int. Standard Org., Geneva

ITTC (2017), *1978 ITTC Performance Prediction Method, ITTC – Recommended Procedures and Guidelines 7.5-02-03-01.4, revision 04*, Int. Towing Tank Conf.

RAVEN, H.C. (2016), *A new correction procedure for shallow-water effects in ship speed trials,* PRADS, Copenhagen

RICHTER, J.; KLUWE, F. (2019), *On speed/power predictions and full scale recordings*, STG Sprechtag “Vorhersage der Propulsion von Schiffen unter realen Bedingungen“, Berlin

STRECKWALL, H.; GREITSCH, L.; MÜLLER, J; SCHARF, M.; BUGALSKI, T. (2013), *Development of a strip method proposed to serve as a new standard for propeller performance scaling,* Ship Technology Research

New Measurement Facility: Enhanced Skin-Friction Measurement over Large-Scale Plates in a Channel Flow

Irma Yeginbayeva, Jotun AS, Sandefjord/ Norway, irma.yeginbayeva@jotun.no
Angelika Brink, Jotun AS, Sandefjord/Norway, angelika.brink@jotun.no
Vilde Emilie Aas, NTNU Trondheim/ Norway, vilde.e.aas@ntnu.no

Abstract

The paper will present technical details of the flowcell built 2021 in Jotun used for skin-friction measurements for marine anti-fouling coatings under various conditions. Validation experiments with smooth plates and sand-grain surfaces will be shown and compared to available publications using similar devices. Further measurements of anti-fouling surfaces of different chemistry and roughness will be presented. A new approach using Power Spectrum Density Functions calculated over spatial frequencies will be introduced to describe surfaces in a holistic way and relate it to drag. This will be done in comparison to a single value-based roughness approach like Rt50 and Rq.

1. Introduction

Channel flow or duct flow is very attractive to experimentalists due to its similarities with pipe flows where the frictional loss can be determined by measuring a pressure gradient between two pressure tapping points. Moreover, the sample handling of coated flat plates used in rectangular ducts is more convenient than other hydrodynamic test equipment. Fully developed channel flow is also favorable for computational fluid dynamics (CFD) specialists due to the simple geometry and applicability of Cartesian coordinate systems. Complications arise in pipe flow simulations in cylindrical coordinates, particularly accounting for the singularity which appears at the centerline (r=0). Several numerical methods have been proposed in *Boyd (2001)* to overcome this difficulty in cylindrical coordinates.

The pioneering work on skin friction dependency on Reynolds number for a smooth wall in rectangular duct flow is that of *Laufer (1948)*. *Laufer (1948)* is an impressive and important reference, as it is the benchmark study which took a rather large leap forward by measuring turbulent velocity fluctuations for the smooth wall in the channel for the first time. Such measurements require high-frequency response anemometers, necessitating the use of hot-wire anemometry technology which was in its infancy in 1950. Almost 30 years after Laufer's work, *Dean (1978)* collected numerous data from different investigators (27 sources from 1928 to 1976) for hydraulically smooth channel flows. This above-mentioned data was used to illustrate in one diagram a change of skin friction coefficient with Reynolds number. Based on this dataset, Dean developed his correlation for friction factor with Reynolds number in Eq.(1).

$$C_f = 0.073{Re_m}^{-0.25} \tag{1}$$

Dean's curve is widely accepted and numerous study results, *Monty (2005), Zanoun et al. (2009), Hoyaz and Jimenez (2006), Schultz and Flack (2013)*, are close to his correlation. For representation of wall skin friction data, Zanoun *et al. (2003)* suggested a slightly modified equation, which is:

$$C_f = 0.058{Re_m}^{-0.243} \tag{2}$$

Experiments with high aspect ratio (AR), which is defined as ratio of the channel width (W) and the channel height (H), for rectangular channels are generally intended to simulate a true channel flow, which would be the flow between infinitely wide parallel plates. If the aspect ratio is high enough, the flow toward the center of the channel can be considered nominally two-dimensional. This means there is no measurable spanwise variation in mean streamwise velocity. Based on compiled channel flow data, Dean postulated that the minimum aspect ratio to ensure two-dimensional flow in channels was 7:1. *Vinuesa et al. (2014)* carried out experiments in a variable AR duct flow facility with the aim to study the flow development and skin friction dependence on the duct AR, which was varied from 12.1

to 48. The first conclusion of this study was that two-dimensional turbulent channel flows cannot be reproduced experimentally. According to *Vinuesa et al. (2014)*, skin friction becomes independent of AR at ratios 24 and higher, and flow becomes truly fully developed for development length, *x/H* values larger than 200. Both are nearly double what was previously thought sufficient for channel flows. Note that experimental and numerical studies on high AR and longer channel lengths are rare. *Vinuesa et al. (2014)* also noticed that for high Reynolds numbers, smaller values of *x/H* such as 120 may be adequate.

A channel flow device has recently been introduced into the research and development department of Jotun A/S to meet the need for hydrodynamic testing of marine coatings in terms of their frictional drag characteristics, Fig.1. To our best knowledge is this device the first flow channel device with several unique features that may be advantageous in the research of surface testing. These features are as follows: a wider and longer testing panels and ability to heat or cool the water in the channel. This article discusses this new device based on the carried out CFD study to establish the main dimensions and share preliminary pressure gradient results collected for selected test surfaces in four main parts.

Fig.1: Overview of the flowcell in Jotun laboratory

2. CFD study establishing main parameters for the flowcell

CFD has become an integral part of the engineering design. CFD is used in many areas to predict the performance in the design process before manufacture and implementation. In this study, CFD was carried out at full-scale using a RANS flow model and "Realizable k-epsilon" turbulence model in the STAR-CCM+ software. The flow was simulated at a water temperature of 15 °C and corresponding density of 1025.9 kg/m^3. The flowrate was varied from 21.6 m^3/h to 216 m^3/h. The computations were carried out by using an unstructured, hexahedral mesh consisting of approximately 7 300 000 cells. The meshed geometry for the investigated geometry is presented in Fig.2.

Fig.2: Computational mesh for the flowcell (side view)

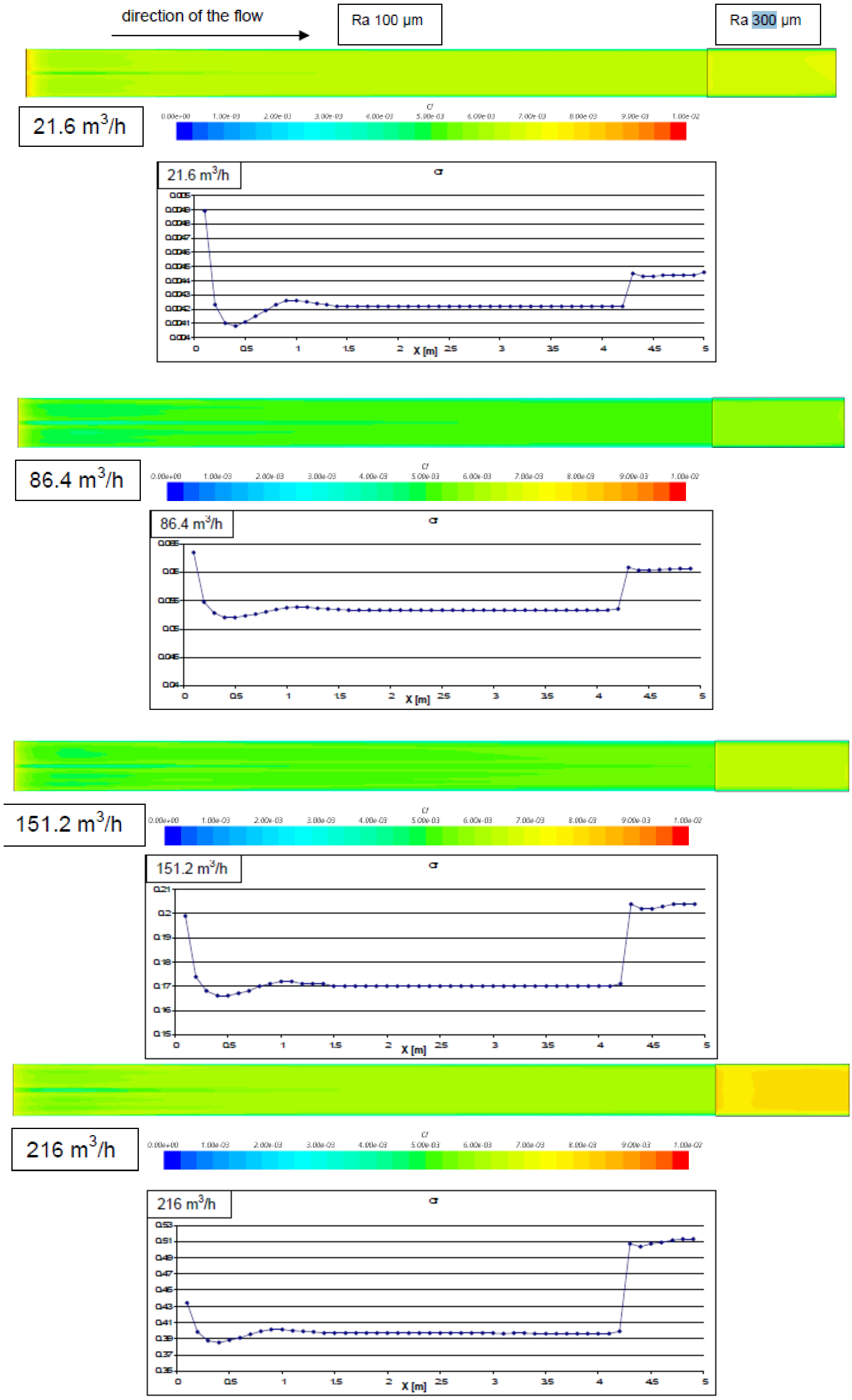

Fig.3: Distribution of the skin friction coefficient (C_f) at different flowrates in '300 mm x 20 mm' cross section of the flowcell

The average roughness of the entrance length of the flowcell was set to 100 μm, whereas the testing section roughness was 300 μm for the simulation purposes, Fig.3.

The aim of this CFD study was to:

- evaluate and visualize the velocity in the flowcell (FC) with a test section dimension of 300 mm x 20 mm and 400 mm x 20 mm;
- evaluate the shear stress distribution in the FC for the same dimensions mentioned above;
- choose the optimal dimension of the FC to proceed with detailed design and manufacture.

Based on the CFD results, the two tested cases (300 mm x 20 mm and 400 mm x 20 mm testing sections) were found to be similar in terms of wall shear stresses and pressure distributions. The only difference was that 300 mm x 20 mm channel was less influenced by the flow separation in the diffuser located at the end of the test section. From the practicality and cost efficiency point of view 300 mm x 20 mm was more favorable. Therefore, this testing section dimension was selected as the final for the flowcell.

Fig.3 shows the distribution of the C_f along the development length with Ra=100 μm and the testing section with Ra=300 μm at flowrate changing from 21.6 m^3/h to 216 m^3/h for the '300 mm x 20 mm' cross section of the flowcell. Fig.3 shows the increase of the C_f with increasing flowrate. Sudden increase in the C_f along the testing section (or x=4.2-4.8 m) is associated with roughness increase from Ra=100 μm to Ra=300 μm.

Fig.4 shows that the velocity at x=2 m and x=4.2 m (before the test surface) is identical, meaning that the flow is already fully developed at x=2 m or x/H=100.

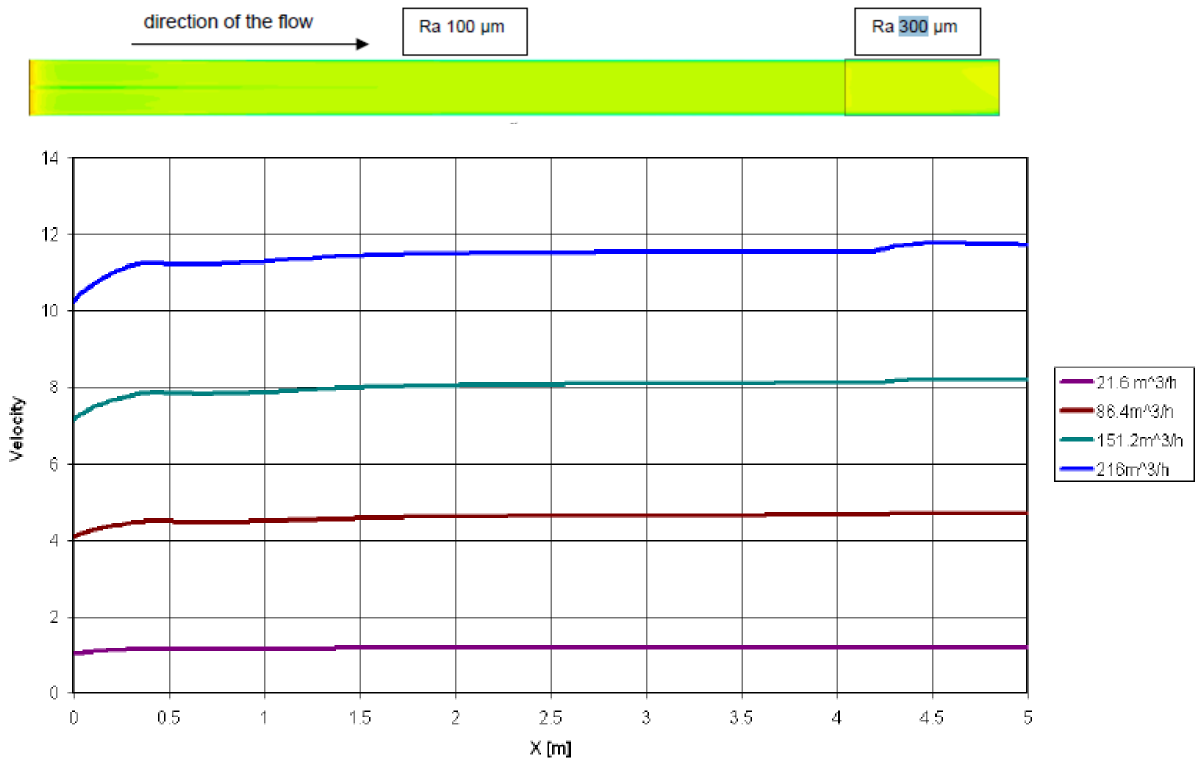

Fig.4: Velocity distribution at the channel centerline along the development length and test section with 300 mm x 20 mm in cross section for different pump-rates.

3. Experimental setup

3.1 Flowcell testing section

The pressure drop (or pressure gradient) experiments were carried out at Jotun, Norway using the flowcell device. The dimension of the cross-section of the channel were as described above 300 mm x 20 mm, providing a channel aspect ratio (AR) of 15:1. This aspect ratio is approximately two times larger than the recommended ratio by Dean (1978), satisfying the criteria to ensure a two dimensionality of the flow. The total length of the flowcell is 9.5 m. The fluid flow is provided by a centrifugal pump with the capacity ranging from 21.6 to 216 m^3/h. This flowrate range results in velocities from 1 m/s up to 10 m/s in the channel as proposed by the CFD study.

Unique features of the flowcell are as follow:

- Larger wetted test area: the length and width of the test panel is 800 mm and 300 mm, respectively.
- The tests can be carried out in variable temperature conditions, 2 °C to 50 °C. For this purpose, the flowcell is equipped with a cooling and heating systems. This system is designed to heat up or cool down the water to the desired temperature and maintain it with a deviation ±1 °C.

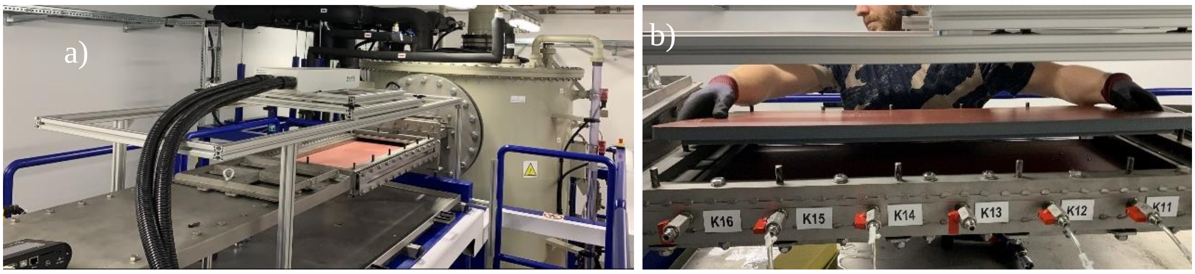

Fig.5: a) Testing section of the flowcell with installed coated panel at the bottom b) Installation of the top panel for pressure drop measurements

The testing section of the flowcell was made from stainless steel 316L, Fig.5a,b. One side of the testing section is made of PMMA glass in optical quality serving as side window to observe and to capture images e.g. by means of high-speed camera of the Particle Image Velocimetry (PIV). The other side is equipped with a set of taps with hoses, connected to differential pressure transducers of three different resolution. Pressure taps are installed at the middle of two parallel panels at different distances from the leading edge of the test panels to read the water pressure at this specific point, Fig.6.

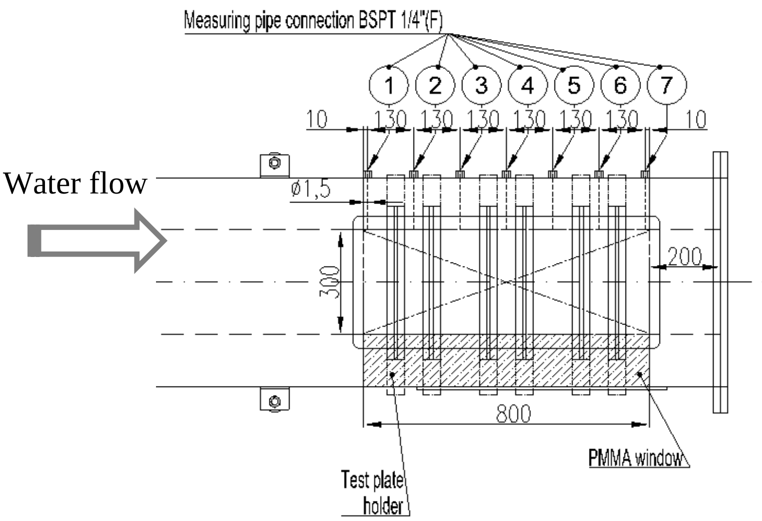

Fig.6: Number of pressure tapping points along the test panel length

The pressure difference between leading edge (tap 1) and trailing edge (tap 7) was used to evaluate the differential pressure for the calculation of drag over the whole test panel. The distance between taps 1 and 7 is 780 mm, covering 97.5% of the panels' total length. The flowcell has a development length of 210 times the height (x/H=200) to ensure that the flow is fully developed before entering the test panel area.

3.2 Test surfaces

The validation of the flowcell was carried out by using a pair of smooth and rough samples, so-called sand-grain surfaces. The results of these panels can be validated and compared with the results of previous similar works and current CFD study, assuring the quality of measurements. Panels machined from transparent polymethyl methacrylate (PMMA) acted as a smooth reference. Rough surfaces were obtained by using two different sizes of black silicon carbide particles. PMMA panels were sprayed with an epoxy base layer and silicon particles were applied to the surface by dipping, assuring a fully covered rough silicon-grit surface. Black silicon carbide consists of crystalline silicon carbide and was produced by Kuhmichel Abrasiv GmbH. FEPA standardized F220 silicon carbide particles with average grain size of 53-75 μm and F80 silicon carbide particles with average grain size of 150-212 μm were used to achieve a finer and courser sand grit surface, respectively.

The coating types tested after the validation stage of the flowcell include:

- Foul-Release Coating (or FRC);
- Self-polishing biocidal antifouling coating (BAC):
  - with high-quality application finish (BAC highq);
  - with low-quality application finish (BAC lowq).

4. Experimental results

4.1 Surface characterization-power spectral density functions

A first attempt is made in this paper to use the power spectral density function as a holistic surface approach. The power spectral density function (PSDF) allows us to draw out information from the measurements of the surface while avoiding dependency on size and resolution of the measurements, making 3D surface measurements form different devices comparable. The PSDF allows to combine measurements from different microscopes at different resolutions in a so-called Master-PSDF. The power spectral density function is a Fourier transformation of the auto-correlation function of a signal, in this case the XYZ signal of a physical surface. By utilizing the PSDF on the data of a surface one can decompose it to contributions from different spatial frequencies. The PSDF of a surface can be used to calculate estimates of the root-mean-square (RMS) roughness, slope and curvature. One can then use these values to explore their effect on drag performance. The RMS roughness will represent contributions from large scale roughness whereas rms slope and curvature represent smaller scale roughness, *Jacobs et al. (2017).*

After processing the data collected using a roughness profilometer, Gwyddion program was used to calculate the one-dimensional PSDF in one direction, $C(q)^{1D+}$. In Fig.9, q is the spatial frequency and is inversely proportional to the wavelength of the roughness features.

From Fig.7a and b, which are the plots used to calculate the RMS roughness and slope respectively, one can see a clear peak for the BAC with low-quality application (or BAC lowq). This implies that for this particular rough coating type, a contribution from low (or longer wavelength/larger-scale roughness features) and medium spatial frequencies are significant. For the course grit, the peak is observed at the spatial frequency of q≈40000, which corresponds to the roughness wavelength of ~157 μm. This is in agreement with the particle size of the course grit, which is 150-212 μm. For the panel covered with the fine silicon grit, the peak starts to rise at the spatial frequency of $q≈10^5$, that corresponds to the roughness wavelength of approximately 60 μm, also in agreement with the particle size of 57-75 μm. For the smooth panel no peaks at the spatial frequencies from the data was detected.

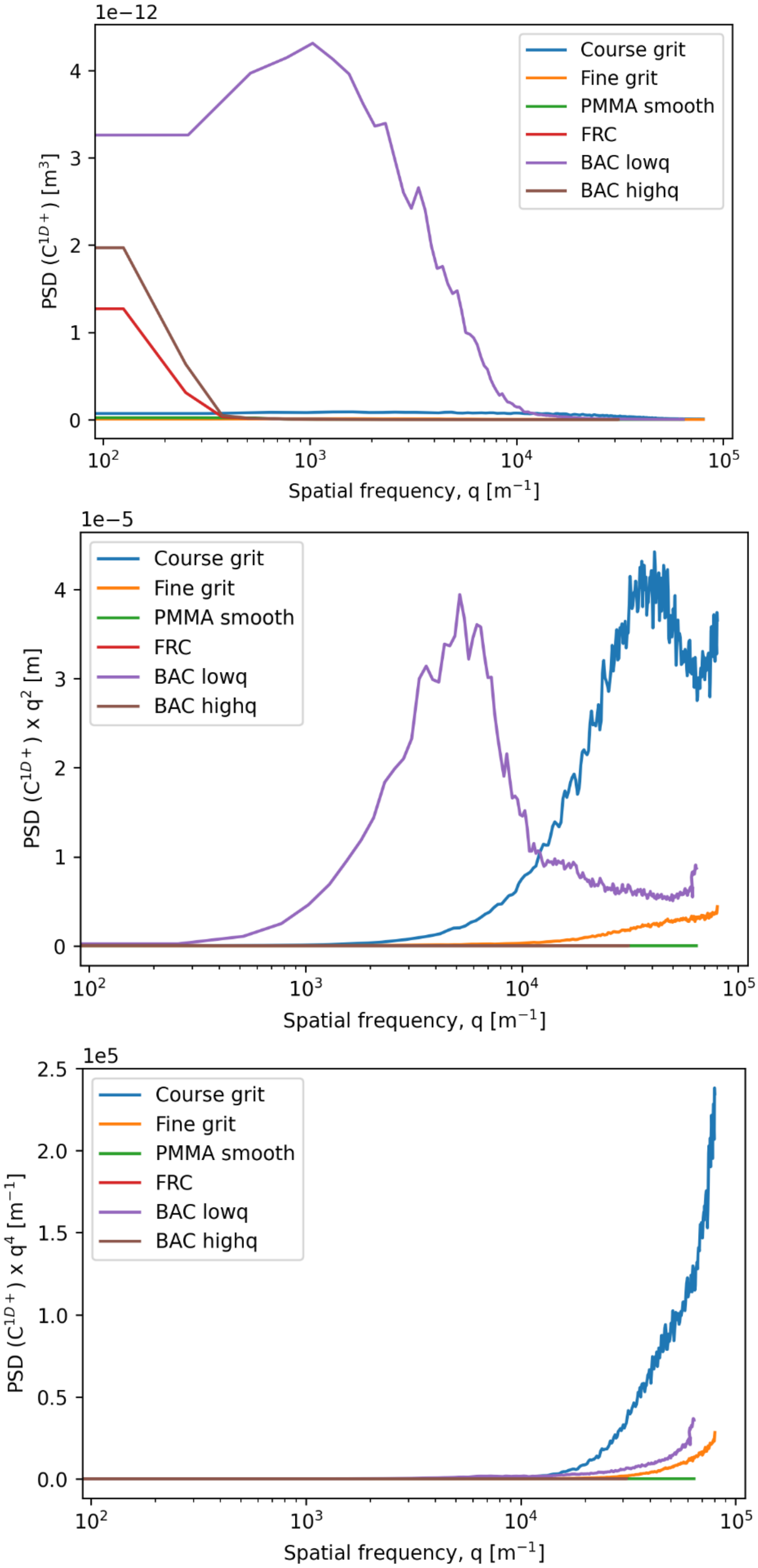

Fig.7: a) PSDF for RMS roughness calculation b) First derivate of PSDF for RMS slope calculation c) Second derivate of PSDF for RMS curvature calculation for test surfaces extracted by integration

This means that for smoother surfaces the resolution of the used microscope was not enough and higher spatial frequencies need to be included by combining low- and high-resolution measurements in a so-called Master-PSDF. This behavior can also be recognized in the corresponding topographic image for BAC lowq and course grit in Fig.8. No large peaks (or small-scale roughness) are observed for FRC, BAC highq coated panels.

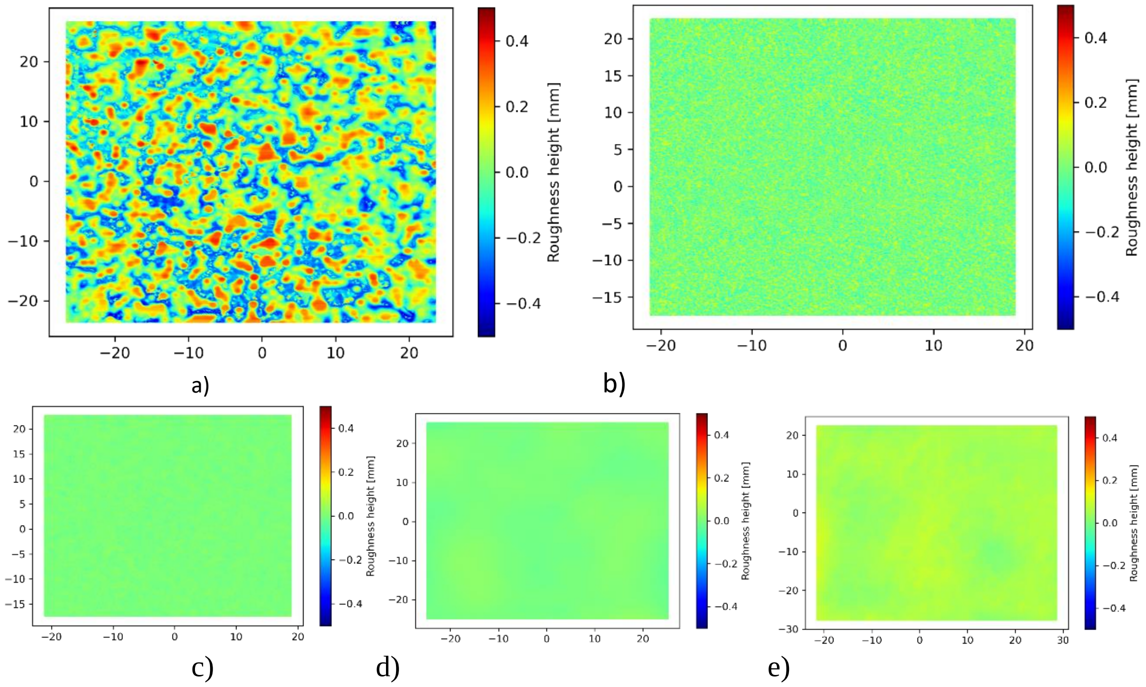

Fig.8: a) Surface topographies for BAC lowq; b) course grit c) fine grit; d) FRC e) BAC highq. Roughness measurements performed by roughness profilometer with 25μm resolution

4.2 Surface characterization-roughness parameters

Roughness parameters like Rq (the root-mean square roughness) and Rt (the maximum peak-to-valley roughness height) were calculated within the 50 mm cut-off length from the data collected from the laser profilometer. Averaged values of the surface roughness for mentioned test surfaces are presented in Same holds true for the course grit and BAC low quality: Rq is ≈44 μm and ≈49 μm for the course grit and BAC low quality, respectively. Although Rt for the course grit (Rt=274 μm) was found to be larger than for BAC low quality (Rt=246 μm), BAC low quality demonstrated higher drag up to mid-range Reynolds number when compared to the course grit data as shown in Fig.10, which is the graph of skin frictional drag performances. This behavior can well be attributed to differences in spatial frequency peaks or in differences in roughness feature wavelengths of these test surfaces.

4.3 Flowcell calibration and preliminary tests

Knowing the flowrate and cross-sectional area of the flowcell test section enables the recalculation of volumetric flowrate for different pump frequencies in terms of mean velocities (U_m), demonstrated in Fig.9. The motor controller was swept through its entire range of frequencies, from 5 Hz to 45 Hz. The pressure difference at the contraction section was measured at corresponding motor frequencies and the velocity at the channel inlet was deduced by applying Bernoulli's equation. According to the measurement results in Fig.9, the bulk or mean velocity in the testing section ranges from 1.1 m/s to 11.3 m/s for a smooth PMMA reference surface.

Table

From Table I one can notice that Rq and Rt parameters of the fine grit shows similar values to that of

FRC and BAC high quality application. However, the peaks for the spatial frequencies are quite different, Fig.7. Same holds true for the course grit and BAC low quality: Rq is ≈44 μm and ≈49 μm for the course grit and BAC low quality, respectively. Although Rt for the course grit (Rt=274 μm) was found to be larger than for BAC low quality (Rt=246 μm), BAC low quality demonstrated higher drag up to mid-range Reynolds number when compared to the course grit data as shown in Fig.10, which is the graph of skin frictional drag performances. This behavior can well be attributed to differences in spatial frequency peaks or in differences in roughness feature wavelengths of these test surfaces.

4.4 Flowcell calibration and preliminary tests

Knowing the flowrate and cross-sectional area of the flowcell test section enables the recalculation of volumetric flowrate for different pump frequencies in terms of mean velocities (U_m), demonstrated in Fig.9. The motor controller was swept through its entire range of frequencies, from 5 Hz to 45 Hz. The pressure difference at the contraction section was measured at corresponding motor frequencies and the velocity at the channel inlet was deduced by applying Bernoulli's equation. According to the measurement results in Fig.9, the bulk or mean velocity in the testing section ranges from 1.1 m/s to 11.3 m/s for a smooth PMMA reference surface.

Table I: *Rt* and *Rq* parameters measured by a laser profilometer

Test surfaces		Description	Roughness parameters from Taicaan Laser Profilometer (50mm cut-off length)	
			Rq, μm	Rt, μm
			Mean±St.dev	Mean±St.dev
Control	'Smooth'	PMMA transparent	2.76±1	12.1±3
	'Fine grit'	Panel covered with silicon carbide F220 grit with average grain size 53-75μm	11.1	82.7
	'Course grit'	Panel covered with silicon carbide F80 grit with average grain size 150-212μm	43.7	274
Coatings	'FRC'	Foul-Release coating	13.1±3	56.9±15
	'BAC highq'	Self-polishing biocidal antifouling coating with high-quality application finish	13.5±5	60.4±19
	'BAC lowq'	Self-polishing biocidal antifouling coating with low-quality application finish	48±7	246.3±36

Because of the roughness effects of surfaces the velocity in the channel is 1.1 % (traditional coating), 2.3 % (fine grit) and 3.8 % (course grit) lower at the maximum pump frequency of 40 Hz. As shown in Fig.9, the relationship between U_m and the pump's motor frequencies can be characterized by the linear equation. The trend demonstrates uniform performance of the selected pump.

Skin frictional coefficients of the different test panels were indirectly calculated by measuring the pressure difference between two pressure taps along the test panel length. The pressure data acquisition time at each pump frequency was more than 40 seconds. In practical in a duct/channel flow the wall shear stress (τ_w) can be related to the head loss due to the friction through the channel. Using a simple momentum balance of turbulent flow in the channel, the relationship for wall shear stress may be given by (3):

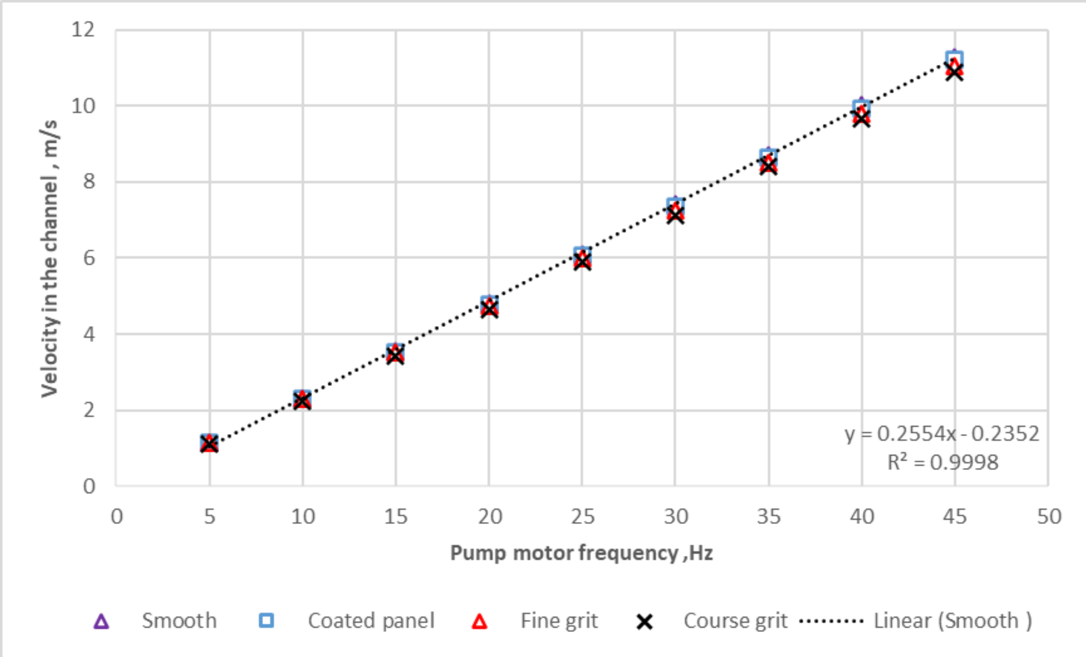

Fig.9: Mean velocity (U_m) as a function of pump's motor frequency

$$\tau_w = -\frac{H}{2}\left(\frac{dp}{dx}\right) \tag{3}$$

Where H is the channel height and $\frac{dp}{dx}$ is the streamwise pressure gradient between pressure tap 1 and 7. The skin friction coefficient C_f is determined by normalizing the wall shear stress with the kinetic energy of the bulk flow:

$$C_f = \frac{\tau_w}{\frac{1}{2}\rho {U_m}^2} \tag{4}$$

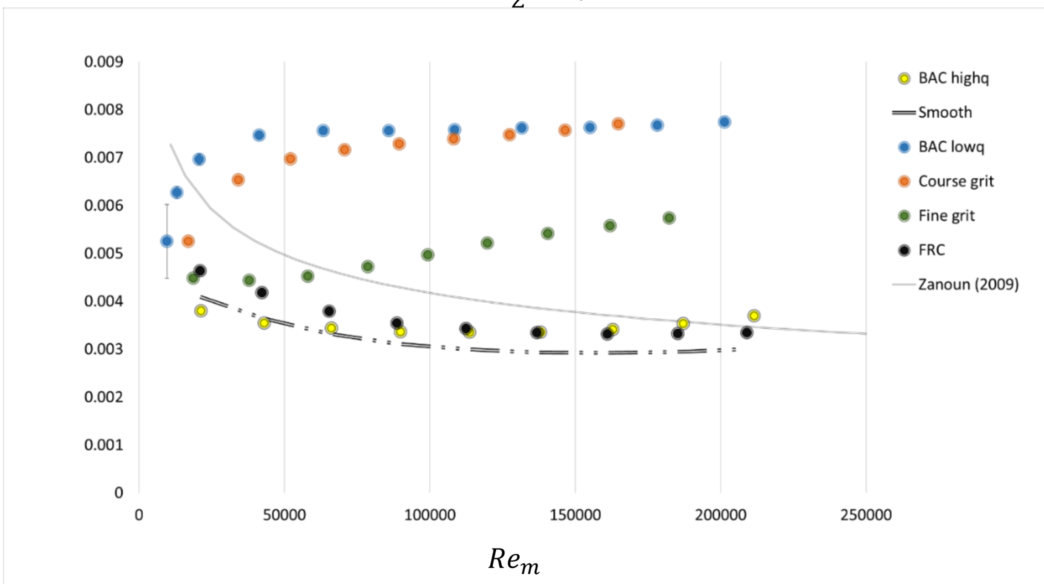

Fig.10: C_f results of surfaces with different surface conditions when compared to smooth wall data

The wall skin friction data (C_f) for reference smooth and other test surfaces discussed in section 3.2 are plotted in Fig.10. In Fig.10, the y-axis represents the skin friction coefficient or drag, acting on surfaces changing with increasing velocities from left to right on the x-axis. The velocity in the channel is expressed in terms of the Reynolds number (Re_m) based on channel half height and mean velocity. A monotonic decrease in the C_f with increase in Reynolds numbers is seen for the smooth reference as the transition from lower to higher speeds occurs. This smooth data was used as a reference to evaluate the roughness effects. The C_f curve for BAC low-quality application diverges upward immediately even at lower Reynolds numbers from the smooth curve, resulting in C_f increase from 126% to 160% in investigated Reynolds numbers. BAC low quality demonstrated higher drag up to mid-range Reynolds number than the course grit as shown in Fig.10, even though Rt for BAC lowq is lower than that of course grit (see Table). This difference in hydrodynamic performance can be due to differences in spatial frequency peaks or roughness feature wavelengths of these mentioned surfaces. The C_f for FRC, BAC high-quality application (except at 1.1 and 2.3 m/s) with normal application finish showed moderate drag increases when compared to the smooth reference. The added drag for FRC was 14 % at $Re_m \approx$ 90 000. One can observe the gain in drag performance (12%) at the higher end of the flow velocities. Whereas, for the BAC high-quality application, we see the gradual increase in the C_f terminating with 23% of drag increase compared to the smooth surface. From Fig.10, it is clear that the course grit panel started to deviate from the smooth wall data already at the lowest Reynolds number of the test with an added drag of 26 %. The fine grit panel demonstrates similar added drag (about 32%) at much later stage of the experiment, namely at $Re_m \approx$60 000. Throughout the tested Reynolds numbers, fine and course grits showed a continuous increase in C_f. At the Reynolds number of $Re_m \approx$90 000 with a corresponding channel velocity of 4.7 m/s, the fine and course grit surfaces compared to the smooth wall data demonstrated about 48% and 119% increase in the C_f, respectively. At the highest pump frequency (≈11m/s), the percentage increase in the C_f reaches 94% and 163% compared to smooth surface. Overall, significant drag coefficient increases were observed over a smooth data when grit size varied from fine (53-75 µm) to course (150-212 µm).

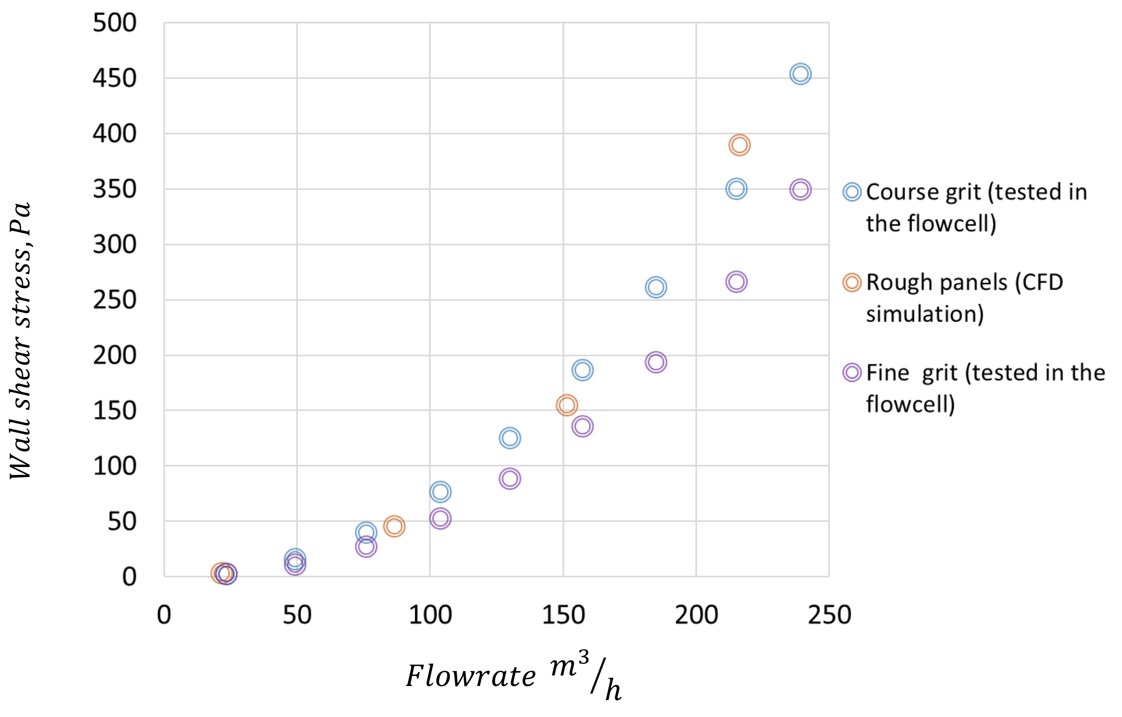

Fig.11: Comparison of wall shear stress (Pa) values of experimental and CFD results

The adverse effect of a higher roughness on the drag performance is also confirmed by the CFD simulation. As it was presented in Section 2, the test plate roughness in the flowcell model was set to Ra=300 µm. From Fig.11 which plots the wall shear stress as a function of flowrate, the wall shear stress values of experimental results for course grit (Rt=274 µm) agrees reasonably well with the results of the CFD simulation, with an average relative error of 12%.

5. Concluding remarks and further work

The present work is about the skin friction measurements of smooth and coated surfaces with various degrees of surface finishes in the newly built flowcell at Jotun A/S. The skin friction coefficients were determined indirectly by measuring repeatably the pressure drop along the test panel. The preliminary results show that roughness amplitude parameters (e.g Rq and Rt) alone are not enough to explain hydrodynamic performance of surfaces. Therefore, next step of this study will be to increase the resolution of surface analysis and include higher spatial frequencies into the evaluation to explore the correlation between RMS roughness, slope and curvature and the drag of tested surfaces.

The understanding of the hydrodynamic performance under various coating conditions depending on application, substrate type and surface preparation; in other words, the “robustness” of a coating to in service application is of great importance. Therefore, more tests are planned for different application conditions. In addition, heat and thermal cycles can be used to test the coatings at different temperatures, as described in section 3.

As part of the future work, the authors also plan to utilize the Particle Image Velocimetry (PIV) setup to accurately resolve the flow structures induced by different test surfaces. Detailed velocity data derived from the PIV will also be used to evaluate two-dimensionality of the flow through the channel. Our PIV analysis is going to provide support for internal numerical modeling studies and shed more light onto the characteristics of complex turbulent flows over coated, aged surfaces. The experimentally obtained data will be used to for full-ship simulations to calculate the impact of the different coatings for different ship hull models.

References

BOYD, J.P. (2001), *Cherbyshev and Fourier Spectral Methods,* Dover Publications

DEAN, R.B. (1978), *Reynolds Number Dependence of Skin Friction and Other Bulk Flow Variables in Two-Dimensional Rectangular Duct Flow,* J. Fluids Engineering 100(2), pp.215-233

HOYAZ, S.; JIMENEZ, J. (2006), *Scaling of the Velocity Flactuations in Turbulent Channels up to Reτ = 2003,* Physics of Fluids 18(01172), pp.1-4

JACOBS, T.D.B.; JUNGE, T.; PASTEWKA, L. (2017), *Quantitative characterization of surface topography using spectral analysis,* Surface Topography: Metrology and Properties 5(1)

LAUFER, J. (1948), *Investigation of Turbulent Flow in a Two-Dimensional Channel,* PhD thesis, California Institute of Technology

MONTY, J.P. (2005), *Developments in Smooth Wall Turbulent Duct Flows,* PhD thesis, University of Melbourne

SCHULTZ, M.P.; FLACK, K.A. (2013), *Reynolds-Number Scaling of Turbulent Channel Flow,* Physics of Fluids 25, pp.1-13

VINUESA, R.; BARTRONS, E.; CHIU, D.; DRESSLER, K.M.; RÜEDI, J.D.; SUZUKI, Y.; NAGIB, H.M. (2014), *New insight into flow development and two dimensionality of turbulent channel flows,* Experiments in Fluids 55(6)

ZANOUN, E.S.; DURST, F.; NAGIB, H. (2003), *Evaluating The Law Of The Wall In Two-Dimensional Fully Developed Turbulent Channel Flow,* Physics of Fluids 15(10), pp.3079-3089

ZANOUN, E.S.; NAGIB, H.; DURST, F. (2009), *Refined cf Relation for Turbulent Channels and Consequences for High Re Experiments,* Fluid Dynamics Research 41, pp.1-12

The Impact of 'Fouling Idling' on Ship Performance and Carbon Intensity Indicator (CII)

Markus Hoffmann, I-Tech AB, Gothenburg/Sweden**,** markus.hoffmann@i-tech.se

Abstract

On January 1, 2023, the International Maritime Organization (IMO) will introduce the Energy Efficiency Existing Ship Index (EEXI) and Carbon Intensity Indicator (CII) measures for every ship above 5,000gt in size as a means to reduce carbon emissions from international shipping. In particular, the CII, as an operational index, will be impacted by biofouling load on the underwater hull surface. This is due to accumulated biofouling creating additional hydrodynamic drag that necessitates a ship to burn more fuel when sailing through water to maintain a set speed. This paper explores the connection between biofouling and ship CII ratings and offers insight and strategies for improving hull performance associated with the use of antifouling coatings. It also highlights the key findings of I-Tech's recent, extensive research into global fleet idling and why ship operators are concerned about the impact of biofouling in terms of both ship performance, profitability, and commercial reputation.

1. Introduction

Biofouling has been a perennial headache for the shipping industry for centuries. Accumulating biological matter on the hull is not a new problem for merchant ships. However, it is a problem that is set to get far worse, particularly for vessels idling in warmer waters. With ocean temperatures rising on a global scale, biofouling hotspots are increasing in size and severity, leaving more ships at risk of the negative impacts of biofouling on ship efficiency. Since fouling species flourish in warmer waters, the risk of them making a home on ship hulls is significantly increasing year-on-year.

In addition to the far-reaching impact of the COVID-19 pandemic on global trade, geopolitical events have continued to render vessels idle in coastal areas. New regulations that seek to reduce the environmental impact of shipping also mean that ship operators will be harder pressed to keep their ships operating efficiently and polluting less than they have done previously.

Biofouling has a threefold effect on ships; slowing them down, increasing fuel use and reducing cargo capacity therefore, its role in decreasing ship efficiency and lessening the impact of fuel saving measures should not be underestimated.

The negative impacts of biofouling are well-documented and increasing attention is being given to the issue by national and international authorities. Port cities are also becoming increasingly sensitive to air pollution and biosecurity risk created by visiting ships.

2. Uncertainty ahead

As the world entered the first few months of 2022, a great deal of uncertainty existed. Differing fiscal policies around the globe, continuing concerns around the COVID-19 virus, and geopolitical risks and growing tensions have made it difficult to foresee the main trends for the year ahead. Anticipations about the escalating situation in the Ukraine sadly came to fruition in 2022 and events in Asia around China, Hong Kong and Taiwan remain to be concerning.

The winter of 2021 also brought soaring energy prices on a global scale putting huge pressures on human populations and industries alike. Inflation is running at levels not seen for 20-40 years in Europe and the US, creating strains on green initiatives at local, national, and regional levels.

In its 2021 Global Trade Outlook report, UNCTAD warned that the forecast for 2022 was uncertain in spite of positive trends for international trade in 2021. Subsiding pandemic restrictions, economic stimulus packages, and increases in commodity prices added to the international shipping industry moving towards returning to business as usual, albeit in a new "normal" world.

Among the factors contributing to industry uncertainty in 2022, UNCTAD cites China's "below expectations" growth in the third quarter of 2021. "Lower-than-expected economic growth rates are generally reflected in more downcast global trade trends," it says, while pointing to "inflationary pressures" that may also negatively impact national economies and international trade flows. UNCTAD's 2021 report also noted that "many economies, including those in the European Union", continue to face COVID-19-related disruptions that could affect consumer demand this year. That is a view that appears both confirmed and contradicted by extended delays for container ships at numerous ports around the world. Queues continue to grow because of labour and capacity issues but consumer demand remains strong even if disrupted by shortages of goods leaving factories.

Fuel costs have also shot up and represent a significant part of the total ship operating costs. As crude prices nudged the US$90 per barrel mark in early 2022, bunker costs were also rising in line. Some analysts believe that 2022 could see crude oil touch the US$150 price point making eyewatering increases in bunker costs inevitable.

3. Incoming environmental regulations

In an attempt to bring the world fleet in line with its greenhouse gas (GHG) reduction programmes, the IMO has initiated two new measures that will be implemented at the beginning of 2023.

The EEXI is a means of applying a similar regime to the Energy Efficiency Design Index (EEDI) for newbuildings to vessels that existed before the EEDI rules became effective in 2011. EEXI is a technical measure and attempts to limit the carbon emissions based upon the equipment and technology installed on the ship. Both the EEDI and EEXI are laudable and effectively make shipping the only industry that has been obliged to reduce emissions on a global scale.

However, both are imperfect because they cannot effectively allow for measures where the impact on emissions is not constant. Battery hybrid ships, dual fuel engines and antifouling coatings are not adequately covered in these rules because they are dependent upon the way the ship is operated.

The CII coming into effect in 2023 will see further pressure on ships to become more efficient. From a coatings point of view, the CII is a regulatory requirement that will be influenced by hull performance, as opposed to the EEXI which is not.

The CII measures how efficiently a ship transports goods or passengers and is given in grams of CO_2 emitted per cargo-carrying capacity and nautical mile. The ship is then given an annual rating ranging from A to E. The rating thresholds will become increasingly stringent towards 2030. If a ship is rated E or D for three consecutive years, the owner will have to submit a corrective action plan to bring the vessel back into compliance. Some analysts believe that more than half of the world fleet will score a D or E rating and will need to take corrective action.

At the same time, other regional environmental regulations present a significant challenge. The EU's ETS scheme will introduce carbon pricing for ship fuel for the first time. There are disputes over who should cover this. Currently it looks as though charterers will be presented with a bill for carbon emissions, almost certainly ensuring they will then pressure shipowners to make ships more efficient.

Biofouling regulation remains to be a national matter, despite IMO guidelines. However, this is evolving. A newly signed initiative is set to provide pilot projects to demonstrate technical solutions for biofouling management in developing countries, address the transfer of invasive aquatic species (IAS) and help reduce GHG emissions from ships.

As new requirements for managing biofouling on international vessels arriving in Australia will begin on 15 June 2022, more countries around the world have already established similar regulations to address the effects of biofouling.

In New Zealand, the Craft Risk Management Standard (CRMS) came into force on 18 May 2018. This mandatory 'clean hull' requirement applies to vessels entering NZ territorial waters and non-compliance can lead to expulsion.

In California, the California State Lands Commission (SLC) Marine Invasive Species Program (MISP) applies to vessels 300 GT and above. These biofouling regulations require the development and maintenance of; a Biofouling Management Plan, a Biofouling Record Book, the mandatory biofouling management of the vessel's wetted surfaces, and mandatory biofouling management for vessels that undergo an extended stay in the same location (45 or more days). An Annual Vessel Reporting Form (AVRF) must also be submitted once per calendar year and at least 24 hours prior to a vessel's first arrival at a California port through a web-based platform.

Also, at the 76th MEPC session, held in June 2021, IMO adopted amendments to the International Convention on the Control of Harmful Anti-fouling Systems in Ships (AFS Convention) regarding controls on cybutryne and the form of the International Anti-fouling System Certificate. The amendments will enter into force on 1 January 2023. From this date, the application or re-application of an AFS containing cybutryne will not be permitted.

4. The biofouling problem

Marine fouling is the biological process of single celled organisms, algae, and hard-shelled organisms, attaching to submerged surfaces and colonising at a rapid rate.

There are approximately 5,000 different fouling species that are found in the world's oceans. These can be classified into "Micro fouling" which comprises slime fouling, and "Macro fouling" which comprises weed fouling and animal fouling (hard, with a shell and soft, without a shell).

Any organisms anchored on the hull create increased drag (commonly referred to as added resistance) which significantly decreases hull performance. Hard (with a shell) animal fouling (calcareous fouling in Table 1) which includes molluscs, bryozoans, tubeworms, and barnacles cause the greatest penalty in terms of hydrodynamic drag when attached to a ship's hull.

A biofouled vessel must burn more fuel to attain the same speed through water when in active service, resulting in higher fuel costs for the ship operator. Therefore, the increase in fuel consumption due to the adverse effect of hard biofouling on hydrodynamic performance is one of the most significant financial penalties for the shipping industry to endure, as detailed in Table I.

Table I: Roughness and Fouling Penalties - Adapted from *Schultz (2007)*

Hull condition	Additional shaft power to sustain speed (%)
Freshly applied coating	0
Deteriorated coating or thin slime	9
Heavy slime	19
Small calcareous fouling or macroalgae	33
Medium calcareous fouling	52
Heavy calcareous fouling	84

In 2019, research commissioned by I-Tech AB quantified the true extent of the barnacle fouling problem across the global shipping fleet. I-Tech contracted independent marine coating consultants, Safinah Group to analyse underwater hull fouling condition on a sample of 249 ships which drydocked over a four-year period between 2015-2019. The sample included all major ship types covering a range of trading activity.

Barnacle (hard) fouling can only occur when a vessel is static for a few weeks in coastal waters. It was found that nearly every vessel surveyed had some degree of underwater hull hard fouling. On 44% of vessels surveyed, over 10% of the underwater hull surface was covered with hard fouling. Anything more than 10% coverage is deemed to cause an ‘unacceptable’ impact on vessel performance.

On many of the vessels surveyed, fouling levels were even worse; approximately 15% of vessels had between 10-20% of hard fouling coverage on the hull, 10% of vessels had 20-30% of hard fouling coverage and the remaining 10% of vessels had between 40-80% of hard fouling coverage.

Extrapolating from published data taken from *Schultz et al. (2011)*, this level of hard fouling could be responsible for at least 110 million tonnes of excess carbon emissions, and an additional US $6 billion spent on fuel per year for the global commercial fleet. The true figure is likely to be higher, as this is a conservative calculation based on relatively low fuel prices in 2019 and only assumes a 10% coverage of hard fouling.

Therefore, the significant extent of hard fouling found across this sample of vessels demonstrates the magnitude of unnecessary demand being placed on engines because of hard fouling, increasing fuel consumption and emissions, and exacerbating speed losses due to increased hydrodynamic drag. According to the study observations, the frequency of hard fouling was relatively higher on vessels with lower activity rates – confirming the link between idling and barnacle fouling risk. 45% of lower activity vessels surveyed suffered from hard fouling coverage of >10% compared to just 27% of higher activity vessels.

This data analysis was carried out before the COVID-19 pandemic therefore, I-Tech anticipates that since this study was conducted, the extent of barnacle fouling coverage across the global fleet will have increased significantly, particularly for the huge proportion of vessels that have laid idle.

Hard fouling on the hull is also extremely impactful on maintenance costs. Costs associated with hull cleaning services are factored into a ship operator’s operating expenditures (OPEX) but as global biofouling risk increases, hull cleaning is likely to be required more frequently, in-creasing maintenance costs. Repeated cleaning of the hull can also remove layers of the antifouling coating, reducing its service life. Abrasive methods to remove hard fouling species, such as barnacles, are particularly damaging to the coating.

5. Quantifying the true extent of idling in the global fleet

An extensive, independent study undertaken by I-Tech and Marine Benchmark of global fleet data up to, and including, the year 2020 explored the issue of idling and resultant biofouling. The results gave novel insight into differences between sectors of the industry confirmed a large increase in vessel idling over the past decade.

Remarkably, no in-depth study has been previously conducted that quantifies the true level of idling in the global fleet or in specific vessel type segments of the global fleet. Many shipowners hold extensive statistics and knowledge on their own fleet’s activity, with statistics on vessel performance and operating parameters such as average speed, fuel use, etc. Also, studies that examine idle capacity of different market segments used as an indicator for available capacity and future price developments can be found. But no current studies include the quantification of idling period length against water temperature and fouling pressure.

The Marine Benchmark web platform used for this study has capability for a full bottom-up AIS based fuel consumption calculation, globally and by countries EEZ (Exclusive Economic Zones). The database uses an online feed from IHS Markit including a feed from their AIS antennas and IMO vessel register.

Its algorithms are run live 24/7 on its 18 servers performing global calculations of distance, speed, fuel consumption, cargo onboard, transport work and Energy Efficiency Operational Indicator (EEOI).

6. Defining "fouling idling"

Disputes often arise between the shipowner and coatings supplier since there remains to be no clear industry definition of idling, which is surprising as idling guarantees are based on this.

To complicate matters further, different coating suppliers may offer their own definition of idling and there is no clear industry standard on how idling is defined. The narrowest definition is a vessel on a defined spot without any movement. But what happens with very short trips or manoeuvring. If an idling guarantee stipulates a maximum period, some shipowners may make a short trip prior to the maximum period being exceeded with the intention to limit the idling time and thereby keeping the guarantee active.

For this idling study, the focus by I-Tech was to look at vessels where idling resulted in high fouling risk in particular. We refer to this as "fouling idling" as a distinct from "commercial idling".

Where the purpose of commercial idling is to measure the commercial activities and inactivity of vessels, the purpose of "fouling idling" is to define idling as a risk for operations due to the resultant biofouling.

For this definition, we link idling to water temperature and how long the vessel is "fouling idling" in an unbroken sequence. As such, "Fouling idling" is defined as any vessel that is idling for 14 days or more in waters of 15ºC or more.

Though all vessels are included in the database it is well known that some ship types, in general, have a trading pattern which can be regarded as idling, these types of vessels include tugboats, fishing boats, bunkering vessels and some type of ferries. These vessels are taken out of the analyses to give a more accurate result. Stationary times at yards were also not counted as fouling idling because the vessels are usually dry-docked and, in most cases, a long stay implies that the vessel will be re-coated with new antifouling coating. However, a vessel waiting to discharge of cargo or sitting stationary due to use as a floating storage may be commercially employed and active but is also idling when it comes to fouling exposure.

The following steps were used to filter the AIS data:

1. Vessels were divided into three segments depending on activity:
- **a.** Stationary - below 1 knot (at yard and outside yards)
- **b.** Manoeuvring - 1 to 6 knots
- **c.** Steaming - above 6 knots

3. To be defined as "fouling idling", the following intermediate activities are allowed:
- **a.** Up to 12 hours manoeuvring is allowed between 2 stationary activities
- **b.** Up to 6 hours steaming are allowed between 2 stationary activities

4. Exclude all yard calls since these vessels are going into drydock.

5. The distance between first and last AIS observation for each fouling idling period is calculated and a maximum distance of 100 nautical miles are allowed.

6. Sea water surface temperatures were divided into three groups: below 15°C (cold), 15°C to 25°C (medium) and above 25°C (warm).

7. The data was divided in number of vessels staying in fouling idling periods: above 14 days, above 30 days and above 45 days.

7. Key study findings

In-depth analysis of the global fleet patterns based on AIS data for all IMO-registered vessels of the global fleet, revealed a substantial increase in the numbers of idling vessels over the past decade.

- The total number of vessels idling has roughly doubled over the last decade.
- A high percentage of idling is occurring in water temperatures above 15°C.
- Many bulker vessels are idling even outside of peaks. The level of idling for this vessel type is regularly above 1000 vessels monthly.
- The number of idling tanker vessels has constantly increased since 2009, peaking at 1421 vessels in 2020.
- During the idling peak in 2020, nearly all idling container vessels were laid up in warm waters and almost half of all container vessels had long idling periods of more than 30 days.
- Cruise vessels at anchor for more than 14 days in 2020 increased from an average of 3% to between 20-30%.
- Depending on season, between 50% - 85% of idling is occurring in water temperatures of above 15ºC.
- During 2020, compared to previous years (2018-2019), the number of vessels idling for more than 14 days increased for most segments within the global fleet.

I-Tech found that 'Fouling Idling', as defined in the study, has increased constantly since 2009, with a starting point of 25.4% to a peak of 35.0% in May 2020. Given the growth of the fleet, this means that the absolute number of vessels idling in the global fleet has doubled between 2009-2020.

Significantly, the study also found that vessels are increasingly idling in so-called biofouling ´hotspots´, where water temperatures above 25°C. Vessels spending the majority of their time sailing in these regions are at acute risk of excessive hard fouling accumulation.

There was a clear peak in June 2020 with 99 container fleet vessels sitting idle in warm temperature waters, 96 vessels idling in medium temperature waters and 2 vessels idling in cold temperature waters giving a total number of 197 vessels being idle. Comparing this to June 2019 when there were only 22 vessels idling in warm temperature waters, 13 in medium temperature waters and 1 in cold temperature waters giving a total number of 36. This represents an increase of over 447% year-on-year.

The effects of the COVID-19 pandemic had an impact within the bulker fleet. There was an increase from 1,100 vessels being idle in the beginning of 2020 to over 1,500 in April 2020. The majority of vessels were idling in water warmer than 25ºC.

For the tanker fleet, idling was at its highest level in May 2020 since 2009, with 15.4% vessels sitting idle. A notable 84.2% of the idling activity happened in medium to warm waters with high risk of fouling. At the peak in May 2020, 1421 tanker vessels were idle for more than 14 days.

The cruise fleet results show an extreme picture. Comparing the time before the Covid break out with after, vessels at anchor for more than 14 days increased from an average of 3% to between 20-30%. In numbers, idling went from less than 10 vessels with long idling periods monthly, to over 60 vessels being laid up.

When looking at the proportion of the global fleet idling for 30 days or more the results were very interesting. For example, looking at the peak in 2015, 5,5% of all container vessels (10000 to 13499 TEU) were idling for more than 30 days, and at the 2020 peak, the number was close to 3%.

For Suezmax tanker vessels (130,000 to 199,900 DWT) idling was peaking to above 4% on regular occasions and during the peak in 2020, 8,5% of vessels were idling for over 30 days.

Capesize bulkers (120,000 to 349,900 dwt), are also part of this trend with several idling peaks between 2009-2020 where 2-4% of all vessels in this segment had idling periods of longer than 30 days.

8. What's the solution to increasing fouling idling and preparing for CII?

Selecting an antifouling technology mix that is suitable for the vessel type, activity, and trading patterns but that also offers an insurance of extended static protection against barnacle fouling during unexpected long idle periods is the best strategy for any ship owner. In combination with a vessel-optimal antifouling coating, ship operators would benefit from planning potential idling periods to take place away from the biofouling high-risk zones.

With unpredictable operations resulting in long periods of idling, it is also more important than ever to examine the idle period guarantees provided by coating manufacturers and identify what components can provide protection during extended idling periods. Apart from ship owners investigating idling guarantees, it has also become clear that there is a need for an industry definition of idling to clarify the meaning of guarantees and make it easier to choose the most suitable antifouling system for a vessel´s operation.

For most antifouling coatings, protection guarantees range between 14 and 21 idle days, with the majority of premium antifouling coatings offering up to 30 days idle guarantee. Some premium antifouling coatings offer idle guarantees over 30 days. However, under tough market conditions such as those encountered during the COVID-19 pandemic, the I-Tech/Marine Benchmark study has proven that it is not uncommon for a vessel to be idling for more than 30 days, and in some cases even longer than 45 days. It is therefore clear that owners and operators need to take into consideration that only the best idling protection guarantees are sufficient.

9. The importance of Selektope® post-2022

Taking future-proofing approach to antifouling coating selection, without any certainty of future trade, is exerting great pressure on the coating suppliers, prospering great innovation and new approaches with fouling prevention technology

For many antifouling coatings on the market, longer idling guarantees are made possible by the inclusion of the biocide, Selektope®. There is increasing demand for antifouling coatings that contain Selektope® from ship owners and operators reflecting the growing issue of increased idling and barnacle fouling.

Selektope® is a biocide that is currently used in Self-Polishing Copolymers coatings. It is not used in Foul Release coating types, yet. Selektope® binds to pigment and other particles in the paint system and is therefore continuously released in the same way as other active substances and components. This contributes to long-term performance as long as the paint remains on the hull. The compatibility between Selektope® and the paint matrix in the marine coatings industry, ensures as slow and steady release secures the antifouling effect over time.

Selektope® has highly favourable antifouling properties at low concentrations (nano Molar). To obtain full protection against barnacle fouling, 0.1 - 0.3% w/w of Selektope® should be used in a wet paint formulation. Just 2 grams Selektope® is used per litre of paint, comparable to 500-700 grams of copper oxide used per litre of paint for barnacle prevention.

Selektope®'s mode of action is completely unique. Barnacles attach to surfaces when in their cyprid larva stage but if a larva comes into contact with a coating containing Selektope, the active agent interacts with the larva's neurological system temporarily stimulating a receptor (the Octopamine receptor), causing a hyperactive swimming behaviour. This makes it impossible for the larvae to attach to the surface. Once out of contact with the Selektope® being leached from the coating, the effect ceases, and the larvae can swim away unharmed to settle elsewhere.

10. Conclusion

Cutting carbon emissions will be an unavoidable necessity post 2023, and ship operators are likely to use various fouling control solutions in their efforts to achieve greater efficiencies.

Most importantly, when it comes to biofouling management, they must ensure that, should any idling take place, the vessel hull remains to be in good condition to perform optimally with no increased emissions. Familiarisation with the individual vessel's risks of biofouling based on its operating footprint is an essential starting point.

When looking at the future trading potential, ship operators need to ensure that their ship is protected, whether it is in constant active service, idle for long periods of time, or at risk of fluctuating between the two. Selektope® takes the role of providing an insurance policy when contained within marine coatings that enables this flexibility due to its ability to prohibit barnacle fouling, even during extended static periods in warm waters.

References

SCHULTZ, M.P. (2007), *Effects of coating roughness and biofouling on ship resistance and powering*, Biofouling 23(5), pp.331-341

SCHULTZ, M.P.; BENDICK, J.A.; HOLM, E.R.; HERTEL, W.M. (2011), *Economic impact of biofouling on a naval surface ship*, Biofouling 27(1), pp.87-98

Continuous Monitoring and Predicting CII based on Ship Operational Data

Wojciech Górski, Enamor Ltd., Gdynia/Poland, wojciech.gorski@enamor.pl
Jerzy Michniewicz, Enamor Ltd., Gdynia/Poland, jerzy.michniewicz@enamor.pl

Abstract

The international shipping industry has joined the global pursuit in reduction and finally the elimination of greenhouse gasses (GHG) emissions. Since the decade International Maritime Organization (IMO) implements various restrictions targeted on the limitation of ship GHG pollutions. These regulations apply to ship design as well as vessel operational aspects. Carbon Intensity Indicator (CII) is a recent mechanism implemented in MARPOL which addresses GHG emissions in ship operation. CII uses CO_2 emission per transport work factor as a key performance indicator and compares it with gradually increasing targets. Owners of the continuously underperforming vessels would have some time to implement remedies or will be forced to leave the market. It is a novel and very powerful mechanism which will impact shipping industry by direct influence on charter rates and vessel market value. Therefore, continuous monitoring and the ability to predict how changes in vessel operation impact CII will become the must-have tool for the shipping market. Enamor R&D team examined operational data collected by the SeaPerformer system in 2020 and 2021 for vessels of various types in order to develop a convenient method for continuous monitoring of CII. Manual entries and high-frequency automatic data acquisition were compared for defining a suitable data collection strategy. A practical method for daily CII monitoring was developed. The initial study revealed high dependency of CII on vessel operational pattern. Therefore, a further study was focused on elaborating an algorithm that combines past data and mathematical modeling for short- and mid-term prediction of CII value. As the result, practical tool for a voyage and operational planning was elaborated. The prediction method was fine-tuned and validated against historical data. Encouraging results allowed the application in the SeaPerformer system which enables ship owners to establish their ship CII rating and plan necessary modifications well before new regulations come into force.

1. Introduction

Ship data collection systems, play an important role in managing ship efficient operation and effective maintenance. Collected data enable performance analytics, operational optimization, maintenance planning and evaluation of effectiveness of various maintenance strategies. Data processing allows also for building predictive models and to implement them in decision making process. Continuous practice of data gathering and processing enables ship performance monitoring thus reacting on gradual or sudden performance disruptions. Data collection systems can be also implemented for regulatory reporting such as MRV, *European Parliament (2015)*, or DCS, *IMO (2016)*, where specific KPIs are used for comparison of ship performance against target reference or with respect to vessels of similar type. Recently IMO introduced another performance index for emissions monitoring i.e., Carbon Intensity Indicator (CII), *IMO (2021)*. Due to the significant impact of this indicator on the assessment of the ship's energy efficiency, and thus on its market value, the use of the data acquisition system only to report the CII value at the end of the year is far from sufficient. Carbon Intensity Indicator shall be monitored on daily basis in order to dynamically react and avoid negative consequences of under-performance. In parallel with monitoring tools, methods of forecasting the influence of parameters and the operation pattern on the value of the CII indicator should also be used.

Once the functionality of data collection system is defined the corresponding data sources and frequency shall be determined. It is relatively straightforward in case of CII monitoring. Following Carbon Intensity Indicator definition described in paragraph 2 it is visible that dataset is not extensive. It comprises of two variables:

- Amount of CO_2 emissions in grams
- Theoretical transport work in Tonnes x Nautical Miles

Although CO_2 emissions can be measured directly this technology is so far considered as unmatured. Therefore, common approach (used also in case of MRV and DCS) is to derive CO_2 emissions from fuel consumption. Each type of fuel used onboard has its emissions factor (i.e., how many tons of CO_2 is produced in burning process out of 1 ton of fuel) and therefore it is sufficient to multiply mass fuel consumption by respective emission factor to derive amount of CO_2 emissions.

Mass fuel consumption can be obtained with use of flow meters installed in the ship fuel system (directly in case of mass flow meters or with use of volume to mass conversions in case of volumetric flowmeters). Fuel consumption depends on load of fuel consumers (e.g., main engine and generators) therefore shall be considered as dynamic process and data acquisition shall be performed at sufficient frequency in order to avoid errors due to interpolation.

Fuel type thus appropriate emission factor shall be recognized by monitoring of so called “switch over” events. Since these are relatively infrequent events it is possible to monitor by crew manual entries. Practice however reveals that human errors in this case may be a source of significant inaccuracies therefore it is strongly recommended to apply automatic monitoring with this respect either directly on switching valves or via vessel alarm and monitoring system (AMS).

The accuracy of fuel consumption determination (and accuracy of CO_2 emissions as a result) strongly depends on installed ship fuel system infrastructure, especially flow meters. Wrong localization or position of flow meter may result in false readings. Improper selection of flow meter (e.g., using high-capacity flow meter for small consumptions) results in large errors. Fuel system arrangement shall be also considered especially in case of differential measurement or complicated fuel systems. In each case determination of fuel consumption by each consumer and each fuel type is necessary and often requires some degree of engineering (including replacement of components which do not guarantee trustworthiness).

In order to simplify and automatize the process of fuel consumption data collection SeaPerformer system offers dedicated module for fuel monitoring. EFCM is specialized system which handles data acquisition from volumetric or mass flow meters, monitoring of switching valves (or temperature-based recognition of fuel type) and process data according to fuel system topology (e.g., handles differential measurements). As the result fuel consumption is provided in mass units and divided among different consumers and fuel types. EFCM is a modular system which can be adjusted towards specific ship needs. System can be integrated with SeaPerformer or any other data collection or AMS systems or can be used as standalone with its own human-machine interface.

With respect to transport work, as the actual value may be difficult to obtain, supply-based or theoretical value can be used. It is a product of distance over ground and vessel capacity and therefore it is sufficient to collect distance with use of onboard GPS. Similar to fuel consumption sufficient data collection frequency must be assured. Capacity as the vessel design parameter does not need continuous monitoring however it shall be possible to modify this parameter as appropriate with respect to major vessel modification.

Data gathering process described above is sufficient for the purpose of CII monitoring. However, in case of CII prediction it must be enhanced as appropriate for building predictive models. In order to enable prediction of CII with respect to operational parameters and voyage profiles, predictive models for fuel consumption in various operational conditions must be developed. For this purpose, apart from fuel consumption, navigation and operational parameters including ship speed over ground, ship speed through the water, ship drafts as well as environmental conditions shall be collected. Majority of these signals has dynamic character therefore automatic, high frequency data collection is recommended.

As indicated above although data collection seems to be relatively simple it may be a source of serious discrepancies or errors if not properly handled. As data set is a mixture of different frequency data manual reporting may lead to problems. As the example of data collection system, SeaPerformer provides the means for data acquisition both automatically and manually. As it is an open, scalable platform, it accommodates data of different dynamics and multitude of sources. System simplifies connectivity due to built-in interfaces for most popular standards. What is most important, SeaPerformer provides variety of data validation tools very important in case of using manual entries prone to human errors.

2. Carbon Intensity Indicator

Carbon Intensity Indicator is recently introduced measure or key performance indicator (KPI) which quantifies ships' emissions performance. The measure describes amount of CO_2 emissions per unit of transport work as described in the introductory paragraph.

$$CII = \frac{mass\ of\ emitted\ CO_2}{transport\ work}$$

Note: Above formula does not include correction factors that are under development at present.

In practice CII shall be calculated according to the following formula:

$$CII = \frac{\sum(mass\ of\ fuel_i \times\ emission\ factor_i)}{ship\ capacity\ \times distance\ travelled}$$

Nominator in above formula includes sum over all types of fuel used onboard. Indicator shall be calculated for 12 months period. First year for which CII report shall be prepared is 2023 therefore data collection must be started on January 1st 2023 the latest. Report shall be prepared and submitted at the beginning of year 2024.

Based on attained value of CII vessels will be ranked in categories A to E which reflect major superior to inferior performance respectively. In order to rank particular vessel a reference value is calculated based on overall performance of the world fleet. Reference performance is based on IMO DCS data collected for year 2019 and is prepared by the regression analyses, Fig.1, within ship type groups and with respect to vessel capacity, *IMO (2021)*.

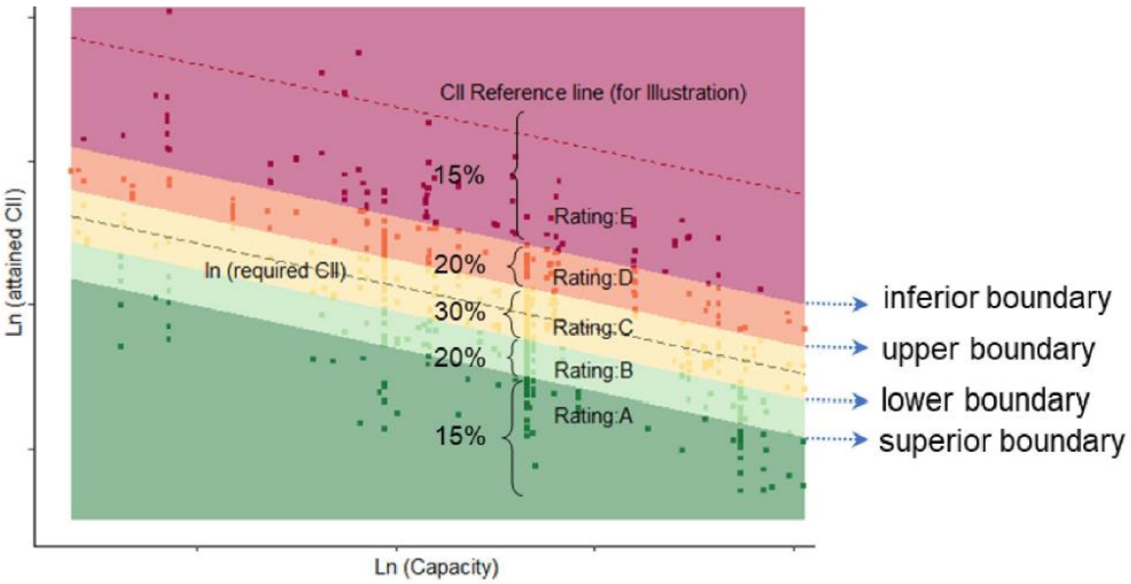

Fig.1: CII distribution of individual ships in year 2019, *IMO (2021)*

Reference calculation mechanism includes the performance upgrade driver. For each consecutive year starting from 2023 a reduction factor shall be applied for the reference value obtained based on data of year 2019. Reduction factors amounts to 5%, 7%, 9% and 11% until year 2026 and will be further tightened based on data gathered following year 2019. This mechanism imposes a continuous pursuit for better emission performance of the vessel since ship which receives C rank (moderate performance) for year 2023 and continues operation on the same performance level will gradually fall into D and E rank in following years. Underperforming vessels (i.e., receiving rank D for 3 consecutive years or rank E for 1 year) need to prepare, approve and implement the performance recovery plan. On the other side, incentives will be provided by administrations, port authorities and other stakeholders to ships rated A or B.

Ship rating based on Carbon Intensity Indicator has been recognized by maritime industry as a very powerful mechanism which will impact business by influencing charter rates and vessel market values. It introduces a shared responsibility of building yard, vessel owner and operator for meeting demanding environmental requirements. Attained CII value results from vessel technical performance (yard and owner responsibility) and operational performance (charterer responsibility) therefore requiring closer cooperation among them which will be reflected in revised building and charter party contracts.

Significant business impact of the IMO regulation demands development of proper tools supporting performance screening and decision making. Data collection and annual reporting is far from sufficient. Revealing ship rank only after completing data for entire year poses high risk for vessel owner. It does not provide any means for making decisions if performance need to be improved during the year and may result in serious business disruption in case of inferior performance. Therefore, CII daily monitoring and prediction is a must-have tool for managing risks connected with stringent environmental requirements. These tools have also prime importance for making decisions which will secure vessel competitiveness on the market and therefore enable achieving expected return of investments level.

3. Motivation

Onboard data collection systems proved to be a practical choice for gathering information required for environmental reporting imposed by international regulations, *Gorski (2017)*. SeaPerformer for example supports reporting of EEDI, MRV and DCS as well as daily reporting and voyage summary reports. In case of CII data set is the same as in case of DCS, therefore systems supporting this IMO requirements provide sufficient data collection for CII purpose. It is important, however, that the system used for environmental reporting provides tools for data validation and allows for mixing high frequency data and manual entries. It is important to implement automatic and continuous data acquisition based on sensors as much as practically possible in order to improve data trustworthiness. Manual entries shall be minimized and used only for information which is difficult to obtain automatically. With respect to CII not only ship distance traveled but especially amount and type of fuel consumed shall be collected automatically. Collected data shall be validated (e.g., SeaPerformer provides data validation against historical data and fuel consumption models) in order to reduce data errors due to e.g., sensor failures.

In case of SeaPerformer system, range of collected data is much wider comparing to CII requirements. Navigation, machinery and environmental data are collected as well. Extensive dataset describes vessel operational characteristics in different conditions. In the connection to continuous CII monitoring broad dataset is indispensable for recognition of root cause of trend change. Understanding the reasons for CII changes, especially in case emission performance is getting worse, is a prime factor for improvement. What is possibly even more important, multifarious and diverse collection of data allows for building vessel operational models. With reference to CII data can be used for development of fuel consumption models and employ them for prediction of different operational scenarios' impact on CII value. Performance modelling based on collected data allows for short- (i.e., voyage) and mid-term (i.e., by the end of year) predictions of CII. Ability of predicting resulting CII value is a vital tool for vessel owner and operator in pursuit for meeting new IMO environmental requirements.

4. Methods

Three new functionalities have been introduced in SeaPerformer system to face new regulations. Monitoring of current CII value (4.1) together with end-year CII forecasting (0) form a tool designed to give the user full control over the level of emissions during ongoing year.

Attained CII shall be aggregated at the end of each calendar year, however controlling its temporal value allows for making most informed decisions. Additionally, CII prediction complements the current value with expected trend and gives a clear input for decision-makers on the probable rating on the year closing (Fig.2). The last feature enhances SeaPerformer route planning tool by CII evaluation (0), showing more detailed prediction related to a specific voyage.

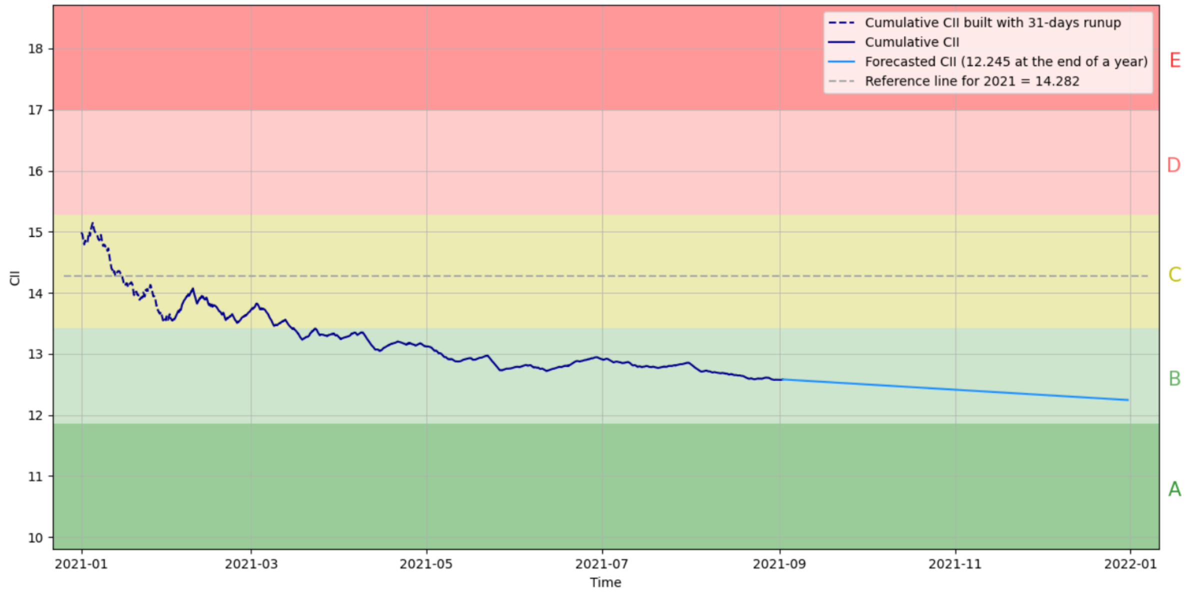

Fig.2: CII monitoring for ongoing year

Below, brief description of algorithms is presented.

4.1. Monitoring of CII

Current CII is calculated generally as a cumulative number, from the beginning of a year until the last data measurement. Reference line level and relevant rating bands shown on Fig.2 are determined for ongoing year, as described in guidelines, *IMO (2021)*.

Typically, in first weeks of the year standard cumulative indicator looks highly unstable (continuous line on Fig.3). Depending on the starting point, either during sea passage or at port call, it takes very high or very low values at first and stabilises after a certain period. This period has been experimentally identified as about one month. In order to achieve smooth and more informative trend line from the start, we have applied a run-up, allowing the use of data from the previous year. Within the unstable period indicator aggregates data from last month in a moving window (dashed line on Fig.3).

4.2. Prediction of yearly CII based on average operational conditions

For pure CII value calculation, measured CO_2 mass M and measured distance D_t are only required. To provide a plausible prediction, accurate modelling of emissions is essential.

$$CII_{fcasted} = \frac{M + M_{fcasted}}{(D_t + D_{fcasted}) \cdot C}$$

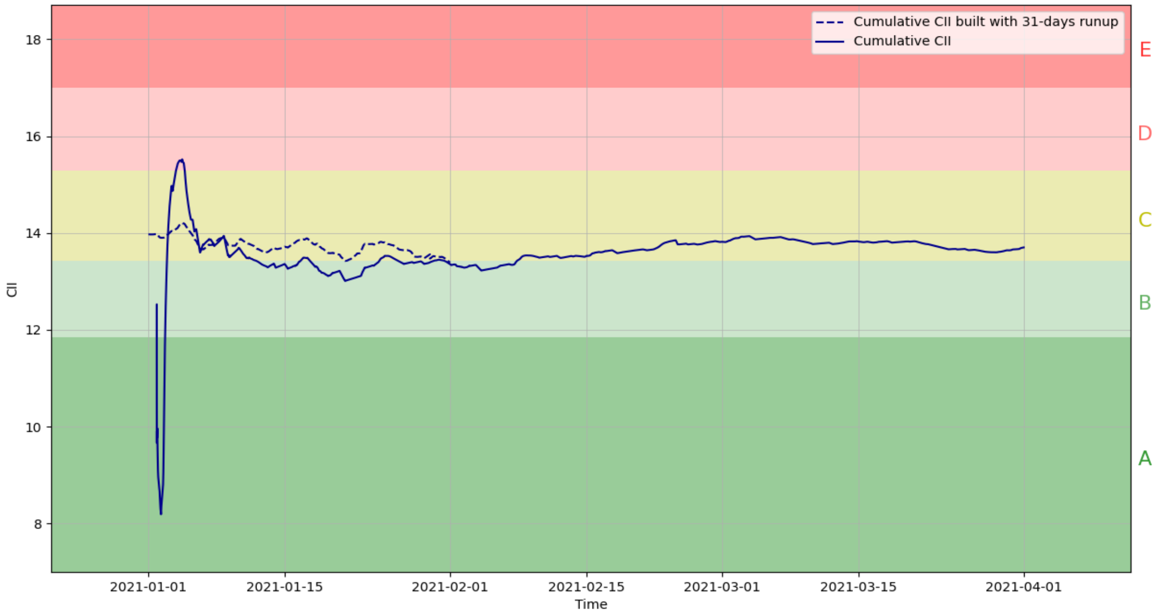

Fig.3: Cumulative CII with 1-month run-up

Forecasted emissions depend on assumed transit time ratio (TTR) and modelled emission rates for vessel underway and during stops respectively:

$$M_{fcasted} = t \cdot \left(TTR \cdot m_{transit} + (1 - TTR) \cdot m_{stop}\right)$$

where:

t: time of the forecasted period,
TTR: ratio of transit time to overall time of operation
(1 - TTR) represents the ratio of stop time to overall time
$m_{transit}$: CO2 emission rate for vessel underway
m_{stop}: CO2 emission rate for vessel at stop

$D_{fcasted}$ is estimated as:

$$D_{fcasted} = v_s \cdot t \cdot TTR$$

where:

v_s: transit speed specified by the user

Transit time ratio *TTR* and transit speed v_s are input parameters given explicitly by user or, by default determined based on measured data from the certain last time of operation. Similarly, emission rates are based on last vessel operation. Harbour/anchorage rate m_{stop} is represented by a constant average value, while emission rate underway $m_{transit}$ is described with 1-dimension model dependent on the specified transit speed.

For certain last time of vessel operation, temporal data sampled every minute are collected including fuel consumption and vessel speed. These are not filtered in terms of loading conditions nor weather conditions, because of long-term prediction character. Overall CO_2 emission is calculated for all fuel types used and consumers. Fig.4 presents data points of overall emission plotted against speed.

The resulting emission-speed model is given by general equation of:

$$y = a + b \cdot x^c$$

where:

x: vessel service speed
y: CO_2 emission rate for vessel underway
a, b, c: fitting coefficients

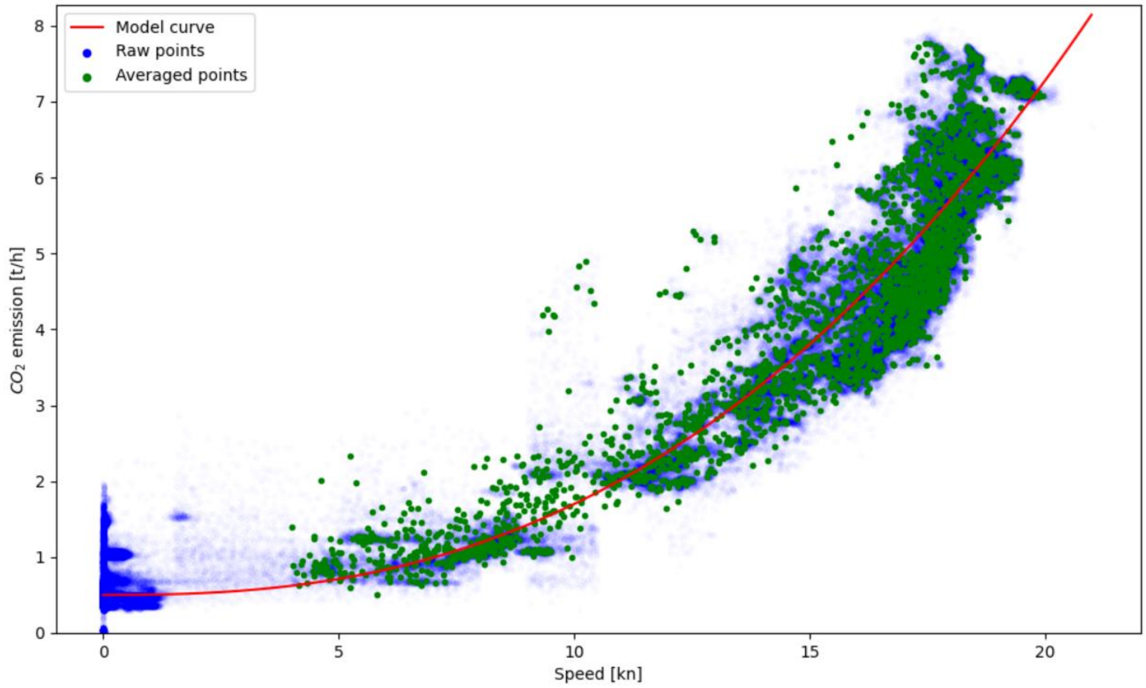

Fig.4: Underway emissions model

Formula's coefficients are determined by fitting curve on operational points in speed-emission domain. In order to get a proper shape of power-speed curve, selection is constrained with explicitly set allowed limits for each coefficient, e.g., $b > 0$. After distribution-based outliers' removal, high-frequency data points are used to define these limits. In the next step points of manoeuvring speeds up to 4 knots are being cut off, because those shall not be subject to modelling. The rest is averaged to 1-hour granularity (marked in green on Fig.4). Model curve is then fitted using least squares method.

4.3. Prediction of voyage impact on CII

Somewhat different algorithm is used to estimate the planned voyage indicator, in order to keep more accuracy, as input information on single route is more detailed than operational pattern to the end of the year. In this case, forecasted times, speeds and geographical paths comes directly from a route-planning tool for a given set of departure- and destination coordinates. For each leg of the planned voyage fuel consumption estimation is made.

Estimation is based on reference consumption and a certain surplus. The reference part, representing clean hull and calm weather comes out of ship performance model for certain speed and loading condition. The surplus includes both statistical weather impact and current state of hull and fuel consumers. For each data point from certain last time of vessel operation surplus coefficients are calculated as:

$$s_c = \frac{(cons_{meas} - cons_{ref})}{cons_{ref}}$$

For each leg, average surplus coefficient of speeds and drafts close to leg's assumptions, is then used to increase the reference consumption. Estimated consumption is turned into emissions and finally together with projected distance into CII.

As an outcome three indicator values are presented with their corresponding ratings, to show the impact of planned voyage on the future CII level:

- Current indicator
- Indicator assessing the sole route being planned
- Forecasted indicator at the end of the planned route

4.4. Impact of data granulation

The example in Fig.5 demonstrates that low-frequency data for consumption and distance produce trend that generally follow high-frequency data and are sufficient to control CII level during the reporting year. Presented trend was plotted with voyage-by-voyage granularity, one point occurs typically every few days. In case of data provided manually, sufficient quality must be maintained, preferably through input validation made already on user interface stage.

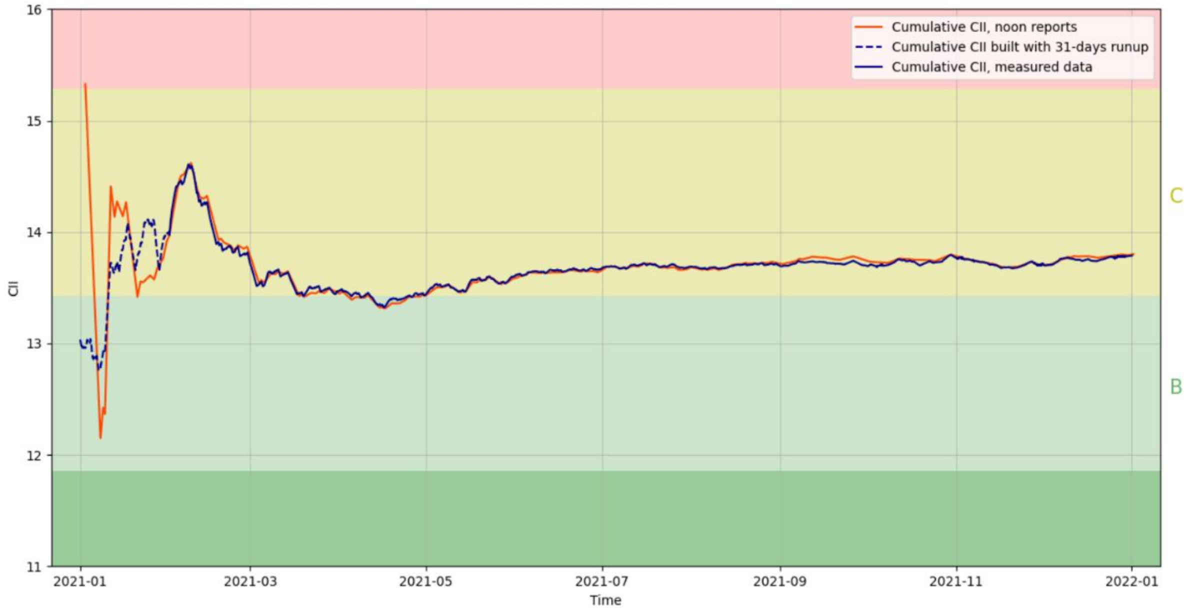

Fig.5: CII monitoring based on voyage-reported and high-frequency data

Although CII monitoring can be practically realised with use of low-frequency data predicting CII in short- or mid-term requires higher data density. Taking into account large time-window averaging, higher scatter and increased probability of gross errors using low-frequency data for building predictive models results in lower prediction accuracy. Therefore building predictive models in SeaPerformer is based on high-frequency, 1-minute data.

5. Verification and validation of CII algorithms

CII calculation algorithm has been verified against two simplified scenarios. The first assumes non-stop sailing with constant average speed and consumption. In the second scenario full year is divided into two operational modes in a specified ratio. One pattern describes vessel underway with the same characteristics as above, the other represents stopped vessel assigned with zero speed and constant harbour consumption level. Verification tests proved proper implementation of CII computational algorithm.

Forecasting method has been validated by making prediction for a year already covered with measured data. For each month in 2021, CII value at the end of the year was predicted, assuming that the algorithm knows only past data for the end of the month. Predicted values were compared with real indicator value calculated from all measured data explicitly. Fig.6 presents how relative error of the prediction converges to zero with time. Presented ships, tagged with their id's represent different sizes of container vessels and bulk carriers. Even though reference CII level differs between both functional types, all lines show similar pattern, resulting in less than 15% relative error at the beginning of September.

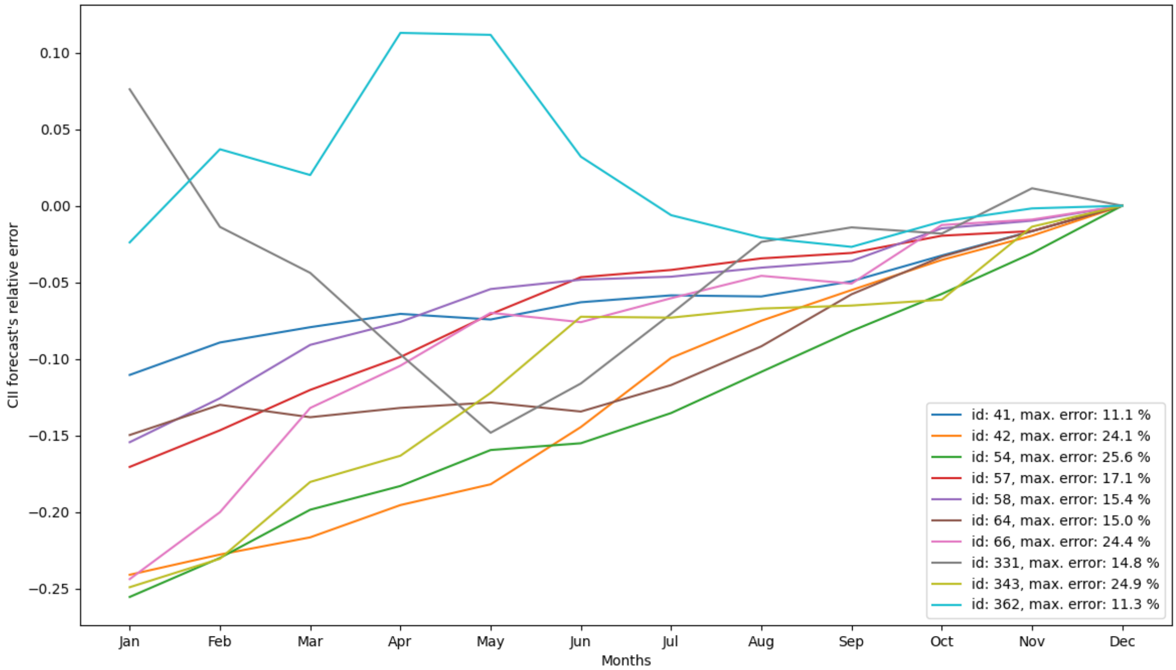

Fig.6: Convergence of annual forecast's relative error

6. Application of CII monitoring and prediction methods

Vessel rating according to CII may significantly impact shipping business by influencing charter rates or even ship value therefore monitoring of CII shall become a daily routine. Early detection of CII deterioration allows for taking corrective measures. Once these are applied CII monitoring provides possibility to evaluate effectiveness of actions. SeaPerformer system provides convenient tool for daily CII monitoring. It is based on high frequency data therefore provides sufficient sensitivity and clearly identifies trend changes. Application of the CII monitoring is illustrated based on the data collected during operation of 3500 TEU container vessel. Vessel is equipped with SeaPerformer system and collects vital operational data including navigation and fuel consumption. Since vessel is equipped with volumetric flow meters arranged in mixed differential topology EFCM sub-system is used to derive mass fuel consumption divided among each consumer and each type of fuel which greatly simplifies calculation of CII value. Fig.7 presents CII trend graphs prepared during vessel operation.

Initially, until mid-May vessel performed satisfactory within C rating (**Fig.7:** Changing charter partyFig.7, period A). However, around 12th of May operational pattern had been greatly modified as vessel was engaged in new charter. At the end of May drastic change of trend was clearly visible (Fig.7, period B). Unfortunately, new operational pattern characterized by higher average vessel speed and shorter port stays had been continued until end of the year. Although shorter port stays reduce CII value the effect of increased speed had been prevailing and finally vessel attained overall rating E (Fig.7, period C). Details of vessel speed pattern in first and second half of year can be compared based on speed histograms (Fig.8, Fig.9).

Based on the vessel in question, influence of average speed and transit time ratio (TTR) on yearly CII prediction may be presented. For the moment of charter party change and resulting change in operational pattern, four scenarios were considered with different sets of input parameters.

Table II: Impact of transit time and speed on CII forecast

Scenario	1	2	3	4
Average speed [kn]	16.0	18.5	16.0	18.5
TTR [-]	0.51	0.51	0.7	0.7
Forecasted CII [-]	10.14	12.85	9.84	12.79

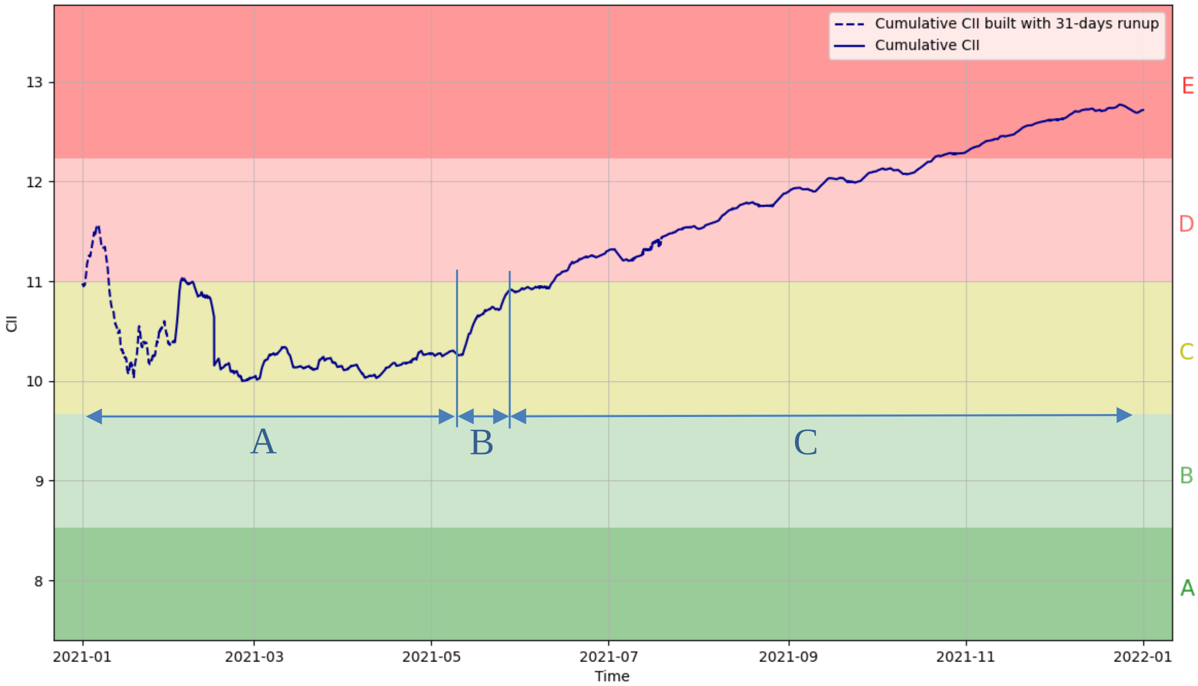

Fig.7: Changing charter party

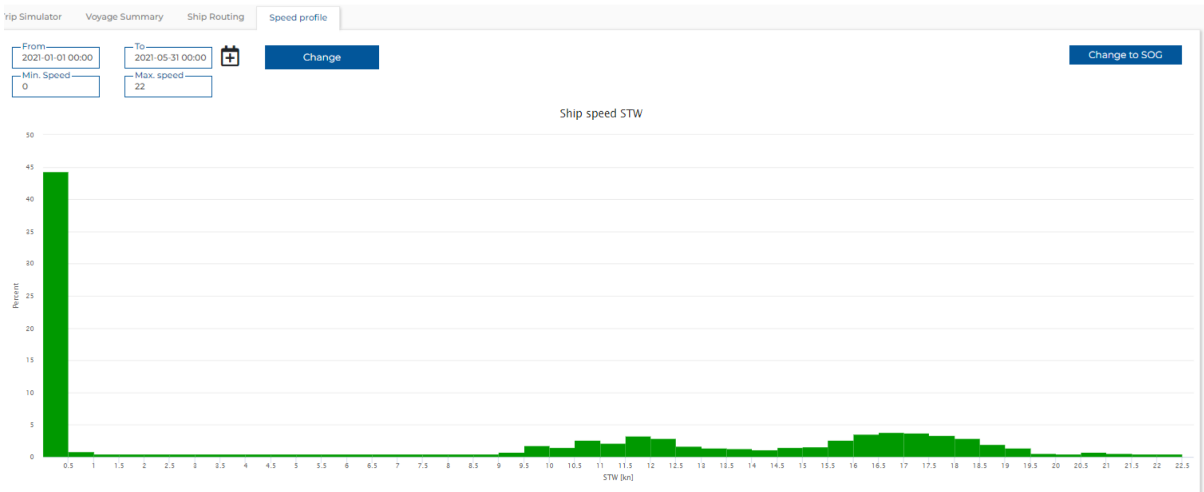

Fig.8: Speed distribution until May

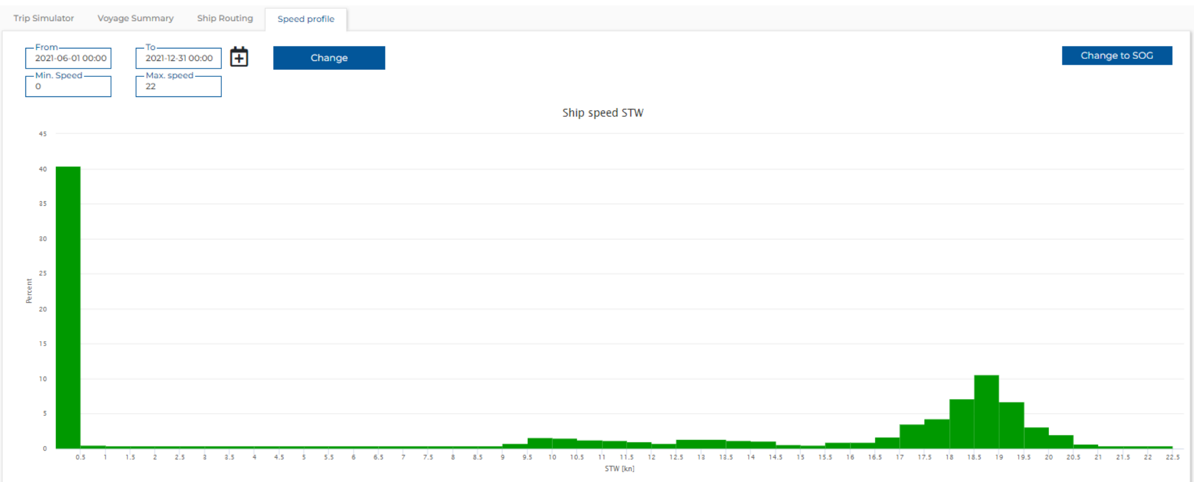

Fig.9: Speed distribution since May

Continuing the same operational pattern, with average speed of about 16 kn would result in CII at the level achieved in May (scenario 1). Speed of 18.5 kn with TTR = 0.51, corresponding to the period until 12th of May, results in CII almost matching the real value at the end of the year (scenario 2). This example reveals significant influence of vessel speed on forecasted indicator's level, which may possibly lead to change in final rating. Changing TTR to 0.7, which represents high improvement in operation, does not affect CII number significantly.

Impact of vessel operation on the CII value shall be assessed whenever new voyage is planned. SeaPerformer provides handy tool for this purpose which offers short term CII prediction. It enables precise estimation how CII would change if certain voyage scenario is realized. For convenience it is coupled with a route planning tool, therefore apart from usual input, the user must provide only port stay duration to enable CII estimate. Fig.10 presents typical evaluation of voyage planning. For a fixed route modification of average vessel speed and port stay duration was considered in terms of CII. Example corresponds to case of fixed time of arrival and variable date of departure i.e., due to elongated port operations. Extended time in port is compensated by higher average vessel speed in order to meet required ETA. Results obtained for 1700TEU container feeder revealed that for a given route increase of port stay by 24 hours results in 11% speed increase. Total impact of increased port stay and higher transit speed results in 12.3% of CII increase in planned voyage. Total attained CII increased by 2% however it must be noted that final year-based CII value would depend on vessel performance and operational parameters in remaining part of the year.

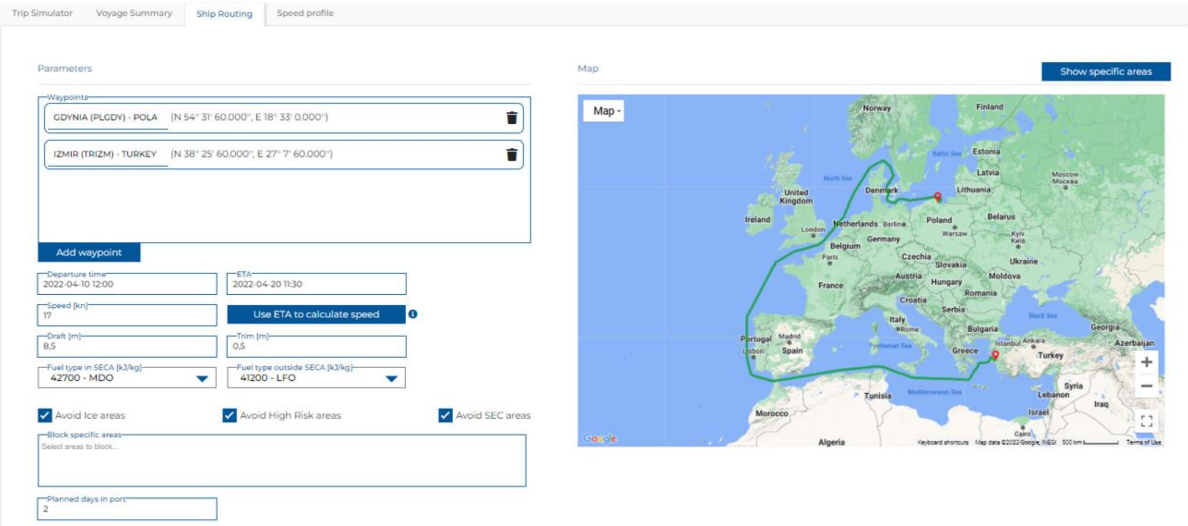

Initial voyage plan

Voyage summary		Estimated fuel consumption		Carbon Intensity Index		Rating
Departure time:	2022-04-10 12:00:00	Inside SECA - MDO:	112.905 t	Current CII:	13.58	C
Arrival time:	2022-04-20 11:30:26			CII of the planned route:	11.802	B
Duration:	239 hours 30 minutes	Outside SECA - LFO:	233.114 t	Current CII including planned route:	13.266	B
Average speed:	17 kn	In Port:	10.390 t			
Distance:	4071.63 NM	Total:	356.409 t			

Voyage plan for delayed departure

Voyage summary		Estimated fuel consumption		Carbon Intensity Index		Rating
Departure time:	2022-04-11 12:00:00	Inside SECA - MDO:	125.489 t	Current CII:	13.58	C
Arrival time:	2022-04-20 11:29:52			CII of the planned route:	13.25	B
Duration:	215 hours 30 minutes	Outside SECA - LFO:	259.096 t	Current CII including planned route:	13.522	C
Average speed:	18.894 kn	In Port:	15.583 t			
Distance:	4071.63 NM	Total:	400.168 t			

Fig.10: Route planning with CII impact calculator

7. Conclusion

IMO (2021) regulation regarding Carbon Intensity Indicator has to be seriously considered as it influences the economy of ship transportation. It has been discussed in the paper that CII evaluation once a year (as to fulfill IMO requirements) is insufficient. Therefore ship performance system SeaPerformer was enriched with a consistent CII toolbox helping owners and operators to cope with new requirements. These tools enable:

- continuous CII monitoring which allows for early detection of trend change thus enabling ship crew, owner office and operator to adjust operational strategy or recover technical performance of the vessel,

- building predictive models based on high frequency data and using them for short- and mid-term predictions which allows for selecting optimum strategy with respect to expected CII level.

SeaPerformer CII package provides essential measures for managing risks resulting from new IMO regulations.

References

EUROPEAN PARLIAMENT (2015), *Regulation (EU) 2015/757 of the European Parliament and of the council of 29 April 2015 on the monitoring, reporting and verification of carbon dioxide emissions from maritime transport, and amending Directive 2009/16/EC*, Official Journal of the European Union

GORSKI, W. (2017), *Automatic MRV reporting with use of onboard performance management systems*, 2nd HullPIC, Ulrichshusen

IMO (2016), *Amendments to the annex of the protocol of 1997 to amend the international convention for the prevention of pollution from ships, 1973, as modified by the proto-col of 1978 relating thereto (Inclusion of regulations on energy efficiency for ships in MARPOL Annex VI),* Resolution MEPC.278 (70), Int. Mar. Org., London

IMO (2021), *CII Guidelines (G1),* Resolution MEPC.336(76), Int. Mar. Org., London

IMO (2021), *CII Reference Lines Guidelines (G2),* Resolution MEPC.337(76), Int. Mar. Org., London

IMO (2021), *CII Reduction Factors Guidelines (G3),* Resolution MEPC.338(76), Int. Mar. Org., London

IMO (2021), *CII Rating Guidelines (G4)*, Resolution MEPC.339(76), Int. Mar. Org., London

Improving Performance Prediction using Hindcast Weather and AIS Data

Dimitris Georgousis, Vessel Performance Solutions, Lyngby/Denmark, dge@vpsolutions.dk
Najmeh Montazeri, Vessel Performance Solutions, Lyngby/Denmark, nmo@vpsolutions.dk
Jakob Buus Petersen, Vessel Performance Solutions, Lyngby/Denmark, jbp@vpsolutions.dk

Abstract

The digitalization journey of shipping opens for new and exciting options to improve the modeling of a ship's behavior at sea. At the same time the modeling of a vessel's performance is not an exact science and the scatter in performance predictions is a concern for everyone involved. This paper is showing steps in how digitalization can help us improve performance prediction capabilities by using data fusion. In the last couple of HullPIC conferences there were discussions about the use of AIS data and hindcast weather. In this paper the improvements in the performance prediction reliability from using AIS data and hindcast weather are quantified. The improvements are demonstrated by using AIS data and hindcast weather for wind and waves to normalize for the environmental impact. Further, it is shown and quantified how hindcast currents can be used to improve the prediction of the vessel's speed through water.

1. Introduction

There is high interest in the shipping industry in the evaluation of a vessel's performance in relatively short time after a dry-dock, hull cleaning or a propeller polish. For a vessel performance analyst to achieve this, accurate noon reports are needed, in the absence of autolog data. Even if one assumes that the reported fuel consumption and sailing distance are accurate, the weather conditions are still dubious, since the noon reports typically cover a 24-hour period. The wind, waves and currents are averaged and subject to human interpretation over the duration of a noon report. In many noon reporting systems, the crew is asked to report the observed weather over the entire noon report, while in other noon reporting systems the crew is asked to report the weather at the time of the observation. In real life, even with clear principles described in the reporting procedures, the crew often mixes them. This introduces further uncertainty in performance predictions.

This issue can be significantly improved by enriching the noon reports with AIS and hindcast weather data. Typically, the spatial and time resolution of the AIS points throughout a noon report are significantly higher than the observations from the crew. Hindcast wind, waves and currents are introduced at the AIS timestamps and positions of the vessel and then the weather impact on the vessel is evaluated. This process increases the confidence in the estimation of the vessel's performance, and thereby reduces the time to reach the same confidence of the result compared to the standard analysis using the reported weather. Finally, apart from noon reports, use of hindcast weather increases the confidence of the autolog-based calculations as well. The accuracy of the calculated Added Resistance due to fouling of the vessel is quantified with the method of Confidence Interval, Assoc. Prof. Gang Chen in personal communication.

2. Literature review

VPS has developed an advanced Vessel Performance system (VESPER) that utilizes noon, autolog, AIS and hindcast data to estimate the resistance due to fouling. In *"ShippingLab"*, http://shippinglab.dk/en/front-page/, one of the objectives is to develop a digital twin of the vessel and optimize the accuracy of the vessel's performance estimation. The optimization is based on quantifying the prediction accuracy. In previous HullPIC conferences, a methodology for using autolog data for performance analysis has been presented. As explained in *Montazeri et al. (2019)*, the autolog signals are filtered based on stationary period detection and average values are used to smoothen the analysis. The stationary periods are identified by the theory of probability of detection of a change in the mean and standard deviation, *Lajic (2010).*

This study follows *Montazeri et al (2020)*, where two bulk carriers have been studied for their performance with both noon and autolog data. It was concluded that the method of autolog stable periods was superior to noon data as the estimation reliability was improved. It was also mentioned that speed through water, from reliable speed logs, led to higher consistency compared to speed over ground, while the same consistency was not observed when enriching speed over ground with hindcast currents. However, the hindcast current resolution and reliability has been increased by the hindcast data provider since that time.

The current study goes one step further to repeat these analyses with the higher resolution hindcast weather data applied on both noon and autolog data and also enriching noon reports with AIS data. This study is conducted on numerous vessels and fleets, which can lead to more generalized conclusions.

3. Hindcast data vs measurements

The resolutions of the hindcast weather parameters are summarized in Table I.

Table I: Resolution of Hindcast data

Hindcast parameter	Time resolution	Spatial resolution
True wind at 10 m	6 h	0.125°
Significant Height of Combined Wind Waves and Swell	6 h	0.125°
Currents	24 h	0.083°

3.1. Hindcast wind vs Anemometer measurements

It is a standard method throughout the evaluation of a vessel's performance to filter out weather conditions above 4-5 Bft. Severe weather conditions introduce unnecessary scatter in the analysis due to the typical simplistic modelling of wind and wave ship response in performance systems. However, in this study no weather filtration has been applied, so a clear conclusion can be extracted for the correlation between the measured wind and the hindcast wind. More sophisticated wind and wave models are being investigated in the ShippingLab project, which may capture the impact of more severe weather conditions more accurately.

Fig.1 shows the measured true wind speed (autolog) against hindcast wind speed for 11 vessels, covering, in total, around 24 vessel years. The anemometers onboard the vessels, which were used in this study, are placed around 37 m above sea level, much higher than the 10m reference height of the provided hindcast wind. Therefore, as expected, the measured data (green points) show higher wind speeds than the hindcast data. The measured data are extrapolated to the 10m reference height, using the following wind profile power law:

$$U = Ur\left(\frac{Z}{Zr}\right)^{\wedge a}$$

where: Z = the reference height above sea level equal to 10m
U = wind speed to be calculated at the reference height Z
Zr = height of the anemometer equal to 37m
Ur = measured wind speed at height Zr
α = wind shear exponent equal to 0.1 for open sea

Using the corrected wind speed (blue points) vs the hindcast wind speed the offset from the diagonal is reduced. However, the measurements remain higher than the hindcast wind speeds. The residual error could originate either from the flow disturbances caused by the ships' superstructures or from underestimation of the wind speed by the hindcast modelling or from sensor offset.

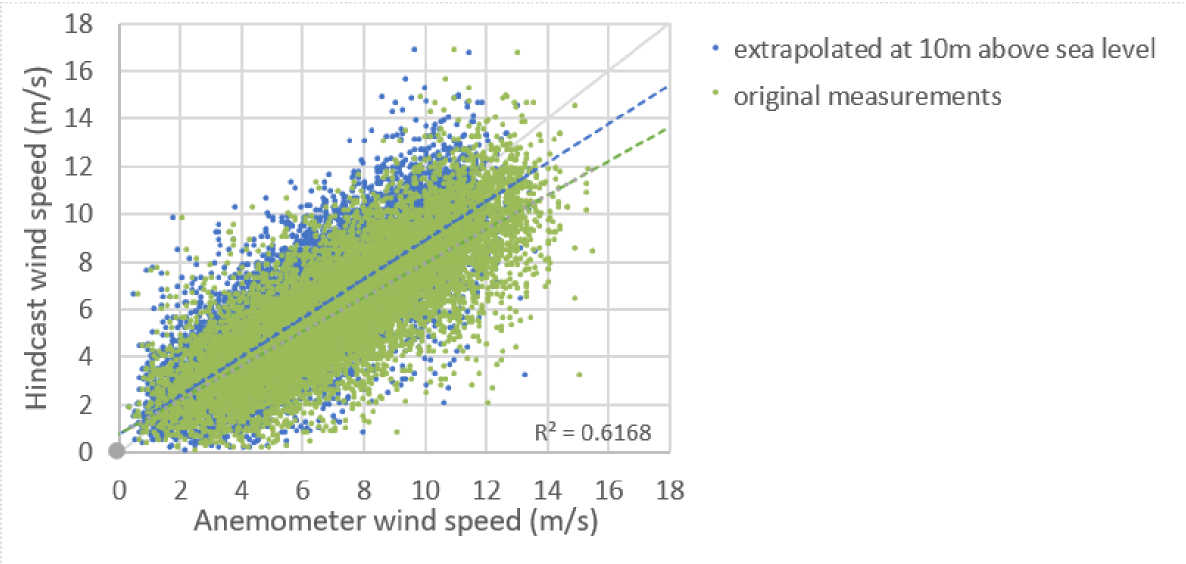

Fig.1: Anemometer against hindcast wind speed (m/s)

3.2. Hindcast currents vs Speed log currents

Fig.2 shows the comparison between autolog-measured current from the speed log of the same vessels against the hindcast current. The speed log provides speed through water measurements (STW) at the position of the speed log sensor and the vessel's GPS provides speed over ground measurements (SOG). Thus, the projection of the current at a ship's course is calculated as:

$$projection\ of\ speed\ log\ current = measured\ SOG - measured\ STW$$

The projection of the hindcast current is calculated as:

$$projection\ of\ hindcast\ current = current\ speed * \cos(relative\ current\ direction),$$

where relative current direction is relative to the vessel's course.

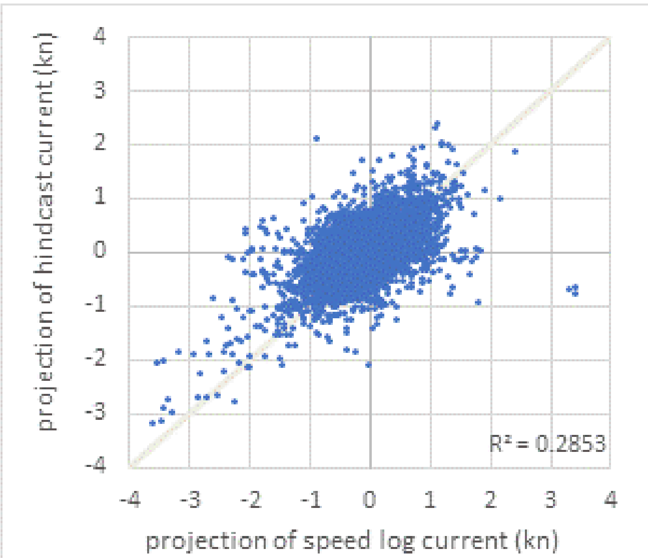

Fig.2: Measured against hindcast current speed (m/s), projected at the ship's course

The R-squared coefficient $R^2 = 0.29$ is low showing low correlation between the two quantities. This could originate from both the quality of the hindcast current modelling and the vessels' measurements.

The projected current from the speed log is calculated from two autolog signals (SOG and STW), which may contribute to higher scatter. It is worth mentioning that the history of the ratio between STW and SOG has been plotted for each vessel, to check for any possible offset or drift of the speed log. No significant offset or drift was found.

4. Enriching noon reports with hindcast weather at AIS positions

The noon reports usually cover a period of 24 h. The resolution of the AIS positions depends significantly on the vessel's location (satellite coverage) and other parameters, i.e. interference with other vessels, functionality of the transmitter etc. In the current set-up of VESPER, it ranges from 0 to some hundreds of points during the noon report period. After filtration of the unnecessarily high number of points to match the hindcast data resolution, a typical average number of AIS positions ranges between 20-50 points during a noon report.

Fig.3 shows a typical sketch of how the AIS and hindcast points are distributed throughout the duration of a noon report.

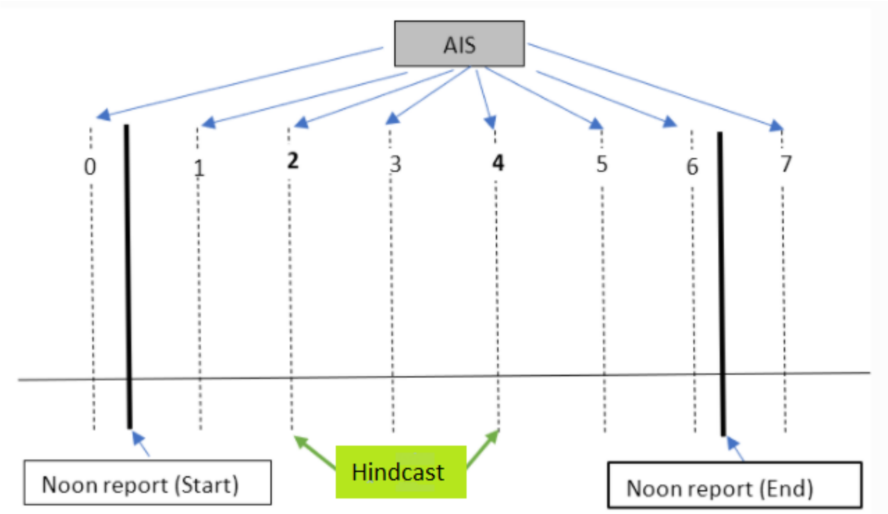

Fig.3: Sketch of distribution of Noon, AIS and hindcast points

The time resolution of hindcast data (summarized in Table I) is usually coarser compared to the resolution of AIS points. As shown in the sketch, there are available hindcast data close (timewise) to the AIS points 2 and 4. Thus, hindcast winds, waves and currents are introduced at the AIS point number 2 and the same values are distributed to AIS points number 0 and 1. Likewise, the AIS points 4 to 7 get identical hindcast data with the introduced hindcast data at AIS point 4, while the data introduced to AIS point number 3 are identical to AIS point number 2 or 4, depending on which one is closer.

The impact of the wind and waves is calculated at each AIS point and quantified in power value (kW) or integrated to chunks of energy for each point (kWh). The chunks of energy are summarized over the noon report period and subtracted from the reported propulsion power. Then, the baseline propulsion power in clam seas is also subtracted, so that the remaining power is the power needed to overcome the resistance due to hull and propeller degradation.

The hindcast current correction is applied to the speed over ground of the vessel at each AIS position as described below:

- The AIS-based SOG is calculated by dividing the distance between two consecutive AIS points with the duration between them
- then, the hindcast current is introduced at the second AIS point,

- the current projection is calculated by using the AIS-based ship's course and the current's speed and direction (Eq.2),
- then the projected hindcast current speed is added to the AIS-based SOG to produce the Current Corrected SOG (CCSOG),
- then the weighted average of the CCSOG values from all AIS chunks during the noon report is calculated to produce the final CCSOG corresponding to the noon report,
- and finally, the weighted averaged AIS-based SOG is also calculated for each noon report. In the cases that the AIS-based SOG deviates significantly from the reported SOG (due to maybe low AIS data quality), then these noon reports are filtered out from the analysis.

5. Impact of using hindcast and AIS data on performance prediction accuracy

As described above, the estimation of Added Resistance due to fouling is based on various inputs. Critical to the accuracy of the calculations are parameters such as the speed, the propulsion power or fuel and the weather conditions. Even without known weather conditions or speed through water, the added resistance can be calculated with reasonable accuracy. This is because the averaged effects of the wind, waves and currents at the power needed for propulsion cancel out after a long period from a dry-dock, hull cleaning or propeller polish. However, this period may range from several months to a year, which may be too late for vessel's performance evaluation. An additional disadvantage of not including the wind, waves and currents in the analysis is that sudden changes in the fouling resistance are very difficult to detect, since they could be incorrectly camouflaged in the resistance due to the scatter arising from the different weather conditions.

By using high resolution weather input in the calculations, the scatter is significantly reduced, which is quantified with the Confidence Interval method.

5.1. Performance prediction and Confidence Interval of a case study

In this section, a case study is carried out. The Added Resistance history of a vessel at the same period is calculated firstly by using standard noon reports, and then by noon reports which are enhanced with AIS and hindcast data. Finally, the two methods are compared. The Added Resistance is calculated by VESPER and the confidence level is set at 95%.

The Added Resistance in Fig.4 is based on reported speed over ground and reported wind and waves. The Added Resistance due to fouling is calculated at 23.3% with a ±7.5% Confidence Interval.

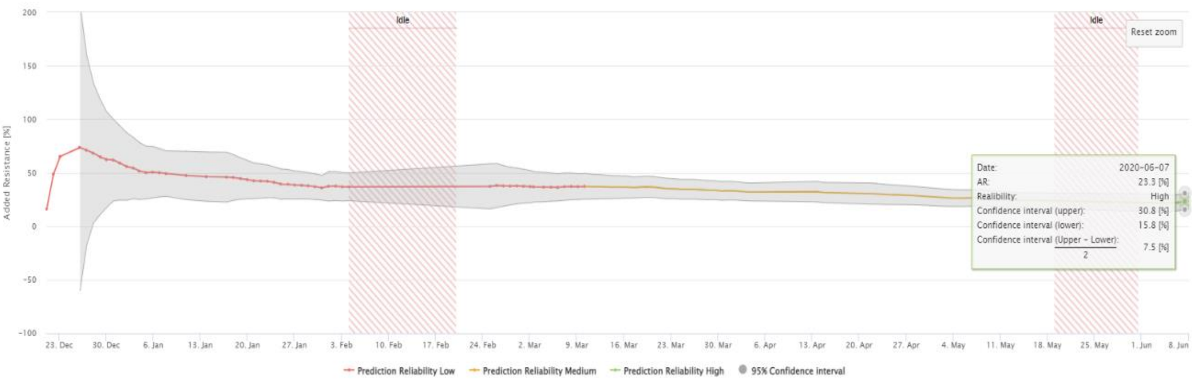

Fig.4: Added Resistance history based on reported SOG and weather

The same noon reports have been enhanced with AIS and hindcast data, then analyzed by VESPER and the result is illustrated in Fig.5. The speed over ground is corrected with the projection of hindcast currents at AIS points at the ship's course, as described in section 4. The weather input is hindcast wind and waves (significant wave height of combined wind waves and swell). The Added Resistance is calculated as 23.1% at the same date with ±5.4% Confidence Interval. This confidence interval is thereby reduced by 28% compared to the analysis based on the original noon reports. In the figure, the date at which the Confidence Interval is ±7.5% is also depicted. This confidence value is achieved at the date 12/03 vs 07/06 in Fig.4, which correspond to almost 3 months earlier. Therefore, enhancing the noon reports with AIS/hindcast data, the time needed to achieve the same confidence level has been reduced more than 50%, in this specific case study.

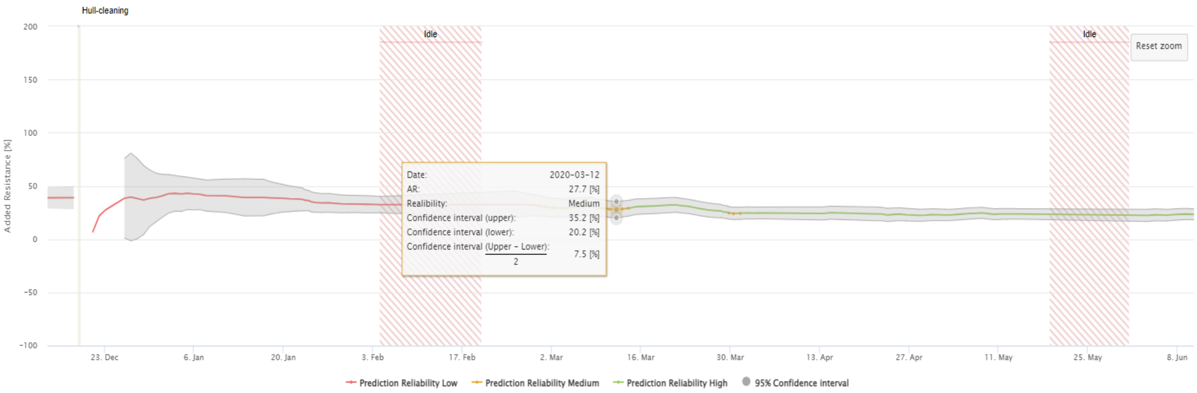

Fig.5: Added Resistance history based on enhanced SOG with hindcast currents and enhanced hindcast weather at AIS points

5.2. Noon-based Added Resistance and Confidence Interval of a whole fleet

In the previous section, the example described covered a period without any major events such as propeller polish, hull cleaning or dry-docking. In this section, the previous analysis is repeated and generalized, covering not one vessel but a whole fleet. The study utilizes 105 event periods from 34 vessels, covering 106 vessel years. Again, results are compared which are based on vessel observations versus AIS/hindcast enhanced noon reports. So, the average improvement of the confidence intervals over 105 event periods is measured.

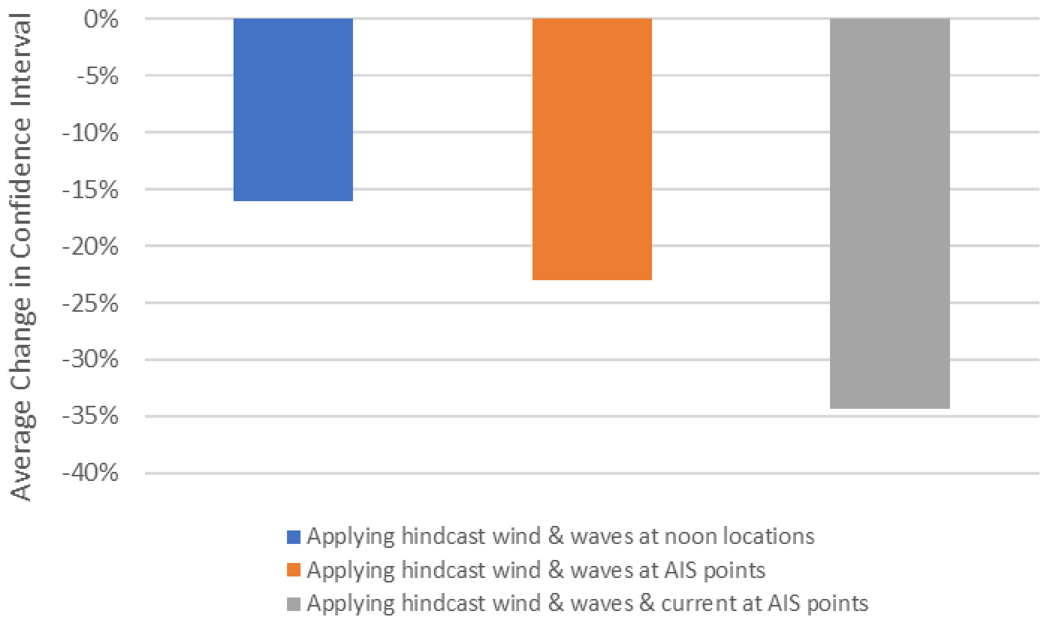

Fig.6: Average change of Confidence Intervals of all event periods by using enhanced noon reports compared to the original noon reports

Fig.6 shows the average change of Confidence Interval of Added Resistance trends after enhancing the noon reports with AIS and hindcast data. By introducing hindcast wind and waves at the noon reported locations (blue column), i.e. two points evenly distributed over the noon report, but keeping the reported

SOG, an improvement of 16% of the confidence interval is achieved. By enhancing the noon reports with AIS points and hindcast wind and waves (orange column), the confidence interval is improved even more, 23% in average. Finally, by correcting speed over ground with hindcast currents (grey column), the average confidence interval is further improved by 34% of the standard noon reporting method.

Fig.7 shows the distribution of the changes of the Confidence Intervals after enhancing the noon reports with AIS and hindcast data. By using hindcast wind and waves at the noon reported locations (blue distribution), 85% of the trends showed improvement. By further enhancing the noon reports with AIS points and hindcast wind and waves (orange distribution), 94% of the trends showed improvement. Finally, by introducing hindcast currents to correct the speed over ground (grey distribution), 93% of the trends showed improvement. After applying hindcast currents, a deeper visual inspection of the not improved trends was carried out. It was found that in rare cases, the introduced hindcast currents had very high values, which led to outliers. These outliers imposed uncertainty and the issue needs to be addressed in VESPER for future analysis.

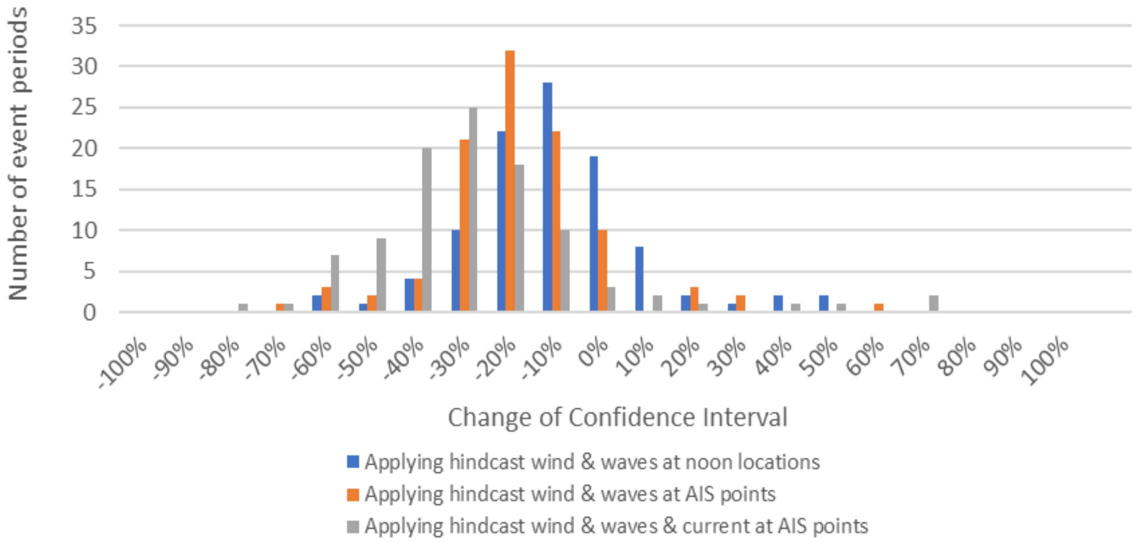

Fig.7: Distribution of the changes of the Confidence Intervals of all event periods by using enhanced noon reports compared to the original noon reports

5.3. Autolog-based Added Resistance and Confidence Interval of a whole fleet

The same study is conducted on another fleet, but this time on autolog data. The analysis includes 13 event periods from 11 vessels, covering 13 vessel years, which are based on original and enhanced autolog reports.

The autolog datasets of this study do not include wave measurements (availability is rare in general). Due to absence of wave measurements, it is assumed that the combined wave height or significant wave height of all the sea states components is highly correlated with the measured wind climate, *Lakshmy-narayanana et al. (2017)*. Consequently, in this section the wave climate is estimated from the autolog wind climate, which could be an extra source of uncertainty.

Fig.8 shows the average change of Confidence Intervals of Added Resistance trends after enhancing the autolog reports with hindcast data. An improvement of 16% in the average confidence interval is achieved by introducing hindcast wind and waves at the autolog timestamps and locations. By further introducing hindcast currents to correct the autolog speed over ground, the average confidence interval is further improved by 22% in total.

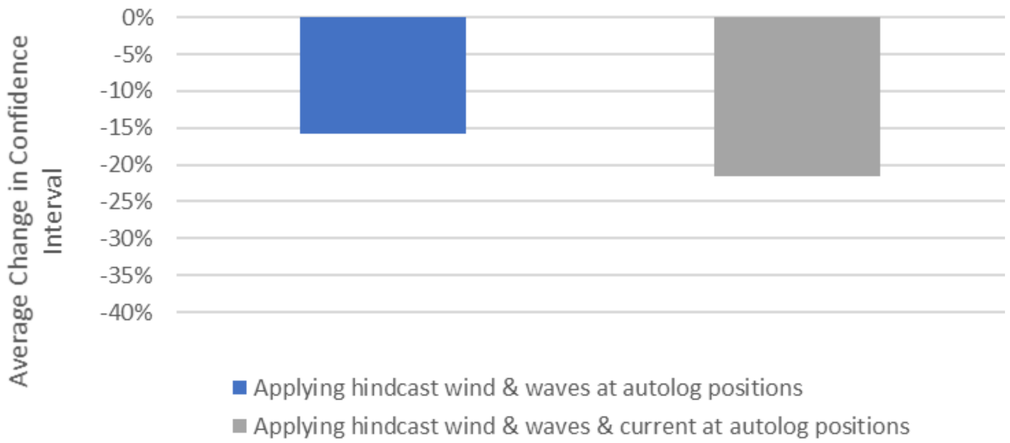

Fig.8: Average change of Confidence Interval of Added Resistance trends by using enhanced autolog reports compared to the original measured autolog reports

Fig.9 shows the distribution of the changes of the Confidence Intervals of Added Resistance trends after enhancing the autolog reports with hindcast data. By introducing hindcast wind and waves at the autolog locations (blue distribution), 84% of the trends showed improvement. By further introducing hindcast currents to correct the speed over ground with hindcast currents (grey distribution), 93% of the trends showed improvement.

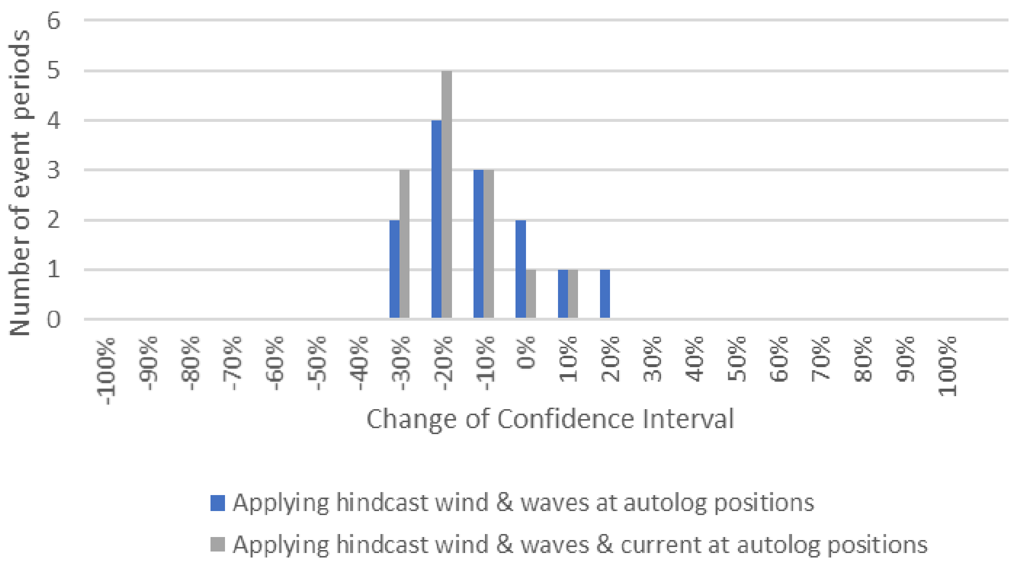

Fig.9: Distribution of the changes of the Confidence Intervals of all event periods by using enhanced autolog reports compared to the original autolog reports

6. Summary

The present study demonstrated some steps in how digitalization in shipping can help us improve performance prediction capabilities by using data fusion. Wind and wave climate from hindcast models replaced the measured wind climate from the autolog systems. Hindcast waves also replaced the wave climate, which was firstly estimated from the measured autolog wind climate, due to lack of wave measurements. Hindcast currents were also applied at the autolog timestamps and positions to correct the measured speed over ground. This way, an alternative speed through water was estimated to replace the speed log data, which are often considered unreliable. The enrichment of autolog data with hindcast data improved the reliability significantly. Apart from fusing hindcast with autolog data, similar fusion was applied to noon reports. Noon reports are still the primary source of data for predicting ship's performance, which cover usually a 24-hour period. The weather varies significantly throughout a noon report, so the reported weather (either at the time of the observation or averaged) is subject to human interpretation, which provokes uncertainty in performance estimation. The enrichment of AIS and hindcast data throughout the noon report improved the reliability of using noon reports significantly.

The Vessel Performance system (VESPER), developed by VPS, was used in the present study to predict performance. The provided power for the ship's propulsion was corrected for the impact of the weather, temperature etc., then the baseline power (model) was subtracted and thus, the residual power corresponded only due to fouling (or more precisely, hull and propeller degradation), which was called added resistance in this study. The method of confidence interval was used to quantify the reliability in the estimated added resistance, which was calculated at the end point of each added resistance trend.

The analyses were conducted twice, once on event periods of vessels with autolog data and once for a fleet with noon reports. It was found, that by enriching the autolog data with hindcast winds, waves and currents, the average confidence interval was reduced by 22% in total. Around 90% of the event periods of all vessels improved their confidence level, after the fusion with hindcast data, while 10% showed worsening. Deeper investigation of the latter trends showed that some hindcast current outliers provoked uncertainty, which can easily be filtered out in the future.

The study based on noon reports showed similar results. By enhancing the noon reports with AIS data and introducing winds, waves and currents at the AIS timestamps and locations the average confidence interval was reduced by 34% compared to the result based on the standard noon reporting method.

An alternative way to quantify the impact of data fusion in the calculations is to measure how much time is saved to reach the same confidence interval compared to the calculations without data fusion. The case study, that was conducted at one vessel, showed that same confidence was achieved in less than 50% of the time needed by using the standard noon reports. However, this estimation may vary significantly and should not be generalized.

References

LAJIC, Z. (2010), *Fault-tolerant onboard monitoring and decision support systems*, PhD thesis, Technical University of Denmark

LAKSHMYNARAYANANA, P.A. (2017), *Is wave height necessary to determine ship performance in calm water from measurements?*, 3rd HullPIC Conf., Darlington

MONTAZERI, N.; PETERSEN, J.B.; HANSEN, S.V. (2019), *Autolog data processing for vessel performance application*, 4th HullPIC Conf., Gubbio

MONTAZERI, N.; HANSEN, S.V.; PETERSEN, J.B. (2020), *A Study on Improving Reliability of Performance Indicators*, 5th HullPIC Conf., Hamburg

Impact of hull coating on EEXI and CII

Keng Khoon Tan, Jotun A/S, Sandefjord/Norway, keng.khoon.tan@jotun.com
Sergiu Paereli, Jotun A/S, Sandefjord/Norway, sergiu.paereli@jotun.com
Angelika Brink, Jotun A/S, Sandefjord/Norway, angelika.brink@jotun.com

Abstract

Decarbonization and sustainability is high on the international agenda and shipping, as a global industry can either lead or follow. This is a highly complicated matter, since the direction that shipping must take is not well defined and there is high uncertainty on how to achieve ambitious carbon neutral targets. Decisions required now will have great impact on the entire ecosystem for the next twenty or thirty years, mainly driven by soon-to-be implemented IMO regulations on EEXI and CII. All elements that impact ship performance will play a role, especially factors influencing Hull Performance. In this very complicated and uncertain landscape, we discuss the impact of hull coatings on EEXI and CII and their respective magnitudes of significance. We discuss commercial implications and what operators should consider before making decisions and investments in coating technologies. Finally, we quantify the impact and discuss limitations and uncertainties in such quantification attempts.

1. Introduction

Ocean-going vessels transport up to 90% of the goods consumed globally. Despite being the most energy efficient mode of transportation, the sheer scale of demand for shipping by sea means that these vessels make up 3% of total annual carbon dioxide emissions from human activities, *IMO (2020)*. In respond to calls for stronger actions to reduce this carbon footprint, the International Maritime Organization (IMO) has set a target of halving emissions by 2050, leading towards zero by the end of the century. The Energy Efficiency Design Index (EEDI) was implemented in 2013, requiring greater energy efficiency for newbuild vessels. Given the lifespan of vessels is over 20 years, EEXI and CII were introduced as additional, short-term measures to drive action on existing vessels, and to reduce actual emissions, not just theoretical calculations.

EEXI is a measure on technical efficiency of a vessel, modelled after EEDI, and adapted for existing vessels already in service. Vessels that fail to meet the required level of EEXI will not be issued an International Energy Efficiency Certificate (IEEC), effectively barring them from operating across international borders.

Calculating attained EEXI can be based purely on technical calculations from existing documentation or include a new sea trial – depending on whether and which upgrades have been retrofitted to the vessel. Among “Innovative Energy Efficiency Technologies” listed on the guidance from IMO, “low friction coatings” is classified under Category A – where the effect on reduction of main engine power cannot be measured, calculated, or certified in isolation from the overall performance of the vessel, *MEPC (2021)*. This implies the effect of antifouling coatings on EEXI improvement can only be considered in the case of a sea trial, where a new power-speed reference curve will be determined. We will discuss the impact of hull coatings on EEXI in Section 2.

Carbon Intensity Indicator (CII) is the short-term measure implemented by IMO that focuses on operational efficiency. Instead of theoretical models and sea trials at a fixed point in time, CII calculates the carbon intensity of vessels based on actual fuel consumption during operations, and rates vessels from A (best) to E (worst) on an annual basis. The rating bands will get stricter progressively from 2023 to 2026, demanding further improvements in energy efficiency from vessels bound by CII requirements. Vessels that achieve an E rating in a single year, or a D rating for three consecutive years, will need to develop a corrective action plan on how to achieve the required CII as part of their Ship Energy Efficiency Management Plan (SEEMP). The plan must be approved by class societies and will be subject to company audits.

While CII ratings will only commence from 2023, and correction factors for special operational circumstances remain to be finalized, the mechanism for collecting necessary fuel consumption data is already in place through IMO Data Collection System implemented since 2019. The EU Monitoring, Reporting and Verification (MRV) scheme, while applicable only to vessels sailing through the EU, makes the carbon intensity of each vessel available publicly.

Much attention has been placed on dual- and alternative fuels that help lower carbon conversion factors, retrofits with energy saving devices, route optimization to avoid powering through bad weather, and so on. The wide array of technologies to consider on areas of technical efficiency, alternative propulsion, operational efficiency and business strategy efficiency, *Maersk (2021)*, as well as decisions on where and how much to invest, can be overwhelming.

Fundamentally, calculating energy efficiency based on actual fuel consumption means the ability of the vessel's chosen hull coating to effectively control biofouling over a span of 36 to 90 months will become a critical factor. Less effective hull coatings will result in growth and accumulation of biofouling, resulting in significantly higher frictional resistance, increased fuel consumption, a worse CII rating – and vice versa.

2. Impact of hull coating on EEXI

It is established that the effect of antifouling coatings on EEXI improvement is to be considered only through sea trials, as the contribution cannot be separated from the overall performance of the vessel. Results of a sea trial will depend on the roughness and condition of the hull. Different cases can be assumed:

(1) a sea trial with a newly coated ship hull, or
(2) a sea trial after an outfitting period at quay side.

For case (1) the initial roughness of the antifouling coating might be the main impact on the hull performance. This initial roughness can be far more significantly influenced by the type and quality of surface preparation (e.g. sweep blast, spot blast, full blast) and paint application (e.g. dry spray due to wrong angle or strong winds), than the innate properties of the paint.

For case (2) it is the antifouling property, meaning how well the coating performed in keeping the hull free from biofouling in the idle outfitting period, rather than having a very smooth initial hull roughness, that plays a bigger role.

EEXI improvements from the hull coating in cases (1) and (2) do not necessarily translate into long-term technical efficiency of the vessel. Smooth application of a topcoat without antifouling properties could contribute more to EEXI sea trials than a roughly applied high-performing antifouling, despite the fact that only the antifouling will help keep the hull free from biofouling and help retain a smooth surface on the underwater hull. The potentially significant effect on energy efficiency of a vessel as a result of varying antifouling performance between coatings over the 5-year drydock cycle is not factored in EEXI assessments.

Still, the listing of "low friction coating" in category A has led to many shipowners and managers enquiring for ways to separately quantify the improvement from hull coatings on a vessel's EEXI, to minimize the required Engine Power Limitation (EPL) for compliance.

Since EEXI calculations are essentially based on EEDI, one may be tempted to leverage on the ITTC prediction model to seek an improvement in technical efficiency based on "low friction coating" and without a sea trial.

The ITTC model provide the hull surface roughness allowance with the following equation:

$$\Delta C_F = 0.044\left[\left(\frac{k_s}{L_{WL}}\right)^{1/3} - 10\,Re^{-1/3}\right] + 0.000125, \qquad (1)$$

with L_{WL} as length of the water line and k_s as roughness of hull surface.

Where no measured data for k_s is available it also suggests 150 µm as a standard value, coinciding with the Rt50 value observed for an average surface roughness of newly coated hulls. It follows that here it is meant to introduce the Rt50 for k_s value after paint application, not considering a change in roughness over time either due to polishing or due to biofouling roughness.

The term k_s can lead to confusion since k_s is in literature used for the equivalent sand-grain height used to scale roughness with the velocity in a so-called roughness function. k_s in literature is normally calculated based on measured shear velocities and Rq roughness value and plotted against the deviation of the near wall velocity profile. Different surface roughness profiles can also have the same Rt50 values but different effect on frictional resistance, and it is beyond the scope of discussion here.

The ΔC_F for an industry average hull coating application with Rt50 of 150 µm and a high-performance smooth application with a full-blasted hull with Rt50 of 80 µm are $1.29 \cdot 10^{-4}$ and $5.38 \cdot 10^{-5}$ respectively, for an assumed L_{WL} =200 m and $Re = 1.378 \times 10^9$ calculated for a speed of 14 kn and a water temperature of 20° C.

An increase in Reynolds number, meaning an increase in operational speed would translate into an increase in ΔC_F which is in accordance with the boundary layer theory and the logarithmic wall law. But the formula is also set up in such a way, that $\Delta \mathrm{C_F} = 0$ would be possible and even a negative ΔC_F can be reached.

For our case calculated above a Rt50 of 45 µm reveals already a negative ΔC_F. Roughness below that value would decrease the ΔC_F even further. ΔC_F-values below zero are physically impossible. Moreover, it is left to the executer to decide how to determine the Rt50 value and under what condition. It is described that a laboratory study on Rt50 values is valid. However, under laboratory conditions most coatings can be applied in such way, that negative ΔC_F- values can be reached. For the above calculated case a coating with an Rt50 of 45 µm would reveal a negative ΔC_F.

A decrease in Reynolds number would also automatically lead to a transition from positive to negative ΔC_F values at increased roughness-values.

These calculations and scenarios exemplify the limitations of the ITTC model and caution against overextending beyond its original intention. EEXI is a one-off certification for the remaining lifespan of the vessel, while the hull is usually repainted every 36 to 60 months. It would be inconceivable to shipowners that the vessel be required to achieve the same Rt50 values used for EEXI calculations at every drydocking – and depending on the executer, locked into using the same "low friction coating" for subsequent hull coating applications.

The purpose of EEXI regulations is to achieve global reduction in carbon emissions – whether through vessel retrofits or a reduction in speed through engine power limitation. Yet the above shows that this climate action goal can be undermined if the recommendation of "low friction coating" is interpreted and implemented in ways described above that give a perception, but do not actually contribute to actual improvement in energy efficiency and reduction in carbon emissions of the vessel.

3. Impact of hull coating on CII

On our opinion, the impact of hull coatings on CII has been understated given the broad technical, operational and environmental factors that can affect fuel consumption and carbon intensity. While hull coatings that have been part and parcel of every drydocking maintenance may seem a trivial topic, they are in fact a low hanging fruit requisite to any action plan on a vessel's CII rating. A simulation was done, shown in Fig.1 to project the CII development of a vessel over a 5-year docking interval on different options for hull coatings. In the graph, the vessel has a potential CII rating of A at that short instance of sailing out of dock. However, as biofilm catches hold of the hull in minutes of going into the water, there are alternative outcomes over time depending on the hull coating of choice at drydocking maintenance, and how well these coatings can keep fouling growth at under control.

With a market average antifouling with an average speed loss of 5.9% over 60 months, the CII rating of the vessel can be expected to increase progressively and significantly over its service interval, from an A rating by the end of the first year, to E by the end of the 5th year, all else being equal. So even if the vessel drydocks at that time and restores its hull efficiency, the E rating will remain with the vessel until the next year. The E rating also means corrective actions have to be developed as part of its SEEMP and approved. A poor rating can mean difficulty to attract charters, financing, and present a favorable ESG profile for stakeholders.

In the simulation, the vessel had a D rating (borderline to E) prior to drydocking and had been using a medium range antifouling. It is projected that the vessel is technically and operationally less efficient that CII requirements, and hull maintenance alone is unable to help the vessel attain an improvement beyond the D rating band. The potential efficiency of A rating at outdocking would require major investments into technical upgrades and retrofits, operational optimizations and potentially costs in business strategies (for example, carrying less cargo) with the aim of achieving good CII ratings. A decision to opt for a market average antifouling would effectively sabotage these efforts and negate the expected returns of investments.

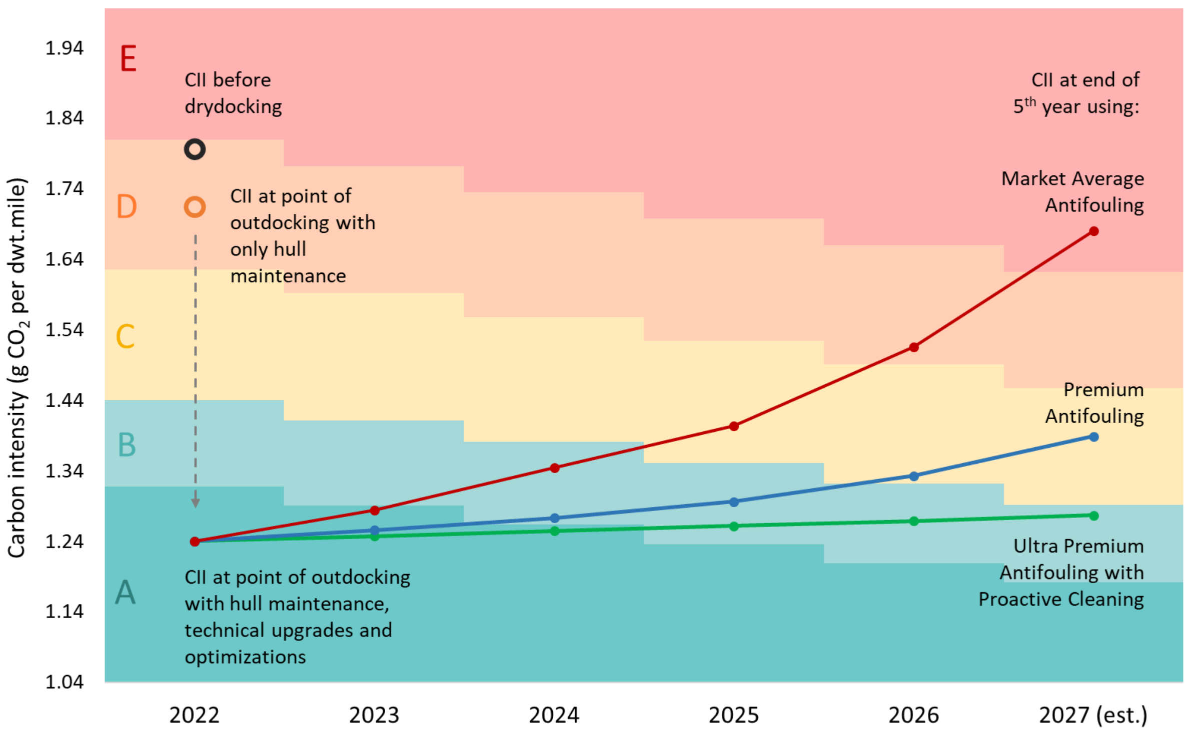

Fig.1: Carbon intensity factor over a 5-year drydocking period for different hull protection solutions

If a premium antifouling had been selected instead, the vessel's CII rating would have stayed within the bands of A, B and C throughout the service interval. Proactive cleaning of the hull, enabled by recent developments in robotics, in combination with an ultra-premium antifouling, would enable an almost flat development curve, with the slight gradient attributed primarily to inevitable mechanical damages caused at berthing.

Against this projected increase of CII are rating bands that would progressively becoming stricter, at a rate of 2 percentage points per year between 2022 to 2026. The graph assumes another 2-percentage point reduction for 2027. Without the tightening requirement, an ultra-premium antifouling with proactive cleaning would have retained the A rating of the vessel over the 5-year period.

These simulations of CII development against tightening requirements underscore the importance of selecting an effective antifouling solution, even if the most pressing decisions now are focused on EEXI. Additional measures like retrofits and optimizations are required if the vessel design and its operational patterns are in themselves less efficient than CII requirements. Otherwise, the consequences of selecting a poor antifouling can nullify energy efficiency gains expected from major investments into technical upgrades on the vessel.

4. Quantifying the impact of hull and propeller performance on CII

To exemplify the correlation between CII and hull and propeller performance, three sister vessels have been chosen. For all three vessels noon data is available for full drydocking cycles from period 2014-2020. Among other parameters fuel oil consumption was logged in noon reports and it is therefore possible to calculate CII with the following formula:

$$CII = \frac{Total\ yearly\ FOC \times carbon\ conversion\ factor}{Total\ yearly\ distance\ sailed \times DWT} \quad (2)$$

where the carbon conversion factor is 3.114, considering that the vessels burnt HSFO. Calculated CII values are plotted in Fig.2.

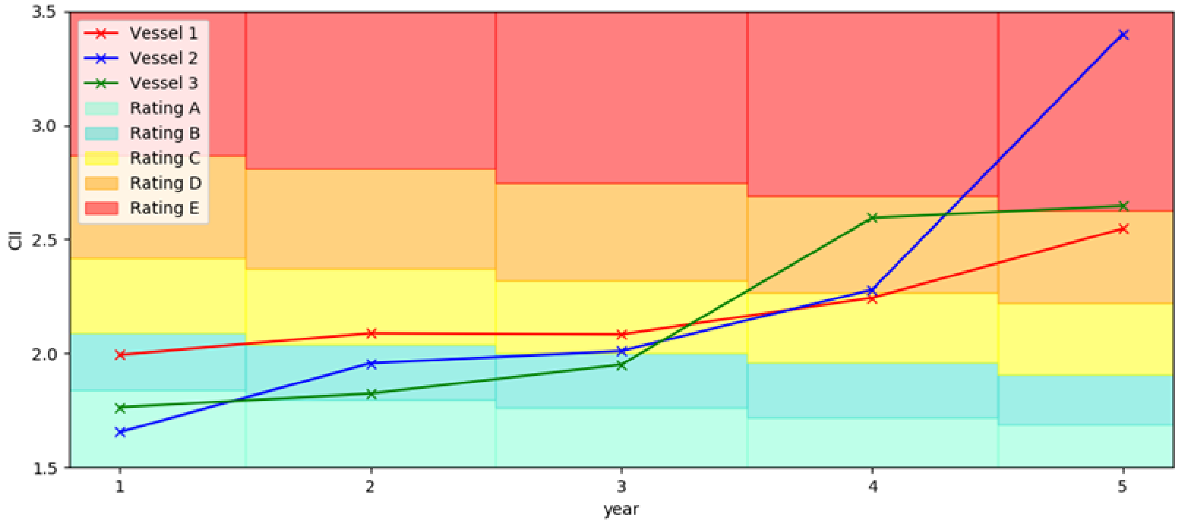

Fig.2: Carbon Intensity correlation of 3 different sister vessels using available hull performance data

In Fig.2, each marker represents the yearly average CII value for each of the three vessels. The background color of the plot is reflecting the rating bands (A-E) for the years 2022-2026. If one is to project the sailing pattern and vessel performance from the drydocking periods 2014-2019 and 2015-2020 to the period 2022-2026, then it is possible to visualize the yearly rating vessels would have had. CII values are steadily increasing from year 1 to year 5 for all vessels.

Considering the above formula, one could say that the increase can be attributed to different factors, such as fuel quality, engine performance, hull and propeller performance, operational performance. It is known though that all three vessels have been using the same type of fuel and that their operational profile has not undergone significant changes during the drydocking period. Furthermore, it is known that all three vessels did not have a good and stable in-service performance, Fig.3. Speed deviations, computed based on ISO19030, are for vessel 1, 2 and 3, 3.3%, 4.2% and 4% respectively. The bad in-service performance of the reported vessels is attributed rather to the lower quality of antifouling which has been applied on the underwater hull, and not to very challenging trade conditions. If one assumes engine performance relatively stable throughout the analysis period, then the correlation between hull and propeller performance, computed based on ISO19030, and CII becomes obvious.

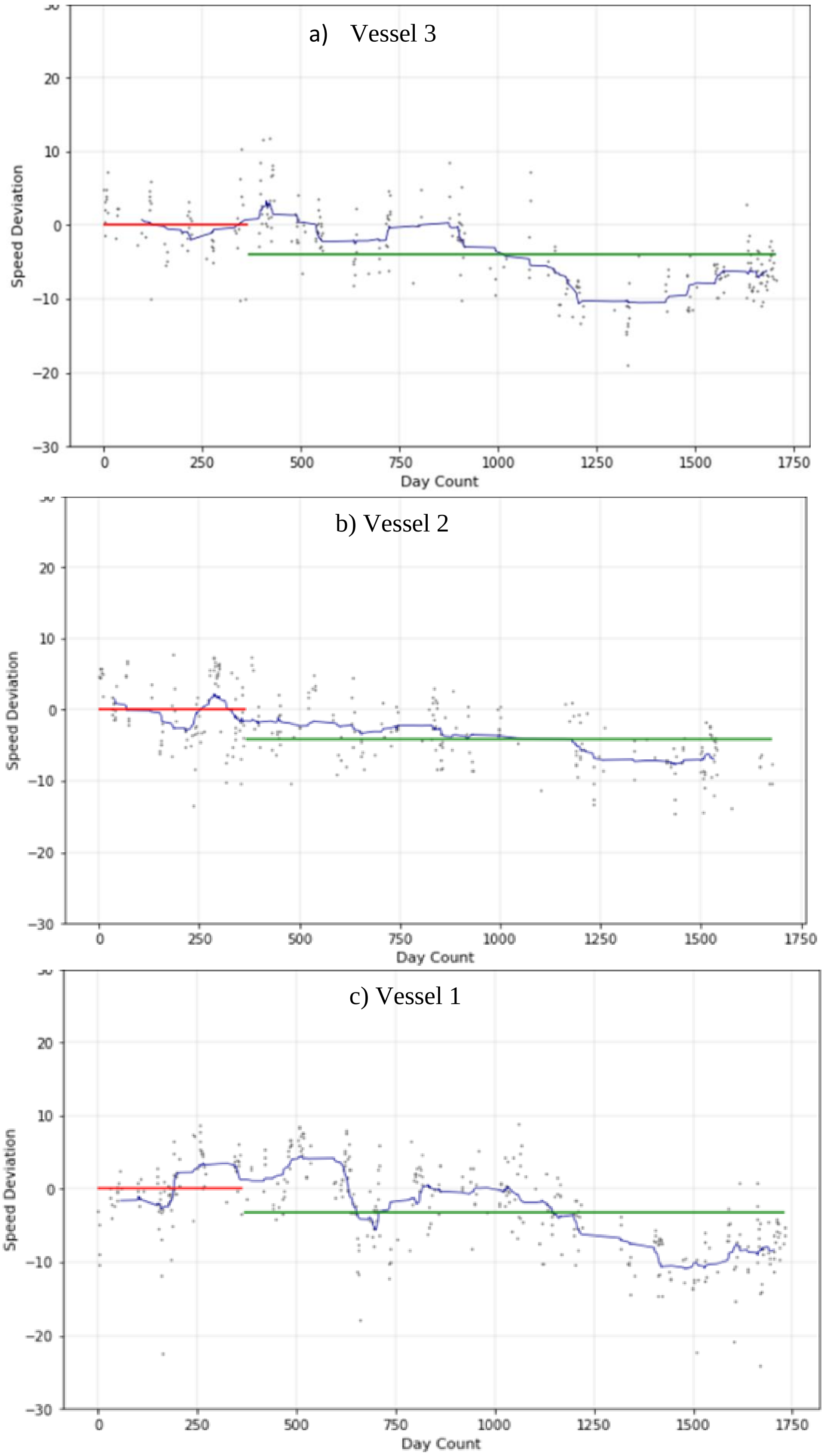

Fig.3: Speed deviation for the three vessels with presented CII factor in Carbon Intensity correlation of 3 different sister vessels using available hull performance data

If the underwater hull of all vessels had been coated with a premium antifouling which can ensure a minimum degradation in hull and propeller performance, and assuming the same starting point in terms of CII index, the CII rating at the end of the drydocking period would have perhaps been B or C and not a bad D or way above that in E.

5. Commercial implications – consideration from operators

The more immediate and severe implication of EEXI non-compliance has resulted in many shipowners and managers placing excessive focus on EEXI, with a consequence of underestimating the potential impact of EEXI-oriented decisions on CII ratings and corresponding setback on the business.

For majority of shipowners, non-compliance with EEXI mean one or a combination of the following:

a) restricting the vessel to transportation only within local waters (which may not fit with the business model),
b) retrofitting – require significant upfront costs, which not all shipowners may be in financial position to do so; or does not make economic sense for remaining lifespan of the vessel
c) reducing engine power (which effectively reduces the speed of vessel but may not meet schedule requirements). This can be detrimental to vessels on charter, and may require more vessels to meet global transportation demand. It might as well be the intention from IMO to drive newbuilding of more energy efficient vessels to replace their aged counterparts.

Many vessels are expected to opt for (c) because an engine power limitation (EPL) is the most cost-effective solution to meet EEXI requirements. It is important that they consider the following into their decisions:

1. Opting for an antifouling coating that touts low surface roughness out-of-dock, and as such an improvement in EEXI, may not necessarily come to fruition without the right surface preparation and application. Should sea-trial results fail to deliver the expected improvements, it would be impossible to pinpoint the measure causing the shortfall – antifoulings being a Category A technology. Further retrofits would be unlikely due to time and cost, resulting in a greater EPL than planned.
2. An effective antifouling coating is crucial to retain as much vessel speed range as possible. By restricting the maximum engine power available, except under life-threatening circumstance, EPL lowers the maximum speed of the vessel. Without an effective antifouling coating, accumulation of biofouling will progressively increase hull friction, and reduce the vessel speed range even further. Towards the later part of docking cycle, vessel speed range would be further restricted than what was initially imposed by the EPL. This means sailing time is likely to increase, total trips the vessel can make in a year could be reduced, and with it revenues and profits for the shipowner or charterer.

With CII, there is a direct correlation between fuel consumption and carbon emissions. In Section 4, it has been shown through actual data that vessels with low quality antifoulings would end up with increasing fuel consumption, translating into poor CII ratings. It can be implied that vessels with comparatively better CII ratings will consume less fuel for the same operations.

For charterers, CII ratings become a strong indicator on the fuel efficiency of vessels for hire. In addition, CII ratings can be used as part of their companies' environmental, social and governance (ESG) agenda. This can lead to setting an ambition, for example, to charter only vessels with a CII rating of A or B. Shipowners of vessels below the targeted CII rating would risk losing such charters or may have to make concessions on charter rates and contractual terms.

On the front of investors, financiers and underwriters, vessels with poor CII ratings will also find it harder to secure financing and insurance. The Poseidon Principles has amassed signatories among major banks for the shipping industry. Signatory banks make a commitment to measure the average carbon intensity of their shipping portfolio, assess the alignment relative to IMO decarbonization target trajectories, and report their progress on an annual basis, *Poseidon Principles (2021)*. Vessels with poor CII ratings may not be able to secure financing or may be offered less attractive financing terms that will affect the overall business profitability. On the flipside, major shipping companies have started using CII rating ambitions as an opportunity to access additional funds exclusively earmarked for sustainability efforts, and to gain lower interest rates on such loans. A similar framework has been launched for marine insurance, *Chambers (2021)*.

CII will leverage on these market dynamics in the shipping ecosystem to enact incentives and penalties, to implore shipowners to reduce the actual carbon intensity of their vessels – be it through technical measures, alternative propulsion, operational optimizations or business strategies.

6. Summary

This paper presents the impact of hull coating on the Energy Efficiency Existing Ship Index and Carbon Intensity Indicator. EEXI is a technical measure that assesses the vessel efficiency at a fixed point in time. As such the contribution of hull coatings is when the vessel undergoes a sea trial. Surface treatment and paint application also play a significant role ensuring a low hull surface roughness. EEXI fails to consider the potential development of roughness as a result of biofouling growth over the drydocking interval. Yet the listing of "low friction coating" as an energy efficiency technology may lead to attempts on theoretical EEXI improvement that undermines the global ambition to reduce carbon emissions.

Effective antifouling coatings is requisite in mitigating the impact of Engine Power Limitations on vessel speed and minimizing the increase in a vessel's CII rating over the drydocking interval. A low performing antifouling can easily negate efficiency improvements delivered from costly investments into technical upgrades. The impact of different antifouling coatings was illustrated and also supported with actual vessel data. Wide commercial implications of both EEXI and CII further underscores the need for shipowners to make the right decisions on antifouling coatings. While EEXI compliance is the most immediate concern, decisions made now will have far reaching consequences on their businesses in the years ahead.

References

CHAMBERS, S. (2021), *Poseidon Principles for Marine Insurance launched*, Splash 24/7, https://splash247.com/poseidon-principles-for-marine-insurance-launched/

IMO (2020), *Fourth IMO GHG Study*, Int. Maritime Org., London

MAERSK (2021), *Industry Transition Strategy*, Maersk Mc-Kinney Moller Center for Zero Carbon Shipping

MEPC (2021), *2021 Guidance on the Treatment of Innovative Energy Efficiency Technologies for Calculation and Verification of the Attained EEDI and EEXI*, MEPC.1/Circ.896, Int. Maritime Org, London

POSEIDON PRINCIPLES (2021), *A Global Framework for Responsible Ship Finance*, Poseidon Principles

Saving AI from its Own Hype:
Getting Real about the Benefits and Challenges of Machine Learning for Ship Performance Modelling Aimed at Operational Optimizations

Camille Colle, Toqua, Gent/Belgium, camille@toqua.ai
Casimir Morobé, Toqua, Gent/Belgium, casimir@toqua.ai

Abstract

This paper compares different approaches for ship performance modelling, with the goal of finding the modelling technique best suited for operational optimizations. Extra emphasis is placed on the potential and challenges of data-driven methods such as machine learning. The added value of using data driven methods based on sensor data compared to noon reports is quantified. Next to industry-standard approaches, a new approach based on physics-informed machine learning called 'ship kernels' is proposed. Ship kernels are shown to outperform the other approaches considered here in short-term accuracy. This makes them an ideal building block for operational optimizations (such as routing and speed optimization) that require predictions for a broad range of conditions. The ship kernels are shown to have excellent long-term accuracy compared to other approaches, making them a valuable tool for performance monitoring use-cases such as maintenance planning related to hull & propeller performance. This paper concludes with general remarks and warnings on the challenges of operationalizing machine learning.

1. Introduction

The terms AI and ML have been overused and misused in the last years to the point where they have lost any meaning to most people. According to *Yan (2021)*, 40% of AI start-ups don't use AI. This fact shows how many companies want to become part of the trend. Nevertheless, using Machine Learning should not be a goal by itself. It is a means to an end. Actually, a general rule of machine learning is to start without machine learning, *Voncent (2019)*. Machine Learning requires high-quality data, robust data pipelines and costly engineers to maintain these systems in production. For most problems a simple heuristic or approximation will give comparable results for a fraction of the costs and effort. It is only in very few cases that these few extra percentages of accuracy due to Machine Learning merit the effort. This paper argues that Ship Performance Modelling for operational optimizations (routing, maintenance planning/fouling detection and speed optimization) is such a case, if sensor data is available.

2. Qualitative analysis of ship performance modelling approaches for operational optimizations

The most common modelling approaches used in the industry today are compared in Fig.1. The solution presented here, developed by Toqua, is denoted "Ship Kernels". In general there is a trade-off between accuracy and implementation cost. Below this trade-off is discussed in detail for the different approaches.

Computational Fluid Dynamics (CFD) is highly accurate and generate interpretable results, with the drawback of requiring niche expertise, long computation times and high costs. As a result, CFD are considered infeasible for operational optimizations where a high number of predictions have to be made for a broad range of weather conditions in a limited time span.

Sea trial curves are highly practical and easy to use but have limited accuracy and flexibility. They cannot account for changing factors such as weather conditions, which have a large influence on the vessel's performance.

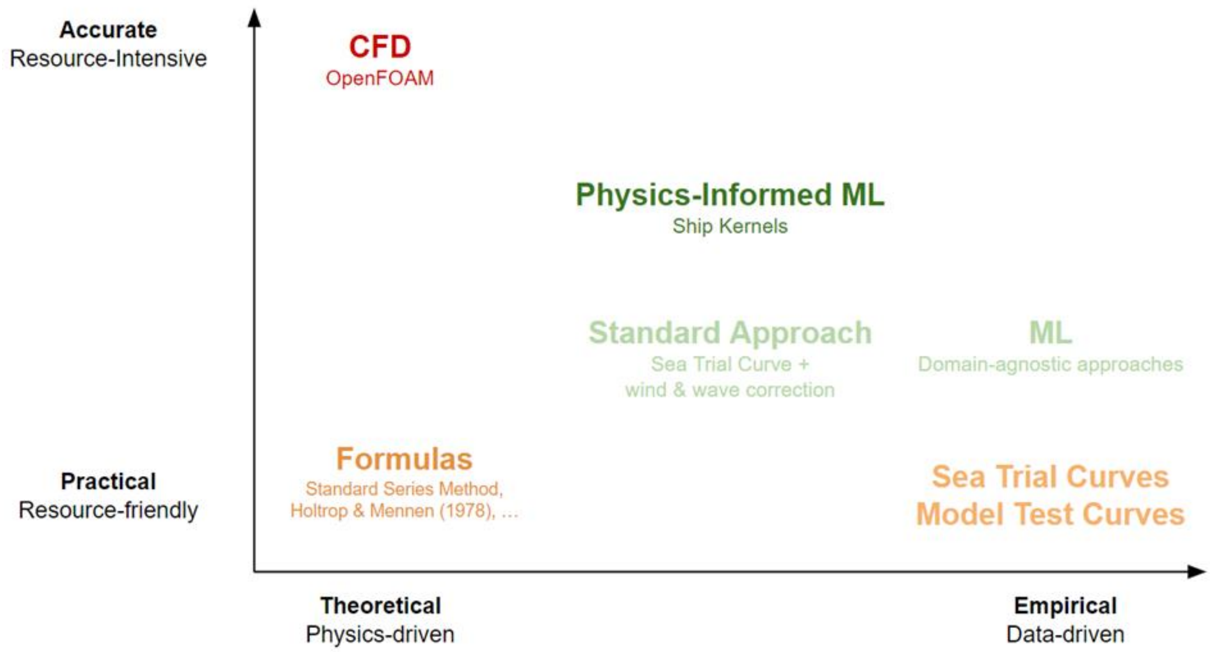

Fig.1: Overview of different approaches in current vessel performance modelling solutions

Formulas based on analytical expressions like the Standard Series Method, *Taylor (1910)*, and the approximate power prediction method of *Holtrop and Mennen (1982)* are highly transparent with low computational cost compared to CFD calculations. These expressions often require a large number of empirical coefficients not readily available for a given vessel. As such simplifications have to be made that reduce accuracy. Even though highly practical and low-cost, both sea trial curves and formulas as stand-alone solutions are considered rather inaccurate due to oversimplifications and data limitations.

Domain-agnostic ML approaches - under the motto ‘chuck in some data and see what happens’ - can generate fairly accurate results under the prerequisite high-quality data is available and predictions are made for operating conditions similar to training conditions. This approach may generate unreliable and unrealistic results for operational optimizations that consider weather & operating conditions not (frequently) observed in the data. This can lead to incorrect and costly business decisions.

A standard approach frequently used in the industry combines sea trial curves with theoretical formulas such as ISO-15016, *ISO (2015)*, or Kreitner’s formula, *Kreitner (1939)*, that corrects the sea trial curves for the added resistance due to wind and waves. These combinations still have a limited complexity, low computational cost and can improve the accuracy compared to uncorrected sea trial curves significantly. As a result, variants of this combination are often the default ship performance model used for operational optimizations in shipping today.

Finally, this paper presents a new approach for ship performance modelling that combines the benefits of sensor data availability and traditional theoretical insights based on physics and naval engineering. This is the domain of Physics-Informed Machine Learning, *Karniadakis et al. (2021)*, a new and quickly developing domain aiming to combine the benefits of data-driven and physics-driven approaches. Toqua has developed Physics-Informed Machine Learning models for ship performance, called ‘Ship Kernels’. Given data of sufficient quality, these ship kernels can outperform sea trial curves, formulas, domain-agnostic ML and correction-based approaches, while still being highly flexible, low-cost and reliable. We argue that ship kernels strike the right balance between accuracy and usability, to become the new standard ship performance model for operational optimizations like routing, maintenance planning (fouling detection) and speed optimization.

3. Why sensor data is a must for accurate ship performance modelling

In Table I and II, we compare how well Noon Report (NR) data approximates High-Frequency Data (HFD) measured by sensors. The goal is to understand the measuring error by NR data for parameters like Speed Through Water (STW) and Main Engine Power. In the first scenario we consider HFD averaged over 24 hours to be the ground truth (1 averaged point per day). In the second scenario, we consider the HFD averaged every 5 minutes to be the ground truth (288 points per day). The error is expressed as the Mean Absolute Percentage Error (MAPE).

The first column shows the error metrics in the case NR data is compared to HFD data averaged over 24h (the timespan covered by the NR). The second column takes the un-averaged HFD data and compares it to the corresponding NR by assuming the NR data is valid for the HFD datapoint that falls within its covered timespan. Note that this increases the error as we are effectively upsampling or interpolating the NR data to the HFD frequency. The second column shows the added value of HFD data while the first is more useful in showing the added value of HFD while the first mainly shows the effect of manual corrections or wrong entries in NRs.

Table I: Speed through water

MAPE - STW	**NR compared to 24h averaged HFD**	**NR compared to 5 min averaged HFD**
Ship 1	0.9%	4.1%
Ship 2	1.1%	4.1%
Ship 3	1.7%	3.1%
Average	**1.2%**	**3.8%**

Table II: Power

MAPE - Power	**NR compared to 24h averaged HFD**	**NR compared to 5 min averaged HFD**
Ship 1	2.6%	7.6%
Ship 2	1.9%	8.1%
Ship 3	13.2%	14.0%
Average	**5.9%**	**9.9%**

In the second column it can be observed that NR data has an average error of about 3.8% for STW and an error of 9.9% for power. It can be seen that the power shows large differences between NR and HFD data. We can conclude that using NR data instead of HFD measured by sensors adds a significant error to STW and Power. This inaccurate measurement severely limits the potential to create and validate ship performance models. In the absence of HFD measured by sensors, NR data is too inaccurate to be used as a ground truth to build and validate models with a power prediction error of less than 10% (MAPE).

4. Methodology

4.1. Measuring Accuracy for Ship Performance Modelling

We advocate for the next 3 metrics to become industry standard, given they are comparable over multiple ships and can be linked directly to certain operational optimization use-cases.

- R^2 = Determination Coefficient - How much of the variance in power is explained by the model:

$$R^2 = 1 - \frac{\sum_{i=1}^{n}(y_i - \hat{y}_i)^2}{\sum_{i=1}^{n}(y_i - \bar{y})^2}$$

Use: Estimating the goodness of fit.

- MAPE = Mean Absolute Percentage Error - The relative error per single prediction expressed as a percentage. Given we consider high-frequency data on power at 5-minute intervals as the ground truth, this is the error made per 5-minute interval.

$$\text{MAPE} = \frac{1}{n}\sum_{i=1}^{n}\left|\frac{y_i - \hat{y}_i}{y_i}\right|$$

Use: Operational Optimizations like weather routing and speed optimization that make a trade-off between a wide variety of operating conditions, also considering shorter time periods. Short term performance monitoring to quickly identify severe underperformance issues

- MAMPE = Mean Absolute Monthly Percentage Error - The error in estimating the performance averaged over a month of sailing. MAMPE is similar to MAPE, but has the crucial difference that instead of averaging the absolute relative error for all data points, it calculates the average relative error per month of sailing before taking the mean of the absolute values. This allows over- and underestimations due to sensor measuring volatility to even out.

$$\text{MAMPE} = \frac{1}{m}\sum_{i=1}^{m}\left|\frac{1}{n}\sum_{j=1}^{n}\frac{y_{ij} - \hat{y}_{ij}}{y_{ij}}\right|$$

Note that the first summation indexed by i loops over months (m) while the second summation indexed by j loops over n data points within a month.

Use: Performance monitoring and fouling detection over the longer term.

4.2 Modelling Scope

ML models are trained and validated on different separate datasets. This ensures the accuracy metrics represent the performance of the models for unseen data, as this is the way the models would be used in practice. When calculating the accuracy, the sensor data is considered as the true value, even if the model is only trained on noon report data. It is expected that sensor data is a more reliable ground truth than noon report data, if the sensors are well calibrated and checked for outliers.

To set a correct baseline for a “normal mode of operation” for the vessel the training data is selected to be in time intervals closely following a dry-docking. This allows for an accurate estimation of the power overconsumption and speed loss due to fouling, hull degradation, and other time-dependent factors that impact the performance of the vessel.

It is crucial to recognize that ship performance modelling consists of multiple conversions or modelling steps. Some steps are straightforward and can be well approximated by empirical formulas (speed over ground (SOG) to speed through water (STW), power to fuel consumption). For the STW-RPM-Power relationship however, significant accuracy increases can be reached by using machine learning compared to a combination of sea trial curves and correction formulas. This is due to the high-dimensionality and high complexity of the relation, an ideal challenge for Machine Learning algorithms when sufficient high-quality data is available.

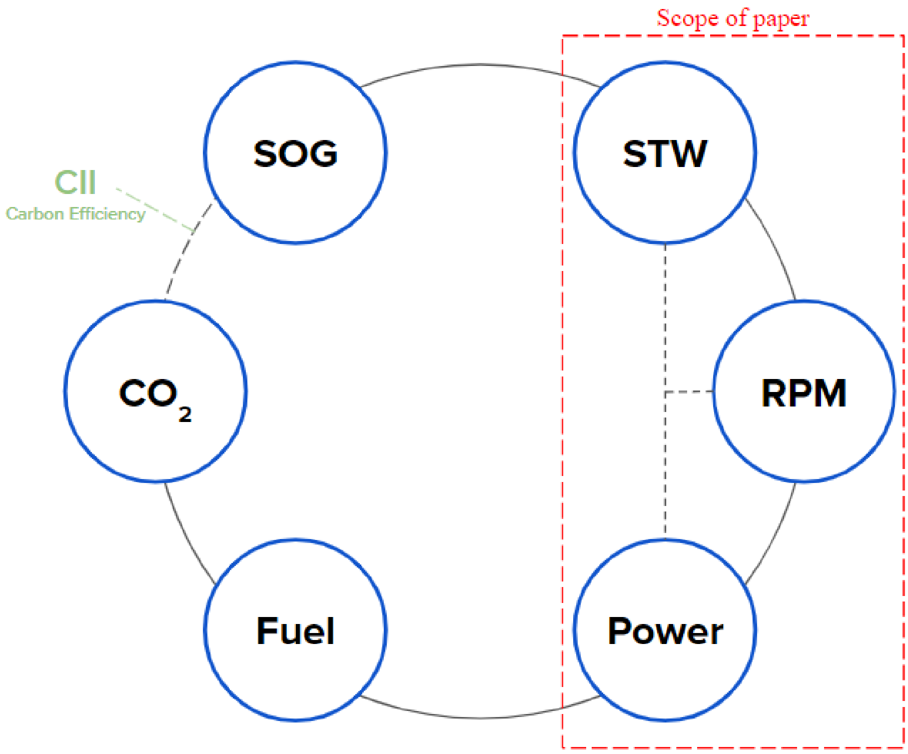

Fig.2: Sub-relations in a Ship Performance Model, red zone indicating the scope of this paper. Note that the accuracy metrics are not necessarily equal in both directions. (For example suppose that a range of 10% in STW corresponds with a variation of only 5% in RPM. Predicting STW->RPM in this range will lead to errors of at most ~5% as there is only 5% variation in the target, while the inverse relation, RPM->STW can have errors of up to 10%.)

This paper focuses on the conversion from STW to power. This relation is the most difficult to model accurately and its accuracy dictates how well hull performance can be analysed.

4.3 Modelling Approaches

In order to quantify the improvement of the ML models, its predictions are compared to other approaches, ranging from a simple baseline model to more advanced semi-empirical formulas.

A baseline model widely used in the industry are sea trial curves or model tests. This is a simple function translating STW to power which does not take any other operational factors or weather conditions into account. This method is used to set a baseline to compare the other approaches with. Although this method can be regarded as an oversimplification, it is sometimes used in the industry.
A common approach to improve the baseline sea trial curves or model tests consists of correcting the power prediction for weather factors such as wind and waves using formulas. Here we use the ISO15016 standard for wind correction and *Kreitner's (1939)* method for wave correction.

Next, a Machine Learning model trained on noon report data, enriched with third-party weather data, is investigated. The ML model is trained to predict the main engine power using weather information and vessel conditions such as STW, draft, ... Note that noon report data is only entered once every 24 h and is subject to human errors. As such it can be expected that these models are still far from the best solution possible.

Finally a new ML approach denoted "Ship Kernels" is detailed. The Ship Kernels are trained using sensor data combined with weather data. The regression task is basically the same as the NR models but as much more data is available, more ML solutions, such as neural networks (NN) become feasible. Several known physical relations from naval engineering are enforced to create physically consistent models. This can be achieved using Physics-Informed Machine Learning, *Karniadakis et al. (2021)*. It is a highly non-trivial task and is one of the major strengths of our models compared to other data-driven solutions.

5. Results

Fig.3 shows the "learning curve" for the 4 modelling approaches outlined above. A learning curve shows how the accuracy of the model changes as more data becomes available. The sea trial curve and the "sea trial + correction" approach are not fitted to any data, leading to horizontal lines on the learning curve figure. For data-driven techniques like machine learning, the amount of training data has a large influence on the accuracy. Both data-driven methods improve in accuracy until they stabilise after approximately 5 months of training data.

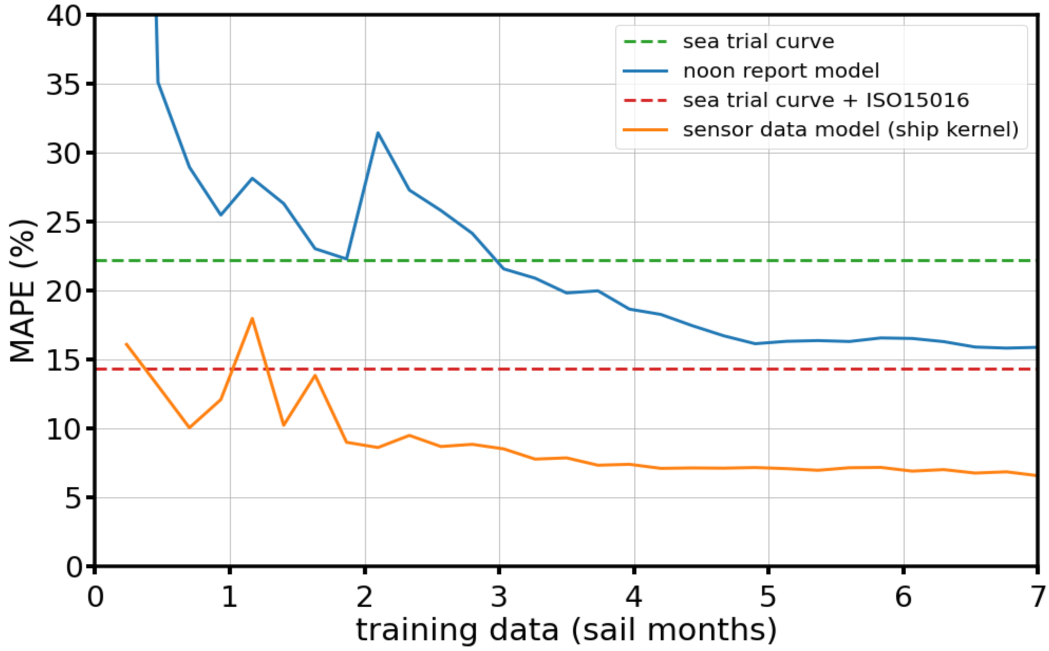

Fig.3: The learning curves using MAPE for the different approaches outlined in this paper

Table III lists the accuracy metrics for all 4 modelling approaches. Ship kernels have the highest goodness of fit, followed by 'sea trial + corrections'. The NR model trained on NR data and validated on sensor data has a very bad goodness of fit, possible due to misreporting and inaccuracies in the NR data. Sea trial curves are the least accurate approach, as was to be expected from an approach that can't account for changing conditions.

STW to Power	Sea trial	NR model	Sea trial + correction for wind & waves	Sensor data model (Ship Kernel)
R^2	0.38	0.26	0.73	0.86
MAPE	22.2%	15.9%	14.3%	6.7%
MAMPE	21.9%	13.6%	13.7%	2.6%

The standard 'Sea trial + correction' approach has a comparable accuracy to ship kernels when only NR data is available (14% and 16% MAPE respectively). However, in a scenario where sensor data is available, the ship kernels have the best accuracy metrics. With a MAPE of 6.7%, the ship kernel is more than twice as accurate as the 'sea trial + corrections. Investigating the MAMPE shows that the data-driven approach of ship kernels drastically outperforms other approaches, making it a much more accurate option to analyse long-term ship performance related to hull & propeller fouling.

6. How to increase the operational usability of Machine Learning

A disadvantage of Machine Learning for ship performance modelling is that it requires 3-6 months of operational data before an accurate model can be made. A second barrier is the requirement of sensor data, while the majority of ships only have NR data today.

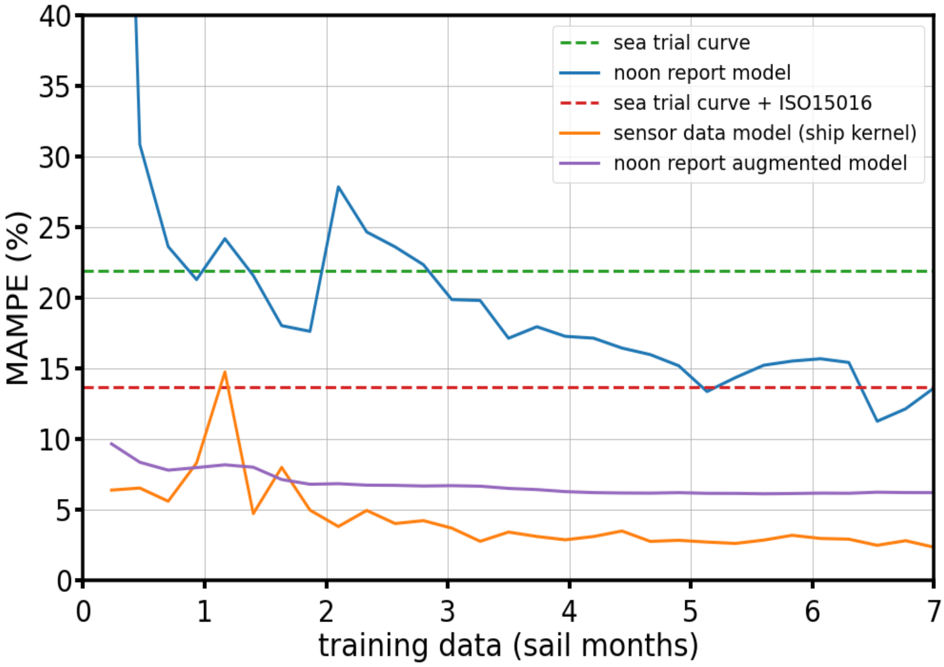

Fig.4: The learning curves using MAMPE for the previous approaches and the ‘augmented approach’

Toqua has solved this disadvantage by creating models that draw from prior knowledge learned by ship kernels for vessels of similar design with sensor data. (A detailed explanation of this method is deemed to be outside the scope of this paper) This approach is denoted as the “augmented approach” and its learning curve is displayed in Fig.4. A MAMPE of around 7% is possible for a ship that only has NR data. This makes this ‘augmented approach’ the most accurate solution for vessels that only have NR data, outperforming the ‘sea trial + corrections’-approach that has a MAMPE of 16%. Nevertheless, to reach the highest accuracy sensor data is still required. We argue that the additional accuracy merits the investment cost in sensor data, since more accurate performance understanding leads to better decision making and even the smallest relative fuel savings outweigh the absolute investment cost of sensor data.

7. The real challenge of using ML in shipping

According to *NN (2018)*, 85% of ML projects fail. We expect that number to hold true in the shipping industry as well. The real challenge does not lie in creating the most accurate and sophisticated models but in getting those models operational at scale in a cost-friendly and reliable way. Most ML projects die after a Proof-Of-Concept stage. A machine learning model can quickly show promising results, but putting that model into production and serving it to the world adds many new challenges and development costs causing projects to lose momentum, go over budget and eventually be cancelled.

In the evolution of ship performance modelling, the first challenge is gathering high-quality, high-frequency data. Today more and more companies with sensor data have reached a stage where their data is ML-ready. The second challenge is to create accurate and robust models from this abundance of data. As this paper illustrates, physics-informed Machine Learning models like Ship Kernels can deliver on that promise. The final and largest challenge before the benefits of digitalization in shipping can really be achieved is getting these models operational at an industrial scale. The costs, time and people required to get ML in production (MLOps) are a multiple of the resources required to create a Proof-Of-Concept model, *Clemmedsson (2018), Srivastava (2022), Lee and Shin (2019)*. We view this as the largest challenge the industry will be facing in the next few years in achieving the efficiency-gains promised by operational optimizations powered by digitization and better ship performance modelling.

8. Summary

A qualitative analysis is presented of the ship performance modelling techniques available to the industry today. Current techniques are graded on their suitability for operational optimizations, requiring high amounts of predictions for a wide range of combinations of speed, draft and weather conditions. A case is made in favour of techniques drawing from a combination of physics-driven and data-driven insights.

Secondly, the measuring inaccuracy of STW and power for Noon Report data is quantified by comparing it with High-Frequency Sensor data. A significant measuring error is found due to Noon Report data (MAPE = 3%-14%). This prompts the authors to conclude that sensor data is an undeniable requirement in order to create and validate highly accurate data-driven ship performance models.

Next, a quantitative analysis is made comparing the accuracy of different modelling approaches for the conversion from STW to ME-Power. It is found that ship kernels (ML, developed by Toqua) trained on sensor data have a much lower error (MAPE=6.7%) compared to other approaches (Sea trial curves: MAPE = 22%, 'sea trial + wind & wave correction': MAPE = 14%, ML on noon report data: MAPE = 16%).

Finally, a fair warning is given that the real challenge in capturing the value of ML & sensor data, does not lie in creating accurate models, but in getting these models operational at an industrial scale, in a reliable and cost-effective manner (MLOps).

References

CLEMMEDSSON, E. (2018), *Identifying pitfalls in machine learning implementation projects: A case study of four technology-intensive organizations*, KTH, Stockholm

HOLTROP, J.; MENNEN, G.G.J. (1982), *An approximate power prediction method*, Int. Shipbuilding Progress 29/335, pp.166-170

ISO (2015), *ISO 15016:2015 - Ships and marine technology — Guidelines for the assessment of speed and power performance by analysis of speed trial data*, Int. Standard Org., Geneva

KARNIADAKIS, G.E.; I. G. KEVREKIDIS, I.G.; LU, L.; PERDIKARIS, P.; WANG, S.; YANG, L. (2021), *Physics-informed machine learning*, Nat. Rev. Phys.

KREITNER, J. (1939), *Heave, Pitch and Resistance of Ships in a Seaway*, Trans. INA 81/440, p.203

LEE, I.; SHIN, Y.J. (2019), *Machine learning for enterprises: Applications, algorithm selection, and challenges*, Bus. Horiz.

NN (2018), *Gartner Says Nearly Half of CIOs Are Planning to Deploy Artificial Intelligence*, https://www.gartner.com/en/newsroom/press-releases/2018-02-13-gartner-says-nearly-half-of-cios-are-planning-to-deploy-artificial-intelligence

SRIVASTAVA, S. (2022), *Estimating the Time, Cost, & Deliverables of an ML App*, Appinventiv, https://appinventiv.com/blog/machine-learning-app-project-estimate/

TAYLOR, D.W. (1910), *The Speed and Power of Ships: A Manual of Marine Propulsion*, Wiley&Sons

VINCENT, J. (2019), Forty percent of ‘AI startups’ in Europe don’t really use AI, claims report, The Verge, https://www.theverge.com/2019/3/5/18251326/ai-startups-europe-fake-40-percent-mmc-report

YAN, E. (2021), *The First Rule of Machine Learning: Start without Machine Learning*, https://eugeneyan.com/writing/first-rule-of-ml/

Full-Scale Power Prediction for Vessel Equipped with Energy Saving Device

Alex A. Shiri, **Sofia Werner**, SSPA Sweden AB, Gothenburg/Sweden, Alex.Shiri@sspa.se
Rickard E. Bensow, Chalmers University, Gothenburg/Sweden

Abstract

Energy Saving Devices are considered as a solution to improve propulsive efficiency in marine vessels. However, performance prediction of ESD presents many challenges; both for full-scale CFD simulation and for empirical methods used to scale-up the power prediction in model test. This paper evaluates practice of power gain prediction for the well-known KVLCC2 with an energy saving device. A duct with pre-swirl stator was designed and studied in a workshop with full-scale CFD simulation using different commercial codes. Model scale tests were performed, and full-scale power gain was predicted using ITTC recommendations. The comparison between different CFD codes and numerical techniques which was used to setup a self-propulsion simulation showed that reliable power prediction with CFD requires further improvement. On the other hand, the Reynolds number scaling of the small appendages with complicates flow regime, put forward many questions on model test prediction practices for ESD efficacy. Despite these issues, combining the existing tools, full-scale CFD and model test, should be the base for ESD design and could be confirmed only with sea-trial. Today, especially in industry, automated mesh generation are used to decrease the cost of setup and meshing in CFD simulations. Most of these methods are developed for resistance prediction in vessels. This paper discusses the considerations in evaluating the quality of simulation method for the purpose of ESD power gain estimation.

1. Introduction

EEDI requirements and global warming pushes the transportation industry to employ every measure for reducing CO2. Fuel price volatility also incentivizes ship owners to investigate all possible methods to decrease fuel consumption of their fleet. In addition to hull performance enhancement of new vessels designed by using combined computational and experimental tools, there is always an interest in further improvement of existing vessels by retrofitting and additional appendages.

For hull designers and model test basins, evaluating a new energy saving device, requested by costumer, is a challenging task. An ESD designed to operate with a particular hull might deliver different performance for a similar, but not identical, vessel depending on how well optimized the initial hull design is. Therefore, it is imperative to evaluate ESD performance with reference to the specific hull.

Principal mechanisms of Energy Saving Device are explained in several references, including *Terwisga (2013), Wald (1965)* and *Dyne (1995),* investigate the role of momentum manipulation components in the flow as energy loss or gain. The summation of these gains and losses presents system performance. This method of investigation discusses optimization of components (like PSS) separately and disregards the interaction of components.

Kim et al. (2014) described in detail that designing the appendage like ESD requires the complete information about full-scale wake region and boundary layer flow which is not provided by model scale test and simulations. They concluded that in full-scale hull, the effect of ESD is less significant compared to model scale due to Reynolds number dependency and ESD design should always be based on the full-scale wake flow. Studies by *Broberg and Orych (2013)* and *Kim et al. (2012)* follow a similar approach by investigating the performance of different pre-swirl and ducted ESDs using SHIPFLOW viscous flow solver combined with Lifting-line propeller modeling of the full-scale hull.

As described by *Carlton (2012)*, Energy Saving Devices are the appendages on hull for propeller thrust augmentation. In a conventional propulsion-hull system, the regions in which hydrodynamic power loss occur are divided into three zones, Fig.1. In zone I, ESD manipulates the boundary layer flow and reshape the wake behind the skeg to increase the uniformity of the inflow to the propeller (increase Relative Rotative Efficiency η_R). Pre-swirl fins and wake equalizing ducts are examples of the ESD used in this zone. Ducted propeller and boss fin in zone II attempt to modify the slipstream of the propeller and increase Propeller Efficiency (η_0). In Zone III, Rudder-Bulb operates behind the propeller to reduce the hub vortex and recover the energy loss due to propeller rotation.

The overall effectiveness of the ESD presents itself in different components of the Quasi-Propulsive Coefficient:

$$QPC = \frac{P_E}{P_D} = \eta_0 \, \eta_H \, \eta_R$$

where the ratio of effective power (P_E) to delivered power (P_D) depends on propeller efficiency (η_0), relative rotative efficiency (η_R) and hull efficiency (η_H)

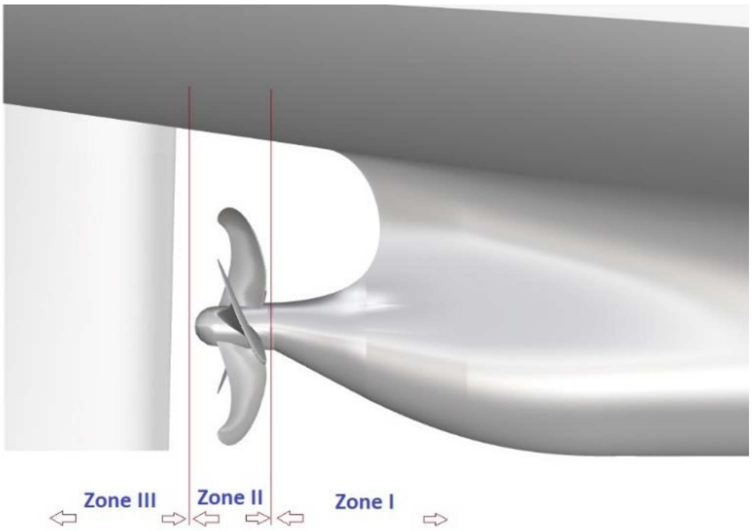

Fig.1: Propeller thrust enhancement regions

New guidelines are proposed in 29th ITTC by the specialist committee on ESD for scaling wake fraction for vessels with pre-swirl device, *Lee et al. (2021),* which includes Pre-Swirl Stator (PSS) and Pre-Swirl Duct (PSD) installed at zone I. Two approaches are discussed in the guideline. First method considers PSS – Propeller system as a combined propulsor which should be tested in open-water and self-propulsion tests as one unit. The common scaling problem of laminar flow on model device occurs in this method and needs to be addressed.

The other approach, which is selected by this study, assumes ESD as a part of hull and two sets of resistance and propulsion test are carried out for hull with and without ESD. Open Water test is performed on propeller without appendages. The scaling process for the wake uses, *Lee et al. (2021)*:

$$w_s = (t_{M0} + 0.04) + (w_{M0} - t_{M0} - 0.04) \times \frac{C_{FS} + C_A}{C_{FM}} + (w_{Ms} - w_{M0})$$

The role of PSS is mainly considered as increasing in the angle of attack for propeller blades and viscous effects of the ESD is neglected. Therefore, Relative Rotative Efficiency is assumed to be scale independent, but Pre-Swirl devices create tip vortices and might generate local separation zones along the fins.

There are some attempts by *Kim et al. (2017)* to improve pre-swirl device prediction by introducing correction factors separately for axial and tangential velocity components. The study is based on limited studies on selected hulls. All these studies indicate that more effort is required to scale model test results of hull with ESD. Full-scale CFD computation of a self-propelled ship, if performed properly, might offer a better alternative.

Nowadays ESDs are designed by evaluating the wake flow either in model test or full-scale CFD simulation. CFD simulation of a vessel, free to heave and pitch in two-phase viscous flow with free surface, have improved in recent years and hull resistance computed for model scale hulls are very close to model test measurements. However self-propulsion simulations with the same setup still requires validation. More specifically when we are dealing with the effectiveness of the appendages near a working propeller.

Many studies like *Shin et al. (2013), Nielsen (2019)* and *Kim et al. (2013)* evaluate the performance of a particular ESD design by comparing CFD result in model scale with a test performed in towing tank. As most commercial CFD solvers are validated for model scale resistance, applying the same setup, such as mesh refinement scheme, wall function and acceptable range of y^+, for simulating full-scale hull with ESD appendages can raise some questions. Isolated studies of a particular hull with and without ESD might show improvement in required power, but a general methodology for evaluation is not available yet.

Karsilnikov (2019) studied the effect of turbulence model and free surface simulation on nominal wakes and *Kim et al. (2014)* performed full-scale self-propulsion simulation on various ESDs using Lifting-Line propeller model. Study by *Andersson et al. (2022)* includes hull roughness as a contributing factor in full-scale simulation comparisons. Much of the CFD simulations nowadays are performed using commercial softwares and although some are dedicated marine hydrodynamic codes, there is a verity of numerical models to select from.

The miniscule power gain from ESD and lack of accurate sea-trial measurements always bring the reliability of the full-scale CFD into the question. Therefore, naval architects and model test basins are faced with these choices to estimated ESD performance:

1. Using model test result and collect enough sea-trial measurements to find correction factors and translate the ESD effectiveness into the full-scale performance.
2. Perform full-scale CFD simulation.
3. Combined CFD and EFD.

Strategy one is the approach presented in ITTC, *Lee et al. (2021)*, which is highly design dependent and hard to be employed as a general guideline for all different types of ESDs. Second strategy has the benefit of correct Reynolds number scaling and is the method being used in many current studies but the problem of reliability of CFD models are still an open question. Until we reach a point that accurate computations are available with reasonable computational costs, there should be a solution to combine CFD and model test result and achieve a better estimation for ESD performances.

This paper presents our effort to define a test case for both model test investigation and computations using state of the art CFD codes. The KVLCC2 test case was selected for a benchmark study organized by SSPA Sweden and Chalmers University with 10 participants. Results of the workshop were published in *Andersson et al. (2022).*

2. Test Case

We selected a vessel equipped with energy saving device in zone I. The vessel is a single skeg KVLCC2 tanker with the length (L_{PP}) of 320 m. SSPA has designed a ducted PSS for this vessel to be installed before propeller. Main particulars of these the vessel is listed in Table .

2.1 Pre-Swirl Stator with Duct – KVLCC2

KVLCC2 is the second variant of tanker developed by MOERI to be used as a test case for CFD investigations. This hull is used in several numerical studies including Gothenburg 2010 Workshop, *Larsson et al. (2014)*. Along with computational simulations, extensive model tests were carried out on this hull, *Kim et. al (2012),* and the SIMMAN 2014 workshop. The vessel has a short skeg with a sharp gradient of hull-lines toward propeller hub. Pre-conditioning of the wake flow into the propeller using duct and pre-swirl stators was a good choice of ESD for KVLCC2. SSPA designed a ducted PSS, Fig.2, and manufactured a hull model in scale of 1:45.714 with and without ESD for testing in towing tank.

Table I - Main Particulars of the KVLCC2 hull

Length between perpendiculars	L_{PP} (m)	320.0
Length at waterline	L_{WL} (m)	325.48
Beam at waterline	B (m)	58.0
Draft	T (m)	20.8
Displacement	Δ (m^3)	312 784
Wetted area hull without ESD/Rudder	S_w hull (m^2)	27 249
Wetted area rudder	S_w Rudder (m^2)	273.3
Wetted area ESD	S_w ESD (m^2)	81.8
Propeller Diameter	D_P (m)	9.860
Hub Diameter	D_{Hub} (m)	1.528
Number of blades	N	4
Expanded blade area ratio	A_E/A_O	0.426
Propeller Pitch	P/D, 0.70R	0.721

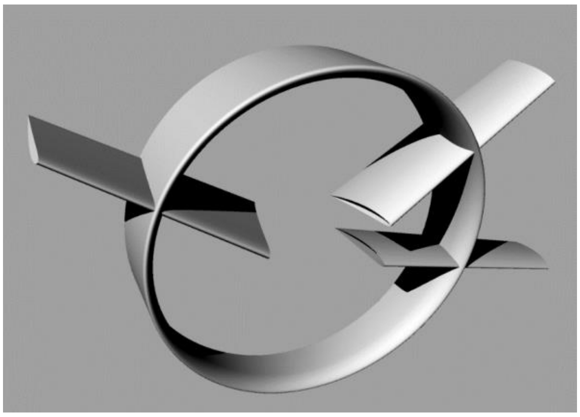

Fig.2: Combined Duct/PSS designed by SSPA for KVLCC2

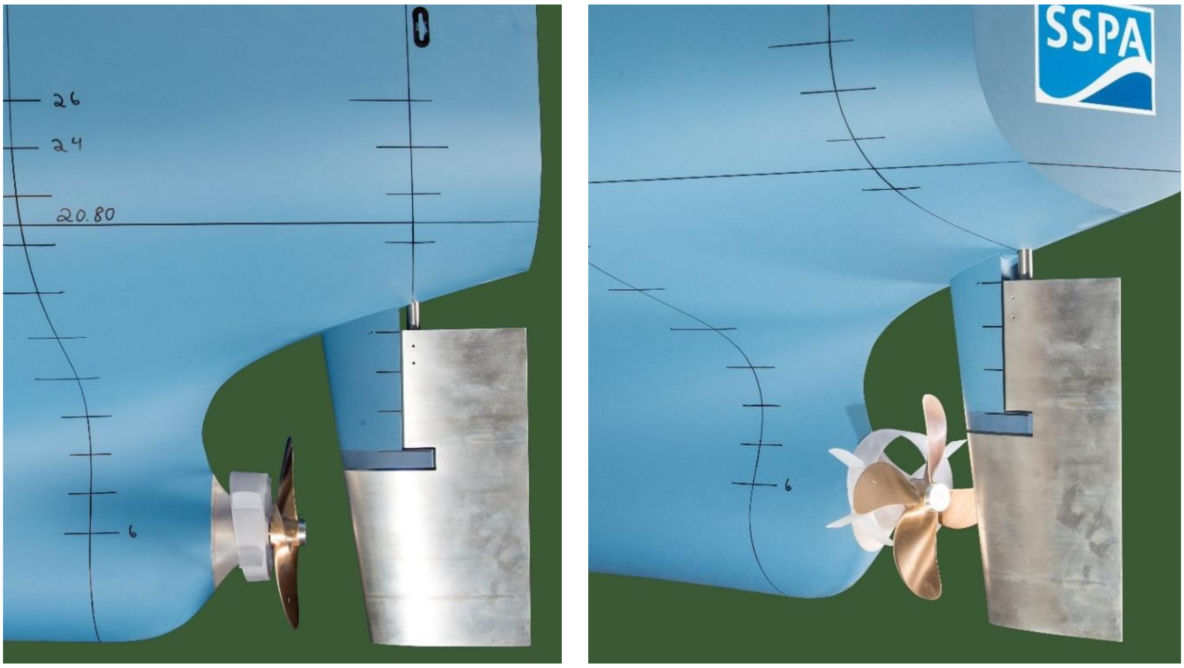

Fig.3: KVLCC2 model hull with propeller and ducted PSS installed

The device is a combination of a duct and PSS which has three blades; two are located on the port side and one on the starboard side, Fig.3. The additional wetted surface of 82 m^2 is considered in the evaluation. Hull geometry was slightly modified for the purpose of manufacturing. Propeller was manufactured based on propeller KP458 designed by MOERI provided in SIMMAN workshop.

Towing tank tests were performed on a manufactured model in SSPA facility. Propeller open water test, resistance test, self-propulsion test and wake measurements were performed for model with and without ESD installed. Tests were performed in free to heave and pitch condition with loading at design draft equivalent to 20.8 m in full-scale and a range of speed from 12 to 16 kn.

The design of ESD was based on full-scale simulations performed by SHIPFLOW viscous RANS solver. The predicted power saving for full-scale ship according to SHIPFLOW computation was 2.9% in 15 kn speed with 2% RPM reduction. Total Wake Fraction in full-scale, without working propeller, is shown in Fig.4 for hull with and without ESD.

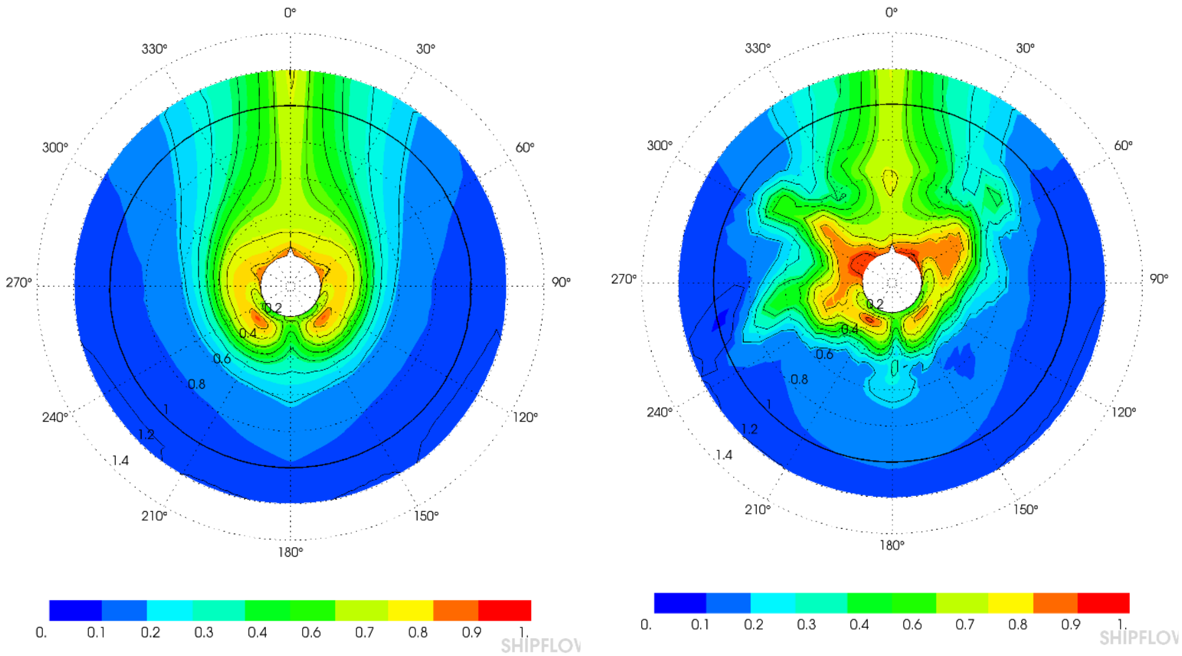

a. Bare hull b. With ESD

Fig.4: SHIPFLOW simulation, Total wake fraction for Full-scale KVLCC2 in 15 kn and design draft, with and without ESD

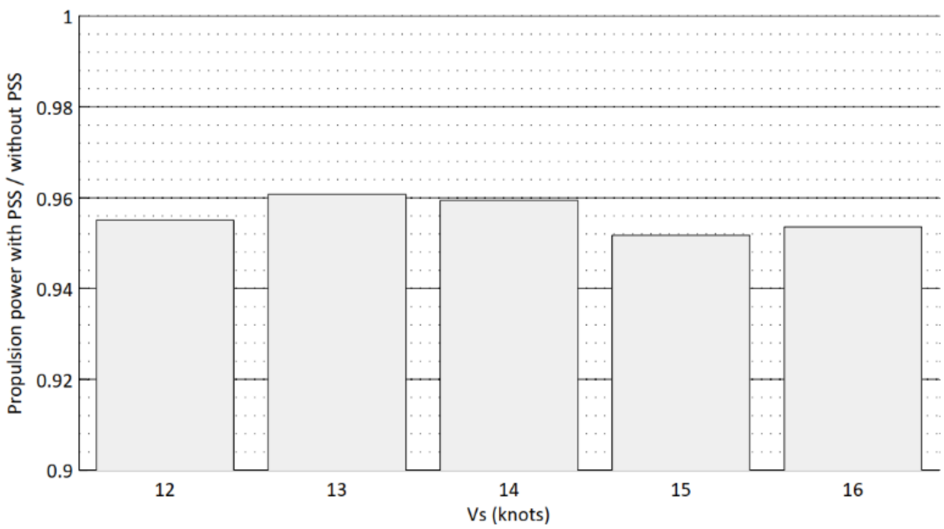

Fig.5: Full-Scale prediction from model test KVLCC2 (modified ITTC 1978 evaluation)

Results of the full-scale prediction from model test based on modified ITTC78 method are presented in Fig.5. The prediction presents ~5% power reduction in speed of 15 kn with the ESD. The total wake fraction measured for design draft in 15kn speed is presented for the hull with and without ESD in Fig.6. For the comparison, wake fraction simulated by SHIPFLOW is presented for model scale in Fig.7.

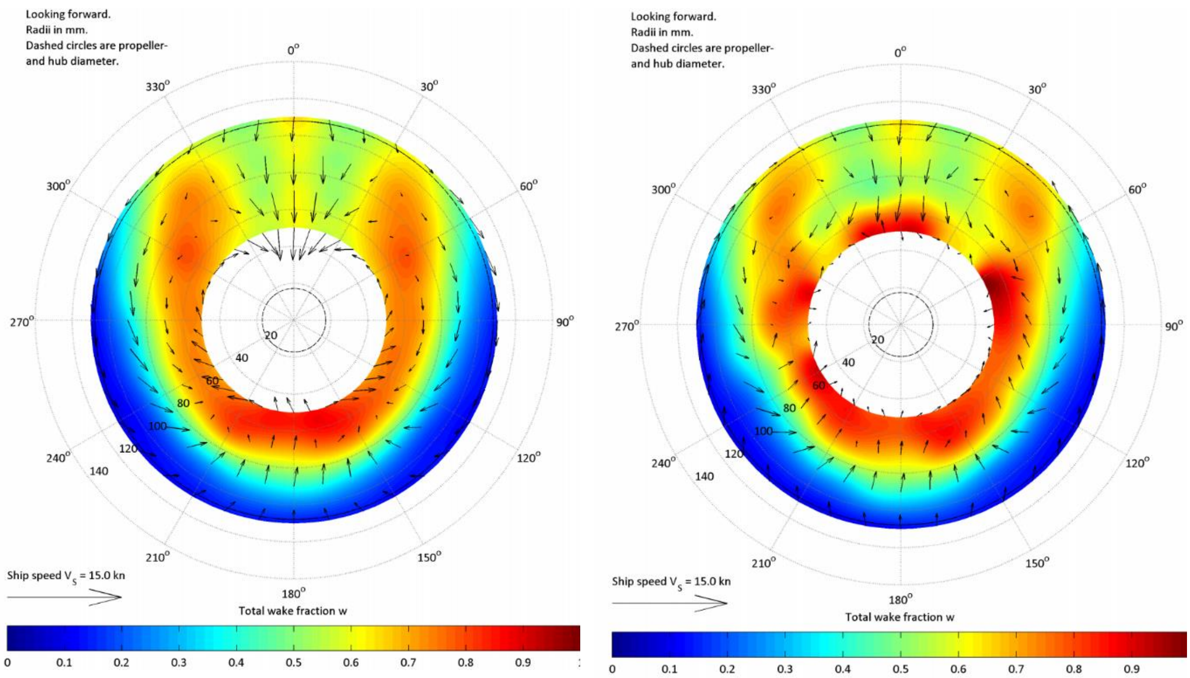

a. Bare hull b. With ESD

Fig.6: Total wake fraction for KVLCC2 model in 15 kn and design draft, with and without ESD

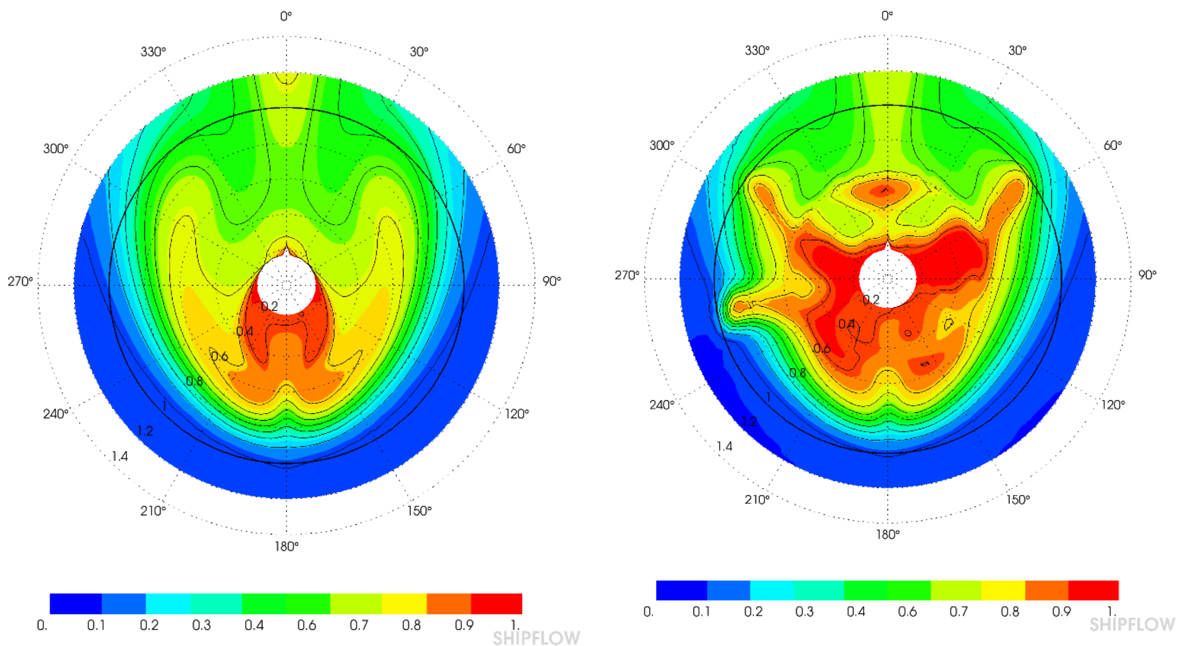

c. Bare hull d. With ESD

Fig.7: SHIPFLOW simulation, Total wake fraction for KVLCC2 model in 15 kn and design draft, with and without ESD

3. Numerical Method

Not all the CFD methods have the same reliability when it comes to evaluating the effectiveness of the ESD. Some modeling techniques are not capable of capturing the complicated flow regime created by the ESD appendages. On the other hand, simulating a full-scale ship with working propeller and hull motion in free surface is very challenging and costly. Meshing strategy should aim to simultaneously satisfy the necessary resolution for propeller and ESD and at the same time simulate the full-scale boundary layer flow over large hull surface.

For designing the Ducted PSS on KVLCC2 hull, we used SHIPFLOW 6.5 together with lifting line approach for propeller thrust simulation. Wave resistance and sinkage and trim of the hull were simulated by potential flow solver in SHIPFLOW and added to the double-body viscous self-propulsion simulation. The EASM turbulence model was used on a structured mesh with 28 million cells and $y^+=1$. Average Hull Roughness was considered aa AHR=100 micron. The transverse projected area above the water line of the KVLCC2 hull was assumed $A_T=1200$ m^2 and was included in the resistance estimation using ITTC empirical formula.

The next series of CFD simulations were performed using NUMECA/FineMarine 9.2. Unsteady RANS simulation with free-to-heave and pitch, full-scale hull was performed. Sliding mesh was used for the rotating propeller in self-propulsion simulation. The modelling approach for free-surface was Volume of Fluid (VoF) and SST k-ω was selected as turbulence model. Equivalent sand grain height of 90μm was considered as equal to the AHR=100μm and for all the surfaces (except deck), No-Slip boundary condition was used with wall-function.

Hexpress 8.2 was used to create two domains belong to hull and cylindrical sliding mesh around propeller. In total 16 million unstructured cells were used in the computation which consisted of 6.5 million cells for propeller domain. The wall function was used with $y^+=250$. Fig.8 shows a cross-section of the mesh, including sliding mesh around the propellers.

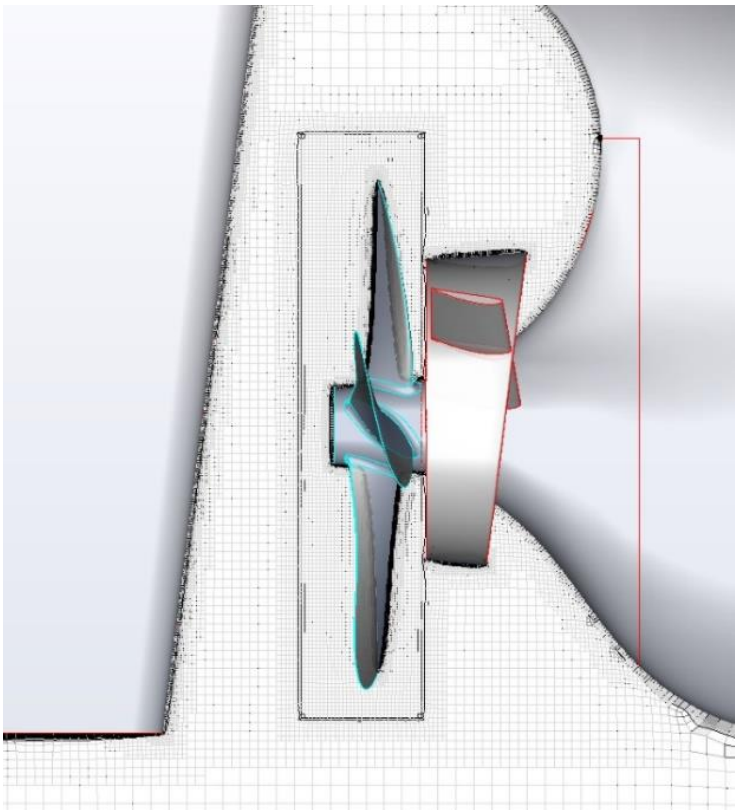

Fig.8: HEXPRESS mesh for KVLCC2 hull with propeller sliding mesh

For self-propulsion simulation, initial quasi-static time-marching simulation was performed to ramp the hull speed and allow the hull motion to stabilize. Then computation continued with unsteady, rotating propeller with much smaller time steps to balance the resistance and thrust forces. A built-in PID controller was responsible for automatically changing the propeller RPM to achieve the force balance.

4. Simulation Results for KVLCC2

FineMarine simulation for the full-scale hull without propulsion provided hull resistance, sinkage, and trim values. Axial velocity component contour is presented in Fig.9 for hull with and without ducted PSS. The azimuthal distribution of hull wake is modified with the stators and duct.

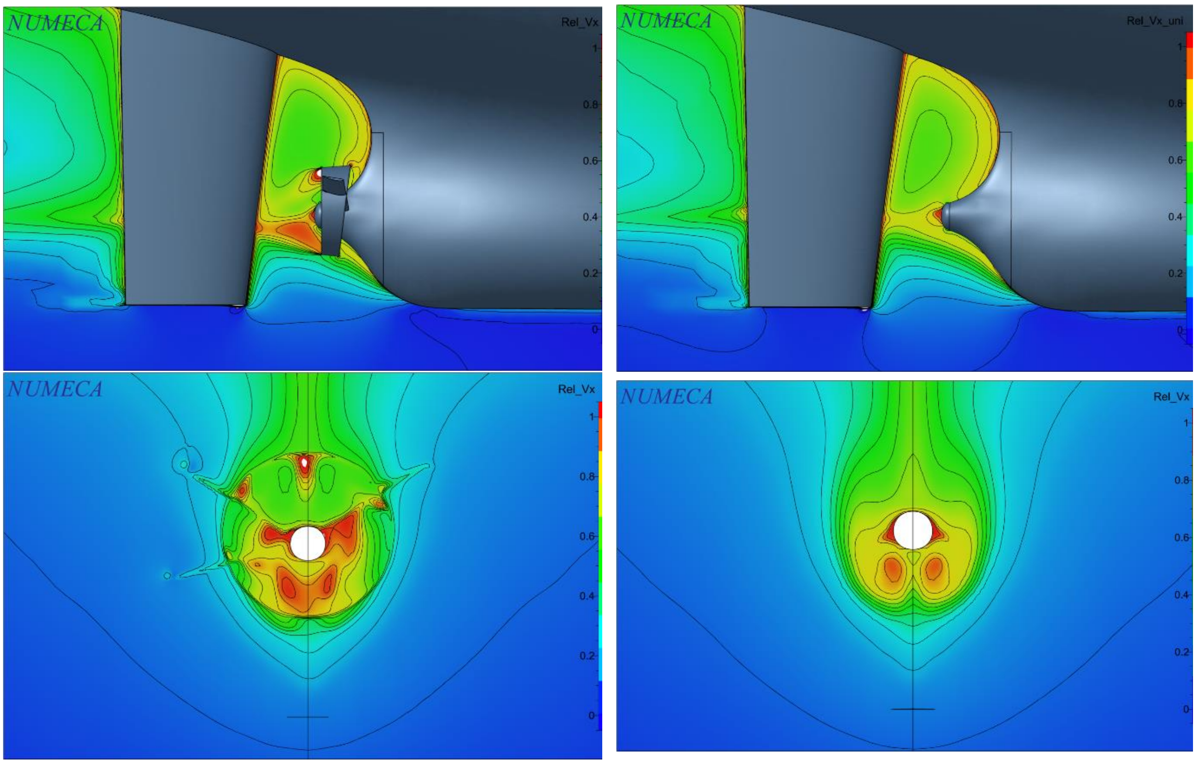

a. KVLCC2 hull with ESD

b. KVLCC2 hull

Fig.9: Full-scale resistance simulation of KVLCC2 with and without ESD at 15 kn

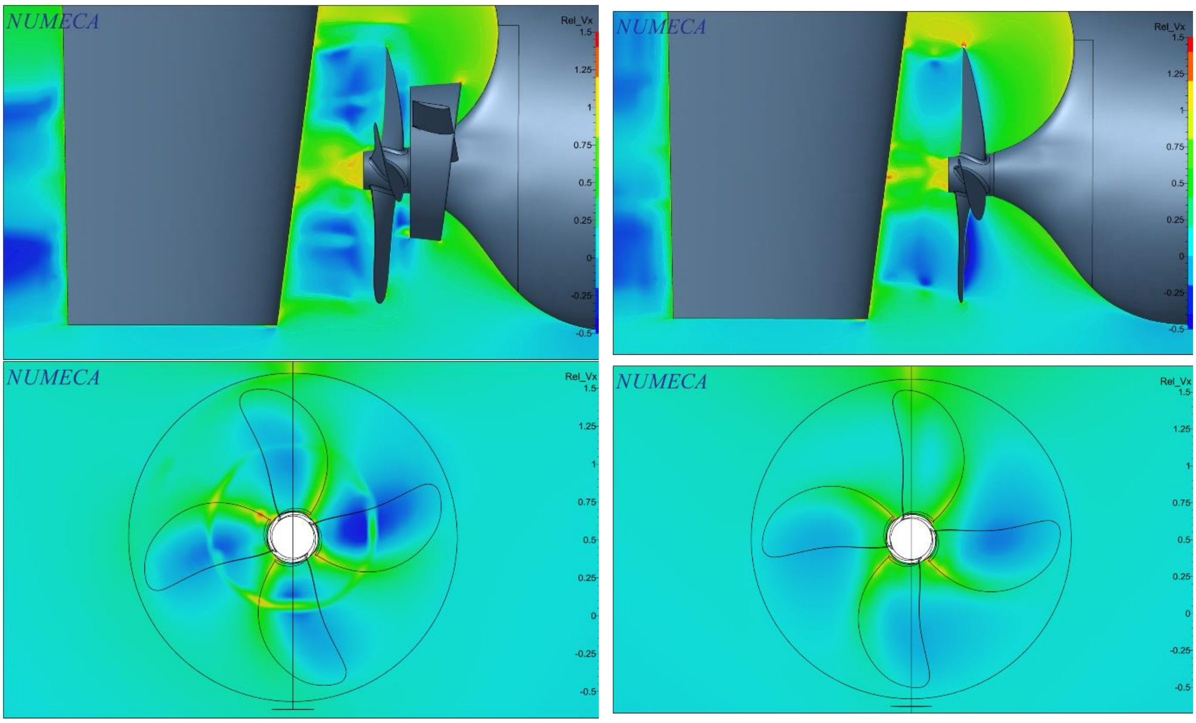

a. KVLCC2 hull with ESD

b. KVLCC2 hull

Fig.10 – Full-scale self-propulsion simulation of KVLCC2 with and without ESD at 15kn.

The self-propulsion FineMarine simulation result over-predicted the adjusted RPM and ESD showed adverse effect on delivered power required for self-propelled hull. Surface roughness value selected for hull played an important role on full-scale self-propulsion computation in which it directly increased thrust required to overcome the hull resistance.

Fig.10 is a snapshot of the axial velocity field with the working propeller with and without ESD at speed of 15 kn. Transverse cross-section contour is located after ESD and before propeller. Modified wake has a balanced distribution of velocity on the entire circumference of the propeller. The computational results were submitted to a workshop and published in *Andersson et al. (2022).*

6. KVLCC2 Benchmark Study and Conclusion

The result of KVLCC2 simulation using FineMarine was presented in a workshop organized together with Chalmers university where in total 10 different participants submitted their computations for the hull with ESD designed in SSPA, *Andersson et.al (2022)*. Eight different CFD codes were used in the study and power difference predictions are presented in Fig.11. The submitted results included some outliers, but even the rest of computations were not conclusive in providing performance enhancement for the hull with ESD.

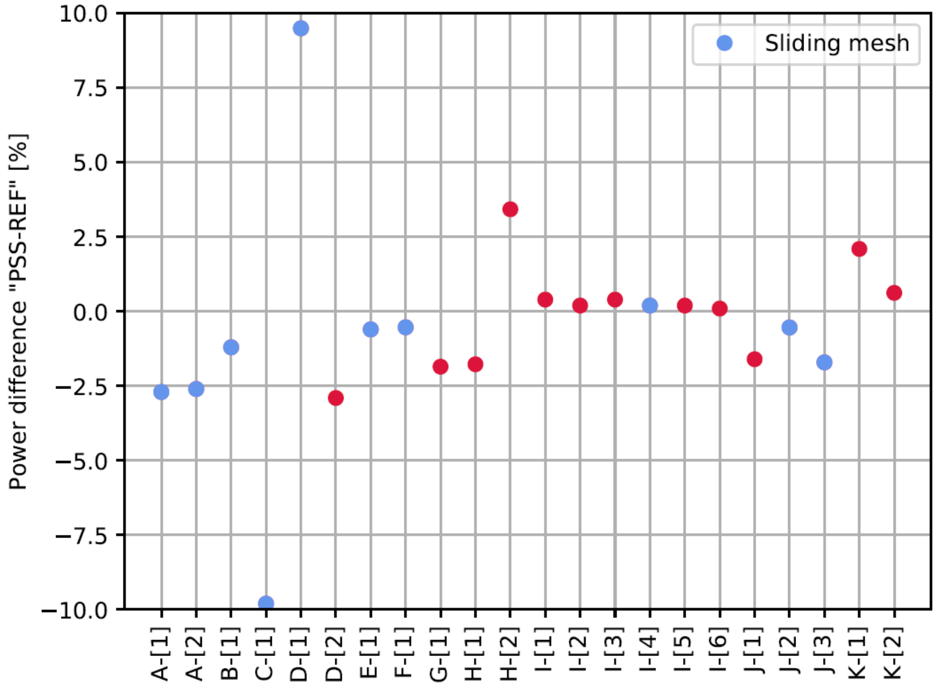

Fig.11: Delivered Power difference for 22 computations by 11 participants submitted in the workshop

Scatter in the result suggests the influence of different propulsion models, either a fully modelled propeller with sliding mesh (blue dots) or simplified potential-flow based models (red dots). Participant were asked to consider full-scale hull roughness equivalent to AHR=100µm, there was also different approach on implementing the roughness effect, either directly in CFD computation or by empirical correction. As roughness plays and important role on wake field formation, different approaches might have predicted the performance of ESD differently.

Overall, the workshop result showed important factors to be considered while performing direct full-scale self-propulsion CFD simulation. There are direct links between assumed roughness, correct trim angle and sinkage and propulsion model with the required hull thrust. Self-propulsion simulation uses PID controller and adjust propeller RPM to compensate for the total hull resistance. The inflow and outflow conditions of the propeller would augment the flow condition for ESD therefore makes it difficult to compare ESD efficiency in different simulations.

A propeller is designed or selected for specific hull with a given resistance and hull wake. Since propeller re-design is not included for the ESD evaluation process, additional appendages change the hull resistance and required thrust. Using the same propeller constitute a change in the propeller RPM to deliver the thrust, which is reflected in delivered power change as rotational speed directly correlates with the delivered power ($P_D = Q \times \omega$). This closed feedback loop affects the simulation result independent of the computational quality of the simulation or CFD model selection. Clearly, we need a well-defined strategy for full-scale CFD simulation to reduce inter-dependent parameters for comparing the results.

Acknowledgements

The study was supported by the Swedish Transport Administration (TRAFIKVERKET), grant number TRV 2018/76544.

References

ANDERSSON, J.; SHIRI, A.; BENSOW, R.; YIXING, J.; CHENGSHENG, W.; GENGYAO, Q.; DENG, G.; QUEUTEY, P.; XING-KAEDING, Y.; HORN, P.; LUCKE, T.; KOBAYASHI, H.; OHASHI, K.; SAKAMOTO, N.; YANG, F.; GAO, Y.; WINDEN, B.; MEYERSON, M.; MAKI, K.; TURNOCK, S.; HUDSON, D.; BANKS, J.; TERZIEV, M.; TEZDOGAN, T.; VESTING, F.; HINO, T.; WERNER S. (2022), *Ship-Scale CFD Benchmark study of a Pre-Swirl Duct on KVLCC2*, Applied Ocean Research 123

BROBERG, L.; ORYCH, M. (2013), *Energy Saving Device Evaluation in Full Scale Computational Fluid Dynamics,* Int. Conf. Ship and Offshore Technology, ICSOT India

CARLTON, J.S. (2012), *Marine Propellers and Propulsion*, 3rd Edition, Elsevier

DYNE, G. (1995), *The Principles of Propulsion Optimization,* RINA spring meeting, London

KIM, K.; LEER-ANDERSEN, M.; WERNER, S.; ORYCH, M.; CHOI, Y. (2012), *Hydrodynamic Optimization of Pre-Swirl Stator by CFD and Model Testing,* 29th Symp. Naval Hydrodynamics, Gothenburg

KIM, K.; LEER-ANDERSEN, M.; ORYCH, M. (2014), *Hydrodynamic Optimization of Energy Saving Devices in Full Scale,* 30th Symp. Naval Hydrodynamics, Hobart

KIM, K.S.; KIM, Y.C.; KIM, J.; LEE, Y.Y.; AHN, H.S.; YIM, G.T.; LEE, C.Y.; VAN, S.H. (2013), *Practical Application of CFD for Design of Energy Saving Devices Mounted on Ship Stern,* 23rd Int. Offshore and Polar Eng. Conf., Anchorage

KIM, M.C.; SHIN, Y.J.; LEE, W.J.; LEE, J.H. (2017), S*tudy on Extrapolation Method for Self-Propulsion Test with Pre-Swirl Device.* 5th Int. Symp. Marine Propellers (SMP17), Espoo

KRASILNIKOV, V.; KOUSHAN, K.; NATALETTI, M.; SILEO, L.; SPENCE, S. (2019), *Design and Numerical and Experimental Investigation of Pre-Swirl Stators PSS,* 6th Int. Symp. Marine Propulsors (SMP19), Rome

LARSSON, L.; STERN, F.; VISONNEAU, M. (2014), *Numerical Ship Hydrodynamics - An assessment of the Gothenburg 2010 Workshop,* Springer

LEE, I.; GOSE, J.; CORADDU, A.; CHEN, J.; HINATSU, M.; QUEREDA, R.; LI, T. (2021), *The Specialist Committee on Energy Saving Methods,* Final Report and Recommendations to the 29th ITTC

NIELSEN, J.R.; JIN, W. (2019), *Pre-Swirl Fins Adapted to Different Operation Conditions,* 6th Int.

Symp. Marine Propulsors (SMP19), Rome

SHIN, H.J.; LEE, J.S.; LEE, K.H.; HAN, M.R.; HUR, E.B.; SHIN, S.C. (2013), *Numerical and Experimental Investigation of Conventional and Unconventional Pre-swirl duct for VLCC,* Int. J. Naval Architecture and Ocean Eng. 5, pp.414-430

VAN TERWISGA, T. (2013), *On the Working Principles of Energy Saving Devices*, 3rd Int. Symp. Marine Propulsors (SMP13), Launceston

WALD, Q. (1965), *Performance of a Propeller in a Wake and the Interaction of Propeller and Hull*, J. Ship Research 9(02), pp.1-36

On the Evaluation of Uncertainty of AI models for Ship Powering and its Effect on Power Estimates for Non-ideal Conditions

Efthymia Ofelia Tsompopoulou, DeepSea Technologies, Athens/Greece, E.Tsompopoulou@deepsea.ai
Andreas Athanassopoulos, DeepSea Technologies, Athens/Greece, A.Athanassopoulos@deepsea.ai
Elli Sivena, DeepSea Technologies, Athens/Greece, E.Sivena@deepsea.ai
Kyriakos Polymenakos, DeepSea Technologies, Athens/Greece, K.Polymenakos@deepsea.ai
Vasileios Tsarsitalidis, DeepSea Technologies, Athens/Greece, V.Tsarsitalidis@deepsea.ai
Antonis Nikitakis, DeepSea Technologies, Athens/Greece, A.Nikitakis@deepsea.ai
Konstantinos Kyriakopoulos, DeepSea Technologies, Athens/Greece, K.Kyriakopoulos@deepsea.ai

Abstract

Accurate modelling of vessel behaviour has never been more important in the shipping industry. While data-driven methods and deep learning approaches are rapidly gaining popularity, the lack of an established and universal process for assessing the accuracy of a vessel's model is a significant obstacle to widespread adoption throughout the sector. In this work, we present an evaluation methodology, based on a dataset-splitting scheme, that aims to reveal a given model's robustness or deficiency in the face of the distributional shifts that inherently characterise many maritime datasets. As part of this process we examine the results through the lens of predicted uncertainty, yielding useful information about a model's fitness in dealing with uncertain and noisy regions in the modelled dataset. We introduce a realistic synthetic dataset allowing for the systematic study of model's performance under a distributional shift. In the proposed dataset: a) we model all aspects of drag as described by the literature, including the rate of hull fouling through time; b) our input features are real samples from on-board sensors collecting data at high frequency; and c) we inject different patterns of noise to measure the model's predictive uncertainty performance. The outcome is a repeatable and robust methodology that allows for the assessment of vessel performance models within the context of their used environment - having a direct impact on a models' deployability and, ultimately on their ability to deliver meaningful insights.

1. Introduction

Environmental regulations, fuel prices, and societal factors all push stakeholders to work even harder to reduce the shipping industry's carbon footprint. At the moment, simply doing their best and/or purchasing equipment labelled "eco" is insufficient. Vessel performance must be measured and evaluated on a continuous basis to establish changes over time and benchmark against the global fleet. With the introduction of EEXI and CII, as well as emissions trading schemes, every vessel will need to be set on a path of continuous improvement, as well as objective measurement of performance. To this end, each stakeholder will have to employ a variety of tactics, ranging from technical retrofits to alternative fuels, condition-based maintenance, and operational measures. One of the most accessible means of boosting performance is to develop a new layer of understanding about what really influences vessel performance. Modelling the real-world performance of the hull and propeller will allow safer decisions on timely cleaning. Furthermore, such modelling can aid in the evaluation of other investments (e.g., antifouling paint, ESD retrofits, etc.) and provide a clearer image of each vessel's operational capabilities, such as charter party description or bunker budgeting. Using the same data, legislators and authorities can estimate the environmental impact of best practices and thus plan future regulations. With detailed vessel performance models in hand, operators can optimise a ship's route and speed profile to reduce fuel consumption. Such a strategy has been widely recognized as the most immediate way of making an impact on emissions, with potential for remarkable results yet requiring low up-front investment. However, the extent to which this approach translates into realised emissions and fuel savings is highly dependent upon the accuracy and granularity of the models that underpin it.

All of the above strategies necessitate an objective method for measuring their impact on reducing fuel consumption and tracking progress in decarbonization efforts. With the advent of ISO 19030, *ISO*

(2016), a standard that levels the playing field was introduced, and a reference frame to follow was set for everyone who cares about their vessels' performance. A good framework was set, consisting of minimum required data to be collected, and criteria for outliers and basic filtering (even though it can be very restrictive). In the core of ISO 19030 the major point of strength, but also vulnerability, is the Reference Model, which (for now) can only be constructed using towing tank tests, sea trials and "detailed" CFD calculations. As discussed in *Tsarsitalidis and Rossopoulos (2018)*, special attention is needed to the quality of the model, which makes its production more expensive for the owner, while also maintaining a series of potential issues. Missing Hull, Propeller and Appendages information, push the model builder to make assumptions with serious impact and possibly several trial-and-error iterations until a safe model is reached, if at all.

Hull interaction factors can be difficult to estimate, especially in the case of retrofits, while even if experimental data are available, they are usually collected for a narrow set of conditions (speeds, drafts) and very rarely simulated for rough (i.e. non-calm) sea. Additionally, the effects of swell are completely disregarded. Even when everything is executed perfectly, the ISO provides a reliable and objective evaluation of performance change only in good weather and steady conditions. It is safe to assume that an improvement in hull roughness and drag measured in good weather will remain an improvement in rough seas or unsteady conditions, but it cannot be taken for granted that any hydrodynamic retrofit will maintain its good characteristics in non-ideal conditions. Furthermore, the current version of the ISO does not permit such testing to confirm or disprove any technology.

In response to such problems, data driven methods are on the rise, where deep learning is showing serious promise, *Górski et al. (2021), Levantis et al. (2020), Gonzalez et al. (2019), Park et al. (2018)*, but even these are not void of limitations and potential problems. A fundamental issue with such models is the lack of formal performance guarantees that would specify sufficient conditions before training for the models to reach a certain level of performance. Consequently the accurate model evaluation after training but before deployment is of paramount importance. In practice, these complex models are usually evaluated on some part of the available dataset that has been held-out during training, based on one or more simple error metrics, such as the root mean square error and the mean absolute percentage error.

The underlying assumption of this standard evaluation practice is that the training, validation and deployment datasets are independent and identically distributed (i.i.d.) and thus testing on the available dataset is indicative of performance at the deployment phase. Unfortunately, this assumption does not hold in real world applications, where the data distribution of the training and the validation set shift from the distribution the model faces when finally deployed, *Malinin et al. (2021)*. Recently, significant research effort has been invested into the accurate evaluation of ML models, especially in high risk or sensitive contexts, *Amodei et al. (2016)*.

Furthermore, even assuming that we have a unique and accurate numerical estimate quantifying the average predictive accuracy of a model, there is still essential information missing. A model that is overall fairly accurate can be wildly inaccurate in a relevant subset of the dataset, and this mismatch between the on-average and the worst-case performance can lead to catastrophic down the line decision making (e.g. weather routing). The notion of predictive uncertainty, where the model provides not only a prediction, but also an estimate of how confident it is for that particular prediction, allows for more nuanced risk analysis and more effective planning. Although there is a plethora of methods for estimating predictive uncertainty that can be compatible with deep neural networks, a solid evaluation procedure is needed to assure that the researched models are producing well calibrated uncertainty estimates.

Supporting this effort, we introduce a synthetic dataset (from SHIFT 2.0 challenge competition, https://www.deepsea.ai/datasets) along with a well-thought split that could help in the direction of systematic evaluation of deep learning models. We show that predictive uncertainty can reveal important information regarding the distributional shift between training and testing but also regarding the dataset splits and the noise levels of the target signal. Although working with a synthetic dataset we are not limited by it, since the same process can be transferred in real datasets. We hope that this work will positively impact the shipping industry into trusting and adopting deep learning methods with predictive uncertainty in vessel performance modelling.

2. Background

In recent years, Machine Learning and Artificial Intelligence (AI) methods have achieved state-of-the-art (SOTA) performance utilising large amounts of data, becoming the default option to solve fundamental problems in various domains such as computer vision, *Krizhevsky et al. (2012)*, speech recognition, *Hinton et al. (2012),* natural language processing, *Mikolov et al. (2013),* and bioinformatics, *Alipanahi et al. (2015); Zhou and Troyanskaya (2015), Ramsundar et al. (2015)*. These advances have brought an increasing number of practical production level autonomous decision systems with high-risk outcomes for their users, such as in finance, medicine, autonomous vehicles and in shipping *Coraddu et al. (2019)*.

The key argument in favour of ML methods is that while traditional methods rely relatively more heavily on expert prior knowledge and expensive computation at inference time, i.e. whenever predictions are needed, ML methods utilise more efficiently larger datasets and computational resources at training time, which can be done offline, with relatively smaller prediction costs. Given the clear trend towards larger and larger datasets, and the development of increasingly sophisticated computational resources dedicated for ML applications, a strong case can be made for the future of ML methods in shipping. While a plethora of ML methods have been presented, each with its unique pros and cons, at the current state of ML research, deep neural networks tend to be the default choice for a great number of tasks, especially those with abundant, unstructured datasets.

Machine learning in shipping is relatively new. A good review of early attempts can be found in *Coraddu et al. (2019)*. A machine learning approach to outlier detection and filtering was shown by *Gonzalez and Arango (2019)*, where it was proven to be extremely difficult to distinguish between anomalies and ship operation induced bias (despite the use of high quality sensors and very low overall noise), while the need of ship specific parameters in filtering was recognized. *Gorski et al. (2021)* displayed the potential of unsupervised learning algorithms, by means of clustering and identifying the most frequent modes of operation of a vessel and building the baseline model for these conditions, with the obvious limitation of being restricted to the specific modes of operation. Thus, the problem of reliable generalisation remains, and uncertainty modelling is possibly our best way of measuring (and then improving) the quality of our models.

2.1. Uncertainty and Modelling

In machine learning there are two distinct types of uncertainty that can be modelled: aleatoric and epistemic uncertainty, *Kiureghian and Ditlevsen (2009)*, while the term total uncertainty refers to their sum. Aleatoric uncertainty captures the inherent stochasticity of the problem, with the rolling of a dice being the prototypical example. This type of uncertainty is not reduced with additional data, as the extra data do not affect the stochastic nature of the problem. Epistemic uncertainty on the other hand captures the uncertainty introduced by incomplete information about the data generating process. As we obtain more data, epistemic uncertainty can be reduced.

There has been significant effort in recent years to combine the power of deep neural networks with the probabilistic techniques that allow for uncertainty estimation and decomposition. Various terms have been used in the research community: Bayesian deep learning (BDL), *Wang and Dit-Yan (2020)* usually refers to a general framework that combines probabilistic thinking with deep learning, that sometimes includes self-supervision and active learning, while Bayesian Neural Networks (BNNs), *Goan and Fookes (2020),* usually refer to deep neural networks augmented with appropriate techniques to support uncertainty quantification. The most popular methods are based either on variational inference, dropout, or ensembles of networks, *Lakshminarayanan et al. (2017)*.

2.2. Generalisation and Distributional Shift

Training a ML model usually involves minimising an error metric on the available dataset (empirical risk minimization, ERM), while the actual goal is to minimise the expectation of the error over the unknown data generating distribution, also referred to as the risk, *Hardt and Recht (2021)*. The generalisation gap is defined as the difference between the empirical error and the risk, and intuitively is the difference in performance of the model on the data it has been trained on, compared with unseen data from the same distribution. Distributional shift takes the notion of generalisation a step further, taking into account the model's performance when evaluated on unseen data coming from a different data generating distribution, in comparison to its performance on unseen data from the same distribution as the training data. It's worth noting that robustness to arbitrary distributional shifts is impossible: the two distributions have to be in some sense similar for the model to perform well (for a detailed breakdown see *Moreno-Torres et al. (2012)*). Both a large generalisation gap and a large performance degradation due to distributional shift are often interpreted as proof that the model is overfitting. This is partially accurate, since not measurable (within available dataset) overfitting is a necessary but not sufficient condition for good generalisation and robustness. Various inherent biases in the sampling process due to extended missing rate or sailing in specific conditions can significantly bias the model without being detectable within the given dataset by using the common model cross validation procedures. The analysis of such selection biases and to what extent they could affect the model's generalisation ability could be the focus of future work.

Under this scope, we propose an evaluation methodology built around a carefully designed dataset partitioning scheme aiming at exposing a model's robustness to large distributional shifts. For the purposes of this study the dataset is synthetic, but the same methodology could be transferred to real ones. As part of the proposed methodology, we analyse the results through the lens of predictive uncertainty as it can reveal useful information about the model fitness in handling uncertain and noisy regions in the modelled dataset. In order to make the dataset as realistic as possible: a) we model all aspects of drag as dictated by the naval engineering literature including hull fouling effects over time b) our input features are real samples from high frequency on-board sensors (i.e real seeds), augmented with real weather data and c) we inject different patterns of noise to measure the performance of model's predictive uncertainty.

3. Methodology

3.1. Synthetic dataset

In this work we introduce a synthetic dataset based on real vessel's seeds and realistic noise to train and evaluate machine learning models. There are multiple distinct advantages that come with this choice, along with certain drawbacks. First and foremost, a synthetic dataset provides access to the ground truth values of all data points. These values can be corrupted by noise if needed, e.g. to test the model's robustness to noisy training data, while the targets without noise can still be used for evaluation. Additionally, the availability of the ground truth labels gives us complete control over the introduced noise both in terms of its magnitude (as we can control the signal to noise ratio) and its properties (uniform white Gaussian noise, heteroscedastic noise etc.). The synthetic dataset also allows us to create as much data as needed (will be explored in a future work), distributed according to the demands of each particular experiment, while a real dataset would only allow choosing a subset of its data points to simulate such effects. Finally synthetic datasets can eliminate data confidentiality concerns, and as a result promote sharing methods and results. On the other hand, synthetic datasets may deviate from real world data, by failing to simulate realistic scenarios or inaccurately portraying some of their properties, and thus casting doubts on whether the conclusions will hold in practice.

Since the focus of this work is to systematically highlight possible complications with the deployment of neural network models through a well thought dataset partitioning, the need of a well-controlled synthetic dataset was necessary. This is not limiting though, since one could apply the suggested dataset partitioning along with the proposed predictive uncertainty measures to real datasets as well.

3.2. Dataset construction

3.2.1. Synthetic model

The Synthetic model is a generative function ($f_{synthetic}$) taking as input a time-series of features (i.e. signals), as recorded from a real vessel, and calculates the power consumed by the vessel's hull. This function finds the propeller cooperation point after calculating all the components of resistance (bare hull, appendages, wind, waves, fouling drag) for given speed, draft and trim. More specifically, for the generation of synthetic data, a non-linear solver script was created to find the operating point of a given propeller and hull resistance for each desired condition, as described by *Bose (2008)*. The propeller curves (K_T, K_Q) can either be user defined or use the B-Series, *Van Lammeren et al. (1969)*. For the resistance part, the calculation of each component can be described as follows: having the full hydrostatics table of the vessel for the whole range of drafts and trims, along with a series of geometric characteristics (bulb shape and size, transom, appendages etc.), calm water resistance is calculated by employing the Holtrop method for slender ships (i.e. containers, RoRo, gas carriers) and modified Holtrop, *Nikolopoulos and Boulougouris (2018)*, is used for bulkier ships like big tankers and bulk carriers. Following the ISO 15016, *ISO (2015)*, the weather added resistance is found by calculating the wind effect by using the regressions of *Fujiwara et al. (2006)*, while the wave effects are modelled according to STAwave1 and STAwave2 as also introduced by *Tsujimoto et al. (2008)*. Hull Interaction factors are calculated depending on ship type, using empirical formulas, a summary of which can be found in *Carlton (2018)*. Scale effect corrections, cavitation criterion and corrections were also taken from *Carlton (2018)* and *Bertram (2012)*. The effect of wake affecting energy saving devices can be modelled by adjusting the interaction factors. Fine tuning of the method to fit a specific vessel (when there is not enough hydrostatic data, or discrepancies are observed), can be done by using sea trial data and/or detailed factors when available from towing tank report, or actual measurements of well-known conditions. Last but not least, the effect of fouling is modelled as the result of its manifestations (drag, propeller and interaction). The change in drag coefficient is modelled after *Townisn (1981)*, the effect of fouling on the propeller performance is modelled as in *Seo et al. (2016)* (increase in torque coefficient), as also described in *Carlton (2018)* and the change of interaction factors are modelled after *Farkas et al. (2020)*. All the aforementioned models produce the effect of fouling on each component over time, which is measured from each drydock / cleaning event.

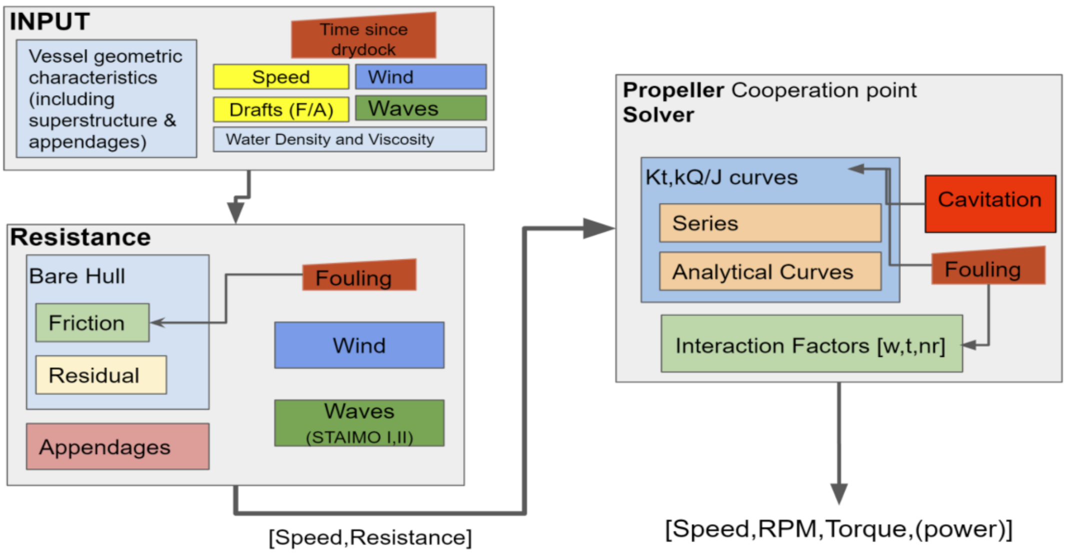

Fig.1: Structure of the synthetic model. The model consists of two main parts, resistance and propulsion solver. The first part (resistance) calculates all the components of resistance for given speed, drafts and weather conditions based on the ship characteristics and time. Then, the Propulsion solver finds the cooperation point for the calculated resistance and speed, with given propeller characteristics and interaction factors.

The resulting program is depicted in Fig.1 and given the characteristics and data of an actual ship, it can estimate the power, rpm and torque, for any given combination of Speed, Draft, Trim, weather conditions, and time since the last drydock, within the limitations of the methods used. The primary vessel particulars are given in Table I for reference.

Table I: Ship Characteristics for bulk carrier

Length Overall	292 m
Length BP	282 m
Breadth (Mld)	45 m
Depth (Mld)	24.8 m
Design Draft	16.5 m
Scantling Draft	18.3 m
Deadweight (at Tdesign)	176364 tdw
main engine MCR	16860 kW
Design speed	14 kn
Operating Speed	13.5 kn

3.2.2. Dataset features

For the current investigation, the dataset is created by combining the real samples with synthetic power labels generated by our synthetic model as described in subsection 3.2.1. The real vessel's records have been sampled on a per minute basis covering a time period of more than four years. The available features as presented in Table II, are recorded by on-board sensors, the global positioning system (GPS) and are augmented with weather data from a global weather provider. The data is preprocessed to remove stationary states, for example when a vessel is at port.

Table II: Available features of synthetic set

Synthetic power	kW	Synthetic propeller shaft power (Target)
Draft aft	m	Vessel's draft at stern from noon reports
Draft fore	m	Vessel's draft at bow from noon reports
Stw	kn	Speed through water
Acceleration	Kn / 3 min	Acceleration over ground
Apparent wind speed	kn	Apparent wind speed
Apparent wind vcomp	kn	Apparent wind component along vessel's direction of motion
Apparent wind ucomp	kn	Apparent wind component perpendicular to vessel's direction of motion
Recurrent vcomp	kn	Relative current component along vessel's direction of motion
Recurrent ucomp	kn	Relative current component perpendicular to vessel's direction of motion
Combined waves height	m	Combined wind(sea) and swell wave height
TimeSinceDryDock	min	Time feature quantifying the time period from the last Dry Docking cleaning event

3.2.3. Dataset Partitioning

The focus of this work is to help with the development of robust models with high quality uncertainty estimates on distributional shifts. Under this scope and motivated by the canonical partitioning of the weather dataset presented in *Malinin et al. (2021)*, we split the synthetic set in two dimensions: time (No cleaning events take place during the time period covered by the synthetic set.) and true wind speed as illustrated in Fig.2, using the wind speed intervals of Table III. The time dimension aims to capture the non-stationary effects of fouling while the wind speed dimension aims to capture weather effects (by being a proxy since wind is correlated with wind-waves) and to better expose the model's performance in bad or uncertain weather. Partitioning the dataset in more dimensions would have added complexity without practical benefits since the most important factors of uncertainty (weather and fouling) are already represented.

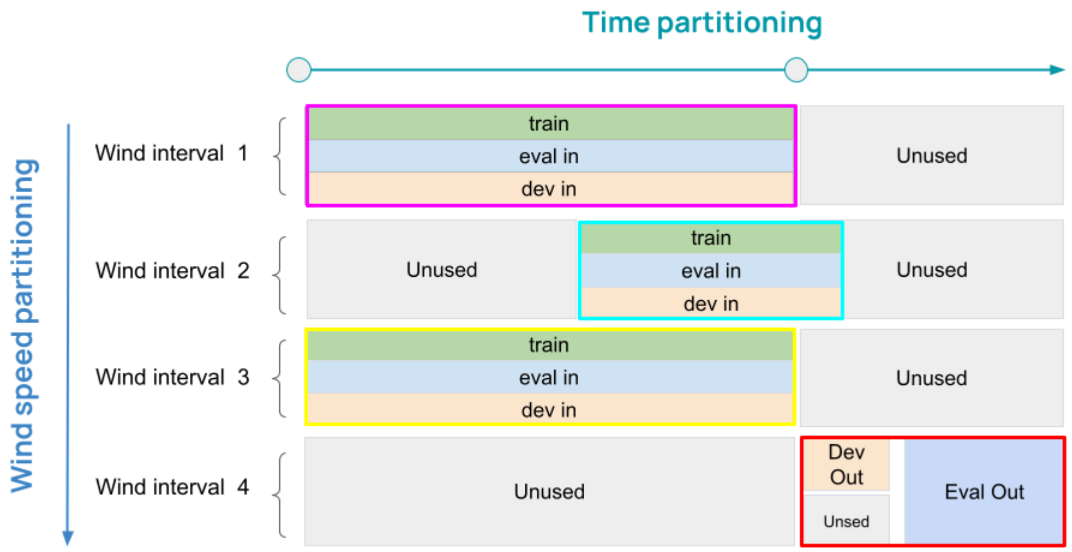

Fig.2: Canonical partitioning of synthetic set

The proposed partitioning has the primary goal of assisting in evaluating the true performance of a model given a real dataset as nearly as possible. To systematically demonstrate its efficacy for this study, we had to employ a synthetic but nonetheless realistic dataset, allowing us to preserve full control over the dataset properties while also having access to ground truth labels.

Three main subsets are created from the proposed partitioning: the train set, used for model training, and the development and evaluation sets, used for the evaluation of the model performance.

In more detail:

- Train set: It covers the time range of 39.4 months starting after a dry-docking cleaning event and includes data with true wind speed up to 19 kn.
- Development set: It consists of an in-domain partition dev_in and an out-of-domain partition dev_out, with equal representatives achieved by downsampling dev_out to match the number of records of dev_in. Dev_in is sampled from the same partitions as the train set while dev_out includes more recent records (time period of 6.6 months) that correspond to wind speeds in range [19, 26) kn.
- Evaluation set: Same as for development set, evaluation set has an in-domain eval_in and an out-of-domain partition eval_out having equal populations (eval_in is downsampled in this case). Eval_in is sampled from the same subsets as the train set. Eval_out is the most shifted partition from the in-domain distribution, including the most recent records covering a time period of 18 months and the most severe wind conditions encountered in the dataset, corresponding to wind speed range [19, 40] kn.

Table III: Wind intervals considered for data partitioning. Beaufort ranges are defined approximately.

Wind interval	Range (kn)	Range in Beaufort
1	[0, 9)	Up to ~3
2	[9, 14)	3-4
3	[14, 19)	4-5
4	≥19	≥ 5

Table IV shows the number of records of the proposed partitions (rows) along with the respective populations in each 2D segmentation of the synthetic set (columns with prefix group).

Table IV: Number of records in the canonical partitioning of synthetic set. The colored borders of the group columns indicate the dataset segmentations from which the partitions are sampled following the same color notation as in Fig.2.

Data	pct (%)	total	Group 1	Group 2	Group 3	Group 4
train	80.3	523190	231626	118698	172866	0
dev_in	-	18108	8017	4108	5983	0
dev_out	-	18108	0	0	0	18108
dev	5.6	36216	8017	4108	5983	18108
eval_in	-	46021	20355	10448	15218	0
eval_out	-	46021	0	0	0	46021
eval	14.1	92042	20355	10448	15218	46021

3.2.4. Target noise

One of the primary goals of this work is to investigate the quality of uncertainty estimation both within and outside of domain areas. Working with a synthetic dataset enables well-controlled noise pattern injection, which should be captured by the model's heteroscedastic predictive uncertainty. We apply two types of Gaussian noise with non-constant variance (heteroscedasticity) to the synthetic target y_i to make the synthetic set realistic for this task:

- heteroscedastic Gaussian noise correlated with power, $\varepsilon_{power,i} = N(0, a \cdot y_i)$. This type of noise simulates the scenario of linear deterioration of the torque meter accuracy as power increases,
- heteroscedastic Gaussian noise correlated with true wind speed, $\varepsilon_{wind,i} = N(0, b \cdot w_i)$. Synthetic data is partitioned based on true wind speed bands as presented in Table III. Therefore adding the noise ε_{wind} with variance linearly increasing with wind speed, results in partitions simulating varying data uncertainty as we move from the in-domain to out-of-domain ones. Such design, aims to capture the empirical observation that the most severe wind conditions encountered in the dataset, being the most uncertain.

where i = 1, …, M stands for the i-th record, w the true wind speed, $a = 0.025$ (at power 40 MW the standard deviation of heteroscedastic power noise is 1 MW) and $b = 25$ (at wind speed 40 kn the standard deviation of heteroscedastic wind noise is 1 MW). The synthetic power with noise is defined as:

$$y'_i = y_i + \varepsilon_{power,i} + \varepsilon_{wind,i}$$

4. Evaluation metrics and results

4.1 Shift metrics

Accurately assessing uncertainty estimation and robustness to distributional shift is a major objective of contemporary ML research, *Malinin et al. (2021)*. Robustness to distributional shift is usually defined as the ability of the model to preserve equally good performance when tested with a shifted dataset, or in other words a dataset that has been generated from a different process. Empirically, robustness is usually assessed by comparing the predictive performance of multiple models on different datasets, one of which is considered to match the original data distribution. The model with the smaller degradation in performance is prefered.

Uncertainty estimation is the ability of the model to provide a quantitative number that represents the model's confidence along with each prediction. It is often expressed in probabilistic terms, with the value of the prediction as the mean of a distribution, and the uncertainty captured with some measure of dispersion (e.g. the variance for Gaussian distributions). Evaluating uncertainty estimation is a challenging task mainly because there is no direct way to evaluate the performance of the models, as there is no "ground truth" for uncertainty scores. Usually uncertainty estimation is assessed by the ability of the model to identify artificially shifted data points. Moreover, there is also an effort to jointly assess robustness to distributional shifts and uncertainty: if a model cannot provide accurate predictions due to distributional shift, it should at least provide high uncertainty estimates. To jointly assess robustness and uncertainty estimation *A. Malinin et al. (2021)* introduce the area under error-retention curves, Fig.3, for the R-AUC retention curve and the F1-AUC retention curve.

The key idea behind error-retention curves for a given error metric is calculating the metric at increasing fractions of the dataset, starting with data points with the least uncertainty, where the model's accuracy is expected to be the highest, and progressively adding points until the whole dataset is considered. For the part of the dataset that is excluded optimal performance is assumed. For an MSE retention curve, *Lakshminarayanan et al. (2017)*, *Malinin (2019)*, for example, every point (x,y) on the retention curve represents the MSE, as calculated for the x (x is between 0-1) fraction of the dataset with the lowest uncertainty, and assuming the error at the rest of the dataset is zero. For x=1 we recover the standard MSE over the whole dataset. The Area Under this Curve (AUC) takes into account both the accuracy of the model (lower MSE leads to smaller AUC) and the correlation between uncertainty and error (stronger correlation leads to smaller AUC). This metric, the area under the MSE retention curve, is referred to as R-AUC. *Malinin et al. (2021)* also propose considering the corresponding metric for the F1 score, namely the F1-AUC, because the R-AUC can be influenced disproportionately by the accuracy of the predictions in comparison to the accuracy of the uncertainty estimates. For the F1 score retention curve, in contrast to the MSE retention curve, the data points are sorted in descending order of uncertainty, and for every retention fraction the most uncertain part of the dataset is considered (see *Malinin et al. (2021)*.

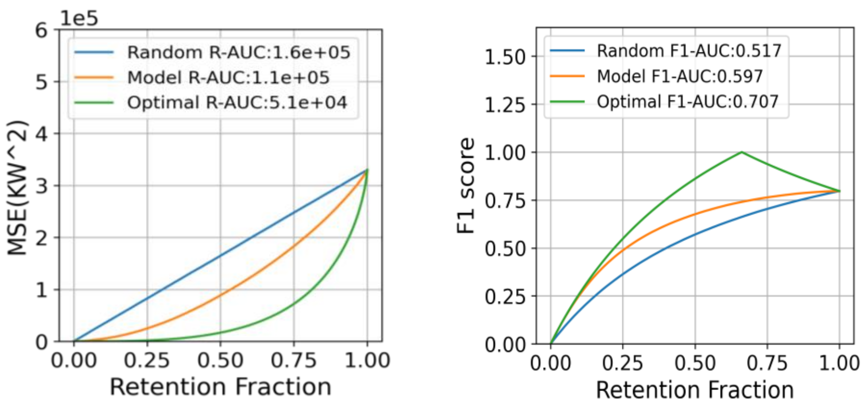

Fig.3: Representative examples of MSE and F1 retention curves

Fig.3 depicts two illustrative examples of retention curves, one using the MSE as the error metric and one using the F1 score. Please note that for the R-AUC a smaller area is better, as smaller MSE is better, while for the F1-AUC on the other hand a larger area is better, since larger F1-score values are better. The two plots refer to models with equal MSE and F1-score respectively, isolating the effect of varying degrees of correlation between uncertainty and error on the AUC metrics. The orange curve corresponds to the error ranking based on the uncertainty estimates of the model evaluated. The blue curve represents the worst-case scenario, where the data points are considered in random order, which is the case when the uncertainty estimates, and the prediction errors are uncorrelated. The green curve represents the case of perfect correlation of error and uncertainty estimates (optimal scenario).

4.2. Experimental results

To evaluate the proposed dataset partitioning through the prism of uncertainty, we use two baseline models, able to capture both epistemic and aleatoric uncertainty, in the form of an ensemble. These are: a) an ensemble of 10 variational inference neural networks (VIs) and b) an ensemble of 10 deep neural networks (DNNs), *Duerr et al. (2020)*. Each model predicts the parameters of the conditional Normal distribution $N(\mu(x_i), \sigma(x_i))$ of the target given x_i. The variance of $\mu(x_i)$ across the members of the ensemble corresponds to the epistemic uncertainty and the mean of $\sigma^2(x_i)$ across the members is a measure of aleatoric uncertainty, *Malinin et al. (2021)*. For both methods we use the same architecture: 2 hidden layers with 50 and 20 nodes and softplus activation function. The output layer has 2 nodes and a linear activation function. To satisfy the constraint of positive standard deviation the second output is fed through a softplus function and a constant 10^{-6} is added for numerical stability as proposed by *Lakshminarayanan et al. (2017)*. For optimization, we use the negative log likelihood loss function and the Adam optimizer with a learning rate of 10^{-4}. The number of epochs is defined by early stopping, with patience set to 20 epochs monitoring the mean absolute error (MAE) of the dev_in set. These two baselines are standard methods for the estimation of the conditional distribution that describes the target and are both reported for completeness, as no significant differences are expected taking into account that they have similar structure.

4.2.1. Power-speed simulations

For qualitative model evaluation, simulations of vessel performance in relation to weather and/or operational conditions are used. The data generation process (synthetic model) of the proposed evaluation protocol, offers a major advantage, allowing for direct comparison between model estimations and the ground truth solution. The variance of the generated synthetic data on the respective conditions, expressing the aleatoric uncertainty, is due to injected noise and is directly compared with the model's predictive aleatoric uncertainty.

Power-speed simulations produced by the baseline ensemble of DNNs for the design draft state and varying true wind conditions are illustrated in Fig.4. The first 3 rows (0 kn, head 16 kn, tail 16 kn) correspond to in-domain wind conditions and the last 2 rows (head 33 kn, tail 33 kn) to out-of-domain conditions. For the in-domain simulations, the estimated average trend is in good agreement with the ground truth solution within total estimated variance. Out-of-domain simulations exhibit a relatively pronounced underestimation of the power-speed trend at high speeds that is not explained by the estimated uncertainty in the case of head wind with speed 33 kn. Another important observation is that the estimated aleatoric uncertainty closely follows the pattern of the real target noise (depicted as blue data points in plots) for all simulated wind conditions. This is a strong indication that the estimated aleatoric uncertainty is well calibrated. Although an incremental tendency is observed at the extrapolated region of high vessel speeds, epistemic uncertainty is not considerable for the in-domain simulations (speeds that exceed the maximum speed recorded in the training data). An interesting out of domain observation is for tail wind with speed 33 kn, where notable epistemic uncertainty is found for both small and high vessel speeds.

<table>
<tr><th>True wind conditions</th><th colspan="2">Simulations</th></tr>
<tr><td>0 kn</td><td>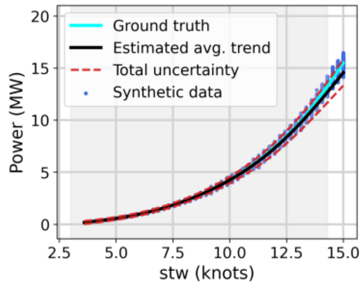</td><td>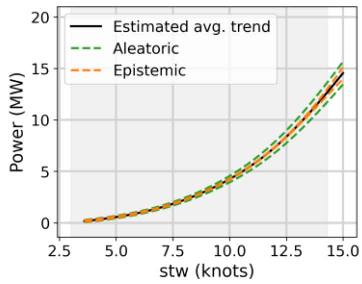</td></tr>
<tr><td>Head 16 kn</td><td>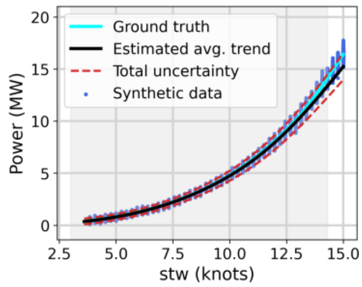</td><td>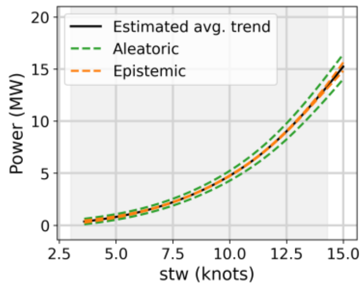</td></tr>
<tr><td>Tail 16 kn</td><td>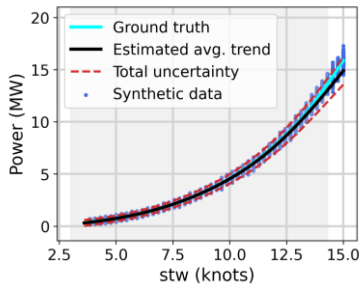</td><td>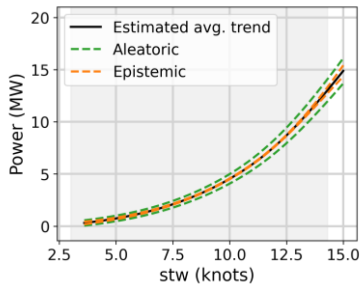</td></tr>
<tr><td>Head 33 kn</td><td>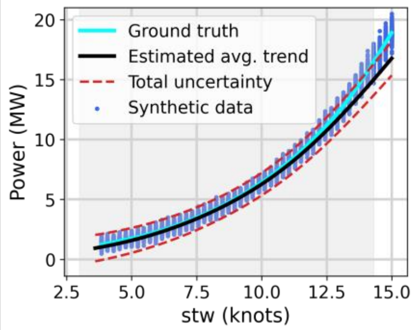</td><td>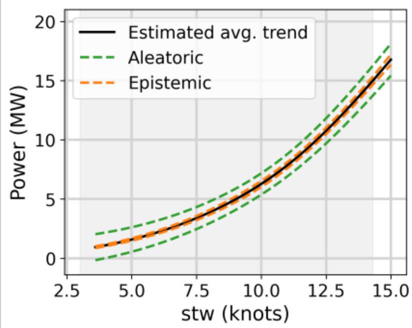</td></tr>
<tr><td>Tail 33 kn</td><td>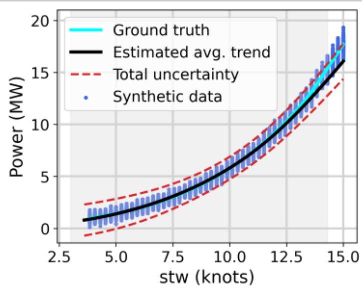</td><td>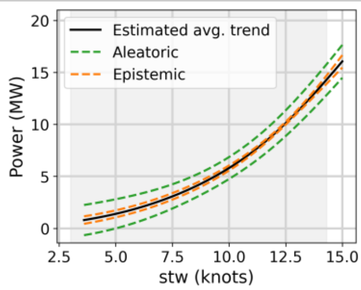</td></tr>
</table>

Fig.4: Power-speed simulations for the design draft state and various true wind conditions estimated by the baseline ensemble of DNNs. In the first column, the average estimated trend (black solid line) and the estimated total uncertainty (red dashed lines) is compared with the ground truth solution (cyan solid line). Synthetic data (blue points) are the noisy data produced by the synthetic model (generator) on the respective simulation conditions. Synthetic data indicate the real data spread due to target noise that should be captured by the estimated aleatoric uncertainty. The second column of plots depicts the estimated aleatoric (green dashed lines) and epistemic (orange dashed

lines) uncertainty along with the estimated average power-speed trend. All uncertainty boundaries correspond to ±3 standard deviations. The grey box in the background of the graphs delimits the speed range of training data regardless of the other feature dimensions. The blue box denotes out-of-domain simulations with respect to wind conditions.

4.2.2. Classical Metrics

For the evaluation of the robustness of models' performance to distributional shifts, we use the RMSE and MAE scores. In Table V, the predictive performance of the two baseline methods, (an ensemble of DNNs and an ensemble of VIs) is presented. It is observed that both methods exhibit the same trends; They have similar scores for the in-domain partitions, while the models' performance deteriorates for the out-of-domain partitions, having greater errors the more shifted the partition is. It is found that eval_out is the most challenging out-of-domain set, as expected, taking into account the partitioning method described in subsection 3.2.3.

Table V: Predictive performance of in-domain and out-of-domain canonical partitions of synthetic set

Data	RMSE (kW)		MAE (kW)	
	Ens. DNN	Ens. VI	Ens. DNN	Ens. VI
Dev in	572	571	436	436
Eval in	574	573	437	436
Dev out	691	703	547	555
Eval out	732	733	574	574

4.2.3. Uncertainty Metrics

Mean square error (MSE) and F1 retention performance metrics (R-AUC and F1-AUC respectively) for two baselines under study are presented in Table VI and the respective retention curves for the ensemble of VIs are illustrated in Fig.5 and Fig.6. Following the methodology proposed by *Malinin et al. (2021)* we use the MSE as the error metric and for F1 scores we consider acceptable predictions those with $MSE < (500\,kW)^2$. As the uncertainty measure, we use the total variance (i.e. due to aleatoric and epistemic uncertainty). A good model should have a small R-AUC and large F1-AUC. The R-AUC metric is comparable for the in-domain partitions, as expected for data that are drawn from the same distribution. Out-of-domain partitions have larger R-AUC indicating that model performance, in terms of robustness and/or uncertainty estimation, degrades when shifting away from the training convex hull, with eval_out being the most challenging set to be modelled, in accordance with the fact that eval_out is the most shifted dataset. Similar trends are observed in F1 retention curves; in-domain partitions result in similar F1-AUC values while F1-AUC decreases for the out-of-domain partitions.

Table VI: Retention performance for in-domain and out-of-domain canonical partitions. F1 scores are defined considering an upper threshold MSE = $(500\text{ kW})^2$ for the acceptable prediction errors

Data	**R-AUC**		**F1-AUC**		**F1 @ 95%**	
	Ens. DNN	Ens. VI	Ens. DNN	Ens. VI	Ens. DNN	Ens. VI
Dev in	112345	112109	0.595	0.596	0.791	0.791
Eval in	111027	110829	0.597	0.597	0.793	0.793
Dev out	206090	210019	0.499	0.498	0.690	0.685
Eval out	218342	217173	0.505	0.505	0.685	0.684

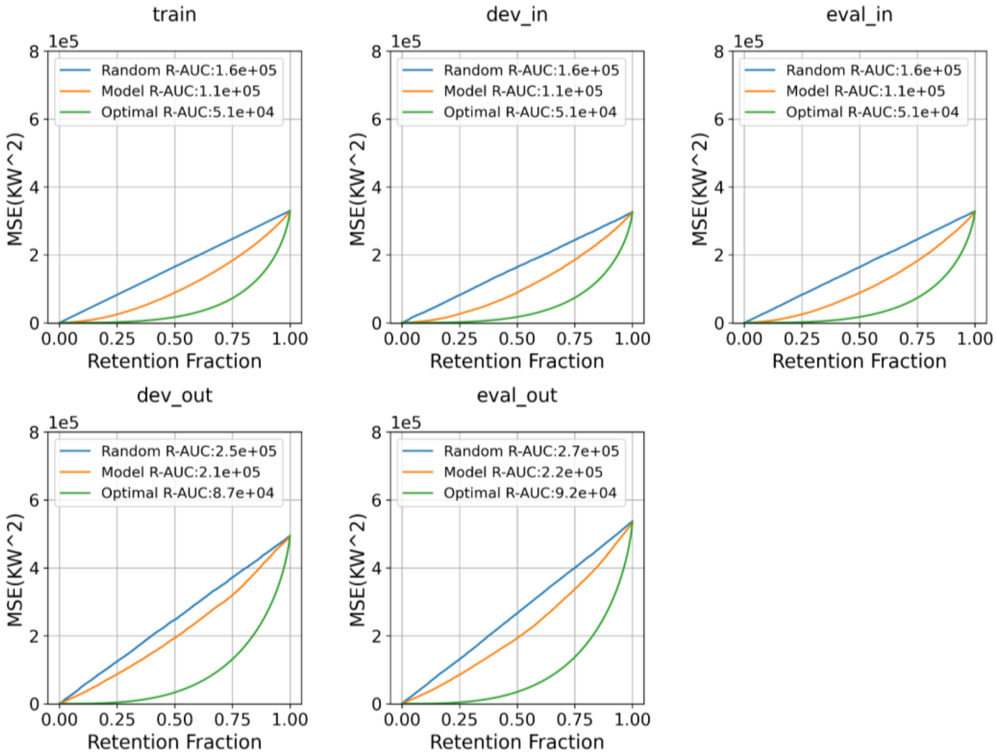

Fig.5: MSE retention curves (R-AUC) of the ensemble of VIs for the canonical partitions of synthetic set. The orange curve is the retention curve of the ensemble. The blue curve represents the worst-case scenario, the green curve the optimal scenario. The R-AUC model score (reported at the legend) is comparable for the in-domain partitions and increases the more shifted the dataset set is.

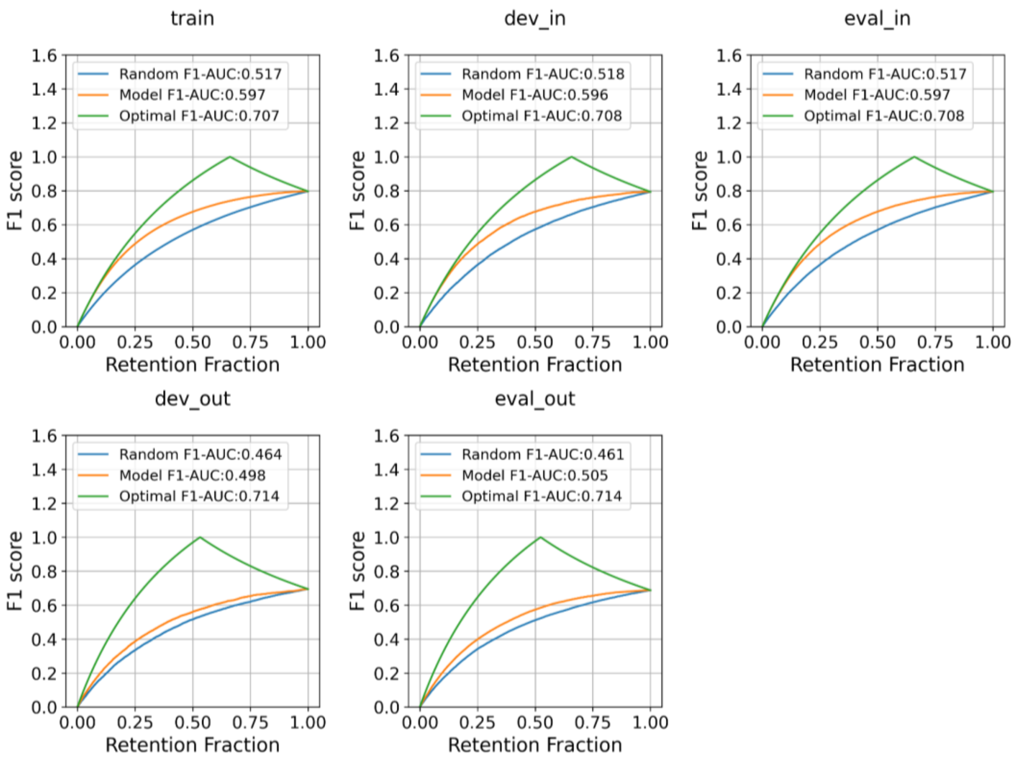

Fig.6: F1 retention curves for the ensemble of VIs under the canonical partitions split. The orange curve is the retention curve of the ensemble. The blue curve represents the worst-case scenario and the green curve the optimal scenario. The F1-AUC model score (reported at the legend) is similar for the in-domain partitions while out-of-domain partitions have smaller scores.

5. Conclusions

In this work, we presented an evaluation methodology based on a well-considered dataset splitting scheme that aims to reveal models' deficiencies to substantial distributional shifts. We examine the results through the lens of predicted uncertainty as part of the process, as this offers useful information about the model's fitness when dealing with uncertain and noisy regions in the modelled dataset. Overall, we find that splitting the dataset in the proposed manner successfully exposes models' performance drop when moving from in-domain to out-of-domain dataset splits, as demonstrated by the classical metrics. More importantly, we showed with two baseline models that predictive uncertainty correlates well with such drops, making it possible to assess the model's performance after deployment, without access to the true target values. We believe that this study encourages the shipping industry to trust and employ deep learning algorithms with predictive uncertainty in vessel performance modelling. Future research could focus on inherent selection biases in the dataset sampling process and how they might affect the model's generalisation ability.

Acknowledgements

We would like to express our thanks to the technical department of Laskaridis Shipping for allowing us to use their data and for the close cooperation in the process of building the synthetic model for their vessel, by sharing design related data and sea trials results.

References

ALIPANAHI, B.; DELONG, A.; WEIRAUCH, M.T.; FREY, B.J. (2015), *Predicting the sequence specificities of DNA-and RNA-binding proteins by deep learning,* Nature Biotechnology 33(8), pp.831-838

AMODEI, D.; OLAH, C.; STEINHARDT, J.; CHRISTIANO, P.; SCHULMAN, J.; MANE, D. (2016), *Concrete problems in AI safety,* arXiv preprint arXiv:1606.06565

BERTRAM, V. (2012), *Practical Ship Hydrodynamics,* Butterworth and Heinemann

BOS, M. (2018), *An Ensemble Prediction of Added Wave Resistance to Identify the Effect of Spread of Wave Conditions on Ship Performance,* 3rd HullPIC Conf., Redworth

BOSE, N. (2008), *Marine Powering Predictions and Propulsors,* SNAME

CARLTON, J.S. (2018), *Marine Propellers and Propulsion,* Butterworth and Heinemann

CORADDU, A.; ONETO, L.; BALDI, F.; CIPOLLINI, F.; ATLAR, M.; SAVIO, S. (2019), *Data-Driven Ship Digital Twin for Estimating the Speed Loss caused by the Marine Fouling,* Ocean Eng.

DER KIUREGHIAN, A.; DITLEVSEN, O. (2009), *Aleatory or epistemic? Does it matter?,* Structural Safety 31.2, pp.105-112

DUERR, O.; SICK, B.; MURINA, E. (2020), *Probabilistic Deep Learning: With Python, Keras and TensorFlow Probability,* Manning Publications, ISBN:9781617296079

FARKAS, A; DEGIULI, N.; MARTIC, I.; DEJHALLA, R (2020), *Impact of Hard Fouling on the Ship Performance of Different Ship Forms,* J. Marine Science and Engineering 8/748, doi:10.3390/jmse 8100748

FUJIWARA, T.; UENO, M.; IKEDA, Y. (2006), *Cruising performance of a large passenger ship in heavy sea,* 16th Int. Offshore and Polar Engineering Conf., Vol. III

GAL, Y. (2016), *Uncertainty in Deep Learning*, Ph.D. thesis, University of Cambridge

GOAN, E.; FOOKES, C. (2020), *Bayesian neural networks: An introduction and survey*, Case Studies in Applied Bayesian Data Science, Springer, pp. 45-87

GÓRSKI, W.; MICHNIEWICZ, J.; SZLENDAK, A. (2021), *Using Unsupervised Machine Learning for Building Ship Performance Reference Model*, 6th HullPIC Conf., Pontignano

GONZALEZ, C.; ARANGO, D.L. (2019), *Techniques for the Automated Detection of Anomalies and Assessment of Quality in High-Frequency Data Collection Systems*, 4th HullPIC Conf., Gubbio

HARDT, M.; RECHT, B. (2021), *Patterns, predictions, and actions: A story about machine learning*, mlstory.org, arXiv preprint arXiv:2102.05242

HINTON, G.; DENG, L.; YU, D.; DAHL, G.E.; MOHAMED, A.R.; JAITLY, N.; SENIOR, A.; VANHOUCKE, V.; NGUYEN, P.; SAINATH, T.N.; KINGSBURY, B. (2012), *Deep neural networks for acoustic modeling in speech recognition: The shared views of four research groups*, Signal Processing Magazine, IEEE, 29(6), pp.82-97

HOLTROP, J.; MENNEN, G.G.J. (1982), *An approximate power prediction method*, Int. Shipbuilding Progress 29, pp.166-170

ISO (2015), *Ships and marine technology – Guidelines for the assessment of speed and power performance by analysis of speed trial data*, ISO 15016:2015, Int. Standard Org., Geneva

ISO (2016), *Ships and marine technology - Measurement of changes in hull and propeller performance - Part 2: Default method*, ISO19030-2, Int. Standard Org., Geneva

JOURNÉE, J.M.J.; MEIJERS, J.H.C. (1980), *Ship routeing for optimum performance*, TU Delft

KRIZHEVSKY, A.; SUTSKEVER, I; HINTON, G.E. (2012), *Imagenet classification with deep convolutional neural networks*, Advances in Neural Information Processing Systems

LAKSHMINARAYANAN, B.; PRITZEL, A.; BLUNDELL C. (2017), *Simple and Scalable Predictive Uncertainty Estimation using Deep Ensembles*, Advances in Neural Information Processing Systems 30

LEVANTIS, M.; PAERELI, S.; ENSTRÖM, A.; BETZ, W. (2020), *Speed-Power Models – A Bayesian Approach*, 5th HullPIC Conf., Hamburg

MALININ, A. (2019) *Uncertainty Estimation in Deep Learning with application to Spoken Language Assessment*, Ph.D. thesis, University of Cambridge

MALININ, A.; BAND, N.; CHESNOKOV, G.; GAL, Y.; GALES, M.J.F.; NOSKOV, A; PLOS-KONOSOV, A.; PROKHORENKOVA, L.; PROVILKOV, I.; RAINA, V.; RAINA, V.; ROGINSKIY, D.; SHMATOVA, M.; TIGAS, P.; YANGEL, B. (2021), *Shifts: A dataset of real distributional shift across multiple large-scale tasks*, arXiv preprint arXiv:2107.07455

MIKOLOV, T.; CHEN, K.; CORRADO, G.; DEAN J. (2013), *Efficient estimation of word representations in vector space*, arXiv preprint arXiv:1301.3781

MOLLAND, A.; TURNOCK, S.; HUDSON, D. (2017) *Ship Resistance and Propulsion*, Cambridge University Press

MORENO-TORRES, J.G.; RAEDER, T.; ALAIZ-RODRIGUEZ, R.; CHAWLA, N.V.; HERRERA, F. (2012), *A unifying view on dataset shift in classification*, Pattern Recognition 45.1, pp.521-530

NIKOLOPOULOS, L.; BOULOUGOURIS, E. (2018), *A Study on the Statistical Calibration of the Holtrop and Mennen Approximate Power Prediction Method for Full Hull Form, Low Froude Number Vessels,* J. Ship Production and Design 35, 10.5957/JSPD.170034

PARK, J.; KIM, B.; SHIM, H.; AHN, K.; PARK, J.H.; JEONG, D.; JEONG, S. (2018), *Hull and Propeller Fouling Decomposition and Its Prediction based on Machine Learning Approach,* 3rd HullPIC Conf., Redworth

RAMSUNDAR, B.; KEARNES, S.; RILEY, P.; WEBSTER, D.; KONERDING, D.; PANDE, V. (2015), *Massively multitask networks for drug discovery,* arXiv preprint arXiv:1502.02072

SEO; K.C.; ATLAR, M.; GOO, B. (2016), *A Study on the Hydrodynamic Effect of Biofouling on Marine Propeller,* J. Korean Society of Marine Environment and Safety 22/1, pp.123-128

TOWNSIN, R.L.; BYRNE, D.; SVENSEN T.E.; MILNE, A. (1981), *Estimating the technical and economic penalties of hull and propeller roughness,* Trans SNAME

TSARSITALIDIS, V.; ROSSOPOULOS, S. (2018), *ISO 19030 - The Good, the Bad and the Ugly,* 3rd HullPIC Conf., Redworth

TSUJIMOTO, M.; SHIBATA, K.; KURODA, M.; TAKAGI, K. (2008), *A Practical Correction Method for Added Resistance in Waves,* J. JASNAOE Vol.8

VAN LAMMEREN W.P.A.; VAN MANEN, J.D.; OOSTERVELD, M.W.C. (1969), *The Wageningen B-Screw Series*, Trans. SNAME 77, pp. 269-317

WANG, H.; YEUNG, D.Y. (2020), *A survey on Bayesian deep learning,* ACM Computing Surveys (CSUR) 53.5, pp.1-37

ZHOU, J.; TROYANSKAYA O.G. (2015), *Predicting effects of noncoding variants with deep learning-based sequence model,* Nature Methods 12(10), pp.931–934

A Journey to Unique PIV Flow Measurements at Ship Scale

Dmitriy Ponkratov, JoRes project, London/UK, dp@jores.net
Gijs Struijk, MARIN, Wageningen/Netherlands, g.d.struijk@marin.nl
Miloš Birvalski, MARIN, Wageningen/Netherlands, m.birvalski@marin.nl
Martijn Elbertsen, MARIN, Wageningen/Netherlands, m.elbertsen@marin.nl

Abstract

In March 2022, MARIN performed unique PIV flow measurements at ship scale within the JoRes Joint Industry Project. This paper describes the journey towards this achievement starting with previous inspirational attempts done by other researchers in the past. After this, the development of the PIV unit at MARIN, its installation on the vessel in a dry-dock, measurements at sea and finally removal without vessel dry-docking are described.

1. Introduction

It may sound surprising, but in the 21st-century humanity knows a lot about space and the universe, but there is almost no data on water flowing into the propeller of an ordinary ship. All the knowledge available currently is either based on model test experiments (with seriously challenged assumptions) or yet-to-be validated numerical simulations. Up until now, there was no reliable and accurate instrument to measure the flow around a vessel. How are we then supposed to optimise the ship hull and propulsion system if we do not know the details of the flow?

With this question in mind, a group of researchers at MARIN working on the development of the JoRes Joint Industry Project (*Struijk and Ponkratov, 2018*) sat together in 2017 and started to think about how to tackle this challenge. If no one has done this before, it does not mean it is impossible!

In the beginning, it is important to highlight previous attempts to measure the flow around a vessel. The first and most obvious way to do this is by using the Pitot tube. These tubes were invented by Henri Pitot in 1732 to measure the velocity of air or water. Essentially a differential pressure flowmeter, a Pitot tube measures two pressures: the static and the total impact pressure. Nowadays, Pitot tubes are widely used on aeroplanes and in racing cars. They are also used in the maritime industry in towing tanks to measure the flow around a ship model. However, there are practical challenges to using Pitot tubes on a full-sized vessel: the risk of hitting this delicate tool with a floating object, or the risk of fouling by marine growth. Even for research purposes, the most logical scenario would be to develop a retractable Pitot tube, however, the results of these measurements would be velocity points along a line, not the two-dimensional wake field which is necessary for propeller optimisation.

However, there were a few good attempts to measure three components of velocity in the wake. One of the most remarkable cases was the resistance trials of HMS Penelope. Her propellers were removed, the special rake with pitot tubes was installed on the shaft and she was towed by HMS Scylla, *Canham (1974*).

The pitot rake for the wake survey is shown in Fig.1, viewed from the forward with protective covers fitted over the pitot heads. The arms of the rake carried four five-hole spherical-headed Pitot tubes for measuring tri-axial components of flow velocity and four normal axial type Pitot tubes, disposed of as follows: Pitot tubes at adjacent radii were located on opposite arms of the rake to avoid interference effects. The rake was designed to take measurements in the plane of the starboard propeller and extended beyond the radius of the propeller disc. A photograph of one of the five-hole pitot heads is reproduced in Fig.2. Some results of measured wakes at ship scale and model scale are presented in Fig.3.

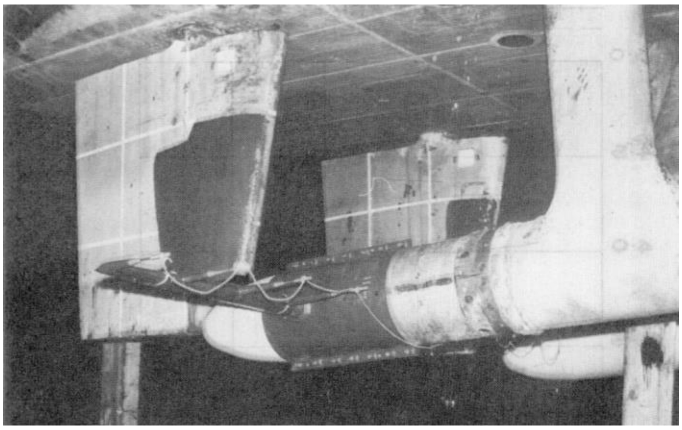

Fig.1: Pitot rake for full scale wake survey, HMS Penelope, *Canham (1974)*

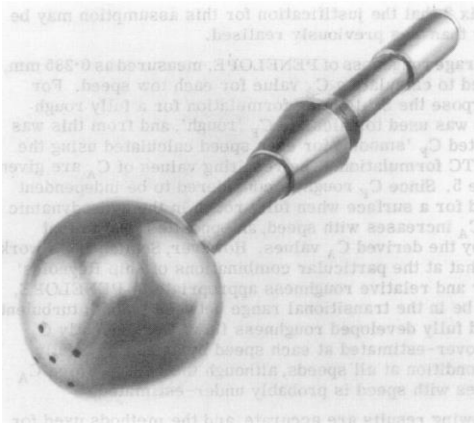

Fig.2: Five-hole spherical headed pitot, HMS Penelope, *Canham (1974)*

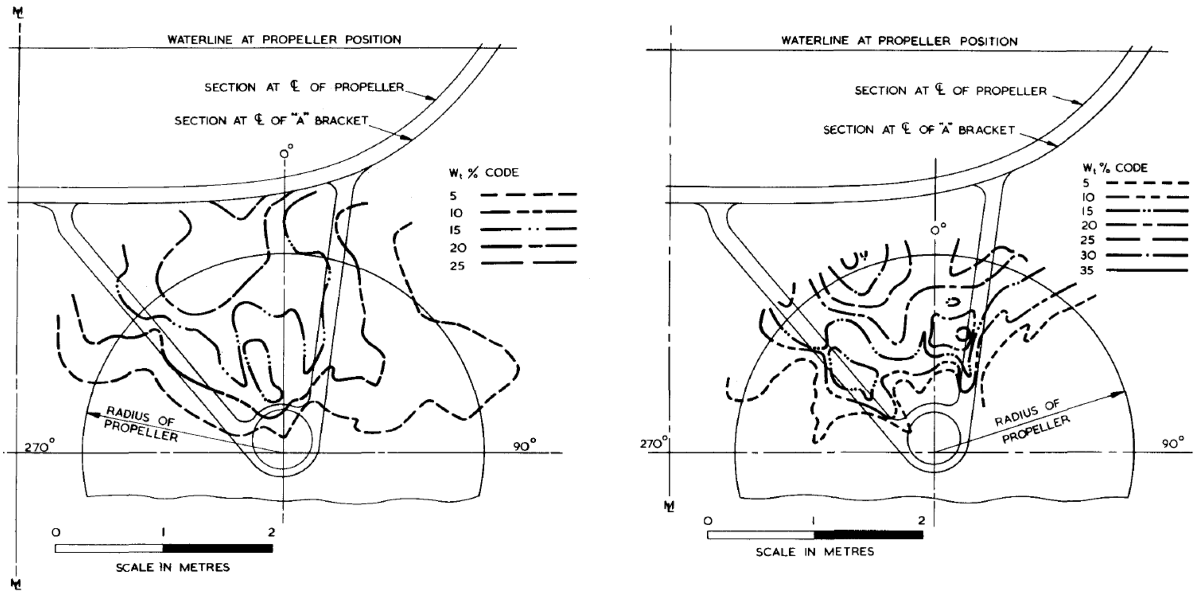

Fig.3: Wake pattern at 17 kn, HMS Penelope, *Canham (1974)*, ship scale (left) and model scale (right)

Another option to measure the flow around a ship could be to use LDV (Laser Doppler Velocimetry). LDV is a technique that uses the Doppler shift of laser light to measure the velocity of fluid flows. This works by crossing two beams of coherent laser light. Transmitting optics focus the beams to intersect at their waists, where they interfere and generate a set of interference fringes. As particles (either naturally occurring or artificial) contained in the fluid pass through the fringes, they reflect light that is then collected by receiving optics and focused on a photodetector. The particle and thereby the fluid velocity can be determined from the Doppler shift of the light hitting the photodetector.

The LDV technique is widely used in model tests to measure the wake field; there were comparatively few attempts to use LDV at the ship scale. For example, MARIN attempted to measure the flow on MV Valovine within the GRIP EU research project in 2014, *Prins (2015)*. Unfortunately, those measurements were not successful. One of the challenges was related to setting up the unit on a vessel; vibrations in the aft end of the ship (due to machinery and propeller cavitation) make intersecting the two beams very challenging. Furthermore, the data rate of LDV that measures in only one point might be limited, requiring long measurement times. Finally, intersecting one set of beams is challenging, resulting in one component of velocity; for the second component, another set of beams would need to be intersected at the same point where the first pair of beams is, increasing the complexity and likelihood of measurement failure even further.

Fig.4: LDV unit during flow measurements on the MV Valovine, *Prins (2015)*

An encouraging project measuring the propeller inflow was done in 2014 by a group of researchers, *Kleinwächter et al*. *(2015*), from the University of Rostock and the Potsdam Model Basin (SVA) using Particle Image Velocimetry (PIV). PIV is a technique that uses a strong light source (typically a laser) to illuminate particles contained in a 2D plane of the flow. The reflected light is captured by a camera, after which the particle images are analysed to determine the velocity field in the part of the flow illuminated by the laser.

Fig.5: PIV measurement setup inside the steering gear room, MV Amandine, *Kleinwächter et al. (2015)*

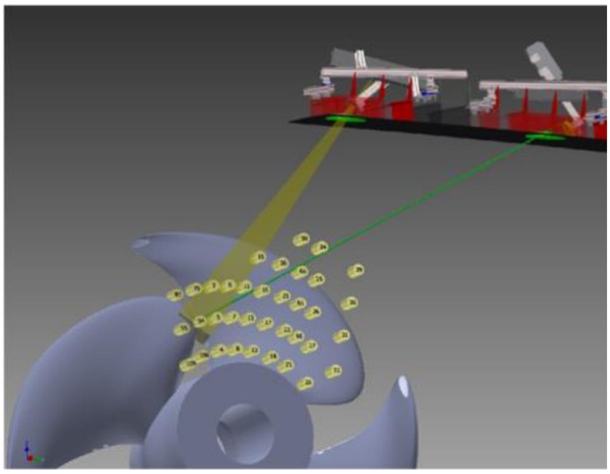

Fig.6: Visualisation of PIV measurements, MV Amandine, *Kleinwächter et al. (2015)*

The RostockUni/SVA group made a series of portholes in the aft end of a ro-ro vessel and operated a PIV system through the portholes, Fig.5 and Fig.6. This was likely the first successful PIV measurement at the ship scale. However, there were a few limitations that made this measurement less than ideal. For example, the limited view from the windows did not allow making a large sector scan; the measurements needed to be made in small areas that were first averaged (producing one measurement point) and then combined to form a larger flow field. Furthermore, the measurements were not done during a well-controlled sea trial (i.e. with reciprocal runs and careful measurement of all the relevant environmental conditions), making it difficult to use the results in CFD validations. Nevertheless, these measurements showed that PIV at full scale is possible which motivated us to develop our full-scale PIV system. This work was done within JoRes Joint Industry Project aiming to collect ship scale data for CFD validation and create a benchmark for energy-efficient solutions.

2. Laboratory tests with sea water at MARIN

The most important limitation that a researcher attempting to apply PIV at full-scale (i.e. at sea) is facing is the inability to control the 'seeding' size and concentration. Namely, PIV requires particles – seeding - in the flow which reflect laser light and whose velocity is determined as a proxy for the local flow velocity. In laboratory applications, the seeding is added by the experimenter. At sea, one would have to do with whatever is naturally present in the water, which is algae, plankton and inanimate solid particles.

To verify if the natural seeding is of the correct size and in sufficient quantity for performing PIV, MARIN performed two studies. In the first, 2D2C (two-dimensional, two-component) PIV was done at ~1 m scale in North Sea water. The water was either unfiltered or filtered to reduce the number of particles, thereby approaching the particle content of clearer oceanic waters (Atlantic, Mediterranean, Adriatic, etc.).

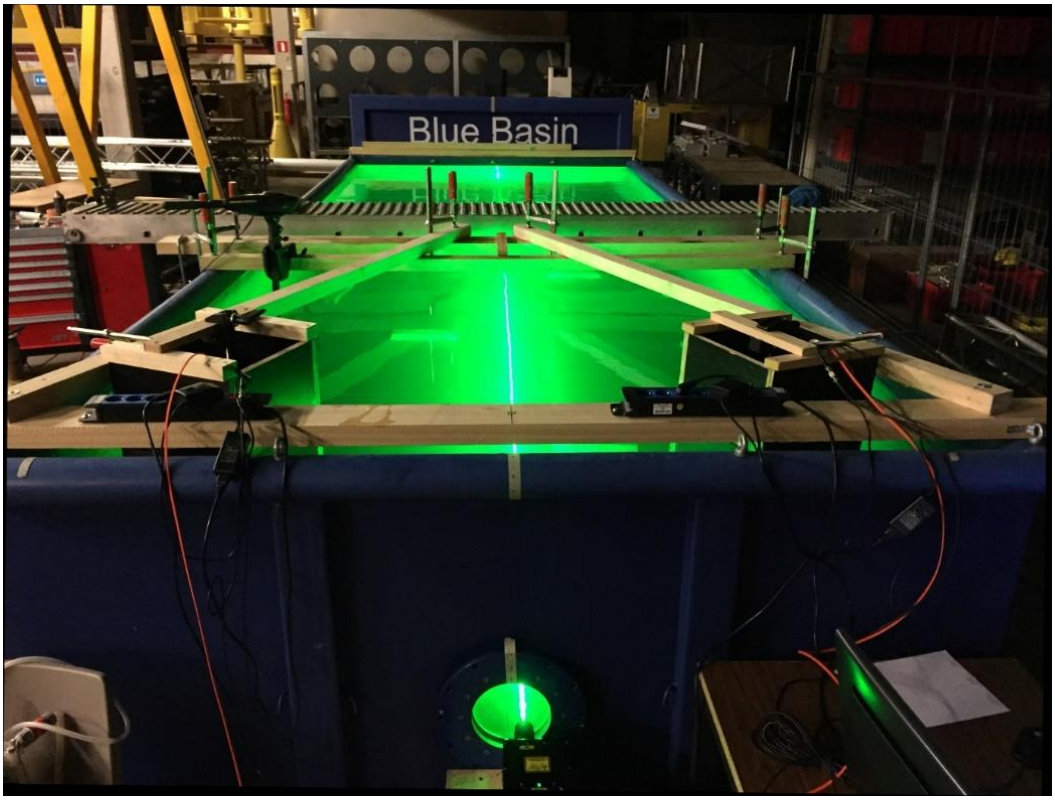

Fig.7: PIV experiments with sea water at MARIN, 2019

It was particularly important to measure the attenuation of laser light through water, thereby quantifying its transparency. This and other (visual) methods of judging water quality will be later used to decide if a full-scale PIV measurement is feasible in a certain region of the sea and in a certain season (the transparency changes due to biological activity, which is seasonal).

In the second test, MARIN used filtered seawater again, but increased the complexity of the PIV system to 2D3C (stereo-PIV) and increased the scale of the system to ~3 m, thereby reaching the size and type of PIV system that could usefully be applied at full-scale. Since this test was also successful, MARIN was confident that measurements at sea would have a high chance of success, so they proceeded with developing the full-scale device.

3. Design and development of PIV unit

After establishing the viability of the PIV measurement principle at full scale, the design and development of the PIV unit started. Based on previous experience measuring with complex optical devices, it was decided to make the unit:

1. As robust and as sturdy as possible, since it needs to withstand harsh conditions (vibrations, flow forces, salt water) when installed, as well as during transport and handling. The device should be water-tight and include various levels of protection against leakage both into the device, as well as into the vessel.
2. As universally applicable as possible, meaning not dependent on the specific position of port-holes or internal structures of the ship. This means mounting the unit outside on the shell plate, thereby also having an unobstructed view of the flow.
3. Able to measure in a large field of view, such that a sufficiently large part of the flow coming into the propeller is measured. This requires the laser energy and the camera efficiency and resolution to be high. Further, the acquisition frequency of the system needs to be as high as possible to gather large amounts of data in the limited time available in a run.
4. Free from the requirement to calibrate the device after installing it on the ship. Having to perform calibration in a ship environment was identified as a possible source of large uncertainty. The device would therefore only require alignment, calibration and other sensitive activities to be performed in the laboratory, after which the device should be able to work without further intervention in the difficult environment of a sea trial.
5.

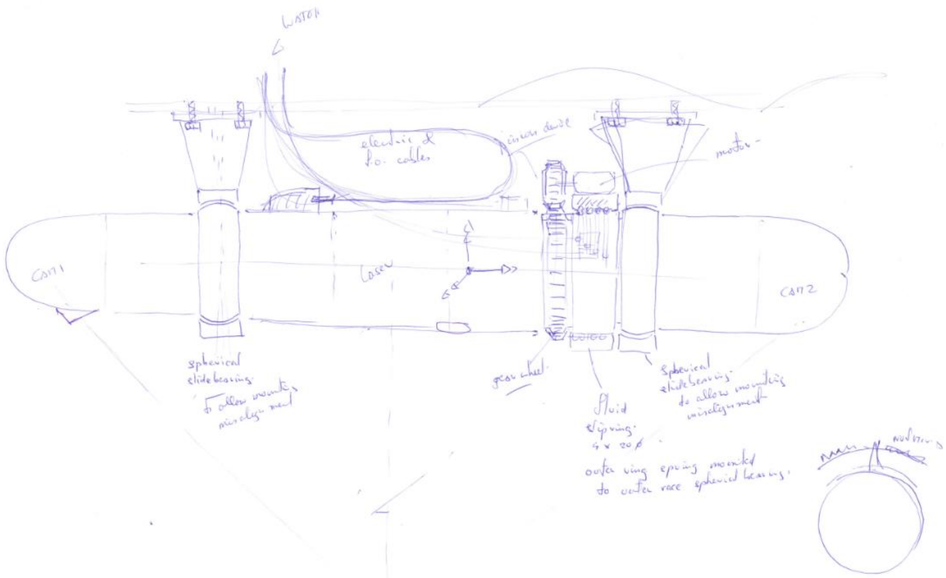

Fig.8: The first sketch of the FlowPike (PIV unit), MARIN, 2019

With these requirements outlined, it was also decided to divide the work between MARIN and LaVision GmbH (Göttingen, Germany) in the following way: MARIN will lead the overall development and perform the design and engineering of all the mechanical parts of the system whilst LaVision will perform optical design and deliver the necessary optical and electrical components of the system. After this, MARIN will perform the final system assembly, testing and commissioning.

The optical design included simulating and selecting the individual components necessary to create a large (1 m wide, 3-4 m long) laser sheet, as well as applying special camera mounts that were resistant to vibration and therefore possible misalignment. Besides this, a custom design was made for all the electrical and optical cables and the air and water hoses necessary for the operation of the cameras, the laser and electrical motors used for lens controls. All these needed to extend from the unit mounted under the ship to the power/control equipment inside the ship, a distance of 10 m, passing through several water-tight bulkheads.

The biggest challenges of mechanical design included making a strong yet streamlined body that will be relatively easy to mount and dismount from the vessel, either in a dry dock or at a port in ballast conditions. This included designing a cradle for the device that is used for lifting and a dummy frame used for aligning the hull penetration and unit supports that need to be cut and welded onto the ship hull. Further, to enlarge the measurement area, the unit needed to be able to turn around its axis to a given angle and maintain the angle against the flow forces acting on it. This was achieved by placing a motor, an encoder and a brake in the front part of the device. Naturally, the water-tightness of the static and rotational seals and of the cable feed-throughs on the bulkheads needed to be ensured as well.

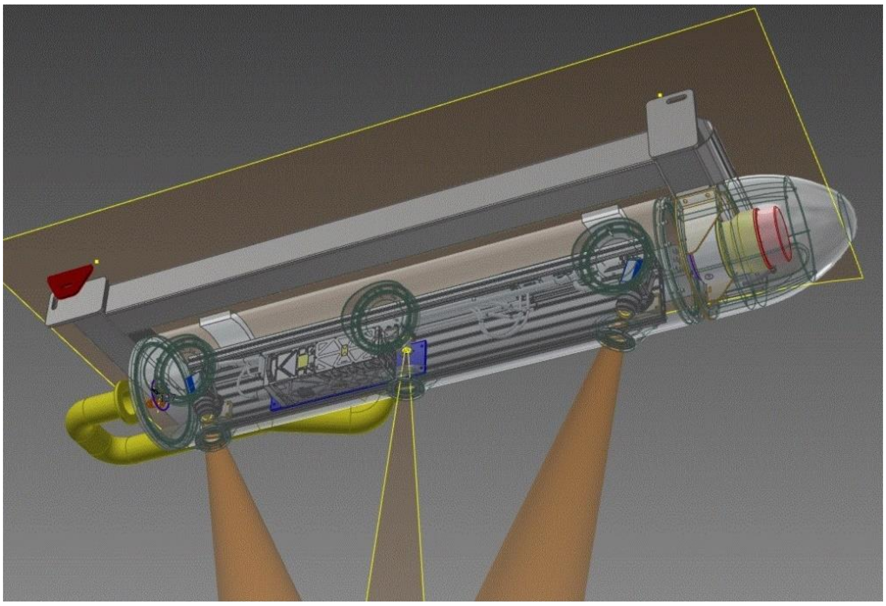

Fig.9: Design of the PIV unit, MARIN, 2019

After all, the optical and mechanical components of the new PIV unit (FlowPike) were manufactured and delivered to MARIN, and the final assembly and testing took place. Special attention during the assembly process was given to securing all the bolts inside the unit to prevent them from coming loose due to exposure to vibration when installed in the vicinity of a cavitating propeller.

The testing was performed in MARIN workshops as well as in MARIN's Deepwater towing tank. In the dry, the working of all the subsystems were tested (cameras, laser, electrical motor for turning, pressure-tightness of the containment, fit and alignment of cable conduits, etc.). Then, the cameras and the laser were aligned using a specially ordered calibration plate, after which they were tightly secured in place.

Once all this was done in the dry, the unit was closed and placed underwater. There, the system was calibrated using the same large calibration plate previously used for alignment. After successfully calibrating the unit, the final test was to mount the unit onto the tank carriage and perform a day of testing in the basin. During the test, runs with increasing speed were performed. The PIV unit was pointed into the flow, its measurement area is vertical, with the main component of velocity directed through the laser sheet; this is the same configuration as in the intended application on the full-scale vessel. The resulting free-stream velocity can be compared to the speed of the carriage, which was increased from 0.5 m/s to 4 m/s. The PIV unit was able to measure the velocity with several per cent errors.

The final field of view of the unit was approximately 0.6 m wide by 1.5 m long, with the centre of the area being 2.5 m away from the device. The FlowPike is, therefore, able to measure a 10-degree wide sector of the flow, starting at approximately 1.7 m away from the device, up to 3.3 m away. By rotating the device, a total angle of 160° can be measured. The measurement frequency is 10 Hz. With this, the testing of the FlowPike was considered complete and the unit was declared ready for deployment.

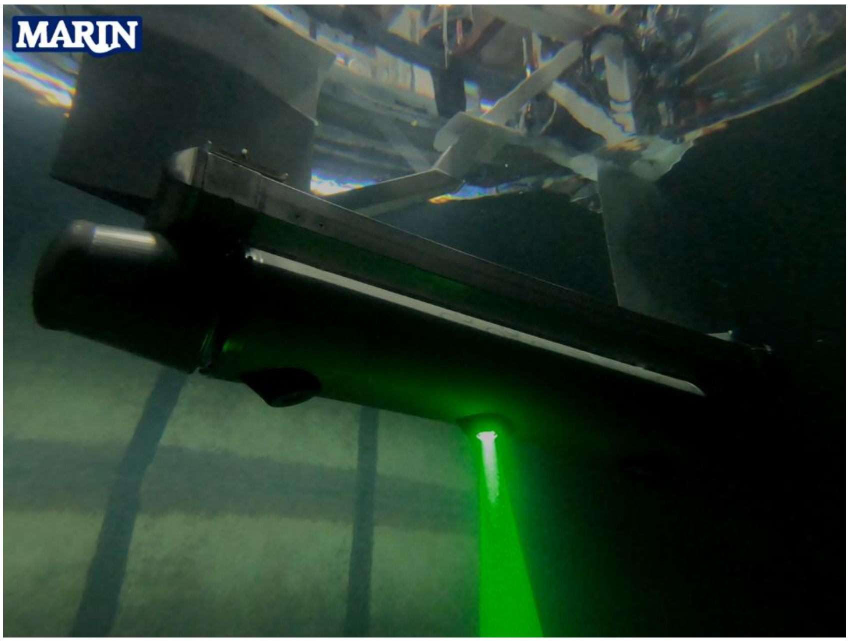

Fig.10: Testing the PIV unit in MARIN's Deepwater towing tank, 2020

4. Installation of the PIV unit in dry-dock

The unit and the welding dummy frame were delivered to the dry dock in early 2022. All necessary approvals by Class were obtained beforehand. As soon as the vessel was dry in the dock, the normal maintenance process of sandblasting the hull was started. It was important to start this process from the aft end to give access to the PIV installation area as early as possible.

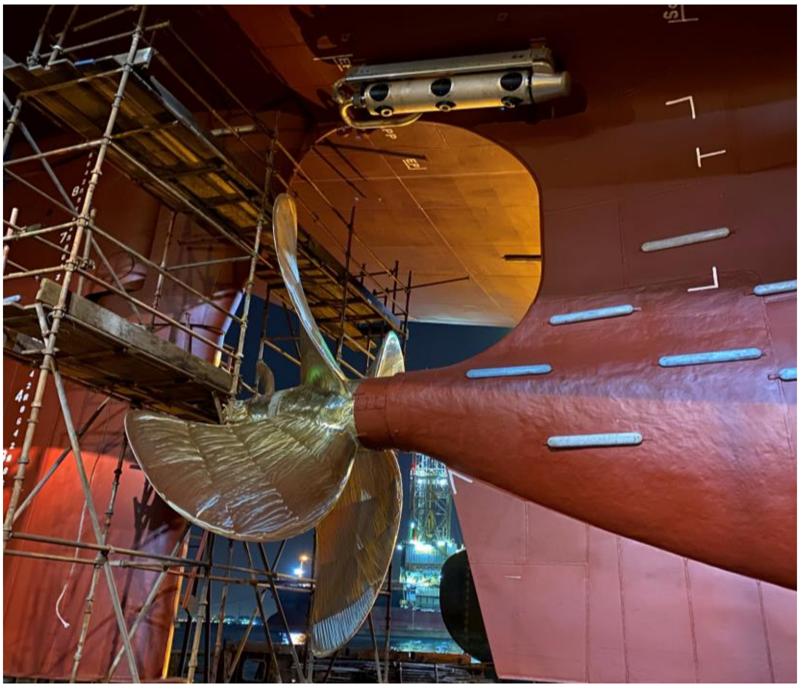

Fig.11: PIV unit installed on the JoRes1 tanker, early 2022

At the beginning of dry-docking, the feedthrough flange was welded in the hull. Four lifting eyes were also welded to the shell plate in the area of the future PIV unit. After that, the dummy frame (which has the same dimensions as the actual PIV unit) was lifted and the dummy feedthrough pipe was attached to the feedthrough flange. This gave the required alignment of the entire frame. While the frame was held by chain blocks, the next step was to weld brackets onto which the PIV unit will be fixed in the correct locations indicated by the dummy frame. Then the frame was bolted to the bracket to check the alignment of the entire structure. The next step was to remove the dummy frame to allow painting the newly installed feedthrough flange, brackets and lifting eyes. The window was closed from the inside to avoid paint coming into the hull. When the area was painted and the paint was dry (on the last day of dry-docking) the PIV unit was lifted by chain blocks and bolted to the brackets. The final operation of that day was a pressure test to ensure the water-tightness of the entire structure.

5. JoRes1 tanker sea trials and PIV measurements

As mentioned before, the main objective of these measurements was to collect ship scale data for further CFD validation within the JoRes Joint Industry Project. For this purpose, a lot of activities took place before the actual trials: the hull and propeller roughness measurements were performed in the dry dock, strain gauges were installed on the propeller shaft to measure propeller torque, the optical sensor was installed next to the shaft to measure propeller shaft speed, anemometers were installed on the antenna mast to get wind characteristics, etc. It should be also mentioned that the PIV unit was pressurised with nitrogen. If the unit lost its water tightness for some reason, the water would not come inside the unit and the hull. The nitrogen was selected to avoid moisturisation of the PIV equipment and especially the unit windows.

The sea trials were conducted according to the ISO15016:2015 standard. Before the trials, the vessel was stopped at sea to deploy the wave buoy, record vessel draughts and measure water properties. Later on, after the trials, the vessel was stopped again to record vessel draughts and measure water properties. The trials were performed at four shaft speeds (60, 75, 90 and 96 RPM). Normally, the ISO standard requires conducting 2 runs for each RPM setting (minimum of 10 min each), however, as it was expected that 10 min would not be enough for sufficient PIV measurements, the decision was made to make the duration of each run 40 min. Moreover, for 75 and 90 RPM settings, 4 runs were performed, resulting in a total of 12 performed runs.

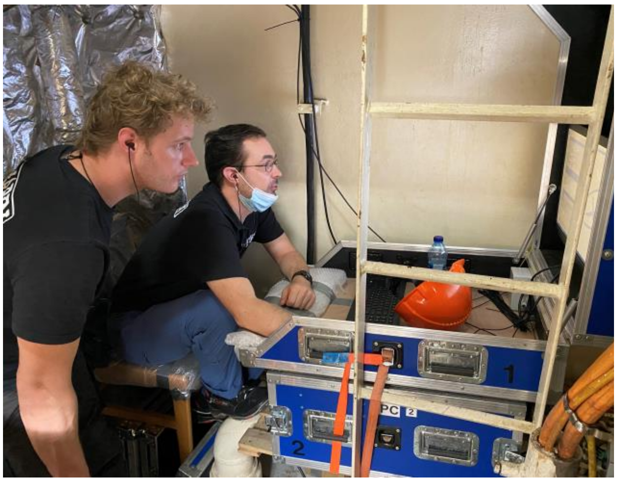

Fig.12: MARIN team performs PIV measurements on JoRes 1 tanker, 2022

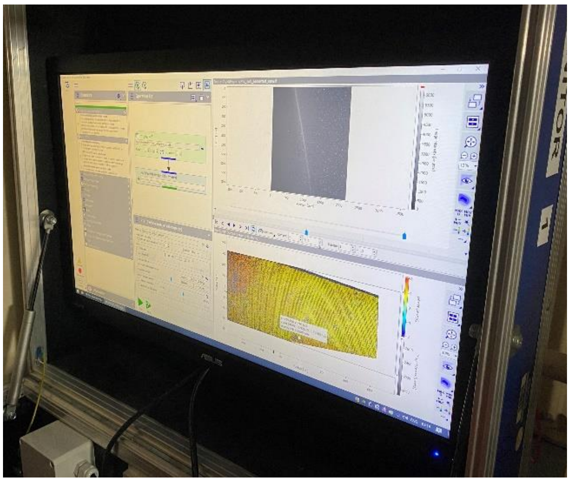

Fig.13: First PIV results

The main part of the PIV measurements was done at two speeds (75 and 90 RPM). Additionally, PIV measurements were done at a third speed (96 RPM), where a limited program could be executed. Each run consisted of measuring at different rotation angles of the FlowPike for either 80 s or 120 s; this amounted to either 800 or 1200 images per one angle. The device was rotated to cover a total sector of either 70° or 140° (the first of the double runs had a 70° sweep, the second a 140° sweep), which is a large part of the wake. The centre of each sweep was pointed at the expected position of the wake peak. Repeat measurements were also performed systematically; in fact, most angles were measured twice within one run, which will result in better statistics and will enable to investigate that there are no large scale flow effects that could bias the measurements.

Overall, the quality of the PIV images was very good, comparable to what was achieved with the FlowPike in the model basin previously. The concentration of the seeding particles was somewhat lower than ideal, but this will not have a large influence on the resulting quality. Likewise, the PIV inter-frame time needed to be kept low due to the high flow velocity through the laser sheet, but the resulting particle displacement is considered sufficiently high for a good dynamic range. In total 6.5 terabytes of PIV data were recorded and it will take some time to post-process and analyse it.

6. Removal of PIV unit after the trials

Performing comprehensive measurements on an ordinary cargo vessel implies some serious limitations as the ship owner normally seeks to have off-hire time as short as possible. Sea trials may be planned well in advance and it is relatively feasible to stick to the schedule provided there is no significant traffic in the trials area. Removal of the unit was a very uncertain operation because no one has done this before. Placing the vessel in dry-dock again to remove the unit would be prohibitively expensive to a research project, so the plan was to remove the unit when she is at the ballast draught (and the unit is above the water) and alongside. An appropriate pontoon was sourced at the yard and stability calculations were performed checking whether it is possible to lower the PIV unit (the total weight is more than 1000 kg) to the pontoon. After a few loaded tests, it was decided not to put the unit on the pontoon, but use it for chain blocks operators. It was agreed to move the unit towards the stern of the vessel by chain blocks (additional existing lifting eyes in the rudder area were used for that). Another challenge was related to the propeller: as mentioned before, it was important to have ballast draught to keep the unit above the water. At the same time, this meant that the pontoon and the PIV unit may be too close to the propeller blades. To mitigate the risk of damaging the propeller, the blades were moved by turning gear as far as possible from the unit and the pontoon. The operation was constantly monitored by divers to ensure all was kept clear of the propeller.

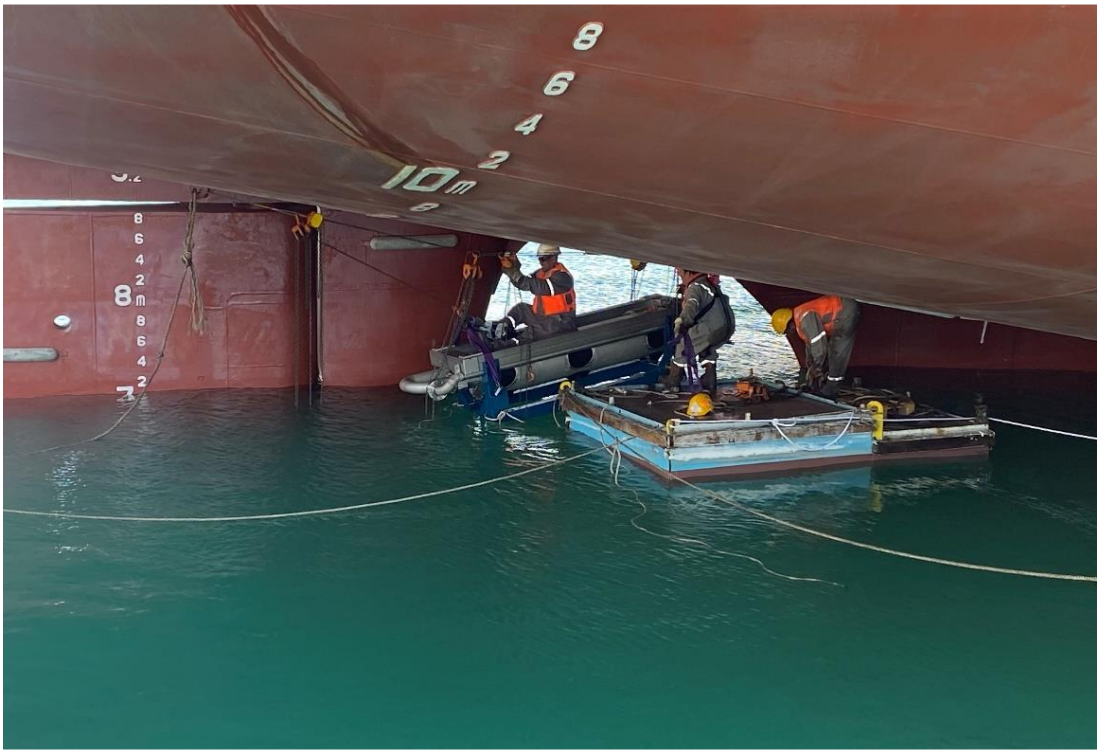

Fig.14: Removing the PIV unit while the vessel is alongside, 2022

In the end, the operation was done smoothly and the unit was safely moved towards the transom where it was picked up by the yard's crane. In total it took about 6 hours to complete the operation. The hull feedthrough flange was closed with a plexiglass window and secured with a blind flange on top of it, as intended in design. The class surveyor checked and approved the installation after that.

7. Conclusions

Naval architects and propeller designers always knew the importance of propeller inflow measurements at ship scale. The initial motivation was to compare the measured wake with model tests and derive recommendations for wake scaling procedures. Nowadays, the main intention is to validate ship scale CFD and better understand and utilise the energy efficiency potential of vessel propulsion. Developing measurement technologies enabled the design and realisation of a new and robust flow measurement tool which is not dependent on vessel geometry and porthole locations. The successful PIV measurements performed on the tanker within the JoRes project showed that this technology works and can be used on other vessels. The installation, performance and removal activities may be aligned with normal vessel operations (dry-docking, post docking trials) and do not require significant off-hire time which makes it attractive for further comprehensive investigations on other vessels.

References

CANHAM, H. (1974), *Resistance, Propulsion and Wake tests with HMS 'PENELOPE'*, Trans. RINA, pp.61-94

KLEINWACHTER, A.; HELLWIG-RIECK, K.; EBERT, E.; KOSTBADE, R.; HEINKE, H.J.; DAMASCHKE, N. (2015), *PIV as a Novel Full-Scale Measurement Technique in Cavitation Research*, 4th Int. Symp. Marine Propulsors (SMP), Texas

PONKRATOV, D.; STRUIJK G. (2018), *JoRes JIP – a unique Joint Industry Project to close the knowledge gap on Ship Hydrodynamics*, Full Scale Ship Performance Conf., London

PRINS, H.J. (2015), *GRIP Green Retrofitting through improved propulsion*, EU project 284905, Final report, pp.34-35

From Performance Monitoring to ShaPoLi System

JanWienke, DNV, Hamburg/Germany, jan.wienke@dnv.com

Abstract

This paper gives some insights into the upcoming IMO requirements on EEXI. The IMO strategy on reduction of GHG emissions from ships demands the reduction of carbon emission per transport work by 40% until 2030. This carbon intensity can be improved by installing smaller engines with less power into new ships, for existing ships a power limitation is regarded as feasible solution. The power limitation can be installed directly at the engine by reducing the available fuel amount (EPL) or with a ShaPoLi system which is based on a shaft power meter.

1. Introduction

Performance monitoring is often based on data from a shaft power meter. This measuring device will get a new relevance with implementation of EEXI in 2023. In MARPOL Annex VI new requirements on the carbon intensity of existing ships are introduced that are measured with the EEXI for each individual ship. Compliance with EEXI requirements is needed for issuance of the International Energy Efficiency Certificate (IEEC) in 2023, meaning that it is not a recommendation but a strict requirement and a ship that does not fulfill the EEXI requirement cannot be operated or requires an exemption from flag state.

Compliance with EEXI can be achieved with the installation of a power limitation in most cases. The ShaPoLi system measures the actual shaft power and compares the current value with a limit value of the maximum propulsion power which is calculated from the EEXI requirement.

2. Energy Efficiency eXisting ship Index (EEXI)

In June 2021, the 76th session of the IMO's Marine Environment Protection Committee (MEPC 76) adopted the introduction of the EEXI. The EEXI guidelines are part of the measures to reduce carbon emission of international shipping. These measures include technical measures which are related to the design of ships as the EEXI and operational measures as the CII.

The EEXI is the transfer of the Energy Efficiency Design Index (EEDI) from newbuilding to existing ships. The EEDI was already introduced in 2013. As it only covers newbuildings it is obvious that the carbon intensity of the whole fleet will only slowly improve with this measure. According to IMO initial strategy on reduction of GHG emissions from ships [MEPC.304(72)], the carbon intensity, meaning the CO_2 emission per transport work, should be reduced by 40% in 2030 compared to 2008. Transferring the requirements to the existing fleet allows for a distinctly faster improvement of carbon intensity.

There are differences between the EEDI and the EEXI. As the EEDI is already considered during design of a new ship, dimension and especially main engine can be selected regarding the EEDI requirements. For existing ships, improvements can only be realized in a small range, e.g. performance improvement by installation of energy saving devices or enlargement of transport capacity. The largest potential for improvement is the limitation of the propulsion power by technical means.

The required EEXI as defined in MARPOL Annex VI regulation 25 is depending on ship type and size. It is based on the reference lines of the fleet in 2008. Reduction factors are defined, which are similar to the reduction factors considered for EEDI in 2023. For part of the ships, in 2023 already phase 3 of EEDI is valid (e.g. container ships), whereas other ship types are still in phase 2 (e.g. bulk carrier and tanker). The strictest reduction factor is valid for large container ships with 50%, bulk carrier and tanker have reduction factors of 20%, ro-ro cargo and passenger ships only 5%.

The attained EEXI is calculated from the CO_2 emission rate per transport power. The emission rate is related to main and auxiliary engines and calculated from installed main engine power, specific fuel consumption at a defined load and a fuel dependent conversion factor. The according values are taken from test bed measurements of the engines and if not available, standard values can be applied. The transport power is defined as product of the capacity which is usually the deadweight (but 70% of DWT for containerships) multiplied with the ship speed at defined load.

An overview of the different ship types and sizes being subject to EEXI is given in Table I. The attained EEXI must be calculated and be submitted in the form of an EEXI Technical File to the EEXI verifier for all cargo ships with more than 400 GT and conventional propulsion. Not for all these ships a required EEXI is defined. For the limit value there is an additional consideration of the size, so that small ships have no required value and will not face any power limitation.

Table I: Application of EEXI depending on ship type and size

Ship type/characteristics		**Attained EEXI**	**Required EEXI**
Conventional propulsion	Bulk carrier	≥ 400 GT	≥ 10,000 DWT
	Gas carrier	≥ 400 GT	≥ 2,000 DWT
	Tanker	≥ 400 GT	≥ 4,000 DWT
	Container ship	≥ 400 GT	≥ 10,000 DWT
	General cargo ship (except livestock carrier, barge carrier, heavy load carrier, yacht carrier, nuclear fuel carrier)	≥ 400 GT	≥ 3,000 DWT
	Refrigerated cargo carrier	≥ 400 GT	≥ 3,000 DWT
	Combination carrier	≥ 400 GT	≥ 4,000 DWT
	Ro-ro vehicle carrier	≥ 400 GT	≥ 10,000 DWT
	Ro-ro cargo ship	≥ 400 GT	≥ 1,000 DWT
	Ro-ro passenger ship	≥ 400 GT	≥ 250 DWT and ≥400 GT
	Cruise ship	N/A	N/A
	Passenger ship (except ro-ro passenger and cruise)	N/A	N/A
	Other ship with conventional propulsion, (e.g. heavy load carrier, livestock carrier, offshore)	N/A	N/A
LNG carrier with any propulsion system		≥ 400 GT	≥ 10,000 DWT
Cruise ship with non-conventional propulsion		≥ 400 GT	≥ 25,000 GT
Bulk carrier, gas carrier, tanker, container ship, general cargo ship (except livestock carrier, barge carrier, heavy load carrier, yacht carrier, nuclear fuel carrier), refrigerated cargo carrier, combination carrier, ro-ro vehicle carrier, ro-ro cargo ship and ro-ro passenger ship with non-conventional propulsion		N/A	N/A
Livestock carrier, barge carrier, heavy load carrier, yacht carrier, nuclear fuel carrier, passenger ship and other ship (e.g. offshore) with non-conventional propulsion, and Category A Polar Code ship		N/A	N/A
Platforms including FPSOs and FSUs and drilling rigs		N/A	N/A

With the installation of a power limitation the calculated CO_2 emission in the attained EEXI calculation is reduced due to the lower power value to be considered but at the same time the according ship speed will decrease, and the specific fuel consumption will increase.

The considered power value is usually 75% MCR as the EEXI calculation should represent normal seagoing conditions. Sea margin and engine margin are deducted from the total installed propulsion power. In case of overridable power limitation, the engine margin is not needed anymore and therefore the power value for the EEXI calculation is 83%MCR_{Lim}.

This means that for a bulk carrier built before 2008 and in agreement with the performance of the average bulk carrier fleet at that time an improvement by 20% for the attained EEXI is needed which corresponds to a power limitation about MCR_{Lim} = 62% MCR (ignoring increase in specific fuel consumption) or even less available propulsion power. Such power limitation has significant impact on operation of the ship as the available ship speed is distinctly lower.

It means as well that for cases where the attained EEXI is only slightly above the required value, the minimum power limitation is above 10%. In such cases alternative improvement measures, e.g. optimized fuel nozzles to reduce the specific fuel consumption might be preferable.

3. ShaPoLi requirements

In the 2021 IMO guidelines on the shaft / engine power limitation system to comply with the EEXI requirements and use of a power reserve [MEPC.335(76)] the overridable shaft power limitation (ShaPoLi) is defined as a verified and approved system for the limitation of the maximum shaft power by technical means that can only be overridden by the ship's master or the officer in charge of navigational watch (OICNW) for the purpose of securing the safety of a ship or saving life at sea.

The following six functions of a ShaPoLi system are needed to be in line with the requirements as stated in MEPC.335(76):

1. <u>Power limiter</u> - The system is to restrict the maximum available propulsion power in agreement with the EEXI calculation to comply with the required EEXI. Unintended use of a propulsion power exceeding the limit value must be avoided.

2. <u>Override</u> - The originally installed power exceeding the limited power should be available as power reserve in defined cases to ensure safety of shipping. With this release option, the minimum propulsion power requirement as defined in the guidelines for determining minimum propulsion power to maintain the manoeuvrability of ships in adverse conditions [MEPC.1/Circ.850/Rev.3] is fulfilled even in cases when the limited power is below the requirement. The minimum propulsion power is only defined for bulk carriers and tankers (and combination carriers as well) and was introduced by IMO when the EEDI requirement for newbuildings led to the installation of smaller engines in new designs of these ship types.

3. <u>Alarming</u> - In case of relevant failure modes the crew must be informed that the ShaPoLi system is not correctly working. The alarm must be given at relevant locations preferably on the bridge.

4. <u>Indications</u> - The status of the ShaPoLi system and measurements to be displayed, if feasible on the bridge. It should be indicated whether the system is in normal operation mode below the power limit, whether the limit is released or whether the propulsion power is even exceeding the power limit using the power reserve. The current measured shaft power should be part of the display and indicates proper operation of the ShaPoLi system. Besides, information about the potential activation of the override and recording of data must be shown.

5. <u>Recording</u> - The system must be able to log relevant events and during unlimited mode the measured shaft power must be recorded. Relevant events are the occurrence of failures, changes in the setting of the ShaPoLi system and release of the power limit. Constant recording of the shaft power including original measured values of torque and shaft speed is required when the power limit is released.

6. <u>Tamper proof operation</u> - This requirement includes on the one hand that the setting of the shaft power meter cannot be changed by crew and on the other hand that reliable recording

by the ShaPoLi system is ensured. Access to the shaft power meter setting is forbidden for crew so that the gain cannot be changed. The according factor to be determined from shaft diameter and standard G-modulus of 82,400 N/mm². Only in case actual shaft torsional tests are available different values for the G-modulus might be applied. Acceptable change of the sensor setting is restricted to a regular zero-setting following the maker's instructions. Usually, for zero setting the shaft must be turned with the turning machine by a full turn in both directions and the zero setting is determined from the mean torque. The control unit must be tamper proof as well, meaning that the limit value cannot be changed and the system cannot be switched off without recording of the event.

4. Shaft power measurements

The shaft power measurement is based on a torque and a shaft speed measurement. With a high measuring frequency, the torque measurement will show strong variation within each turn of the shaft due to torsional vibration. Besides, the torque will change with the sea state and rudder movements by autopilot to keep course. With a measuring frequency of 1 value each 15 seconds the mean shaft power for this 15 second interval will average these variations. Further variation of the shaft power signal will be due to changes in wind speed and rudder angles to change the course. A five-minute average taken each 15 seconds as proposed by ISO 19030 will give a stable shaft power measurement.

In the engine automation the shaft power measurement will not be applied to govern the engine. For fixed pitch propeller arrangements, the fuel index will be controlled by the shaft speed. PID controllers allow to stabilize the control loop. The shaft power will simply be integrated as additional limit value. To avoid instability of the governor a stable input is essential, and the 5-minute average is a feasible approach.

5. Power limit for ShaPoLi and EPL

Generally, the power limit value is the same whether engine or shaft power limitation is installed to comply with EEXI requirements. There are two cases where differences appear:

The first case is the multiple engines or shaftline arrangement. With a ShaPoLi solution the total propulsion power is restricted whereas the EPL is installed on the individual engines. This gives additional flexibility for the arrangement with the ShaPoLi installation as in case less engines are operated at a time these engines can run on higher power than an EPL would allow.

By the way, there is also one special case where the EPL can restrict the total engine power of several engines instead of the individual power of each single engine, which is the EPL for electric propulsion engines where the power converter allows to restrict the total propulsion power. Diesel-electric propulsion arrangements are only considered for cruise passenger ships and LNG carriers in the context of EEXI. The diesel engines will not be restricted to comply with EEXI but the electric propulsion motors will be restricted in accordance with the EEXI requirements.

The second case is the arrangement with a shaft generator. As part of the engine load is assigned to the electric power of the shaft generator, the limit value of the EPL is higher than the according value of the ShaPoLi.

When the main engine is below 10 MW, the nominal auxiliary power P_{AE} is set to 5% MCR; for larger main engines the auxiliary power is 2.5% MCR + 250 kW. If the shaft generator has an electric power above P_{AE} / 0.75, the PTO covers the total auxiliary power in the EEXI calculation and the CO_2 emission from auxiliary engines can be ignored.

In the EEXI calculation the PTO power can be deducted from MCR. Therefore, the EPL limit value differs from ShaPoLi limit value as shown in Fig.1.

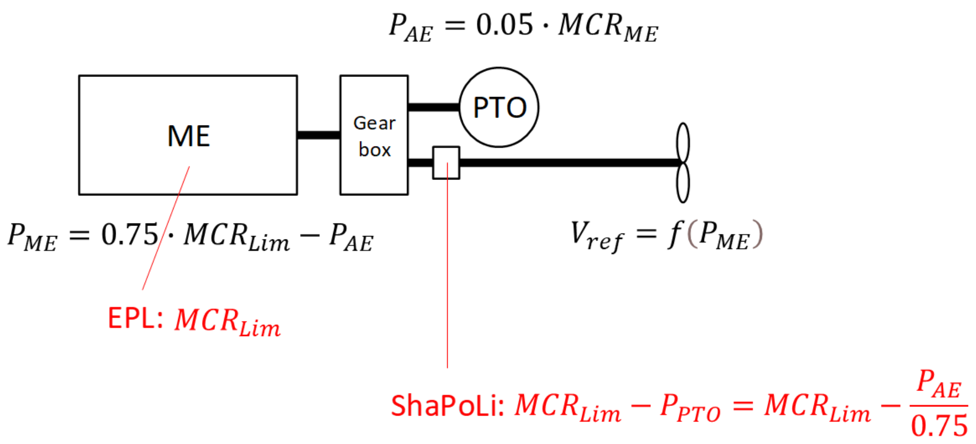

$$EEXI_{required} \geq EEXI_{attained} = \frac{0.75 \cdot MCR_{Lim} \cdot C_F \cdot SFC_{ME}}{DWT \cdot V_{ref}}$$

Fig.1: Comparison of EPL/ShaPoLi for small main engines (<10 MW) and large PTO

From this follows that there is additional flexibility in operation for EPL in this case as complete MCR_{Lim} can be used for propulsion only when PTO is switched off and additional auxiliary engines deliver the auxiliary power. This means that a higher maximum ship speed is possible than with a corresponding ShaPoLi system.

On the other hand, the ShaPoLi solution offers more flexibility in case high auxiliary power is needed, e.g. for reefer container. The shaft generator can cover the auxiliary power independent from the applied propulsion power, meaning that higher main engine power is available than with EPL.

6. Conclusions

The ShaPoLi solution will be applied for EEXI compliance. For some arrangements the ShaPoLi system is a favourable solution such as shaft generator systems, multiple engine or shaft line arrangements and steam turbine systems on LNG carriers. The application of shaft power limitation systems for simple direct diesel engine driven propeller arrangements will depend on the required effort to integrate the independent ShaPoLi system into the engine automation.

References

MARPOL Annex VI, *Regulation 23 & 25 as amended by MEPC.328(76)*, IMO, July 2021

IMO MEPC.335(76), *2021 Guidelines on the Shaft / Engine Power Limitation System to comply with the EEXI Requirements and use of a Power Reserve*, July 2021

Data Models for Environmental and Safety Improvements and Innovation

Martin Karlstad, DNV, Høvik/Norway, martin.karlstad@dnv.com

Abstract

The DNV Master Model was developed by DNV in collaboration with the Norwegian Coastal Administration (NCA) initially to estimate ship emissions along the Norwegian Coast. The DNV Master Model with supporting data sources is now finding relevance for a range of stakeholders including new use cases for NCA, ship brokers, and charterers. This paper aims to exemplify how the model and/or data sources not only can be re-used, combined, and scaled but also how it provides the basis for better decision support and innovation for managing shipping risks and environmental performance for a range of stakeholders.

1. Introduction

The DNV Master model: Mapping of Ship Tracks, Emissions and Reduction Potentials (DNV Master Model) was initially developed in 2010 for use for NCA havbase.no to model fuel consumption and emissions for all ships along the Norwegian Coastline but has today global coverage including world fleet of ships.

The DNV Master Model is a bottom-up approach by using a range of public available commercial and open-source data, internal DNV sources, customers' data sources and applying commonly accepted models/algorithms, Fig.1, on the DNV Veracity platform.

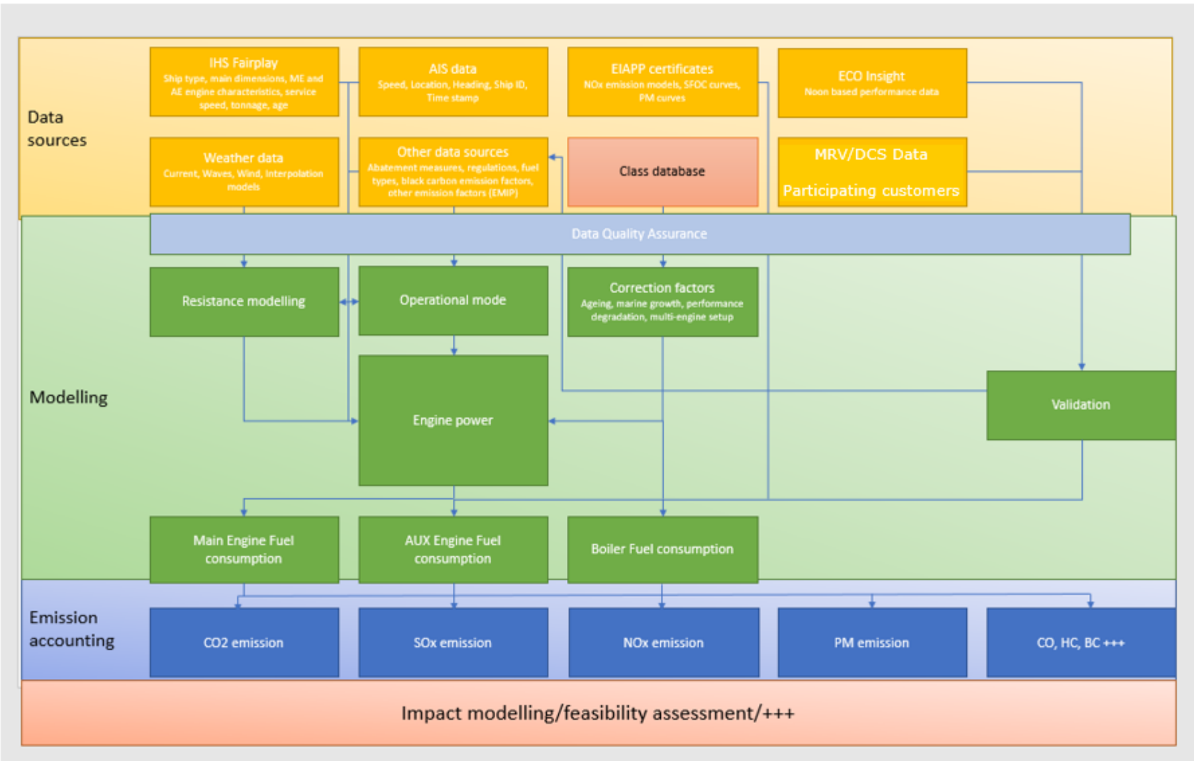

Fig.1: DNV Master Model overview

This includes vessel particulars, AIS data from multiple sources, weather data, ship engine certificates, ship/spill drift models, Port Shapes, and a range of other sources. The modelling includes commonly accepted calculations and algorithms related to resistance modelling, operational modes, ME/AUX/Boiler fuel consumption, alternative fuels, and emission abatement technologies. The model is calibrated and further expanded by use of empirical data e.g., from participating vessel owners and DNV's EU MRV and IMO DCS services covering regular reports on actual consumption for 10.000+ vessels. The result is that factors such as distance sailed, consumption and emissions to air are calculated ~16 million timed daily for more than 80.000 vessels. For this paper, the DNV Master Model refers to both the modelling, the data orchestration and underlying Veracity platform capabilities such as security, identity, and data management/validation as these are fully or partly applied to the various use cases.

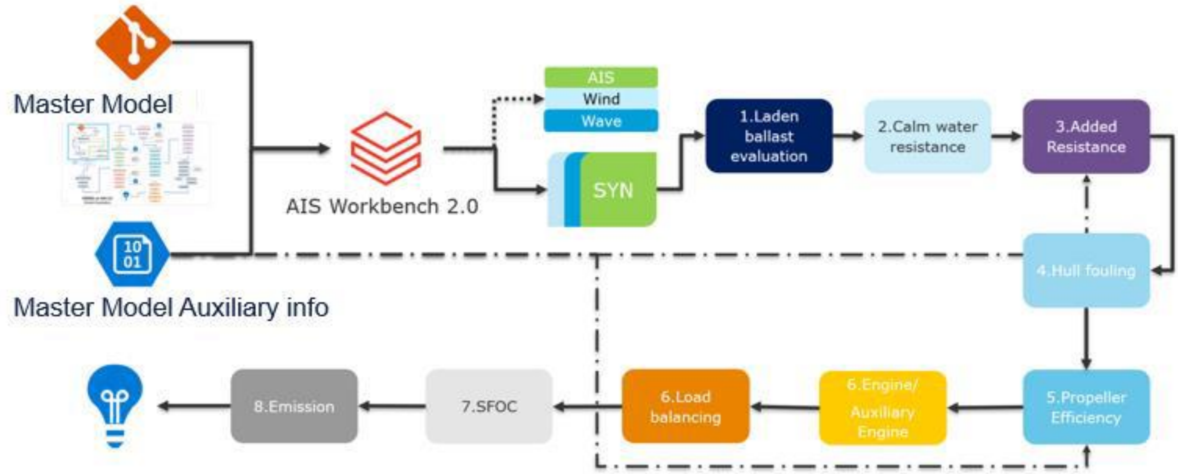

Fig.2: DNV Master Model workflow

2. Multiple stakeholders

The highly intensified focus on decarbonization, environmental issues and digitalization within the marine industry entails that the DNV Master Model become relevant as a basis for a range of new use cases. This includes additional use cases for NCA but also for other stakeholders such as ship owners, equipment and machinery manufacturers, banks, insurance, charterers, and ship brokers, Fig.3.

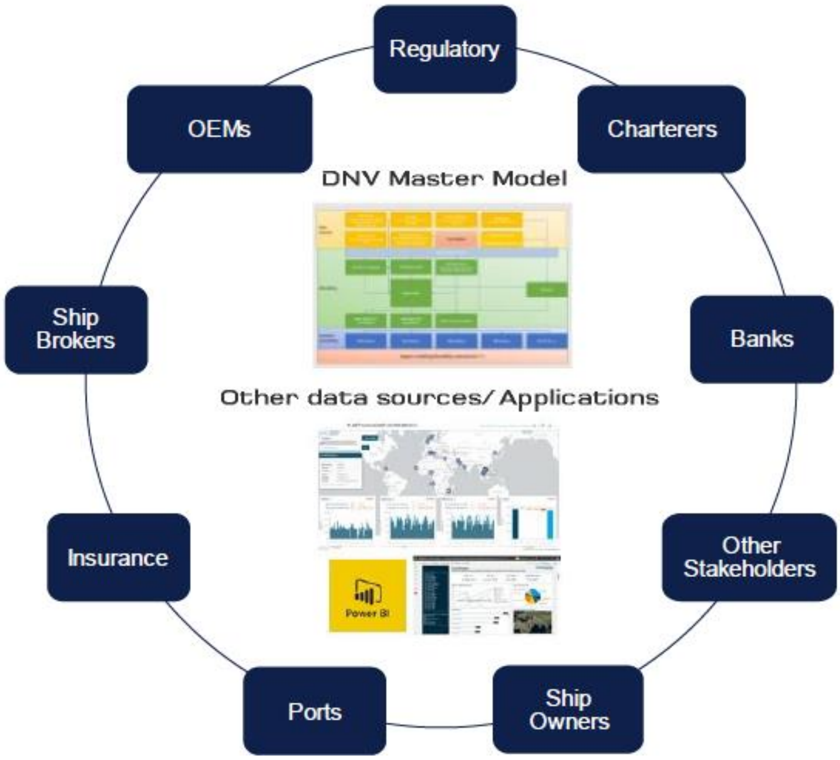

Fig.3: DNV Master Model for multiple stakeholders

NCA: Havbase - The initial use case from NCA was to calculate emissions every six minute from each ship along the Norwegian Coastline, www.havbase.no, (translates to 'oceanbase'). Havbase is based on the principles of environmental accounting and the system is made publicly available, Fig.4. It is used by NCA in an integrated, ecosystem-based marine management approach for calculating emissions to air and planning measures.

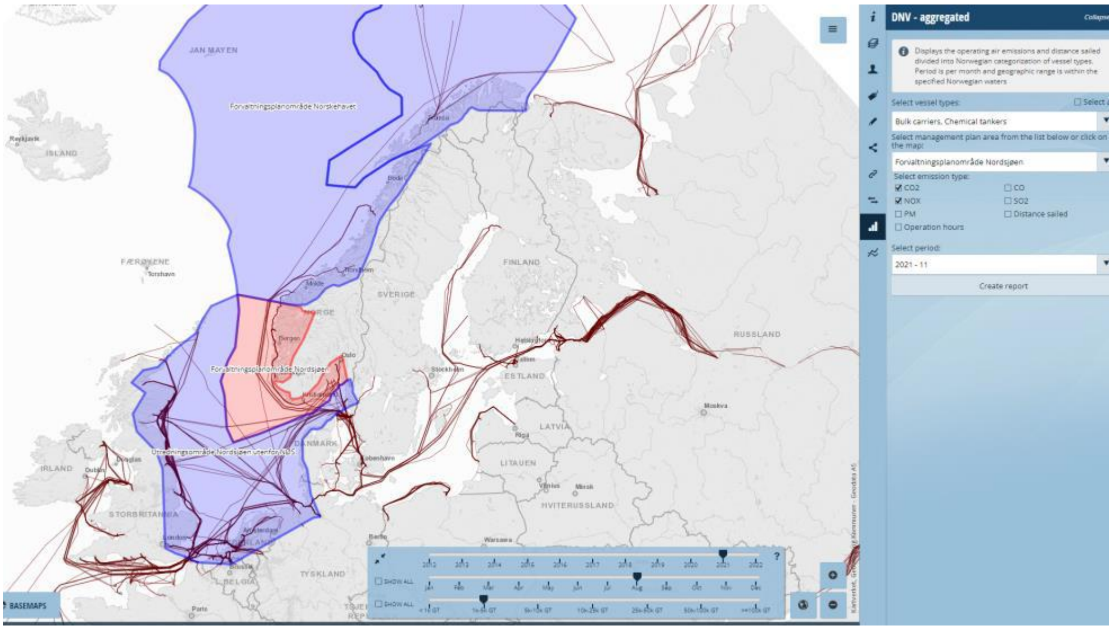

Fig.4: havbase.no showing emissions along the Norwegian Coast

NCA: AISyRISK - NCA had for some time used aggregated AIS data to estimate accident risks related to collisions, groundings, fire/explosion and foundering along the 100.000 km long Norwegian Coastline- thus a statistical methodology based on x nautical mile and y number of vessels, will provide z number of incidents based on vessel density in an area. As the pattern of ships traffic is changing with more seaborne trade, cruise vessels along the coast during the winter, and more bulkers and less tankers; NCA needed an automated and more granular system / methodology for tracking each single ship and create a transparent and updated systems to

- monitor trends related to frequency of accidents and oils spills
- identify high risk areas
- provide updated information to their stakeholders/government regarding risk development as sea borne traffic patterns change
- use information for emergency preparedness- what type is required, where etc.

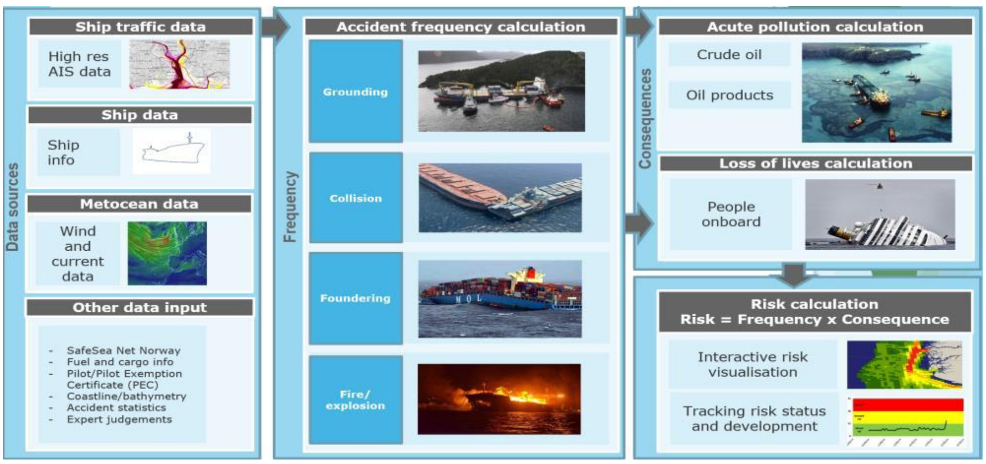

Fig.5: overview of AISyRISK

The DNV Master Model are combined with other data sources such as high resolution AIS data delivered by NCA (up to 2 s resolution), detailed drafts and bathymetry data, pilot status onboard, weather information, what type/size of vessel (e.g. passenger vessels vs oil tankers) and risk models, Fig.5. The application is available for the public on www.aisyrisk.no.

To illustrate the collision model; each ship is given a dynamic safety zone calculated from the ship size and speed over ground (SOG) and high resolution AIS data as shown to the left in Fig.6.

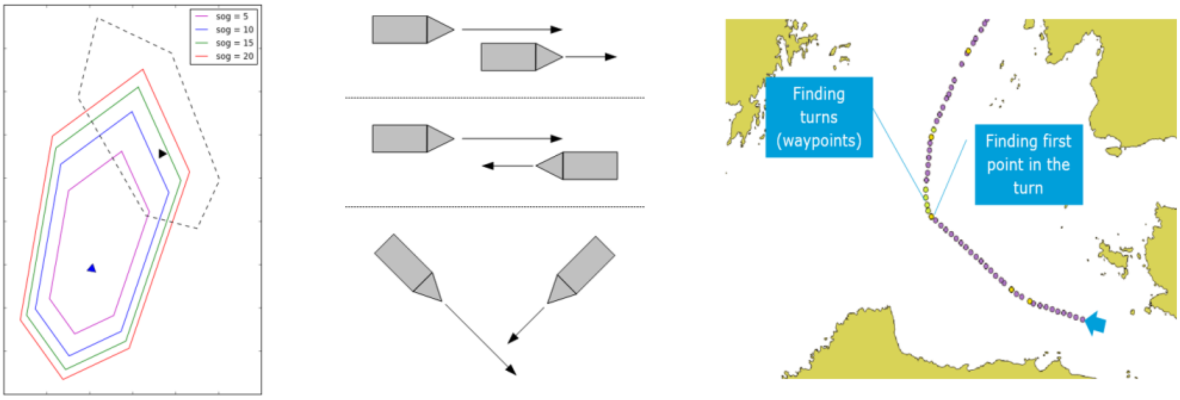

Fig.6: AISyRISK dynamic safety zones based on SOG, type of collisions and powered grounding

AISyRISK tracks each single ship within the vicinity/dynamic safety zone and looks at the risk based on possible collisions based on overtaking, head-on or crossings as illustrated in the middle of Fig.6. The powered grounding model looks at differences in course over ground between adjacent points higher than 5° as shown to the right in Fig.6.

Thus, by tracking each single ship with related details such as ship type/size, speed, loaded or ballasting, type of fuel/cargo, present weather conditions, pilot onboard or not, time of the day, and a range of other factors; AISyRISK provides data richness and granularity for analytics way beyond the initial aggregated/density model. NCA can do detailed analytics such as what type and volume of oil onboard in possible oil spills (e.g. crude vs diesel) which then leads to which type of flanges are required, are better navigational aids required related to risk of powered groundings, seasonal variations, pilot requirements and a range of other analytics scenarios related to all parts of NCA. This provides much better empirical data for decision support, Fig.7, and consequently for getting funding and implementing the relevant risk reduction measures.

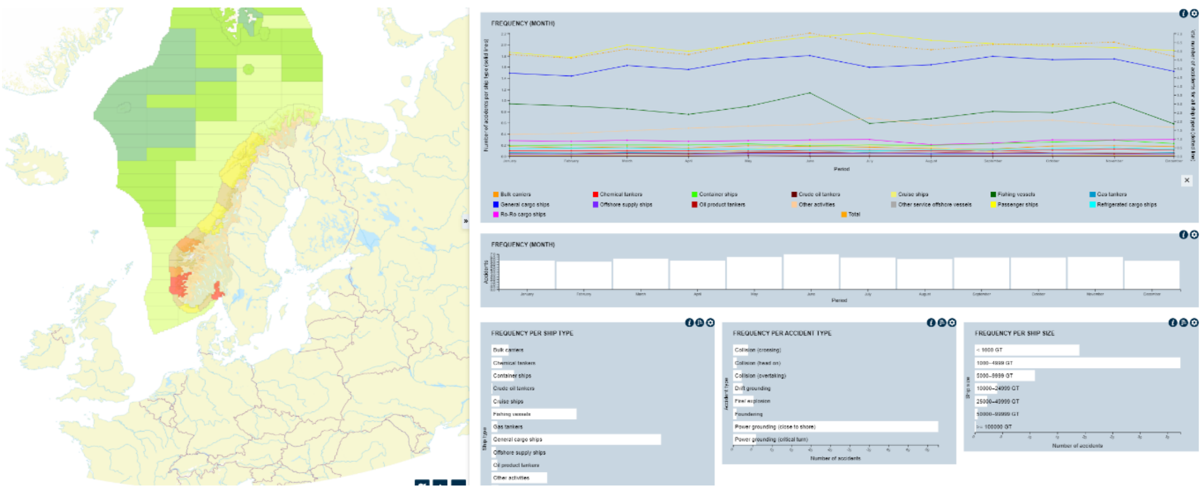
Fig.7: AISyRISK statistics

NCA: EnviRisk **-** NCA combines the DNV Master Model with environmental data sets and oil drift models to calculate the environmental risk - i.e. also for incidents in neighboring countries/seas with possible adverse effects for the Norwegian coast. This will provide detailed information about the area, ecosystem, species, vulnerability, and estimated recovery time.

Fearnleys and other shipbrokers: Emission Prediction Calculator (EPC) - As an additional variable for offering a ship for a charter, Fearnleys will use the DNV Master Model to estimate emissions to air when offering ships from ship owners to charterers by simulating voyages for a high number of ships/voyages per day. The EPC will use additional inputs such as ballast/voyage legs, estimated vessel speed and duration, and location proxies for the possible voyage/charter. The initial modelling of the EPC estimates that there will be millions of calls per day and the DNV Master Model will provide the required assurance and trust between the stakeholders in emissions predictions.

Charterers - ESG Scope 3 emissions - DNV is working with large charterers such as BHP to use the DNV Master Model towards charterers' requirements related to sustainability analytics, ESG Scope 3 reporting and benchmarking towards industry factors and trajectories. This includes supplementing emissions calculations from the chartered ships where there is missing or bad quality data/ information. This is particularly related to voyages/contracts where data is not uniform from the various ship owners/managers, only partly received and in need of validation.

3. Next steps

The current focus on environmental issues and risks from all maritime stakeholders makes the DNV Master Model more relevant than ever. The DNV Master Model combined with additional data sources is applicable for a range of use cases and stakeholders which was not foreseen when the project started 12 years ago. There is a need for data and the DNV Master Model is an important and scalable brick in building new and innovative solutions to address the industry challenges.

Increasing Fuel Efficiency by Sharing Operational Insights with the Crew

Martin Köpke, Hapag-Lloyd AG, Hamburg/Germany, martin.koepke@hlag.com

Abstract

Today a vessel's crew is entering and sending a detailed set of operational data to shore. However, what they mostly receive in reply are instructions, schedules and if at all a very limited abstract of their performance. In order to achieve a higher level of transparency and mutual understanding Hapag-Lloyd introduced automated feedback to vessel crews for all 250 operated ships. The idea behind this automated crew feedback is to display the results of the vessels' actions and reports. Each reported value is compared to an expected value, which is based on a virtual model of each individual ship. This way the crew is immediately aware of reporting errors, measurement errors and possible excess consumptions. This paper elaborates the background of the feedback, crew awareness and will analyse the impact on data quality, vessel operation, and efficiency. Further, bottlenecks and obstacles will be analysed which are hindering the crew to gain from such a tool. The feedback to crew module was a development with the innovation project ShippingLab.

1. Introduction

Decarbonisation is one of the biggest challenges for the shipping industry today and tomorrow. The shipping industry has clear GHG reduction targets released by *IMO (2018)* and *EU (2021)*. Beyond these mandatory reduction schemes, shipping lines, as Hapag-Lloyd, published even more ambitious targets towards decarbonisation of shipping, https://www.hapag-lloyd.com/de/company/ir/calendar-events/capital-markets-day.html#tabnav.

For newbuildings, regulations exist, e.g. with the Energy Efficiency Design Index, *IMO (2011)*. Certainly new, carbon-free propulsion technologies are required. However, there is still a large existing fleet, which is being to a certain extent modernised towards operation that is more efficient. Nevertheless, these vessels operate on fossil fuels. Therefore, the vessel operation itself needs to be as efficient as possible. IMO addressed this with various levers, such as the introduction of the Ship Energy Efficiency Management Plan (SEEMP), the Data Collection System (DCS) and the Carbon Intensity Indicator (CII), *IMO (2017)*, *IMO (2022)*. The CII will have significant impact on the current fleet, by increasing the required energy efficiency on a yearly level. To reach these targets, speed instructions will have a big impact; however, also the efficient voyage execution is even more in focus than before.

Similar to IMO's initiatives, the EU introduced the Monitoring, Reporting and Verification (MRV) scheme, where shipping companies report their emissions in European waters. EU already announced that an Emission Trading System will follow, where shipping companies need to pay for their emitted GHGs.

Together with IMO's DCS, this gives a new importance to the quality of reported operational data from ships.

This paper will discuss the roll-out of a fleet-wide performance feedback to crew platform. Aim of the crew feedback is to achieve a higher level of transparency and awareness towards fuel efficiency and data quality for the captains and senior officers on board. To begin, the relevant Key Performance Indicators (KPI) will be introduced. Followed by an analysis of the impact on performance and a discussion of the obstacles of such a roll-out. The introduced crew feedback module is a development within ShippingLab. ShippingLab is a nonprofit innovation and project partnership in Blue Denmark, https://shippinglab.dk/.

2. Key Performance Indicators

Operational data quality and fuel consumption are in the focus of shipping companies as well as authorities and policy makers. Therefore, it needs to be determined what is needed by the crew to improve these.

The fleet operated by Hapag-Lloyd consists of more than 250 container vessels varying in size from 350 to 19,000 TEU. About one-half of the fleet is owned, while the other half is chartered. This means communication, on-board systems, technical equipment and training of the different crews vary. With regard to operational data reporting, this means the traditional noon report is the one common ground all vessels can provide. In case of Hapag-Lloyd, all vessels report in the same tool to have comparable and unified data for each vessel. Hence, in the first roll-out of the feedback to crew, all analyses rely on manual noon data.

This awareness campaign targets especially Captains, Chief Officers, Chief Engineer and 2nd Engineer, since they hold the main responsibilities for the nautical and technical speed and power management of a ship. Furthermore, they are also responsible for the operational reporting. To achieve the targets towards higher data quality and more efficient voyage execution, the following requirements to the feedback to the crew were established:

- Visualise reported figures to the crew
- Enable the commands to see their impact of their own actions
- Quantify data quality and vessel performance
- Compare themselves to (anonymised) peer vessels / sister vessels

The operational data quality is shown as KPI as well as percentage of errors, which triggered a plausibility check. Further, the respective errors for each day are displayed.

The main engine's total consumption as well as the specific fuel oil consumption are displayed. The consumptions are shown in relation to the expected consumption based on fuel tables and shop test, respectively. Furthermore, speed-consumption data in relation to weather and a load diagram are available to support the vessels crew in their voyage planning. The actual and the expected boiler consumptions are displayed.

In order to stimulate the professional pride and completion, the KPIs of the anonymised sister vessels are available to the crew.

In general, most of these data was available to the vessel command also before the crew feedback platform was rolled out; however, on the platform also the expected values are shown. This helps to with reporting, but also senior related issues. By providing sister vessels' KPIs, the board command can also see what is possible with regard to efficient operations on other vessels.

3. Impact review

The impact review is done on two levels, on one side the perception (qualitatively) of the implementation of the crew feedback platform is evaluated. On the other side, the implementation is quantitatively evaluated with regard to the KPIs.

3.1. Qualitative review

For the review of how the crew feedback was perceived on board, a survey form was sent to vessels. The answering of the survey was anonymous in order to avoid biased results. About 20% of the fleet filled out the survey form. About 7% of the vessels wrote back that they had technical issues to fill out the form and the rest did not respond.

The vessels were asked questions in different categories, such as frequency of usage, utility, system performance, practicality, and completeness of the platform.

The answers of the survey show that the general perception of the feedback on board is very positive. The vast majority (96%) answered that they deem the feedback to crew as useful and 2/3 of the vessels answered that they use the tool at least once per week, Figs.1 and 2. Furthermore, most vessels stated that the crew feedback improves the overall voyage execution as well as quality of the reported data, Figs.3 and 4.

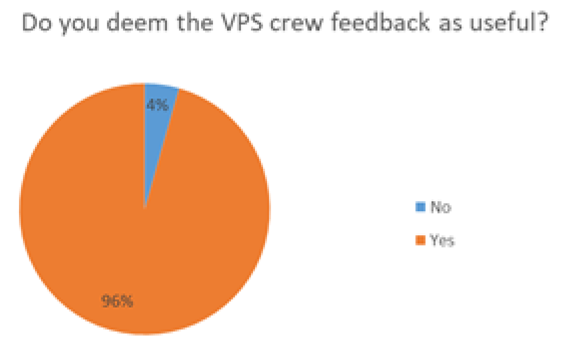

Fig.1: Usefulness

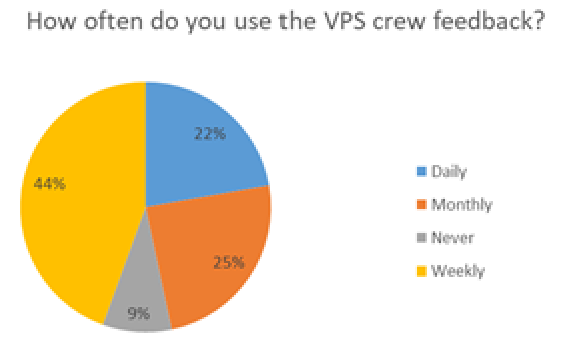

Fig.2: Usage frequency

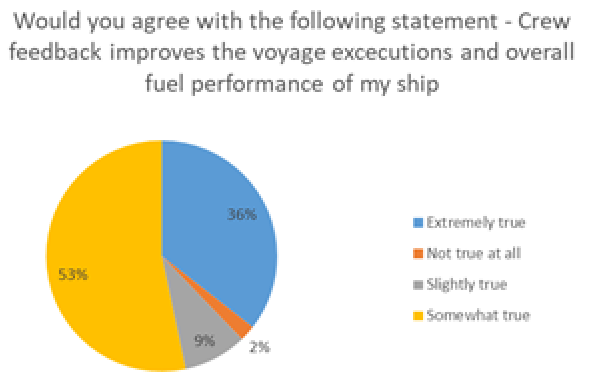

Fig.3: Perception of voyage execution and overall fuel oil consumption improvement

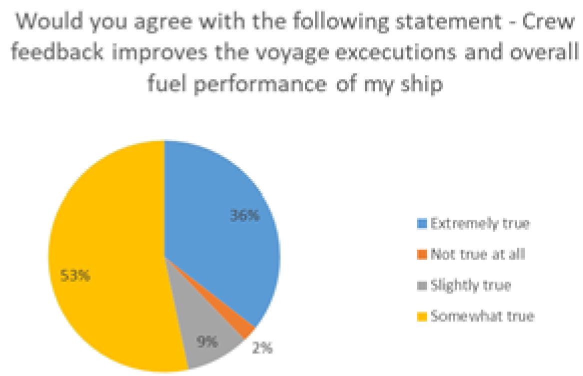

Fig.4: Perception of operational data quality improvement

One assumption behind the introduction of the feedback to crew model was that the board management would appreciate the transparency and perceive it as additional motivation. The vessels were asked for brief testimonials how they perceive the feedback. In general, these statements reflect that the crew appreciates the feedback to crew module. Exemplarily, some statements are shown below; please note that two captains sent their testimonial via email and therefore, with their consent, are not anonymised:

"This performance monitoring tool is very useful in order for us to improve our machineries performance in general and to rectifying the warnings and errors as well." – Anonymous

"Mainly for curiosity, to compare our performance with other ships." – Anonymous

"The best is speed and consumption for future voyage calculation." – Anonymous

"Monitoring for highest amount of errors and analyse where are they coming from. Analysing performance of Main Engine and comparing with benchmark." – Anonymous

"We can see performance of vessel during voyage and we can see various graphs and it help us to identify performance and maintenance issues". – Anonymous

“The automated crew feedback software gives us a feedback of the quality of our reported data and proves to us that our efforts in collecting and reporting these data produce actual results. Comparing our data to peer values and to anonymized sister vessels can help us find abnormalities in the data reported, enabling us to improve the quality of our noon reports or even vessel performance as a whole. With a generally increasing workload of documentation and reporting on board, it is nice to have a tool that uses data, which we already provide anyway, without creating additional work.” – Dennis Schwartz, Master Mariner

“For several years we have been using the same reporting tool on all ships in the HL fleet to report a large number of parameters from daily ship operations, e.g. positions and times at the start/end of the voyage, midday position, miles travelled, observed weather data, consumption of main engine, auxiliary diesel and boiler etc. The “Fleet Analytics” team on land evaluates this data. The positions are forwarded to our weather provider for weather routing. With the crew feedback, we get a visualisation on-board. This enables to compare data we previously entered voyages and as well as corresponding values of the sister ships. The latter is particularly important in my service trade area with five sisters in the same service. The tool also enables us to check the quality of the data entered. In the medium and long term, even possible technical defects can be identified that occur gradually and are therefore not noticeable in daily on-board operation (e.g. defective valves that cause higher boiler consumption).” – Björn Kropp, Master Mariner

3.2. Quantitative review

The quantitative analysis investigates if there are measurable improved since the introduction of the crew feedback. For this, a subset of 38 owned and by Hapag-Lloyd managed vessels is analysed. This subgroup of vessels is used to ensure the vessels were continuously in the fleet for the whole period that this paper looks into, which could not be guaranteed for chartered vessels.

The focus of the quantitative analysis in this paper is on the data quality and not the consumptions. The reason are different external parameters that have an impact on the consumptions that are beyond the crew feedback. To illustrate this, the monthly average consumption of the oil-fired boiler is analysed, six months before and six months after the crew feedback was introduced. The chosen subgroup of vessels show that the boiler consumptions increased by around 10%. However, the six months after the introduction of the crew feedback are the months from October 2021 to March 2022. All analysed vessels operated in the majority of that period in the northern hemisphere. Therefore, it is concluded that the boiler consumptions correlate to the lower average temperatures, Fig.5. However, even on a year-to-year comparison, the consumptions slightly increase. Yet, no clear conclusion on the additional consumption could been derived. There is consensus that this increase is not caused by providing additional data to the crew.

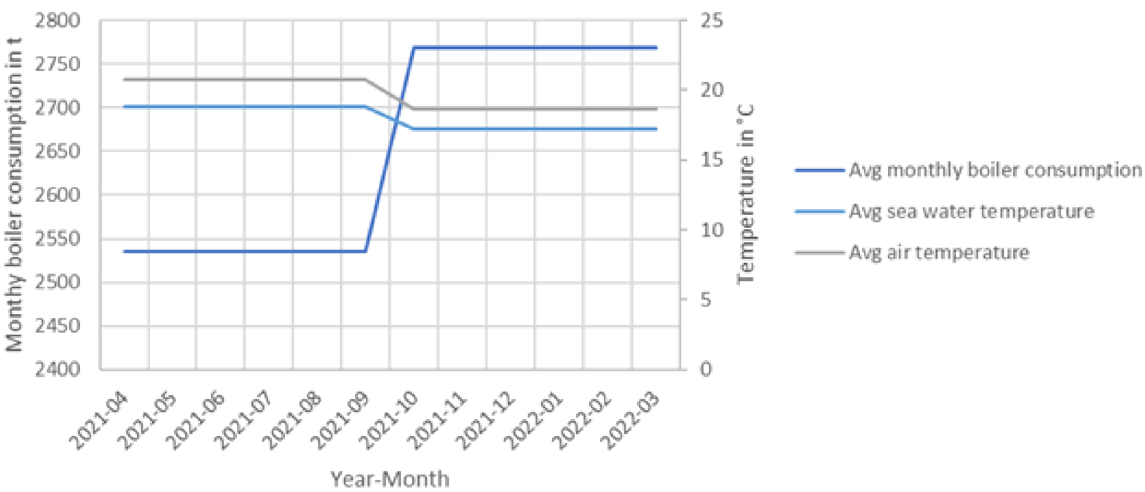

Fig.5: Monthly avg. boiler consumption at sea and sea water / air temperature

To quantify the impact on the reported noon data quality, the weekly average number of errors is counted. An error in this context means that a plausibility check is triggered, and the respective reported value is outside expectations. Again, the earlier defined subset of vessels is used. For all analysed vessels, the data quality improved by about 7%, i.e. 7% fewer errors are detected. However, it became also apparent that some vessels showed a decay in the data quality. It seems unlikely that by focusing on data quality, the actual data quality would decrease. In this context, it should be noted that the actual usage of the crew feedback tool could not be tracked. Therefore, it is considered that the tool where data quality decreased was not in use.

When filtering out the vessels, which may not use the tool, the improvement on data quality is much higher. The increase of data quality is about 21%, Fig.6.

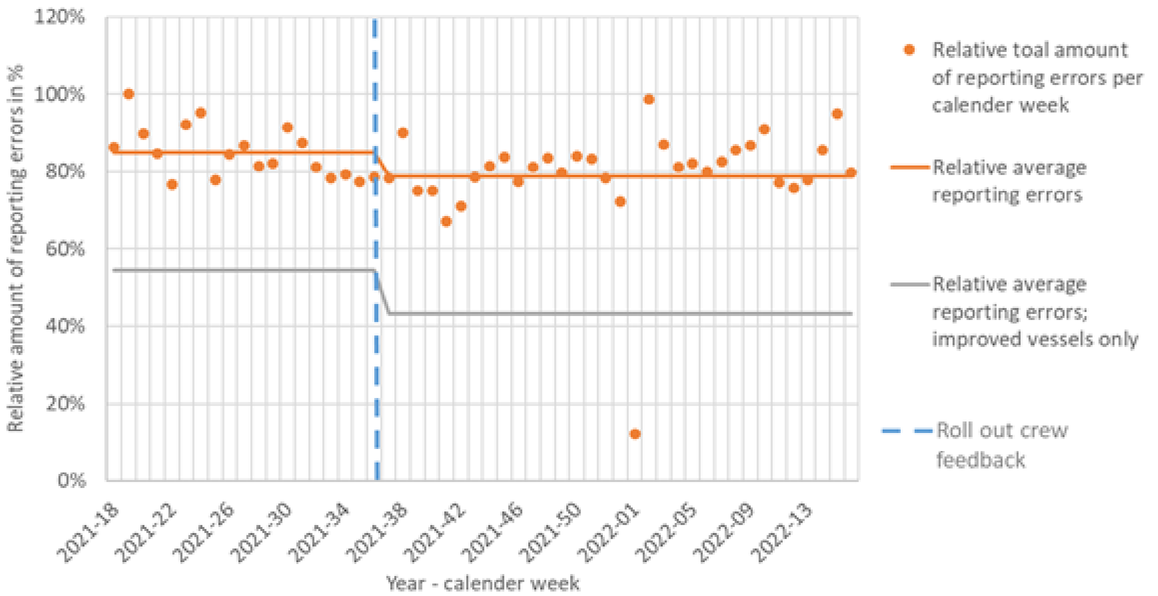

Fig.6: Operational data quality

4. Lessons learnt

Within the roll-out of the feedback to crew module, some observations were made. First, about 5% of the chartered vessels have no internet access, except for emails. This could not be solved during the project, beyond discussing the issues with the managers/owners, and hence the tool could not be rolled out to these ships at all.

Furthermore, about 25% of the chartered in vessels could initially not reach the webpage of the crew feedback, because it was blocked. The IT departments of the respective ship managements needed to whitelist the webpage. This was necessary for internet security reasons and company policies.

In addition, on the owned and managed vessels, the crews reported at the beginning that the performance of the system was very low, resulting in inconvenient waiting times. In some cases, the waiting time were so frustrating that captains would not use the tool. After some investigations with Hapag-Lloyd's IT, it was found that the reason for the low performance was related to internet security settings. The settings of the involved systems could be configured resulting in much faster performance of the system.

Initially it was planned to track the usage of the crew feedback module using Google Analytics. After continuously monitoring lower than expected number of users, the presumed non-users were asked for the reasons why not using the tool. It turned out that many of the presumed non-users stated that the tool is in use. This led to an investigation if the tracking of clicks in Google Analytics works sufficiently. It turned out that depending on the settings of individual computers (basically cookie settings), satellite communication, company internet security settings, etc. Google Analytics would not count all clicks. Hence, a new tracking needs to be developed.

To stimulate the usage of the tool as well as receiving feedback by the vessels, weekly newsletters were sent to the fleet introducing functions and features of the tool. In addition, improvements for data quality, which could be related to the use of the tool, were communicated.

5. Conclusions

The presented analysis shows that the crew feedback tool is perceived very positively within the fleet. The increased level of transparency provides information for more efficient voyage execution, supports voyage planning, and helps to identify efficient operational practice.

Furthermore, the analysis showed measurable improvement of operational data quality. By increasing operational data quality, the reliability of efficiency evaluation is improved. This applies to all consumers as well as hull efficiency evaluation. For the latter, higher reliability and more accurate data lead to quicker conclusions and hence actions, in case of a performance decrease is detected, e.g. due to biofouling.

Even though this paper does not quantify benefits in consumptions, there is consensus that voyage execution and hence consumptions are improved. This is also stated by on-board management.

As a next step, in order to reach also vessels with no internet access (except emails), vessels with slow internet connections, and on-board management simply not clicking the tool, regular performance reports will be sent on board.

Acknowledgement

I thank all involved captains and officers of the Hapag-Lloyd's operated fleet for their valuable comments and feedback. In addition, I thank all members of the ShippingLab innovation project for the constructive collaboration, bright ideas and developments.

References

EU (2021) *Use of renewable and low-carbon fuels in maritime transport and amending*, Directive 2009/16/EC, European Union

IMO (2011), Res MEPC.203(62), Int. Mar. Org., London

IMO (2017), *Existing IMO activity related to reducing GHG emissions in the shipping sector*, Int. Mar. Org., London, https://wwwcdn.imo.org/localresources/en/OurWork/Environment/Documents/ISWG-GHG%201-2.pdf

IMO (2018), *Initial IMO Strategy on Reduction of GHG Emissions from Ships*, Res. MEPC.304(72), Int. Mar. Org., London

IMO (2022), *Annual operational carbon intensity indicator (CII) and CII rating*, Int. Mar. Org., London, https://www.imo.org/en/MediaCentre/PressBriefings/pages/42-MEPC-short-term-measure.aspx

Vessel Technical Performance Analysis using Accurate Weather and Speed Through Water Data

Vemund Svanes Bertelsen, Miros Mocean, Asker/NO, vsb@miros-group.com
Alfredo Carella, Miros Mocean, Asker/NO, ac@miros-group.com
Rune Gangeskar, Miros Mocean, Asker/NO, rg@miros-group.com
Gunnar Prytz, Miros Mocean, Asker/NO, gp@miros-group.com
Michael Schmidt, Copenhagen Commercial Platform, Rungsted Kyst/DK, mhs@ccp-platform.com

Abstract

A wide range of maritime stakeholders including owners, operators, charterers, suppliers and regulators currently have a large focus on monitoring and reducing fossil fuel consumption and associated emissions. The fuel consumption and the corresponding technical performance of a vessel depend on a range of factors related to the vessel itself and the surrounding environment. Environmental factors like ocean waves, currents and temperature, as well as wind, all have a significant impact on vessel performance. Until recently, the impact of the environment on vessel performance has been hard to quantify accurately, and consequently, vessel performance analyses have been tainted with large uncertainties. With recent improvements in measurement technologies, it is now possible to measure environmental parameters and vessel performance accurately. By combining high-frequency, accurate data with detailed models for how the key environmental factors influence a vessel, the actual vessel performance in typically occurring weather conditions can be estimated accurately. This paper presents a solution for how the impact from the environment can be separated from the technical performance of a vessel, together with some examples using data from real-life situations.

1. Introduction

193 countries have adopted the United Nations 2030 Agenda for Sustainable Development and its 17 Sustainable Development Goals. The overall objective is to promote prosperity while protecting the planet. As formulated by the IMO (the International Maritime Organization - a specialized agency of the United Nations which is responsible for measures to improve the safety and security of international shipping and to prevent pollution from ships), most of the elements of the 2030 Agenda will only be realized with a sustainable transport sector supporting the world trade and facilitating the global economy. Goal number 14, "Conserve and sustainably use the oceans, seas and marine resources for sustainable development", is particularly central for shipping, although many of the other goals are also in some way related to shipping.

The UN sustainable development goals underline the present global focus on efficient usage of energy and reduction of pollution and emissions in all aspects of society. Looking at shipping, there is a vast range of initiatives, technologies, concepts and regulations aimed at reducing emissions of ships in order to improve the sustainability of global transportation. The primary objective of many innovations within energy saving devices, hull and propeller coating and cleaning solutions, as well as hull and propeller designs, is to improve vessel performance. On top of this comes new developments within areas such as voyage optimization and performance-oriented contracts.

The validation of new technologies and solutions requires accurate insight into how vessels perform. Traditionally, there has been a lack of accurate data measured in service related to some of the crucial input and output factors, and this has made the task of accurately describing vessel performance difficult. The key inputs would be fuel, cargo and weather (e.g. waves, wind and current), and the output would be the resulting speed of the vessel through the water. Other input factors related to the vessel hull and propeller condition (e.g. fouling), the vessel loading condition (e.g. draft and trim) and how it navigates (e.g. rudder movements and engine speed variations) are also important. From this perspective, the speed of a vessel can be seen as a measure of the output or transport efficiency of a vessel at a given input of fuel, cargo, weather etc.

Well proven and sufficiently accurate instrumentation exists to determine how much fuel a vessel has consumed (e.g. via mass flow meters or tank soundings) and how much cargo it is carrying (e.g. by measuring draft). It is however challenging to accurately determine the most important measure of the vessel output, the Speed Through Water (STW), as this is often measured with low accuracy by speed logs or estimated based on GPS data and weather models with limited spatial and temporal resolution and insufficient accuracy. Adding to the challenge is that data is often available as one point per day (e.g. noon report data) or with a few data points per day (e.g. forecast/hindcast data). The situation is similar with weather data, where some parameters like wave height and direction might even be visually assessed just once a day, which further adds to the challenge of doing accurate performance analysis.

A certain input of fuel results in a certain speed through water of the vessel. A set of factors influence this relationship, including:

- The quality of the fuel (i.e. the energy content)
- The efficiency of engines and drivetrain
- The amount of cargo carried
- The condition of hull and propellers
- The draft and trim of the vessel
- The weather conditions (waves, current and wind)
- The water conditions (temperature, salinity and depth)
- The influence of navigation (e.g. rudder movements, speed changes)

To reach a new level of in-service accuracy within technical vessel performance analysis, there is a need to have accurate data on key input and output factors including weather and STW. In addition, the data update frequency has to be in the minute range as this is the rate of change of some of the input factors like the weather or navigational changes. For some use cases like speed optimization related to performance contracts or time-of-arrival conditions, the data must be made available in real-time in an actionable manner. For other use cases, like vessel performance analysis, it is sufficient to have the data available in retrospect.

The fuel going into the engines produces a certain amount of shaft power which moves the vessel forward. The shaft power is consumed by a number of processes and effects related to both the actual movement of the vessel and the environment surrounding the vessel, fig.1.

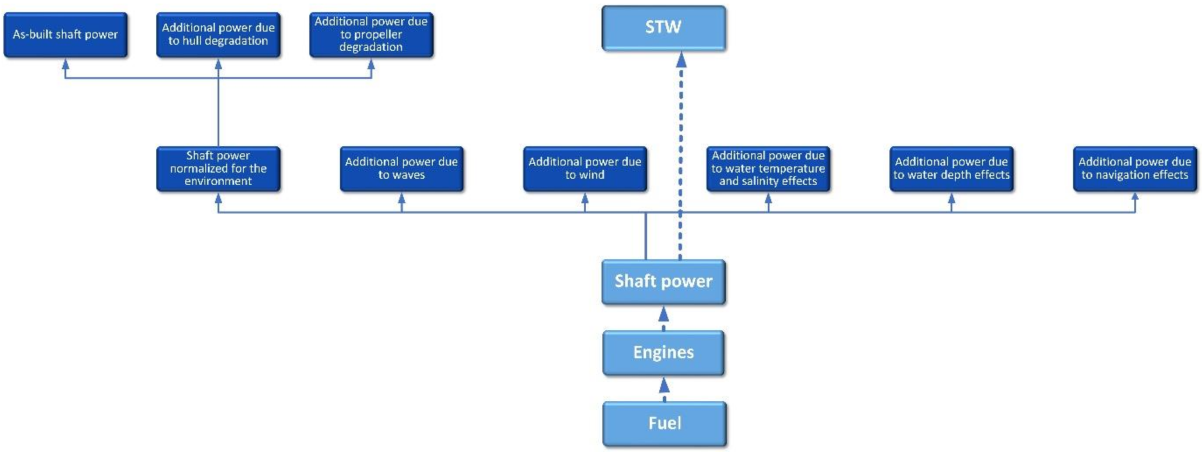

Fig.1: Process from fuel to speed through water. Shaft power is divided into its components.

A considerable amount of shaft power can be consumed in countering the effects of the waves in situations with bad weather. The amount of power consumed due to waves depends on wave height, direction and period. In situations with several wave systems present, each wave component will add different power contributions. In some situations, there can be a positive effect from the waves, i.e. the waves contribute positively to the forward motion of the vessel.

The situation is similar for wind, which can have a significant impact on the forward motion of a vessel. The effect varies with the wind magnitude and direction. The wind power can be both negative and positive, as is obvious for sailing vessels. The depth of the water also influences the amount of power required to move a vessel forward. In areas with low depth (lower than 5-10 times the mean draft of the vessel), more power is required to move the vessel forward than in deep water areas. Furthermore, the ocean water temperature and salinity influence how much power is needed to maintain a certain speed through the water.

In addition to the above, power is lost by vessel navigation, i.e. when the vessel changes speed or course. Changing the trim state (i.e. the difference between forward and aft draft) will also influence the vessel and the amount of power required to propel the vessel forward.

There is a need to isolate the influences of the environment and vessel navigation in order to arrive at the actual, technical vessel performance. The isolation of weather effects is normally referred to as weather normalization, and a set of available methods can be applied for this purpose (e.g. ISO-15016-2015). The correction due to water temperature and salinity effects is sometimes also included in weather normalization. Weather normalization is a key topic of this paper and will be discussed further in the sections below.

Similarly, navigational effects can be removed by removing time periods where the vessel is changing speed or course. Due to the inherent time lag in such a system, there might be a need to also remove a certain time period (e.g. 30 minutes) after the change to allow the vessel speed to settle.

This paper presents some examples of vessel performance analysis using accurate, high-frequency vessel data. The data is normalized for weather and other effects and the resulting actual performance is estimated.

2. Analyzing the technical performance of vessels

Newer vessels have their new build performance established with standard tests and a sea trial (i.e., procedures from ITTC, ISO-15016, etc.). The sea trial, setting the vessel specific technical performance, is conducted under controlled circumstances and within certain weather limits. Following how a vessel's performance develops over its lifetime is more difficult as equally accurate performance data are hard to obtain while the vessel is in service. Important parameters like speed through water and weather have not been measured with sufficient accuracy. Also, established and suggested indexes have a tendency to mix together technical vessel performance with vessel operation.

DNV, Copenhagen Commercial platform (CCP) and Miros Mocean are collaborating in a project that aims to develop a Vessel Technical Index (VTI), *Guo et al. (2021)*, *Svanes Bertelsen et al. (2021)*. The VTI is an index that aims to describe a vessel's in-service performance normalized for environmental and operational effects. This will enable relevant stakeholders to use the VTI to describe the current technical performance of a specific vessel compared to its new build reference performance and follow it during its lifetime and manage their vessels based on better information. For the time being, two main use cases have been identified for the VTI:

- Assess and advice on the need for hull cleaning/propeller polishing (maintenance) based on VTI score over time.
- Evaluate and verify the effects of energy efficiency devices and other technical measures.

An important part of the project has been to quantify the uncertainty in the VTI. Sources of uncertainty have been identified and their contribution to the resulting VTI quantified for different scenarios of data input accuracy and environmental conditions. An important aspect in this context is how the uncertainty in the model used to calculate the effect of the environment, is dependent on the prevailing environmental conditions themselves. This puts constraints on how data inputs and results should be filtered to obtain an accurate enough VTI, useful for specific operational decisions.

3. Vessel Technical Index (VTI) – calculation and data inputs

Guo et al. (2021) and *Svanes Bertelsen et al. (2021)* described and discussed a procedure for how to calculate a VTI, which is defined as:

$$VTI = \frac{P_m - P_{env}}{P_0} \tag{1}$$

Here P_m is the delivered power measured at the propeller shaft. To correct the calculated VTI for the effect of the environment the vessel is operated in, P_{env}, the power to overcome environmental effects, is subtracted from the measured power. This difference, $P_m - P_{env}$, is referred to as normalized power.

P_0 is the reference power, the power the vessel should use to achieve the measured speed through water for the given loading condition, based on the vessel's reference performance, measured in tank tests and the sea trial.

The model for the power correction P_{env} suggested in *Guo et al. (2021)*, can be written as follows*:*

$$P_{env} = P_{wave} + P_{wind} + P_{temp} \tag{2}$$

As *Guo et al. (2021)* describes, P_{wave} is calculated based on a formula presented in *Liu and Papanikolaou (2020*) for added resistance induced by waves from arbitrary directions. As discussed in section 4, two approaches have since then been analyzed. The first approach applies the measured directional wave spectrum from a Miros Wavex solution directly. The second approach applies a synthesized Pierson-Moskowitz spectrum based on the integrated wave parameters calculated based on the measured wave spectrum: significant wave height H_{m0}, primary wave peak period T_{p1}, and the primary peak direction D_{p1}.

The added resistance from the wind is calculated using formula C.1 in Annex C of *ISO 15016:2015(E) (2015)*. Likewise, added resistance due to water temperature effects is calculated based on *ISO 15016:2015(E) (2015)* Annex F.

The power P_{env}, consisting of P_{wave}, P_{wind} and P_{temp}, is calculated by multiplying the added resistance by the measured speed through water:

$$P_{env} = \left(\mathrm{R_{wave}} + \mathrm{R_{wind}} + \mathrm{R_{temp}}\right) \cdot \mathrm{V_{STW}} \tag{3}$$

An expression for the reference power P_0, as a function of speed through water and displacement, is obtained by interpolating tank tests and sea trial data as described in *Svanes Bertelsen et al. (2021)*. The expression has a valid area limited by the speeds and displacements covered by tank tests and sea trial data, but relevant combinations of speed, displacement and power for a vessel in transit are covered.

Figs.2 and 3 gives an overview of data inputs collected from sensors onboard, external sources, and parameters calculated by the Miros Mocean system used to obtain the results presented in section 4.

The power consumption $\mathrm{P_m}$ is measured by a shaft meter based on a strain gauge technique at the propeller shaft. The Miros Mocean system includes a Miros Wavex solution, a state-of-the-art radar-based sea state measurement device, that can measure ocean waves, ocean currents and STW accurately under widely varying conditions and with high availability and reliability *Gangeskar (2018a, 2021)*. Measurements are based on marine X-band navigation radar images. Fig.4 illustrates how configurable measurement areas are extracted from polar radar images, for wave, current and STW measurements in local areas of interest, at a couple of hundred meters from the vessel. The images are processed by algorithms designed to obtain real-time wave spectra, integrated wave parameters, surface current vectors and STW data, *Gangeskar et al. (2018)*, *Prytz et al. (2019)*.

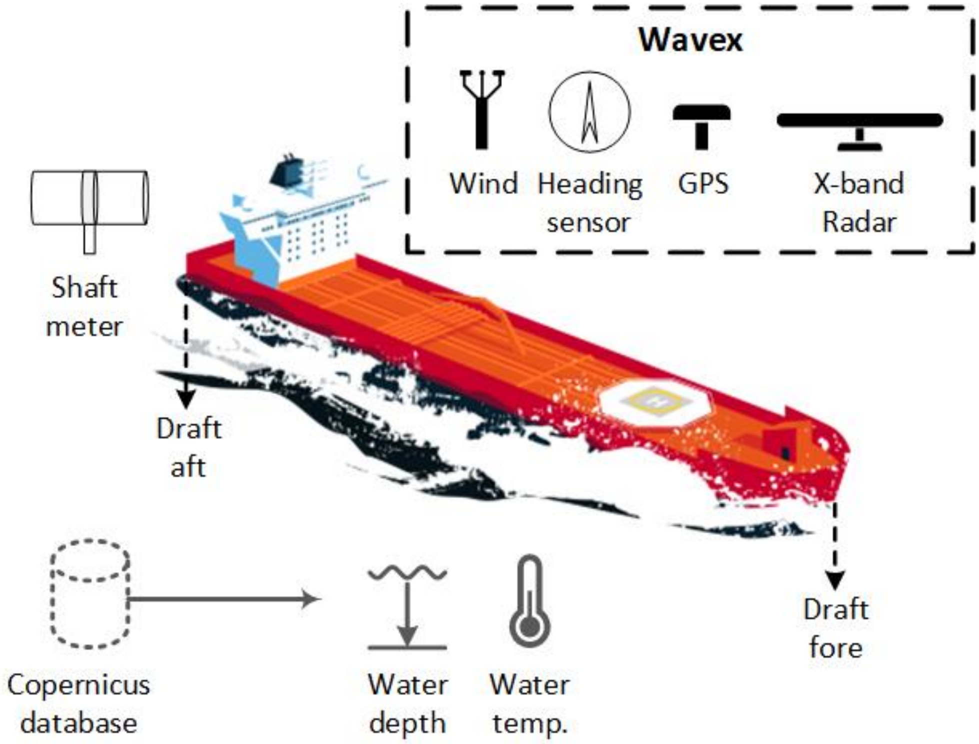

Fig.2: Required sensor and data inputs used to calculate the VTI

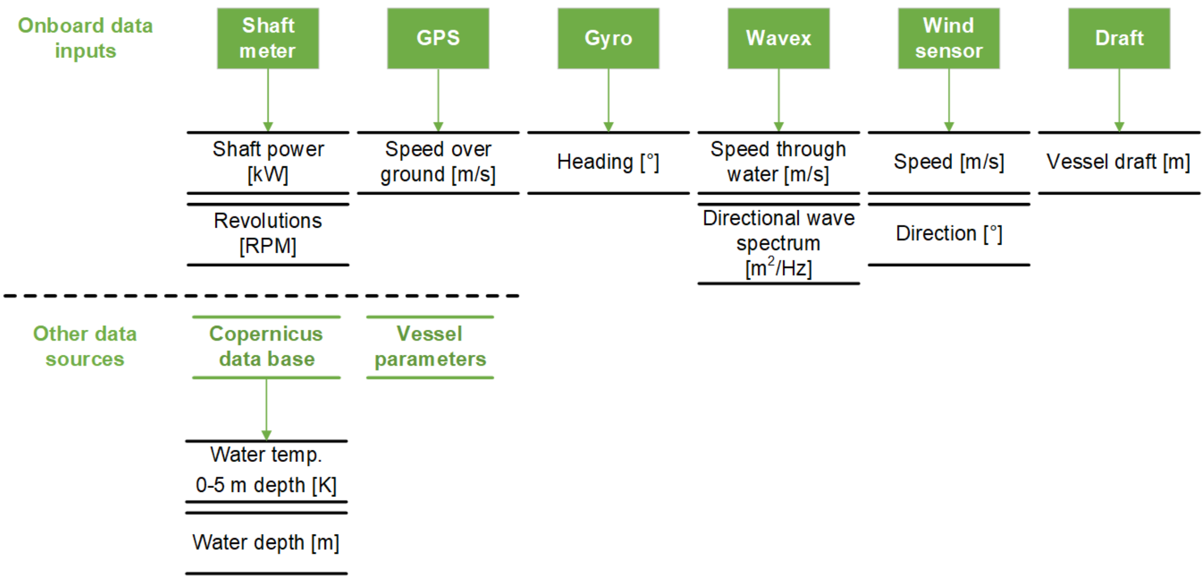

Fig.3: Overview of data inputs used to calculate the VTI

During the recent years, data quality has been improved in various conditions, and significant resources have been put into test and verification of the high measurement accuracy provided by Wavex, *Gangeskar (2017, 2018a,b,c, 2019, 2021), Prytz et al. (2019), Svanes Bertelsen et al. (2020)*. For further details on the basic components of a Wavex system installed on a moving vessel, refer to *Prytz et al. (2019)* and *Svanes Bertelsen et al. (2020)*.

The Miros Wavex solution provides the Miros Mocean system with continuous timeseries of accurate wave spectra and integrated wave parameters, required to calculate P_{wave}, and the most essential parameter for accurate VTI calculations: accurate speed through water.

Wind measurements are collected and relevant parameters for the calculation of P_{wind} are computed.

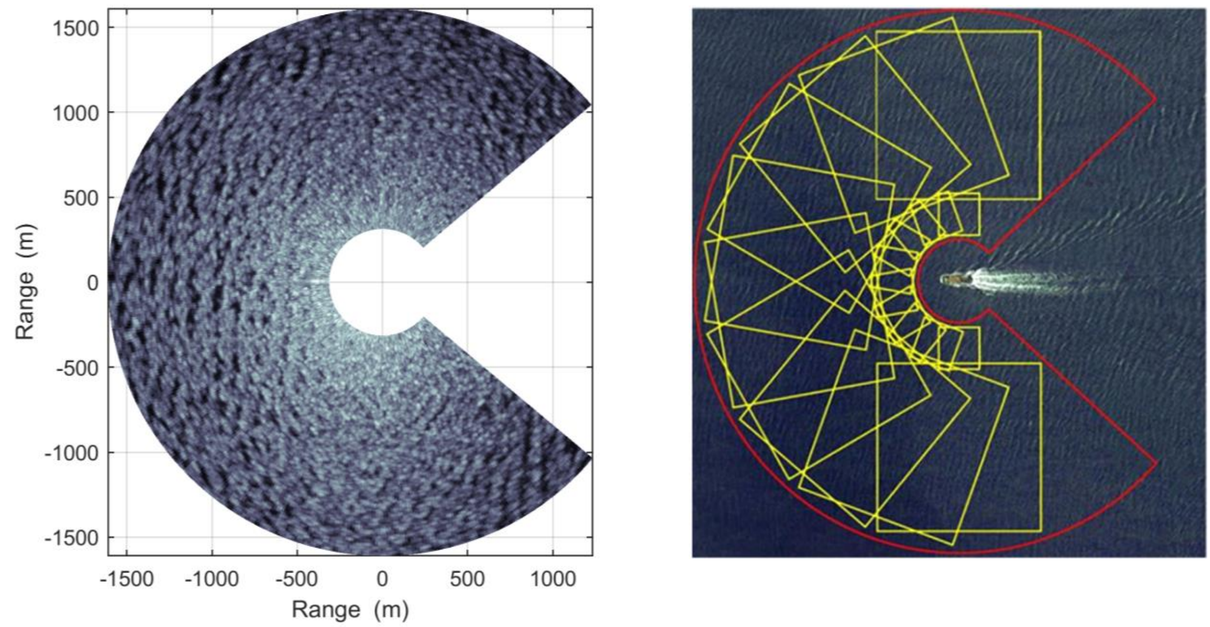

Fig.4: How measurement areas can be extracted from a polar radar image

Values for fore and aft draft are based on voyage draft surveys and daily readings calculated by the onboard loading computer.

P_{temp} is calculated using sea temperature data read from the Copernicus database, *GEBCO (2020)*.

Vessel properties required to calculate P_0, P_{wave}, P_{wind} and P_{temp}, i.e., regarding hull shape, hydrostatic tables, engine properties, etc., are acquired from standard vessel documentation.

A combination of heading from gyro, speed over ground and position from the GPS, is used to motion compensate collected data. Position data was in addition used to geo locate data and look up water temperature and water depth in the Copernicus database, *GEBCO (2020)*.

4. Data analysis

To demonstrate how the VTI can be utilized as a technical index during and across voyages, this section includes two concrete calculation examples. The first one helps to identify the main contributors in the environmental power term P_{env} and demonstrates how the normalization for weather works. The second example illustrates how the VTI can be utilized for monitoring the effect of a hull cleaning. In addition, we discuss the differences between using a set of wave parameters as input to the model for calculating the power consumed to overcome the waves P_{wave} vs. using the full directional wave spectrum.

4.1 Weather normalization

Weather normalization provides an estimate of how waves, wind and water temperature affect vessel performance. By continuously measuring the delivered shaft power P_m and calculating the additional power P_{env} from environmental effects, it is possible to visualize how the power spending is distributed between vessel propulsion and environmental effects.

A transatlantic voyage made by BW RYE between April 24th and May 6th 2020 forms the basis for discussing the normalized power used in the VTI calculation, to account for the effect of the encountered weather, fig.5.

Fig.5: Voyage 1, conducted by BW RYE during April-May 2020

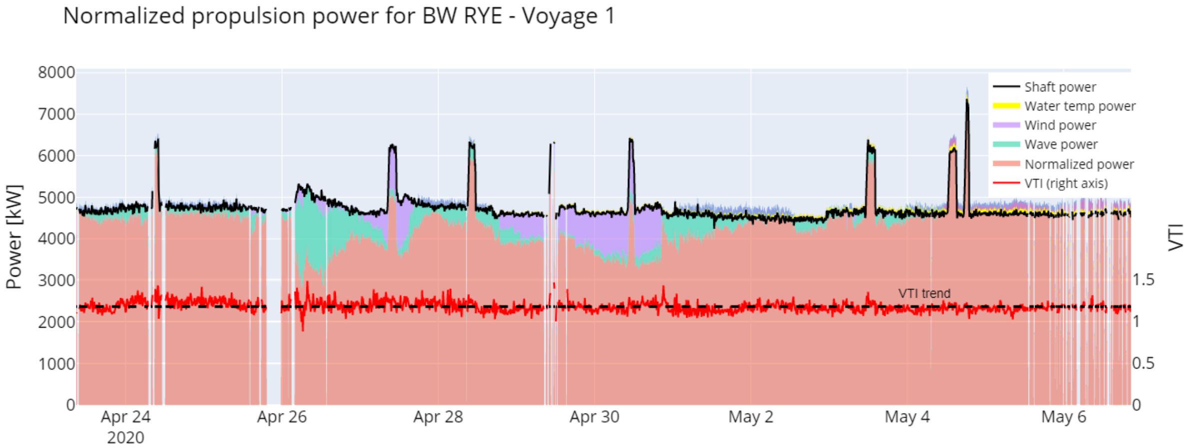

Fig.6: Normalized power calculated at 1-minute intervals from raw data. The black line shows power consumption in kW, measured at the engine shaft. The colored subareas of the graph represent power terms of P_{env}. The red line corresponds to the calculated VTI values at each time. Blank segments correspond to timestamps where data is missing, or data inputs have been tagged with an invalid status flag.

Fig.6 shows the measured power at the propeller shaft, and the resulting normalized power after accounting for environmental effects. The measured propeller shaft power P_m is here represented by the continuous black line. The environmental power term is further split into contributions from waves, wind, or temperature. The colored subareas of the graph represent the following power terms of P_{env}:

- Yellow - the power P_{temp} used or gained from temperature effects compared to the reference condition for P_0.
- Magenta - the power P_{wind} used or gained from the drag effect of the encountered wind.
- Green – the power P_{wave} used or gained from the effect of the encountered sea state.

If the power contribution from one of these terms has a negative effect on the ship performance, it shows up underneath the black line, as can be seen in fig.6. If the contribution is positive, it shows up above the black line.

Data has only gone through an initial stage of cleaning:

- Measured values tagged with invalid status codes are considered invalid and discarded.
- Normalized power values falling outside the combinations of speeds and displacements covered by tank tests and sea trial data are considered invalid and discarded.

Note that the peaks in the measured power correspond to brief increases in the engine load as part of soot blowing procedures.

Fig.6 shows that, most of the time, the normalized power is lower than the measured power consumption. Performance can also occasionally be increased by the weather conditions. A calm sea, tail wind, and a higher water temperature during the last days of the voyage result in the normalized power being higher than the measured power consumption, i.e., the vessel should sail slightly faster than what the measured power indicates.

An interesting aspect of the data shown in fig.6 is how the consumed power is distributed between the terms P_{wave}, P_{wind}, and P_{temp} and how this distribution varies during the voyage in correspondence with the measured weather. Important measured weather parameters are shown in fig.7.

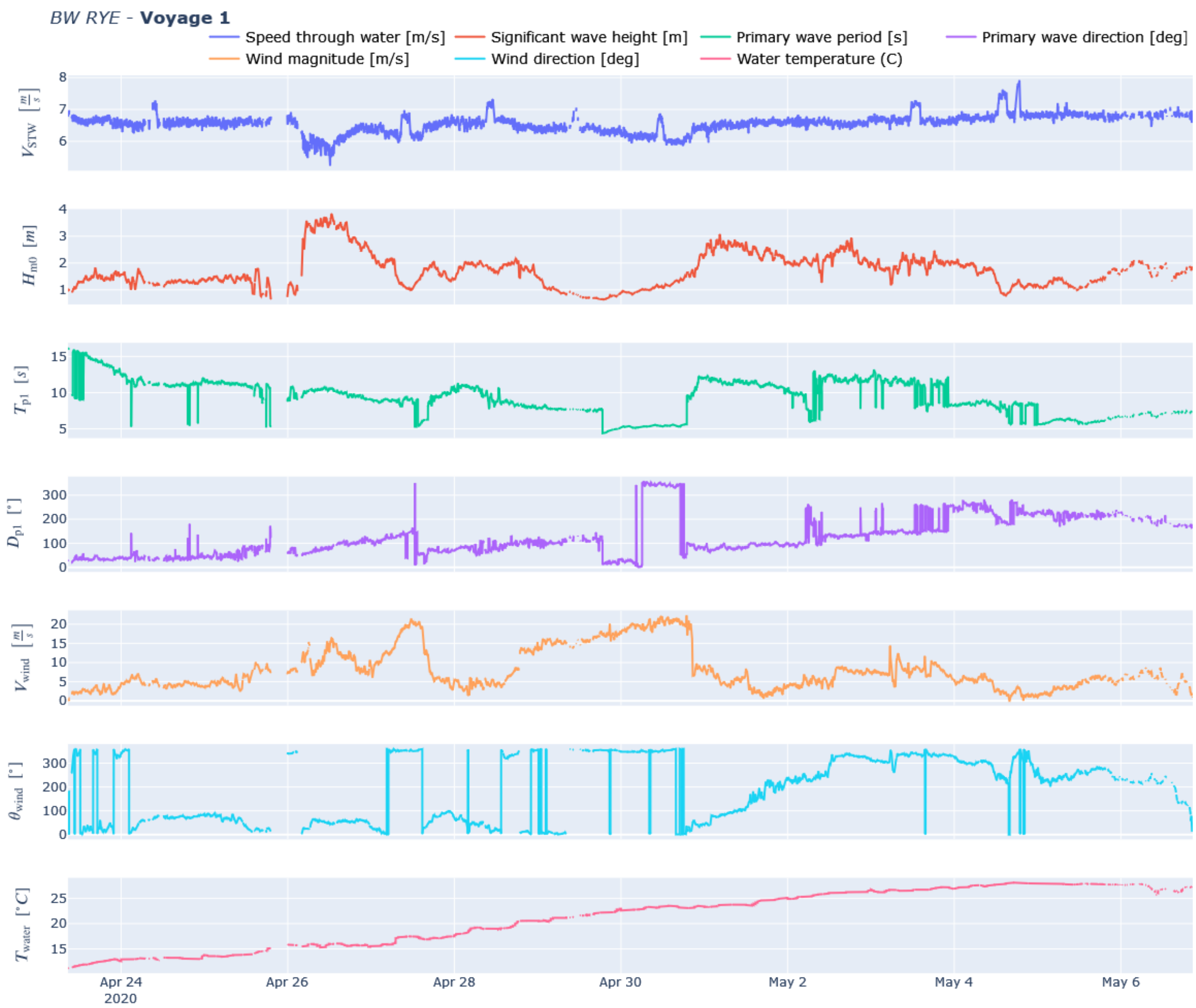

Fig.7: A timeseries plot of important parameters in the discussion of weather normalization and power consumption due to weather. Wave and wind directions are defined "as coming from" relative to the vessel, i.e., 0° correspond to from heading, 90° from starboard, and 180° from astern.

In fig.6 we can observe a significant increase in the term P_{wave} on April 26th. In fig.7 we can observe the cause, the sea state changes from a situation with a significant wave height H_{m0} of approximately

1.0 - 1.5 m, to a situation with a significant wave height of 3.0 – 4.0 m, and then proceeds down again. The primary wave direction relative to the vessel changes slowly but steadily from 50° to around 140°. We see significant changes in P_{wave} in this period. Although the VTI is noisier in this period, the average value is not significantly altered by the high sea state, nor the varying wave direction. This indicates that the wave model based on *Liu and Papanikolaou (2020*) captures the effect of this sea state event with sufficient accuracy to be used to normalize the VTI for the effect of this weather component. However, *Liu and Papanikolaou (2020*) discuss inaccuracies and limitations in the validity of the model. Limits based on vessel parameters, wave energy amplitude, and how wave energy is distributed in direction and frequency will be considered in further work.

From Fig.6, we can also observe that the wind power contribution can be significant. For example, both April 27th and April 30th we have true wind speeds reaching 15 m/s (29 kn) and more, while the wind is coming from ahead. The wind model seems to catch these situations well as the VTI does not significantly change during these events.

Water temperature is generally the least significant factor affecting P_{env}; a slightly negative contribution to P_{env} (i.e. aiding ship sailing) becomes visible during the last few days of the voyage.

As mentioned, identifying reasonable limits for the environmental conditions that can support application specific requirements to VTI accuracy, will be important in further work. The relevant procedures in ISO-19030 have restrictive limits for under what weather conditions data can be included in the performance analysis, as the effect of the environment is not measured with sufficient accuracy to compensate for it. As the aim of the VTI is to get closer to a continuous performance measure, a similar approach is not suitable. The ISO-15016 uses a combination of procedures and weather restrictions to ensure that a sea trial is conducted in conditions that can be accounted for by using specified correction models. Wind and temperature models have been adopted from this standard and so far, results seem satisfactory. To increase the weather window where the VTI is valid, the model of *Liu and Papanikolaou (2020*) was adopted. *Liu et al. (2020)* describes several relevant filtering schemes, among them limits on wave height and direction.

In the end, a good indicator of the combined validity of the measured data and the weather normalization procedure is to what extent the variations in the weather parameters are correlated with changes in the calculated VTI. If the weather is measured with good accuracy and the models work well, variations in the weather should not significantly affect the VTI.

4.2 VTI use case

As stated in section 2, one of the aims for the VTI is to improve the basis for decision making related to maintenance operations. An accurate assessment of P_{env} is necessary for a continuous monitoring of the vessel performance, which in turn can be used to estimate and anticipate to what degree the hull is fouled. This allows to quantitatively evaluate the need for maintenance.

A comparison of the VTI for periods immediately preceding and following a hull and propeller cleaning is presented in fig.8. VTI values are based on the same initial data cleaning as described in the previous section. The timeseries plot shows the result of this process, the magenta-colored dots being the data points discarded as a result of the cleaning. Two histograms based on the remaining black points from each period are presented at the bottom of the figure.

The positive effect of the hull and propeller cleaning is clearly demonstrated by a reduction in the average VTI from 1.35 to 1.16. This corresponds to a reduction in the normalized power consumption by 19% of the reference power.

In practice, a wider data distribution implies the need to measure the VTI for a longer period to obtain a meaningful result. The VTI histograms in fig.8 are somewhat broad, corresponding to the dispersion observed in the time series. Note, however, that these raw results are simply a baseline, prior to any filtering or averaging. The reference power P_0 from Eq.(1) is a valid benchmark only when the ship is running at steady state. Work is currently underway on reliably identifying periods where the ship condition is not stationary (such as acceleration and maneuvering). Automatically detecting and discarding invalid data points will contribute to reduce the dispersion in the VTI index and move the VTI one step closer to continuous monitoring of ship performance.

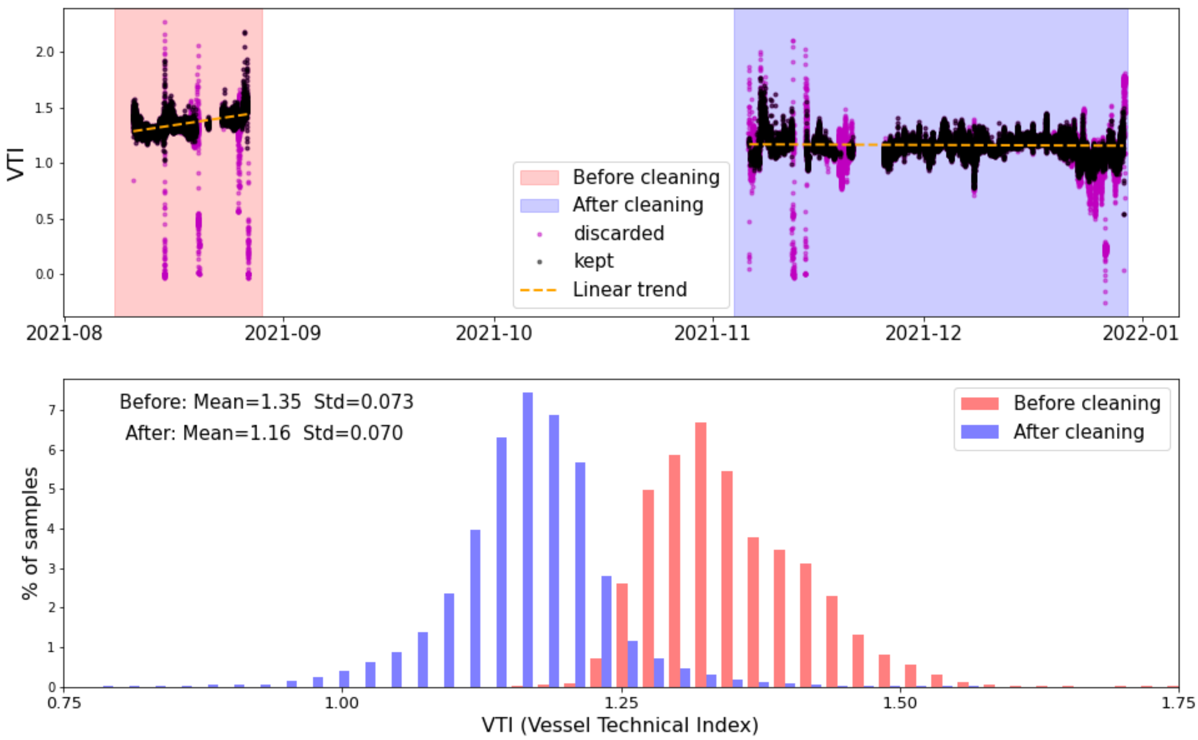

Fig.8: Unfiltered VTI comparison for BW RYE before and after hull cleaning, performed on November 3rd. The histograms in red and blue correspond to the time periods highlighted in the time series. Discarded points (magenta) are not included in the histograms.

4.3 Improving wave power estimation

A challenging part of accurately calculating the normalized power $(P_m - P_{env})$ is to obtain a good estimate of the added resistance due to waves R_{wave} (presented in Eq.(3)). This constitutes a main source of inaccuracy in the weather normalization part of the VTI calculations.

R_{wave} is calculated by linear superposition of the directional wave spectrum E and the response function of mean resistance increase in regular waves R_{RF}, from *ITTC 7.5-04-01-01.2 (2014, Rev. 01)* Section 4.3.2):

$$R_{wave} = 2\int_0^{2\pi}\int_0^{\infty} \frac{R_{RF}(\omega,\ \alpha,\ V_{STW})}{\xi_A^2} E(\omega,\alpha) d\omega\ d\alpha \tag{4}$$

with
R_{RF}: mean resistance increase in regular waves,
ξ_A: wave amplitude,
ω: circular frequency of regular waves,
α: angle between ship heading and incident regular waves
V_{STW}: speed through water
E: wave directional spectrum

The R_{RF} transfer function, *Liu and Papanikolaou (2020)*, depends mainly on:

- ship geometry (such as length, beam, radius of gyration);
- shape of the displaced water volume (e.g., water displacement, block coefficient, draft); and
- speed through water (V_{STW}).

Of these variable groups, the first one is usually available in standard ship documentation and the second one is easily derived from a combination of hull geometry and draft measurements. Speed through water, on the other hand, needs to be measured accurately *Svanes Bertelsen et al. (2021)*, as it is an important factor also for the accuracy in the added power due to waves.

The directional wave spectrum E should ideally be measured directly *ITTC 7.5-04-01-01.2 (2014, Rev. 01)*. When direct measurements are unavailable, the recommendation is to calculate it as:

$$E(\omega,\alpha) \approx S_f(\omega)G(\alpha), \quad (5)$$

where
S_f is a Pierson-Moskowitz frequency spectrum, and
G is a predetermined angular distribution function.

The frequency dependency S_f is approximated as a function of just two parameters: significant wave height H_{m0} and primary wave peak period T_{p1}. The angular dependency G is given by the primary wave peak direction D_{p1}.

A limitation of this approach is that Eq.(5) takes the full energy content in the wave spectrum (captured by H_{m0}) and allocates it to a standard spectral shape S_f, adjusted to its main frequency component $f_{p1} = 1/T_{p1}$, around the direction D_{p1} corresponding to that frequency component. One intrinsic limitation of this is that it assumes that the ship is exposed to a single dominant wave system. When two or more wave systems are present, this assumption breaks down, and the accuracy of the approximation deteriorates.

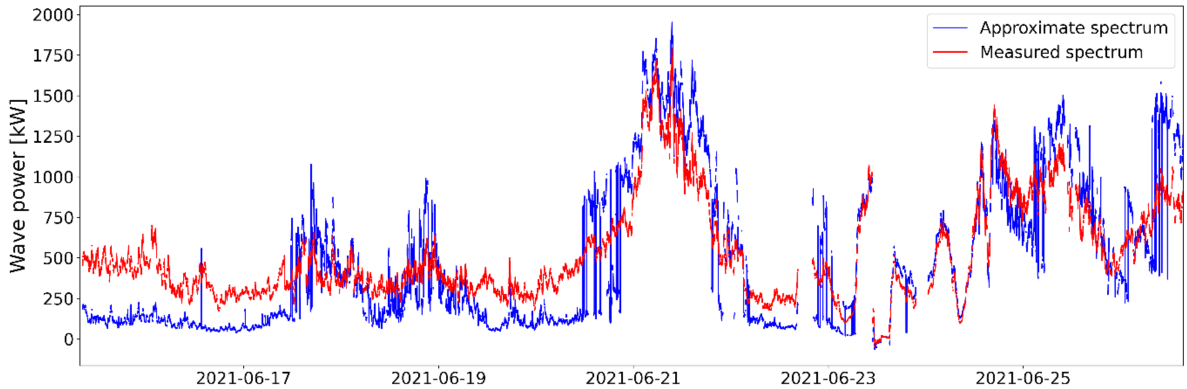

Fig.9: Calculated wave power ($P_{wave} = R_{wave} \cdot V_{STW}$) resulting from using as input the measured wave spectrum (red) and the approximation from Eq.(5) (blue). The jumps in the blue line occur when the primary and secondary wave frequency components have similar amplitudes.

An illustration of how this affects R_{wave} can be seen in fig.9, which shows P_{wave} values measured on board the BW RYE for two weeks (ship location in fig.10). The wave power estimate using the approximation in Eq.(5) allocates all the wave energy to a Pierson-Moskowitz spectrum with its peak at the main frequency component f_{p1}. This results in simultaneously overestimating the wave resistance due to the main frequency component f_{p1} and underestimating the contribution of the secondary frequency component f_{p2}. When the energy content in two frequency bands is similar, minor sea state variations can cause the spectral amplitudes of the two main frequencies f_{p1} and f_{p2} to switch places and result in unrealistic discontinuities. This is particularly evident in the data for June 20th and 21st, when two wave systems are present.

Fig.10: Route followed by BW RYE between June 15th and 26th 2021 as part of a voyage

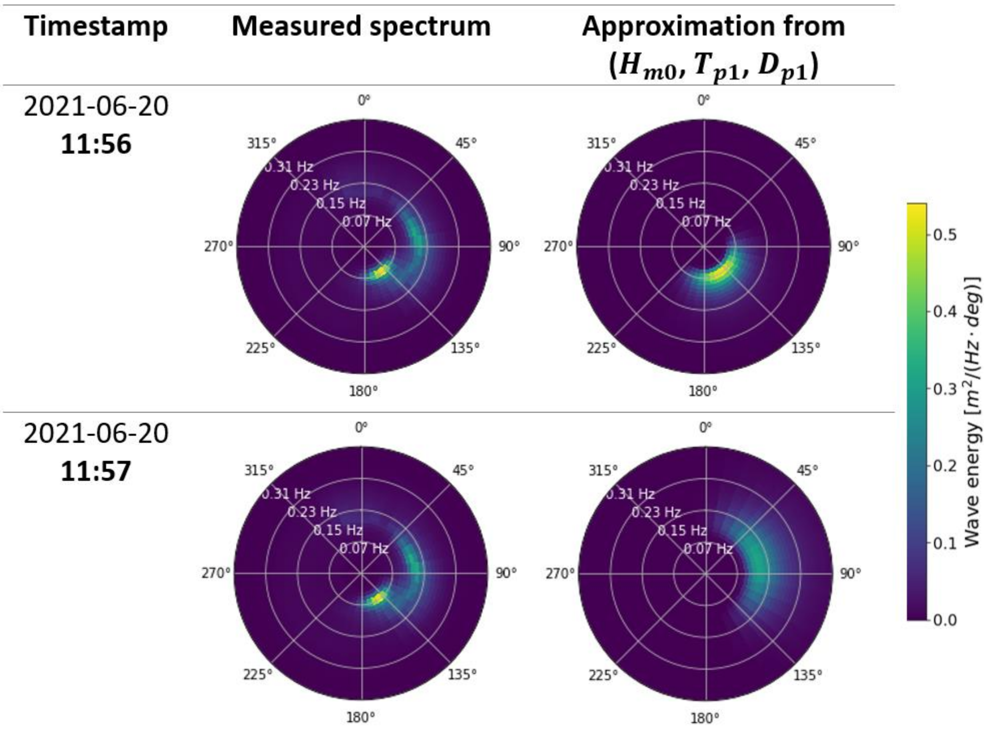

Fig.11: Side by side comparison of the measured wave spectrum and its approximation according to Eq.(5) for two consecutive points in the time series. Spectra consisting of two or more wave systems can be significantly distorted. Head waves correspond to 0°, waves from starboard 90°

Fig.11 shows the measured wave spectrum side by side with its approximate reconstruction according to equation (5) for two consecutive data points. Two wave systems are present in this measurement. One of them (swell) consists of low frequency waves coming mainly from behind the ship, while the other one corresponds to higher frequency beam waves (wind sea).

The change in the measured wave spectrum within a minute is barely noticeable, as expected, while its approximate reconstruction changes dramatically. Consequently, the wave power P_{wave} calculated using the full wave spectrum as input slowly drifts from 539.7 kW to 541.0 kW, while using the approximation yields unrealistic values of 161 kW and 881 kW respectively.

Direct wave spectrum measurements provide more stable and reliable wave power estimates and therefore a more stable and accurate VTI, especially when multimodal sea states are encountered. The practical outcome of this increase in accuracy is a consequent reduction in the number of data points required to obtain significant information about the technical condition of a vessel.

5. Discussion

This paper has presented how a vessel technical index (VTI) can be calculated based on earlier work presented in *Guo et al. (2021)*. Data presented shows examples of the extent of the power used to overcome or that can be gained from the environment, and how this power is distributed among the different environmental factors accounted for in the weather normalization process of the VTI.

A use case showing how the VTI can be used to see the effect of a hull and propeller cleaning was presented in section 4.2. The VTI is also undergoing an accuracy study that looks at how input data accuracy propagates through the VTI model. Based on this, the results are expected to be further improved by limiting used data to ranges where model uncertainty is within acceptable limits for a specific application and applying steady state identification.

High confidence VTI data also relies on accurate data input. In section 4.3 the effects of using a measured directional wave spectrum versus a model Pierson-Moskowitz spectrum, to calculate the power used to overcome the waves a vessel is encountering, were discussed. In situations where a vessel is exposed to multiple wave systems like wind sea and swells, i.e., waves coming from more than one direction and with different wave periods at the same time, the measured wave spectrum gives a better description of the situation. This is reflected in an improved weather normalization and an overall more stable and reliable VTI.

The VTI model application area has so far been limited to dry cargo vessels and tankers. Work is currently in progress to apply the VTI calculations on a wider range of vessels. To extend the application area the VTI models apply to, it will be tested based on data collected from more vessels and vessel types.

Future work is planned to develop the use of the VTI to be able to rate and compare the technical (hydrodynamical) performance of two vessels. The VTI can be used to estimate how much power your vessel will use with its current technical performance, to achieve a certain speed through water, in a certain loading condition. By using engine data describing how much fuel is consumed to achieve a specific power output, this can be used to calculate the fuel two different vessels will consume for a certain cargo load transported at a specific speed, and hence aid a user to choose the best suited, or most environmentally friendly vessel for a certain cargo transport.

Another possible advantage of the methodology outlined for the VTI in this paper, and accurately measuring the effect of weather at full scale for in-service vessels, is that it can allow to further develop vessel specific performance models to further increase accuracy and the range of environmental conditions it can reliably cover.

6. Conclusion

A long list of factors influences the technical performance of a vessel. The condition of the hull and propellers play a crucial role and is often the focus of attention in vessel performance analysis. Such analysis work is complicated by the strong impact of the weather surrounding the vessel. Weather data related to ocean waves, current and wind has traditionally been inaccurate and often with only one or a few data points per day. The crucial STW parameters have also been littered with inaccuracies. Recent advances within technology have, however, made accurate, high-frequency weather and STW data available.

This paper has shown that accurate weather data can be used together with advanced models and accurate STW data to estimate real-time vessel performance with much better accuracy than before. By subtracting the influences of the weather on the vessel in this manner, it is also possible to determine the state of the hull and propellers with significantly higher confidence than before. This is useful for improved scheduling of hull and propeller maintenance activities. The methodology laid out in this paper can also be used to improve how the effects of new hull designs, hull and propeller coatings and energy saving devices can be determined.

The proposed VTI is a factor that estimates the difference between actual vessel performance and the performance of the vessel when it was new. VTI was defined as the ratio of the actual, measured power normalized for environmental effects and the reference power based on sea trial and tank test data. The VTI can be used to monitor how the performance of the vessel develops over time and how it changes due to hull cleanings, new paints or other energy saving devices and schemes.

As shown in *Svanes Bertelsen et al. (2021)*, inaccurate STW data has a very large influence on the accuracy of the VTI. Furthermore, the weather normalization models also require accurate, high-frequency data. In complex sea state scenarios, this paper has shown that using a directional wave spectrum is advantageous.

Further work is needed in quantifying the financial gains associated with accurate insight. Although everyone appreciates accuracy, there is a need to understand the economic impact on hull maintenance scheduling, methods and pricing. The same goes for assessing the value of energy saving devices, hull coating technologies. It also seems clear that accurate insight into performance can be used to reduce margins in performance-oriented contracts and thereby improve competitiveness and even transparency. An additional next step would be to take the VTI concept further by investigating how it can be scaled to allow comparison between vessels. This would simplify the process of identifying the most efficient vessels for a certain transportation task.

References

GANGESKAR, R. (2017), *Automatically calibrated wave spectra by the Miros Wavex system – Accuracy verified*, Miros AS, Asker

GANGESKAR, R. (2018a), *Verifying High-Accuracy Ocean Surface Current Measurements by X-Band Radar for Fixed and Moving Installations*, IEEE Trans. Geosci. Remote Sens. 56/8, pp.4845-4855

GANGESKAR, R. (2018b), *Ocean Surface Current Measurement by the Miros Wavex System*, Miros AS, Asker

GANGESKAR, R. (2018c), *Surface Current Measurements from Moving Vessels by Wavex – Verified*, Miros AS, Asker

GANGESKAR, R. (2019), *Measuring the speed through water by Wavex*, Miros AS, Asker

GANGESKAR, R. (2021), *Automatic Radar Data Quality Control – Applying Deep Learning, AI to Ocean Wave, Current Measurements*, Sea Technology 62/2, pp.23-27

GANGESKAR, R.; PRYTZ, G.; SVANES BERTELSEN, V. (2018), *On-Board Real-Time Wave & Current Measurements for Decision Support*, 3rd HullPIC, Redworth, pp.223-233

GEBCO (2020), *GEBCO 2020 Grid, used to look up sea water temperature and water depth data*, GEBCO Compilation Group, https://resources.marine.copernicus.eu/product-detail/GLOBAL_ANALYSIS_FORECAST_PHY_001_024/INFORMATION

GUO, B.; ROGNEBAKKE, O.; TVETE, H.A.; ADAL, C.; STORHAUG, G.; SCHMIDT, M.; BRUSET, T.; PRYTZ, G. (2021), *Setting the standard for evaluation of in-service technical ship performance*, 6th HullPIC, Pontignano

ISO-15016 (2015), *Ships and marine technology - Guidelines for the assessment of speed and power performance by analysis of speed trial data*, Int. Standard Org., Geneva

ISO-19030 (2016), *Ships and marine technology - Measurement of changes in hull and propeller performance*, Int. Standard Org., Geneva

ITTC 7.5-04-01-01.2 (2014, Rev. 01), *Recommended Procedures and Guidelines – Analysis of Speed/ Power Trial data*, Int. Towing Tank Conf.

LIU, S.; PAPANIKOLAOU, A. (2020), *Regression analysis of experimental data for added resistance in waves of arbitrary heading and development of a semi-empirical formula*, Ocean Eng. 206

LIU, S.; LOH, M.; LEOW, W.; CHEN, H.; SHANG, B.; PAPANIKOLAOU, A. (2020), *Rational processing of monitored ship voyage data for improved operation*, Applied Ocean Research

PRYTZ, G.; GANGESKAR, R.; SVANES BERTELSEN, V. (2019), *Distributing Real-Time Measurements of Speed Through Water from Ship to Shore*, 4th HullPIC, Gubbio, pp.114-127

SVANES BERTELSEN, V.; GANGESKAR, R.; PRYTZ, G.; SCHMIDT, M. (2020), *Accurate Voyage Sea State and Weather Measurements Improve Performance-Based Vessel Management*, 5th HullPIC, Hamburg, pp.157-171

SVANES BERTELSEN, V.; BRUSET, T.; GANGESKAR, R.; PRYTZ, G.; SCHMIDT, M. (2021), *Accurate Speed Through Water Measurements Enable Accurate Vessel Performance Management*, 6th HullPIC, Pontignano, pp.112-123

To What Extent can SHaPoLi Accelerate Digitalization of the Shipping Industry

Hauke Hendricks, Hoppe Marine GmbH, h.hendricks@hoppe-marine.com
Andre Blaurock, Hoppe Marine GmbH, a.blaurock@hoppe-marine.com

Abstract

This paper provides an overview of the MEPC Resolution 335 (76) Shaft Power Limitation (SHaPoLi) system. It is described as a technical measure to comply with Energy Efficiency Existing Ship Index (EEXI) requirements. This paper will explore the possibilities of SHaPoLi as an accelerator of digitalization installations within the maritime industry.

1. Regulatory framework – EEXI and MEPC Res. 335 (76) in a nutshell

With the global drive for decarbonization the shipping industry is facing the challenge to comply with more stringent regulations related to greenhouse gas emissions (GHG). The current IMO targets are CO_2 reduction by 40% in 2030 and 70% by 2050, compared with the level of 2008. The overall GHG reduction should be at least 50% by 2050, https://www.imo.org/en/MediaCentre/HotTopics/Pages/Reducing-greenhouse-gas-emissions-from-ships.aspx.

The EEXI is one major milestone to achieve GHG reduction. It was adopted by the International Maritime Organization (IMO) during the Maritime Environmental Protection Council (MEPC) meeting in June 2021.

The MEPC Res. 335 (76) – Guidelines on the shaft/engine power limitation system to comply with the EEXI requirements and use of a power reserve is part of the EEXI. The EEXI builds upon the EEDI (Energy Efficiency Design Index; for newbuildings) formula. For most ships, the CO_2 target is a function of dead weight tonnage but for cruise ships a function of gross tonnage. It looks as follows:

$$EEXI = \frac{CO2\ emissions}{Transportation\ work}$$

$$\text{EEXI} = \frac{(\prod_{j=1}^{n} f_j)(\sum_{i=1}^{nME} P_{ME(i)} C_{ME(i)} SFC_{ME(i)}) + (P_{AE} C_{AE} SFC_{AE}) + ((\prod_{j=1}^{n} f_j \sum_{i=1}^{nPTI} P_{PTI(i)} - \sum_{i=1}^{neff} f_{eff(i)} P_{AEeff(i)}) C_{FAE} SFC_{AE}) - (\sum_{i=1}^{neff} f_{eff(i)} P_{eff(i)} C_{FME} SFC_{ME})}{Capacity\ v_{ref} f_i f_c f_l f_w f_m} \quad (1)$$

The general concept of the EEDI and EEXI is to compare the impact to society (CO2 emissions) with the benefit to society (transportation work).

All vessels above 400 gross tonnage and ships of another category (non- conventional propulsion e.g., diesel-electric propulsion, hybrid propulsion, gas-turbine propulsion) are required to have a valid EEXI technical file on board. The technical file is the basis of a new IEEC (International Energy Efficiency Certificate). The main purpose of it is to show the calculation of the ship's attained EEXI (calculated for individual ship) in comparison with the required EEXI (maximum allowed value; the attained EEXI needs to be less the required EEXI). Also, it contains general information about the ship, and information about values were used to calculate attained and required EEXI, https://www.dnv.com/maritime/insights/topics/eexi/advisory-service-technical-file.html.

For ships delivered before 1st January 2023 the first EEXI certification will take place at first annual, intermediate or renewal survey of IAPPC (International Air Pollution Prevention Certificate). Ships delivered on or after 1st January 2023 have to certificate their EEXI at their initial survey.

Resolution MEPC.335(76) describes requirements to the shaft/engine power limitation system to comply with the EEXI and use of a power reserve. It provides the technical and operational conditions SHaPoLi and Engine power limitaion (EPL) systems should comply with. As this paper is about SHaPoLi system, EPL regulations will not be further considered.

Main technical requirements for SHaPoLi are sensors measuring torque and rotational speed of the shaft delivered to the ship's propeller, a data recording and processing device for tracking and processing provided data and a control unit for calculation and limitation of the power transmitted by the shaft to the propeller. General system requirements are non- permanent power limitation, but to use the full power it needs a deliberate action of the master or OICNW (Officer In Charge of Navigational Watch). If the engine is electronically controlled and the limit is overwritten, it needs a clear warning for master and/or OICNW. Also it needs to be tamper-proof and data like shaft rotational speed, shaft torque and shaft power should be recorded and shown constantly.

As the system is non- permanent it is still possible to use unlimited power but is only allowed for the purpose of securing the safety of a ship or saving life at sea. As soon as the power is unlimited it needs to be manually recorded in the OMM (Onboard Management Manual) and automatically by the system, https://wwwcdn.imo.org/localresources/en/OurWork/Environment/Documents/Air%20pollution/MEPC.335(76).pdf.

2. Market impact – Who is affected

Table I shows the average EEXI exceedance per vessel type and age. The need for EPL and within this SHaPoLi retrofits for ships built from 1970 to 2019 is present. Ships built after 2019 mostly comply with EEDI regulations which are similar to EEXI regulations. The table also shows a receding MCR for newer ships as more modern design of vessels has already led to lower attained EEXI values.

Table I: Need for EPL/ SHaPoLi solutions for ships built before 2019

Ship type	Parameter	Build year			
		1970-1984	1985-1999	2000-2014	2015-2019
Container	EEXI exceedance	+51%	+26%	+28%	-1%
	EPL required	45%	29%	30%	9%
	% MCR allowed	55%	71%	70%	91%
Oil tanker	EEXI exceedance	+43%	+26%	+23%	+23%
	EPL required	42%	30%	27%	22%
	% MCR allowed	58%	70%	73%	78%
Bulk carrier	EEXI exceedance	+62%	+25%	+25%	+13%
	EPL required	49%	27%	27%	15%
	% MCR allowed	51%	73%	73%	85%

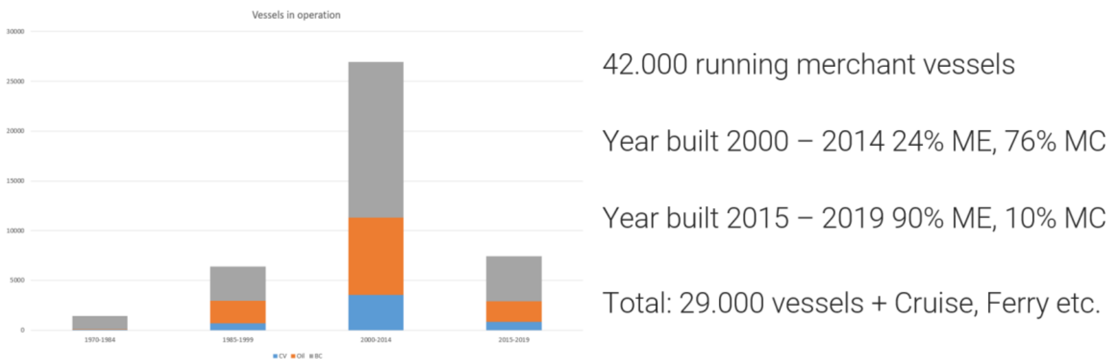

Fig.1: Merchant vessels in operation and engine type

Especially vessels with mechanical engines will face the challenge of a technical EPL or SHaPoLi solution. More modern vessels with an electronic engine might just require a software update to properly comply with overridable power limitation.

The total number of merchant vessels (tanker, bulkers and containers) with mechanical engines are around 29,000 of a total 42,000 as seen in Fig.1.

It is obvious that there will be a big market impact. Every part of the shipping industry will be affected – it starts from ship owners and suppliers, as retrofits are needed to comply with the newest regulations as mentioned above, continues with the vessel crew as they need to consider the new limitation, to service companies for maintaining new systems. Finally, also to solutions providers, who work with ship to shore data to enable a better and more efficient ship performance and ensure compliance with EEXI. For this companies more data coming from the propulsion system is also helpful to monitor specific fuel and oil consumption and evaluate hull and propeller efficiency in a more detailed way. Due to this digitalized way coming within the new SHaPoLi regulatory it will be easier for the ship owners to save costs and operate their ships in the best economic way.

3. SHaPoLi – IACS interpretation

The IMO has verbalized their basic requirements within the MEPC Res. 335 (76). There are two measures to limit propulsion power (overridable): SHaPoLi and EPL. EPL limits engine power e.g. by reducing the maximum amount of fuel supplied to the engine via the fuel racks at mechanically controlled engines or by fuel index for electronically controlled engines. SHaPoLi measures shaft power by a shaft power meter and the limitation is based on this value. The power limitation needs to be overridable, https://wwwcdn.imo.org/localresources/en/OurWork/Environment/Documents/Air%20pollution/MEPC.335(76).pdf.

However, the definitions within the resolution are not formulated to such an extent that a vessel owner can follow the resolution and implement a system. Therefore, MEPC has given the task to the Recognized Organizations to develop guidelines on the implement of EEXI. The recognized Organizations are the classification societies respectively their umbrella organization International Association of Classification Societies (IACS). A draft of these guideline has been released on the 27th of April by the IMO, Fig.2. The final words on the IACS guideline will be confirmed at the MEPC 78 from 6th to 10th of June 2022.

6.6 Onboard Management Manual (OMM)

- Regarding resolution MEPC.335(76), section 2.1.1.3 *"a control unit for calculation and limitation of the power transmitted by the shaft to the propeller(s)"* : It is clarified that this control unit can be independent from the engine automation. Override of limitation should be indicated by giving an alarm on the bridge which has to be acknowledged by ship's master or OICNW. Any use of power reserve to be automatically logged by the data recording device as defined in section 2.1.1.2. The OMM should clearly define this confirmation of the alarm as the deliberate action in agreement with requirement in chapter 2.2.1.

Fig.2: IACS interpretation of SHaPoLi systems

The current IACS guideline allows a 'stand-alone' SHaPoli system. It means there will not be an active engine power limitation by an interface. The responsibility for EEXI compliant operation of the vessel lies with the master or OICNW.

4. Possibilities for digitalization with SHaPoLi solution

With the need for adoption of the shipping industry to GHG reduction also chances for technology development, digitalization and efficiency are apparent. Some of the possible improvements, which can come along with a SHaPoLi installation, are listed below.

- Ship-to-Shore infrastructure: With SHaPoLi systems being data loggers or IoT devices there is a possibility to build a proper (stable, low bandwidth, cyber-secure etc) ship-to-shore infrastructure. It will be possible to monitor all essential parameters of the SHaPoLi system and connect additional sources of data without major efforts. With data collected and stored in the cloud it is possible to analyze and evaluate data for a longer period of time. With the stored long period high quality data, it is possible to improve the ship's performance and investigate smaller and major issues.

Fig.3: Ship-to-Shore infrastructure

- EEXI compliance notifications: As a manually operated SHaPoLi solution is currently foreseen in the IACS EEXI interpretation guideline, a stand-alone SHaPoLi system is a likely solution to ship owners. The master or OICNW carries the responsibility of EEXI compliant vessel operation. In order support the crew, automatic notifications to the shore personal can be added to SHaPoLi systems. This will facilitate collaboration between vessel's crew and the shore personal. Collaboration can increase awareness, training level and prevent undeliberate use of power reserve or a near-miss. See Fig.4 for an example of power reserve exceedance.

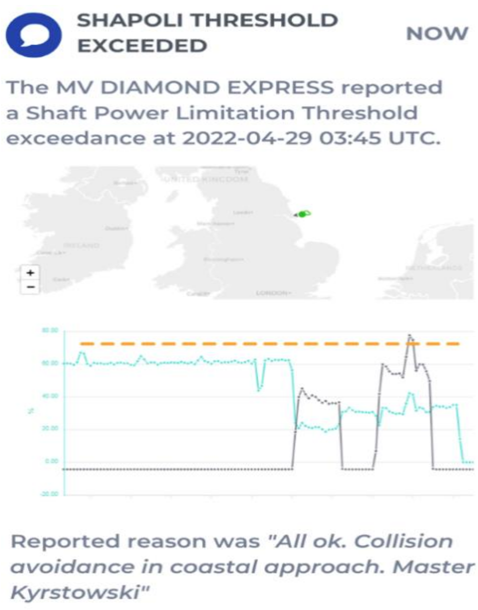

Fig.4: Power reserve exceedance notification

- Data sharing and collaboration: Modern cloud solutions allow easy integration between suppliers, ship-owners, charters etc. Web Application programming interfaces (APIs) have been adopted within the industry. Testing and identifying the benefit of a new application on a set of high-quality high-frequency data has never been as easy as it is today. Decision support tools for hull-cleaning, weather routing, and engine maintenance are much easier to integrate nowadays. Barriers for collaboration can be reduced and time for integration is lowered.
- Data and Event logging: With Data and Event logging, alarms and unpredicted events can be identified by the SHaPoLi operator or the shore personal. With the ship to shore infrastructure and stored data it is easier to react to events and provide the crew and owner with reasons how

this event or alarm occurred and how to solve it. Also, it is possible to see if similar events happened in the past and identify patterns of undesired actions.

- Remote Updates and support: With the establishment of a permanent ship-to-shore connection remote updates and services will be available. A reduction of service attendances and improvement of mean time to recovery has been identified within remote-enabled systems within Hoppe products. In additional travel requirements are reduced, helping to reduce the general carbon footprint.

5. Conclusion

Decarbonization is one of the biggest challenges, if not the biggest, in the 21st century. As an integral part of a globalized world, the shipping industry will have to contribute to decarbonization and GHG reduction by lowering the carbon footprint, lowering GHG emissions and facilitate energy efficiency.

With EEXI coming into force 2023 retrofitting a limitation system will become mandatory for many ship owners for their existing fleet. The very short timeline from finalization, during MEPC 78, of the regulations and guidelines until adoption within 2023 will be a challenge for ship owners affected by the EEXI. Therefore, it will be mandatory to get acceptance by the IACS of stand-alone SHaPoLi solutions for ship owners. This will improve availability of solutions from the supply side, lower the costs and reduce lead time.

However, SHaPoLi solutions can also be considered as a door-opener to wide-spread adoption of modular and upgradeable high-frequency data loggers. Standardized cloud-based data infrastructure will improve data-sharing and collaboration within the industry. The request for collaboration with other suppliers has increased by 200% within Q1/2022 compared with the whole year of 2021.

Especially ship owners with ageing vessels and limited budget will have the opportunity to update and digitalize their fleet. Increased digitalization will allow a more economic, ecologic, and cost-efficient operation, e.g. by faster implementation of new optimization tools.

Hull Data is Big Data –
How Much Can We Improve Hull Performance Using Real Hull Data?

Solène Guéré, Nicolas Gambini, Notilo Plus, Marseille/France, solene@notiloplus.com

Abstract

Fleet Performance has witnessed major optimizations in the last decades. One of the aims of these algorithms is to estimate the fuel performance loss due to hull fouling, and thus decide when it is time for hull cleaning. However, these methods are largely reactive and tend to postpone cleaning until no doubt remains of its need. The authors open the discussion on how much could be saved by feeding these fleet performance algorithms with the actual state of the hull, and how it could help to reach CII and green shipping targets more easily. Notilo Plus uses Artificial Intelligence to create reproducible data out of ship hull inspections. Here, we share preliminary work and thoughts on how some machine learning and digitization techniques could be used to assist in hull performance review and performance prediction. Digitalizing the hull thus opens a new world of opportunities to move from reactive hull cleaning to predictive maintenance.

1. Introduction

In today's globalized world, more than 90% of consumer goods transit by sea, creating 3% of worldwide CO2 emissions, *Buhaug et al. (2009), Smith et al. (2014), IMO (2020).* In a Business-as-Usual scenario, the emissions of the maritime industry would increase by 50% between 2008 and 2050, which would make Paris agreements nearly unachievable.

Yet, a significant part of these greenhouse gas emissions is purely released in the atmosphere with no added value for the shipowner: increased hull roughness caused by fouling overconsumption can keep the energy consumption up by around 10% of the worldwide fleet, *Molland et al. (2014), Wang and Lutsey (2013).*

Additionally, this overconsumption creates a burden on the energy costs of the vessels, decreases the average speed, and accelerates the wear of engines and mechanical parts. With the lookout of ever more stringent regulations like CII, hull optimization becomes a need that aligns the three targets of climate protection, cost reduction and regulation compliance.

Many digital tools have been developed to calculate hull roughness out of speed loss data and sensor data. However, this optimization is still focused on reactive maintenance, whereas actual hull data could optimize it further.

Rather than guessing the state of the hull from the performance tools calculation, what would be the consequence of inputting it into these tools?

2. The road to optimization

2.1. AIS data and noon reports

The need for optimizing ship performance is a focus of ship managers since fuel consumption largely depends on it. It is essential with vessel planning and especially hull cleaning, as important biofouling could be responsible for a significant drop in performance.

Historically, the most common practice for assessing a ship's performance is filling noon reports: this report provides the vessel's position and other relevant standardized data. These data can be collected by hand, even only on a sheet of paper, and help assess the performance of the ship based on its speed, weather conditions... The information provided by the noon report is essential but partial and only little analysis can follow as it may not be linked to performance tools: there is indeed only one additional datapoint every day, covering the last 24 hours of navigation. Being also filled by hand implies more frequent errors, and overall, it renders it nearly impossible to analyze efficiently.

Linking the fuel consumption in noon reports to AIS (Automatic Identification System) data can be considered as the first level of ship optimization. AIS is an automatic tracking system that uses transceivers on ships. Information provided by AIS equipment can include unique identification, position, course, and speed. In some cases (Authors discussion with industry players), just making the crew aware of good practices for ship management allowed them to save around 20% of fuel consumption, without using any sensor. Hull performance can be deduced by a drop in fuel efficiency, and cleaning planned accordingly.

However, noon reports and AIS data remain vague and quite general. This explains the need for ship managers and captains to access more precise data, and therefore the development of sensors and big data dashboards, which are associated with new challenges.

2.2. Sensor data, cleaned data

The goal of sensor data is to acquire many data points, concerning precise phenomenon, and use algorithmic tools to give a clear picture of the vessel performance at any given moment. For example, depending on the sensors used on a ship, one ship manager can access engine revolutions per minute, wave height, current speed in a very precise manner. These sensor-data is often linked to powerful calculation tools, giving access to optimization KPIs with prediction, within an API.

However, sensor-based data can be considered a double-edged sword. Indeed, a huge amount of data is collected, and the data quality is very variable. Data analysts strive to clean up the data, by removing outliers or noisy data points, and considering an ever-growing number of operational and natural phenomena.

Although the quality of prediction is increasing every year, even if this data comes from cutting edge sensors analyzing real-world phenomena, predictions that the algorithm draws from the observations may fall short from reality. For instance, *Seah et al. (2021)* noted that there was a difference in model predictions and actual consumption of around 20%, as shown in Fig.1.

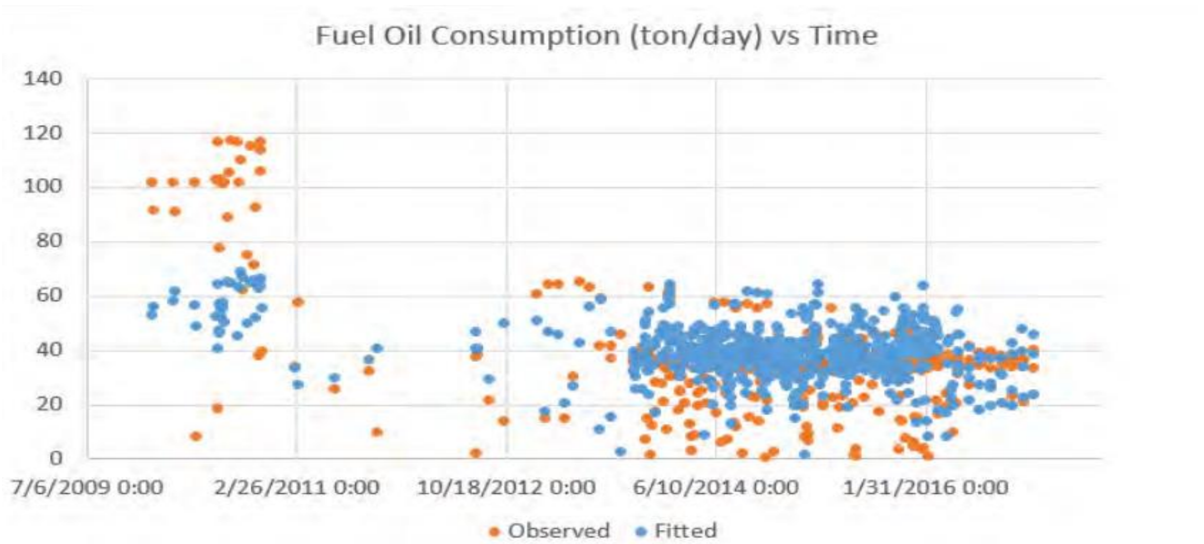

Fig.1: Observed data vs Fitted data; *Seah et al. (2021)*

In short, sensor-based data has allowed a significant step forward for vessel performance optimization, but there is still a significant difference between theoretical computations and real consumptions, and data is scattered.

In the operational life of vessels, immobilizing a vessel for a hull cleaning, and taking the risk to damage the coating, are decisions that can't be taken if any uncertainty about the state of the hull remains.

Therefore, in the context of clean hulls and biofouling, this situation results in the following common practice: ship managers wait until there is an average of 10% to 15% of overconsumption before carrying out a pre-cleaning inspection and cleaning (Authors discussions with various fleet managers). Above a given threshold, the performance engineers advise the fleet managers to perform an inspection and cleaning.

Though partly optimized, this practice is still based on reactive cleaning and the hull condition still has a strong impact on vessel performance. The real hull data would be necessary to get one step further: to predictive maintenance.

3. Problems and Solutions for real-life hull data

3.1. Real-life hull information is still very difficult to analyze

Though fouling is directly related to the drag of the vessels, it has proven very difficult to estimate precisely to what extent.

The studies that are reaching a consensus in the industry are mainly studying plate data in controlled environments, *Schultz (2004)*, or sometimes data from a single ship analysis.

The results generally agree that there is a general increase of drag and CO2 emissions of 10-20% with light slime, 25%-40% with heavy slime, and up to 50% with small hard fouling or large weed, *CHI (2022)*.

Nevertheless, it is still very difficult to link this information to day-to-day performance analysis and to normalize it to the actual operation & sensor data of the vessels. To our knowledge, it hasn't been used for daily operations and optimization of the vessels.

The reason for this is that ship hull inspections are generally ordered for a single use: check what to do at a given time on the hull, and not collecting data.

Therefore, the quality and quantity of data collected during ship hull inspections is often too poor for detailed analysis. Data points are dispersed and difficult to correlate in real data, *Brink (2022)*.

What's more, these inspections are performed by hundreds of different service providers all around the world. The outputs and reports vary widely depending on the conditions of inspections, the technology used, the service provider skills, and the reporting style.

Up to now, this lack of consistency has made it impossible to normalize inspection data and to fit it in performance dashboards.

Efforts from the industry, *AMPP (2022), BIMCO (2021), NZ (1993)*, to improve the quality of underwater inspection reports will help get a better understanding at the hull and create reliable decisions. However, they are still all based on a small number of pictures, analyzed by the human eye, which is prone to errors: calculating the surface coverage of fouling in one image, for example, is very difficult to estimate with accuracy, *Brink (2022)*.

3.2. What technology can bring to make it compatible with performance dashboards

To ramp up the quality of underwater inspection reports, there is a need for some changes in good practices of hull data collection:

- more data: the surface of the hull of a 200 m vessel averages 10000 m^2, meaning 1.5 soccer fields. There should be more than just a dozen pictures to thoroughly know its state. Thousands of images should be taken to analyze the hull at the scale of the vessel.
- locate pictures: when it comes to knowing the state of the hull precisely, it's important to know where each of these thousands of pictures come from. Ship hull inspections should include information about the places or zones that were inspected, for each image or portion of videos.

Similarly, to make it useful and feasible, reporting should be adapted to the needs of big data:

- automated technology: whoever wishes to analyze thousands of pictures, says they should be assessed automatically, and report creation should be fast.
- removing human errors: the automated technology should create consistent dashboards for the service provider, for any water conditions and technology.
- presenting API-able dashboards: instead of PDF reports, analysis of inspections should be presented as smart, dynamic dashboards with a possibility to get overall scoring or to dive into picture-by-picture checks. All information should be made available to other data lakes through dedicated APIs.

Artificial intelligence is a tool that can automate and speed-up data analysis, as well as creating smart reports. Computer vision algorithms can be trained through neural networks to recognize fouling intensity, coating defects, and niche areas.

Notilo Plus has developed a combination of Hardware and Software to enable this change management. On the one hand, our ROV SEASAM locates collected data to perform hull inspections easily. It can be used as a Remotely Operated Vehicle after a very short training as the remote control makes it intuitive to pilot. Equipped with a high-definition low-light camera and compatible with powerful lights and extra-sensors (such as keeping distance to the hull or sea-chest explocam), it is a perfect tool to perform inspections on the hull with rich metadata such as depth, zones of the vessel, distance to the hull, etc.

On the other hand, more than 25,000 pictures were classified to train our dataset and enable Notilo Cloud to determine a fouling score with around 90% accuracy, *Guéré (2021)*. Various additional algorithms were created to detect defaults on coating, identify niche areas and to categorize the images according to their visibility.

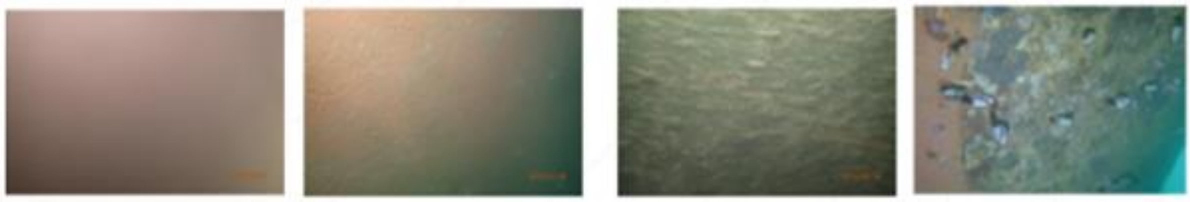

Fig.2: Classification rules for fouling AI analysis

This tool creates reproducible data that can be compared and included into statistical analysis: Notilo Cloud analyzes hours of videos and thousands of images and take them all into account to create a meaningful report.

On average, 10 hours are required to edit a traditional report with real world data - compared to 30 min with an automatic Notilo Cloud report and its algorithms.

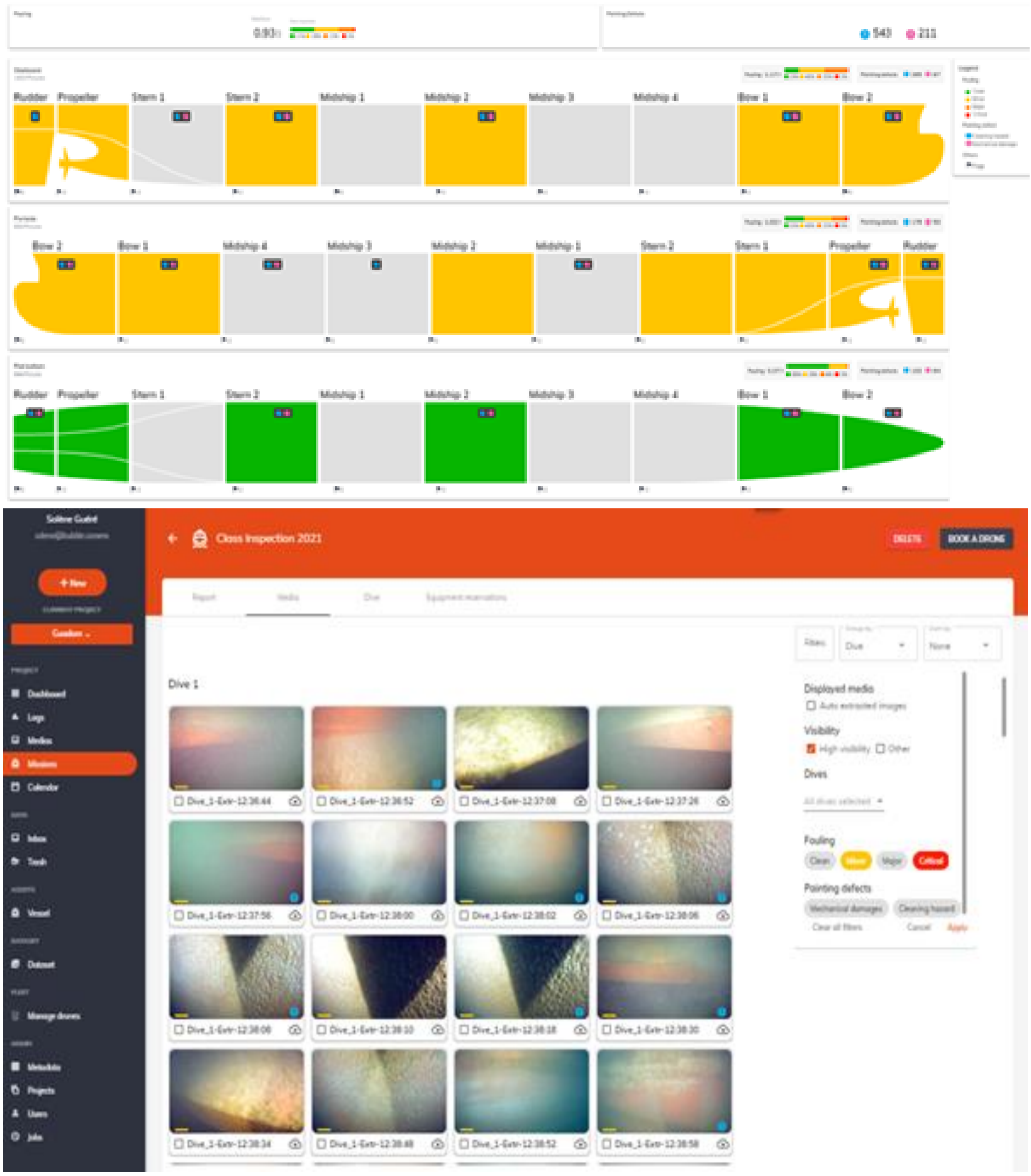

Fig.3: Screenshots of Notilo Cloud smart report and AI media filters

The hull reports generation requires several tasks and four different algorithms:

- A first algorithm extracts video frames where the hull can be seen. Only images showing the hull will be selected. After the frame extraction, a preprocessing algorithm adapts the format of the data to make it compatible with the other classifiers.
- A second algorithm precises if the frame consists in a niche area, and in that case, which niche area
- A third algorithm evaluates the level of fouling from 0 to 3, for each single relevant frame
- A fourth algorithm determines if any coating defect is present: painting defect or mechanical damage
- Finally, every image keeps its metadata about depth and zone around the vessel.

All these combined actions lead to the creation of a report, with 30 hull sections that have color and information on the status of each area, and a total of 120 zones with detail by draft.

This automatic evaluation makes the most out of hull videos, and by creating API-able smart reports, opens the way for more in-depth performance analysis.

4. What big hull data could bring to performance

These hull reports being digitalized on Notilo Cloud, we open a discussion on how much could be saved in fuel and CO2 emissions if they were bridged to hull performance data.

4.1. Check the zones that need cleaning

One major difference between theoretical and real-life hull data is the fact that real fouling is combined, and sometimes differently distributed all around the hull. In real-life, some patches are done, coating types vary, places are more exposed, and the hull has rarely a constant fouling type all around.

High scale, located data has an immediate effect: focusing the cleaning effort only on the parts that really need it and not to go over the clean parts.

This way, time required for cleaning operations is shortened if the cleaning is only performed on fouled areas. For a vessel cleaned only on half of the hull, the price of cleaning would be arguably 30% lower. Cleaning being shorter, the idle time of the vessel is lessened, with a smaller loss of profitability. When calculating the hourly cost of such an operation, we quickly understand the interest of optimizing them to reduce these costs and focus more on profitable operations. The idling time could drop from 18 hours to 12 hours, increasing operational time, resulting in savings that depend on the market conditions, but that could peak at hundreds of thousands of dollars if the cleaning was not well anticipated.

More importantly, most cleaning technologies damage the hull, leading to more frequent subsequent cleaning. It is frequent that the first cleaning would be performed 3 or 4 years after dry dock, whereas the following ones would need to be planned every 3 to 6 months, because fouling comes back more quickly once the coating has been scratched by cleaning tools. With Notilo Cloud tool, we delay coating deterioration as long as possible - and subsequent cleaning could also be partial cleanings.

Last but not least, by avoiding successive hull cleaning, the risk of paint residues going into the water and polluting the seabed is significantly reduced.

Fig.4: Fouling score by zone of the Starboard, with a detail by draft section – Example of report where only the bottom part of the vertical sides would need to be cleaned

By assessing more precisely the zones that need to be cleaned, the combined savings could reach between USD 50,000 and USD 100,000 of savings per cleaning.

4.2. Act preventively and with certainty

One of the major consequences of hull fouling on ship performance is the impact on fuel consumption. Indeed, the cleaner the hull, the less frictions of the water on the hull and therefore the less fuel consumption for a given speed. Moreover, fuel consumption is synonymous with money spent and emissions of greenhouse gasses.

The following list shows various common practices to help decide when it is time for hull cleaning:

- The rule of thumb, or no optimization, would regularly wait until there is 60% of overconsumption before planning a cleaning (Author's discussion with industry players).
- Low-data decisions, with low-frequency and low-quality data point, enables to recognize fouling when there is an overconsumption of around 30% and to plan fouling accordingly
- Current sensors and optimization of performance dashboards set up thresholds that vary depending on the specificity of each ship, but that would be around 15% of overconsumption. The reason is the impact of cleaning the hull when it is not required, that would be huge with economic consequences.

With more certainty about the state of the hull, the ship manager can act with confidence to order a cleaning.

In the example of the Fig.4, the fuel penalty would probably be average in the performance dashboards, and no cleaning would be planned.

However, it could be the right time to clean the bottom part of the vessel, and therefore lower fuel consumption without waiting for the 15% threshold. We anticipate that, in average, regular "data-rich" hull inspections would enable to lower the threshold to 5 to 7% of overconsumption.

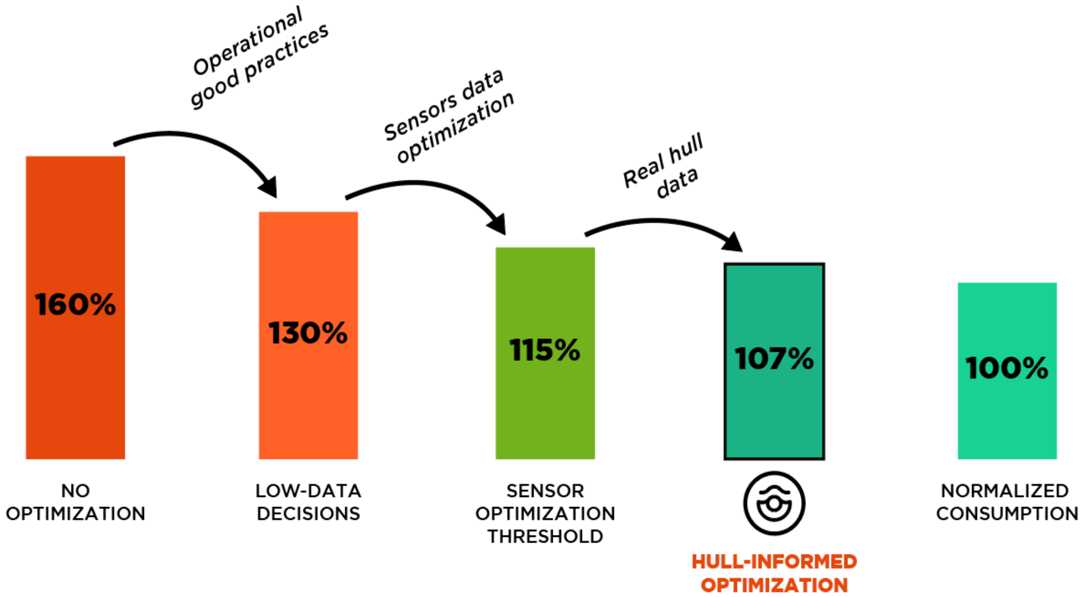

Fig.5: Fuel overconsumption threshold before cleaning, with various industry practices

Let's try to estimate the savings associated with real hull data analysis, compared with sensor-based optimization.

With sensor optimization, as high consumption triggering hull cleaning is around 115%, we can assume for this first calculation that the average over-consumption is around 7.5% in that case.

With hull-informed optimization where the trigger would be at 7% of over-consumption, let assume that it averages 3.5% of over-consumption.

On this basis, considering a vessel daily consuming 150T of fuel after dry dock, we can draw these results from the previous assumptions:

- Based on sensor optimization, over-consumption is in the range of 7.5% a day, which equals to 11.25 t additional fuel and 35.6 t additional CO_{2e} per day
- Based on real hull data optimization, over-consumption is in the range of 3.5% a day, which equals to 2.1 t additional fuel and 16.6 t additional CO_{2e} per day

In the end, getting from sensor-based optimization of hull condition to hull-informed allows ship owners to avoid yearly consumptions of 2,190 t of fuel, amounting to USD 1,916,000 (at USD a bunker price of 875 per ton) per year and 6,935 t of CO_{2e} emissions per year.

These considerable cost savings for just one vessel, would also render CII compliance easier.

4.3. Optimize decisions from one dry dock to another

Data's power of optimization is exponential as soon as it is merged with multiple data sources. This is what renders performance optimization algorithms so important. Adding hull data to fuel performance will enable the industry to understand with much better the adequacy of various types of coating, various technologies of cleaning, depending on the specificity of each vessel. On top of what is already developed to calculate fuel efficiency, hull data can improve knowledge about

- number and types of coating defects
- speed of fouling bloom after dry dock for a given paint
- speed of fouling boom after cleaning with a specific cleaning method
- efficacy of service providers cleaning
- and more…

The accuracy of these computations will be satisfying with AI methods, creating comparable data and remove human error.

In short, real hull data merged with performance creates new data sets that will give strong scientific information to help choose the right paint and the right cleaning method for each vessel.

This optimization would enable shipowners to anticipate the exact savings associated with higher quality paints, and ensure it is taken care of correctly.

It also widens the way for paint contracts with a lifetime paint warranty, making it available for many more vessels. By bringing more transparency all along the value chain of hull care, it will help shipowners and ship managers make more informed decisions, and the overall value of decreasing uncertainty and reaching new optima with paint care, industry-wide, has a tremendous potential.

For a given vessel, some paint suppliers claim that applying best-in-class paintings could amount to 6% of consumption decrease, *Hempel (2018), Wallentin (2012)*. Normalizing these numbers, not only with sensor data and weather data, but also using actual hull data, would enable them to certify these numbers, and perhaps find new creative ways to finance better performing paints, pushing the speed of the industry transition to better coatings.

Making the right coating and cleaning decision at the right time could, without any doubt, add a few percent points to the yearly savings of fuel.

Even one additional percent of optimization for the above example, with a vessel consuming 150 t of fuel daily, would amount to close to USD500k and more than 1,700 t of $CO_{2e.}$

5. Discussion and Challenges

Our preliminary results show that the economic optimum for ship hull maintenance decisions, including coating types, cleaning time and cleaning method is not yet found, and that real hull data would help get a step closer, potentially resulting in millions of dollars of savings each year for a single vessel. It would also make compliance to CII easier over the long run.

These results are still theoretical and would need to be backed by use cases on real vessels.

All findings point towards the need of better-quality hull data, creating more transparency. This transparency is essential, especially in complex industrial relationships involving many parties: shipowners, ship managers, charterers, coating manufacturers, service providers.

Reproductible dashboards would create an industry standard on which every party could build sustainable business cases and assumptions.

The reason why it has not been done, up to now, is that the world of ship hull inspections is very poorly digitized. Performed by a myriad of SMEs active in local ports around the world, the output lacks the coherence and consistency that would be necessary for data analysis.

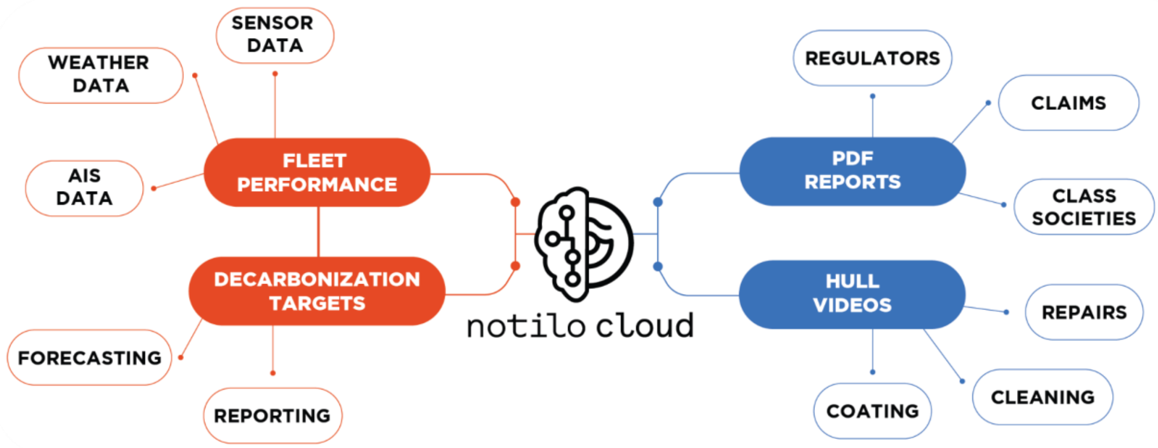

Fig.6: Connecting performance monitoring and in-water inspection

The industry players need to work together to increase the quality and quantity of data from hull inspections, to bridge the gap between hull reports and performance dashboards. Technology is readily available; the shipowners and ship managers should now organize the market by asking digitized reports to their vendors.

Working on use cases to validate the assumptions in this article would path the way to new algorithms, closer to the economic optimum and reducing climate consumption. It will accelerate the move from reactive cleaning to predictive cleaning.

It would also be useful to assess the impact of new cleaning methods such as proactive cleaning, in an emerging market where many technologies are released yearly.

Finally, the route to Net Zero carbon footprint technologies will require other sources of fuel, which all have in common to be more expensive than current oil sources. Hull optimization will therefore be crucial to keep costs down and make these climate-friendly technologies economically viable.

5. Conclusion

Fleet hull optimization is still a relatively "low" hanging fruit, reaching both climate targets and savings needs of industry players.

However, uncertainty in the world of ship hulls maintenance is still huge, and there is an overall lack of transparency between all parties involved including: ship managers, shipowners, paint manufacturers, and service providers.

Consequently, despite these being financially feasible, the optimum of hull coating and cleaning is not yet reached. This is the so-called 'energy efficiency gap', which is caused by an unrealized potential for improvement, and affects many other fields, *Johnson et al. (2014)*. One of the barriers for the implementation of new energy efficiency improving technologies is the lack of actual data to work on. With artificial intelligence technology, hull data can become a new brick of technology that will be a game changer for hull maintenance, and vessel performance in general.

This will help the shipping industry reach their sustainability goals and protect Planet Earth for the years to come.

References

ACCIARO, M.; HOFFMANN, P.; EIDE, M. (2013), *The energy efficiency gap in maritime transport* J. Shipp. Ocean Eng. 3(1-2)

AMPP (2022), SC19 | TR21517 - *Grooming and Remote Inspection of Ship Hull Surfaces*, Association for Materials Protection and Performance

BIMCO (2021), *Industry standard on in-water cleaning with capture*, BIMCO, Copenhagen

BRINK, A. (2022), *Biofouling impact on vessel performance and GNG emissions*, Clean Hull Initiative launch

BUHAUG, Ø.; CORBETT, J.J.; ENDRESEN, O.; EYRING, V.; FABER, J.; HANAYAMA, S.; LEE, D.; LINDSTAD, H.; MJELDE, A.; PALSSON, C.; et al. (2009), *Second IMO greenhouse gas study*, Int. Maritime Org., London, https://www.imo.org/en/OurWork/Environment/Pages/Second-IMO-GHG-Study-2009.aspx

CHI (2022), *Impact on Ships' Biofouling on Greenhouse Gas Emissions,* CHI launch event, Oslo

CORADDU, A.; ONETO, L.; BALDI, F.; CIPOLLINI, F.; ATLAR, M.; SAVIO, S. (2019), *Datadriven ship digital twin for estimating the speed loss caused by the marine fouling*, Ocean Eng. 186, 106063

GUÉRÉ, S.; GAMBINI, N. (2021), *Hull Reports at Scale – Notilo Cloud AI Platform,* 6th HullPIC, Pontignano

HEMPEL (2018), *10 Years of Savings with Silicone Coatings*, https://www.hempel.com/news/2018/10-years-of-savings-with-silicone-coatings

IMO (2020), *Fourth IMO greenhouse gas study*, Int. Maritime Org., London URL https://docs.imo.org

JOHNSON, H.; JOHANSSON, M.; ANDERSSON, K. (2014), *Barriers to improving energy efficiency in short sea shipping: an action research case study*, J. Cleaner Prod. 66, pp.317-327

MOLLAND, A.; TURNOCK, S.; HUDSON, D.; UTAMA, I. (2014), *Reducing Ship Emissions: A Review of Potential Practical Improvements in The Propulsive Efficiency of Future*, Trans. RINA 156, Part A2, pp.175-188

NZ (1993), *Requirements for Vessels Arriving in New Zealand*, New Zealand - Biosecurity Act 1993, Biosecurity New Zealand Standard

SEAH, Y.H.; CHEN, H.L.; KIDD, B. (2021), *Feature Engineering-Enhanced Vessel Performance Prediction and Modeling*, 6th HullPIC, Pontignano

SCHULTZ, M.P. (2004), *Frictional resistance of antifouling coating systems*, ASME J. Fluids Eng. 126, pp.1039-1047

SMITH, T.; JALKANEN, J.; ANDERSON, B.; CORBETT, J.J.; FABER, J.; HANAYAMA, S.; O'KEEFFE, E.; PARKER, S.; JOHANSSON, L.; ALDOUS, L.; RAUCCI, C., TRAUT, M., et al. (2014), *Third IMO greenhouse gas study*, Int. Mar. Org., London, https://www.imo.org/en/OurWork/Environment/Pages/Greenhouse-Gas-Studies-2014.aspx

WALLENTIN, B. (2012), *The illusion of fuel savings – an urgent need for improved transparency in marine hull coatings*, Jotun, http://cdn.jotun.com/images/the-illusion-of-fuel-savings_tcm29-10267.pdf

Index by Authors

Aas 149
Athanassopoulos 218
Bekiaris 75
Bensow 207
Bertelsen 260
Berthelsen 4
Bertram 16,24
Bingham 63
Birvalski 234
Blaurock 275
Brink 149,190
Carella 260
Colle 198
Deymier 63
Elbertsen 234
Fritz 107
Gambini
Gangeskar 260
Gatin 30
Georgousis 181
Giordamlis 75
Gorski 169
Guere 280
Gundermann 63
Hansen 111
Hendricks 275
Hoffmann 161
Kalajdžić 30
Karlstad 249
Kluwe 141
Köpke 254
Kuroda 36
Marioth 111
Michniewicz 169
Mittendorf 63
Montazeri 181
Morobé 198
Nielsen 4,63
Nikitakis 218
Nisbet 124
Olsson 124
Paereli 190
Pang 50
Parkes 50
Petersen 181
Polymenakos 218
Ponkratov 234
Prytz 260
Richter 141
Schmidt 260
Schmode 63
Shiri 207
Sivena 218
Struijk 234
Sogihara 36
Tan 190
Tolias 75
Tsarsitalidis 218
Tsompanoglou 91
Tsompopoulou 218
Tsujimoto 36
Wagner 141
Werner 124,207
Wienke 244
Yeginbayeva 149
Zervos 75

8th Hull Performance & Insight Conference (HullPIC)

Merged with 4th PortPIC Conference

Pontignano/Italy, 28-30.8.2023

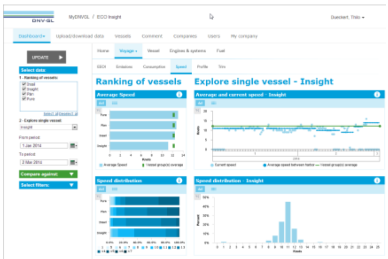


Topics: ISO 19030 and beyond / sensor technology / human factors in reporting & understanding performance / information fusion / big data / uncertainty analysis / hydrodynamic models / business models / cleaning technology / coating technology / ESDs

Organiser: Volker Bertram (VB conferences)
Morten Sten Johansen (Jotun)

Advisory Committee:

Francesco Bellusci	Scorpio Group	**Jeppe S. Juhl**	BIMCO	**Geir Axel Oftedahl**	Semcon
Jasper Cornelis	Port of Zeebrugge	**Jan Kelling**	Hasytec	**Beom-Jin Park**	KRISO
Simon Doran	HullWiper	**Manolis Levantis**	Jotun	**Buddy Reams**	NACE
Johnny Eliasson	Chevron Shipping	**John Lewis**	ES Link Services	**Runa Skarbø**	Bellona
Wojciech Gorski	Enamor	**Carsten Manniche**	Ultranav	**Aron Sorensen**	BIMCO
Solene Guere	Notilo Plus	**Richard Marioth**	Idealship	**Geoff Swain**	FIT
Erik Hagestuen	Kyma	**Justin McDonald**	Gov. Western Australia	**Burkhard Watermann**	Limnomar
Gilyong Han	Intertanko	**Ivana Melillo**	D'Amico	**Sofia Werner**	SSPA
Liz Haslbeck	NSWC-CD	**Alex Noordstrand**	FleetCleaner	**Diego M. Yebra**	Hempel
		Tor M. Østervold	ECOsubsea		

Venue: The conference will be administered in Hamburg/Germany and held in Pontignano/Italy

Format: Papers to the above topics are invited and will be selected by a selection committee.
The proceedings will be made freely available to the general public.

Deadlines:

anytime	Optional "early warning" of interest to submit paper / participate
21.03.2023	First round of abstract selection (1/3 of available slots)
21.04.2023	Second round of abstract selection (remaining slots)
21.07.2023	Payment due for authors
21.07.2023	Final papers due

Admin. Fees: **800 €** – early registration (by 30.06.2023)
900 € – late registration

Fees are subject to German VAT

Sponsors: Jotun, Tutech Innovation, COACH Solutions, Enamor, Hasytec, Hempel, Hoppe Marine, HullWiper, Idealship, Kyma, Miros Mocean (further sponsors to be announced)

Information: volker@vb-conferences.com or volker.bertram@dnv.com